



Seismic bridge design and retrofit – structural solutions

Seismic bridge design and retrofit – structural solutions

State-of-art report

prepared by Task Group 7.4,

Seismic design and assessment procedures for bridges

May 2007

Subject to priorities defined by the Technical Council and the Presidium, the results of <i>fib</i> 's work in Commissions and Task Groups are published in a continuously numbered series of technical publications called 'Bulletins'. The following categories are used:	
category	minimum approval procedure required prior to publication
Technical Report	approved by a Task Group and the Chairpersons of the Commission
State-of-Art Report	approved by a Commission
Manual, Guide (to good practice) or Recommendation	approved by the Technical Council of <i>fib</i>
Model Code	approved by the General Assembly of <i>fib</i>
Any publication not having met the above requirements will be clearly identified as preliminary draft.	
This Bulletin N° 39 was approved as an <i>fib</i> state-of-art report by Commission 7, <i>Seismic design</i> , in 2006.	

This report was mainly drafted by the following members of Task Group 7.4, *Seismic design and assessment procedures for bridges*:

G. M. Calvi^{1,6} (Convenor, Univ. degli Studi di Pavia and ROSE School, IUSS, Italy), K. Kawashima^{1,11} (Convenor, Tokyo Institute of Technology, Japan), I. Billings⁸ (Beca Carter Hollings, Auckland, New Zealand), A. Elnashai¹⁰ (Univ. of Illinois, USA), C. Nuti⁹ (Univ. di Roma Tre, Italy), A. Pecker⁵ (Géodynamique et Structure, France), P. E. Pinto^{7,10} (Univ. di Roma La Sapienza, Italy), N. M. J. Priestley^{2,3} (ROSE School, IUSS, Italy), M. Rodriguez⁴ (Univ. Nacional Autonoma do Mexico, Mexico)
^{1,2,.....} chapter number for which this TG member was the responsible author

Further relevant contributions to individual chapters were provided by
L. Di Sarno¹⁰ (Univ. degli Studi del Sannio, Italy), P. Franchin^{7,10} (Univ. di Roma La Sapienza, Italy),
D. Pietra⁶ (Ph. D. student, ROSE School, Italy; also assisted in proof-reading and reviewing all chapters),
I. Vanzi⁹ (Univ. G. D'Annunzio, Italy).
^{1,2,.....} chapter numbers

The valuable support, through discussions and comments, of other Task Group and Commission members not mentioned here is gratefully acknowledged by the authors. Full address details of Task Group members may be found in the *fib* Directory or through the online services on *fib*'s website, www.fib-international.org.

Production note

The authors regret that some photos and diagrams for publication in this Bulletin could not be made available in accordance with the usual *fib* quality requirements for off-set printing. As a result, a number of figures were unsuitable for colour printing, and some may be difficult to read. As a service to readers of this Bulletin who may wish to refer to the original (low-resolution) colour images, a number of figures have therefore been made available for electronic viewing in a colour PDF file, which can be downloaded, free of charge, from the *fib* website at www.fib-international.org/publications/fib/39. This is indicated in the Bulletin, where applicable, by a note accompanying the relevant figures. The *fib* secretariat regrets any inconvenience caused by this procedure.

Cover photo: The Rion-Antirion Bridge near Patras (Greece), one of the winners of the 2006 *fib* Awards for Outstanding Structures, *Civil Engineering Structures* category

© fédération internationale du béton (*fib*), 2007

Although the International Federation for Structural Concrete *fib* - fédération internationale du béton - does its best to ensure that any information given is accurate, no liability or responsibility of any kind (including liability for negligence) is accepted in this respect by the organisation, its members, servants or agents.

All rights reserved. No part of this publication may be reproduced, modified, translated, stored in a retrieval system, or transmitted in any form or by any means, electronic, mechanical, photocopying, recording, or otherwise, without prior written permission.

First published in 2007 by the International Federation for Structural Concrete (*fib*)

Postal address: Case Postale 88, CH-1015 Lausanne, Switzerland

Street address: Federal Institute of Technology Lausanne - EPFL, Section Génie Civil

Tel +41 21 693 2747 • Fax +41 21 693 6245

fib@epfl.ch • www.fib-international.org

ISSN 1562-3610

ISBN 978-2-88394-079-6

Printed by Sprint-Digital-Druck, Stuttgart

Preface

This Bulletin represents a further evidence of the continued power of *fib*, heir of the illustrious associations CEB and FIP, of attracting experts from all over the world to participate in tasks that are most frequently challenging from both the intellectual as well as the material point of view, with no other reward than the pleasure of learning from each other, of comparing experiences, and producing worthy documents.

Consider the topic: bridges and earthquakes, and imagine a group of experts from places as diverse as Japan, New Zealand, Europe, North and South America, having their first meeting to discuss content and character of the future document. The initiative is voluntary, and the higher decision bodies of *fib* rely on the seismic commission and its groups for the most appropriate choice of the content. Opinions on best balance differ, being almost as many as are the prevailing orientations of the members: design, analysis, assessment, isolation, strengthening, experiment, reliability-based approaches, foundations, etc.

Agreeing on the titles in the list of content has been then a first successful effort, only to be followed, however, by a continuous, patient, work, lasted for more than three years, of placate and less placate discussions on exactly what material and in what form should be included or not under each title. As one can understand, the problem was one of abundance, not of scarcity, given the wealth of knowledge available within the group, and a great merit goes to the convenors for their steering and to the active members for their goodwill to temperate their opinions with those of the others.

What can be said about the outcome? It is my true belief that this Bulletin rates quite high in terms of comprehensiveness, state-of-the-art global information, clarity and rigour of presentation. It is a small “summa” of the present state of knowledge regarding bridges subjected to seismic action: it is more specialised than a textbook, but it is equally profitably readable by engineers seriously engaged in the non-trivial task of seismic bridge design.

Paolo Emilio Pinto
Chairman of *fib* Commission 7, *Seismic design*

Contents

PART I – INTRODUCTORY REMARKS

1	Introduction	1
1.1	Bridges and dreams	1
1.2	Bridge structural solutions	2
1.3	Current design practice and trends	2
1.4	Current developments	3
1.5	Problems with existing bridges	3
1.6	Dreams and reality	3

PART II – CURRENT DESIGN PRACTICE AND TRENDS

2	Pier section for bridges in seismic regions	5
2.1	Introduction	5
2.2	Single-column or multi-column piers	5
2.3	Column section shape	5
2.4	Hollow section columns	7
2.5	A regional review of design choices	10
	References	18
3	Pier/superstructure connection details	19
3.1	Introduction	19
3.2	Advantages and disadvantages of support details	19
3.3	A regional review of design choices	21
	References	22
4	Superstructure	23
4.1	Introduction	23
4.2	Section shapes for superstructures	23
4.3	Movements joints	25
	4.3.1 Design practice in California – 4.3.2 Design practice in Japan – 4.3.3 Design practice in Greece	
4.4	Stresses in bridge superstructures subjected to seismic actions	28
4.5	A regional review of design choices of bridge superstructure	29
	References	40
5	Design of foundations	41
5.1	Overview of bridge foundations design	41
5.2	Spread foundations	42
	5.2.1 Force evaluation – 5.2.2 Stability verifications –5.2.3 Structural design	
5.3	Pile foundations	46
	5.3.1 Pile types for bridge foundations – 5.3.2 Modeling techniques – 5.3.3 Pile integrity checks	
5.4	Design of foundations in a liquefiable environment	54
	5.4.1 Shallow foundations – 5.4.2 Pile foundation	
	References	61

PART III – CURRENT DEVELOPMENTS

6	Design for enhanced control of damage	65
6.1	Basic concepts for enhanced damage control	65
6.2	Seismic structural control strategies	65
6.3	Bearings, isolators and energy dissipation units	66
	6.3.1 General features – 6.3.2 Elastomeric bearings – 6.3.3 Sliding devices – 6.3.4 Metallic and Friction Dampers – 6.3.5 Viscous and Viscoelastic Dampers – 6.3.6 Self-Centering Dampers – 6.3.7 Electro and Magnetorheological Dampers – 6.3.8 Electro-inductive devices	
6.4	Active and semi-active control systems	109
	6.4.1 Optimal force control – 6.4.2 Optimal displacement control	
6.5	Design concepts and analysis of deck – isolated bridges	110
	6.5.1 Analysis concepts – 6.5.2 Basics of capacity design – 6.5.3 Considerations on input characteristics	
6.6	Foundation rocking and pier base isolation	115
	6.6.1 Basics of foundation rocking 6.6.2 Soil – Structure Interaction (SSI) 6.6.3 Pier base isolation	
6.7	Controlled rocking of piers and built-in isolators	116
	6.7.1 Controlled rocking of combined concrete members – 6.7.2 Response of partially prestressed coupled members – 6.7.3 Design and analysis of segmented piers – 6.7.4 Unbonded columns and isolator built – in columns	
	References	123
7	Design for spatial variation of ground motion	129
7.1	Introduction	129
7.2	Analytical modelling	130
	7.2.1 Model of spatial variability – 7.2.2 Generation of samples	
7.3	Review of relevant past studies	134
	7.3.1 Monti, Nuti and Pinto 1996 – 7.3.2 Lupoi, Franchin, Pinto and Monti 2005 – 7.3.3 Sextos, Kappos and Pitilakis 2003 – 7.3.4 Shinozuka, Saxena and Deodatis 2000 – 7.3.5 Monti and Pinto 1998 – 7.3.6 Nuti and Vanzi 2004, 2005	
7.4	Concluding remarks	155
	References	156
8	Design for active fault crossing	159
8.1	Introduction	159
8.2	Fault effects and ground displacements	162
8.3	Planning issues	163
8.4	Performance requirements and design philosophy	164
8.5	Design steps	165
8.6	Design concepts	166
	8.6.1 Design of fault crossing bridges	
8.7	Retrofit design	167
8.8	Project examples	167
	8.8.1 Bolu viaduct retrofit, Turkey – 8.8.2 Thorndon overbridge retrofit, New Zealand – 8.8.3 Taiwan high speed rail project - Tuntzuchiaofault crossing – 8.8.4 Fujimi Dori Torii route bridge, Japan – 8.8.5 Rion Antirion bridge, Greece – 8.8.6 I10/I215 interchange ramp, California	
	References	172

PART IV – PROBLEMS WITH EXISTING BRIDGES

9	Screening of bridges for assessment and retrofit	175
9.1	Introduction	175
9.2	Classification of the methods	176
9.3	Review of the methods	177
	9.3.1 Methods based on physical models only, (i.B): Kawashima et al., 1990, Nielson et al., 2003 – 9.3.2 Methods based on engineering judgement and cost of failure, (i.A) (ii,A,B): ATC, 1983, FHWA, 1995, WSDOT, 1991, Basoz and Kiremidjian, 1996 – 9.3.3 Methods based on physical models and cost of failure, (i.B) (ii.A or B)	
9.4	Classification of minimisation problems	192
9.5	Conclusions	193
	References	194
10	Fragility assessment	197
10.1	Introduction	197
10.2	Structural deficiencies	197
	10.2.1 Span failure – 10.2.2 Pier failure – 10.2.3 Joint failure – 10.2.4 Abutment failure – 10.2.5 Footing failure	
10.3	Limit states	204
	10.3.1 Requirements for comprehensive limit states for assessment – 10.3.2 Observational limit states – 10.3.3 Limit states of functionality – 10.3.4 Analytical limit states	
10.4	Methods of assessment	211
	10.4.1 Observational methods – 10.4.2 Analytical methods – 10.4.3 Example applications	
10.5	Fragility assessment	226
	10.5.1 Approaches for fragility assessment – 10.5.2 Background to probabilistic fragility assessment – 10.5.3 Example applications	
	References	241
11	Seismic retrofit	247
11.1	Introduction	247
11.2	Retrofit of columns and piers	247
	11.2.1 Introduction – 11.2.2 Steel jacketing – 11.2.3 Reinforced concrete jacket and shear wall – 11.2.4 Composite material jackets – 11.2.5 Precast concrete segment jacket	
11.3	Retrofit of beam-column joints	271
	11.3.1 Retrofit of cap beams – 11.3.2 Retrofit of cap beam/column joint regions	
11.4	Retrofit of foundations	277
	11.4.1 Introduction – 11.4.2 Retrofit of foundations to instability of surroundings soils – 11.4.3 Shear and flexure retrofit of footings – 11.4.4 Cost-effective dry-up construction method – 11.4.5 Micro piles – 11.4.6 Retrofit of abutments	
11.5	Retrofit of superstructures	286
11.6	Retrofit using dampers and isolation	287
	11.6.1 Introduction – 11.6.2 Retrofit using seismic isolation – 11.6.3 Retrofit using brace dampers	
11.7	Other measures for seismic retrofit	292
	References	294

1 Introductory remarks

1.1 Bridges and dreams

“Imagine a world without bridges.”

This is the incipit of Petroski’s book ‘Engineers of dreams’¹ where he describes how *“bridges have become symbols and souls of cities, and each city’s bridges have been shaped by, and in turn shape, the character of that city”*.

There is no question about the role that bridges have played in the development of civilization, and no question about their power of evocation on people, as symbols of scientific and technical advancement, of richness, and of power.

Bridge structures have also always occupied and still occupy a special place in the affection of structural engineers, probably because in bridges the structural conception is more strictly related to aesthetics and functionality than in most other construction types. For the same reason bridges give the impression of being rather simple structural systems, whose seismic response could be easily predicted. On the contrary, in recent earthquakes bridges did not perform well, showing an increased need of research and understanding of different potential problems and collapse mechanisms.

In recent years progress in design and assessment procedures have been achieved all over the world and practices have changed.

Beautiful bridges have been built in high seismicity areas, such as the splendid Rion – Antirion bridge, that recently won several awards for its excellence in design and construction.

Large viaducts were severely challenged by intense seismic action, such as in the case of the Bolu Viaduct, that sustained significant damage during the November 1999, Duzce Earthquake and had to be subjected to a complex and innovative repair and retrofit process.



Fig. 1.1: The Rion – Antirion bridge.
(Figure available electronically on *fib* website; see production note on p. ii)

¹ Petroski, H., *Engineers of dreams*, Knopf, 1995

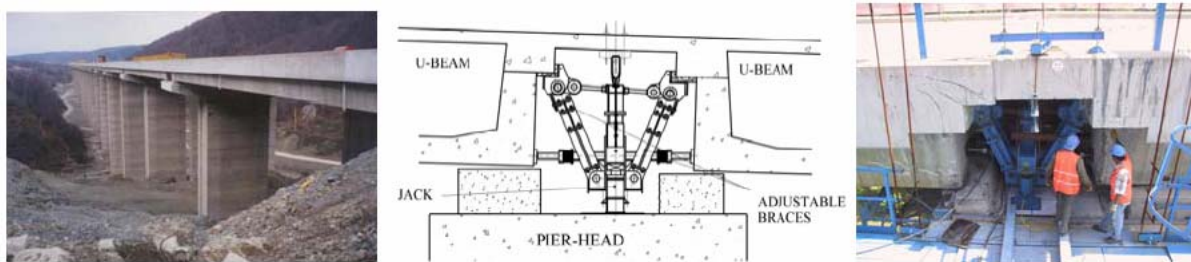


Fig. 1.2: The Bolu Viaduct, design and operation for repositioning the superstructure
(Figure available electronically on fib website; see production note on p. ii)

1.2 Bridge structural solutions

In this context, it was felt useful and appropriate to present, discuss and critically compare structural solutions for bridge seismic design and retrofit developed and used all over the world, ten years after the publication of the last comprehensive manual on the subject².

For this purpose, a truly international team of experts came together and cooperated actively and intensely for more than three years, holding six meetings, in Greece, USA, Canada, France, Italy, and Japan.

It was decided that the Bulletin should address problems with current design (comparing current design practice and trends), current developments in specific areas (such as enhanced damage control, spatial variability of ground motion and fault crossing) and problems to be encountered when dealing with existing bridges (screening, assessment and strengthening).

These choices are reflected into the organization of the contents of the Bulletin, which is briefly overviewed in the next sections.

1.3 Current design practice and trends

Consistent with the above discussion, the first four chapters of the Bulletin essentially present a regional review of design choices, comparing and discussing design practice all over the world, and pointing out relative merits and potential problems.

In **chapter 2** pier sections are considered, discussing essential practices which are required to design columns with sufficient strength and ductility capacity. Single vs. multi – columns, solid vs. hollow shapes, a review of regional design choices and pier reinforcement details is presented.

In **chapter 3** superstructure – pier connections are described with an emphasis on advantage and disadvantage of monolithic moment-resisting vs. bearing supported connection. A review of regional design choices of connection and type of bearing describes presented.

In **chapter 4** superstructure are addressed. Section shape, stiffness and weight of superstructures, movement joints and seat length, precast vs. cast-in-place superstructures, seismic analysis consideration and a review of regional design choices of superstructures is introduced.

In **chapter 5** design of foundations is tackled, discussing design of spread vs. pile foundations and design of foundations in a liquefiable environment. A description of the typical regional practice of type and design of foundations is also presented.

² Priestley, M. J. N., F. Seible and G. M. Calvi, Seismic design and retrofit of bridges, Wiley, 1996

1.4 Current developments

Current developments are treated in the next three chapters, with particular emphasis on design for enhanced damage control, for spatial variation of ground motion and for fault crossing.

In **chapter 6** control strategies are discussed and presented in relation to possible choices of bearing, isolation and dissipation units, foundation rocking, base isolation, controlled rocking of piers and built in isolators.

In **chapter 7** different models to represent the spatial variability of ground motion are introduced, with reference to loss of coherence, wave passage and soil profiles.

In **chapter 8** fault effects and ground displacements, planning issues, design philosophy and concepts, retrofit choices and relevant case studies are presented, in relation to the general subject of fault crossing.

1.5 Problems with existing bridges

The last part of the Bulletin presents a summary of current issues related to existing bridges.

In **chapter 9** screening approaches for assessment and retrofit are introduced, presenting methods based on physical models and on engineering judgement.

In **chapter 10** methods for assessment of existing bridges are overviewed, with reference to structural deficiencies, limit states, observation vs. analytical methods of assessment, and fragility analysis approaches.

Finally, in **chapter 11** aspects of retrofit design and examples are introduced, with specific reference to columns and piers, beam column joints, foundations, superstructure, and application of dampers and isolation to seismic retrofit.

1.6 Dreams and reality

As discussed in 11 chapters, extensive technical developments have been taking place in the last two decades to make a reality of the dream that bridges serve as a most important transportation infrastructure with limited damage during earthquakes. It is obvious from the contents of this Bulletin that the effort towards this objective has been tremendous. Because shapes and contents of the dreams depend on regional seismicity, system of transportation, seismic performance goals, culture and peoples, design and construction practices with a wide range spectrum are presented and discussed in this Bulletin.

The history of seismic design has been too often a repetition of damage produced by earthquakes and consequent modification of design practices. We need to develop insight and technology to solve hidden problems behind visible damage to make the dreams come true.

2 Pier sections for bridges in seismic regions

2.1 Introduction

Pier Section design is more critically affected by seismic considerations than other parts of the bridge, with the possible exception of the foundations, since it will normally be the case that lateral resistance to seismic forces and displacements will be provided by the piers. With conventional seismic design (as distinct from seismic isolation design – see Chapter 6), ductility, implying potential damage will be expected from the piers under design-level seismic response. This requires the designer to carefully consider different alternatives for section shape, and reinforcement layout to ensure that the required seismic displacement capacity is available without significant strength degradation.

Alternatives to be considered include whether single-column or multiple-column piers are to be adopted, whether circular, rectangular, oval, or special architectural section shapes are more appropriate for the design constraints, whether solid or hollow pier sections are to be used, and how these choices impact on the reinforcement layout in the piers.

An international survey, presented at the end of this chapter, indicates that to some extent the choices between the above alternatives are based on convention and tradition, rather than pure structural considerations, and hence regional differences are apparent. Before discussing these differences, it is appropriate to present general information based on structural considerations. These have been presented elsewhere by Priestley et al. (1996) which is used as a basis for this discussion.

2.2 Single-column or multi-column piers

The choice between single-column and multi-column piers cannot be made independently of the choice of pier/superstructure connection type (see Chapter 3). With bearing-supported superstructures, the single-column design has the attraction that critical seismic response characteristics (strength and stiffness) can be made equal in orthogonal directions, since the pier will respond as a simple vertical cantilever in all directions. The location and performance of the potential plastic hinge will be known to a high degree of certainty. On the other hand, the lack of redundancy associated with a single-column vertical cantilever has led some design authorities to specify lower design ductility levels for this type of design relative to multi-column designs.

Multi-column piers are more appropriate when monolithic pier/superstructure connection details are selected, and also when the superstructure width is large, resulting in a potential for high eccentric live-load moments in single-column piers. When the column has monolithic connections to the superstructure and foundation, it is again simple to make the seismic response characteristics omni-directional. Note, however, that if the superstructure is bearing-supported on a multi-column pier-cap, pier response will be as a vertical cantilever in the longitudinal direction, and by double-bending transversely, resulting in non-uniform strength and stiffness in orthogonal directions.

2.3 Column section shape

Figures 2-1 and 2-2 illustrate different possible section shapes for reinforced concrete columns of bridge piers. The principal choice will be between circular and rectangular

sections, with a secondary choice between solid and hollow section shapes. Additional, more complex section shapes principally chosen on the basis of architectural considerations may be considered, as in the example of Fig.2-2c (Hines et al., 2001). Such sections may present difficulties in seismic detailing, and in assurance of satisfactory seismic performance, unless verified by structural testing. In Fig.2-1, sections A-A and B-B represent the common choice of columns with a circular distribution of longitudinal reinforcement contained within transverse reinforcement in the form of circular hoops or spirals. These sections are efficient, economical and easy to construct. The continuous curve of the transverse reinforcement results in excellent confinement of the core concrete and also provides effective constraint against buckling of the longitudinal flexural reinforcement. Section strength and displacement capacity are independent of direction of seismic response.

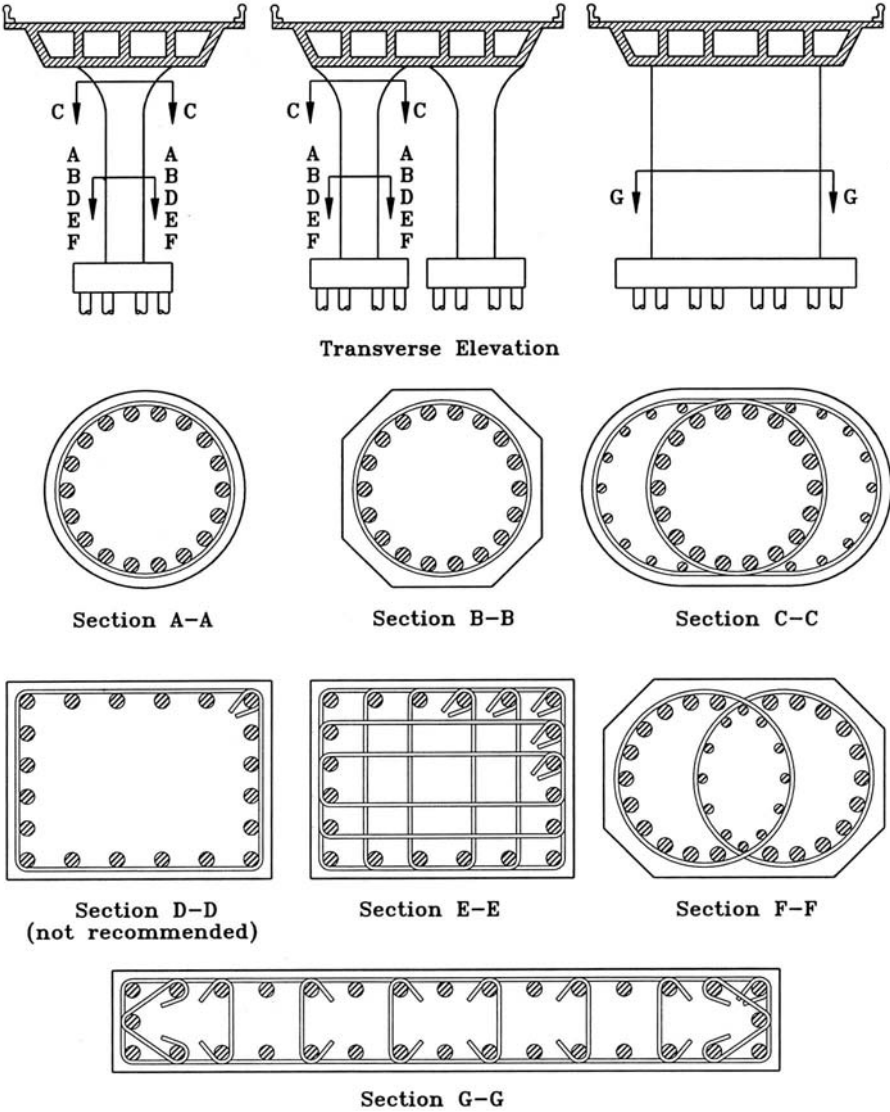


Fig.2-1: Solid section alternatives for bridges (after Priestley et al.,1996)

With monolithic pier/superstructure designs it is common to flare the top of the column to provide better support to the cap beam under eccentric live-load, and also to improve aesthetics. An example is shown in section C-C, Fig 2-1, where the circular longitudinal reinforcement has been supplemented by additional reinforcement in the flare region. For

single-column piers, the flare will normally be contiguous with the pier cap, but for multi-column piers where plastic hinges are expected at the top as well as the base of the columns, the flare is sometimes separated from the superstructure by a gap of about 50mm to provide certainty about the location of the top plastic hinge. This detail is common in California. Although certainty about location of the plastic hinge is assured by this detail, experiments have shown that premature damage to the non-structural flare may occur due to strain incompatibility between the flare and the core plastic hinge.

Rectangular columns, though common in bridge design are less desirable than circular columns from a seismic viewpoint. Sections D-D to F-F of Fig.2-1 show possible alternatives for solid rectangular sections. Section D-D has only peripheral hoop reinforcement, which is ineffective in confining the core concrete and in providing restraint against longitudinal bar buckling, and hence should never be used when ductile response is required of the pier. Providing adequate confinement using rectangular hoops, as is common in building columns, and illustrated in Fig.2-1, section E-E, is possible for only comparatively small bridge columns, since the layout of transverse hoops necessary to adequately restrain all longitudinal bars against buckling becomes impractical when the number of longitudinal reinforcing bars exceeds about 20, the number shown in section E-E.

It should be noted that a further problem with rectangular columns is that when loaded in the diagonal direction, cover spalling will initiate at lower levels of seismic intensity than when loaded in the principal directions. This is because the depth of the compression zone must be larger to provide the required compression force, resulting in lower curvatures corresponding to the extreme-fibre spalling strain. This can have significance when the design requirements include consideration of serviceability levels of response.

In California, the detail of using longitudinal reinforcement contained within intersecting spirals, as shown in Fig. 2-1, section F-F is common for large rectangular columns. Semi-circular ends, or large chamfers are used to avoid excessive cover, with consequent potential spalling problems, and to reduce sensitivity to diagonal attack. The spirals must overlap by a sufficient amount to ensure that shear strength is not compromised.

When longitudinal response of a bridge with comparatively few spans is resisted principally by abutments, an elongated rectangular pier section as shown in Fig.2-1, section G-G may be adopted. In the transverse direction, these sections act as structural walls, with high strength and stiffness, but in the longitudinal directions, they have low stiffness, thus attracting little seismic force. Despite this, tests (Haroun et al., 1994) have shown that significant ductility capacity exists in the longitudinal direction, even when transverse confinement details are poor, as will generally be the case.

2.4 Hollow section columns

When large, long-span bridges have tall bents, hollow columns may be a viable option. These have the advantage of reducing concrete mass, thus reducing inertial response of the piers as vertical beams spanning between foundation and superstructure, and also reduce the tendency for thermally-induced cracking at an early age resulting from heat-of-hydration temperature variations. In Europe, hollow sections with large section dimension (up to 8m maximum section depth or diameter) are common. Fig.2-2 shows alternatives based on hollow circular and hollow rectangular sections.

The hollow circular option of Fig.2-2(a) is less common than the rectangular option of Fig.2-2(b), despite theoretical considerations which would indicate improved seismic performance for the circular option, resulting from similar considerations to those noted above for solid sections. With the two-layer reinforcement pattern shown, with rings of longitudinal and transverse reinforcement adjacent to both outer and inner surfaces of the hollow section,

the inner hoop, if placed in tension by confinement requirements, will tend to induce a radially inwards component on the inner concrete cover, providing a negative confining influence, possibly resulting in implosion. To combat this, cross links must be anchored over the inner spiral or hoop, making for difficult construction. It would thus appear that the inner layer of reinforcement provides little structural benefit, apart from being a location of additional vertical reinforcement. Tests on hollow circular sections subjected to simulated seismic action (Ranzo and Priestley, 2001) have shown that hollow circular columns with all longitudinal and transverse reinforcement placed in a single layer close to the outer surface provide excellent stable hysteretic response provided extreme fibre compression strains are less than about 0.006. At higher extreme fibre strains, external cover concrete spalling can result in a sudden increase in the depth of the neutral axis, increasing the strain at the internal surface of the section to the stage where internal spalling, resulting in implosion, occurs.

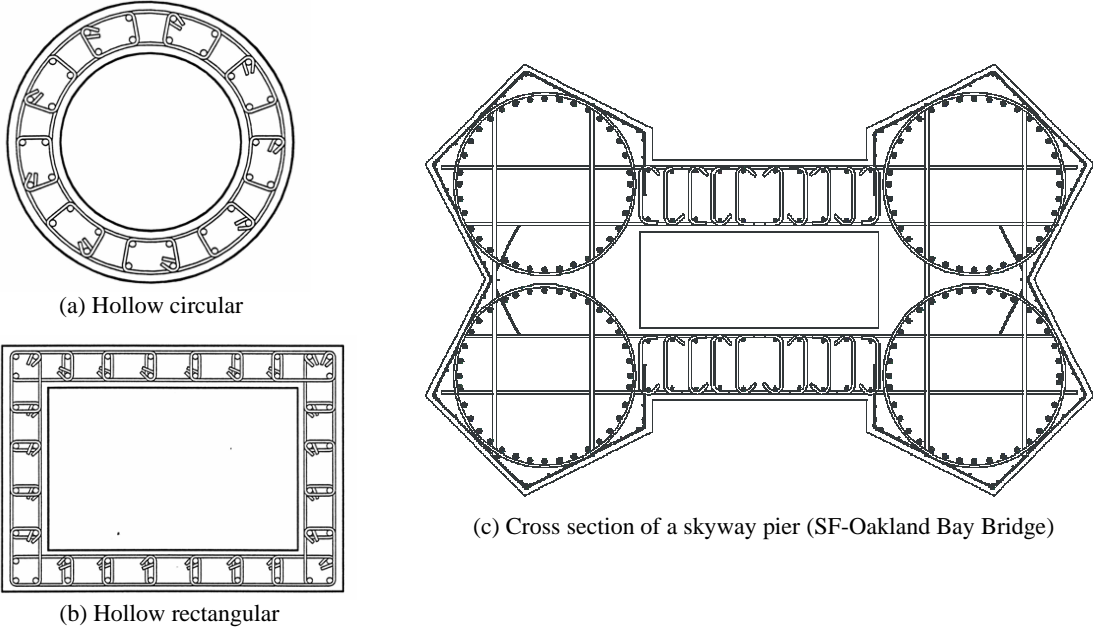


Fig 2-2: Pier section shapes (after Priestley et al., 1996 and Hines et al., 2001)

With a single layer of reinforcement, the hollow circular section becomes extremely economical. In such a design, the wall thickness should be kept to a minimum, to avoid large volumes of concrete without any reinforcement. Note that the outer layer of spiral reinforcement provides confinement for the circumferential direction over the full wall thickness.

With large hollow circular columns, transverse reinforcement has normally been provided by individual hoops, made continuous with lap welds. This can be an expensive detail, especially for large-diameter columns, where the circumferential length of a single hoop may exceed the maximum production length of a reinforcing bar (typically 18m). Efficiency can be improved by replacing the individual hoops by a continuous spiral of unstressed prestressing strand. Test on columns using prestressing strand with an allowable stress for confinement or shear resistance of 1000MPa have indicated improved performance compared with columns reinforced with conventional mild-steel hoops and a design strength of 420MPa (Budek et al., 2001, Ranzo and Priestley, 2001).

Although the rectangular section of Fig. 2-2(b) is less susceptible to confinement failure on the inside surface, effective confinement of the section requires large numbers of transverse links or hoops. As a consequence, construction is time-consuming and relatively expensive. Note that the option of omitting the inner layer of reinforcing, which is acceptable, and even advantageous for hollow circular columns cannot be adopted for hollow rectangular

columns, since the resulting section would essentially be unconfined, and potential buckling of the vertical reinforcement near the centre of the sides would be unrestrained.

It should be recognized that a relaxation of seismic detailing for large hollow columns can often be justified because of the low expected ductility levels. It has been shown (Priestley, 2003) that the effective bi-linear yield curvature for solid circular columns is essentially independent of axial force and reinforcement content, and can be approximated by the expression

$$\phi_y = 2.25\varepsilon_y / D \quad (2-1)$$

where ε_y is the yield strain of the flexural reinforcement and D is the column diameter. The same expression is also a reasonable approximation for hollow circular columns, and, within an error of 10% can be applied to rectangular columns. The yield displacement for a cantilever column of height H can thus be expressed as

$$\Delta_y = \phi_y H^2 / 3 = 2.25\varepsilon_y H^2 / 3D \quad (2-2)$$

Fig. 2-3 plots the relationship implied by eq.(2-2) for reinforcing steel with a yield strength of 500MPa (i.e. $\varepsilon_y = 0.0025$). It is apparent that for tall piers ($H > 40\text{m}$) the yield displacement exceeds 400mm, even for very large diameter piers. Considering that maximum elastic response displacements under excitation corresponding to an M7.0 earthquake at a distance of 10km from the structure are expected to be less than 600mm, (Faccioli et al., 2004) it is clear that in many seismic regions, ductility demand on tall bridges will be minimal.

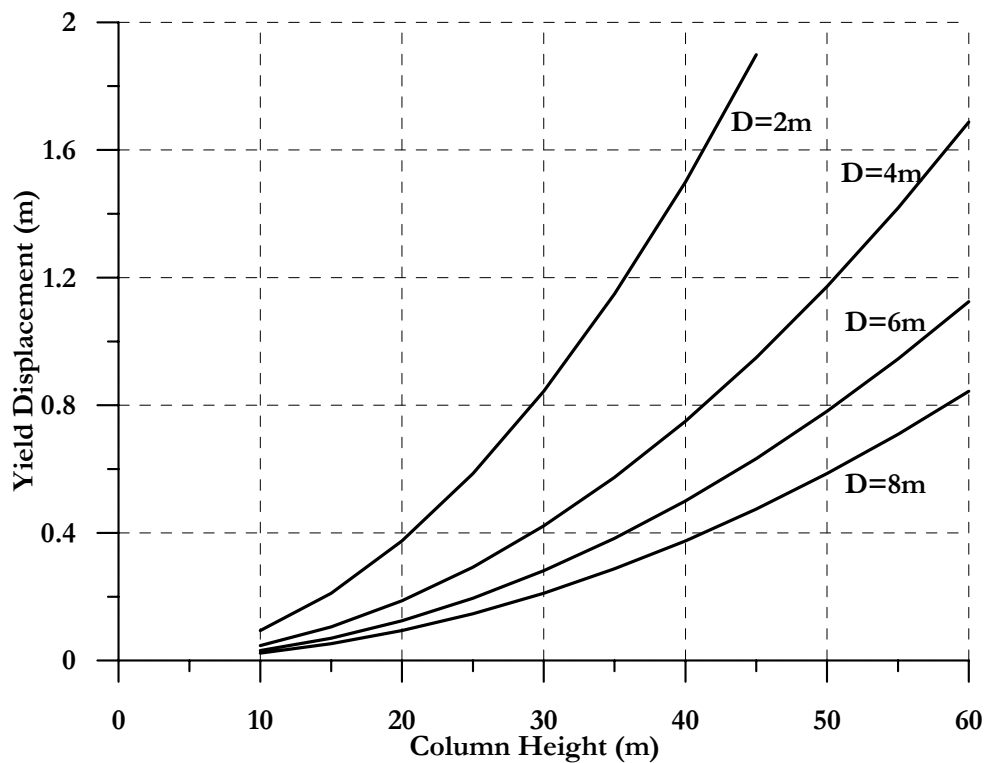


Fig.2-3: Yield displacements of circular cantilever piers

2.5 A regional review of design choices

Results of an international survey on design choices for pier section and detailing are summarized in Tables 2-1 and 2-2. The questions, and a synopsis of the range of answers, are also presented in the following sections.

	USA West	USA East	NZ	Mexico	Japan	Italy	France	Greece	Slovenia
Solid Circ	C 1m	C	C	C	C	C	O	C	C (skew)
Solid Rect	R	C	R	C	C	R	C	C	C
Solid Non Prismtc	O	R	O	O	R	R <30m	C	O	C (I-shape)
Solid Wall Piers	O		O	O	C	O <30m	C	O	R (integral Abut.)
Hollow Circ	R	N	N	O	C	C >30m	O: M-L N: S	N	R
Hollow Rect	R	N	R	O >30m High	C	C >30m	O: M-L N: S	C:M,L	C:L >20m high
Hollow Non Prismtc	R	N	N	R	N	C >30m high	O: L		O >20m high
Drilled Shaft	C	O	R	C	N	R	R		R
Spread	O	O	O	O	C	C	O	O	C
Pile support column	O	C	C	C	R	C	C	C	C
Pile Bent	O	C	C (Rail)	N	R	R	R	O	R
Single Col Bents	C	R L	C	C	C	C	R	C L>40m	C
2 Column Bents	C	O M	O	O	O	C <30m	R	R	R
3 or more Col bents	O	C S	R	O	O	C	R	R	O Highway o'pass

Legend:

C: common O: Occasional R: rare N: not used

L: Large bridges (>300m) M: Medium (150m to 300m) S: Small Bridges (<150m)

Note: Due to large variation in various US States, it is difficult to generalize trends. The above draws largely on experience in California and North Carolina.

Table 2-1: Pier Section Details

	USA West	USA East	NZ	Mexico	Japan	Italy	France	Greece	Slovenia
Lap Splice	Outside hinge	In hinge	Outside hinge	Outside hinge	Outside hinge	In Hinge	Outside hinge	Outside hinge	Varies
ρ_l	>0.01 <0.04	>0.01 <0.04	>0.008 <0.03	>0.01 <0.05	>0.008 <0.020	>0.01 <0.04	>0.005 <0.03	>0.01 <0.03	>1% <2.5%
Long. Bar Size (mm) and Type	32-57 ASTM A706	28-44 ASTM A615	25-32	25-38 ASTM A615	29-51 JIS SD295	16-26	>10	25-32 S500 temcore	16-28 S500
ρ_v	>0.005 <0.012	>0.002 <0.10	>0.005 <0.012	>0.005 <0.020	>0.005 <0.018	>0.002	>0.005	>0.007 sp >0.009 rc	>0.3% <1.5%
Trans. Steel size and spacing (mm)	12-25 50-150	10-12 75	12-20 75-200	12 150	16-32 150	12-20 100-250	>10 <8d _b <0.5B <200	>14 75-150	10-16 100-200
f'_c f_y (MPa) f_u	30-45 420 600	26 420 600	30-45 500 700	25-30 420 630	24-30 >295 440-600	20-35 >430 >540	30-45 500 >600	25-30 500	25-30 500 >600
ALR	0.04 to 0.12	0.04 to 0.10	0.04 to 0.10	0.04 to 0.12	0.03 to 0.08	0.03 to 0.18	Around 0.10	0.07 to 0.15	Around 0.10
Drift Limit	None	None	None	<0.01	None	None	None	None	None
Design Ductility	3-4		<6	2-3	3-4	Varies	3.5	1.5-3.5	1.5-3.5
Seismic Demand	High	Low - Mid	Varies	Varies	High	Low-Mid	Low-Mid	Mid-High	Mid

Legend:

B=section depth

$$\rho_l = \frac{A_{st}}{A_g} \quad \rho_v = \frac{V_{st}}{V_{member}} \quad ALR = \frac{P}{f'_c A_g}$$

Note: Due to large variation in various US States, it is difficult to generalize trends. The above draws largely on experience in California and North Carolina.

Table 2-2: Pier Reinforcement Details –Results of Survey

2.5.1 Solid section vs hollow section: When are hollow sections used in preference to solid sections, and why?

Hollow sections are used to reduce seismic mass, based on economic considerations of the cost saving associated with reduced material and design moments compared with increased construction complexity, and hence increased labour costs. This results in different characteristic column heights above which hollow columns are considered appropriate. In Europe, hollow columns are used for columns as low as 20m (Slovenia) or 30m (Italy), but in the United States, it is rare to use hollow columns for column heights less than 40m.

2.5.2 Solid sections: What section shapes are preferred for solid-section columns?

Typically, solid-section columns are simple in section shape, being either circular or rectangular. Both are common in most seismic regions, though in recent times, the tendency has been towards circular columns, because of simpler detailing of transverse reinforcement. In California, rectangular columns are only used with the intersecting spiral reinforcement layouts of Fig. 2-1, Section C-C. In Italy, rectangular sections generally have rounded corners in recent designs.

2.5.3 Hollow sections: What section shapes are preferred for hollow-section columns?

The range of section shapes for hollow columns is rather wide, and often influenced by architectural considerations. Hollow circular columns are common in parts of Europe (e.g. Italy), whereas hollow rectangular columns are more commonly used in Greece, Turkey and Portugal. In these cases, the section shape is often modified by corner chamfers, as shown in the example of Fig. 2-4, which shows a 1970's design from Slovenia. Current designs would have more robust cross-linking between the layers of reinforcement. Nevertheless, recent testing (Isakovic and Fishinger, 2006) has indicated substantial ductility available from this design. Fig. 2-5 shows a hollow circular column in a recent Italian design, flared at the top in the transverse direction to allow two-bearing support of the steel superstructure, and with a 4.8m diameter column, with a wall thickness of 1m. Note that in this case the mass reduction compared with a solid section is a comparatively modest 34% .

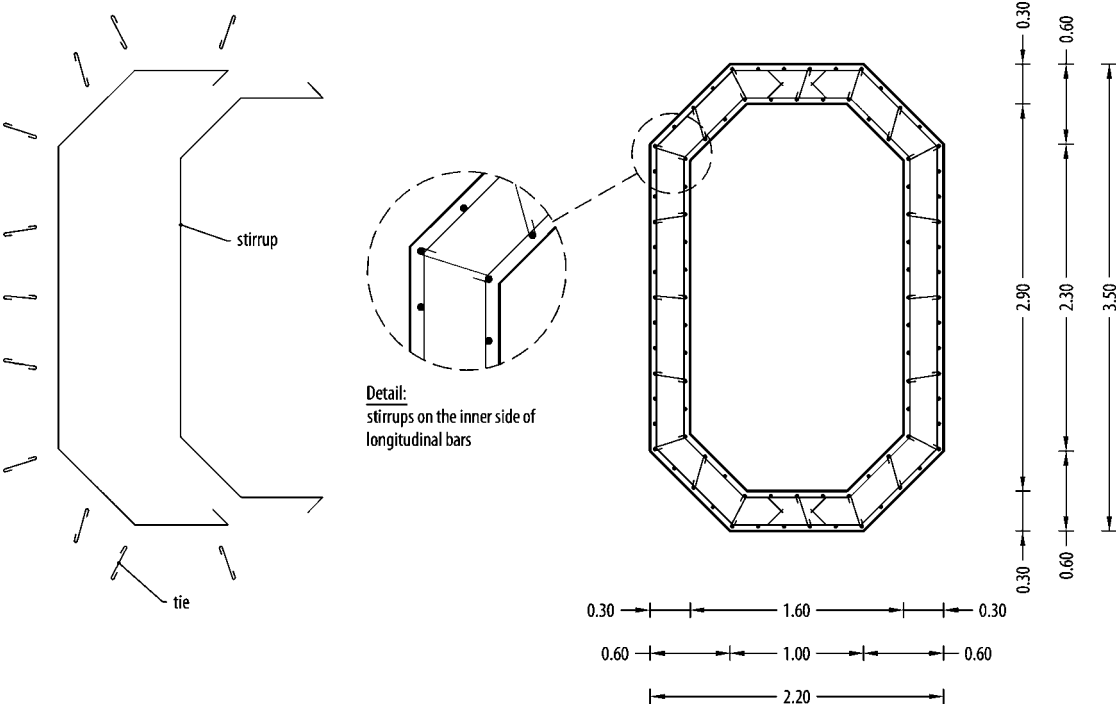


Fig.2-4: Section shape and detailing of Ravbarkomanda Viaduct Columns, Slovenia

As noted above, recently designed hollow section shapes in California have often been strongly influenced by architectural considerations. Earlier designs, from the 1960's to 1980's typically had simpler rectangular section shapes.

2.5.4 Reinforcement layout: What is the preferred layout of both longitudinal and transverse reinforcement for columns. (e.g. cross-links in solid sections; one or two layers in hollow sections; anchorage details for transverse reinforcement)?

Longitudinal reinforcement is always essentially uniformly distributed around sections. In solid sections a single layer is almost always used, though in California, the reinforcing bars may be bundled in two or three bars to increase spacing between bars. With hollow sections, two layers of reinforcement are always used, regardless of country, despite the fact that for hollow circular columns this is not strictly necessary.

Transverse reinforcement in solid rectangular sections invariably includes cross-links to support longitudinal bars against buckling. These are typically anchored back by 45° hooks into the core. With solid circular columns, the transverse reinforcement is generally in the form of circular hoops closed by welding, or by continuous spirals, with lap-welds. Internal cross-links are not usually used in circular sections, since there is no theoretical basis for such a requirement, but some countries, such as Japan have used cross-links in large circular columns. In hollow sections, cross-links are provided as indicated in Figs. 2-2 and 2-4.

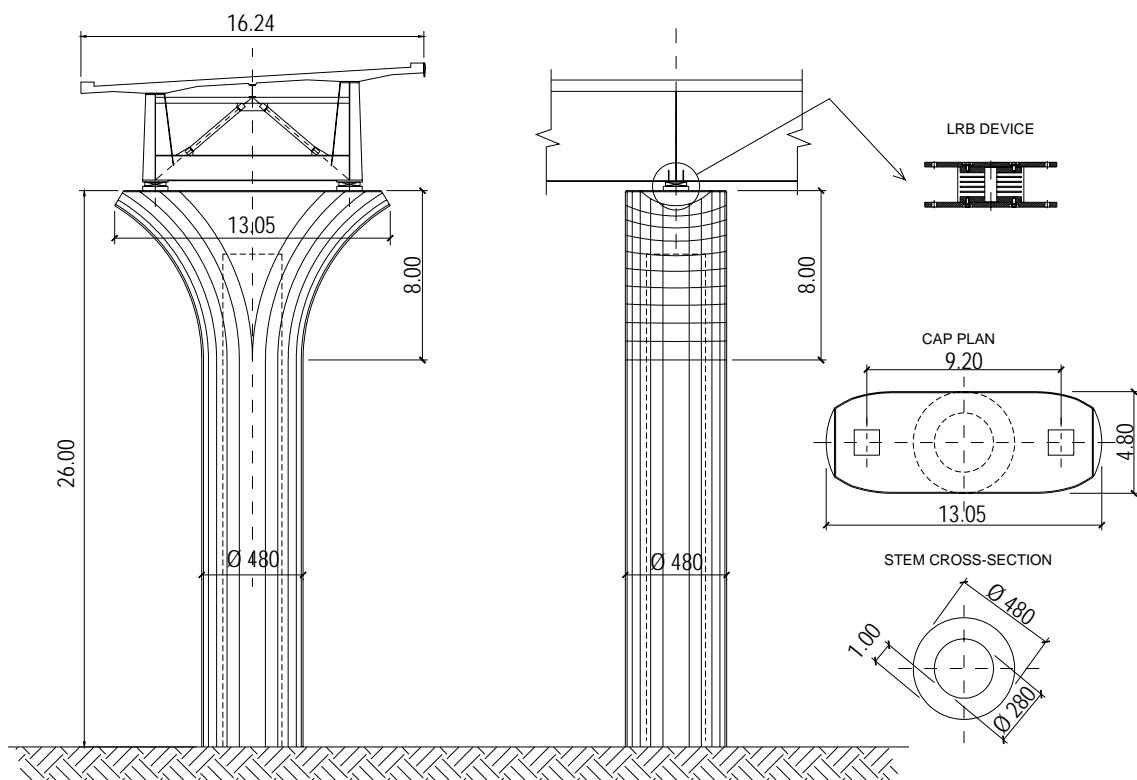


Fig.2-5: Hollow circular column in flared single-column bent, Italy

2.5.5 What are limits for longitudinal and transverse reinforcement

Lower limits for longitudinal reinforcement vary considerably between countries. In Europe and Japan, the lower limit for solid sections until recently has been 0.5%, whereas in the United States and Mexico, a lower limit of 1% has applied. Recently, lower limits for longitudinal reinforcement have increase in Europe to 1%, except in France. In New Zealand, a 0.8% lower limit has applied for many years.

In building columns, where high axial load ratios (up to 0.4) can be common for high rise buildings, a lower limit of about 1% has often been considered appropriate to avoid excessive compression strains in longitudinal reinforcement resulting from creep under the high axial loads. Because of the typically low axial load ratios in bridge columns, this is not a relevant issue for bridges

A more important consideration for seismic response is the necessity for the flexural strength of the column to adequately exceed the cracking strength, to ensure a satisfactory spread of cracking under lateral response. If only a single crack develops at the column base, the plastic hinge may be constrained to the extent that fracture of the longitudinal reinforcement may occur at low displacement ductilities, particularly if small-diameter bars are used for the longitudinal reinforcement.

Fig. 2-6 presents results of analyses relating the ratio of flexural strength to cracking strength, to axial load and reinforcement ratio. It has been noted (Priestley et al., 1996) that provided this ratio is at least 2.0, an adequate spread of plasticity is assured. For reasonable levels of axial force this ratio is provided if the longitudinal reinforcement ratio exceeds 0.5% or 0.7% for circular and rectangular columns respectively. Experiments have confirmed satisfactory ductility with this level of longitudinal reinforcement.

Upper limits to the longitudinal reinforcement ratio are generally specified by codes to be about 4%, though codes applying in the 1960's often permitted ratios as high as 8%. Above 4%, anchorage of longitudinal reinforcement in foundations or cap beams becomes difficult because of congestion, and joint shear stress levels become unacceptably high. Consequently, in modern designs it is uncommon for longitudinal steel ratios to exceed 3%, based on the gross section area, and the most common range is 1.0% - 2.0%. However, Table 2-2 indicates a range of upper limits to longitudinal reinforcement between 2% (Japan) and 5% (Mexico).

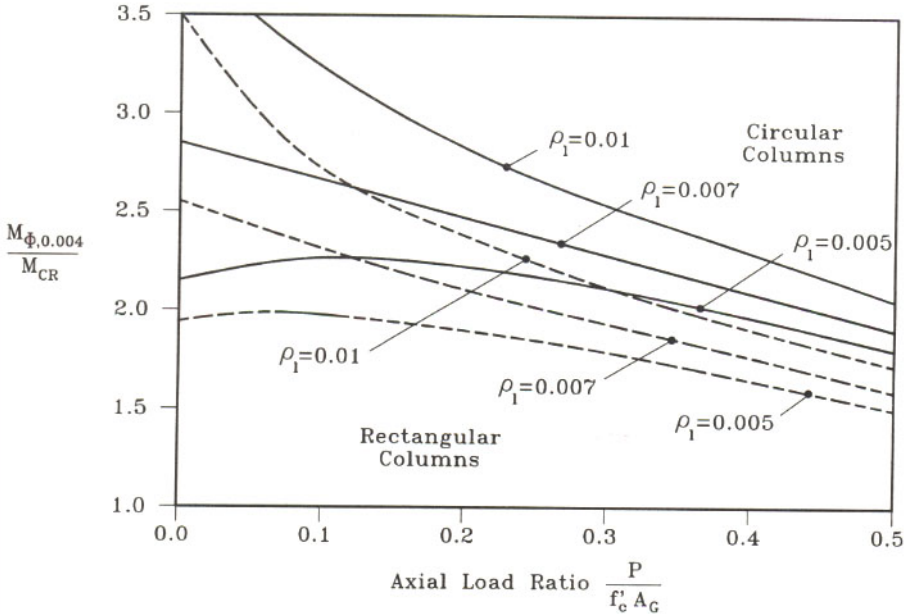


Fig.2-6: Flexural strength: Cracking moment relationship (after Priestley et al., 1996)

2.5.6 What are typical longitudinal reinforcement sizes, strength and properties?

There are large variations in reinforcement bar sizes, with sizes as low as 16mm diameter in Europe, and as large as 51mm and 58mm in Japan and California respectively. Yield strength is generally in the range 400MPa to 500MPa, though a lower yield strength (295MPa) is sometimes used in Japan. A significant difference in the ratio of ultimate strength to yield strength exists, with values of 1.3-1.5 common in the United States and

Mexico, but values of about 1.2 applying in Europe. This has significance to the spread of plasticity in the plastic hinge region. Low ratios of f_u/f_y result in a shortening of the plastic hinge, and hence an increase in reinforcement strain for a given ductility level.

2.5.7 What are typical transverse reinforcement sizes and spacing?

General layout of transverse reinforcement is discussed above in Section 2.5.4. Volumetric ratios of transverse reinforcement in most countries have a practical lower limit of 0.5%, though Italy, Slovenia and USA East Coast report lower values. Upper limits tend to be between 1% and 2%. Bar sizes are typically in the range 12mm-25mm, with spacings along the column axis between 50mm and 150mm, though occasionally wider spacing is used. Note these spacings differ considerably from practice common in the 1960s and 1970s when spacing of transverse reinforcement was typically 300mm.

2.5.8 Are single-column or multi-column bents more commonly used, and in what circumstances? Are wall piers used, and if so, when?

The general trend world-wide appears to be away from multi-column piers with small section size, which were the rule with bridges constructed in the 1950’s to 1970’s, towards a current preference for single-column piers with much larger section size. Exceptions occur with very wide bridges with multiple traffic lanes, but the tendency here has been towards reducing bridge superstructure width by supporting the two traffic directions by independent bridge structures. Multiple-column piers are also common with highway overpasses.

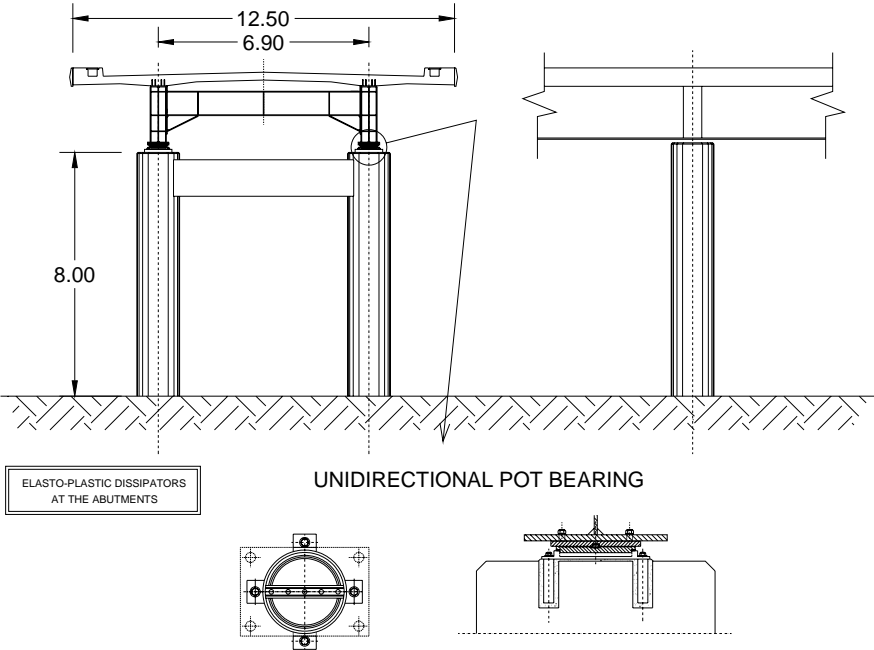


Fig.2-7: Simple portal pier with circular columns, Italy

In Italy, with low-height piers, the simple portal shown in Fig. 2-7 is sometimes used. With this detail, the columns extend above the beam joining the two columns and directly support the superstructure. This details simplifies anchorage of the column reinforcement at the column top, compared with columns which frame into the soffit of the cap beam, and allows

the beam linking the two columns to be designed for ductility, rather than forcing a plastic hinge into the column top, as would be the case in Californian practice.

2.5.9 What is the typical relationship between column section size, and span length?

No uniform trend was observable.

2.5.10 Is the column section size typically governed by gravity or seismic considerations, and is this dependent on local seismicity?

In low seismicity regions the column size may be dictated by eccentric live-load considerations, particularly for single-column piers. In mid to high seismicity regions seismic considerations dictate column size.

2.5.11 Do architectural considerations have a significant influence on section shape and dimensions?

As noted above, this appears more common with hollow columns than with solid columns. To some extent this is because hollow columns tend to be larger and taller than solid columns. As a consequence they are more visible, and also cost more to construct. As such the extra cost of applying the architectural shape or finish is easier to justify.

2.5.12 Are there generic concerns with earlier (historic) designs?

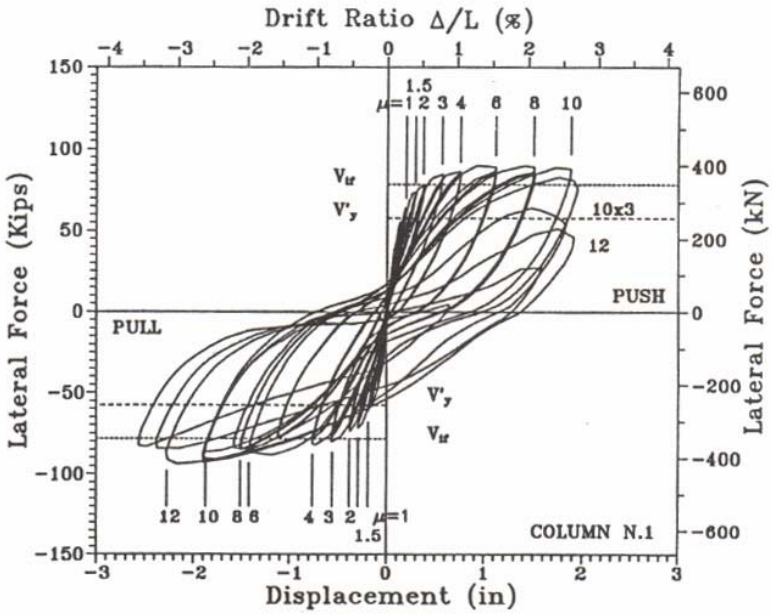
Concerns relating to section size and shape are fairly uniform: Many bridge structures constructed in the 1950's to 1970's were designed without specific consideration of seismic aspects, and certainly without capacity design consideration. Specific column deficiencies are mainly related to:

- Inadequate transverse reinforcement volume to provide adequate confinement to concrete and anti-buckling restraint to longitudinal reinforcement.
- Inadequate transverse reinforcement to ensure dependable shear strength exceeds maximum feasible flexural strength.
- Inadequate detailing of transverse reinforcement to ensure that the required shear strength and anti-buckling roles are effected satisfactorily.
- Premature termination of longitudinal reinforcement in columns, resulting in a propensity for flexural hinging and shear failure at column mid-height.
- Inadequate anchorage of flexural reinforcement in footings and cap beams.
- Lap-splicing of flexural reinforcement at the base of columns, thus limiting the curvature ductility capacity of column-base plastic hinges.

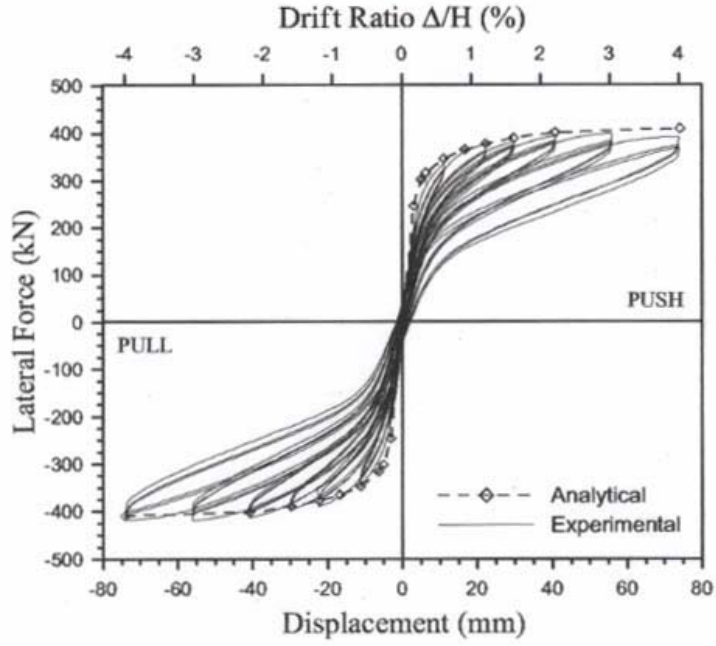
2.5.13 New Developments in Column Designs

Theoretical and experimental research has been carried out recently into the use of unbonded vertical reinforcement to provide the flexural resistance for bridge columns. This type of design facilitates the use of precast column sections, which can be a considerable advantage when overpass bridges are constructed across existing highways. The concept has

been developed from the use of unbonded prestressing in precast buildings (Priestley et al. 1999). Fig. 2-8 compares force-displacement hysteresis response for a conventionally reinforced column, (Priestley et al., 1996) and a column reinforced with unbonded prestressing (Hewes et al., 2001). It will be noted that the unbonded design has very stable hysteretic response, and virtually zero residual displacement but has less energy dissipation than the conventional design. It has been shown that the lower energy dissipation does not result in significantly increased response displacements (Hewes et al.,2001). See Palermo (2004), for additional information on bridge columns with unbonded prestressing.



(a) Conventionally reinforced bridge column (after Priestley et al. 1996)



(b) Column Reinforced with Unbonded prestressing (after Hewes et al.,2001)

Fig.2-8: Force-displacement hysteresis response for bridge columns

References

- Budek, A.M., Lee, C.O. and Priestley, M.J.N. (2001). Seismic Design of Circular Bridge Columns with Unstressed Strand for Transverse Reinforcement. Structural Engineering Report SSRP 2001/06, Univ. of Calif. San Diego
- Faccioli, E. Paolucci,R. and Rey, J (2004). Displacement Spectra for Long Periods. Earthquake Spectra, Vol.20 #2, pp347-376
- Isakovic, T. and Fischinger, M. (2006). Higher Modes in Simplified Inelastic Analysis of Single Column Bent Viaducts. Earthquake Eng. and Str. Dyn. Vol 35 pp 95-114
- Hewes, J. and Priestley, M.J.N. (2001). Seismic Design and Performance of Precast Concrete Segmental Bridge Columns. Structural Engineering Report SSRP2001/25, Univ. of Calif. San Diego, 241 pp.
- Hines, E.M., Dazio, A., and Seible,F. (2001). Cyclic Tests of Structural Walls with Highly Confined Boundary Elements – Phase III- Web Crushing. Structural Engineering Report SSRP 2001/27, Univ. of Calif. San Diego, 260 pp.
- Palermo A. 2004. The use of controlled rocking in the seismic design of bridges. Doctoral thesis, Politecnico di Milano
- Haroun, M.A., Pardoen, G.C., and Haggag, H.A. (1994). Assessment of Cross-Ties Performance in Bridge Pier Walls of Modern Designs. Proceedings, 3rd Annual Caltrans Seismic Research Workshop, Sacramento, Ca. June 1994, 10 pp.
- Priestley, M.J.N., Seible, F., and Calvi, G.M. (1996). Seismic Design and Retrofit of Bridges. John Wiley and Sons, NY, 686 pp.
- Priestley, M.J.N., Sritharan, S. Conley, J.R. and Pampanin, S. (1999). Preliminary Results and Conclusions from the PRESSS Five-Storey Precast Test Building. CI Journal, Vol.44,No.6 Nov-Dec, pp. 42-67
- Priestley, M.J.N. (2003). Myths and Fallacies in Earthquake Engineering, Revisited. IUSS Press, Pavia, 121 pp.
- Ranzo, G., and Priestley, M.J.N. (2001). Seismic Performance of Circular Hollow Columns Subjected to High Shear. Structural Engineering Report SSRP 2001/01 Univ. of Calif. San Diego, 215 pp.

3 Pier /superstructure connection details

3.1 Introduction

It was mentioned in section 2.2 that the choice between single-column and multi-column piers could not be made independent of the connection detail between pier and superstructure.

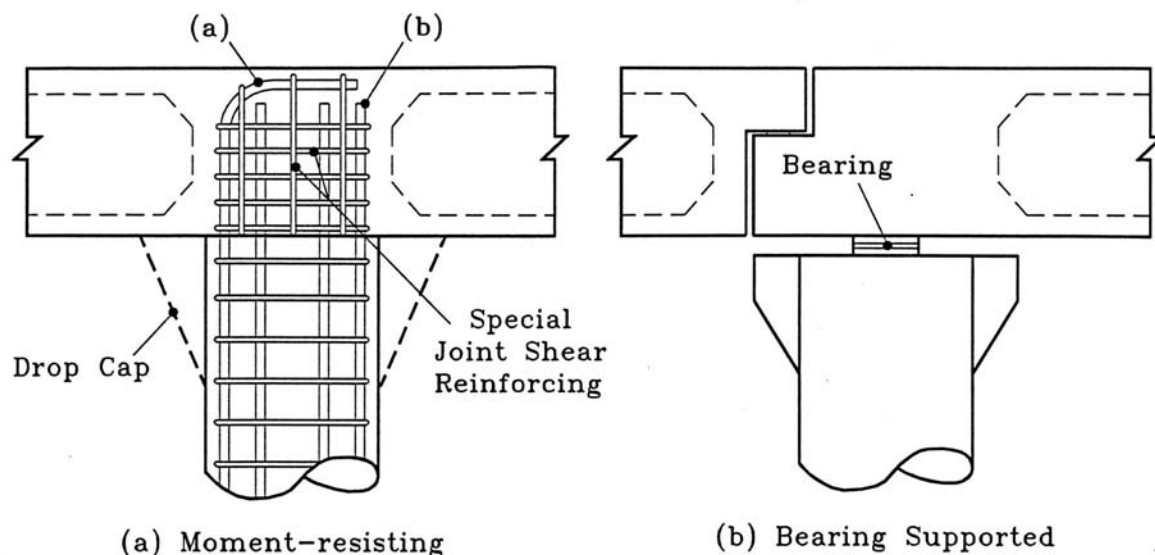


Fig.3-1: Pier/superstructure connection alternatives (after Priestley et al,1996)

Fig. 3-1 shows monolithic and bearing-supported connection alternatives between pier and superstructure. Monolithic connection details (Fig.3-1(a)) are preferred in California when piers are sufficiently slender or short so that thermally induced moments are not critical. The main reason for the popularity of this detail is the robustness for resisting ground motions larger than design level, since unseating of bearings, which has occurred with a number of bearing-supported bridges in recent earthquakes, is not an issue. A secondary reason is the high maintenance costs associated with bearings, and movement joints. Despite this advantage, monolithic connection is less common in Europe.

3.2 Advantages and disadvantages of support details

It is thus of interest to examine other advantages and disadvantages of the alternative details. With a moment-resisting connection, the potential for additional redundancy of energy dissipation exists, since plastic hinges can form at top and bottom of the columns, at least under longitudinal response. With multi-column piers this advantage also extends to transverse response. Lateral resistance will thus be increased for a given column size, and as a consequence, the column dimensions may be reduced. The fixed-top connection detail also allows the designer to consider the option of pinned connections between the column base and foundation, when multi-column piers are utilized. This detail which is common in California, but rare in other parts of the world has the merit of reducing seismic forces in, and hence the cost of, the foundation system.

A major disadvantage of the monolithic connection detail is that seismic moments developed at the top of the pier are transmitted to the superstructure. This adds to the superstructure gravity negative moments at the pier, and may also result in positive superstructure moments. This may increase the cost of the superstructure. Anchorage of the column flexural reinforcement in the cap beam, and joint shear stresses may cause design problems, and special reinforcement details, such as confinement reinforcement, and hooked longitudinal bars (see Fig.3-1(a) may be necessary. Clearly the monolithic detail is only appropriate when the superstructure is continuous over the pier, rather than simply supported. This might be felt to rule out designs where the construction uses precast concrete beams for the superstructure. However, connection details providing fully monolithic response of bridges with precast superstructures have been successfully tested under simulated seismic loading in California (Holombo et al, 1998).

Bearing-supported superstructures have the advantage of avoiding the problems associated with moment transfer from the pier to the superstructure, and the joint-shear and anchorage issues. Different types of bearings may be considered, including pot-bearings, rockers, pte-stainless steel sliders and elastomeric bearings. These are discussed in some detail elsewhere (Priestley et al, 1996). Bearing-supported connection details will almost always be chosen when a decision is made to provide seismic resistance by seismic isolation (see Chapter 6). Seismic displacements of bearing-supported superstructures will generally be larger than those of structures with monolithic connection, and the sensitivity to seismic intensity exceeding the design level will also be increased as noted above.

When there is potential for liquefaction at the bridge site, the pier-superstructure connection detail requires special consideration. One school of thought would claim that the best connection would be bearing-supported simple spans with linkage bolts between spans, on the grounds that this will provide the greatest freedom to accommodate gross displacements resulting from differential liquefaction effects. However, experience in recent earthquakes with this type of detail (e.g. Costa Rica, 1991) have been rather unsatisfactory. An alternative viewpoint is expressed in relation to Fig. 3-2, where monolithic moment connection is adopted, piers are kept as slender as possible, and pier bases are supported on raked piles passing through the liquefiable layers to add rigidity to the foundation system. If necessary, the lateral force resistance can be enhanced by slack tendons restraining the abutments back to “dead men” located beyond the region of expected lateral spreading.

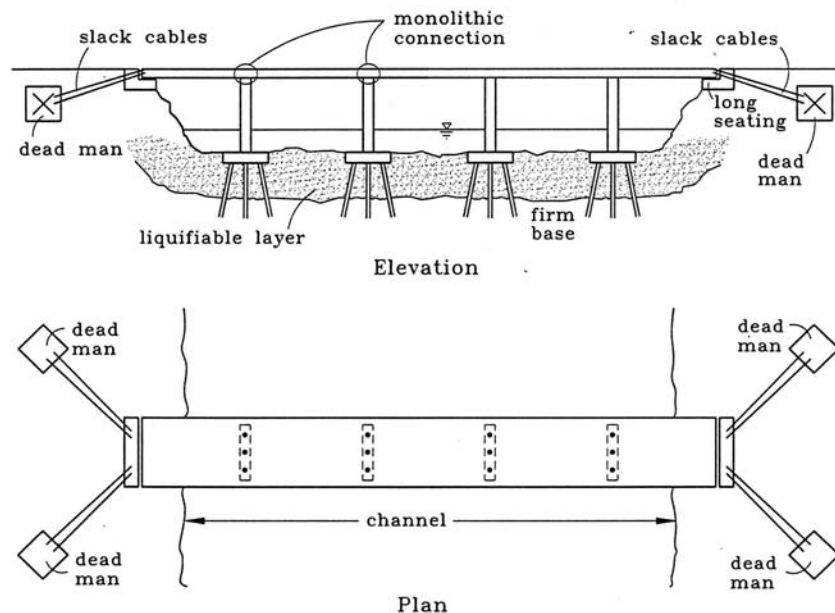


Fig. 3-2: Pier/superstructure connection for a liquefiable site (after Priestley et al,1996)

3.3 A regional review of design choices

Results of an international survey on design choices for pier section and detailing are summarized in Table 3-1. The questions, and a synopsis of the range of answers, are also presented in the following sections.

	USA West	USA East	NZ	Mexico	Japan	Italy	France	Greece	Slovenia
Bearing Support	R	C	R	C	C	C	C	C	C
Pot Bearing			O:M-L R:S	R	O	C	C: M-L	O	C
Rocker Bearing	N		N	N	N	C	N	C spherical	N
PTFE Sliders	R		O	R	C	C	C with pot bearings	C with pot, spherical	C
Elastomeric Bearings	C:LDR R:HDR	C:LDR	C:LDR N:HDR	C:LDR N:HDR	C:HDR	R	C: S-M	C:LDR R:HDR	C:LDR
Lead Rubber Isolation	O		O	N	C	R	N	O	N
Friction Pendulum Isolation	O: L		N	N	N	N	N	O: L	N
Lateral Restraint	R	R	R	C	C	C	C	C	O
Monolithic Support	C	R	C	R	C	R	N except portal frame	C For short bridges	C:L
Integral Cap Beam	C	R	O	R	R	R	O: L R: S-M	C:S	C
Drop Cap Beam		R	C	R	R	R	R	O	R

Legend:

C: common O: Occasional R: rare N: not used
 L: Large bridges (>300m) M: Medium (150m to 300m) S: Small Bridges (<150m)
 LDR: Low damping rubber. HDR: High damping rubber

Table 3-1: Pier/superstructure Connection- Results of Survey

3.3.1 Are superstructures normally bearing-supported or monolithically connected to piers, and what factors affect the choice?

There are distinct differences between design practice in California and New Zealand, where monolithic support is more common, and bearing-supported superstructures are rare and Europe where bearing support is more common. This appears to be a matter of tradition rather than different conditions applying in the different regions. In Japan both bearing support and monolithic support are common.

3.3.2 With bearing-supported superstructures, what are the most common types of bearings chosen

Rocker bearings, which were common in the 1950's and 1960's are now almost never used. Pot bearings are common in Europe but rare elsewhere. PTFE sliders are frequently used in conjunction with pot bearings in Europe.

Elastomeric bearings are common in almost all regions, with the exception of Italy. In most cases the bearings are constructed with low-damping rubber, and are primarily provided to accommodate creep and thermal movements, rather than being placed as a form of seismic isolation. High-damping elastomeric bearings are common in Japan, occasionally used in Greece and California, but almost never used elsewhere.

Lead-rubber isolation bearings (that is, elastomeric bearings with a central lead core) are common in Japan, and occasionally used in other high seismicity areas (NZ, USA West Coast, Greece), but never used in low to mid seismicity areas.

Friction pendulum isolation bearings have occasionally been used on large bridges in USA West Coast and in Greece, but have not been used in other countries.

3.3.3 With monolithic pier/superstructure connection, is the cap-beam typically under-slung below the superstructure, or incorporated within the depth of the superstructure?

Integral cap beams are more common than cap beams that extend below the superstructure soffit, but there is little consistency in the answers provided (see Table 3-1)

3.3.4 Have historical influences resulted in a change in pier/superstructure connection details in the past 50 years?

In Europe following World War II, there was a need for a major bridge-building program as a consequence of the large numbers of bridges destroyed by warfare. As a consequence there was a need for simple, standardized designs. In Italy this led to construction of rather standard bridges of multiple prestressed concrete simple spans supported on multi-column piers of circular or rectangular section. This was progressively replaced in the late 1960's by continuous prestressed concrete superstructures with monolithic connection to the piers. Consideration of seismic response in the design was rare. A similar change from simply-supported precast beams on portal to continuous designs occurred in Slovenia, with the main reason for change being economic, associated with the high maintenance costs associated with simple spans and bearing support.

References

- Holombo J., Priestley, M.J.N. and Seible, F. (1998). Longitudinal Seismic Response of Precast Spliced-Girder Bridges. Structural Engineering Report SSRP 98-05, University of Calif. San Diego, 298 pp.
- Priestley, M.J.N., Seible, F. and Calvi, G.M. (1996). Seismic Design and Retrofit of Bridges. John Wiley and Sons, NY, 686 pp.

4 Superstructure

4.1 Introduction

A review of the seismic resistance in bridges very likely would indicate that the critical structural elements are the bents and substructures. However, it is relevant to review several considerations for the seismic design of superstructures since their properties affect the seismic response of bridges and also because the cost of superstructure is a relevant part in the overall cost of a bridge. As discussed in the following, several alternatives need to be considered in the seismic design of a superstructure, such as section shapes, movement joints, analysis considerations and others.

Results from an international survey are included at the end of this chapter, which suggests, as in the case of Pier Section reviewed in Chapter 2, that choices from above alternatives are made mainly based on convention and tradition, rather than structural considerations. Before presenting these results, this chapter presents general information on structural considerations for the seismic design of bridge superstructures.

4.2 Section shapes for superstructures

Fig. 4-1 (Priestley et al., 1996) shows a number of section shapes for concrete superstructures commonly used in bridge construction. According to Priestley et al. (1996) solid and voided slabs are appropriate for short span bridges, with spans below 15 m. The inverted T section is also used for short span bridges, with spans below 25 m. Typically an in situ deck is cast on the inverted T units, using shear connections between these units and in situ slabs. The I beam is a common section for short span bridges. The double T section is used in the lower end of the medium-span range (25 to 35 m). However, this section is not suitable for bridges curved in the horizontal plane because of poor torsional characteristics. Box girders have the advantage of having high stiffness and strength for minimum weight, and also high torsional characteristics. This last feature makes the sections suited for bridges curved in the horizontal plane.

The choice among the different sections here described depends on several factors such as section depth and section width. For example, multi-cell box girders may be used for very wide bridges. For medium-span bridges (30 to 60 m), a prismatic section will generally be appropriate. For long-span bridges (spans longer than 60 m), box girders are common, with increased section depth toward the supports.

In some countries of Europe, such as Greece, modern roadway bridges and viaducts are constructed with small widths (typically not exceeding 14 m), therefore “twin” structures (see Fig. 4-2) are used, in which each lane of the roadway is carried by a separate bridge. This is dictated mainly by economy considerations, and one of its implications is that multi-cell box girder sections are hardly ever used in Greek bridges.

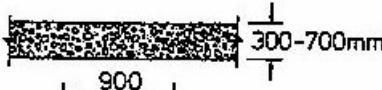
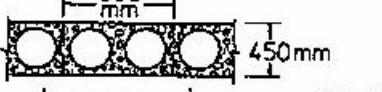
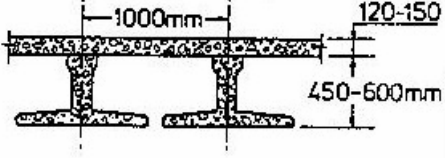
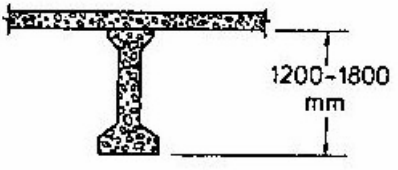
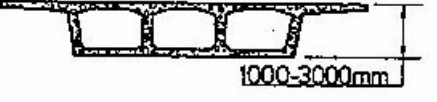
TYPE	EXAMPLE
Solid Slab	
Voided Slab	
Inverted-Tee	
I-Beam	
Double-Tee	
Single-Spine Box Girder	
Multi-Cell Box Girder	

Fig. 4-1: Section shapes for bridge superstructures (after Priestley et al., 1996)



Fig. 4-2: The Votonosi Bridge near Metsovo (NW Greece); the superstructure consists of a post-tensioned single cell box girder (common in modern bridges), and its 230m central span, is the longest span so far in balanced cantilever construction in Greece (Courtesy of A. Kappos).
(Figure available electronically on fib website; see production note on p. ii)

4.3 Movements joints

Movement joints are needed in bridges to accommodate longitudinal expansion and contraction resulting from prestress shortening, creep, shrinkage, temperature variations and earthquake displacement demands. The movement joint layout defines separate frames with their own dynamic response during an earthquake. In addition to movement joints for longitudinal expansions and contraction, other type of movement joints could also allow flexural rotation about the movement joint axis but restrict translation perpendicular to the bridge axis by means of shear keys. Caution should be taken for response of a bridge to transverse seismic demands since frames with bents of unbalanced transverse stiffness could lead to rotation of the bridge superstructure in the plane of the bridge deck. This undesirable behavior could also occur in curved bridges.

Enough hinge seat width needs to be available to accommodate not only longitudinal expansion and contraction resulting from prestress shortening, creep, shrinkage and temperature variations but also expected movements of joints during earthquakes. The trend for modern bridges is to use continuous superstructures, without intermediate movement joints, even for long bridges (for example for the 1036 m long Arachthos Bridge, currently under construction in Greece). In this case, movement joints are typically placed only at the abutments.

4.3.1 Design practice in California

According to Caltrans (Caltrans, 2004), the seat width normal to the centerline of bearings, see Fig. 4-3, needs to be calculated according to eq 4-1 and should not be less than 600 mm. In eq 4-1, the relative earthquake displacement demand, Δ_{eq} is calculated according to eq 4-2.

$$N \geq \left\{ \begin{array}{l} (\Delta_{p/s} + \Delta_{cr+sh} + \Delta_{temp} + \Delta_{eq} + 4) \\ (\Delta_{p/s} + \Delta_{cr+sh} + \Delta_{temp} + \Delta_{eq} + 100) \end{array} \right\} \begin{array}{l} \text{(in)} \\ \text{(mm)} \end{array} \quad (4-1)$$

N = Minimum seat width normal to the centerline of bearing

$\Delta_{p/s}$ = Displacement attributed to pre-stress shortening

Δ_{cr+sh} = Displacement attributed to creep and shrinkage

Δ_{temp} = Displacement attributed to thermal expansion and contraction

Δ_{eq} = Relative earthquake displacement demand

$$\Delta_{eq} = \sqrt{(\Delta_D^1)^2 + (\Delta_D^2)^2} \quad (4-2)$$

$\Delta_D^{(i)}$ = The larger earthquake displacement demand for each frame calculated by the global or stand-alone analysis

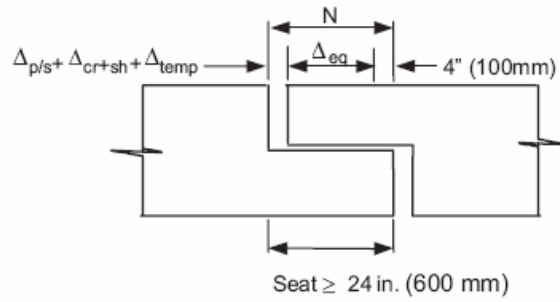


Fig 4-3: Hinge seat width

Due to the fact that lineal elastic modal analysis is commonly used for seismic analysis of bridges in California, Caltrans recommends performing two different analyses using tension and compression models and choosing for seismic design the maximum response quantities from either model. In the tension model all joints are defined with linear elastic restrainer springs. In the compression model all joints are rigidly connected in the bridge axial direction, and they are free to rotate about the vertical axis. It must be pointed out that this dual analysis model approach is used only for estimation of maximum member forces and displacements, and should be not used for prediction of relative displacements at the movement joints. The reason is that modal analysis gives maximum displacements occurring at different times during an earthquake, which overestimates these values as compared to those from nonlinear time-history analysis.

4.3.2 Design practice in Japan

The Japan Road Association [JRA (2002)] specifies that under earthquakes the deck movement relative to substructures may be contributed by two sources: 1) the deck displacement relative to the column due to inertia force, and 2) spatial variation of ground motion. Therefore, the seat length S_E (m) is evaluated as

$$S_E = u_R + u_G \geq S_{EM} \quad (4-3)$$

in which u_R represents the maximum displacement of the deck relative to the pier (m) under the design ground motion, and u_G is the relative displacement of ground (m) resulted from ground deformation during an earthquake. Parameter S_{EM} is the minimum required seat length (m) and it is given as

$$S_{EM} = 0.7 + 0.005l \quad (4-4)$$

in which l is the span length (m).

In eq. (4-3) u_R can be evaluated by a pushover analysis or nonlinear dynamic response analysis of a total bridge system. When soil liquefaction or lateral spreading is anticipated to occur at the site, u_R is evaluated under three conditions: 1) liquefaction-induced lateral spreading occurs, 2) only liquefaction occurs, and 3) neither liquefaction or liquefaction-induced lateral spreading occurs, and the largest u_R is used for design.

On the other hand, u_G is evaluated as

$$u_G = \varepsilon_G L \quad (4-5)$$

in which ε_G is seismic ground strain in the bridge axis and L is the distance between two substructures which control the seat length. ε_G is recommended to be 0.0025, 0.00375 and 0.005 at the sites of Type I, II and III ground conditions (stiff, moderate and soft soil sites), respectively. Examples of the distance L are shown in Fig. 4-4.

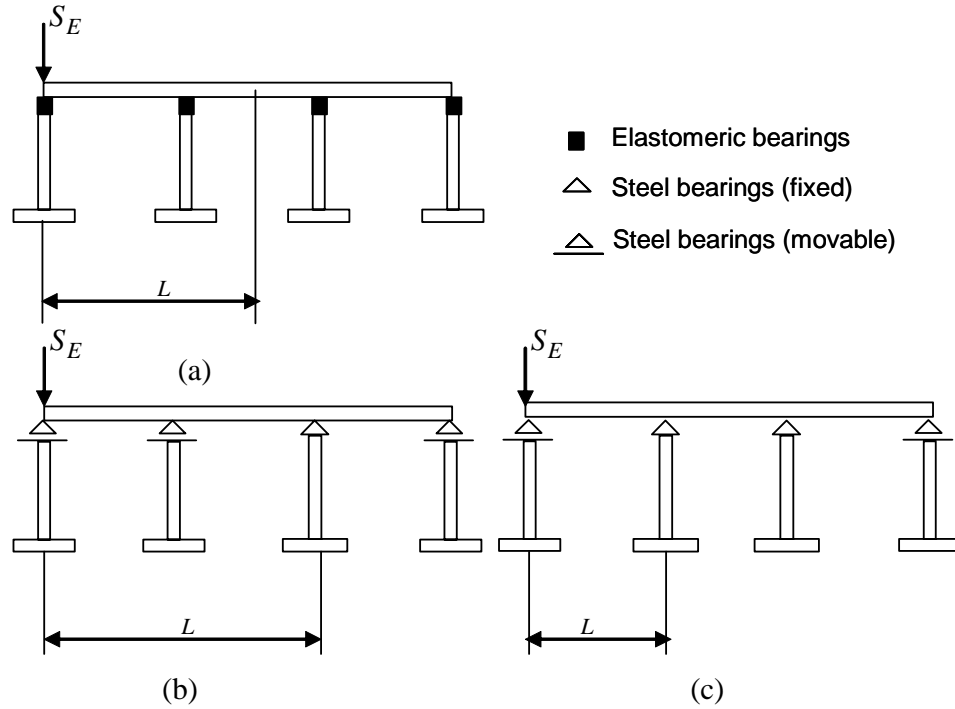


Fig. 4-4: Distance between two substructures which controls the seat length L : (a) bridge supported by elastomeric bearings, and (b) and (c) bridges supported by steel bearings

4.3.3 Design practice in Greece

According to the Greek Code (E39, 1999), the minimum width required at deck joints is

$$d_{td} = \pm 0.4d_E + d_{1t} \pm \varphi_{2T}d_T \quad (4-6)$$

where d_E is the design seismic displacement (if the bridge consists of two independent parts, d_E is estimated as the SRSS combination of the individual displacements), d_{1t} is the displacement due to long-term effects (prestress, creep, and shrinkage), d_T is the displacement due to temperature changes, and $\varphi_{2T} = 0.5$ is a combination factor for thermal actions.

When simply supported spans are used, the problem of potential unseating is addressed by specifying (for both end and intermediate supports) a minimum seat width C (in mm)

$$C = (400 + 2.5L + 10H) \times (1 + s^2 / 8000) \quad (4-7)$$

where L is the length (in m) of the monolithic part of the deck (average of adjacent spans in intermediate supports), H is the pier height (in m) at the support under consideration, and s is

the skew angle (in degrees). When $L > 250\text{m}$, the Eurocode 8 Part 2 Provisions, wherein the effect of spatial variability of ground motion on required seat width is taken into account, should be applied. In general, seat widths provided in Greek bridges are ample, and no unseating has occurred to date, even in older bridges with span hinges (Gerber type).

4.4 Stresses in bridge superstructures subjected to seismic actions

One of the main considerations in modern seismic design of bridge superstructures is that the superstructure must resist the seismic action elastically. The common mechanism of inelastic deformation is expected to develop in plastic hinges in bridge columns. It follows that the superstructure needs to be capacity designed to remain elastic when balancing the flexural overstrength from the column plastic hinge. It is, therefore, relevant to review whether this design assumption is likely to occur when a bridge responds to expected earthquake ground motions. A study along these lines has been conducted by Fishinger (2006) for a typical European viaduct and is briefly described in the following.

The behaviour of the prestressed superstructure of a typical European viaduct (Fig. 4-5 and 4-6) was analysed in the transverse direction for different earthquake intensities (see Table 4-1). The applied accelerograms were based on the EC8 spectrum – soil B.

Maximum and minimum observed stresses in the superstructure are summarized in Table 4-1. Results from this study indicates that the superstructure remained elastic up to the earthquake intensity of 0.5g, which is more than the maximum ground acceleration expected anywhere in Europe. These results indicates that for the analyzed bridge the superstructure is likely to respond elastically to the design earthquake and that inelastic deformations are developed only in plastic hinges of the bridge columns.

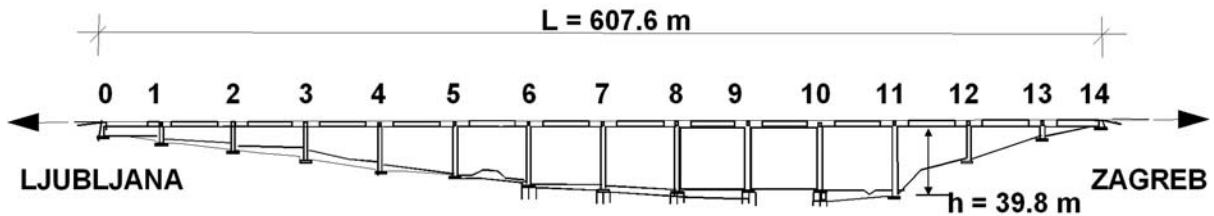


Fig. 4-5: Typical European viaduct

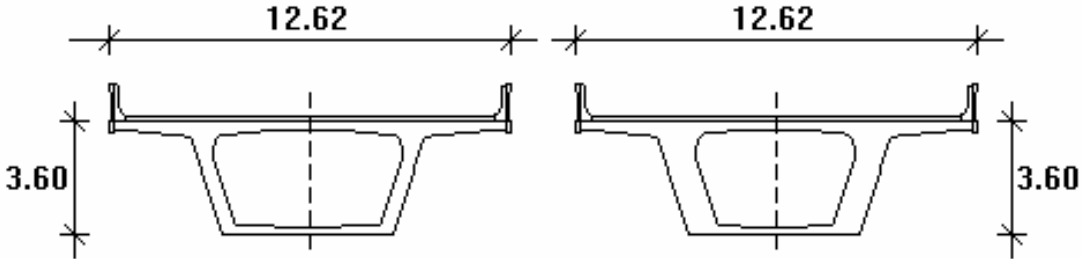


Fig. 4-6: Cross-section of the prestressed superstructure

Bridges in Japan are designed in accordance with three Seismic Performance Levels (SPL). For function evaluation ground motions, superstructures should remain elastic (SPL1). For safety evaluation ground motions, important bridges and standard bridges should be design so that they retain limited damage (SPL 2) and prevent critical damage (SPL 3), respectively [JRA (2002)].

PGA	s_c/f_{ck}	s_t/f_{ctm}
0.50g	0.65	0.55
0.40g	0.60	0.05
0.35g	0.57	in compression
0.30g	0.53	in compression
0.25g	0.49	in compression

PGA – peak ground acceleration

s_c – compression stress

s_t – tension stress

f_{ck} – characteristic cylindric compression strength

f_{ctm} – mean tensile strength

Table 4-1: Stresses in superstructure for different earthquakes intensities

To satisfy the SPL 2, a superstructure should be designed so that it can be used without permanent repair under the safety evaluation ground motion. For such a purpose, the superstructure is designed so that the curvature developed in the superstructure is within the limit states shown in Table 4-2. On the other hand, for satisfying the SPL3, the compressive strain of concrete at the outmost edge of the superstructure should not exceed the design compression strain of 0.002 so that spalling of cover concrete does not occur.

Type of superstructures	Longitudinal Direction	Transverse Direction
Prestressed concrete superstructures	Curvature formed when a PC member reaches the elastic limit state	Curvature formed when the reinforcing bar on the outmost edge of web yields or when a PC member reaches the elastic limit state
Reinforced concrete superstructures	Curvature formed when a reinforcing bar on the outmost edge reaches the yielding	

Table 4-2: Design Curvature of Superstructures for Seismic Performance Level 2

4.5 A regional review of design choices of bridge superstructure

This section presents results from an international survey on seismic design for bridge superstructure. The questions of this survey and a summary of the range of answers are presented in the following.

4.5.1 Simple supported vs Continuous superstructure: when and why they are used, reasons for a preference

It is of interest that in Europe before the 90's, the trend for bridge construction was to use simple supported prestressed superstructures. Fig. 4-8 shows some details of an old precast bridge superstructure built in Slovenia before the 90's. Fig. 4-7 shows a greek bridge, which, although constructed in the 90's, has a superstructure that is typical of older construction. In these cases, the superstructures consist of precast post-tensioned beams connected through a cast in situ top slab.

In the US, after the 1971 San Fernando Earthquake in California, most bridges in the West Coast, long and short, were constructed with support continuity and only few new bridges incorporate simply supported spans and these incorporate restrainers. Bridges in North

Carolina (East coast of the US) are of both types of superstructures. For spans less than 70-80 m, simply supported is the norm. Beyond that, bridges are often simply supported for dead load, and continuous for live load.

In Japan, a load combination of dead weight, thermal force and seismic effect was included in the design code prior to 1980. This load combination generally resulted in larger stress in columns in multi-span continuous bridges than simply supported bridges under seismic effect. As a consequence, simply supported bridges were more common prior to 1980. However, it was evident even prior to 1980 that multi-span continuous bridges in Japan were superior to simply supported bridges because of lower seismic risk of unseating of the decks from their supports and lower maintenance of expansion joints due to less impact force by traffic load. Therefore various attempts were implemented to build multi-span continuous bridges with controlling the increase of stress resulted from the load combination of thermal and seismic effects. For example, damper stoppers that transfer seismic force from the deck to piers and release the thermal movement of the deck were installed between the deck and the piers so that the inertia force of the deck could be distributed to every pier.

Construction of multi-span continuous bridges in Japan became predominant after 1980 when the load combination of dead weight, thermal effect and seismic effect was eliminated. In particular after the 1995 Kobe earthquake multi-span continuous bridges with total deck length over 1 km are encouraged by using elastomeric bearings.

A current trend worldwide for bridge construction is to use continuous prestressed superstructures, even for long bridges (total length more than 1000 m). It is the general belief that bridges with support continuity avoid the necessary maintenance of bearings and expansion joints and the problem of unseating.



*Fig. 4-7: The G2 bridge near Kavala (NE Greece); the superstructure consists of precast post-tensioned beams connected through a cast in situ top slab (typical of older construction) (Courtesy of A. Kappos).
(Figure available electronically on fib website; see production note on p. ii)*

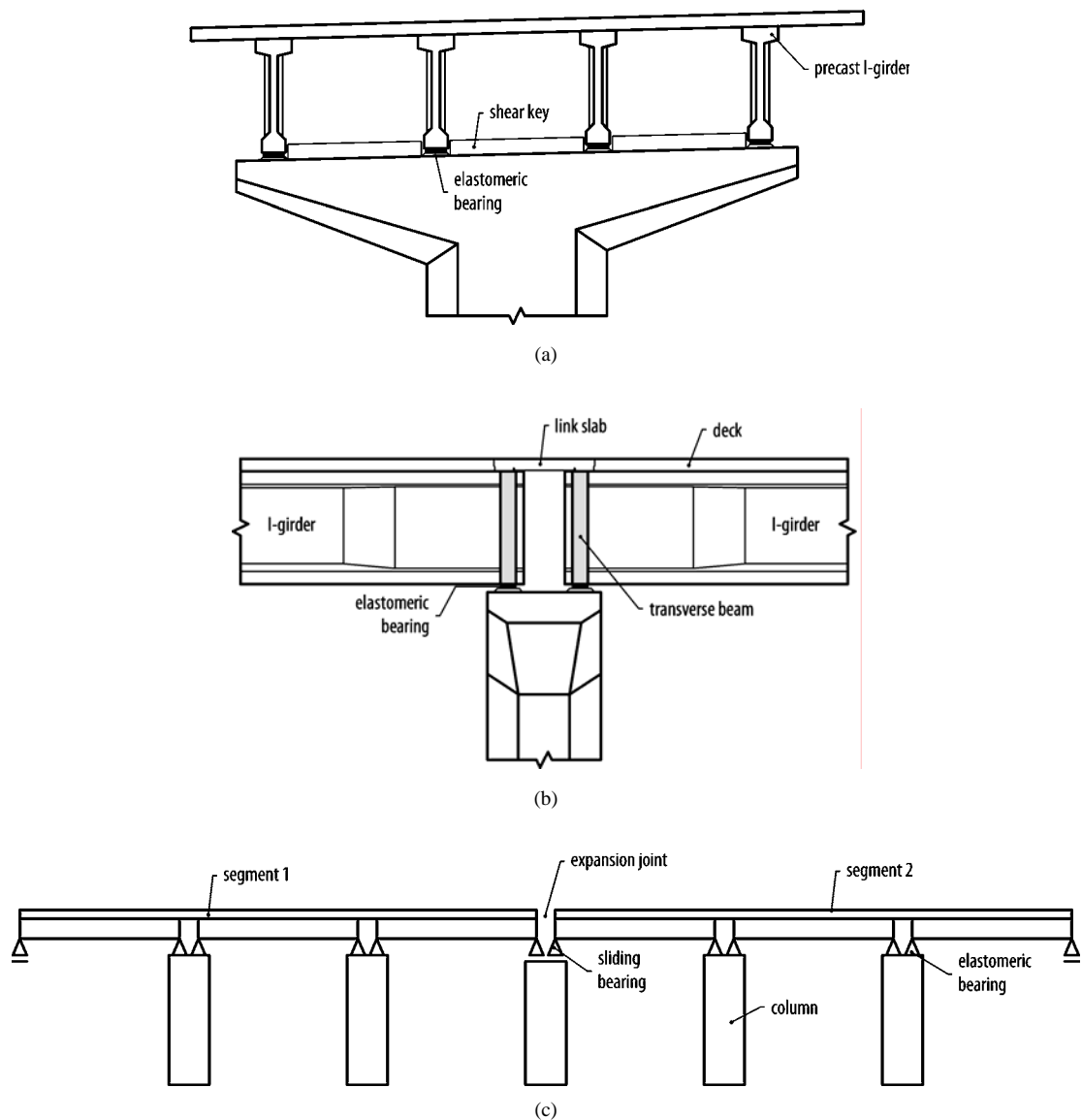


Fig. 4-8: Typical cross section of an old precast superstructure system built in seventies and eighties: (a) transverse and (b) longitudinal direction; (c) structural system of the superstructure.

4.5.2 Precast vs cast-in-place superstructure: factors that affect the decision making process

In Europe, precast post-tensioned or pre-tensioned beams are the most widely used method for deck construction for medium spans of up to about 45m, as they can be constructed both fast and cost effectively. Traditionally, bridge decks consisting of precast beams have been built in Europe without the continuity of the in-situ top slab over the piers. However, the presence of numerous expansion joints has resulted in maintenance and functionality (ride-ability) problems; hence, precast beams in combination with continuous in-situ top slabs are used in modern bridges.

In Japan, both precast and cast-in-place superstructures are used.

Precast and cast-in-place superstructures are used in California. Typical precast/prestressed concrete bridges in California consist of simple supported girder elements which for multispan bridges are made continuous with a cast-in-place deck. Cast-in-place superstructures girders are constructed monolithic with column. In new construction, the use

of cast in place hollow box girders are almost always the choice. However, there are exceptions to this case. Bridges built over environmentally sensitive areas or above water, are built using precast elements. Two options are used: precast concrete segmental construction, or precast concrete I-girders with a continuous deck. Fig. 4-9 shows the precast concrete segments built in a yard and ready for transport for the construction of the new San Francisco-Oakland bay bridge skyway structure. In the East coast of the US almost exclusively precast bridge systems are used. Even for the very short spans, hollow core slab planks are used there. The exception to this is the very occasional cast in place box girder (there are just a few in the region).

Typically precast girders lack a direct positive moment connection with the cap beam, which in the longitudinal direction under seismic demands could turn in a pinned connection. Recent research (Holombo et al., 2000) has confirmed the viability of precast spliced girders with integral column-superstructure details that can resist longitudinal seismic loads. However, according to Caltrans this type of system is considered non-standard until design details and procedures are formally adopted.

It is of interest that a significant portion of Caltrans bridge construction budget nowadays goes into the widening of bridges in existing highways in California. In these widening projects, precast concrete girders seating on a cast in place inverted T bent cap are commonly used, especially in areas where traffic can be disrupted and safety compromised. Fig. 4-10 shows an example of a recent bridge-widening project.



*Fig. 4-9: Precast segmental elements for the construction of the San Francisco-Oakland Bay Bridge Skyway Structure (Courtesy of F. Seible)
(Figure available electronically on fib website; see production note on p. ii)*



Fig. 4-10: Example of use of the use of precast I-girders on a highway bridge widening project in California (Courtesy of J. Restrepo)
(Figure available electronically on fib website; see production note on p. ii)

4.5.3 Seismic analysis considerations such as effective width of superstructure, cracking and yielding, etc.

A common seismic design consideration in Europe and US is that the superstructure must resist the seismic load elastically. The deck is capacity designed to remain elastic when the ductile behavior of a bridge is chosen. However, the international survey indicates some exceptions on this issue. An important viaduct in Mexico City, recently constructed with span hinges (Gerber type), was designed considering inelastic behavior of both piers and superstructure.

The survey indicated that the most common analysis method for new bridges is modal spectral analysis. Bridges that can be modeled as SDOF oscillators, such as single span bridges, multi-span bridges consisting of simply supported spans, or multi-span bridges in general in their longitudinal direction (if the mass of their piers is less than 20% of the total) can be analyzed using the equivalent static method.

Different practices were found in the international survey regarding effective width of superstructure resisting longitudinal seismic moments. In Europe, no specific provisions for effective deck width are considered in the analysis of the longitudinal response of the bridge. Two remarks are in order in this respect: First, the width of bridge is relatively small (typically not exceeding 14m); roadway bridges and viaducts are constructed as ‘twin’ structures (see Fig. 4-2), and second, most bridge superstructures are post-tensioned.

According to Caltran’s recommendations, the effective width of superstructure resisting longitudinal seismic moments, B_{eff} , is defined by eq. 4-8

$$\begin{aligned}
 B_{eff} &= D_c + 2D_s && \text{Box girders \& solid superstructures} \\
 B_{eff} &= D_c + D_s && \text{Open soffit superstructures}
 \end{aligned}
 \tag{4-8}$$

Parameters D_c and D_s are defined in Fig. 4-11. The effective superstructure width can be increased at a 45° angle moving away from the bent cap until the full section becomes effective, see Fig. 4-11.

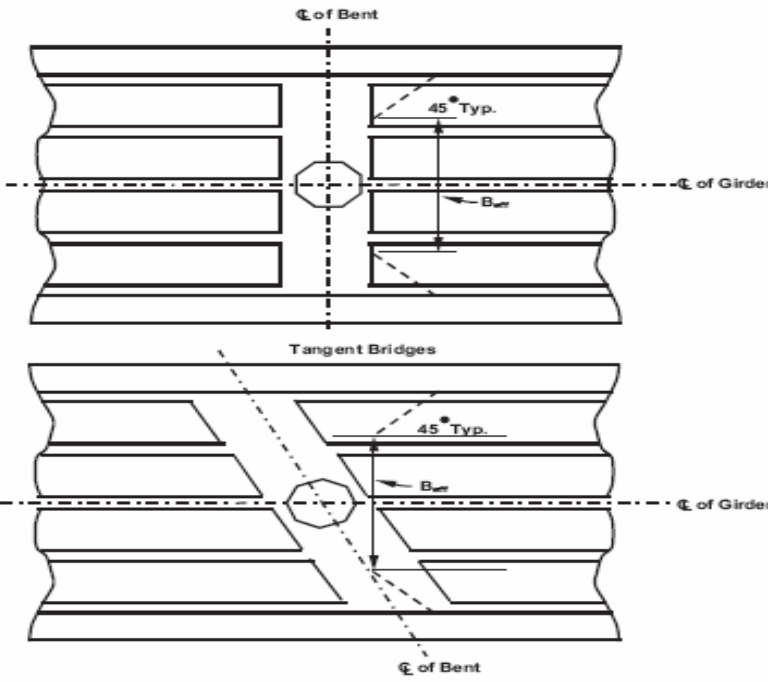
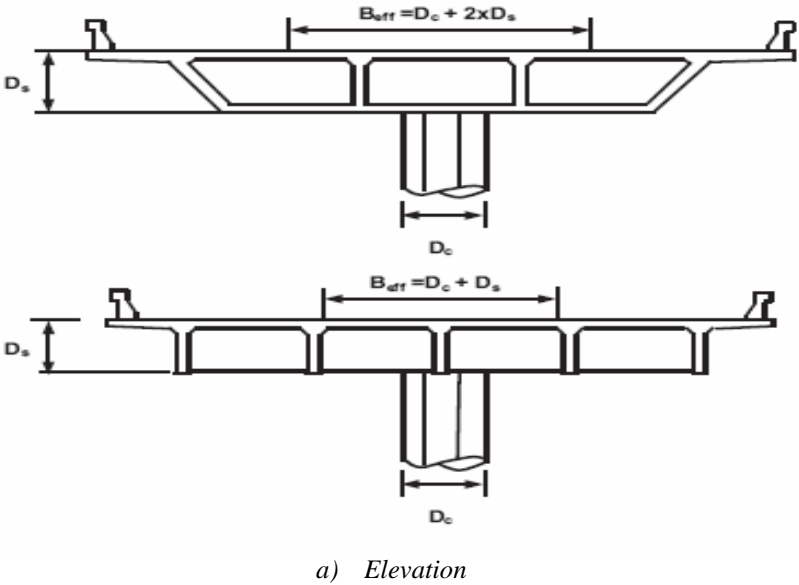


Fig. 4-11: Effective superstructure width (Caltrans)

According to results found in the international survey, since prestressed concrete decks are not expected to be part of the plastic mechanism, in Europe they are modelled using their elastic rigidity (EI_g). Non-prestressed concrete decks are, as a rule, also expected to remain below yield conditions; the Code recommendation in Europe is to model them using the average of the elastic and the yield stiffness values, but it is common in design offices to use

EI_g for RC decks, too. A notable exception is the case of continuity slabs used in decks consisting of precast prestressed beams, simply supported on the piers. For example in Greece, the effective rigidity of the continuity slabs (above the supports) is usually taken equal to 10% to 20% EI_g in the longitudinal analysis of the bridge, to account for the fact that plastic hinges *are* expected to form at these locations.

According to Caltrans, section properties such as flexural rigidity $E_c I$ and torsional rigidity $G_c J$ shall reflect the cracking that occurs before the yield limit state is reached. The effective moment of inertia I_{eff} and J_{eff} shall be used to obtain realistic values for the superstructure's period and the seismic demands from seismic analyses. In prestressed concrete box girder sections, the location of the prestressing steel and the direction of bending have a significant impact on how cracking affects the stiffness of prestressed members. Due to this reason and considering that modal analysis cannot capture the variations in stiffness caused by moment reversal, no stiffness reduction is recommended in California for prestressed concrete box girder sections. For reinforced concrete box girder sections, I_{eff} can be estimated between $0.5 I_g$ and $0.75 I_g$. These values range from lightly reinforced sections to heavily reinforced sections. Reductions to I_g similar to those specified for box girders are used for other superstructure types.

4.5.4 Irregularities on stiffness and mass of bridge superstructure. Indicate how designers consider irregularities for seismic design

In Europe there are no special recommendations regarding stiffness of adjacent bents within a frame, however regular bridges are preferred. Variable width decks are not used, which leads to a uniform distribution of mass along the bridge (assuming the height of the section is kept constant). Designers in Greece (Tokatlidis, 2005) consider the Caltrans recommendations for k_{min} / k_{max} to be rather restrictive (where k_{min} / k_{max} are the smaller and larger effective bent or frame stiffness, respectively), particularly in mountainous areas (very common in Greece) where the use of piers of unequal height is dictated by topography. However, they do use techniques for balancing the stiffness of adjacent bents, such as 'pre-shafts' (upward extensions of the foundation shaft, see Fig. 4-12) that increase the effective height of shorter piers, or the combination of monolithic and bearing deck to pier connections (the latter used in shorter piers). These techniques lead to a more balanced stiffness of adjacent bents, but often tend to increase the overall cost of the bridge.



*Fig. 4-12: Use of a 'pre-shaft' to increase the pier length in an Egnatia bridge (Metsovitikos)
(Figure available electronically on fib website; see production note on p. ii)*

In Japan is considered that irregularity on stiffness and mass in bridges may result in poundings between decks of two adjacent bridges. To limit the effect of pounding, a gap between two adjacent decks S_B is designed by eq. (4-9) (see Fig. 4-13) .

$$S_B = \begin{cases} u_s + L_A c_1 & \text{(between a deck and an abutment)} \\ c_B u_s + L_A & \text{(between adjacent decks)} \end{cases} \quad (4-9)$$

where

$$\Delta T = T_1 - T_2 \geq 0 \quad (4-10)$$

in which u_s is the maximum relative displacement between two adjacent decks which are subjected to the life safety ground motions, L_A is allowance of adjacent decks, T_1 , T_2 and ΔT are the natural period of adjacent decks ($T_1 \geq T_2$) and difference of two natural periods, respectively, and c_B is a modification factor for gap depending on the natural period ratio $\Delta T / T_1$ (refer to Table 4-3). If the natural periods of two adjacent bridges are much different, larger gap is required between adjacent superstructures in terms of c_B . It is noted that c_B stands on the relative displacement response spectra which were proposed based on an analysis of 63 components of ground motions [Kawashima and Sato (1996)].

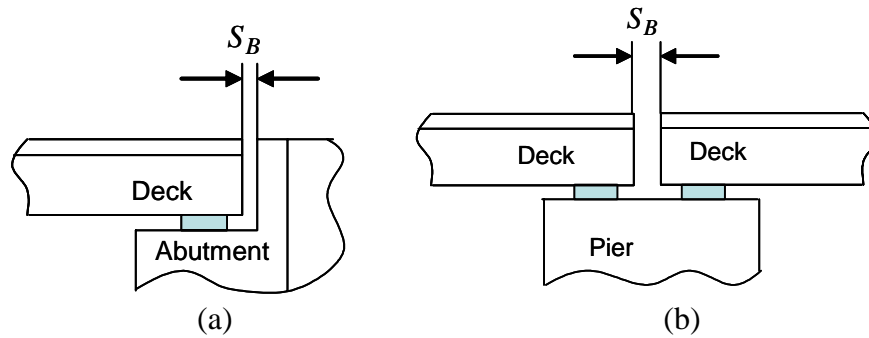


Fig. 4-13: Gaps between adjacent superstructures: (a) deck supported by an abutment, and (b) deck supported by a pier

$\Delta T / T_1$	c_B
$0 \leq \Delta T / T_1 < 0.1$	1
$0.1 \leq \Delta T / T_1 < 0.8$	$\sqrt{2}$
$0.8 \leq \Delta T / T_1 < 1.0$	1

Table 4-3: Modification factor for gaps depending on natural period of two adjacent superstructures

In adjacent bridge frames, Caltrans recommends that the ratio of fundamental period of vibration for adjacent frames in the longitudinal and transverse directions satisfy eq 4-11

$$\frac{T_i}{T_j} \geq 0.7 \quad (4-11)$$

where

T_i = natural period of vibration of the less flexible frame

T_j = natural period of vibration of the more flexible frame

According to Caltrans the consequences of not meeting the fundamental period requirements given by eq 4-11 would increase the likelihood of out-of-phase response between adjacent frames, which would lead to large relative displacement that increases the probability of longitudinal unseating and collision between frames at movement joints.

The level of analysis in the design of bridges in California depends on the category of the bridge. The Caltrans seismic design criteria classifies bridges in ordinary and non-ordinary, which can be standard and non-standard.

Ordinary standard bridges have span lengths less than 90 m, are constructed with normal weight concrete girder, and column or pier elements, the horizontal members are either rigidly connected, pin connected, or supported on conventional bearings by the substructure. Ordinary non-standard bridges satisfy the above requirements but incorporate base-isolation or supplementary damping devices. Irregularities in these bridges are commonly dealt with using conventional modal analysis.

Non-ordinary bridges are special structures that require a two-level design approach to check for functionality and for life-safety. The functional evaluation earthquake is a probabilistically assessed ground motion that has a 40% probability of being exceeded during the useful life of the bridge. The objective is to relate level-of-performance criteria to realistic earthquake levels; level of performance is defined in terms of elastic behavior of the structure during the earthquake as well as the extent and reparability of damage. The safety evaluation earthquake is defined as the maximum credible earthquake and has a probabilistically assessed ground motion with a long return period (1000-2000 years). Typically non-ordinary bridge structures are analyzed using time-history non-linear analyses.

4.5.5 Historical considerations, changes in types of bridge superstructures in the last (about) 50 years

In Japan, first seismic design code was introduced in 1925. Because instability of soils was the major causes of damage, attention was paid for seismic design of foundations at the early days. First attention to seismic design of superstructures was paid when bridges suffered extensive damage due to liquefaction and liquefaction induced lateral spreading in the 1964 Niigata earthquake.

In Italy a strong impulse to the construction of modern road infrastructures dates back to the post WWII period. In the 50s and the 60s due to economic as well as technological constraints the standard solution adopted throughout the Country consisted of simply supported multiple pre-stressed beam decks with standard span length of 30 to 32m. The bearings were almost invariably made of low neoprene pads and the joints between decks were rather primitive. For the crossings of large valleys the solution was still that of the RC arch-bridge with upper deck. This typology was progressively replaced in favour of segmental cast-in-situ pre-stressed concrete bridges with symmetric cantilever construction and span lengths of the order of 100m. Mainly due to limited predictive control of the long-term creep and shrinkage effects, with the ensuing pre-stress losses, the preferred solution was to have a hinged connection at mid-span. During the 70s, while the construction of the highway infrastructure was reaching completion, in the medium to long span range the segmental launching technique replaced the balanced cantilever construction, and the most common typology for short span length (35 to 40m) remain almost unvaried, i.e. simply supported pre-stressed concrete decks. These latter were now made up either of pre-cast pre-tensioned multiple beams, with T or U sections and cast-in-place RC slab, or of pre-cast box-section girders having the full width of the deck, constructed off-site and positioned with launching girders. Bearings did not see any significant evolution until the end of the 70s early 80s when the first pot-bearings made it to the market.

The above described changes in type of bridge superstructures in Italy to some extent also describe the evolution of bridge superstructure in Europe and in the US. California has build significant confidence on cast-in-place concrete continuous box-girders and contractors are very familiar with this type of construction. This is a shift from the construction of smaller simply supported span steel and concrete bridges that were commonly used in the 1950s and 1960s. The West coast of the US has gone more towards concrete and away from steel, although there are still a fair number of steel bridges. Towards the coast, almost exclusively concrete. In Mexico most roadway bridges are built nowadays with simple supported superstructures.

4.5.6 Perceived problems with earlier design

In Japan, unseating prevention devices were first developed and they have been implemented since the 1964 Niigata earthquake. Unseating prevention devices consisted of providing restrainers and seat length for preventing unseating of the superstructures from their supports. In the national seismic retrofit programs which were initiated in 1971 and repeated at approximately every 5 years, providing unseating prevention devices has been one of the most common practices of the seismic retrofit. The extensive damage in the 1995 Kobe earthquake revealed inadequate ductility capacity of columns and inadequate strength of restrainers. Shear failure and premature shear failure of columns with termination of main reinforcements at mid-heights resulted in the extensive damage. Steel jacketing as well as precast segment jacketing and composite materials jacketing was implemented over 40,000 columns since the Kobe earthquake. Design seismic force of unseating prevention devices was increased, and detailings of design for cable restrainers and joint protectors were extensively modified in the code [Kawashima (2000)].

It is of relevance to note that in Italy seismic design considerations for bridges were implemented in this decade, implying that the design of existing bridges and new bridges are quite different. Until the 90's, no proper seismic design code existed and seismic prescriptions were only nominal, limited essentially to conventional forces (maximum spectral acceleration of 0.1g), without any detailing and capacity design indications. The only exception to this rule took place after the 1981 Campania Earthquake, which affected a good number of highway bridges in an area close to the epicentre. The solution for retrofitting these bridges (simply-supported multiple-span viaducts) was to replace all bearings with HDR (High-damping rubber) bearings, and to make the deck continuous at the slab-level. A total of about 150 bridges were treated in this way, a first example of application of modern EE concepts.

In California, Caltrans has made a considerable investment at retrofitting older bridges of significant importance to the community. Most retrofits consist of column jacketing to protect brittle shear failures, to provide suitable confinement to the concrete, and to provide an effective force transfer mechanisms in columns with poorly detailed lap-splices at the column bases. It is of interest that a common retrofitting solution for bridges with simple supported superstructures after the 1971 San Fernando Earthquake was the use of restrainers in the superstructure. In the West coast of the US, perceived problems with earlier design are related to maintenance and designs that are not friendly to the environment.

4.5.7 Bridge superstructure section shapes

Results from the international survey on design choices for bridge superstructure indicate some common trends for the use of superstructure section shapes. In Europe solid slabs are used for short spans (0 to 25 m). The slab mass is effectively reduced by 30-40 % when multi-girder slab is used instead of a solid one. In countries like Slovenia, voided slabs are not used since voids cannot be inspected. In the US, solid and voided slabs are used for road and rail bridges with spans below 15 m. Simple supported prestressed I-beams are used in Europe and US for spans up to 20-25 m.

For medium spans (30 to 60 m) double T section is commonly used in Europe. However it is not recommended for curved bridges because of poor torsional characteristics. In the US, this section is less favored than in Europe since box girders and I-beams are preferred. In California, I-beams are preferred in some specific projects (new bridges over water, widening projects).

In Europe and in the US, box girders is the choice for medium and large spans. They are also used for bridges curved in the horizontal plane due to their substantial torsional stiffness. Variable section height along the length of the bridge can only be economically justified for long spans (100-120 m). As discussed earlier, road bridges and viaducts in some regions in Europe are constructed as “twin” structures (see Fig. 4-2). On the contrary, in the US, either single box-girders or multi-cell box girders are commonly employed. Single box-girders are preferred in two-lane bridges whereas multi-cell box girders are preferred in bridges with four or more lanes.

Table 4-4 shows an example of typical use of superstructure shapes in Greece and illustrates some of the use of different section shapes above discussed.

Deck cross section	Typical span limits
Solid RC slab	simply supported: 15m continuous: 20m frames (e.g. portal): 25m
Solid PSC slab	simply supported: 25m continuous: 30m
Voided slab (cast in situ)	RC continuous: 20m PSC simply supported: 35m PSC continuous: 45m
Precast I-beams (post-and/or pre-tensioned)	RC simply supported: 20m PSC simply supported: 40÷50m (in railway bridges: 35m)
Double-tee beams (post-tensioned)	PSC continuous: 45m
Box girder (post-tensioned)	fixed depth: 120m variable depth: 250m

Table 4-4: Superstructure shapes for concrete bridges in Greece

4.5.8 Weight of superstructure

An effective procedure for reducing weight in a bridge is the use of lightweight concrete which leads to reduced seismic forces. Results from the international survey indicate that lightweight concrete is not used in the construction of bridge decks in Europe. It is argued there that with lightweight concrete is difficult to attain the required concrete strength (particularly in prestressed decks). However, use of several non-solid sections such as voided slabs and several types of 'open soffit' and box sections are commonly used in Europe, which lead to a reduced weight of the superstructure. The US moves towards lightweight, highstrength, and self-consolidating concrete although these are all in general on the horizon except for a few demo structures. An example of the use of structural lightweight concrete in the US is the new Benicia-Martinez Bridge in California. This is a cast-in-place concrete, pos-tensioned box girder bridge in a high seismic zone. In this case, the lightweight concrete density is 1.92 Mg/m^3 with a compressive strength of 45 MPa.

The use of lightweight concrete does not increase the total project cost. For a bridge with a cost of US $800/\text{m}^2$, the use of lightweight concrete results in a cost increase in materials of one percent (Holm and Ries, 2001). This cost increase in materials is offset by the reductions in the cost of slab reinforcement and the reduced size and cost of girders and foundations due to a lower superstructure weight.

References

- California Department of Transportation (Caltrans) 2004. Seismic Design Criteria (http://www.dot.ca.gov/hq/esc/earthquake_engineering/SDC/SDCPage.html)
- European Committee for Standardization. Eurocode 8, Design of Structures for Earthquake Resistance. Part 2. (CEN 2004), Brussels
- Fishing M. 2006. Private communication
- Greek Seismic Code for Bridges (E39/1999)
- Holm T. and Ries J. 2001. Benefits of Lightweight HPC. HPC Bridge Views, Issue No 17, Federal Highway Administration and the National Concrete Bridge Council, (<http://www.portcement.org/br/newsletters.asp>)
- Holombo H., Priestley M.J. and Seible F. 2000. Continuity of Precast Prestressed Spliced-Girder Bridges Under Seismic Loads, PCI Journal, March -April
- Japan Road Association 2002. Part V: Seismic Design, Design Specifications of Highway Bridges. Maruzen, Tokyo, Japan
- Kawashima K. and Sato T. 1996. Relative displacement response spectrum and its application. Proc. 11th World Conference on Earthquake Engineering, 1103, Elsevier
- Kawashima K. 2000. Seismic Design and Retrofit of Bridges. 12th World Conference on Earthquake Engineering, Paper No. 1818, Auckland, New Zealand
- Priestley M.J, Seible F., and Calvi G.M. 1996. Seismic Design and Retrofit of Bridges. J. Wiley & Sons
- Tokatlidis A. 2005. METE-SYSM Design Office, Thessaloniki, Private communication

5 Design of foundations

5.1 Overview of bridge foundations design

Bridges are built on spread footings or on pile foundations, less commonly nowadays on deep caissons. Bridges on spread foundations are supported by firm soil layers or on rock close to the ground surface, and such bridges have performed well during earthquakes. On sites with weak soil layers, bridges are supported by deep foundations that transfer the vertical and lateral forces to the stronger layers of soil beneath the soft material. Bridges on sites with soft clay, silt or loose saturated sand, have been damaged by the amplification of the ground motion or by soil failure during earthquakes. Except when massive soil failures have occurred, pile foundations have performed well during past earthquakes, even when other bridge elements sustained considerable damage. On the contrary, bridges supported on liquefiable soil deposits, or on soft sensitive clays, have been particularly vulnerable to earthquakes: soil liquefaction can cause a loss of bearing capacity and, sometimes, lateral movement of the substructure. These last phenomena have become a major concern after the 1995 Kobe earthquake and specific design procedures have emerged since, which will be reviewed in section 5.4.

Because it is difficult to inspect or to repair foundations after an earthquake, it is a common practice to restrict to a minimum the damages to the foundations so that operation of the bridge can easily restart without repair work to the foundations. However, in some instances this is not possible, for example when the structure possesses a large capacity (controlled by factors other than the earthquake). To achieve the aforementioned objective, bridge foundations are usually not intentionally used as sources of hysteretic energy dissipation and therefore, as far as practicable, are designed to remain elastic under the seismic action. The forces applied to the foundations are obtained either directly from the elastic analysis, when the superstructure remains elastic, or from the capacity of the intended plastic hinges, enhanced by the overstrength factor, when the structure is designed for a ductile behavior; the overstrength factor takes values that typically range from 1.10 to 1.35. However it must be recognized that the above approach is not a requirement; following the Kobe earthquake, the new Japanese Specifications for Highway Bridges (JRA, 2002) recommend a ductility design method, at least for the level 2 motion, to verify the seismic performance of foundations, in which both the capacity and ductility of the foundations are taken into account.

The basic principles of foundation design require that the foundation be able to safely transfer to the ground the applied loads; accordingly they should be mechanically stable and should not cause detrimental displacements. To ensure stability, the foundations must exhibit the required factors of safety against bearing, sliding and overturning failure mechanisms. The items to be checked for the stability verifications differ depending on the foundation type as shown in Table 5-1.

Finally, in addition to the foundation stability requirements, the foundation elements must be structurally designed to resist the applied forces.

In the following sections, the specific aspects related to spread foundations, pile foundations and foundations in a liquefiable environment are examined.

Foundation type	Bearing capacity	Overturning	Sliding	Horizontal displacement
Spread foundation	Yes	Yes	Yes	
Caissons foundation	Yes			Yes
Pile foundations	Yes			Yes

Table 5-1: Foundation stability verifications

5.2 Spread foundations

Spread foundations are foundations that directly transmit loads from the superstructure to the competent ground; they can be defined as foundations for which the ratio of the embedment depth to the foundation width is smaller than 0.5; otherwise foundations are referred to as caisson foundations. Seismic design of spread footings is usually carried out in two steps, using a substructure method: loads transmitted to the foundation are evaluated from a linear soil structure analysis in which the foundation is modeled by its stiffness and damping, and the foundation capacity is subsequently checked for those forces.

5.2.1 Force evaluation

The current state of practice in soil-structure interaction analyses for spread footing involves solving for the response of a rigid footing on a layered elastic half space. From elasto-dynamic formulation, the stiffness characteristics of the foundation consist of two parts: a static component and a dynamic component. The general form of the stiffness matrix for a rigid footing is:

$$[K] = \begin{bmatrix} k_{11} & 0 & 0 & 0 & -k_{15} & 0 \\ 0 & k_{22} & 0 & k_{24} & 0 & 0 \\ 0 & 0 & k_{33} & 0 & 0 & 0 \\ 0 & k_{42} & 0 & k_{44} & 0 & 0 \\ -k_{51} & 0 & 0 & 0 & k_{55} & 0 \\ 0 & 0 & 0 & 0 & 0 & k_{66} \end{bmatrix} \quad (5-1)$$

Degrees of freedom 1 through 3 are translation and degrees of freedom 4 through 5 are rotation. The degree of freedom 3 is the translation in the vertical direction. The vertical translational degree of freedom (k_{33}) and torsional degree of freedom (k_{66}) are uncoupled with the other degrees of freedom in the stiffness matrix provided the foundation geometry is regular and possesses two axes of symmetry. However, the two components of horizontal translation are always coupled with the two degrees of freedom in rocking rotation in the stiffness matrix. When embedment of the footing is shallow, the off-diagonal (cross-coupling) terms are generally neglected.

The stiffness matrix derived from the elastic half space theory is a linear representation of the problem. For tall bridges the most important mode of foundation behavior is the rocking

behavior where base separation can take place and have major effects on the resultant global bridge behavior; consideration of this factor can only be achieved with an incremental non linear analysis. However, in practice base separation and the resulting "softening" of the secant rotational spring is ignored for the evaluation of the inertial forces acting on the foundation; base separation is only taken into account for the stability verifications of the foundation (see section 5.2.2). This implies that base uplift is limited in order to consider that the forces are not significantly affected by this geometrical non linearity; a good rule of thumb is to accept that the linear analysis, without consideration of base uplift, is still valid as long as the uplifted ratio of the foundation is less than 30% to 50%.

5.2.2 Stability verifications

It is still common practice to check separately the resistance to overturning, sliding and vertical bearing capacity by examining the forces and moments equilibrium around an horizontal axis and along horizontal and vertical axes.

The vertical bearing capacity is checked with the well known bearing capacity equation taking into account the load eccentricity and inclination :

$$Q_u = A \left\{ \frac{1}{2} \gamma B i_\gamma s_\gamma N_\gamma + C i_c s_c N_c + q i_q s_q N_q \right\} \quad (5-2)$$

In the above expression i_α and s_α are the corrections factors for load inclination and eccentricity, B and A the foundation width and area, C the soil cohesion, q the lateral overburden and N_γ , N_c and N_q the bearing capacity factors that depend on the soil friction angle. Different expressions for eq. 5-2 exist in the literature; for example the Japanese Road Association (JRA, 2002) makes use of a similar, but different, expression. A safety factor greater than 2 is usually required for the seismic situation. It must however be recognized that the definition of the exact global safety factor is difficult when the code format is based on partial safety factors, like Eurocode 8, or on the LRFD approach (AASHTO).

With respect to overturning it is usually required that the load acts within one sixth (most of the codes) to one third (JRA, 2002) of the footing width from the center, which is equivalent to say that uplift is either not allowed or allowed over half the foundation width. Uplift seems to be more commonly tolerated because it is recognized that rocking of foundation reduces the forces that enter the structure and therefore protects it; however, rocking must be restricted to very good soil conditions to avoid yielding of the soil under the loaded edge, which induces permanent settlement and tilt of the foundation. To appreciate the importance of this behavior, it is recommended that pseudo-static pushover analysis be conducted to examine moment-rotation characteristics of spread footings considering the effects of geometric nonlinearity (uplift of the footing) and soil yielding. Analytical results from these pushover analyses not only yield rotational stiffness parameters, but also provide the geotechnical mode of ultimate moment capacity which can be treated as load fuse in the overall bridge system. For the spread footing problem, geometric nonlinearity (uplift) is the most severe form of nonlinearity, and the foundation cannot develop overturning moments that are higher than the ultimate moment capacity.

Fig. 5-1 presents an example of pushover (rocking) analyses conducted for a spread footing on dense sand at San Diego-Coronado Bay Bridge (Lam and Law, 2000). A vertical dead load was imposed on the spread footing before an increasing moment was applied. From the limit equilibrium, the upper bound value of the ultimate moment capacity may be evaluated from the product of dead load on the footing and the half width of the footing.

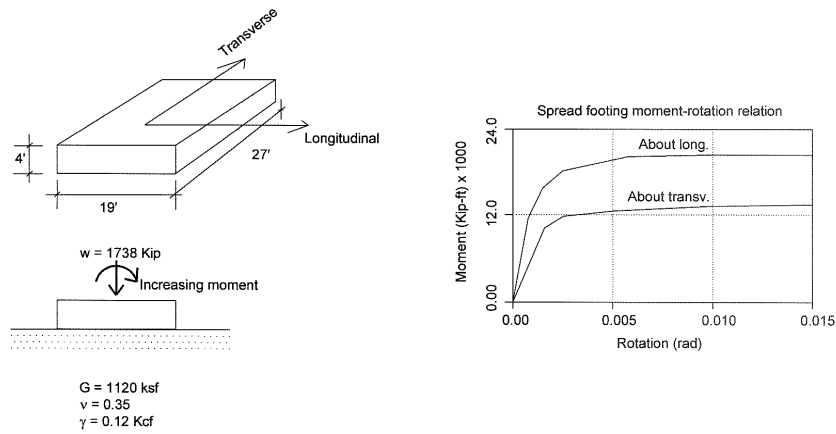


Fig. 5-1: Pushover (rocking) analyses (Lam and Law, 2000)

For the verification against sliding, the contribution of the forces acting at the base of the foundation and, when the foundation is embedded, on the sides and at the front are added; a safety factor ranging between 1.1 and 1.0 is usually required. It must be realized that taking into account the full passive resistance at the front of the footing not only implies that the material against the foundation is correctly compacted, but also that significant displacements take place. If displacements have to be limited to small values it is advisable either to neglect the front resistance or to retain only a fraction of the full resistance; for instance, Eurocode 8 recommends that no more than 30% of the full passive resistance be added to the contribution of the resisting forces. Provided that sliding is not detrimental to the bridge, it is however an efficient source of energy dissipation and, as base isolation systems, protects the superstructure by bounding the forces that enter it. It must be further pointed out that the predicted foundation displacement, when sliding is allowed, is highly dependent on the friction coefficient between the footing surface and the soil, which in turn depends on the surface material, its drainage characteristics and on the construction method; if reliable estimate have to be made, in situ tests are warranted.

Although the aforementioned verifications still represent the state of practice, recent developments in the calculation of the ultimate capacity of a shallow foundation provide the framework for a more direct check. Furthermore, these developments take into account one component of the forces developed by the seismic action that is not considered in the state of practice, i.e. the inertia forces developed through the soil by the passage of the seismic waves. A general formulation for the ultimate capacity of a shallow foundation subjected to a design base vertical force N_{Ed} , shear force V_{Ed} , overturning moment M_{Ed} and inertia force F in the supporting soil is given by Pecker (1997) and has been incorporated in Eurocode 8-Part5. This formulation states that the allowable state of forces (N_{Ed} , V_{Ed} , M_{Ed} , F) lies within a bounding surface defined by:

$$\frac{(1 - e\bar{F})^{c_r} (\beta\bar{V})^{c_r}}{(\bar{N})^a \left[(1 - m\bar{F}^k)^{k'} - \bar{N} \right]^b} + \frac{(1 - f\bar{F})^{c_M} (\gamma\bar{M})^{c_M}}{(\bar{N})^c \left[(1 - m\bar{F}^k)^{k'} - \bar{N} \right]^d} - 1 \leq 0 \quad (5-3)$$

where:

$$\bar{N} = \frac{\gamma_{Rd} N_{Ed}}{N_{max}}, \quad \bar{V} = \frac{\gamma_{Rd} V_{Ed}}{N_{max}}, \quad \bar{M} = \frac{\gamma_{Rd} M_{Ed}}{B N_{max}}$$

N_{max} is the ultimate bearing capacity of the foundation under a vertical centered load;

B is the foundation width;

\bar{F} is the dimensionless soil inertia force, $\bar{F} = \frac{\rho \cdot a_g \cdot B}{\bar{c}}$ for cohesive soil, $\bar{F} = \frac{a_g}{g \tan \phi'_d}$ for cohesionless soils;

a_g is the ground acceleration;

γ_{Rd} is the model partial factor; which takes values in the range 1.0 to 1.5 depending on the soil type.

$a, b, c, d, e, f, m, k, k', c_T, c_M, c'_M, \beta, \gamma$ are numerical parameters depending on the soil type.

If the verifications show that the applied forces lie on, or outside, the bounding surface described by equation 5-3, the induced permanent displacement can be computed using a Newmark type of analysis.

5.2.3 Structural design

As the structural analysis of footings may be difficult, footings are usually designed by treating them as cantilevers supported at the verification sections, simple beams or continuous beams between two columns of rigid frame piers. However, as footings may behave as slab structures and redistribution of the stresses in the footings may be considered, footings can be designed by replacing them by bi-directional beams. The footings should have sufficient thickness to be regarded as rigid bodies.

The section for verification of the bending moments is at the front section of the column as indicated by section AA in Fig. 5-2.

The eccentricity e_N of the resultant force with respect to the center of the footing is defined as:

$$e_N = \left(3 - \frac{12}{4 + \sqrt{6 \left(\frac{M_L}{M_0} \right)^2 - 2}} \right) \frac{M_0}{V} \quad (5-4)$$

where $M_0 = BV/6$ is the moment at the onset of uplift and M_L the moment at the base of the footing.

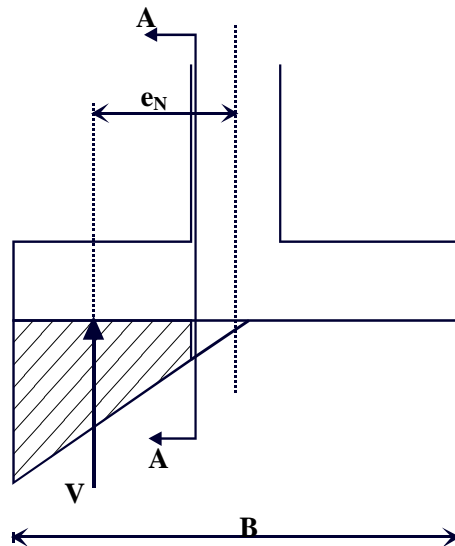


Fig. 5-2: Verification section for bending moments

As the footings are designed as beams, it is necessary to define an effective width of the footing; depending on the motion level considered (1 or 2) the Japanese Road Association defines the effective width as indicated in Table 5-2.

	Seismic level 1	Seismic level 2
Reinforcement at lower section of footing	$b = t_c + 2d \leq B$	$b = B$
Reinforcement at upper section of footing	$b = t_c + d \leq B$	$b = t_c + 1.5d \leq B$

Table 5-2: Effective width of footings (JRA, 2002)

In the above expressions t_c is the pier width, d the effective depth of the footing and B its width.

5.3 Pile foundations

The seismic response of pile foundations to strong earthquake shaking is a very complex process that is controlled by inertial interaction between superstructure and pile foundation, kinematic interaction between foundation soils and piles, and the non-linear stress strain behavior of soils and soil-pile interface. In addition, at some sites high seismically induced pore water pressures or liquefaction add to the complexity. The purpose of this section is not to review all aspects related to pile design but rather to identify some key issues and review how they are dealt with in practice; this state of practice, for the aspects covered below, has been established from a questionnaire distributed among the TG 7.4 members and reflects the most current trends in the following countries: France, Greece, Italy, Japan, New Zealand, Slovenia, Taiwan, USA (California). For a more complete review of pile seismic design, the reader is referred to Finn (2005), Lam and Law (2000), Priestley and Seibel (1997).

5.3.1 Pile types for bridge foundations

Many different materials and shapes have been used for pile designs. Although numerous examples of long span bridges in seismic areas founded on timber piles still exist in California (Priestley and Seibel, 1997), one being the San Francisco Oakland Bay bridge, the current trends involve the use of concrete (reinforced or hollow prestressed) piles, steel (H type, shell and concrete filled shell) piles; a special situation is represented by the integral pile-shaft column arrangement where the piles are not connected to a pile cap but are extended by columns into the superstructure.

In most countries for which information was collected (Table 5-3), reinforced concrete piles largely prevail (>70% and most of the time >90%). Exceptions are represented by Japan with 50% of concrete piles, half of it being prestressed, and USA (California) with only 30% of concrete piles. When steel piles are used they are either concrete filled shell or shell piles with an exception for France where 13% of the steel piles are of the H type. Integral pile shaft columns seem to be used almost exclusively in California and to a much lesser extent in France (respectively 60% and 5% of the total number). Although not explicitly quoted in Table 5-3, prestressed solid piles are sometimes used in California with a square or octagonal cross section, with diameter between 400 and 600 mm.

With regards to the installation techniques almost all the concrete piles are cast in drilled holes, except in Japan and California where 30% of the concrete piles are driven. Steel piles are mainly cast in place (Table 5-3).

			USA - California	France	Greece	Italy	Japan	New Zealand	Slovenia	Taiwan
Pile type	Integral pile shaft columns		60	4						
	Steel piles	H type		4				15		
		Shell		2		5	50 ⁽¹⁾			
		Concrete filled shell	10	20			50 ⁽¹⁾	15		
	Concrete piles	Reinforced	30	70	~100	95	50 ⁽²⁾	70	100	99
		Prestressed shell					50 ⁽²⁾			1
Installation procedure	Concrete piles	Cast in drilled holes	70	69	~100	X	70	60	100	99
		Driven	30	6			30	20		1
	Steel piles	Cast in shell piles		20		X	70			
		Driven		5			30	20		

⁽¹⁾ percentage with respect to steel piles ⁽²⁾ percentage with respect to concrete piles

Table 5-3: Pile type and installation techniques

One controversial topic regarding the pile type relates to the possibility of using raked piles in a seismic environment. From a static point of view, this type of foundation may be advantageous for abutments to sustain the horizontal forces induced by the static earth pressures. However for seismic loading, several codes, like for instance Eurocode8, advise against the use of raked piles. This is based on the observation that these piles frequently suffer substantial head damage during earthquakes. This occurs when the axial stiffness of the pile is much greater than the lateral stiffness (Pender, 1993). In this situation even a small angle of rake gives horizontal and moment stiffness terms of the pile head stiffness matrix considerably larger than those for the vertical pile. The consequence is that when a horizontal displacement load is applied at its head the pile sustains large axial forces; the behavior under this type of loading is obviously less than ductile than when the pile responds mainly in flexure. In addition, during earthquake loading the supporting soil may undergo vertical settlements causing a lack of underneath support to the inclined piles, which still carry the overburden load; these parasitic bending moments must be added to the axial forces. All these issues are design issues that may be accommodated provided the physics of the phenomena are perfectly understood, but this has not always been the case. There is however one situation for which inclined piles seem to have a beneficial effect: when there is potential for liquefaction and lateral spreading at a bridge site the use of inclined piles help reducing the damages to the foundation by limiting the horizontal displacements as shown by the example of the Edgcombe bridge (Berrill *et al*, 2000). Additional means for enhancing the resistance to lateral displacements of the foundation system have been presented in section 3.2.

5.3.2 Modeling techniques

As opposed to spread footings, for which a single method of analysis to determine the forces transmitted by the foundation emerges in practice (based on a substructuring approach and the definition of the foundation stiffness matrix and damping), several modeling techniques are used to model pile foundations in a global bridge model for seismic response studies; the most common methods are the simplified beam on Winkler foundation model and the coupled foundation stiffness matrix (substructuring). These two modeling techniques are illustrated in Fig.5-3 for the complete model and in figure Fig.5-5 for the substructure model (Lam *et al*, 2004).

In the complete model, piles are represented by beam elements supported by linear or non linear, depth-varying, Winkler springs. In the case of earthquake excitation, ground motion would impart different loading at each soil spring and these motions need to be calculated from a separate analysis.

The main drawback of this modeling technique is the large number of degrees of freedom needed to formulate the complete system. The alternative approach employing a substructure system in which the foundation element is modeled by a condensed foundation stiffness matrix and mass matrix along with equivalent forcing function represented by the kinematic motion, may be more attractive; in addition, it more clearly separates the role of the geotechnical engineer and of the structural engineer. The substructuring approach is based on a linear superposition principle and therefore linear soil behavior is more appropriate. In that case, the condensed stiffness matrix may be obtained either from the beam on Winkler springs model or from continuum impedance solutions (Gazetas, 1991). When non linear soil behavior is considered, the condensed stiffness matrix is generally evaluated by a pushover analysis of the pile group and linearization at the anticipated displacement amplitude of the pile head.

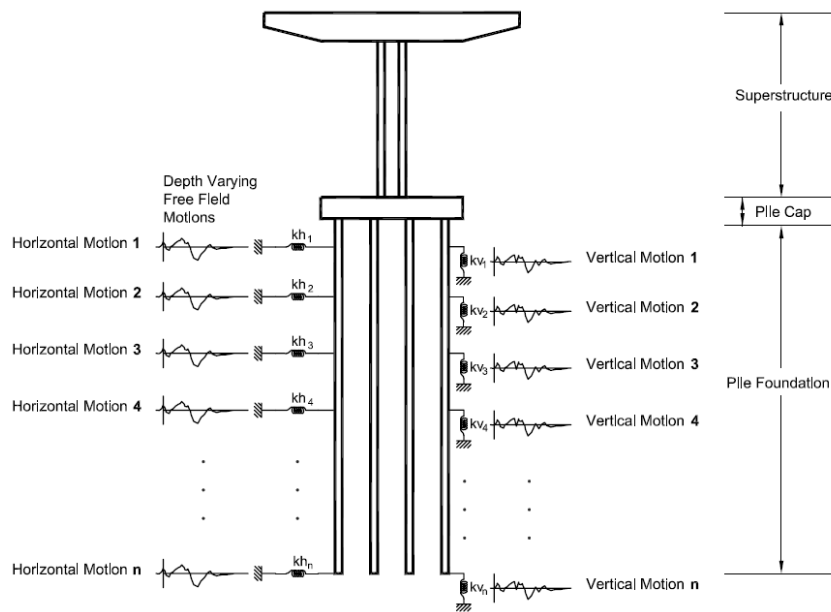


Fig.5-3: Complete pile-structure model

The p-y relation, representing the non linear spring stiffness, is generally developed on the basis of a semi-empirical curve, which reflects the nonlinear resistance of the local soil surrounding the pile at specified depth. A number of p-y models have been proposed by different authors for different soil conditions. The two most commonly used p-y models are those proposed by Matlock (1970) for soft clay and by Reese *et al* (1974) for sand. These models are essentially semi-empirical and have been developed on a basis of a limited number of full-scale lateral load tests on piles of smaller diameters ranging from 0.30 to 0.40 m. To extrapolate the p-y criteria to conditions that are different from the one from which the p-y models were developed requires some judgment and consideration. For instance in Slovenia, values of the spring stiffnesses are derived from the static values, increased by 30%. Based on some field test results, there are indications that stiffness and ultimate lateral load carrying capacity of a large diameter drilled shaft are larger than the values estimated using the conventional p-y criteria as reported by Stevens and Audibert (1979). Pender (1993) suggests that the subgrade modulus used in p-y formulation would increase linearly with pile diameter. Using nonlinear three dimensional finite element analyses, Lam and Law (1996) demonstrated that the increases in stiffness and lateral capacity of large diameter shafts are attributed to additional soil resistance mobilized due to pile rotation.

Studies have shown that Matlock and Reese p-y criteria give reasonable pile design solutions. However, the p-y criteria were originally conceived for design against storm wave loading conditions based on observation of monotonic static and cyclic pile load test data. Therefore, Matlock and Reese's static p-y curves can serve to represent the initial monotonic loading path for typical small diameter driven isolated piles. If a complete total system of a bridge is modeled for seismic response study, individual piles and p-y curves can be included in the analytical model. However, for a large pile group, group effects become important. An example is given in Fig. 5-4 which presents the results of horizontal impedance calculations of the group of piles of half the foundation (22 piles) of one of the pylon of the Vasco da Gama bridge in Lisbon (Pecker, 2003); the group efficiency, computed from elastodynamic theory, is of the order of 1/6 at low frequencies and decreases with frequency due to the constructive interference of diffracted waves from adjacent piles. Typically, for large pile groups it is not uncommon to calculate group efficiency in the range 1/3 to 1/6.

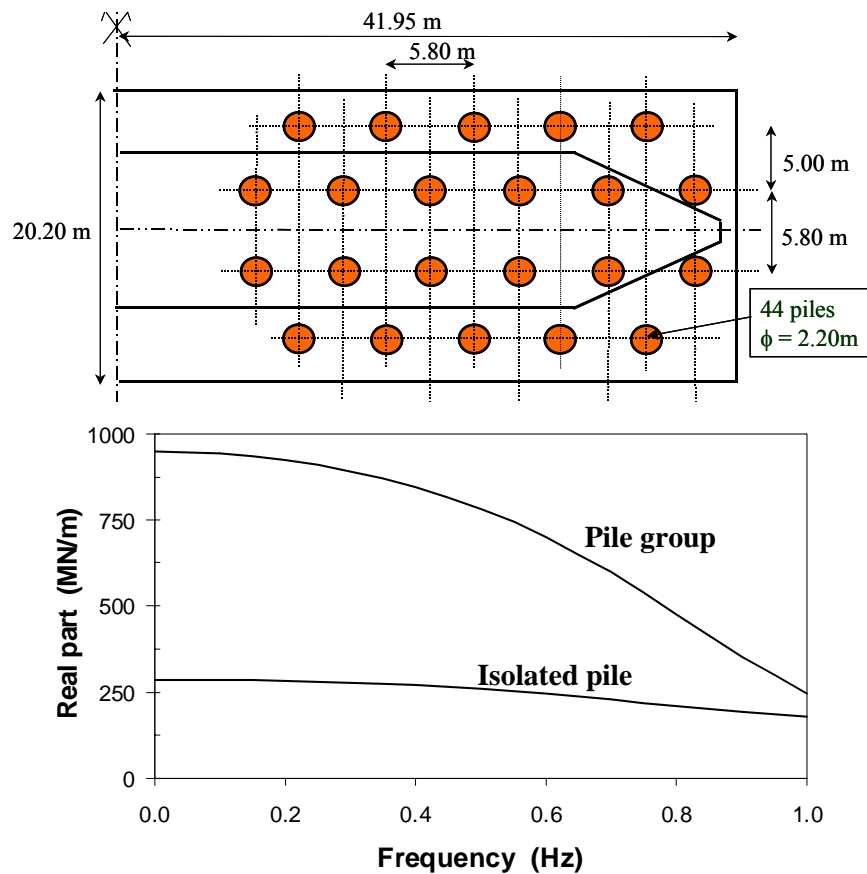


Fig. 5-4 : Horizontal pile group impedance for the Vasco da Gama bridge (Pecker, 2003)

Although the group effects have been a popular research topic within the geotechnical community, currently there is no common consensus on the design approach to incorporate group effects. Full scale and model tests by a number of authors show that in general, the lateral capacity of a piles in a pile group is less than that of a single isolated pile due to so-called group efficiency. The reduction is more pronounced as the pile spacing is reduced. Other important factors that affect the efficiency and lateral stiffness of the pile are the type and strength of soil, number of piles, type and level of loading. In the past, the analysis of group effects were based mostly on elastic halfspace theory due to the absence of costly full-scale pile experiments. In recent years, a number of major studies yielded some high quality experimental data from full-scale or centrifuge model tests (e.g., Ashford *et al*, 1999, Brown, *et al*, 1987, McVay, *et al*, 1995). In addition to group effect, gapping and potential cyclic degradation have been considered in the recent studies. It has been shown that a concept based on p-multiplier applied on the standard static loading p-y curves works reasonably well to account for pile group and cyclic degradation effects (e.g., Bogard and Matlock, 1983; Brown *et al*, 1987; Brown and Bollman, 1996). The p-multiplier is a reduction factor that is applied to the p-term in the p-y curve for a single pile to simulate the behavior of piles in the group. For instance, the values proposed by Brown and Bollman (1996) are given in Table 5-4. Clearly, p-multipliers are dependent on site conditions, soil types, details of stratification and displacement amplitudes (Finn, 2005).

Row spacing	Front row	Second row	Third and more rows
3D	0.80	0.45	0.35
4D	0.90	0.65	0.55
5D	1.00	0.85	0.75

Table 5-4 : *p*-multipliers for pile group design (Brown and Bollman, 1996)

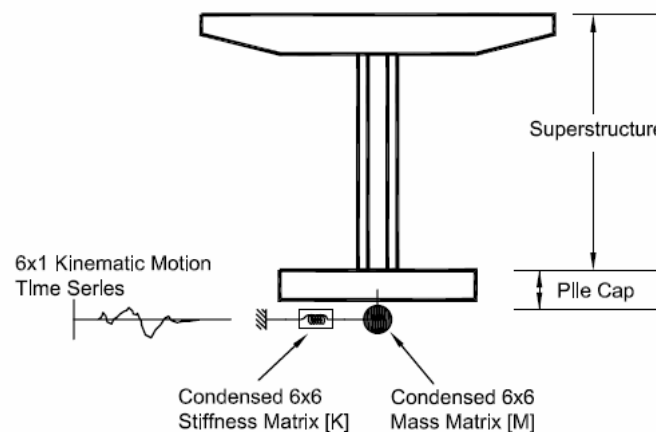


Fig.5-5: Substructure model

Examination of the questionnaire filled by the various countries mentioned above show that in practice only one method of analysis is considered for the analysis of pile foundation: the *p-y* curve method with the exception of France considering both methods (*p-y* curves and continuum analysis) as viable alternatives (Table 5-5). In all countries, but France, group effect is taken into account. Kinematic interaction, which serves to define the effective input motion is only considered in Japan and, for the verification of the pile integrity, in Greece under certain restrictive conditions (high seismicity, bridge of high importance and soft heterogeneous soil profile).

All countries have a specific design code for bridges, based on Eurocode Part 2 in Europe, and on Caltrans specifications in California or AASHTO outside California in the United States, JRA in Japan, AASHTO and own bridge code in Taiwan.

5.3.3 Pile integrity checks

Because of difficulties in investigating pile conditions after an earthquake, it will be normal to design piles to remain essentially elastic under design level seismic response. An exception to this rule applies for the integral pile shaft-column designs, where development of an in-ground plastic hinge is inevitable when the pile and the column have the same diameter and reinforcement; when the pile diameter is larger than the column diameter, as sometimes encountered in New Zealand, the plastic hinge can be placed at the ground level (Fig. 5-6). However, some codes, like Eurocode 8 (part 5), allow for the formation of a plastic hinge in the pile: "Piles should in principle be designed to remain elastic, but may under certain conditions be allowed to develop a plastic hinge at their heads". Nevertheless, in all countries having filled the questionnaire but one, no advantage is taken from this allowance and the piles are designed to remain elastic and the connection pile to pile cap to be fixed.

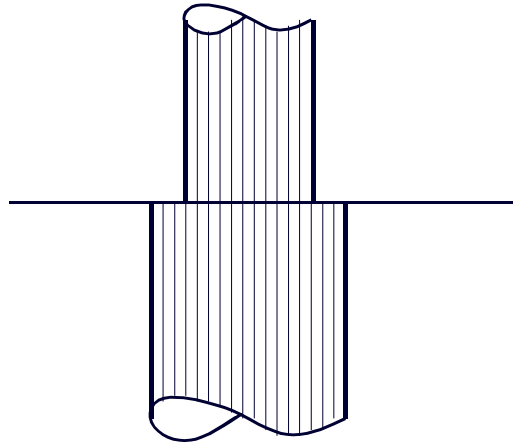


Fig. 5-6 : Example of integral pile shaft column used in New Zealand

			USA - California	France	Greece	Italy	Japan	New Zealand	Slovenia	Taiwan
Connection	Column / base	Pinned or Plastic hinge	50	30						
		Fixed	50	70	X	X	X	X	X	X
	Pile / pile cap	Pinned or Plastic hinge		2						
		Fixed	X	98	X	X	X	X	X	X
Analysis	p-y curves		X	X	X	X	X	X	X	X
	Continuum			Footings						
	Group effect		Yes	No	Yes	Yes	Yes	Yes	Yes	Yes
	Kinematic interaction		Yes	Yes	Yes ⁽¹⁾	No	Yes	No	No	No

⁽¹⁾ under conditions set forth in Eurocode 8 (EN 1998-5).

Table 5-5 : Methods of analysis for pile foundations

Greece is the only exception to the above rule and allows for the formation of a plastic hinge when elastic design is not possible; under that circumstance, confinement of the concrete core at the potential and possible regions of plastic hinges must be effected, as well as capacity shear check of the piles. Potential region for a plastic hinge is considered a region of length $2d$ below the pile cap. In addition, if the pile crosses the interface of successive soil

layers which have much different shear moduli (ratio of shear moduli > 5), then regions of $\pm 2d$ above and below the possible limits of this interface shall be deemed to be regions of possible plastic hinges. In these regions, confinement and bending strength equal to that of the pile top shall be provided. This rule does not apply for the region of the foundation layer for end-bearing piles provided that conditions of full fixity of the piles are not developed there.

For a plastic hinge forming at the pile top with a monolithic pile/cap connection, the plastic hinge length may be taken equal to (Priestley *et al*, 1996)

$$L = 0.08l_c + 0.022f_y d_{bl} \geq 0.044f_y d_{bl} \quad (5-5)$$

where l_c is the distance from the point of contraflexure to the pile cap, f_y is the yield strength of pile longitudinal reinforcement in MPa and d_{bl} is the longitudinal bar diameter.

For in-ground hinge, the hinge length decreases with increasing soil stiffness and with reducing height from ground to the point of contraflexure. The lower limit is approximately given by :

$$L = 1.0D + 0.06H/D \quad (5-6)$$

where H is the above grade height to the point of contraflexure. Recent experiments (Budek *et al*, 1997) have shown that the amount of confinement reinforcement can be reduced in the plastic hinge region because of the beneficial effect of the soil pressure exerted on the compression side of the pile (Fig.5-7); changes in the pile moment profile are caused by soil pressure against the compression side of the pile and results in additional confinement stress being placed on the compression zone of the concrete by the soil, reducing the requirement for confinement reinforcement.

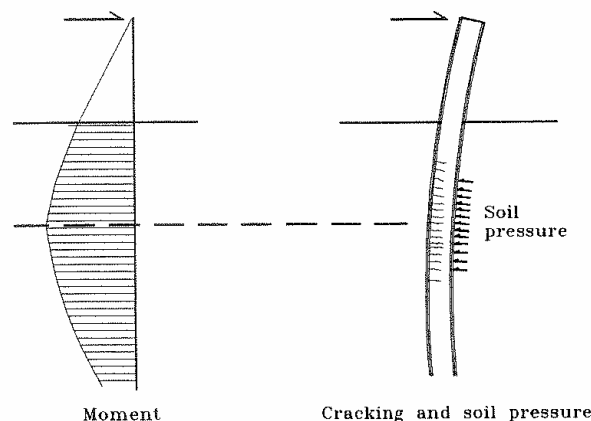


Fig.5-7: Confinement of compression zone by soil pressure for in-ground hinges (after Priestley and Seible, 1997)

To conclude with the integrity checks it is interesting to note that none of the countries that responded to the questionnaire mentions a requirement for a minimum reinforcement ratio for the piles

5.4 Design of foundations in a liquefiable environment

Most of the seismic codes and the current practice recommend that foundations shall not be located on liquefiable deposits; for instance Eurocode 8 –Part 5 states that "if soils are found to be susceptible to liquefaction and the ensuing effects are deemed capable of affecting the load bearing capacity or the stability of the foundations, measures...shall be taken to ensure foundation stability".

When designing a foundation on a potentially liquefiable deposit three situations need to be analyzed :

Stage 1 when limited pore pressures have developed and the soil retains its original stiffness and strength; at this stage the forces applied to the foundation are most likely smaller than the maximum forces that would develop during the earthquake if liquefaction would not occur; the response of the bridge-foundation system is purely dynamic.

Stage 2 when considerable excess pore pressures Δu have developed (typically $\Delta u > 0.50\sigma'_v$ where σ'_v represents the vertical effective overburden) but no widespread liquefaction has yet occurred. At this stage the soil stiffness is drastically reduced but the soil still preserves a non-zero shear stiffness so that the seismic waves can propagate through the soil and affect the foundation; the response of the bridge-foundation system is still predominantly dynamic but significant non linearities take place that reduce the input motion, and therefore the dynamic forces.

Stage 3, which takes place towards the end or after the earthquake loading has ended. Full liquefaction has developed and lateral spreading of the liquefied soil may take place under certain conditions, such as an inclination of the soil layers or ground surface, resulting in a quasi-static, gravity induced loading to the foundation. The response is essentially static.

5.4.1 Shallow foundations

For shallow (footing or mat) foundations the upward flow of water towards the ground surface induces a significant, if not a total, loss of soil resistance; because the bearing layers are at the ground surface, the strength reduction that occurs in stage 2 or 3 causes loss of bearing capacity accompanied by not only vertical settlement but also, in some instances, significant tilt.

The foundation movements that accompany full development of pore pressures are unpredictable and therefore countermeasures need to be implemented; there is no other alternative than improving the ground conditions.

5.4.2 Pile foundation

For pile foundation the situation is somewhat different; the resisting elements can be embedded below the potentially liquefiable strata. Therefore it is conceivable to design pile foundations to accommodate soil liquefaction. This has been done in practice at least to accommodate stage 1 and stage 2. However, until recently (Kobe earthquake, 1995) it has not been foreseen to design pile foundations to accommodate lateral spreading (stage 3), and significant soil improvement needed to be implemented to protect the foundations of bridge piers.

One example of a foundation designed to accommodate stages 1 and 2 is provided by the Nestos bridge in Northeastern Greece (Klimis *et al*, 2004); the bridge is part of the Egnatia Highway and is 1km long with two independent branches, 952m long each with 20 spans (the central span is 120m long). It is located in a seismic area where the design motion has a peak ground acceleration of 0.26g at the rock outcrop. The foundation soils consist of river deposits composed of silty and clayey silty sands, gravels, and of alluvial deposits essentially of sandy nature. Those layers are relatively loose and considerably uneven.

Evaluation of liquefaction susceptibility was carried out according to the state of the art developed in the NCEER 1997 report, based on CPTs (static cone penetration tests) and SPTs. It was concluded that an extensive zone prone to liquefaction exists between 7m and 25m depth below the ground surface (Fig.5-8); lateral spreading towards the river bed was also predicted to be possible due to a slight increase of the ground surface inclination caused by future erosion of the riverbed deposits.

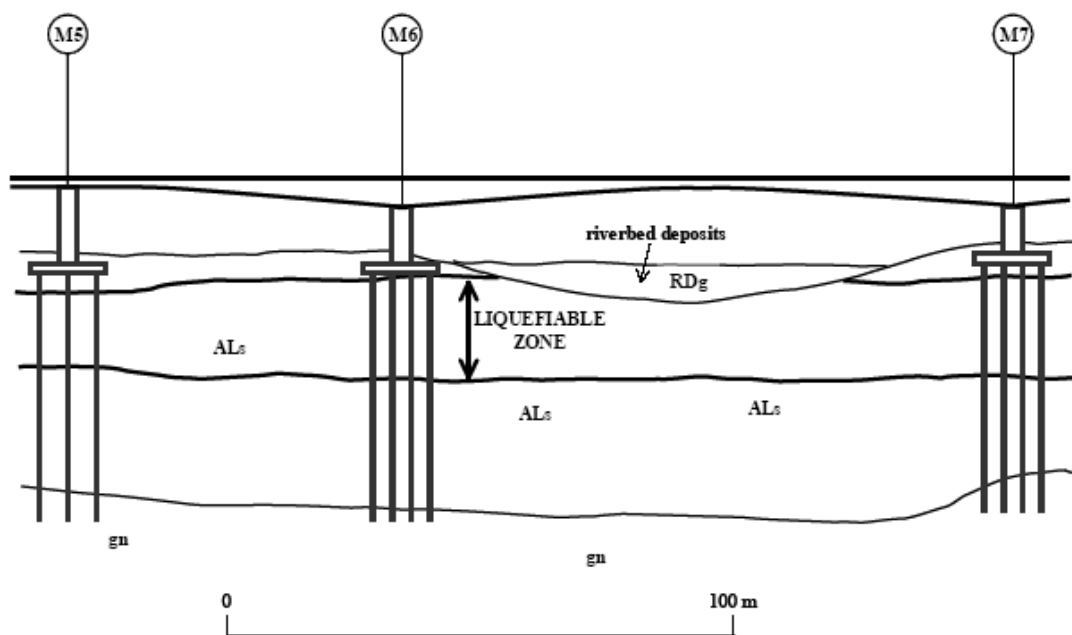


Fig.5-8: Section of the bridge; central span over the river

The piles were designed to accommodate stage 2 above through a numerical dynamic response of the soil-pile system: the model of a beam on Winkler foundation was used but with softer springs than usual to account for the strong soil nonlinearities. The vertical stiffness distribution of the springs is portrayed in Fig.5-9. Dynamic analysis was carried out under the assumption that inertia loading to the pile is negligible because of the strongly reduced accelerations levels; thus a kinematic interaction analysis alone is adequate to predict the total system response under stage 2. The bending moment and shear force distributions along the pile are plotted in Fig.5-10; the results of stage 1 analysis, which does not account for any pore pressure build-up, are also plotted in this figure. It is clear that the slightly liquefied soil has a strong detrimental effect on the response: moments are doubled at the pile cap connection and shear forces are more than doubled in depth.

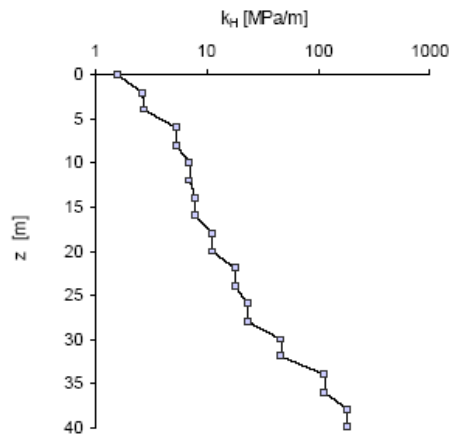


Fig.5-9: Vertical stiffness distribution of Winkler soil springs

With regards to stage 3 analysis, the performance criterion assigned to the foundation was to minimize lateral spreading; consequently, design of piles to accommodate the ground displacement was not considered and ground improvement was implemented for the two piers close to the river bed in order to prevent any additional loading to the piles after lateral spreading onset. Ground improvement consists in the construction of 0.8m diameter jet-grouted columns suitably arranged between the piles, as sketched in Fig.5-11.

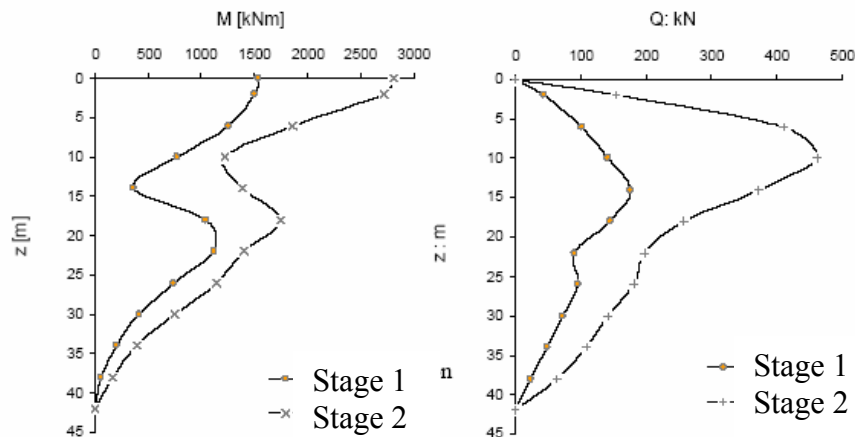


Fig.5-10: Kinematic interaction forces due to soil softening

Soil improvement of the kind depicted in Fig.5-11 may be expensive especially when a wide area is affected by lateral spreading. For instance, the north approach viaduct of the Rion-Antirion bridge (Greece) is located in a zone where extensive lateral spreading was predicted for the design earthquake; a cost benefit analysis showed that designing the piles to resist the forces induced by the soil displacement was more economical than improving the ground conditions.

It is only recently that this kind of analysis has been made possible; extensive back analyses of damages caused to pile foundations during the Kobe earthquake resulted in rational design methodologies (Finn, 2005, Tamura, 2005). The situation to be analyzed is depicted in Fig. 5-12.

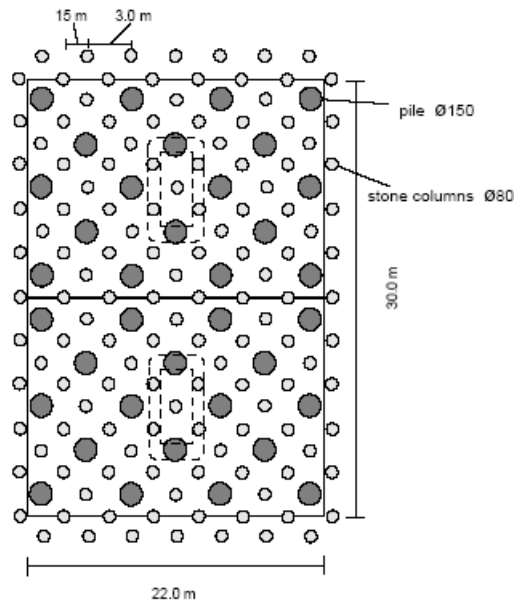


Fig.5-11: Ground improvement with jet grouted columns

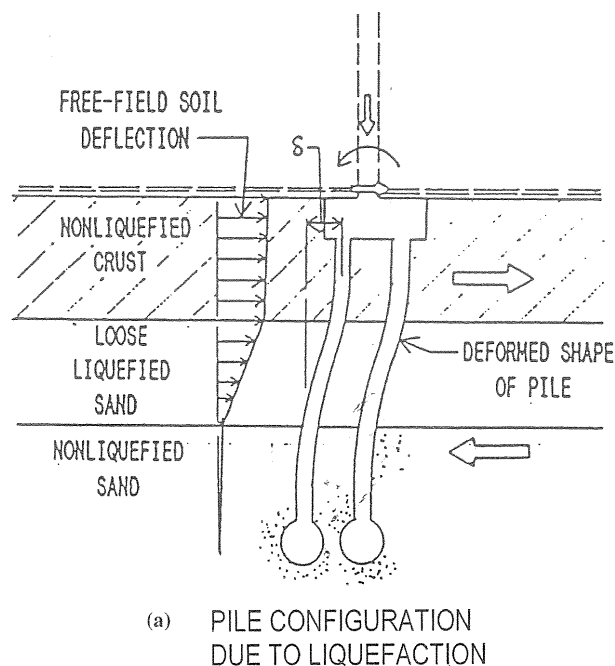


Fig. 5-12: Pile configuration due to liquefaction (Finn, 2005)

After liquefaction, if the residual strength of the soil is smaller than the static shear stress caused by a sloping site or a free surface such as a river bank, significant down slope movement may occur; the moving soil then exerts damaging pressures against the piles, especially if a non liquefied layer rides on top of the liquefied layer. Basically there are two different approaches to evaluate the forces: a force based approach and a displacement based approach.

5.4.2.1 Force based approach

A force based analysis is recommended in the Japanese design code for analysis of pile foundations in liquefied soils (JRA, 2002): the non liquefied surface layer is assumed to apply a passive pressure, q_{NL} , on the foundation; the liquefied layer is assumed to apply a pressure, q_L , less than the equivalent hydrostatic pressure. Fig.5-13 illustrates the forces acting on the foundation.

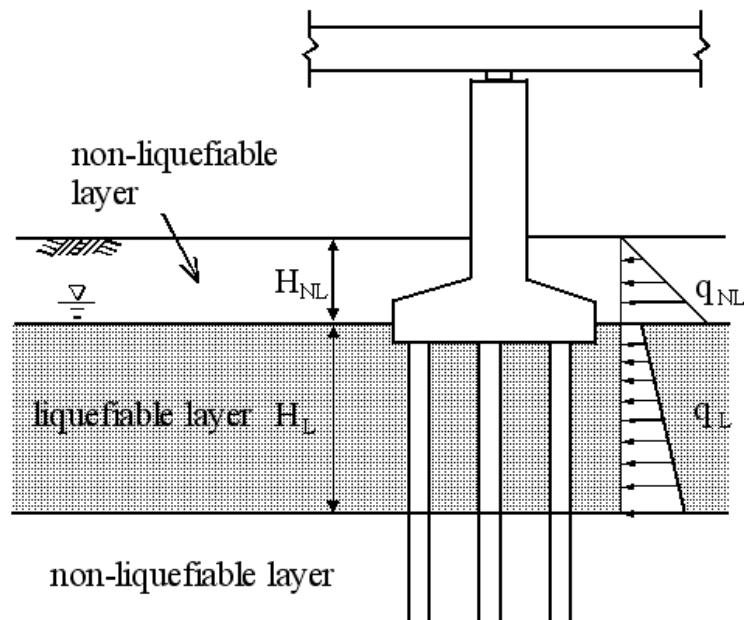


Fig.5-13: Idealization of ground flow for seismic design of bridge foundations (JRA, 2002)

It has been found that the pressure exerted by the liquefied layer may be taken equal to 30% of the overburden pressure. These findings have been confirmed by centrifuge tests (Dobry and Abdoun, 2001) which, in addition, pointed out that the moments in the pile are dominated by the lateral pressure from the non liquefied layer.

The foundation of the north approach viaduct of the Rion Antirion bridge (Greece) have been designed following these concepts. The soil profile is shown in Fig.5-14; the liquefiable deposits are the strata labeled (1), except for the top 4 meters which are non liquefiable being located above the water table. The plane view of the foundation is portrayed in Fig. 5-15 and is located at boring T5. To withstand the forces applied by the ground flow the steel tube piles were driven down to elevation -45 MSL. Furthermore, to minimize the bending moments in the piles arising from the pressures exerted by the top 4m of non liquefied soils, the pile cap has been placed above the ground surface without contact with the in place soils (Fig.5-16).

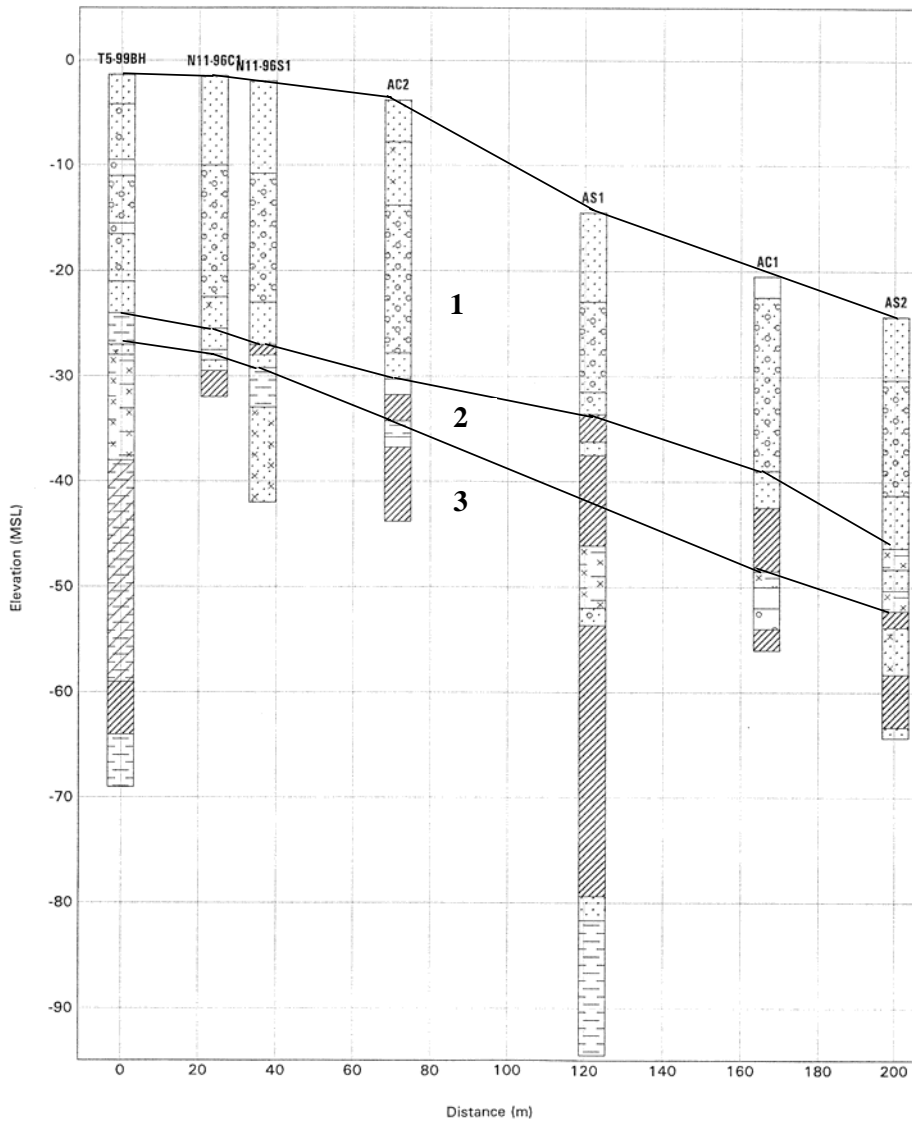


Fig.5-14: Soil profile

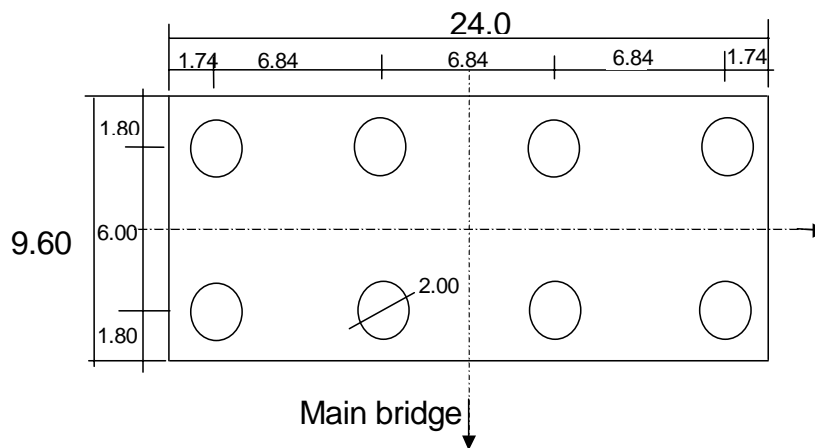


Fig. 5-15: Plane view of the foundation



Fig.5-16: View of the Antirion access viaduct during construction (see pile cap above ground surface)
(Figure available electronically on fib website; see production note on p. ii)

5.4.2.2 Displacement based approach

Following this approach, forces are not applied to the piles but rather free field displacements are imposed at the free ends of the springs in the Winkler model shown in Fig. 5-17. The method requires the knowledge of the free field displacements, which can be estimated using predictor equations: in the US the equations developed by Youd *et al* (1999) are used while in Japan the equation by Hamada *et al* (1986), further updated by the Japan Water Works Association (JWWA, 1997), is preferred.

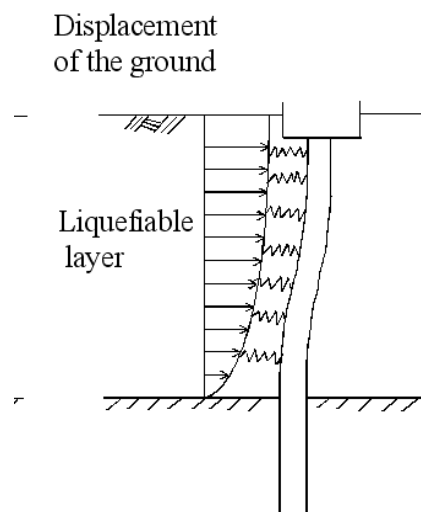


Fig. 5-17: Winkler spring model for lateral spreading analysis

In Japanese practice, reduction in the springs stiffness for use in liquefiable soils depend on the factor of safety against liquefaction F_L . The recommended reduction factors are given in Table 5-6 as a function of the product of the resistance to liquefaction R_L and of the parameter c_w , which depends on the motion type ($c_w=1$ for type 1 motion; for type 2 motion $c_w=1.0$ for $R_L \leq 0.1$, $c_w=3.3R_L + 0.67$ for $0.1 < R_L \leq 0.4$, $c_w=2.0$ for $0.4 < R_L$).

Safety factor F_L	Depth from ground surface $x(m)$	Dynamic shear strength ratio $R=c_w R_L$	
		$R \leq 0.3$	$R > 0.3$
$F_L \leq 1/3$	$0 \leq x \leq 10$	0	1/3
	$10 < x \leq 20$	1/3	1/3
$1/3 < F_L \leq 2/3$	$0 \leq x \leq 10$	1/3	2/3
	$10 < x \leq 20$	2/3	2/3
$2/3 < F_L \leq 1$	$0 \leq x \leq 10$	1/3	1
	$10 < x \leq 20$	1	1

Table 5-6: Reduction coefficients for soil constants due to liquefaction (JRA, 2002)

There is no commonly accepted practice in North America on the appropriate modeling of degraded spring stiffness; the basis of most analysis is a degraded form of the API p - y curves (API, 1993). The practice is to multiply the p - y curves by a uniform degradation coefficient β which ranges in values from 0.3 to 0.1 (Finn, 2005).

There is a great uncertainty in the definition of the free field displacements used as input data to the analysis. The predictor equations are strongly empirical and based on few observations. Consequently, the force based approach is often preferred and recommended (JRA, 2000).

Acknowledgments

In addition to the contribution of the TG7.4 members, the contribution and help of the following individuals, who provided information about the current practice in their own countries, is gratefully acknowledged: Pr G. Martin and Pr L. Restrepo (USA), Dr E. Bouchon, Dr. D. Davi and Dr. D. Criado (France), Pr G. Gazetas (Greece), Dr. R. Franchin and Dr. C. Lai (Italy), Dr. K. Goto (Japan), Dr. I. Billings (New Zealand), Dr. J. Zevnik (Slovenia), Dr. T.Y. Lee (Taiwan).

References

- AASHTO (2002), "Standard Specifications for Highway Bridges", 17th edition. American Association of State Highway and Transportation Officials, AASHTO HB-17.
- API (1993), "Recommended Practice for Planning, Designing and Constructing Fixed Offshore Platforms", American Petroleum Institute
- Ashford S., and Rollins K. (1999), "Full-Scale Behavior of Laterally Loaded Deep Foundations in Liquefied Sand," Preliminary Test Results, Department of Structural Engineering, University of California, San Diego.
- Berrill J.B., Christensen S.A., Keenan R.P., Okada W., Pettinga J.R. (2000), "Case study of lateral spreading forces on a piled foundation", *Geotechnique*, vol. 51 (6), pp 501-517.
- Bogard D. and Matlock M. (1983), "Procedure for the Analysis of Laterally Loaded Pile Groups in Soft Clay," *Proceeding of Specialty Conference on Geotechnical Engineering in Offshore Practice*, ASCE, April, pp 499-535.
- Brown D.A., Reese L., and O'Niell M. (1987), "Cyclic Lateral Loading of A Large-Scale Pile," *Journal of Geotechnical Engineering*, Vol. 113, No. 11, November.

- Brown D.A., Bollman H.T. (1996), "Lateral Load Behavior of Pile Group in Sand," *Journal of Geotechnical Engineering*, ASCE, Vol. 114, No. 11, pp1261-1276.
- Budek A.M., Benzoni G., Priestley M.J.N., "Experimental Investigation of Ductility of In-Ground Hinges in Solid and Hollow Precast Prestressed Piles", Division of Structural Engineering Report SSRP-97/xx, University of California, San Diego, 1997.
- Dobry R., Abdoun T. (2001), "Recent studies of centrifuge modeling of liquefaction and its effect on deep foundations". (S. Prakash ed.), 4th International Conference on Recent Advances in Geotechnical Earthquake Engineering and Soil Dynamics, San Diego CA, 26-31.
- Eurocode 8 (2004), "Design of structures for earthquake resistance-Part 5: Foundations, retaining structures and geotechnical aspects" prEN 1998-5.
- Finn, W.D.L., (2005), "A Study of Piles during Earthquakes: Issues of Design and Analysis". The Tenth Mallet Milne lecture, *Bulletin of Earthquake Engineering*, Vol. 3, n°2, 141-234.
- Gazetas G. (1991), Foundation Vibrations, in *Foundation Engineering Handbook*, 2nd edition, Hsai Yang Fang Eds, Van Nostrand Rheinhold.
- Hamada M., Yasuda S., Isoyama R., Emoto K., (1986), "Study on Liquefaction Induced Permanent Ground Displacement". Association for Development of Earthquake.
- JRA (2002), "Design Specifications for Highway Bridges. Part V Seismic Design". Japanese Road Association
- JWWA (1997), "Seismic Design and Construction Guidelines for Water Supply Facilities". Japan Water Works Association.
- Klimis N., Anastasiadis A., Gazetas G., Apostolou M., (2004), "Liquefaction Risk Assessment and Design of Pile Foundations for Highway Bridge", 13th World Conference on Earthquake Engineering, Vancouver B.C., Canada, paper 2973.
- Lam P.I, Law H (1996), "Soil-Foundation-Structure Interaction-Analytical Considerations by Empirical p-y Method", Proc. 4th Caltrans Seismic Research Workshop, Sacramento, July 9-11.
- Lam P.I, Law H. (2000), "Soil Structure Interaction of Bridges for Seismic Analysis". Technical Report MCEER-00-008.
- Lam P.I, Law H., Yang C.T. (2004), "Modeling of Seismic Wave Scattering on Pile Group and Caisson", Technical report MCEER (in preparation, personal communication from G. Martin).
- Matlock H. (1970), "Correlation for Design of Laterally Loaded Piles in Soft Clay," 2nd Annual Offshore Technology Conference, Paper No 1204, May.
- McVay M., Casper R., and Shang T. (1995), "Lateral Response of Three-Row Groups in Loose to Dense Sands at 3D and 5D Spacing," *Journal of Geotechnical Engineering*, Vol. 121, No. 5, May.
- NCEER (1997), Proceedings of the NCEER Workshop on Evaluation of Liquefaction Resistance of Soils, (T.L. Youd and I.M. Idriss, eds.), Technical report NCEER 97-0022, National Center for Earthquake Engineering Research, State University of New York at Buffalo.
- Pecker A., (1997), "Analytical formulae for the seismic bearing capacity of shallow strip foundations" in *Seismic Behavior of Ground and Geotechnical Structures*, Eds Seco e Pinto, Balkema.
- Pecker A., (2003), "Aseismic foundation design process - lessons learned from two major projects : the Vasco da Gama and the Rion-Antirion bridges", Proceedings 5th ACI International Conference on Seismic Bridge Design and Retrofit for Earthquake Resistance, La Jolla, California.
- Pender M. J. (1993), "Aseismic Pile Foundation Design and Analysis", *Bulletin of the New Zealand National Society for Earthquake Engineering*, Vol 26, No. 1, 49-160.

- Priestley M.J.N., Seible F., Calvi G.M., "Seismic Design and Retrofit of Bridges", Wiley & Sons Inc., 1996.
- Priestley N.J., Seibel F. (1997), "Bridge Pile Foundations Under Seismic Loads- Capacity Design and Issues", Squad Consulting Engineers, Report #97/10.
- Public Works Research Institute- Foundation Engineering Research Team. (2003), "Design of Highway Bridge Foundations in Japan", PWRI N°01-2003.
- Reese L., Cox W., Koop R. (1974), "Analysis of Laterally Load Piles in Sand," 6th Annual Offshore Technology Conference, Paper No. 2080, May.
- Stevens J. B., Audibert J. M. E., "Re-Examination of P-y Curve Formulations", 11th Annual Offshore Technology Conference, Houston.
- Tamura K., (2005), "Seismic Design of Highway Bridge Foundations for Liquefaction-Induced Ground Flow", personal communication.
- Youd T.L., Hansen C.M., Bartlett S.F., (1999), "Revised MLR equations for predicting lateral spread displacement". In Proceedings of the 7th US-Japan workshop on Earthquake Resistant Design of Lifelines Facilities and Countermeasures against Liquefaction, Technical Report MCEER-99-0019, University of Buffalo, N.Y.

6 Design for enhanced control of damage

6.1 Basic concepts for enhanced damage control

A very attractive way to improve the seismic performance of bridges, in order to protect them against undesired failure modes (typically a shear failure of the piers), is given by the possibility of an artificial increase of both the period of vibration and the energy dissipation capacity of the system. This can be obtained by making use of specific artificial elements designed to isolate part of the bridge (typically the piers) from the full intensity of the seismic motion (reduction of the seismic energy transfer into the system) and/or to dissipate a large amount of energy (dissipation of the input energy, thus reducing the plastic deformations of the piers and also concentrating damage in these elements, that can be easily substituted). The first type of elements (Isolation devices) has the main objective to increase the period of vibration of the bridge towards a lower amplification range of the acceleration response spectrum for the design ground motion, thus reducing the input energy (i.e., force demand) into the structure. The second type of elements (Dissipation devices) provides mainly the supplemental damping thus reducing the displacement demand on structural or non-structural elements. The combination of these kinds of devices will define an isolation system.

In bridges, where the objective is usually to protect relatively low-mass piers and their foundations, isolators and dissipators are normally placed between the top of the piers and the superstructure. The viscous damping and hysteretic properties of isolators are generally selected to maintain all the deck's components within the elastic range, or to require only limited ductile actions. The bulk of the overall displacement of the deck, which moves largely as a rigid body mounted on the isolation system, can be concentrated in the isolator's components, with relatively little deformation within the structural elements.

6.2 Seismic structural control strategies

Structural control may be utilized either to reduce the amount of energy transfer into the structure from the ground motion or to absorb some of the earthquake energy after it has been transmitted to the structure. Structural control systems can be classified as either passive, active, semi-active or hybrid.

The firsts, referred as passive since the control system properties cannot be modified after installation, require no external power or computer process for operation. Active control systems utilize actuators to apply control forces to the structure, which are determined by incorporating the actuators within a feedback control system that utilizes the measured response of the structure or the measured ground motion feedback. Semi-active systems may be regarded as passive control systems, which have been modified to allow for the adjustment of mechanical properties. Finally, hybrid systems consist of combinations of the aforementioned control systems. Fig. 6-1 shows the classification of structural control techniques, separating between those which are frequency-dependent (i.e., the control uses the natural frequency of the system) or frequency-independent (i.e., utilizing damping augmentation).

Since passive control strategies represent the most common design choice, passive devices will be extensively described in the following. Finally, the major advantages/ disadvantages related to the alternative control systems will be discussed.

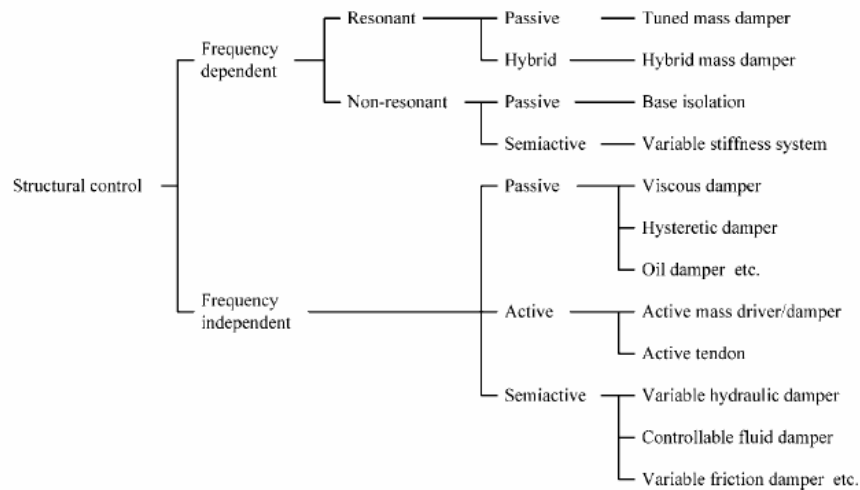


Fig. 6- 1: Structural control systems (from Kurata et al. (2002)).

6.3 Bearings, isolators and energy dissipation units

In most cases the choice of isolation as the design (or retrofit) strategy is adopted in order to increase the period of vibration of the bridge and thus reduce the amount of the seismic input energy into the system. In bridges, which usually have a simple structural configuration, made by a continuous deck supported on the top of the piers by simple bearings only with the function of supporting gravity loads, this can be easily obtained by designing such bearings as isolation devices. Moreover, where the enhancement of the energy dissipation has also to be provided, devices with their own dissipation properties (Isolation/Dissipation devices (I/D)) could replace the simple bearings or could be used in conjunction with them.

6.3.1 General features

The functions of an isolation/dissipation system are generally one or a combination of the following: (i) supporting gravity loads and providing for (ii) lateral flexibility (period shift), (iii) restoring force and (iv) energy dissipation (either of hysteretic, in the case of displacement activated dampers, or viscous nature, in the case of velocity activated dampers); According to their performance, the anti-seismic devices can be grouped in: rigid connection devices (e.g. shear links, lock-up devices), linear devices, non linear devices, viscous dampers, isolators (e.g. sliders, rubber bearings). Common types of anti-seismic devices are:

- Elastomeric bearings: Natural Laminated, Lead and High Damping Rubber Bearings (HDRB);
- Sliding devices;
- Friction Dampers;
- Metallic Dampers (sometimes combined with bearings to form sliders): yielding steel systems, lead extrusion devices;
- Viscous and Viscoelastic Damper;
- Self-centring Dampers: Shape Memory Alloys, Energy Dissipation Restraints, Friction Spring Seismic Dampers;
- Lock-up Devices (sometimes combined with Hysteretic Dampers);

6.3.1.1 Force-Displacement Relationships

In general, the design properties of isolators/dissipators depend on their behaviour, which may be one or a combination of the three different typologies described in the following paragraphs.

6.3.1.1.1 Viscous Behaviour

Viscous behaviour is characterized by a resisting force that depends on the relative velocity of motion of the unit. The force of viscous devices is proportional to v^α , where v is the velocity of motion. This force is zero at the maximum displacement and therefore does not contribute to the effective stiffness of the isolation system. The force-displacement relationship of a viscous device is shown in Fig. 6-2 (right) (for sinusoidal motion), and depends on the value of the exponent α .

6.3.1.1.2 Hysteretic Behaviour

Hysteretic-type response characterizes units that are governed by an inelastic behaviour. The force-displacement relation of the isolator may be approximated by a bilinear curve (Fig. 6-2, left). The parameters of the bi-linear approximation are: the yield force at monotonic loading F_y , the force at zero displacement at cyclic loading F_0 , the elastic stiffness at monotonic loading K_e (equal to the unloading stiffness at cyclic loading), the post elastic (tangent) stiffness K_p and the energy dissipated per cycle E_D at the design displacement d_d , (equal to the area enclosed by the actual hysteresis loop).

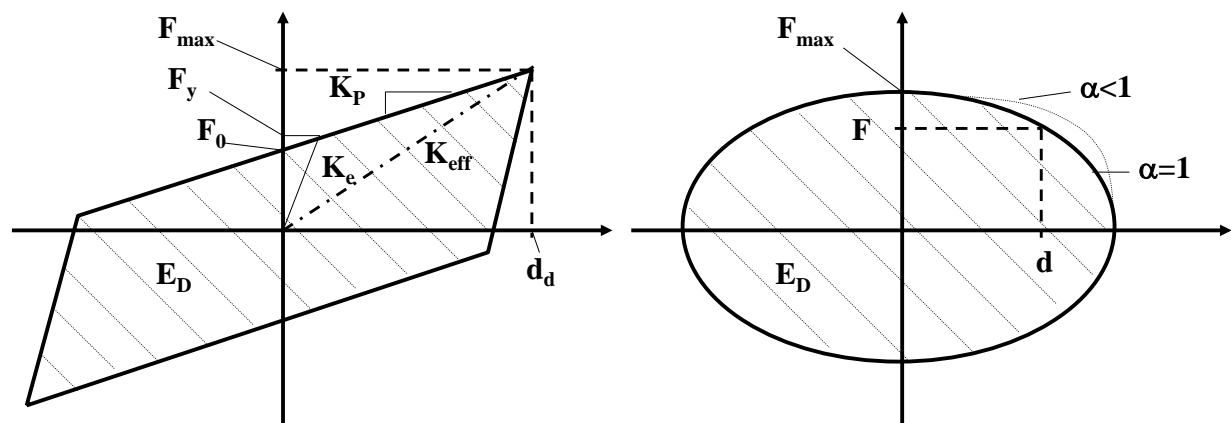


Fig. 6- 2: General Hysteretic behaviour (left), and Viscous behaviour (right).

6.3.1.1.3 Friction Behaviour

Friction- type response is a particular kind of hysteretic behaviour where the yield level depends upon the coefficient of friction (μ_d) at the sliding interface and magnitude of the normal force (N_{sd}) acting on that surface. Depending upon the stiffness after sliding has occurred we should distinguish between two different typologies:

Type 1) Sliding devices, with flat sliding surface, limit the force transmitted to the superstructure to:

$$F_{\max} = \mu_d N_{sd} \text{sign}(\dot{d}) \quad (6-1)$$

where N_{sd} is the normal force through the device (Fig. 6-3, left). Due to the possible substantial permanent offset displacements, they should be used in combination with devices providing an adequate restoring force.

Type 2) Sliding devices, with spherical sliding surface of radius R_b (e.g. Friction Pendulum Bearings), provide a restoring force proportional to the design displacement d_d (eq. (6-2) and Fig. 6-3, right), and a force displacement relationship given in eq. (6-3). Eq. (6-3) refers to a small displacement approximation.

$$F_{\text{restoring}} = \frac{N_{sd}}{R_b} d_d \quad (6-2)$$

$$F_{\max} = \frac{N_{sd}}{R_b} d_d + \mu_d N_{sd} \text{sign}(\dot{d}) \quad (6-3)$$

In either of the two cases, the energy dissipated per cycle E_D at the design displacement d_d is:

$$E_D = 4\mu_d N_{sd} d_d \quad (6-4)$$

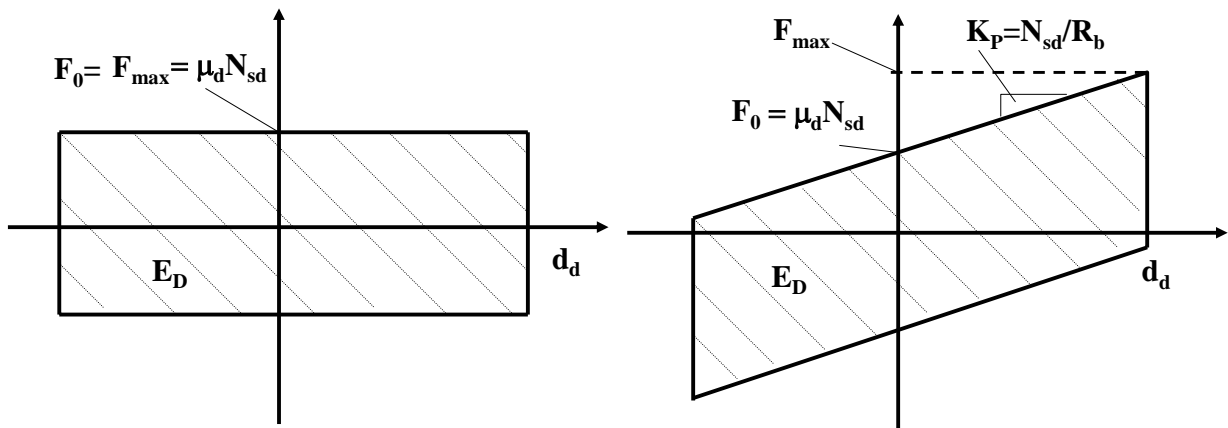


Fig. 6- 3: Sliding Friction Hysteretic behaviour for Flat (left) and Curved (right) Surfaces.

It may also be noticed that the correct evaluation and prediction of the friction coefficient μ_d , and thus the level of the yielding force of the device during the seismic response, is characterized by a relatively high level of uncertainty. In fact, its value depends on several factors such as temperature (see in section 6.3.1.2), normal pressure on the sliding surface and sliding velocity.

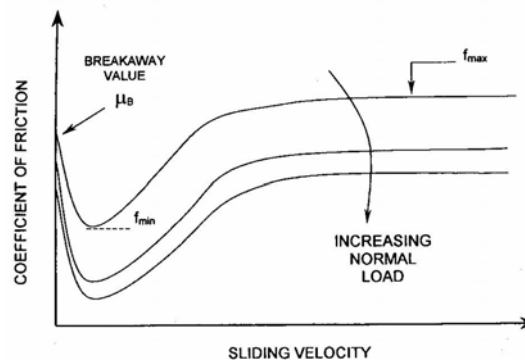


Fig. 6- 4: Friction coefficient of PTFE-polished stainless steel interface at varying velocity and normal load.

In the typical range of earthquake velocity response values the dynamic coefficient of friction can be evaluated using the following expression (Costantinou et al., 1990):

$$\frac{\mu}{f_{\max}} = 1 - \left(1 - \frac{f_{\min}}{f_{\max}} \right) \exp^{-av} \quad (6-5)$$

where the actual value of the coefficient of friction μ correspondent to a sliding velocity v is defined as a function of the maximum and minimum values that it might assumes throughout the hole range of velocity at the given level of normal pressure on the surface (a is a constant). The physical meaning of these parameters is graphically represented in Fig. 6-4.

6.3.1.2 Isolation/Dissipation Systems Issues

A number of issues are related to the employment of isolator and dissipator devices in the design of a bridge.

- In the design of an isolated bridge, not only the required performances in terms of period elongation and energy dissipation have to be taken into account. The yielding force and displacement of the isolation system have to be properly defined according to the design response spectrum, and its elastic stiffness has to be selected in order to control the deformability of the system under frequent quasi-static loads. Moreover, the ultimate displacement and post-ultimate behaviour of the isolators have to be evaluated in order to predict the seismic response of the bridge even after their failure (in case of an event higher than expected) and thus, if required, protect the piers with proper design details.
- Local soil conditions are crucial in the correct prediction of the response of the isolated bridge. At large periods of vibration, as in the case of an isolated system, the shape of the design spectrum widely affects the velocity as well as the displacement demand for which the isolation system has to be designed.
- Isolation devices should also provide the required stiffness under vertical loads for the whole range of their deformation capability. As will be treated in detail in section 6.3.2 the vertical response constitutes one of the governing factors in elastomeric bearings.
- I/D devices also show some inherent problems: their properties, in fact, vary due to the effects of wear, aging, temperature, history and nature of loading, etc.
- The representations of the global force-displacement relationships of the devices, illustrated in section 6.3.1.1, are in general a first approximation of the actual behaviour: the differences in advanced and simplified models may lead to differences in the structural response whose importance has to be evaluated. Once refined models for different isolation

systems are developed, it should be studied how they influence the structural response, in order to find out protection factors for different isolation systems, when a simplified model of the devices is employed. In other words, if the seismic demand on the piers, or generally on the structure, increases when refined models are used, simpler modeling might be allowed, provided that adequate protection factors are accounted for. The concept of Property Modification Factors has been introduced by Constantinou et al. (1999) in order to characterize the variability of the nominal properties of an isolator and understanding the consequences on both the device and the structural response. EC8 provisions require that, in addition to the set of nominal Design Properties derived from the prototype tests, two sets of design properties of the isolation system shall be properly established (Upper and Lower bound design properties). AASHTO provisions indicate similar requirements.

- The problem of re-centring the bearing in its original position after an event that causes any kind of offset is relevant in designing the Isolation/Dissipation system. Only pure springs with zero-damping are perfectly re-centring, while energy dissipation generates residual displacements; particularly, anti-seismic devices based on friction may offset due to thermal effects or small earthquakes as long as the friction force is equilibrated by the re-centring force. On the contrary, the response of hysteretic dampers, up to yielding, is similar to that of perfect springs.
- The heat generation due to the relative movement in the device might be a problem for the correct functioning or the life of the isolator/dissipator itself. Heating might affect the design parameters of the isolator as, for example, the coefficient of friction in PTFE-stainless steel interfaces of sliding devices, by decreasing its value. Marioni (2002) analyzed numerical examples of different devices, having the same characteristics in terms of period of the isolated structure, design displacement and number of cycles during the earthquake. Table 6-1 shows a comparison between devices performances in terms of temperature increase per cycle: it can be easily seen that heat generation might be critical for some kind of energy dissipating anti-seismic devices, for which full scale dynamic tests should be recommended.
- As the whole thrust of seismic isolation is to shift the probable damage level and thereby the damage costs, economic factors need to be considered by an engineer wishing to decide whether a structure should incorporate seismic isolation: maintenance costs should be low for passive systems, whilst the construction costs including seismic isolation usually vary by 5-10% from non isolated options.

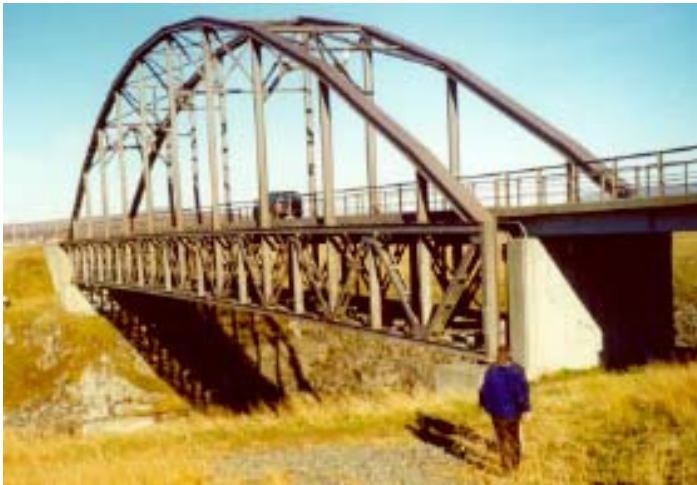
	Thermal Capacity (kJ/kg°C)	Temperature Increase/Cycle (°C)
Hysteretic Steel Dampers (under flexure)	0.502 (steel)	5.33°C
LRB	0.129 (lead)	27.3°C
HDRB	0.8 (rubber)	6.4°C
Friction Device	0.502 (steel)	(temperature given by the solution of Fourier Equation, as a function of time and distance from the interface)
Viscous Dampers		thermal behaviour as a function of the pressure and the size of the damper

Table 6-1: Comparison of Temperature Increase per Cycle for Different Antiseismic Devices.

6.3.2 Elastomeric bearings

Elastomeric bearings have been used for about 40 years to isolate bridge structures from the lateral forces induced by shrinkage and creep of their superstructures (Taylor et al. 1992). More recently, they found application also as a means of decoupling the deck from seismic ground motions.

An elastomeric isolation bearing consists of a number of rubber layers and steel shims, bonded in alternating layers, to produce a vertically stiff but horizontally flexible isolator. The steel layers act to restrain the rubber layers from their tendency to extrude horizontally (bulging) when compressed.



*Fig. 6- 5: The Thjorsa bridge in the South Iceland Lowlands (mceer.buffalo.edu).
(Figure available electronically on fib website; see production note on p. ii)*

This kind of bearings increases the global flexibility and may provide hysteretic or viscous damping, as a function of lower or higher damping properties of the rubber and of the possible insertion of a lead plug that increases the energy dissipation capacity and the initial stiffness, essential for static loads. Consequently they can be grouped in (i) Natural Rubber Bearings, (ii) High Damping Rubber Bearings (HDRB) and (iii) Lead Rubber Bearings (LRB). Fig. 6-5 represents an example of application of such devices to isolate the deck in a single span steel bridge.

The fixation to the structure is not based on friction but on positive connections, recess or dowels (to prevent overturning), as schematically represented in Fig. 6-6.

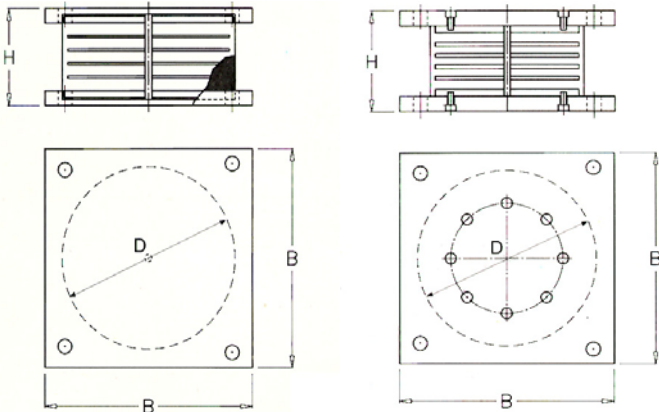


Fig. 6- 6: Schematic representation of (a) recessed and (b) bolted elastomeric bearings.

6.3.2.1 Rubber properties

Elastomers are materials composed of polymers, fillers, oils, accelerators, antioxidants and retarders that are blended and vulcanized in order to create a tridimensional network of crosslinks (sulfur is the most common crosslink agent) between the previously independent macromolecular chains. In engineering applications, the most common elastomers used are natural rubber, neoprene, butyl and nitrile, and often are identified through their hardness, which can be easily measured and relates directly to primary physical properties such as shear and compressive moduli. Other primary properties are tensile strain and strength, and hysteretic energy dissipation. These properties are controlled mainly by the amount of filler agent (typically carbon black in seismic isolation bearings) used in compounding the elastomer. Increasing the proportion of the latter hardness, shear and compressive moduli, and damping increase, whilst the tensile strain at break decreases (Taylor et al. 1992). Physical-mechanical rubber characteristics refer to CNR10018, AASHTO (sec.14/25), BS5400, European Standards pr EN1337. A range of variability of rubber properties is provided in Table 6-2.

Scragging occurs in elastomeric bearings that are subjected to one or more cycles of high shear deformation before testing. Scragged bearings show a significant drop of shear stiffness and damping after the first cycle of loading (Fig. 6- 7, left). This effect is prominent mainly in high damping and in low modulus bearings and the tendency is that the original (virgin) shear stiffness of the bearings is practically recovered within the design life of the structure.

Strain crystallization is an important property of such bearings mainly because it causes an increase in the shear stiffness of the isolator at large strains, as will be explained also in section 6.3.2.7, which tends to limit favorable the seismic displacement, but increasing the force transmitted to the pier.

In the evaluation of the vertical response of elastomeric bearings should also be considered the different stiffness of the rubber in tension and compression: an example of their typical behaviour under cyclic axial load is represented in Fig. 6- 7(right).

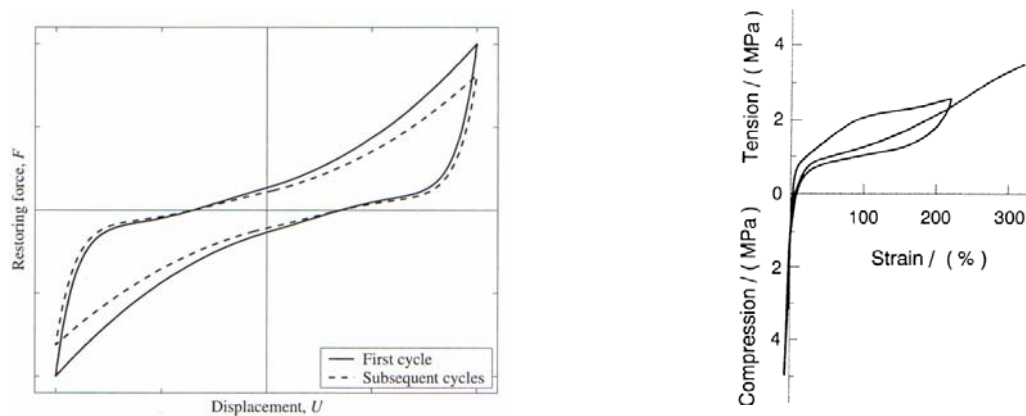


Fig. 6- 7: Comparison between first cycle load and scragged response of an HDRB (left), and Stress-Strain curve for a laminated rubber bearing axially loaded (right).

Rubber properties modifications due to environmental effects such as ozone, corrosion and temperature, and results from laboratory tests considering different loading conditions can be found in Taylor et al. (1992).

Characteristic	SOFT	Compound	
		NORMAL	HARD
hardness (Shore A3)	40±3	60±3	75±3
tensile strain (%)	20	20	18
tensile strength (MPa)	750	600	500
G (MPa)	0.4	0.8	1.4
equivalent viscous damping (%)	10	10	16

Table 6-2: Rubber Properties (Alga Spa, 2003).

6.3.2.2 Laminated Rubber Bearings

Laminated Rubber bearings consist of alternate layers of rubber and steel plates of limited thickness bonded by vulcanization, being able to support vertical loads with limited deflection, due to very high vertical stiffness. As well, they are able to support operating horizontal loads (e.g. wind), with very low displacements. Their life time is over 60 years.



Fig. 6- 8: Section of a Laminated (left) and Lead (right) Rubber Bearings.
(Figure available electronically on **fib** website; see production note on p. ii)

Typical Laminated Rubber Bearings (Fig. 6-8, left) characteristic parameters are the vertical load capacity, the bearing horizontal and vertical stiffnesses, the bearing lateral period, the bearing damping and the allowable seismic displacement, as described hereafter. Low damping elastomeric bearings have an equivalent viscous damping ratio ζ approximately equal to 5% ($\pm 20\%$). Their behaviour may be approximated by that of a linear elastic element, with a secant shear modulus G equal to 1.0 MPa ($\pm 15\%$) and a shear strain of 2.0.

- VERTICAL LOAD CAPACITY W

Since the horizontal behaviour associated with bulging under vertical loads governs the strength, the bearing capacity of such devices depends directly on the shear modulus and the design shear strain level. The vertical load capacity W of a device can be computed from eq. (6-6):

$$W < A'GS\gamma_w \quad (6-6)$$

$$S_{\text{Rectangular Bearing}} = b_x b_y / 2(b_x + b_y)t_i \quad (6-7)$$

$$S_{\text{Circular Bearing}} = D / 4t_i \quad (6-8)$$

where G is the shear modulus of rubber (of the order of 1MPa); A' is the overlap of top and bottom area (A) of bearing at maximum displacement, and it ranges from $0.4A$ to $0.7A$, but a value of 0.6 is typically used for design earthquake; S is the bearing shape factor, i.e. the loaded to force-free area ratio of the rubber layer (which gives an estimate of the confined depth) and it is a function of the inverse of the i^{th} layer thickness t_i , generally ranging from 3 to 40 (typical relations for rectangular and circular bearings are given in equations (6-7) and (6-8)); γ_w is the allowable shear strain and might be assumed equal to $0.2\varepsilon_z$ (Skinner et al, 1993), where ε_z is the failure strain of the rubber in pure tension, typically equal to 4.5 to 7. Finally, b_x , b_y and D define respectively the plane size of a rectangular device and the diameter of a circular bearing.

The allowable vertical stress on the gross area is of the order of $5\div 10$ MPa, but it is indirectly governed by limitation on the equivalent shear strain in the rubber due to different load combinations and stability requirements. Two forms of instability might occur depending on the type of connection to the structure: Euler instability in the case of bolted bearings, which are able to sustain tensile stresses and are prevented from rotating at each end, and Rollout instability with recessed (or doweled) devices (Fig. 6-9). Although some tests have shown that there have been cases where the rubber is capable of sustaining quite high tensile stresses, a conservative assumption is to adopt the rollout value as the displacement limit (equations (6-16) and (6-19)), even when bolted connections are used.

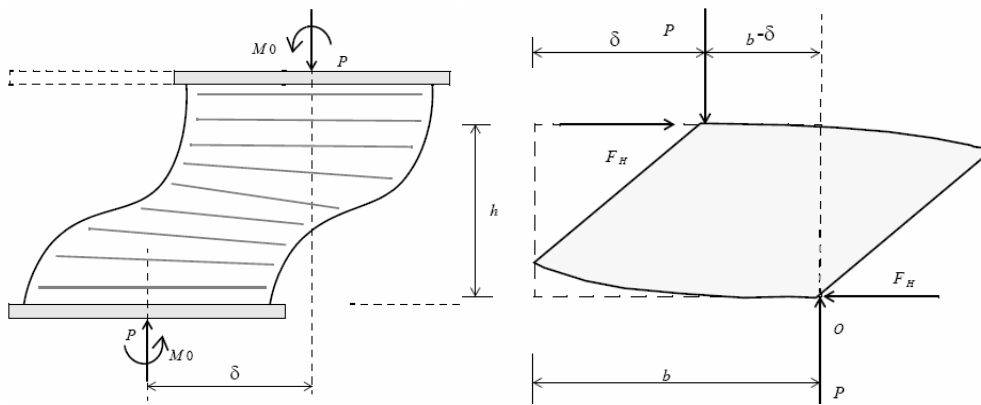


Fig. 6- 9: Euler (left) and Rollout instability (right).

- BEARING HORIZONTAL STIFFNESS K_b AND LATERAL PERIOD T_b

The horizontal stiffness K_b and the lateral period T_b of a device can be computed using the following equations:

$$K_b = GA / h \quad (6-9)$$

$$T_b = 2\pi(M / K_b)^{0.5} = 2\pi(W / gK_b)^{0.5} = 2\pi\left(\frac{1}{gG} \frac{W}{A} h\right)^{0.5} \quad (6-10)$$

And substituting eq. (6-9) into eq. (6-10):

$$T_b = 2\pi(Sh\gamma_w A' / Ag)^{0.5} \quad (6-11)$$

In equations (6-9) and (6-10) h is the total rubber height (i.e. the sum of the layer thicknesses), M is the beard mass and g the acceleration of gravity. K_b is typically of the order of 1÷2MN/m. It is common to obtain period of vibration of the order of 2÷3 seconds. As shown in eq. (6-11) the lateral period results to be a function of the square root of the ratio of bearing height and layer thickness $(h/t)^{0.5}$.

The horizontal stiffness, and the lateral period of the bearing, can be controlled mainly through an adequate selection of the height of the isolator and its shape factor, considering that changes of the latter will also leads to variation in the vertical load capacity.

There will be some reduction in the bearing height with large displacements, partly due to flexural beam action and partly to the increased compression on the reduced loaded area. The resulting inverted pendulum action, which reduces K_b and in extreme cases also the re-centering forces, can be reduced by increasing S up to 10÷20. This problem has been accurately studied by different authors (Kikuchi and Aiken, 1997; Nagarajaiah and Ferrell, 1999; Buckle et al., 2002).

- BEARING VERTICAL STIFFNESS K_v

The vertical deflection of a bearing is the sum of the deflection due to the rubber shear strain and to the rubber volume change. The respective stiffnesses are:

$$\begin{aligned} K_{z-shear\ strain} &= 6GS^2 A / h \\ K_{z-volume\ change} &= \kappa A / h \end{aligned} \quad (6-12)$$

where κ (≈ 2000 MPa) is the rubber compression modulus; the vertical stiffness, corresponding to the two stiffnesses in series is:

$$K_z = 6GS^2 A \kappa / (6GS^2 + \kappa) h \quad (6-13)$$

The resulting value is of the order of 1000÷2000MN/m. This implies a vertical stiffness of the order of one thousand the horizontal one and consequently vertical period of vibration of the order of 0.06÷0.1 seconds (i.e., 3% the horizontal one). Thus, assuming an allowable vertical stress on the gross area of 10MPa, the maximum vertical displacement should be kept satisfactory around values of the magnitude of 1÷2 millimetres, depending on the area of the bearing.

- ALLOWABLE SEISMIC DISPLACEMENT Δ_b

The allowable seismic displacement Δ_b can be limited by either the seismic shear strain γ_s or the overlapping area factor. In the first case, it is given by:

$$\Delta_{b-seismic\ shear\ strain} = h \gamma_s \quad (6-14)$$

where h is the total rubber height.

The allowable limit for the seismic shear strain γ_s , depends on how much shear strain γ_v is mobilized by the vertical load. When rubber is assumed to be incompressible, the shear strain that develop under direct compression by the constraint of the rigid layers to which the elastomer material is bonded is equivalent to $6S\varepsilon_v$ (where ε_v is the axial strain of the rubber). The bearings in fact must withstand the combined rubber shear strains due to structural weight

(γ_v) and seismic displacement (γ_s). Some bridge bearing design codes define a maximum strain criterion for the elastomer (γ_w), including all the strain components, of the order of $0.5\varepsilon_z$ (where ε_z is the failure strain of the rubber in pure tension). For bridges, as will be explained in section 6.3.2.6, additional shear strains due to traffic loads and thermal displacements must be accounted for. The damaging effect of a given rubber strain increases with its total duration of application and by the number of applied cycles. A reference value for the sustainable steady shear strain (i.e., the maximum seismic shear strain) in a rubber bearing (according to the Bridge Engineering standards, 1976) is:

$$\gamma_w = 0.2\varepsilon_z \quad (6-15)$$

where ε_z is the short-term failure tensile strain, which usually ranges from 4.5 to 7. Under combined action of uplift and end moments, the rubber undergoes to large negative pressures, possibly causing small cavities, which grow progressively during sustained and cyclic negative pressures. These effects may cause a large reduction in the axial stiffness, but have normally little effect on the horizontal stiffness. It is usual to design bearings so that negative pressures do not occur, or occur with low frequencies and durations. Higher negative pressures, that may be important for an appropriate modeling of the rubber bearing, can be avoided through a proper detailing.

A limit to the displacement, in order to avoid lateral instability of the bearing, is provided also by the overlapping area ratio (A'/A). Allowing an overlapping area ratio of 0.6, the allowable seismic displacement is of the order of magnitude of $D/3$ and $b/3$ respectively in the case of a circular bearing with diameter D and a rectangular bearing with size b in the direction of the displacement.

In particular, for circular bearings the allowable displacement is given by eq. (6-16):

$$\Delta_b \cong 0.8D \left(1 - \frac{A'}{A} \right) \quad (6-16)$$

with:

$$\left(\frac{A'}{A} \right)_{\text{Circular Bearing}} = 1 - \frac{2}{\pi} (\theta + \sin \theta \cos \theta) \quad (6-17)$$

$$\theta \cong \sin \theta = \frac{\Delta_{b\text{-Circular Bearing}}}{D}$$

For rectangular bearings, accounting for motion that involves both the components along the two principle directions in plan of the unit, the displacement limit along each direction is again given by eq. (6-16) with D replaced by b , and using:

$$\left(\frac{A'}{A} \right)_{\text{Rectangular Bearing}} \cong 1 - \frac{\Delta_{bx}}{b_x} - \frac{\Delta_{by}}{b_y} \quad (6-18)$$

where Δ_{bx} and Δ_{by} are the two components of the bearing displacement in the two principle directions, and b_x , b_y are the dimensions of the element along the same axes. If only the displacement in one direction is taken into account, the displacement of the rectangular bearing might be approximated by eq. (6-19):

$$\Delta_{b-//B} = B \left(1 - \frac{A'}{A} \right) \quad (6-19)$$

Other researchers such as Nagarajaiah and Ferrell (1999) sustain that the aforementioned formulation where the axial load capacity reduces as the shear displacement became larger, which are often adopted in many design procedures (e.g., AASHTO, 1999) might lead, for bolted bearings (where overturning is prevented) with a shape factor of the order of 5÷10, to non conservative estimates of the axial load capacity at low displacements while overestimating that at large deformations (displacement of the order of the bearing size).

6.3.2.3 High Damping Rubber Bearings (HDRB)

HDRB can provide both period shift and energy dissipation: the rubber compound presents damping capability, at least corresponding to 10% of equivalent viscous damping, commonly reaching values of 15-16%, and normally dependent on the bearing displacement. The rubber compound is designed to withstand very large shear deformations, much larger than the standard elastomeric bearings. The rubber compound stiffness is much higher at small deformation levels (up to about 4 times the value at large displacements) and reduces for large deformations. Strain hardening might also develop at very large deformation levels.

As it will be further discussed in section 6.3.2.7 HDRB tend to stiffen after yielding: an experimental study (Kawashima et al., 2002), which analyzed the plastic deformation of RC piers and HDRB system in an isolated bridge subjected to a strong near-field ground motion, shown that large plastic deformations occur in the pier as the intensity of ground motion increases due to the post-yielding stiffness of the bearing. In order to limit such deformations in the piers the authors recommended to adopt a proper safety margin in designing such isolation systems, and they proposed the following requirement in case of extreme seismic design conditions:

$$F_b(u_B) < \alpha P_y \quad (6-20)$$

where $F_b(u_B)$ is the total restoring force of the bearings on a pier at the design displacement u_B , P_y is the yield force of a pier and α is a factor for allowance (within the range 0.7÷0.8) that perhaps needs further studies.

6.3.2.4 Preliminary Design for RB Isolating Systems

In preliminary design of Rubber Bearings Isolating Systems, simplifying assumptions are that the isolators act like perfect springs connecting deck and piers and those piers will be stiff enough to neglect their deformation. Assuming also that the deck behaves as a rigid mass, the whole bridge can be idealized as a single-degree-of-freedom-system (SDOF system) with mass equal to the deck mass and stiffness equal to the isolation system stiffness. Since the mass of the structure is known, the design choices are related to:

- The structural period (normally between 2 and 3 sec.) and the correspondent stiffness (total stiffness of the isolators).
- Whilst the equivalent viscous damping of the HDRB isolators normally ranges between 10% and 16%, in the case of normal laminated rubber bearings typical values are of the order of 5%. From the assumed damping ratio, spectral response values S_a and S_d can be determined and reduced through the parameter η (EC8, prEN 1998-1):

$$\eta = \sqrt{\frac{10}{5 + \xi_{eq}}} \geq 0.55 \quad (6-21)$$

- The design shear strain of the rubber γ . The thickness can be determined through the relative displacement S_d .

$$h = \frac{S_d}{\gamma} \quad (6-22)$$

The net rubber thickness shall be increased to allow for the movements due to temperature, creep and shrinkage (Code provisions are presented in section 6.3.2.6).

Finally, knowing the rubber shear modulus (which value is fairly constant, around 1MPa), the total area of the isolators can be found as a function of the horizontal stiffness (K_b) and the total height of the rubber (h):

$$A = \frac{K_b h}{G} \quad (6-23)$$

The dimensions of the single unit can thus be determined, provided that the allowable vertical pressure is within 7-15 MPa (for $G=0.7-1.4$ MPa) or 4-10Mpa (for $G=0.4-0.7$ MPa) and the displacement capacity of the bearing, as defined in equations (6-16) or (6-19), is higher than the design displacement S_d . Difficulties in the design of these devices arise when an high deformation capacity is required in conjunction with a low level of the vertical load on the device. In these cases, since the large bearing diameter required to provide the displacement capacity, associated with moderate vertical loads, leads to low vertical stresses on the device, thus requiring a very large bearing height in order to get the design period of the isolator (according to eq. (6-10)). The better solution might be to design the device in such a way that the seismic shear strain limitation (instead of the limit imposed by the overlapping area factor) will govern the displacement capacity, assuming an average vertical stress close to the bearing capacity thus containing the height of the bearing.

It is generally necessary, after the preliminary stage, to reduce the number of different types of isolators and to check the manufacturer availability. The preliminary design of the

base isolators has to be followed by a more specific and detailed one, based on the actual parameters.

6.3.2.5 Lead Rubber Bearings (LRB)

In case of standard rubber it is possible the insertion of a lead plug, with diameter of the order of 10% to 20% of the overall bearing diameter, in the laminated rubber bearing to increase the energy dissipation (providing equivalent damping ratios typically of the order of 30%) and to provide the capacity and the stiffness for static loads (Fig. 6-8, right).

The parameters characterizing the system are the yielding shear and the sustainable post-yielding shear force, given in the following equations.

$$V_y = \frac{G_l A_l}{h} \Delta_y + \frac{G_r A_r}{h} \Delta_y = \tau_{ly} A_l + \frac{G_r A_r}{h} \Delta_y \quad (6-24)$$

$$V_d = \tau_{ly} A_l + \frac{G_r A_r}{h} \Delta_d \quad (6-25)$$

where τ_{ly} is the lead yield shear strength (common values may be around 10.5MPa), G_l is the lead stiffness (typically of the order of 130MPa), A_l is the lead area, G_r is the rubber stiffness (\cong 1MPa), A_r is the rubber area, h is the total height of the rubber Δ_y is the displacement corresponding to the yielding shear and Δ_d is the design displacement.

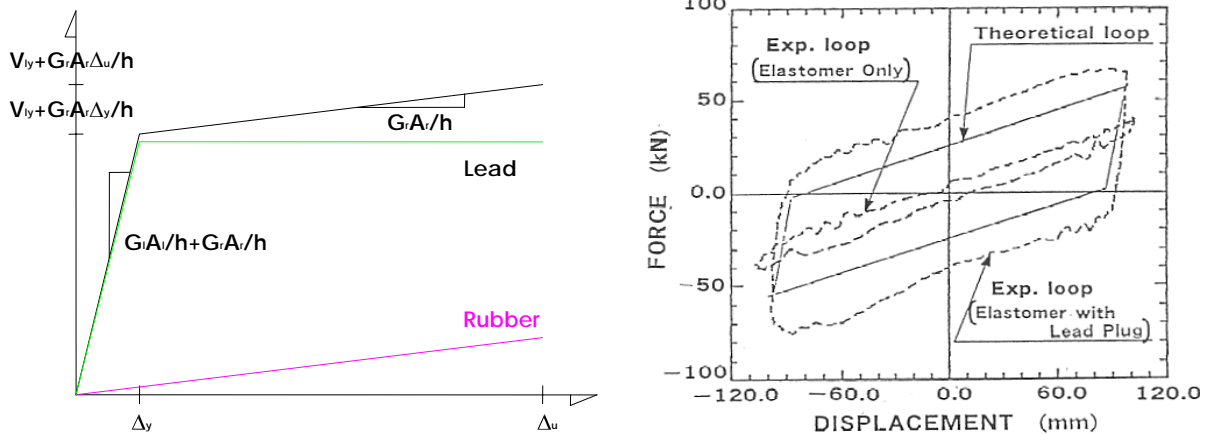


Fig. 6- 10: Schematic Bilinear Constitutive Law (left) and Comparison of shear force-displacement loops for elastomeric bearings with and without lead plug (EERC) (right).

The yielding shear is the total bearing shear at the lead yield displacement and the sustainable post-yielding shear force is the shear at the design displacement of the isolator. The initial elastic stiffness has been estimated from experimental results in the range of 9÷16 times the stiffness of the rubber in a horizontal plane (K_{br}). The size of the lead plug is proportional to the yield strength of the isolator (at this displacement, the rubber contribution is usually neglected, being very small with respect to the lead contribution), while the post yielding stiffness is mainly governed by the rubber bearing stiffness, varying from it by up to $\pm 40\%$, but more likely within $\pm 20\%$.

The maximum force has an uncertainty of the order of 20%. This simplified bi-linear model (Fig. 6-10, right) has a hysteresis loop approximately 20% greater than the actual one.

Mainly, because of the insertion, most of the self-centering property of the laminated rubber bearing is lost, and as shown in Fig. 6- 10 (right) large permanent displacements might occur.

Lead Rubber Bearings have a little strain rate dependence for a wide frequency range, which contains typical earthquake frequencies, have a stable behaviour under repeated loads, and are not strongly dependent on fatigue and temperature excursions within $-35^\circ / +45^\circ$. The effects of vertical load variations on hysteresis are also not relevant if the device is properly designed, with relatively high value of the shape factor S (i.e. $S > 10$).

6.3.2.5.1 Preliminary Design for LRB Isolating Systems

The design of LRB Systems can also be performed, in a preliminary stage, reducing the structural system to an equivalent SDOF system in which the contributions of n isolators in parallel are summed.

The following parameters have to be considered: the total rubber area A_r , and the total lead area A_l , to be split into n isolators; the height of the isolator, h_l , which is the same for the n isolators. The equivalent single LRB can be found comparing the two systems of one isolator, with A_r , A_l and h_l , and n isolators, with A_r/n , A_l/n and h_l , in Table 6-3, where the index i corresponds to the individual isolator unit.

<i>One isolator (with A_r, A_l and h)</i>	<i>n isolators (with A_r/n, A_l/n and h each)</i>
$K_r = \frac{G_r A_r}{h}$	$K_{ri} = \frac{1}{n} \frac{G_r A_r}{h}$
$V_u = \Delta_u \frac{G_r A_r}{h} + A_l \tau_{yl}$	$V_{ui} = \Delta_u \frac{G_r (A_r / n)}{h} + (A_l / n) \tau_{yl}$
	$V_u = n V_{ui}$

Table 6-3: Equivalent SDOF isolator.

It has to be noted that the same stiffness of the two systems can be obtained just imposing that the aspect ratio of the equivalent SDOF isolator be n times the aspect ratio of the n isolators. Nevertheless, this would change the ultimate shear, which depends only on the lead area, and the yielding displacement, which depends only on the lead height. Therefore, the damping characteristics of the system would be altered.

The preliminary design can be based on the following main steps:

- Choose the isolation period T , which is essentially governed by the rubber height.
- Estimate the system damping ratio, and define, by means of eq. (6-21), the correspondent displacement demand S_d .
- Assuming a bilinear inelastic response with a post-yield stiffness (K_2) correspondent to 0.1 the initial one (K_1) and knowing the displacement demand, the yield shear V_y , which is essentially governed by the lead area, and post yielding stiffness are found verifying that the equivalent viscous damping (which is proportional to the area within an hysteresis loop at the design displacement level) matches the chosen damping.

This scheme is not applicable but really efficient, since Δ_d , K_r and V_y are not independent parameters, and this design procedure may eventually results in an unfeasible isolation system due to a series of factors and limitations. The first one is that choosing an ultimate admissible displacement implies a lower bound for the rubber area size (overlapping area limit) and thus a minimum for $K_2 \cdot h$. Then, K_I is a function of K_2 , of the lead area, and the height of the bearing. This is the reason why all the procedure is in reality a function of one parameter: the isolator height, h_I . Based on this observation, the following preliminary design may be proposed, as a function of T_I , h_I , and the admissible Δ_d .

- STEP 0 (Input Data): the input data are the mass, the shear moduli of the rubber and of the lead, and the yield strength of the lead.

Mass	G_{rubber}	G_{lead}	$\tau_{y,\text{lead}}$
M_I	1 MPa	130 MPa	10 MPa

Table 6-4: Input Data.

- STEP 1: T_I , Δ_u , ξ_{eq} are determined. A first trial value of T_I is chosen, and the 5% damped Response Spectra S_a and S_d are determined. A value of ξ_{eq} is chosen, considering that the maximum displacement ηS_d shall be less than Δ_d and the equivalent elastic stiffness K_{eq} for the system is calculated. The ultimate shear capacity V_u for the system might be computed: V_d is checked to be of the same order of magnitude of V_u , nevertheless the shear demand on the system will be determined in a more advanced phase then the preliminary design, possibly through nonlinear analyses of the structure.

T_I	S_d	ξ_{eq}	Δ_u	K_{eq}	V_u	S_a	V_d
(chosen)	(from 5% damping spectrum)	(chosen to properly limit Δ_u)	$g\eta S_d$	$M(2\pi / T_I)^2$	$K_{eq}\Delta_u$	(from 5% damping spectrum)	$W_I\eta S_a$

Table 6-5: Step 1.

- STEP 2: A_r , h_I and h_r (effective rubber height) are found. Maintaining the overlapping ratio limit of 0.6, the minimum size of the rubber for each isolator B_{ri} is derived (from relationships (6-16) or (6-19)) (the fact that the lead plug is inside the rubber area can be neglected at this stage), and A_r is calculated. A trial value of h_I is chosen, and, considering a ratio of 0.9, h_r is estimated.

B_{ri}	A_{ri}	A_r	h_I	$a=h_r/h_I$	h_r
$B_{ri} = \Delta_u / 0.4$	B_{ri}^2	$A_r = nA_{ri}$	(chosen - trial parameter)	(estimate)	ah_I

Table 6-6: Step 2.

- STEP 3: hysteresis loop parameters are determined (Table 6-7). The stiffness of rubber K_r is estimated, and the yielding displacement Δ_y is determined as a function of known parameters (equations (6-26)). The initial system stiffness K_I is determined from the eq. (6-

27), and A_l is defined from the eq. (6-28). The system yielding shear V_y can now be calculated.

$$V_{yl} = K_l \Delta_y = A_l \tau_{yl}; \quad \frac{G_l A_l}{h_l} \Delta_y = A_l \tau_{yl} \quad (6-26)$$

$$V_u = K_1 \Delta_y + K_r (\Delta_u - \Delta_y) \quad (6-27)$$

$$K_1 = K_r + \frac{G_l A_l}{h_l} \quad (6-28)$$

K_r	Δ_y	K_1	A_l	V_y
$\frac{G_r A_r}{h_r}$	$\frac{h_l \tau_{yl}}{G_l}$	$\frac{V_u - K_r (\Delta_u - \Delta_y)}{\Delta_y}$	$(K_1 - K_r) \frac{h_l}{G_l}$	$A_l \tau_{yl} + K_r \Delta_y$

Table 6-7: Step 3.

- STEP 4: known the system hysteresis loop parameters, actual equivalent viscous damping is calculated (eq. (6-29) and Table 6-8).

$$\xi_{eq} = \frac{A_{loop}}{4\pi A_{elastic}} \quad (6-29)$$

where A_{loop} is the area enclosed in one complete idealized hysteresis loop and $A_{elastic}$ represents the elastic strain energy stored in an equivalent linear elastic system, with stiffness equal to the secant stiffness at the design displacement of the inelastic model, under static conditions.

A	b	c	d	ξ_{eq}
$\Delta_u - \Delta_y$	Δ_y	$V_U - V_y$	V_U	$2 \frac{ad - ac - cb}{\pi d(a + b)} \times 100$

Table 6-8: Step 4.

- STEP 5: h_l is adjusted by a trial and error procedure. The value of h_l selected in Step 2 is adjusted until $\xi_{eq(STEP5)}$ matches $\xi_{eq(STEP1)}$. In order to avoid heavy mathematical expressions arising from Step 5 to Step 1, this can be carried out by means of a simple trial and error procedure, easily achieved by setting up an electronic worksheet and changing the values of the lead height.

The only parameters governing the procedure are T_l , h_l , and the admissible displacement Δ_u (based on the overlapping area ratio), whilst other quantities are evaluated deterministically from their values. The last step is to calculate the real maximum admissible displacement, based on the real B_{ri} , considering that overlapping areas includes the lead area; equations (6-30) refer to the case of square bearing and monodirectional displacement.

$$B_{ri} = \sqrt{A_{li} + A_{ri}} \quad (6-30)$$

$$\Delta_{admissible} = 0.4B_{ri}$$

This value, which should not differ very much from the ultimate displacement estimated in step 1, will be compared with the maximum displacement coming from non linear analyses on simplified or refined models of the structure in more advanced design phases.

6.3.2.6 Allowable shear strain and other code recommendations

6.3.2.6.1 AASHTO (1999) Recommendations

In the AASHTO code (1999), shear strain components for isolation design are:
The shear strain due to compression by vertical loads γ_v given in the following equations:

$$\gamma_v = \begin{cases} \frac{3SP}{2A_r G(1+2\bar{k}S^2)} & , S \leq 15 \\ \frac{3P(1+8G\bar{k}S^2/K)}{4G\bar{k}SA_r} & , S > 15 \end{cases} \quad (6-31)$$

where k is the bulk modulus of the elastomer, to be taken as 2000 MPa if not measured, and \bar{k} is an elastomer material constant related to hardness.

The allowable vertical load is indirectly governed by limitations on the equivalent shear strain in the rubber due to different load combinations and stability requirements. Creep effects on the elastomer shall be added to the instantaneous compressive deflection, when considering long term deflections.

The elastic modulus of the rubber E varies in the range of $(3.8 \div 4.4)G$, with an average of E equal to $4G$ that leads to the following equations to estimate the bearing compression modulus of the bearing E_b :

$$E_b = \begin{cases} 4G(1+2\bar{k}S^2) & \text{incompressible rubber} \\ \frac{1}{\frac{1}{8G\bar{k}S^2} + \frac{1}{K}} & \text{compressible rubber} \end{cases} \quad (6-32)$$

where k is the bulk modulus of the elastomer, S is the shape factor of the bearing and G is the shear modulus of the rubber, determined from the secant modulus between 25% and 75% shear deformation. For bearings with large shape factors, the assumption of rubber incompressibility leads to overestimate the compression modulus, and the second eq. (6-31) is used, based on the empirical relation for the compression modulus given in the second eq. (6-32).

The shear strain $\gamma_{s,s}$, due to imposed non seismic lateral displacement Δ_s , the shear strain $\gamma_{s,eq}$, due to earthquake-imposed lateral displacement d_t and the shear strain γ_r , due to the design rotation θ (i.e., the maximum rotation of the top surface of the bearing relative to the bottom), can be estimated according to the following equations:

$$\gamma_{s,s} = \frac{\Delta_s}{T_r}; \quad \gamma_{s,eq} = \frac{d_t}{T_r}; \quad \gamma_r = \frac{B^2 \theta}{2t_i T_r} \quad (6-33)$$

where T_r is the total rubber height, B is the size of the bearing, and t_i is the layer thickness. The load combinations within it is required to perform verification are:

$$\begin{aligned} \gamma_c &\leq 2.5 \\ \gamma_c + \gamma_{s,s} + \gamma_r &\leq 5.0 \\ \gamma_c + \gamma_{s,eq} + 0.5\gamma_r &\leq 5.5 \end{aligned} \quad (6-34)$$

6.3.2.6.2 EC8 Recommendations

According to EC8 (EC8, prEN 1998-1), the total design shear strain (ε_{td}) shall be determined as the sum of the following components: the shear strain due to compression ε_v , the shear strain due to the total seismic design displacement ε_s and the shear strain due to angular rotations ε_α :

$$\varepsilon_{td} = \varepsilon_v + \varepsilon_s + \varepsilon_\alpha \quad (6-35)$$

Maximum allowable values of shear strains ε_v , ε_s , and ε_{td} are given in Table 6-9.

<i>Shear Strain</i>	<i>Maximum Value</i>
ε_v	2.5
ε_s	2
ε_{td}	6

Table 6-9: Maximum Allowable values of Shear Strain (EC8).

The shear strain due to compression is calculated according to the following equation:

$$\varepsilon_c = \frac{1.5 \sigma_e}{S G} \quad \text{with} \quad \sigma_e = N_{sd}/A_r \quad (6-36)$$

where G is the shear modulus of the elastomer, σ_e is the maximum effective normal stress of the bearing, given by the ratio of the maximum axial force N_{sd} on the bearings resulting from the design seismic load combination, over the minimum reduced effective area of the bearing A_r . The latter is given in equations (6-37) and (6-38)-(6-39), respectively for rectangular

bearings with steel plate dimensions b_x and b_y (without holes) and for circular bearings with steel plate of diameter D .

$$A_r = (b_x - d_{Edx})(b_y - d_{Edy}) \quad (6-37)$$

$$A_r = (\delta - \sin\delta)D^2/4 \quad (6-38)$$

$$\delta = 2\arccos(d_{Ed}/D); \quad d_{Ed} = \sqrt{(d_{Edx}^2 + d_{Edy}^2)} \quad (6-39)$$

In the above equations d_{Edx} and d_{Edy} are the total relative displacements under seismic conditions, in the two principal directions in plan, of the bearing, including the design seismic displacements (with torsional effects) and the displacements due to the imposed deformations of the deck (i.e. shrinkage and creep where applicable and 50% of the design thermal effects). d_{Ed} is the total seismic design displacement, and S is the shape factor of the relevant elastomer layer.

The shear strain due to the total seismic design displacement d_{Ed} , including torsional effects, shall be determined as in eq. (6-40):

$$\varepsilon_s = d_{Ed}/t_t \quad \text{with:} \quad t_t = \sum t_i \quad (6-40)$$

where t_i is the total thickness of the elastomer.

The shear strain due to angular rotations shall be determined as in equations (6-41) and (6-42), respectively for rectangular bearings of dimensions the b_x and b_y and for circular bearings of diameter D .

$$\varepsilon_\alpha = (b_x^2\alpha_x + b_y^2\alpha_y) / 2t_it_t \quad (6-41)$$

$$\varepsilon_\alpha = D^2\alpha / 2t_it_t \quad (6-42)$$

$$\alpha = \sqrt{(\alpha_x^2 + \alpha_y^2)}$$

where α_x and α_y are the angular rotations across b_x and b_y . Normally in bridges the influence of ε_α is negligible for the seismic verification.

6.3.2.7 Basic Hysteretic Behaviour and Advanced Analytical Hysteresis Models

Force-displacement relationship of typical elastomeric isolation bearings is non-linear because it is sensitive, in particular for HDRB, to the strain level and axial load effects. Experimentally obtained shear force-displacement relationships for elastomeric bearings show strong non-linearities and stiffening behaviour dependent on shear strain magnitude. Experimental tests revealed that beyond a certain strain level the high-damping bearings exhibit a clear stiffening behaviour (Fig. 6-11). This stiffening is a material property of filled rubbers.

The lead-rubber bearing (Fig. 6-11 (c)), which was made from unfilled rubber and had doweled shear connections, did not show the large-strain stiffening effect (Kikuchi and Aiken,

1997). The reduction of the seismic forces in the piers caused by the fundamental period lengthening may be accompanied by large horizontal displacements in the isolators, which might lead, associated with large axial loads, to instability of elastomeric bearings and thus a significant reduction of their (i) bearing capacity, (ii) shear stiffness and (iii) rotational stiffness; as a consequence, the height, the damping and the overturning strength (in case of doweled connections) of the bearing result to be affected.

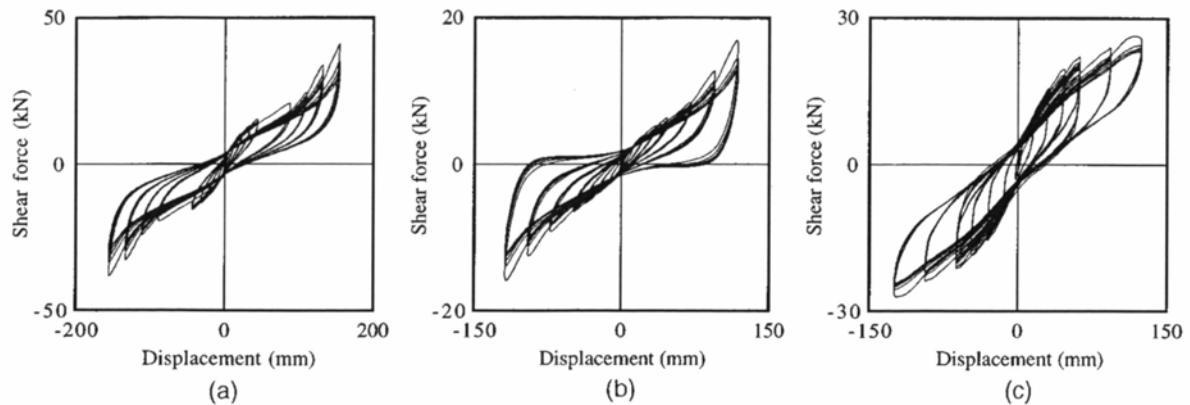


Fig. 6- 11: Lateral force-displacement relationships of typical elastomeric bearings: (a) RB, (b) HDRB, (c) LRB.

Analytical models were developed by Nagarajaiah and Ferrell, (1999), and Hwang et al. (2002)). Nagarajaiah and Ferrell, with the aim to numerically study the buckling of elastomeric bearings at high shear strains, developed a theoretical model that explicitly includes the complex nonlinearities that occur in the elastomeric bearings at high shear strains. An analytical model for HDRB has been developed by Hwang et al. (2002), which seems to predict seismic response time histories of a bearing with a practically acceptable precision.

Doudoumis et al. (2005) developed finite element micromodels for the evaluation of the response of LRBs. Since the confinement of the core depends on manufacturing details, two separate models are proposed, neglecting and accounting for the contribution of the interaction between the lead core and the steel shims and rubber layers respectively, in order to define bound responses.

The behaviour of HDRB, in particular at high strain levels, is also strain rate dependent and may be modeled through the adoption of a viscoelastic response, as proposed by Hwang et al. (1001) and Tsai et al. (2003). Other factors that are difficult to represent are the variation in horizontal stiffness with temperature and ageing effects.

6.3.3 Sliding devices

This class of devices consists of sliding supports providing for frictional damping forces. Modern sliding bearings are defined through a sliding interface and a rotational element needed for maintaining the full contact at the sliding interface. The rotational element may take various forms such as in pot bearings, spherical bearings, disc bearings, articulated slider in friction pendulum bearings or in elastomeric bearings.

The type of material at the slider interface may be:

- Unlubricated polytetrafluoroethylene (PTFE): unlubricated interfaces consisting of highly polished austenitic stainless steel in contact with PTFE or similar composites (as those used in friction pendulum systems);
- Lubricated PTFE: lubricated interfaces consisting of highly polished austenitic stainless steel in contact with unfilled PTFE; lubrication is applied by grease stored in dimples.
- Bimetallic interfaces: interfaces consisting of stainless steel in contact with bronze or similar metals impregnated with a lubricant such as lead, PTFE or graphite.

Stainless steel – PTFE bearings are widely used in bridge design to accommodate slow thermal movements. The friction coefficient of PTFE on steel is $0.02\div 0.03$ (lubricated and unlubricated PTFE respectively) for very slow slip rates. For typical seismic velocities and typical pressure for bridge bearings, the friction coefficient increases to values of the order of $0.10\div 0.15$, depending on lubrication.

In a system isolated with a set of PTFE bearings, the first period of vibration of the system corresponds to the period of the non-isolated bridge since arises from the conditions before sliding (i.e., piers jointed to the deck). Thus, it might be short, leading energy into higher modes, while the second period (i.e., the isolated period), since the stiffness of the device after sliding is negligible, tends to infinity. The overall response results favorable in avoid resonance under seismic loading. In fact, as the first mode attracts high frequencies components of the seismic energy enough to activate the devices (i.e., sliding occurs) the structure begins to soften, and, as the displacement response increases, the effective period of the system progressively shifts towards higher values, thus reducing the potential for an unbounded response.

The approximately rectangular force-displacement loop produces very high hysteretic damping but does not provide any restoring force to the system. Thus, they are generally coupled with other devices like rubber bearings or steel dampers, which provide the required re-centring capability. In the latter case, the entire load is carried by the PTFE bearings and the friction coefficient should be kept as low as possible, while centring force, and even additional damping, are provided by the dampers. In the former case, they can be mounted in parallel, thus sharing the vertical load, or they can be mounted in series to provide flexibility at force levels lower than the bearing sliding forces. In both cases, part of the vertical load is sustained by the rubber.

Moreover, sliding bearings may be used, through a proper definition of the friction force level, to effectively direct loads away of elements of the substructure, which are least capable of resisting them, thus protecting low strength piers, which remain essentially elastic in strong earthquake excitation (Kartoum et al., 1992).

Friction Pendulum Systems represents an innovative and extremely efficient alternative with respect to commonly adopted multi-directional sliding bearings in seismic design of bridges, and thus they will be described in detail in the following sections.

6.3.3.1 The Friction Pendulum System

The Friction pendulum system (FPS) is a sliding recentering device based on the principle of the pendulum motion. It consists of two sliding plates, one of which with a spherical stainless steel surface, connected by a lentil-shaped articulated slider covered by a Teflon-based high bearing capacity composite material (Fig. 6-12, left). The slider is generally locked on a vertical stud with a special hollowed end, which allows free rotation of the slider and a perfect contact with the sliding surface at all times (Fig. 6-12, right). During the ground shaking, the slider moves on the spherical surface lifting the structure (Fig. 6-13) and

dissipating energy by friction between the spherical surface and the slider, essentially resulting in a pendulum motion with period of vibration given by the following equation:

$$T = 2\pi \sqrt{\frac{R_0}{g}} \quad (6-43)$$

where R_0 is the radius of curvature of the spherical surface and g is the acceleration due to gravity.

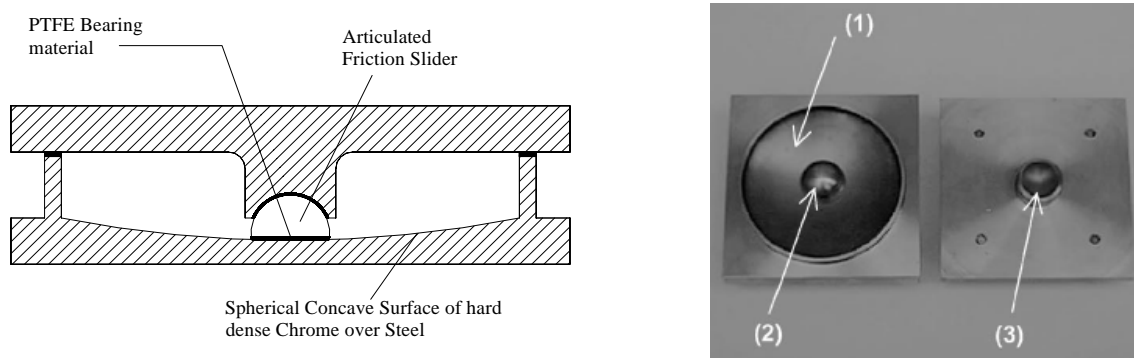


Fig. 6- 12: Radial section of the FPS device (left) and Components of a typical FPS (right): (1) spherical surface, (2) slider, and (3) stud.

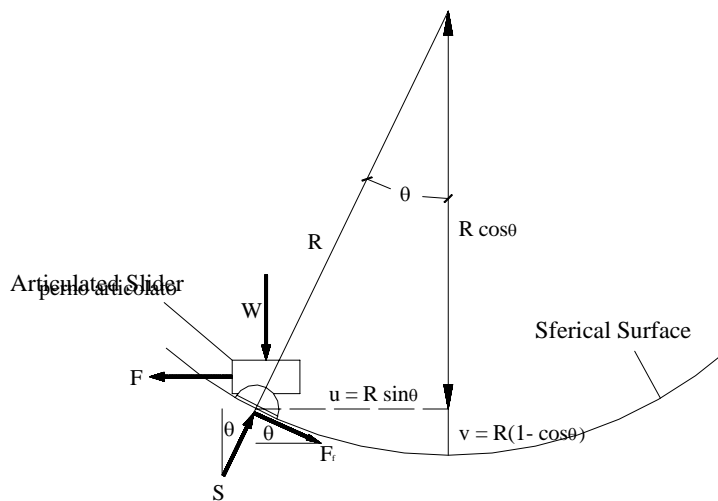


Fig. 6- 13: Static equilibrium scheme of the FPS device.

The behaviour of such devices, and thus their design, is governed only by two parameters: the friction coefficient at the sliding interface and the radius of the spherical surface. Since the first, neglecting its variability with velocity and pressure that slightly effect the peak response of the system (Almazan et al. 1998), might be estimated with a constant value of the order of 5-7% (since typical values ranges between 2-10%), the only one parameter in the hands of the engineer is the radius of the spherical surface. It completely defines the isolation period (Eq. (6-43)) and governs the post-yielding stiffness of the device (Eq. (6-44)). One of the most relevant features of the FPS is that residual displacements are reduced due to the self-centering action induced by the concave spherical surface. Typically, a FPS device may

provide equivalent dynamic periods of vibration within the range from 2 to 5 seconds and displacement capacities greater than 1 m, which is essentially bounded only by the requirement to contain the correspondent vertical component of the displacement.

Considering a system with mass M , the system stiffness K is easily obtained, as shown in equations (6-44).

$$T = 2\pi\sqrt{\frac{M}{K}} = 2\pi\sqrt{\frac{F_V}{gK}} \quad (6-44)$$

$$\frac{F_V}{gK} = \frac{R_0}{g} \Rightarrow K = \frac{F_V}{R_0}$$

where F_V is the total weight on the device and R_0 is the radius of the spherical stainless steel surface.

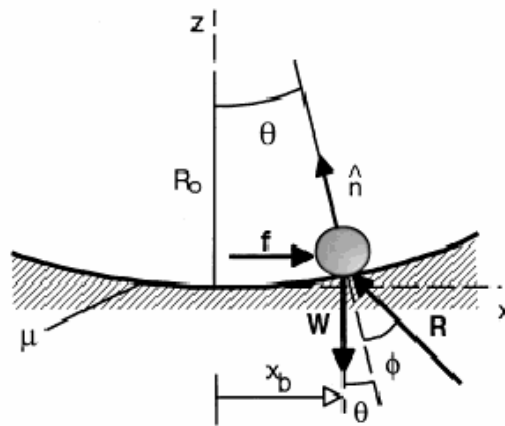


Fig. 6- 14: FPS Equilibrium diagram: planar model.

The resulting isolator force consists of two main components, namely, the restoring force due to the tangent component of the self-weight, always contributing to the restoring mechanism, and the frictional force always opposing the sliding, thus contributing to resist the restoring force depending on the direction of motion. The peculiarity of the FPS is the association of the concave sliding surface to a friction-type response: the consequent coupling between the lateral and vertical motions may produce large deformations in the isolators, but it is not considered in the small deformation theory used in most theoretical formulations, because generally a small-deformations hypothesis is accurate enough for estimating global response quantities. The exact force–deformation constitutive relationship of the isolator may be carried out at different levels of complexity.

Considering the planar system 2D in Fig. 6- 14 the simplest form of the constitutive law is the well-known force–deformation relationship of the FPS system in one dimension and small deformations, resulting from the horizontal equilibrium of the isolator:

$$F = \frac{F_V}{R_0} x + \text{sign}(\dot{x})\mu F_V \quad (6-45)$$

where the total acting vertical force F_V can be identified with the weight W acting on the device.

If the small displacements approximation is overcome, the vertical and horizontal equilibrium equations lead to:

$$\theta = \arcsin\left(\frac{x}{R_0}\right) \quad (6-46)$$

$$N = \frac{F_v}{\cos \theta - \text{sign}(\dot{x})\mu} \quad (6-47)$$

$$F = F_v \text{tg} \theta + \text{sign}(\dot{x})\mu \frac{N}{\cos \theta} \quad (6-48)$$

Detailed descriptions of the basic principles of the FPS devices can be found in relatively recent works (Almazan et al., 2002, Wang et al., 1998; Tsai, 1997).

The device can be either mounted in an upward or downward position (Fig. 6-15), conceptually equivalent in terms of isolation effect, but different for the design implications on deck and piers: in the downward position, the P- Δ effect is transmitted to the pier, while if the FPS is positioned upward, a loading eccentricity corresponding to the displacement results on the deck.



Fig. 6- 15: FPS bearing in downward (left) and upward (right) position.

FPS bearings have been used in both the retrofit (e.g. Priestley and Calvi, 2002) or in the design of new bridge structures (e.g. the American-river bridge in California, and the With-river bridge in Canada). The feasibility of using friction pendulum bearings for seismic isolation of bridges has been also investigated by Wang et al. (1998).

6.3.3.1.1 Basics Hysteretic Behaviour

The hysteretic loop of an FPS is often approximated using a rigid plastic model with post yielding hardening. The actual hysteresis loop is more complex, depending on a series of factors, the main of which is the strong dependence of its response on the axial force variation on the device. Both the yielding shear force and the post elastic stiffness are influenced by temperature, wearing state and level of axial force on the sliding surface, resulting in hysteresis loops that may significantly vary with respect to the standard constant shape shown in Fig. 6-16. Whilst all the aforementioned phenomena modify the response since they affect

the value of the coefficient of friction, the level of the vertical pressure also influence directly both yield strength and inelastic stiffness.

The stiffness of the device seems to be affected by the sliding velocity. Moreover, this dependence appears to be of the same kind of the friction coefficient. Experimental measures of the actual device stiffness record an increase of up to 10% of its theoretical value. The reason of this still needs further investigation.

Simplifications in the modeling of the FPS constitutive law lead to an essentially constant, regular, parallelogram shaped hysteresis loop: specifically these simplifications consists in small angles approximations, in neglecting the friction at the interface of the socket of the slider, in neglecting the non-punctual transfer mechanisms of the forces and in neglecting the axial force variations. This last aspect is probably the most relevant in affecting the real behaviour of the isolator.

6.3.3.1.2 Modeling Issues of the Friction Pendulum System

Earlier studies developed simplified analytical models capable of representing the predominantly bilinear FPS behaviour: most of the theoretical formulations were carried out considering small-deformations, however, due to recent seismic event observations, the large-deformations and the associated P- Δ effects have been addressed to be a concern. For these reasons, large-deformations models should be used in the design of FPS isolated bridges, for which is particularly important the consideration of the axial force in the isolators as it can induce accidental torsion effects not accounted for in the current design procedures.

- **Modeling of the axial force variation Influence**

The modification of the response of the FPS due to axial force variations, as mentioned before, is probably the most relevant one. In fact, the latter is characterized by a variable yield point and a post-elastic stiffness that depends on the acting axial force, resulting in a non-linear post-elastic branch. Calvi et al. (2004) developed and tested an analytical model of FPS, which takes into account the effect of the axial force variations on the isolators. The formulation models both the yielding shear and the post-elastic stiffness of FPS as a function of the acting axial force, resulting in hysteretic loops characterized by non-linear post-elastic branch, as evident in Fig. 6-16. The following figure shows the responses of two isolators sensitive to the axial force variations, one subjected to an increasing compression and the other to a decreasing axial load, and a third FPS insensitive to the axial force variations.

The model of the isolator has been implemented by means of a three-dimensional 2-joint finite element, characterized by cylindrical symmetry. The actual behaviour of the isolator has been found to be of relevance in terms of the general response quantities of bridge structures. Whilst the displacement demand on the isolator results almost independent upon changes of the axial force level on the isolators, the shear demand at the top of the piers might significantly be affected, with variations that could exceed 60÷70% in curved bridge configurations. With low values of the ratio pier/deck mass, also the shear demand at the pier base could significantly change and its shear capacity might be exceeded. Moreover, if differential (i.e., with different sign) variations of axial load on the two isolators could occur, a significant torsional moment demand, large enough to possibly induce collapse, might develop at the top of the pier.

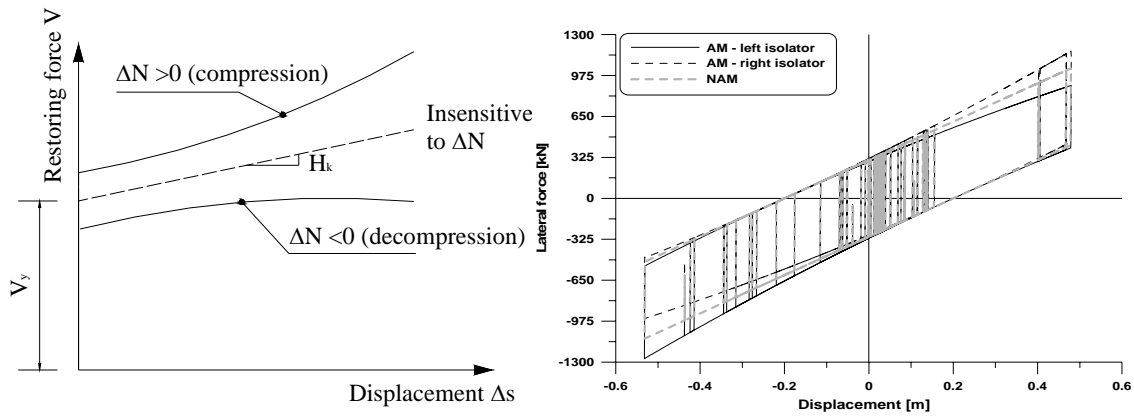


Fig. 6- 16: Constitutive laws (left) and hysteresys loops (right): simplified and advanced models.

These variations depend mainly upon the geometric configuration of the bridge and the magnitude of the vertical ground motion. In particular, large values are expected (i) as the radius of curvature decreases, (ii) the pier/deck mass ratio decreases, and (iii) the vertical component of the record is considered. Should be noticed that, whilst in straight bridges variations of the axial load on the isolators are significant (of the order of 25÷35%) only if the vertical component of the ground motion is considered, in curved bridges they are of relevance even neglecting this component of the record.

- Analytical Model for the Teflon-Metal Interface and of the Local Bending Effects

With the aim to simulate accurately the behaviour of the Teflon-metal interface in FPS devices, including the effects of axial forces and velocities, Tsai (1997) developed an analytical model based on visco-plasticity theory. Numerical simulations, performed only on multi-storey structures, have shown that nonlinear local bending moment effects are substantially important and that axial force variations on the isolators are of relevance for the friction force calculation in this kind of isolators.

- A physical model for the FPS uplifting

In order to include possible uplift and impact, Almazan et al. (1998) defined a physical model for the FPS, including a uniaxial gap element between isolator and sliding surface and a kinetic energy reduction factor which accounts for the energy loss during the impact in the isolators in which uplift occurs. The resultant vertical impact of the slider and the spherical surface leads to two effects: column base shear may increase due to increase in normal force at the isolators interface; this in fact results in the instantaneous stop of the slider from sliding and in the transmission of significantly larger shear forces to the supported columns.

Although local effects such as variation in the normal contact forces, large deformations and uplift do not seem to effect considerably the global system response, Almazan et al. (1998; 2002) recommend to consider them in the isolation modeling and design to compute local responses such as the superstructure deformations and the normal isolator forces, especially for near-field earthquake with strong initial acceleration pulses and for statistically correlated horizontal and vertical expected ground motion components.

6.3.4 Metallic and Friction Dampers

This kind of dampers, relatively economic, are used when a control is needed on the level of the provided force, when an increased initial structural stiffness is needed, and/or when the main concern is to reduce displacement as opposed to acceleration demand. The macroscopic model and the analysis of the dynamic response of bridges equipped with metallic and friction

dampers is basically the same, due to the essentially equivalent elastic-perfectly plastic response exhibited by the devices.

Friction dampers dissipate the seismic energy by friction developed between two solid bodies sliding relatively one to another. With the term friction dampers we are referring to elements that, as in the case of the previously presented sliding devices, make use of friction mechanisms to develop the resisting force and energy dissipation, but differ from the latter since they do not carry any vertical load. Such devices are usually adopted within braced-frame structural systems, and thus they are not often used in bridges (unless for multi-bent bridges), they will be only mentioned here (Filiatrault, 2003; Pall et al., 1980; Tremblay and Stimer, 1993; Tyler, 1983). Typical examples of these devices are:

- Slotted-bolted connections;
- Pall devices;
- Sumitomo Devices.

Metallic dampers take the advantage of hysteretic behavior of metals when deformed into the post-elastic range. A wide variety of different types of devices have been developed, with basic shapes cut from thick steel plates, among these:

- C/E-shaped Hysteretic Dampers;
- EDU device;
- ADAS and TADAS Elements;
- Lead Extrusion Devices;
- Torsional beams, bell dampers, steel tubes, etc;

6.3.4.1 Friction Dampers

Friction dampers might be placed in multi-bent bridge configurations, fixed to cross braces and then clamped together in order to control the transversal response.

In the case of friction dampers, the design philosophy to enhance the structural performance is to provide a way for the structure to yield without damaging the existing structural members: seismic energy is dissipated by means of friction, i.e. by making steel plates sliding one against the other, while bolts hold the steel plates together providing the normal component of the friction force. At a given sliding load, P_y , the plates begin to slide and dissipate energy. Varying the sliding load will alter the seismic energy attracted by the structure

6.3.4.2 Steel Hysteretic Dampers

Hysteretic dampers dissipate energy by flexural, shear or extensional deformation of the metal in the inelastic range. Typically, mild steel plates with triangular or hourglass shapes are used, in order to provide a constant strain range for each section and optimize the use of the damper material. These devices are able to sustain repeated cycles of stable yielding, avoiding premature failure. Further, they are reliable, maintenance free, not sensitive to temperature variations and not subjected to ageing.

The steel used for these devices must be characterized by a very high elongation at failure and a low hardening, in order to provide a very high low cycle fatigue life with negligible performance decay after many cycles.

In continuous span bridges, they may be located either in one position (e.g. one abutment) to allow free movements of the bridge (in this case they are normally designed for large forces), or distributed in several locations to allow thermal movements of the structure (usually used in conjunction with hydraulic shock transmission units).

There are three typical kinds of steel dampers, according to their working principle:

- Uniform moment bending beam with transverse loading arms;
- Tapered-cantilever bending beam;
- Torsional beam with transverse loading arms;

Several devices developed in the early 1980's shown some limits, such as: difficulty to provide large displacement capacity and uniform response in any direction; limited capacity to resist yield cycles without breaking; characteristics degradation after first cycles with progressive reduction of the yield force up to failure; asymmetry of the load-displacement cycles with stiffness variations in tension and compression.

New devices overcoming these limits have been then developed. For example, relatively complex devices, based on the combination of C-shaped elementary energy dissipators, have been designed specifically in bridges with a limited total weight and large displacement capacities. Tests on these devices have shown long cyclic life, almost no cycle deterioration before failure and very good dissipation capacity, as shown in the typical hysteresis loop of Fig. 6-20.

These devices may constitute the dissipative part of a system of seismic isolation of the bridge deck, as well as they may simply act as dampers by themselves. Then they can be arranged to be a part of one-directional or multidirectional bridge bearings.

The conceptual design of the single damper unit is based on optimization criteria, i.e.:

- An optimized shape allows almost constant strain range for each cross section (uniform diffusion of plasticization);
- Particular design arrangements neutralize the effects of geometry changes, that otherwise can cause strain hardening or softening behaviour and/or asymmetrisation of the hysteresis cycles, at large displacements. The dissipation effectiveness is thus improved, and large displacements and damping of response in all directions are allowed.

6.3.4.2.1 C-shaped Device

Typical C-shaped elements have a semicircular shape (Fig. 6-18, left), with constant radius r , while the depth of the section varies in order to ensure a uniform plasticization of all sections. The maximum depth in the middle decreases towards the supports, obviously not zero, but small enough to guarantee the shear and axial load transmission to the supports). The angular opening of the device is generally of 180° , or greater when the displacement demand is particularly high.

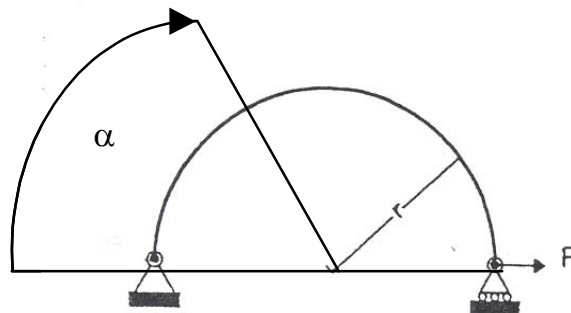


Fig. 6- 17: Schematic representation of a C-Shaped element with an angular opening of 180° .



Fig. 6-18: C-shaped Device (left) and EDU Device (right).
(Figure available electronically on fib website; see production note on p. ii)

Equations (6-49) give the yielding and plastic quantities of the device when α does not exceed 180° , where α is polar coordinate referring to an horizontal axis passing through the centre of the C device, as schematically represented in Fig. 6-17.

$$\begin{aligned}
 b(\alpha) &= b_{\max} (\sin\alpha)^{1/2} \\
 M_y &= \sigma_y \frac{sb(\alpha)^2}{6} & M_p &= \sigma_y \frac{sb(\alpha)^2}{4} \\
 P_y &= \sigma_y \frac{sb_{\max}^2}{6r} & P_p &= \sigma_y \frac{sb_{\max}^2}{4r} \\
 \delta_y &= 4.824 \frac{r^2}{b_{\max}} \varepsilon_y & \delta_{\max} &= 4.824 \frac{r^2}{b_{\max}} \varepsilon_{\max} \\
 \mu &= \frac{2}{3} \mu_l & K &= 0.03455E \frac{sb_{\max}^3}{r^3}
 \end{aligned} \tag{6-49}$$

where b_{\max} is the maximum depth of the element section (for α equal to $\pi/2$), $b(\alpha)$ is the depth at any other section, s is the width of the section; r is the radius of the element, s_y is the yield strength of the steel, M_y and M_p are the yield and plastic moments of the section, P_y and P_p are the correspondent value of the force applied to the element, ε_y and ε_{\max} are the yielding and plastic strains of the steel, d_y and d_{\max} are the displacements at yielding of the device and at the attainment of its capacity, μ_l is the local ductility of the section (equal to $\varepsilon_{\max}/\varepsilon_y$), μ is the global displacement ductility of the element and K is the elastic stiffness of the device.

The response of each one of these units, described by the equations (6-49), considers only bending deformation, and do not account for axial effects (softening in tension and hardening in compression). These effects, however, became negligible as a consequence of coupling several units as in the device shown in Fig. 6-18 (right).

Other devices, with a different shape, like the E-Shaped device, (Ciampi and Marioni, 1991) were developed, following the same principle to achieve a uniform plasticization throughout the member.

6.3.4.2.2 The EDU Device

The EDU Device is a multi-composed device made up with C-shaped elementary energy dissipators (Fig. 6-18, right): they are combined in such a way that they are forced to deform anti-symmetrically, i.e. for each compressed one, another is in tension; combination of them with radial symmetry allows uniform behaviour under earthquake loading acting in any direction. This device can be used in conjunction with conventional pot-bearings carrying the vertical loads (as has been done in the design of the Bolu Viaduct in Turkey, Fig. 6-19), and they can also be coupled with hydraulic shock transmitters in parallel.



Fig. 6-19: View of the Bolu Viaduct (Priestley and Calvi, 2003) (left) and detail of the pier top (Marioni, ALGA S.p.A.) (right). (Figure available electronically on fib website; see production note on p. ii)

The EDU device has been tested by Marioni (1996) with a real earthquake of 7.4 magnitude with 0.8g PGA confirming that it dissipates a significant amount of energy (Fig. 6-20) and fulfill European standards for in-service conditions. It shows self-centering properties for thermal effects and small earthquakes, but it has to be coupled in parallel with other devices, characterized by a linear, spring-like response, if the residual displacement is a concern and need to be reduced. Obviously, any reduction of the potential residual displacement implies a reduction of the hysteresis loops area and of the global equivalent damping.

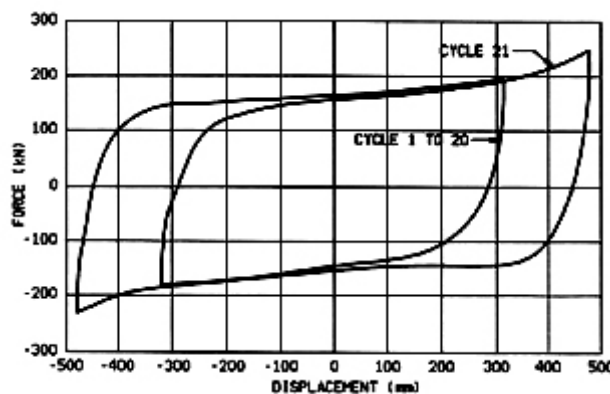


Fig. 6-20: Load Deflection Plot of the EDU device (Marioni, 1996).

6.3.4.2.3 ADAS and TADAS Elements

The Bechtel Added Damping and Stiffness (ADAS) device is another example of a hysteretic damper (usually installed in conjunction with a chevron brace assemblage in multi-bent bridges). ADAS elements are designed to dissipate energy through the flexural yielding

deformation of X-shaped mild-steel plates configured in parallel between top and bottom boundary connections (Fig. 6-21). The particular advantage of an X-plate is that, when deformed in double curvature, the plate deformation is uniform over its height, and when deformed into its plastic regime, the yielding will be distributed.

The primary factors affecting an ADAS element behaviour are the elastic stiffness, yield strength, and yield displacement (Bergman, 1987).

Possible shortcomings with X-shape ADAS are that the stiffness of the device is very sensitive to the tightness of the bolts and generally lower than that predicted by assuming both ends fixed, through the flexural behaviour might be weakened when the device is subjected to axial loads.

Triangular ADAS (TADAS) devices using triangular steel plates welded at bottom and bolted at top (Fig. 6-22) were developed to avoid these inconveniences: Stiffness varies linearly along the height, implying constant curvature, thus avoiding curvature concentration and assuring also in this case a distributed plasticity throughout the whole device.

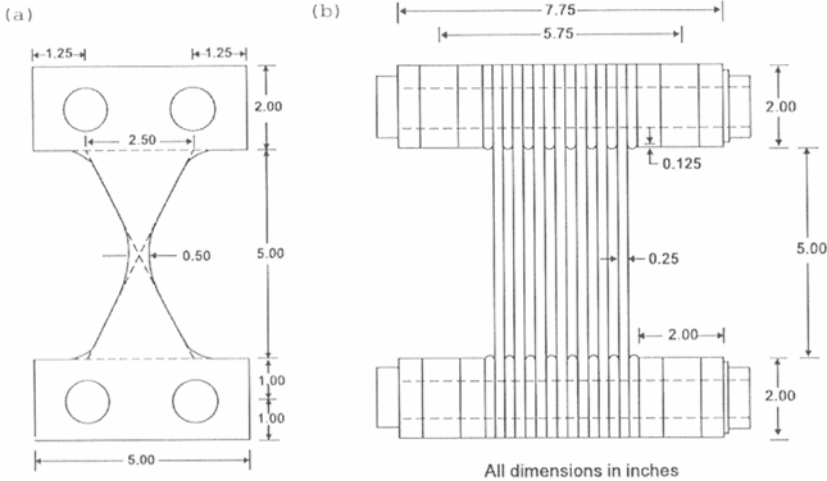


Fig. 6- 21: Added Damping and Stiffness (ADAS) Element.

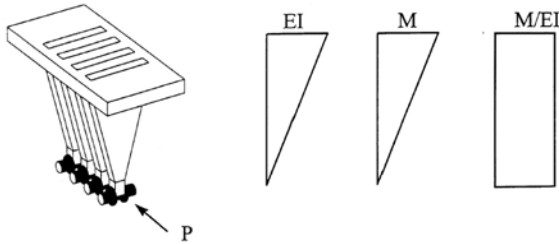


Fig. 6- 22: TADAS Element.

6.3.4.2.4 Lead Extrusion Devices (LEDs)

Lead Extrusion Dampers are based on the properties of lead when it is forced through orifices.

Fig. 6-23 illustrates two types of lead extrusion dampers: the constricted tube, which forces the extrusion of the lead through a constricted tube, and the bulged shaft, that uses a bulged shaft through a lead cylinder.

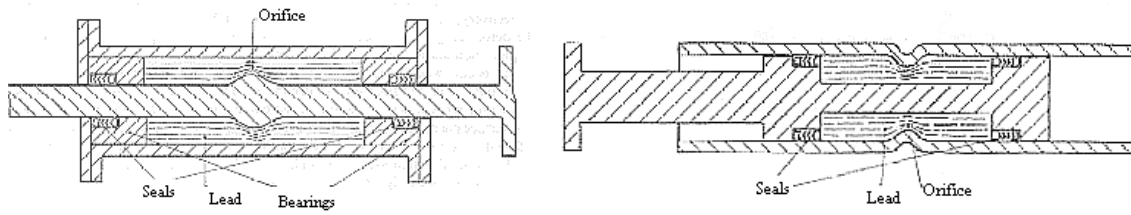


Fig. 6-23: Longitudinal Section of a bulged-shaft (left) and of a constricted-tube (right) extrusion energy absorber.

The main characteristics of these devices are that (i) Lead hysteretic behaviour is essentially rectangular, stable and unaffected by number of load cycles (Fig. 6-24); (ii) it is not influenced by any environmental factor; (iii) fatigue is not a major concern; (iv) strain rate has a minor effect and (v) aging effects are insignificant. Although, they are rarely adopted on bridge structures since they do not have any re-centering capability of the deck and they cannot be efficiently designed for both large displacements and large forces because of the possibility of buckling of the internal shaft during compression.

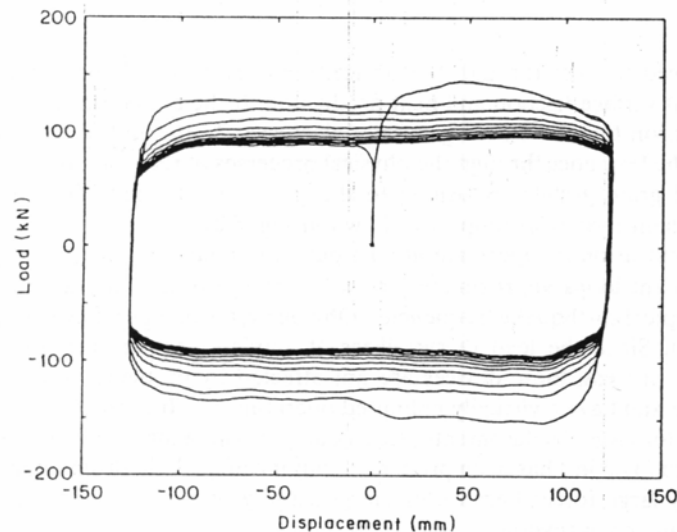


Fig. 6-24: Lead Force Displacement Curve.

6.3.4.2.5 Conceptual Design: concepts of yield/slip shear and Optimization criterion

The design of bridges equipped with metallic/friction dampers, since the main design parameter of such devices is the level of the resisting force that they provide before that sliding occurs (F_y), has the objective to define the latter in order to efficiently control the seismic response of the bridge. The design procedure can be divided in four stages: (i) the estimation of the optimum parameters (i.e., values that provide a minimum for a considered design objective function) for dampers and adjacent elements by hand- calculation (such as the force at yielding or the slip shear for metallic and friction devices respectively); (ii) the design of dampers and adjacent elements to meet the determined optimum parameters; (iii) the application of capacity design checks for all members of the structure under the expected ultimate force generated by the metallic/friction dampers, in order to preserve them against damage until the isolation system will be activated; (iv) nonlinear time history analyses checks of the whole equipped structure are required after the preliminary design phase.

The definition of the optimum parameters of the devices is certainly the crucial aspect in the design of the isolated bridge. Park and Otsuka (1999) proposed a design procedure for bilinear seismic isolators for bridge applications where the optimal yield level of the isolator is defined through the minimization of the total strain energy that the structural members have to sustain. The optimal ratio of yield force of the isolator to the total weight of the structure (mentioned as OYR in the paper) corresponds to the attainment of the maximum ratio of absorbed energy by the isolator to the total input energy (called RAE). The authors found that the latter relates directly to structural responses of the prototype bridge models, since maximum displacement, acceleration and shear demands generally approach low values as RAE increases. Relationships developed relate the OYR with the earthquake amplitude and are suggested in a preliminary design stage of bilinear type seismic isolation devices

6.3.5 Viscous and Viscoelastic Dampers

6.3.5.1 Viscous Dampers

Linear devices produce damping forces proportional to the velocity of the damper deformation, greatly attenuating the higher-mode seismic response, which is only relatively reduced by isolators with a high level of hysteretic damping. Hydraulic dampers (Marioni, 1999 and 2002) make use of viscous properties of a fluid to improve structural resistance against earthquake. Such devices have been commonly adopted in the past as shock transmitters, able to allow slow movements (in service conditions) without valuable resistance, and react stiffly to dynamic actions.

More recently, it became possible to develop effective velocity dampers, of the adequate linearity, using the properties of high-viscosity silicone liquids: a double-acting piston drives the silicon fluid cyclically through a parallel set of tubular orifices, giving high fluid shears and hence the required velocity-damping forces. The force generated by the device can be described by the following equation:

$$F = CV^\alpha + A \quad (6-50)$$

where F is the force applied to the piston, V is the piston velocity, C , A , α are constants depending on the fluid and circuit properties; α may range between 0.1 and 2, according to the type of valves. Force-displacements plots for devices with different values of α subject to sinusoidal input are elliptical-shaped.

Fig. 6- 27 (left) illustrates the relationship that occurs between force and velocity, for different values of α . The parameter α equal or higher than 1 is preferred when the difference of force at low and high velocity shall be maximized, allowing slow movements, due to thermal variations, creep and shrinkage and to become rigid in case of dynamic actions (braking force and earthquake), or when energy dissipation is not required: in this case they are called Shock transmission Devices (STD) or Hydraulic Couplers. When energy dissipation is required, a value of α lower than 1 is preferred in order to increase the hysteretic area and maximize the dissipated energy per cycle. In this case they are called viscous dampers (VD), for which a reference value of α is generally 0.1.

Some practical examples for the application of viscous dampers to bridge structures are provided in Fig. 6-25. Such devices can either act in the longitudinal direction, usually at location of thermal gaps, or be used to control the transversal response of cable-stayed bridges, as in the case of the recently opened Rion-Antirion bridge (Fig. 6-25, left). In this

case, four dampers connect the deck at the top on each pier and limit the pendulum movement of the latter during an earthquake. The dynamic relative movement during an extreme seismic event will be in the order of 3.50m while velocities may exceed 1m/s.



Fig. 6- 25: Representation of the viscous damper units in the Rion-Antirion bridge (<http://www.gefyra.gr>) (left), example of viscous dampers application to a bridge located at Yen-Chou in Taiwan (Hwang and Tseng, 2005) (right). (Figure available electronically on **fib** website; see production note on p. ii)

6.3.5.1.1 Basic Hysteretic Behaviour of Viscous Dampers

Assuming that the axial force in the element is linearly proportional to the relative velocity between its two ends when subjected to a sinusoidal relative axial displacement history ($x(t) = X_0 \sin(\omega t)$, where X_0 is the relative amplitude between the two ends of the element and ω is the excitation frequency), the force-displacement relationship is represented by eq. (6-51) and the energy dissipated per cycle by eq. (6-52). Eq. (6-51) describes an elliptical loop (Fig. 6-26, left), in which the amplitude of the maximum induced force in the element is linearly proportional to the damping, to the displacement amplitude and to the excitation frequency: for this reason, in MDOF systems, each mode has an assigned viscous damping. It is worth noting that during a seismic excitation, the frequency continuously varies, and in the same way the amplitude of hysteresis loops. Thus, the energy dissipated/cycle will continuously change with the excitation frequency, since, as previously mentioned, it is proportional to the square of the maximum displacement, which could differ from cycle to cycle.

$$\frac{F}{X_0 C \omega} = \pm \sqrt{1 - \left(\frac{x}{X_0}\right)^2} \quad (6-51)$$

$$E_D = \int_0^{2\pi/\omega} F(t)x dt = \pi C \omega X_0^2 \quad (6-52)$$

where F is the axial force induced in the element, x is the relative axial displacement between the two ends of the element, E_d is the energy dissipated in one cycle, C is the viscous damping constant, X_0 is the relative displacement amplitude between the two ends and ω is the excitation frequency.

An important characteristic of linear viscous dampers is that the resisting force provided by the damper is out of phase with the deck acceleration, and this is useful in limiting it. Nevertheless, the fact that the viscous damper force is directly proportional to displacement,

implies that there is no limit to the damper force itself, that is virtually unbounded, while e.g. in friction dampers it is limited by the damper yielding.

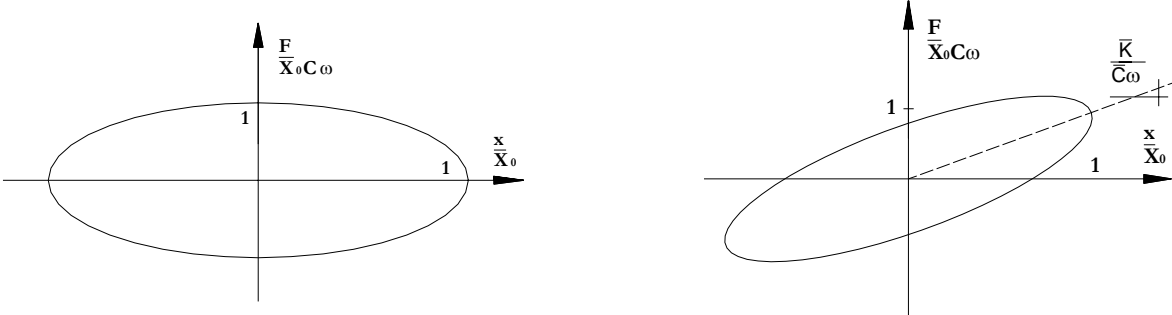


Fig. 6- 26: Cyclic Response of a pure Linear Viscous Element (left), Cyclic Response of a pure VE Damper (right).

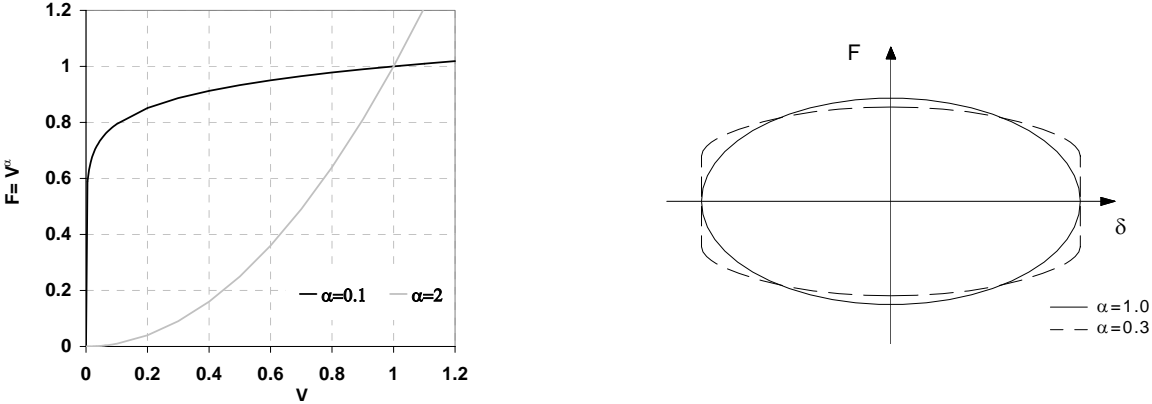


Fig. 6- 27: Force-velocity type dependence for different values of the parameter α (left), Hysteresis Loop of a viscous damper with different values of α (right).

Non linear viscous devices with α lower than 1 provide a limit for the increase of the force with displacements (Fig. 6-27, left). In the practical range of velocity and exponential coefficient (0.2 to 1) the ratio between the nonlinear damping constant (CNL) and the damping constant of an equivalent dissipating linear system (C) can be approximated, equating the energy dissipated per cycle, through eq. (6-53). Consistent units must be used since eq. (6-53) is not dimensionally homogeneous.

$$\frac{C_{NL}}{C_L} \cong \frac{\sqrt{\pi}}{2} (\omega X_0)^{1-\alpha} \tag{6-53}$$

where X_0 is the relative displacement amplitude between the two ends, ω is the excitation frequency, and α is a property of the fluid and the type of device selected.

6.3.5.1.2 Design considerations

The design process, in the case of bridges isolated with viscous dampers, has the main objective to achieve the level of equivalent viscous damping specified by the designer in order to satisfactory reduce the displacement demand due to seismic loading.

Whilst several studies have been performed in the field of develop design procedures for viscous dampers for multi-storey braced frames, only few focused their attention on bridge structures. Recently Hwang and Tseng (2005) developed and proposed the design formulas for supplemental viscous dampers to highway bridges. They can be used to determine the damping coefficients of linear or non-linear viscous dampers corresponding to a desired system damping ratio of the bridge in which different component damping ratios may be assumed for the elastomeric bearings, piers and abutments. Through this concept of composite damping ratio the possibility that bridge components might have different stiffnesses, lumped masses and damping ratio can be taken into account. The derived formulas have been numerically validated by comparing the seismic responses of a three-span bridge equipped with viscous dampers with those of the same bridge without dampers but with the assigned target damping ratio. The authors, since the good agreement obtained between the seismic responses of the two models, suggested the formulas for practical applications.

6.3.5.1.3 Fabrication and Detailing Issues

Fluid dampers mounted in a structure are essentially a “bolt-in” item, of a relatively compact size. A brief discussion on the implementation of fluid dampers is provided in terms of fabrication issues (Size vs. Cost) and detailing (Attachments and Brace Styles). If a given structure requires a specific amount of total macroscopic damping, the latter needs to be divided among the number of dampers. The end result is a maximum force and damping constant for each individual damper. The question arises if the engineer should select a large number of small dampers, or a lesser number of large dampers.

Maintenance is not required for a properly designed and manufactured fluid damper used for seismic and wind damping in structures. Usually, visual inspection of the dampers should occur after a major seismic event: in this case, the damper mounting pins may bend or shear. In some cases, regional codes may require that a few dampers be randomly removed from the structure, and subjected to testing in order to verify the damping output.

6.3.5.2 Viscoelastic Dampers

Typically, used viscoelastic dampers are made of copolymers or glassy substances; they are often incorporated in bracing members (in multi-span bridge piers or deck) and dissipate energy through shear deformations of the Viscoelastic material (Fig. 6-28).

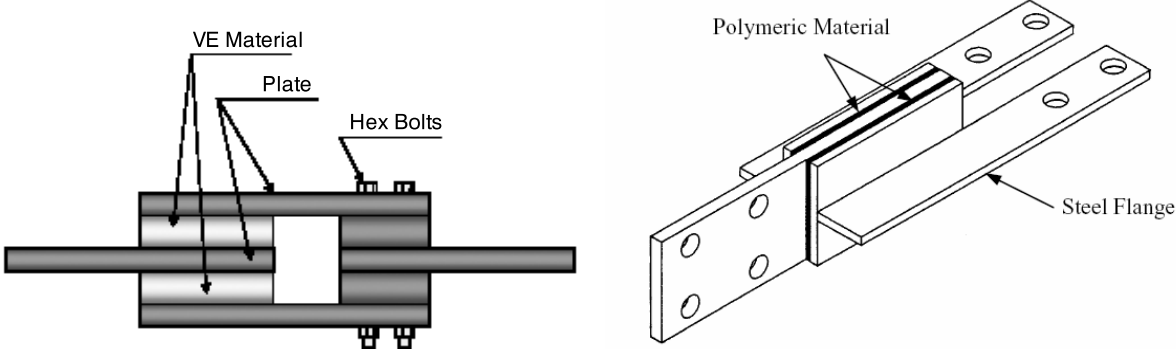


Fig. 6- 28: VE Damper part of a bracing member: typical schemes. 2D (left) and 3D (right) representations.

6.3.5.2.1 Basic Hysteretic Behaviour of VE Dampers and Dynamic Analysis of VE Dampers Equipped Structures

The response of this kind of dampers is analogous to the previously mentioned viscous behaviour with an added elastic component. The device is represented by means of G_E and G_C , respectively the instantaneous elastic response and the shear viscous damping constant exhibited by the viscoelastic material.

The solution for a sinusoidal excitation describes an elliptical shaped loop Fig. 6-26 (right), and eq. (6-55)) inclined with respect to the principal axis of a quantity corresponding to the instantaneous elastic stiffness: the response can be easily viewed as the sum of a linear elastic component and a viscous elliptical component: still maximum force does not occur at maximum displacement, and optimum phasing can be obtained by adjusting the material properties \bar{K} and \bar{C} (equations (6-54)).

The energy dissipated per cycle is easily shown to be given by the eq. (6-52), with C replaced by \bar{C} : this can be also deduced observing that the elastic component does not contribute to the energy dissipation.

The equivalent viscous damping ratio $\bar{\xi}$ of the element is shown in eq. (6-56):

$$\bar{K} = \frac{G_E A}{h} \quad ; \quad \bar{C} = \frac{G_C A}{h} \quad (6-54)$$

$$\frac{F}{X_0 \bar{C} \bar{\omega}} = \frac{\bar{K}}{\bar{C} \bar{\omega}} \left(\frac{x}{X_0} \right) \pm \sqrt{1 - \left(\frac{x}{X_0} \right)^2} \quad (6-55)$$

$$\begin{aligned} \bar{\xi} &= \bar{C} / 2\bar{\omega}m = G_C \bar{\omega} / 2G_E = \eta / 2 \\ \bar{K} &= \bar{C} \bar{\omega} / \eta \end{aligned} \quad (6-56)$$

where $\bar{\omega}$ is the oscillating circular frequency of the element.

In viscoelasticity, G_E is the Shear Storage Modulus, that is a measure of the energy stored/recovered per cycle, and $G_C \bar{\omega}$ is the Shear Loss Modulus, measure of the energy dissipated per cycle, and the ratio of the two is called Loss Factor, $\eta = 2\bar{\xi}$.

Chang et al. (1993) found that both G_E and $G_C \bar{\omega}$ decrease with an increase of the ambient temperature, but the Loss Factor remains fairly constant. In addition, damper properties, for different temperatures and frequencies, remain fairly independent with respect to the strain level when the latter is below values of the order of 20%.

6.3.6 Self-Centering Dampers

Generally, dampers are unable to limit the residual displacements after a seismic event. Some recently developed damper systems, characterized with a so-called flag-shaped hysteretic loop, incorporate re-centering capabilities thus reducing permanent offsets when the structure deforms inelastically. Among these, might be mentioned the Shape Memory Alloys Dampers (SMAs), which take advantage from peculiar material properties, and other devices,

such as the Energy Dissipating Restrain (EDR) and Friction Spring Seismic Dampers, which make use of the geometry of the device in order to provide the required restoring forces.

6.3.6.1 Shape Memory Alloys Dampers (SMA)

Several experimental tests on SMA Dampers has been conducted in the past by DesRoches and Delmont (2002), Dolce et al. (2000) and Aiken et al. (1993), and analytical models were developed by DesRoches and Delmont (2002), Ivshin and Pence (1994), Liang and Rogers (1990) and. Recently, within the MANSIDE project (memory alloys for new seismic isolation and dissipation devices) founded by the European Commission, an extensive study on SMAs has been performed where devices have been implemented and tested for passive control of different structural systems (Cardone et al., 1999 (a)(b), Dolce and Marnetto, 1999).

Results show that Shape-Memory Alloys (SMAs) possess several favorable characteristics for use as restrainers in bridges since they might be designed to undergo large strains and subsequently recover their initial configuration. The basis for this behaviour, as it will be discussed in the following section, is that, rather than deforming in the usual manner of metals, shape-memory alloys sustain a stress-induced transformation from the austenitic to the martensitic crystal phase (Hodgson, 1988). Combinations of SMAs, which are stable in one of the two states, are also adopted.

The most important feature of SMAs is, together with the simplicity of the functioning mechanism, their great versatility, which allows the designer to calibrate, according to any particular individual needed, the shape of the cyclic behaviour, from fully recentring to highly dissipating (Fig. 6-29(a)(b)(c)), by simply varying the number and/or characteristics of the SMA components (Dolce et al., 2000). Moreover, Dolce et al. (2000), whose researches fall within the MANSIDE project, pointed out that SMAs presents an extraordinary fatigue resistance under large strain cycles, long-term reliability (negligible relaxation effects of the pretensioned SMA wires), great durability (corrosion resistance and no degradation due to ageing), limited sensitivity to temperature, and substantial independence from the oscillation frequency.

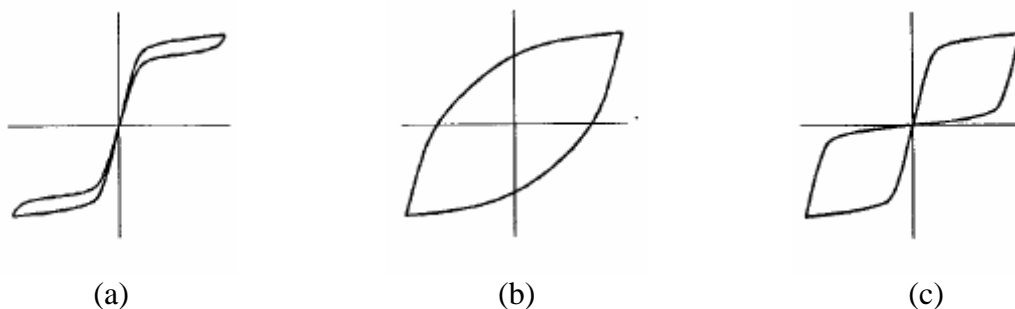


Fig. 6- 29: SMAs: (a) austenitic state (re-centring component), (b) martensitic state (dissipating component), (c) combination of re-centring and dissipating groups.

When designed to develop a double flag-shaped hysteresis loop, SMAs provide re-centring forces to restore the initial configuration of the system, good energy dissipation and high stiffness for small displacements to avoid deformations due to wind or braking loads. Furthermore, Nitinol (NiTi) shape memory alloys, as shown in Table 6-10, give other several advantages over typical structural steel elements, such as large elastic strain range, hysteretic damping, highly reliable energy dissipation (based on a repeatable solid state phase transformation), strain hardening at strains above 6%.

Property	Ni-Ti shape memory alloy	Steel
Recoverable elongation	8%	0.2%
Young's modulus	8.7E4 MPa (Austenite), 1.4-2.8E4 MPa (Martensite)	2.07x10 ⁵ MPa
Yield strength	200-700 MPa (Austenite), 70-140E4 MPa (Martensite)	248-517 MPa
Ultimate tensile strength	900 MPa (fully annealed), 2000 MPa (work hardened)	448-827 MPa
Elongation at failure	25-50% (fully annealed), 5-10% (work hardened)	20%
Corrosion performance	Excellent (similar to stainless steel)	Fair

Table 6-10: Comparison of NiTi SMA properties with typical structural steel.

6.3.6.1.1 Macroscopic Hysteretic Behaviour of the SMA

SMA's are binary or ternary metallic alloys that can be found in two different phases (for example NiTi (nickel-titanium), CuAlNi (copper-aluminum-nickel), CuZnAl (copper-zinc-aluminum)) austenite and martensite, capable of experiencing thermo-elastic solid transformations; each phase is stable at different thermo-mechanical states. Austenitic structure has a higher degree of symmetry and is stable at higher temperatures and lower stresses, while martensitic structure is generally met at lower temperatures and higher stresses. For some SMA's, such as Nitinol, the phase change can be stress-induced at room temperature if the alloy has the appropriate formulation and treatment. The austenitic phase of the material is stable before the application of stress. However, at a critical stress level the martensite becomes stable, yielding and showing a stress plateau, as shown in Fig. 6-30. At large strains the stiffness increases since they cause the martensite state to be loaded elastically.

From these peculiar features of SMA materials directly became (i) the *memory effect*, i.e. the aptitude to recover the initial shape by heating, and (ii) the *superelasticity*, i.e. the aptitude to recover the initial shape as soon as the external action is removed, important in engineering applications.

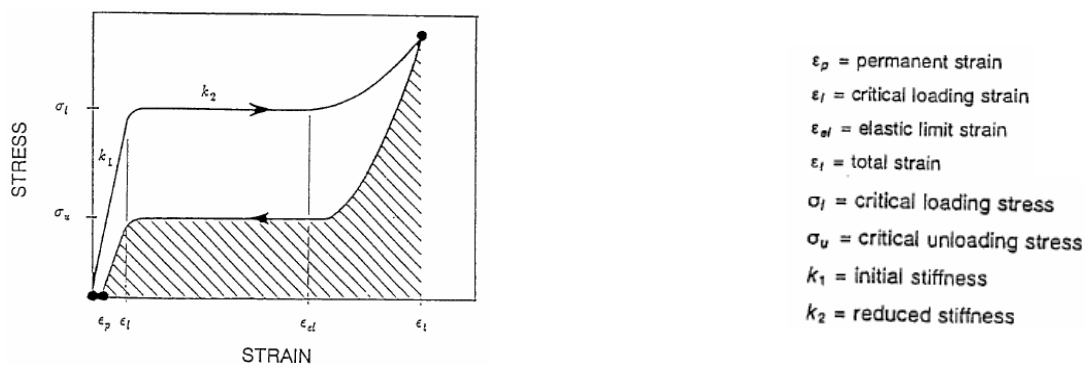


Fig. 6- 30: SMA's: stress-induced material state change.

6.3.6.1.2 Application and effectiveness of SMA restrainer to multi-span bridges

The use of the SMA restrainers in multi-span simply supported bridges at the hinges and abutments can provide an effective alternative to conventional restrainer systems: SMA's can be designed to provide sufficient stiffness and damping to limit the relative hinge displacement. Preliminary steps in the design of SMA are (i) the selection of the most suitable

alloy for the kernel components (elements where the phase change is stress induced or a combination of materials which are stable in the austenitic or martensitic state might be adopted), the selection of (ii) the shape of each component, and (iii) the range of stresses within they should work.

From the experimental performances of SMAs, Dolce et al. (2000) suggested that the optimal manner to provide self-centring capability require pre-tensioned (to get a rigid-linear behaviour) austenitic superelastic wires to be arranged in such a way as to be always stressed in tension (re-centring group), coupled with martensitic bars or austenitic superelastic wires to provide energy dissipation (dissipating group). Considering the limited workability of the material, kernel components for devices can only be drawn from wires (up to 2mm diameter), used only in the austenitic phase, or bars (up to 8mm and 50mm diameter for commercial and special production bars respectively), which might be employed in either the two states (Dolce et al., 2000).

The SMA devices may be connected from pier cap to the bottom flange of the girder beam in a manner similar to typical cable restrainers, as shown in Fig. 6- 31. The restrainers are typically used in a tension-only manner, with a thermal gap to limit the engaging of the restrainer during thermal cycles, or, if adequate lateral bracing is provided, can be designed to act in both tension and compression.

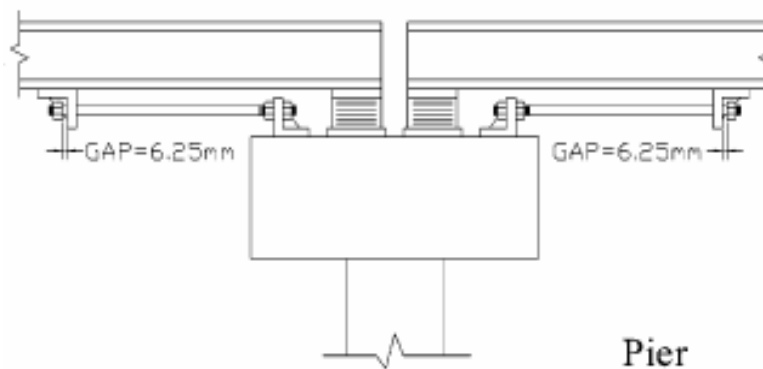


Fig. 6- 31: Configuration of shape memory alloy restrainer bar used in multi-span simply supported bridges.

DesRoches and Delemont (2002) investigated the effectiveness of the SMA restrainer bars through an analytical study of a multi-span simply supported bridge. Results shown that SMA restrainers reduce relative hinge displacements at the abutment much more effectively than conventional steel cable restrainers. The large elastic strain range of the SMAs allows them to undergo large deformations while remaining elastic and, due to their superelastic properties, they are able to maintain their effective stiffness for repeated cycles, differently with respect to conventional restrainer cables once yielded. Moreover, the increase stiffness at large strains, which induce the martensite material state to be loaded elastically, protects the deck against unseating.

Finally, evaluation of multi-span simply supported bridges subjected to near-field ground motions shown that the SMA restrainer bars are extremely effective for limiting the response of bridge decks. Instead, in conventional cable restrainers, large pulses induced by near-field records produced early yielding of such elements, thus reducing their effectiveness and resulting in large relative hinge displacements for the remainder of the response history.

6.3.6.2 The Energy Dissipating Restraint and The Friction Spring Seismic Damper

Self centring dampers, which make use, instead of the peculiar properties of the material as in the case of SMA, of particular geometric configuration, in order to obtain the required restoring forces, have been also developed. Among these, for bridge applications, might be mentioned the Energy Dissipating Restraint (EDR) and the SHAPIA seismic damper.

The first, developed and tested by the Fluor Daniel, Inc., consists of an external cylinder with an internal spring with bronze friction wedges (Fig. 6-32). When the spring reaches the stop that is located at the end of the range of motion normal forces develops and the energy dissipation is provided by the friction force that develops. The spring then provide the required restoring force. A full description of the EDR mechanical behaviour and detailed diagrams of the device are given by Nims (1993).

The SHAPIA seismic damper, also known as friction spring damper, uses a ring spring to dissipate earthquake-induced energy (Kar and Rainer 1995, 1996; Kar et al. 1996). A section through a typical ring spring assembly consists of outer and inner rings that have tapered mating surfaces. As the spring column is loaded in compression, the axial displacement is accompanied by sliding of the rings on the conical friction surfaces: the outer rings are subjected to circumferential tension (hoop stress), and the inner rings experience compression. The force-displacement response of SHAPIA Dampers has been further investigated by Filiatrault et al. (2000).

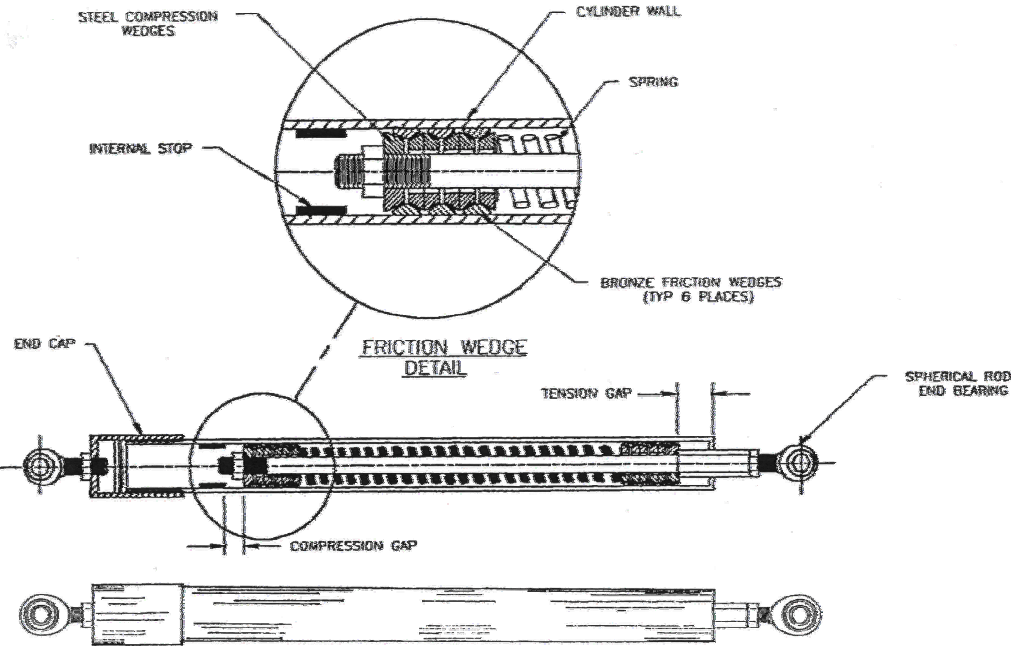


Fig. 6- 32.External and internal views of the EDR, Nims et al. (1993).

6.3.7 Electro and Magnetorheological Dampers

Magneto-Rheological Dampers (MRDs) typically consist of hydraulic cylinders containing micron-sized magnetically polarizable particles suspended within a fluid. With a strong magnetic field, the particles polarize and offer an increased resistance to flow. Varying the magnetic field strength has the effect of changing the apparent viscosity of the MR fluid. The term “apparent viscosity” is used since the carrier fluid exhibits no change in viscosity as the magnetic field strength is varied. Upon exposure to a magnetic field, the MR fluid as a whole will appear to have undergone a change in viscosity. They may be used within a semi-

active system (as discussed in section 6.4) by varying the magnetic field, the mechanical behaviour of the MRD can be modulated from a viscous fluid to a yielding solid within millisecond and the resulting damping force can be considerably large with a low-power supply. Magneto-rheological Damper hysteretic behaviour is nonlinear, and can be represented by various hysteresis models, as proposed by Bingham (in Shames and Cozzarelli, 1992), Spencer et al. (1997), Bouc, (1967), Wen, (1976), etc.

Electro-Rheological Dampers (ERDs) are the electric analogue ones. ER fluid contains micro-sized dielectric particles and their behaviour can be controlled by subjecting the fluid to an electric field.

Magneto-rheological fluids are an alternative solution to electro-rheological ones when very compact devices are needed, as the rheological behaviour is similar to the ER-fluids but with higher yield stresses. In the case of steady fully developed flow, the shear resistance of MR/ER fluids may be modeled as having a friction component augmented by a Newtonian viscosity component.

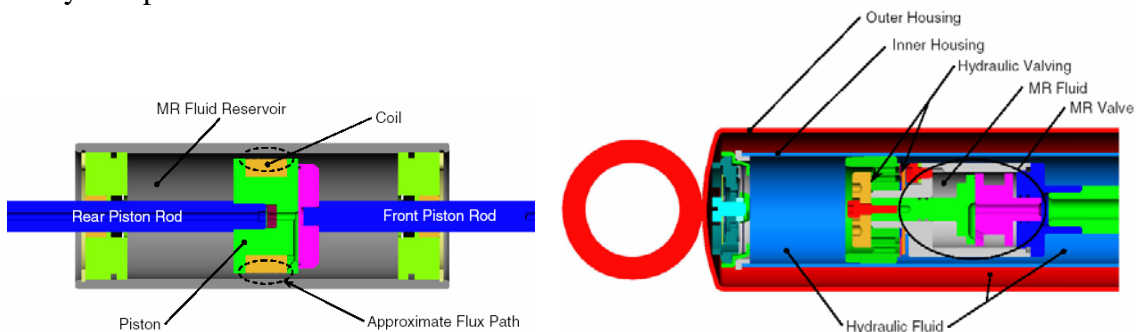


Fig. 6-33: Double-ended MR damper (left) and MR piloted hydraulic damper (right). (Figure available electronically on *fib* website; see production note on p. ii)

(Figure available electronically on *fib* website; see production note on p. ii)

Among the MR devices have to be mentioned the Monotube and the Twin-Tube Dampers, and also the double-ended MR damper (Fig. 6-33, left) and the MR piloted hydraulic dampers (Fig. 6-33, right) (Casarotti, (2004)).

6.3.8 Electro-inductive devices

Principles of operation of the electro-inductive devices are: (i) the generation of electrical power from seismic vibration as a primary energy source for the device mechanical input (passive and semi-active devices); (ii) the regulation of the sign and of the amount of the instantaneous power flow exchanged between earthquake and device in order to achieve a real time control of the vibration modes of the structure to be protected (when designed as active devices).

Two possible working schemes are addressed by Marioni (2002): a linear dissipator (Fig. 6-34, left), basically composed by two plates with permanent magnets and an inner plate of conductive non magnetic material moving between the previous two; and a rotating system (Fig. 6-34) where the linear earthquake motion is converted into a rotational one through a screw: the advantage of this solution is the possibility of amplifying the relative velocity by a suitable selection of the ratio between linear and rotational motion.

Advantages of these devices are low maintenance, no ageing effects, no limitations on life cycles, low scattering of the response and no temperature sensitivity. Whilst passive energy dissipating systems have inherent limitations such as they are generally tuned to the first vibration mode, active ER dampers can be effective over a much wider range of frequencies.

The electro-inductive dissipators can be compared to the viscous dampers, due to their capability of providing both viscous and friction-type forces. The damping force developed

by ER Damper depends on physical properties of the used fluid, on the pattern of flow in the damper and on its size. When an electric field is applied, the behaviour of the ER fluid is nearly viscoplastic, and the shear stress in it has to exceed the developed ‘yield’ stress to initiate flow. This mechanism is responsible for their controllable viscoplastic behaviour. The force produced by a linear viscous fluid device, is proportional to the velocity of the piston in the fluid, up to a limiting frequency, beyond which the device becomes viscoelastic; the resulting damping force $f_{ER}(t)$ in the ER damper is given in eq. (6-57):

$$f_{ER}(t) = C_d \dot{x}(t) + F \text{sign}[\dot{x}(t)] \quad (6-57)$$

where C_d is the viscous characteristic of the viscous ERD, x is the displacement at the damper location and F is the controllable yield force.



Fig. 6- 34: ER Dampers: linear (left) and rotating (right) working schemes (Marioni, 2002).
(Figure available electronically on fib website; see production note on p. ii)

6.4 Active and semi-active control systems

Active, semi-active as well as hybrid control systems represents an innovative and appealing alternative with respect to passive systems. As discussed in section 6.2 active systems utilize actuators to apply forces to the controlled structures, and thus their effectiveness is limited under large earthquakes due to the greatly increased energy requirement as the vibration disturbance becomes larger (Kurata et al. 2002). Such limitation might be overcome by semi-active devices that require only power to operate calculators and small electric devices for modifying their mechanical properties. Semi-active systems combine the reliability and much easier maintenance of passive systems with the adaptability of active devices (Symans and Kelly, 1998). Moreover, incorporate semi-active systems into an isolation system, thus defining a semi-active hybrid system, seems to be favorable against the adoption of passive dampers, since they may provide a reduction of the bearing displacements without further increase in forces and pier drifts (Saharabudhe and Nagarajaiah, 2005). For the above-mentioned reasons, international societies have recognized semi-active control as a structural control system that can deal with large earthquakes.

Several kind of devices might be implemented within semi-active control strategies, such as MR (Saharabudhe and Nagarajaiah, 2005; Spencer, 2001; Abe et al. 2000; Dyke and Spencer, 1996) and ER (Symans, 1997; Makris, 1997; Makris et al., 1996) controllable fluid dampers, friction dampers (with a variable friction force) (Yang et al., 1994) and variable hydraulic dampers (where the movement of the fluid is controlled through an orifice) (Jung et

al., 2004; Kurata et al., 1999). Although several theoretical and experimental studies have been carried out on all these typologies, only the latter has been used in real applications, as in the case of the Walnut Creek Bridge (USA) (Patten et al. 1999).

6.4.1 Optimal force control

The force control strategy has the main objective to calibrate the force generated in the semi-active dampers as the response of the system changes.

Only the damper force, F_d due to the yielding shear stress in fluids can be controlled through the change in the applied electric or magnetic field.

The concept of the clipped Optimal force control is the following (Ribakov and Gluck, 2002): when the j^{th} damper is providing the desirable optimal force, the voltage applied to the damper should remain at the present value; if the magnitude of the force produced by the j^{th} damper is smaller than the magnitude of the desired optimal force, and the two forces have the same sign, the voltage applied to the damper has to be increased; otherwise it has to be set to zero.

6.4.2 Optimal displacement control

The displacement control strategy, since the optimal displacement vector cannot be directly controlled, acts on the damper force F_d in order that the measured displacement vector traces the optimal displacement vector as close as possible.

The concept is the following (Xu et al., 2000): when the j^{th} damper displacement is approaching the desirable optimal value, the friction force in the damper should be set to its minimum value so as to let the damper reach its optimal displacement as soon as possible. When the j^{th} damper moves in opposite direction to the optimal displacement, the friction force F_{dj} in the damper should be set to its maximum value (or to the j^{th} damper force if smaller, otherwise it stops moving and no vibration energy can be dissipated) so as to prevent the damper motion away from the optimal target at most.

6.5 Design concepts and analysis of deck – isolated bridges

6.5.1 Analysis concepts

The structural behaviour of isolated bridges cannot be easily predicted since several factors, as for example axial force levels, large displacements, and temperature, might significantly affect the dynamic response of the isolators. Thus, modeling of this kind of elements might not be an easy task and a progressive refinement of the structural model should be adopted in order to simplify the design process.

A static linear SDOF analysis, instead of a non-linear dynamic one, can be adopted in a preliminary design phase or in the case of bridges with a regular geometric layout and a regular mass distribution. In these cases, the coupling effect of the deck can be neglected and the design of each bent will be independent from the others.

The single bent will be modeled as a SDOF system with an appropriate tributary mass, effective global stiffness and effective global damping. The SDOF parameters can be defined by:

- Effective global stiffness:

$$K_g = \frac{1}{1/K_{py} + 1/K_{DE}} \quad (6-58)$$

where K_{py} is the secant stiffness at yielding of the pier and K_{DE} is the secant stiffness at the expected maximum displacement (displacement demand on the isolator) of the isolation system;

- Effective global damping:

In the case of isolation systems with essentially linear response and viscous dampers as dissipative devices:

$$\xi_g = \frac{\Delta_p \xi_p + \Delta_D \xi_{DV}}{\Delta_p + \Delta_D} \quad (6-59)$$

where ξ_p is the equivalent viscous damping of the soil-foundation-pier system, ξ_{DV} is the viscous damping provided by the device and Δ_p, Δ_D are respectively the displacement of the pier, and the displacement of the isolation system.

In the case of isolation systems with essentially hysteretic energy dissipation, the term ξ_{DV} has to be replaced by the effective damping equivalent to the dissipated hysteretic energy (ξ_{DE}):

$$\xi_{DE} = \frac{2(1 - 1/\mu_G)}{\pi} \quad (6-60)$$

where the effective global ductility of the soil-pier-isolation system can be obtained by:

$$\mu_G = 1 + (\mu_D - 1) \frac{\Delta_{DE}}{\Delta_S + \Delta_{DE}} \quad (6-61)$$

Eq. (6-61), where Δ_{DE} represents the elastic deformation of the isolation system, shows that the damper ductility (μ_D) will be reduced by the additional flexibility of the soil-pier system (Δ_S).

In the case of bridges with irregular height of the piers and deck-mass distribution, with the assumption of having a rigid deformation of the deck, might be also represented at this design stage by means of a SDOF model.

The procedure (Calvi and Pavese, 1997), according to a displacement-based strategy, can be described in the following steps:

- The design displacement (Δ_e) will be decided, and it will apply to all piers and abutments.
- The yielding displacement of each pier will be calculated. Assuming a single-bending moment connection:

$$\Delta_{Py,i} = \frac{\Phi_{Py,i} H_i^2}{3} \quad (6-62)$$

where $\Phi_{py,i}$ is the yield rotation (which may be estimated from approximate relations (Priestley et al., 1996)) and H_i is the height of the i -th pier;

- Define the effective displacement of each isolator ($\Delta_{DE,i}$), assuming, according with capacity design principles (as it will be explained in section 6.5.2), that the force in each isolator at the expected displacement will be 85% of the yield force of the pier:

$$\Delta_{DE,i} = \Delta_e - 0.85\Delta_{Py,i} \quad (6-63)$$

- The ductility demand desired for the isolators at the effective displacement (μ_{DE}) will be decided, by applying an appropriate factor to the isolator ductility capacity, to avoid collapse in the case of an extreme seismic event. Then the yield displacement ($\mu_{Dy,i}$) of each device can be calculated:

$$\Delta_{Dy,i} = \Delta_{DE} / \mu_{DE} \quad (6-64)$$

- The effective ductility demand of each foundation-pier-isolation system will be calculated as:

$$\mu_{E,i} = \frac{\Delta_e}{\Delta_{Dy,i} + \Delta_{Py,i}} \quad (6-65)$$

- The corresponding effective damping (ξ_i) will be calculated according to eq. (6-60) or alternatively from an appropriate $\mu - \xi$ curve.
- Estimate the global effective damping of the bridge through the weighted average of the different damping ratios:

$$\xi_b = \frac{\sum M_i \xi_i}{M_d} \quad (6-66)$$

Where M_i is the tributary mass of each pier and M_d is the total mass of the deck.

- Knowing the design displacement and equivalent damping, the period (T_b) of the equivalent SDOF model might be determined from the design spectrum, and the equivalent stiffness of the bridge evaluated (K_b).
- Assuming proportionality between stiffness and tributary mass, the stiffness of each foundation-pier-isolation system might be computed:

$$K_i = \frac{M_i K_b}{M_d} \quad (6-67)$$

- Finally, the design forces for each pier can be obtained by multiplying stiffness by displacement. Might be observed as the design of the pier reinforcement will result, since the higher bending moments demand, in larger reinforcement percentage in taller piers, in opposition of what usually happens for non-isolated bridges.
The displacement-based design procedure could be refined accounting for the flexibility of the deck and restraint conditions at the abutments following a procedure in all analogous to the one reported in section 6.7.2.

A non-linear dynamic analysis is always recommended after the preliminary design phase, mainly in order to refine the accuracy in modeling the isolators' response. The MDOF model should be progressively refined according to the design earthquake intensity. For the maximum credible earthquake, the deck-isolated bridge should be modeled considering in a more refined way:

- I/D devices: it is more appropriate to use at least a tri-linear spring model (instead of a linear equivalent highly damped element), with the third branch to simulate a possible strain hardening (that can develop for example using steel dampers) or the simulation of displacement-limiting devices;
- Piers: in the case of a large-than-expected earthquake also the piers could have to sustain a plastic deformation with the ductility demand that could soon become excessive, and thus a more refined bi-linear model should be used (a value of 2% should be adopted for the equivalent viscous damping ratio). In order to evaluate the non-linear behaviour of the piers in the last version of the AASHTO recommendations (1999) response modification factors (R-factors) are proposed for the substructure of seismically isolated bridges to calculate the design forces in the piers from the demand obtained with the assumption that they behaves within the elastic range. Might be underlined that the proposed R-factors differs from those adopted for non-isolated bridges, because numerical analysis results show that the displacement ductility demand in the piers is higher in isolated bridges with respect to non-isolated systems if they are designed for the same response modification factor.

It is also important to account for the actual mass distribution along the pier height in order to consider a possible amplification of the higher modes components associated with the response of the pier alone, possible when the lower-frequency modes involving the deck mass are isolated;

- Deck: modeled as linear beam elements, with a proper mass distribution;
- A linear model of the soil response is adequate in most cases.

When the reinforcement of the piers of a bridge is already given, for example, when it is required to design the retrofit of a bridge, or when it is desired to keep the reinforcement obtained from non-seismic constraints, it will be difficult to design the isolation system to obtain a regular response as in the previous case. Since the strength of the piers will be known, the strength of the isolators at design response could be set at 85% the strength of the correspondent pier. An other possible choice is to design the isolators using the strength of the weakest pier as reference (Calvi and Pavese 1997). In both cases, the coupling effect of the deck could be important and a time-history analysis is fundamental to check the design.

6.5.2 Basics of capacity design

The main design objective in a deck-isolated bridge is to concentrate most of the damage in the I/D devices thus preventing damage of the remaining part of the structure, whose

response is therefore principally linear elastic with some possible damage localized at movement's joints due to large structural displacements.

The design procedure for such structures will follow the same general Capacity Design (CD) principles. The protection factor to be applied depends on the reliability of the mechanical characteristics of the isolation system: in most cases it is required that the actual strength of an I/D device does not differ by more than 10% from its design strength. Then, requiring that the strength of the device at the expected displacement be equal to 85% of the design nominal strength of the pier, we will obtain a protection factor against the pier yielding.

The CD principles still have to be applied, although it will no longer be necessary to ensure that column shear strength exceeds column flexural strength. Therefore, it is required only to assure an adequate inelastic rotational capacity at the pier base. According to basic CD principles, the estimate flexural strength M_n , reduced by a reduction factor Φ_f has to be larger than the required strength M_r (according to eq. (6-68)). Capacity protection factors have also to be applied to the strengths of supports, connections and abutments.

$$\Phi_f M_n \geq M_r \quad (6-68)$$

6.5.3 Considerations on input characteristics

Local seismicity aspects, mainly due to different soil conditions rather than source mechanisms, are significant in the design of non-isolated bridges and represent a crucial aspect in case of an isolated system. In fact, the frequency content of the expected ground motion can be of the utmost importance in the case of isolated bridges, particularly if a period shift rather than adding damping is considered as the design objective. If the possibility of different spectra, characterized by high displacement response at longer periods (induced by soft soil conditions), cannot be excluded, an artificial period elongation could result in a catastrophic situation.

Moreover, near-field ground motions (characterized by high frequency spike and low-frequency, low-acceleration pulses) include large pulses that may greatly amplify the dynamic response of long period structures, particularly if structures deform in the inelastic range. In recent years, several seismologists have doubted that base-isolated structures are vulnerable to large pulse-like ground motions generated at near-fault locations. Makris and Chang (2000), observing that near source ground motions are particularly destructive to some structure because not of their PGA, but of their 'incremental' ground velocity, sustained that seismic isolation could be effective against near-source ground motions provided that the appropriate energy dissipation mechanism is assured. Lee and Kawashima (2004) analyzed the effectiveness of supplementary dampers to mitigate the large deck displacement in case of strong near-field motion and the correspondent inelastic demand in the piers, residual displacement and also to prevent from unseating that it might produce. The response of both active control devices (MRDs are considered) and passive systems (VDs are considered) are evaluated and compared in the paper. They had shown that the effectiveness is nearly the same with both the supplementary dampers typologies, which satisfactorily reduce the deck displacement, as well as the pier displacement ductility, demand. Moreover, this research highlighted that the magnitude of the damper force required for control depends on the characteristic of seismic excitation, and thus the designer has to pay attention on the type of ground motion to maintain the stability of the control.

A detailed analysis of the expected seismic motion is therefore of fundamental importance in the design of isolated bridges.

6.6 Foundation rocking and pier base isolation

6.6.1 Basics of foundation rocking

It has been observed after several earthquakes that a number of structures had responded to seismic excitation by rocking on their foundation, and, in some cases, this enabled them to avoid failure. Such behaviour will occur principally in structures like elevated water or storage tanks, characterized by large masses at some distance from the ground and comparatively narrow bases. In these slender structures the overturning moment at the base will govern the response and, if rocking is possible, it can be limited to the moment needed to lift the weight of the structure against the stabilizing moment due to gravity, thus reducing the magnitude of the internal forces and the deformation demand throughout the structure. For these reasons the rocking mechanism will often be considered as a satisfactory response in assessment of existing bridges or useful as an alternative approach in the design of new ones, where geometry, mass distribution and foundation characteristics could favor a controlled rocking response in the transverse direction, according to the capacity of the superstructure to accommodate such movements.

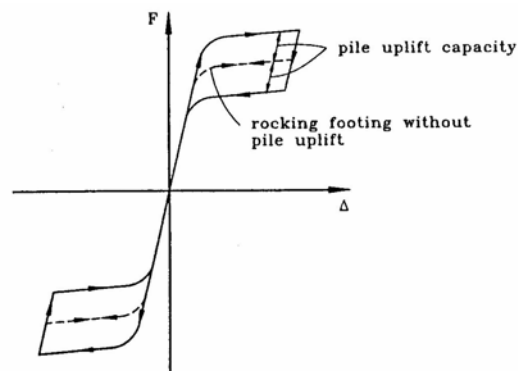


Fig. 6- 35: Rocking response of a footing with uplifting piles.

The seismic response of a rocking bridge is similar with that of a bridge isolated by FPS, because it follows the same inverted pendulum concept. The correspondent hysteretic behaviour will be approximately rigid-plastic with a substantial re-centering force given by the uplift force itself. Rocking, either of spread footings or pile-supported footings without tension connections between piles and footings, will result in an approximately non-linear elastic behaviour; instead when tension connection between the piles and footings is assessed to be competent (analyses may show that pile uplift is expected under the column plastic moment capacity) an additional lateral strength, due to the pile tension capacity, and an additional damping, due to the Coulomb friction associated with pile friction, will develop (Fig. 6-35).

6.6.2 Soil – Structure Interaction (SSI)

Soil-structure interaction can have the same qualitative effect as base isolation on the bridge response. Rocking and uplifting of foundations, as described above, is only one aspect of soil structure interaction; other non linear effects may also take place such as sliding of the foundation. Sliding bounds the forces transmitted to the superstructure, to a value equal to the

dead weight times the friction coefficient, but its counterpart is the occurrence of permanent displacements. Provided permanent displacements can be accommodated and the coefficient of friction is well controlled, sliding may be an efficient and attractive base isolation system.

These two examples of soil-structure interaction involve non linear effects that may be difficult to analyze and to keep under control; however, even linear soil structure interaction can substantially modify the response, with respect to a fixed base analysis, and have a beneficial effect. The translational and/or rotational flexibilities of the supporting soil lengthen the periods of vibration of the foundation and move them towards regions of smaller spectral accelerations. This statement is clearly related to the standard, smoothed, shape of code spectra, which almost invariably possess a gently descending branch beyond a constant spectral acceleration plateau. However, there is evidence that, for structures founded on unusual soils, soil-structure interaction may increase the response and makes the structure more vulnerable. Examples of such cases are given by Gazetas and Mylonakis (1998) for instance.

6.6.3 Pier base isolation

Seismic isolation at the base of the piers has rarely found application in real cases. Although, one example of such design procedure is represented by the Benten Viaduct, one of the bridges of Hanshin Expressway route 3 in Japan. The 19-span bridge has been damaged after the Hanshin/Awaji earthquake (January 1995), and reconstructed adopting continuous rigid-frame configuration with seismic isolators installed underneath the steel piers (Yoshikawa et al., 2000). Whilst the rigid pier-deck connections prevent bridges from falling down, the isolation devices reduce the force demand on piles, with respect to rigid or hinged connection, thus avoiding additional reinforcement. LRB have been used in this case.

6.7 Controlled rocking of piers and built-in isolators

6.7.1 Controlled rocking of combined concrete members

In order to design (or assess) a rocking bridge a substitute structure design method can be followed, assuming, similar to the case with isolation devices, that the response will depend only on the equivalent elastic characteristics (period and damping) at peak response.

The entire structure can be analyzed, in a preliminary phase, considering separately each single bridge bent modeled as a rigid SDOF oscillator with constant damping and period of vibration proportional to the amplitude of rocking. In fact, the period of vibration of the rocking response will increase with displacement amplitude and thus a trial-and-error design procedure has to be performed.

This design procedure takes its basic principles on the rocking mechanism of a rigid block and it is characterized by the following main steps:

- Definition of weights: at the deck level will act the seismic weight W_s and at the footing level the total weight W (which includes also the weight of the pier, not included in the seismic weight and the footing weight);

The foundation could be modeled as a rigid block and at the soil-footing interface can be assumed to develop a rigid perfectly plastic pressure distribution in compression and tension (pc, pt); this results in a rectangular stress block (Fig. 6-36) with width a in the compression zone given by the following equation:

$$a = \frac{BLp_t + W}{B(p_c + p_t)} \quad (6-69)$$

where B is the footing width, L is the footing length and W is the total weight at the footing level.

- The magnitude of the lateral overturning force corresponding to the total displacement Δ (that includes also the structural displacement, for slender piers), can be evaluated, from the moment equilibrium, with the following equation:

$$V_E(\Delta) = \frac{R_t L / 2 + W(L - a) / 2 - W_s \Delta}{H + \Delta_r (L - a) / 2H} \quad (6-70)$$

where R_t tension force acting at the soil-footing interface and H is the distance between the center of the seismic weight (W_s) and bottom of the footing.

Simplifications may occur in the above relationship:

- if the pier is stiff the structural component Δ_c of the total displacement Δ can be neglected: $\Delta_c \cong 0 \rightarrow \Delta \equiv \Delta_r$;
- if the pier is tall might be assumed that the displacement due to the rocking motion Δ_r is given by: $\Delta_r (L - a) / 2H \cong 0$;
- or, when no tension occurs at the footing level: $R_t \cong 0$;

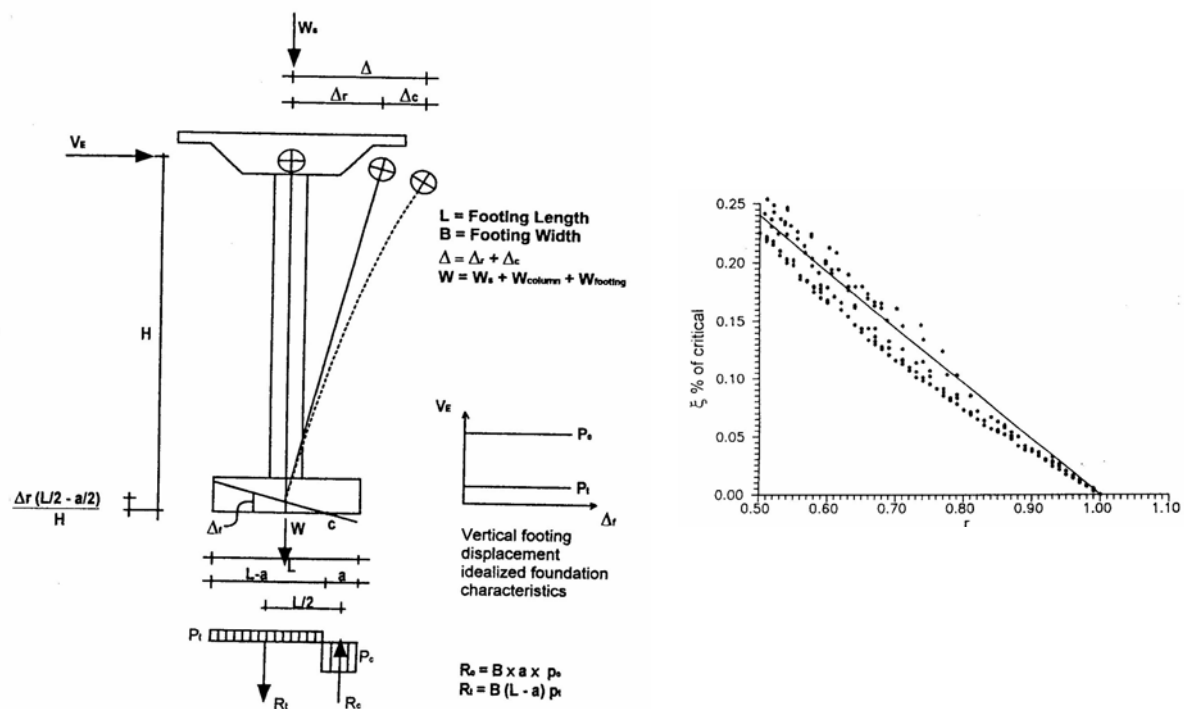


Fig. 6-36: Rocking mechanism of a single pier (left) and approximate relationship equivalent viscous damping – energy reduction factor (right).

- The effective stiffness of the rocking pier, if the single bent rocking mechanism is more likely to develop, can be defined by:

$$k_{pier} = V_E(\Delta) / \Delta \quad (6-71)$$

where $V_E(\Delta)$ is provided by eq. (6-64).

- Instead, when a stiff superstructure connects several bents, rocking of the whole structure will occur and the effective stiffness for n bents can be combined, considering the lateral overturning force of each bent $V_{E,n}$, to an effective frame stiffness of the bridge:

$$k_{frame} = \sum_n V_{E,n} / \Delta \quad (6-72)$$

- Accounting for the tributary seismic weight of each bent $W_{s,n}$, the characteristic rocking period of the whole bridge will be:

$$T = 2\pi \left(\sum_n \frac{W_{s,n}}{gk_{frame}} \right)^{0.5} \quad (6-73)$$

- Energy dissipation: in the foundation rocking mechanism of a rigid block, an important role is played by the energy dissipation, in the form of radiation to the soil half space, which could develop because of the block-soil collisions, if these are assumed purely inelastic impacts. This phenomenon, expressed through the kinetic energy reduction factor r (obtained by equating momentum before and after the impact) leads to a progressive reduction of the peak displacement amplitude (expressed as a dimensionless quantity Δ_n , equal to the actual displacement divided by the width of the foundation) as the number of impacts n increases. The peak nondimensional displacement after n impacts (Δ_n) is predicted as a function of the nondimensional initial displacement (Δ_0) by:

$$\Delta_n = 1 - \left\{ 1 - r^n \left[1 - (1 - \Delta_0)^2 \right] \right\}^{0.5} \quad (6-74)$$

Then, considering that the equivalent viscous damping ξ of a SDOF oscillator is related to the relative amplitude of different displacement peaks after m complete cycles by the expression:

$$\xi = \frac{\ln(\Delta_0 / \Delta_n)}{2\pi m} \quad (6-75)$$

and considering that in the rocking response there are two impacts per cycle the equivalent damping ratio of a rigid rocking system can be found. Under the hypothesis of $\Delta_0 < 0.5$ and $n = 2m < 16$ this relation is rather insensitive to the value of the initial displacement and the number of cycles, and a linear expression can be used ((6-76), Fig. 6-36 (right)):

$$\xi = 48(1-r) \quad (6-76)$$

In the case of bridge structures a simplified expression, neglecting the contribution of pier and foundation mass and assuming deck width larger than the deck height in the computation of the mass moment of inertia, r can be evaluated through the following equation:

$$r = \left(1 - \frac{R^2(1 - \cos(2\alpha))}{R^2 + b^2/12} \right)^2 \quad (6-77)$$

where R is the distance between the mass centroid and the center of rotation, α is the angle between a vertical line and the line connecting the mass centroid and the center of rotation and b and h are the width and height of the deck.

The definition of the amount of damping involved in the rocking phenomenon is one of the most important issues regarding the rocking mechanism; here only the soil radiation damping contribution is considered, but also the amount due to hysteretic response of dampers can be introduced in those cases where these kinds of devices are used.

Based on these basic principles a response spectra design approach for rocking bridges can be pursued, following these steps:

1. Model a bridge bent as a rigid SDOF oscillator with constant damping and period of vibration proportional to the amplitude of rocking, using equivalent values at peak response;
2. Use the initial no-rocking period and damping ratio to evaluate if the elastic response acceleration will induce rocking;
3. compute the kinetic reduction factor r and then the equivalent damping ratio ξ of the rocking response through the eq. (6-76);
4. Assign a displacement Δ_1 , calculate $V_E(\Delta_1)$ through the eq. (6-70) and the correspondent period of vibration T_1 ;
5. Calculate from the displacement response spectrum a new displacement $\Delta_2 = S_d(T_1, \xi)$;
6. Iterate until convergence of a couple of values of period and displacement. In order to achieve a stable response, the use of linearly increasing displacement response spectra should be avoided, which also does not correspond to reality;
7. Design the structure to behave linearly until rocking takes place and to be able to accommodate the expected displacement;
8. Time-history analyses are finally recommended to check the design (or assessment) of the rocking bridge since all the simplified expressions used in this procedure can be considered adequate only for a preliminary design.

6.7.2 Response of partially prestressed coupled members

Unbounded post-tensioning techniques might be used where segmented piers are adopted or as a useful alternative in the design of rocking bridges creating jointed ductile connections at pier-foundation or pier-deck interface. They will accommodate the inelastic demand within the connection itself and maintain the structure in the elastic domain, thus limiting the damage to pier elements achieving the maximum target displacement. The same approach might be

used also in the case of segmented piers, creating ductile connections at every connection between two pier segments.

This kind of connections are usually defined by a prestressed elastic anchorage or bar/tendon and eventually an energy dissipation devices (typically mild steel reinforcement added at critical sections to the unbounded post-tensioned elements): the restrainers will provide a smaller rotation (i.e. a reduced value of the kinetic reduction factor r) preventing the toppling of small slender rocking blocks, and the dissipative element will increase the energy dissipation capacity of the system.

The combination of such elements (called *controlled rocking systems* or *hybrid rocking systems*) will lead to a flag-shaped hysteresis loop, which properties can be calibrated by changing the design parameters of each element, such as the magnitude of the post-tensioning load in the unbounded members or the additional strength provided by the mild steel bars. The main design parameter that will govern the design of these connections is the ratio λ between the resisting moment provided by the axial load components (the weight component M_N and the contribution due to the post-tensioning load M_{pt}) and the moment M_s provided by the mild steel elements.

$$\lambda = \frac{M_{pt} + M_N}{M_s} \quad (6-78)$$

As this latter contribute became larger the global response will approximate the elasto-plastic behaviour, resulting in an higher energy dissipation but loosing its re-centering properties; instead, as λ increases the response will approach the non-linear elastic behaviour with any dissipation properties but providing full re-centering of the system.

Several analytical and experimental studies have been performed in order to evaluate the response of hybrid foundation rocking systems (Palermo, 2004), in terms of their moment-rotation relationship and their efficiency and potentiality as an alternative solution in the seismic design of bridges. They have pointed out not only the primary role of the parameter λ in their design procedure, but also, as in the case of reinforced concrete sections (Priestley and Kowalsky, 1998), the invariance of the yielding curvature with mechanical parameter. Consequently, the definition of a coefficient K_{θ_y} , constant with respect to structural and sectional parameters, is occurred for every section profile:

$$K_{\theta_y} = \frac{\vartheta_y h}{\varepsilon_{sy} L} \quad (6-79)$$

where θ_y is the yielding rotation, ε_{sy} the yielding strain of the mild steel, h the height of the section and L the height of the pier. Through the comparison of the performance of controlled rocking designed bridges and monolithic systems under static cyclic forces as well as time-history records, it has been found that, independently from the regularity of the bridge configuration (pier heights), deck stiffness and abutment restrain conditions, the use of these hybrid systems can lead to significant improvements of the bridge response. In fact, the added re-centering capability can reduce the amount of the residual drift and also produce a more symmetrical hysteresis loop, with respect to what we may have if plastic hinges will develop at the piers base, with a better employment of the material properties.

These studies have defined also that the most effective approach in the design of controlled rocking connections will be to have a uniform distribution of λ among all the piers,

with magnitude of about 1.5: in this way full re-centering properties can be combined with a significant energy dissipation in the most effective way (Fig. 6-37).

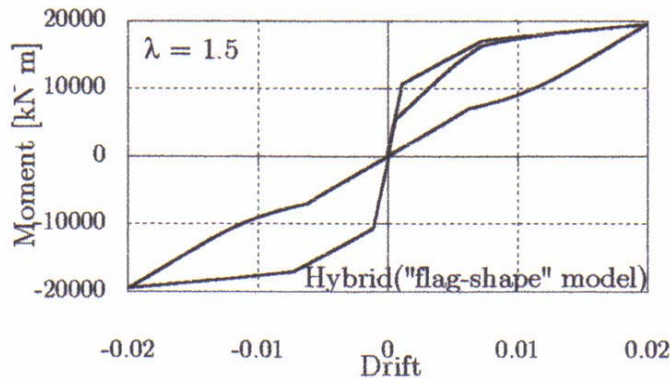


Fig. 6-37: Optimal Flag-Shaped hysteresis loop.

Controlled rocking bridges can be designed, according to a direct-displacement-based design approach, adopting the following procedure:

1. Assume a parabolic displacement shape as a first trial solution for the bridge transverse response (constant, instead, in the longitudinal direction);
2. Identify the target design displacement that any pier can exceed;
3. Compute the equivalent SDOF system parameters, knowing the tributary mass (m_i) and the design displacement (Δ_i) at each bent (i.e., pier) location:

$$\Delta_{eq} = \frac{\sum m_i \Delta_i^2}{\sum m_i \Delta_i} \quad (6-80)$$

$$M_{eq} = \frac{\sum m_i \Delta_i}{\Delta_{eq}} \quad (6-81)$$

4. Evaluate the equivalent hysteretic damping ratio of each individual pier member adopting damping-ductility relationships available in literature (e.g. proposed in Priestley, 2002). Moreover, Palermo (2004) proposed equations where also the hybrid system properties (identified through the parameter λ) are accounted for.
5. Compute the equivalent damping ratio of the entire bridge (ξ_{eq}), weighting each pier contribution (ξ_i) in proportion to the pier base shear V_i , which is evaluated with an iterative procedure (Priestley and Calvi, 2003):

$$\xi_{eq} = \frac{\sum V_i \xi_i}{\sum V_i} \quad (6-82)$$

6. Find, from the displacement response spectrum the equivalent period of vibration, and the correspondent stiffness of the SDOF system. The total base shear then will be:

$$V_{eq} = K_{eq} \Delta_{eq} \quad (6-83)$$

7. Distribute the base shear among the different piers, and perform a static analysis of the structure under this static lateral force pattern:

$$F_i = \left(\frac{m_i \Delta_i}{\sum m_i \Delta_i} \right) V_{eq} \quad (6-84)$$

8. Evaluate the deformed shaped and the pier base shear obtained in the static analysis and iterate until convergence of the maximum displacement to the target one.

6.7.3 Design and analysis of segmented piers

The use of precast segmental construction for concrete bridges represents an attractive design approach in order to increase the seismic performance, thus reducing repair interventions to the minimum, also shortening construction periods with respect to conventional R.C. designs.

Unbonded post-tensioned precast concrete segmental bridge piers are constructed by stacking precast segments one on top of the other and then connecting the assembly structurally with vertical post-tensioned prestressing tendons passing through ducts located in the precast segments. The tendons are anchored at the foundation below the column and in the bent cap at the column top.

When displaced laterally, a wide flexural crack forms at the interface between the base of the precast column and the foundation, and the pier rotates rigidly about its compression toe. Moreover, since the tendon is unbonded (thus, the incremental strain is distributed along the whole tendon), the column can be fully restored to the undeformed position if the initial prestress level has been carefully selected. Special detailing, transverse spiral reinforcement or a steel shell, are required to confine the concrete in the plastic end region (pier base) where large compression strains might develop as the column rigidly rotates about its base.

Experimental tests (Hewes and Priestley, 2001) shown that such economic and efficient design method, enhance the capability of the column to sustain earthquake-induced deformations, reducing the overall damage in the column and providing a stable response under cyclic loading, avoiding significant residual drifts. Damage, in the forms of spalling of cover concrete and concrete crushing, is minimal and limited to the region near the compression toe of the pier. Moreover, no residual cracks in the column will develop, and footing damage resulting from strain penetration of longitudinal bars into the footing, typical of R.C. columns, will not be present. Experimental tests, where circular piers with different aspect ratio (H/D), variable amount of confinement (thickness of the steel shell) and different levels of initial prestress have been considered, shown that for moderate design drifts and low tendons prestress force, a relatively low level of confinement (transversal steel ratio of the order of 1.9%) may be sufficient. Instead, for higher design drift or prestress force, an increased level of confinement is required (transversal steel ratio of the order of 3.9%) in order to contain satisfactory the column damage.

6.7.4 Unbonded columns and isolator built – in columns

Alternative techniques to enhance the ductility capacity and reduce the residual drift of R.C. bridge columns have been recently proposed and tested by Kawashima.

The first consists in mitigate the concentration of damage at the plastic hinge by unbonding the longitudinal bars at the critical region, by wrapping them by plastic tubes (Kawashima et al., 2001). The deformation of longitudinal bars in tension results in a rocking motion, reducing the flexural deformation of the column, and thus limiting its flexural failure. Experimental (Kawashima, 2005) tests shown that this technique results effective in increasing the ductility capacity of the pier. Although, the proper definition of the unbonded length (L_{ub} , Fig. 6-38 (left)) needs further studies.

Alternatively, Kawashima and Nagai (2002) proposed to replace the concrete in the plastic hinge region, where inelastic deformations occur, by an appropriate material (high damping rubber has been studied for this purpose). The latter has to be softer than concrete, in order to reduce the flexural deformation of the column, stable under repeated seismic loading, durable for long term use and able to provide enough deformation and energy dissipation, preferably through the deformation of the material. The isolator is built-in with column (Fig. 6.38, right): longitudinal bars are continuous through the laminated rubber unit and prestressed tendons are inserted in order to prevent sudden deterioration of the restoring force and to mitigate residual drift. Shear-keys are also required to prevent an excessive lateral displacement of the column, relative to the footing, when the isolator is thick. Such designed columns result effective in limiting the concrete failure, thus increasing the ductility capacity of the column (Kawashima, 2005). However, ductile bars have to be used to prevent rupture, and consequent strength deterioration, because strain of bars here is extremely high.

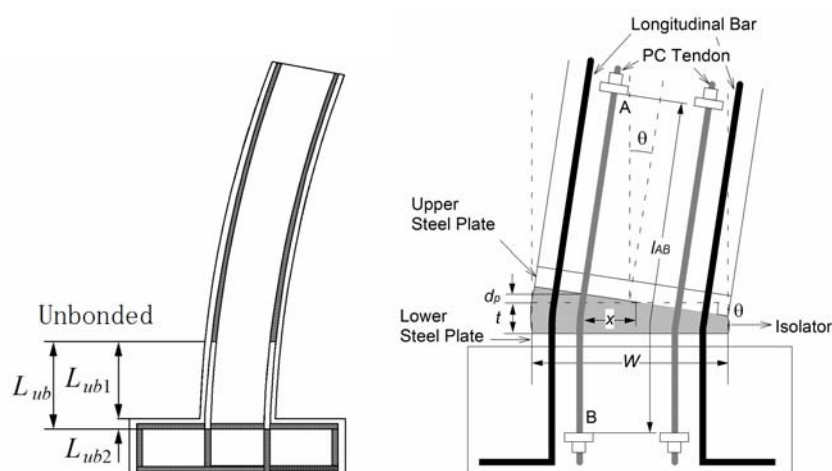


Fig. 6- 38: Unbonded column (left) and built-in column (right).

References

- AASTHO (1999), “Guide specifications for seismic isolation design”, American association of state highway and transportation officials, Washington DC, 76 pp.
- Abe M., Erkus B., Fujino Y., Park K.-S., (2000), “Applicability of semi-active control for seismic protection of bridges”. Proceedings of the international conference on advances in structural dynamics (ASD2000), 13-15 December, Hong-Kong, China, pp. 311 –318.

- Aiken I.D., Nims D.K., Whittaker A.S., Kelly J.M., (1993), "Testing of passive energy dissipation systems", *Earthquake Spectra*, Vol. 9, No. 3, Earthquake Engineering Research Institute California.
- Alga Spa, 2003, *Algasism HDRB*, manufacturer instructions.
- Almazan J.L., De la Llera J.C., (2002), "Analytical model of structures with frictional Pendulum isolators", *Earthquake engineering and structural dynamics*, 31, pp. 305–332.
- Almazan J.L., De la Llera J.C., Inuaudi J.A., (1998), "Modeling aspects of structures isolated with the Frictional pendulum system", *Earthquake engineering and structural dynamics*, 27, pp. 845–867.
- Bergman, D.M., and Goel, S.C., (1987), "Evaluation of Cyclic Testing of Steel-Plate Devices for Added Damping and Stiffness," Report UMCE, 87-10, Dept. of Civil Eng., Univ. of Michigan, Ann Arbor.
- Bouc R., (1967), "Forced vibration of mechanical systems with hysteresis", *Proceedings of the 4th Conference on Non-Linear Oscillations*
- Calvi G.M., Ceresa P., Casarotti C., Bolognini D., Auricchio F., (2004), "Effects of axial force variation on the seismic response of bridges isolated with friction pendulum systems" *JEE*, Vol.8 (Special Issue 1), pp.187-224.
- Calvi G.M., Pavese A., (1997), "Conceptual design of isolated systems for bridge structures" *JEE*, Vol. 1, No. 1, pp.193-218.
- Cardone D., Dolce M., Bixio A., Nigro D., (1999(a)), "Experimental tests on SMA elements" *Proceedings of final workshop on the BRITE-MANSIDE (memory alloys for new seismic isolation and energy dissipation devices) project*, Rome, Italy.
- Cardone D., Dolce M., Nigro D., (1999(b)), "Experimental tests on SMA-based devices" *Proceedings of final workshop on the BRITE-MANSIDE (memory alloys for new seismic isolation and energy dissipation devices) project*, Rome, Italy.
- Casarotti C., (2004), "Bridge isolation and dissipation devices: state of the art review in bridge isolation, structural seismic response and modeling of modern seismic isolation and dissipation devices" *ROSE School, MSc Dissertation*.
- Chang K.C., Lai M.L., Soong T.T., Hao D.S. and Yen Y.C., (1993), "Seismic behavior and design guidelines for steel frame structures with added viscoelastic dampers" Report No. NCEER 93-0009, National Center of Earthquake Engineering Research, Buffalo, N.Y.
- Ciampi V., Marioni A., (1991), "New types of energy dissipating devices for seismic protection of bridges" *3rd World Congress on Joint Sealing and Bearing Systems for Concrete Structures*, Toronto, Canada.
- Costantinou M.C., Mokha A., Reinhorn A., (1990), "Teflon Bearings in Base Isolation. II: Modeling", *Journal of Structural Engineering*, Vol. 116, No.2, pp. 455-474.
- Costantinou M.C., Tsopelas P., Kasalanati A., Wolff E., (1999), "Property Modification Factors for Seismic Isolation Bearings", Technical Rep. No. MCEER-99-0012, Multidisciplinary Center for Earthquake Engineering Research, State Univ. of New York at Buffalo, Buffalo, N.Y.
- DesRoches R., Delemont M., (2002), "Seismic retrofit of simply supported bridges using shape memory alloys", *Engineering Structures* 24, pp 325–332.
- Dolce M., Cardone D., Marnetto R., (2000), "Implementation and testing of passive control devices based on shape memory alloys" *Earthquake engineering and structural dynamics*, Vol. 29, pp. 945-968.
- Dolce M., Marnetto R., (1999), "Seismic devices based on shape memory alloys" *Proceedings of final workshop on the BRITE-MANSIDE (memory alloys for new seismic isolation and energy dissipation devices) project*, Rome, Italy.
- Doudoumis I.N., Gravalas F., Doudoumis N.I., (2005), "Analytical modeling of elastomeric lead-rubber bearings with the use of finite element micromodels" *5th GRACM International Congress on Computational Mechanics*, Limassol, 29 June-1 July.

- Dyke S.J., Spencer Jr B.F., (1996), "Seismic response control using multiple MR dampers". Proceedings of the 2nd International Workshop on Structural Control, Hong Kong, pp. 163–173.
- EC8, prEN 1998-1, Revised Final PT Draft (preStage 49).
- Filiatrault A., (2003), "SE 223 Advanced Seismic Design of Structures Class Notes", UCSD.
- Filiatrault A., Tremblay R., Kar R., (2000), "Performance evaluation of friction spring seismic damper", Journal of Structural Engineering, Vol. 126, No. 4, pp. 491-499.
- Gazetas G., Mylonakis G., (1998). "Seismic soil structure interaction: new evidence and emerging issues". Geotechnical Earthquake Engineering and Soil Dynamics, ASCE, II, pp. 1119-1174.
- Goel R.K., (1998), "Effects of supplemental viscous damping on seismic response of asymmetric-plan systems", Earthquake engineering and structural dynamics, Vol. 27, No. 2, pp.125-141.
- Hewes J.T., Priestley M.J.N., (2001), "Experimental testing of unbonded post-tensioned precast concrete segmental bridge columns", Proceedings of the 6th Caltrans seismic research workshop program, Sacramento, California, 12-13 June, Div. of engineering services, California department of transportation, Sacramento, 8 pages.
- Hodgson, D.E., (1988), "Using Shape Memory Alloys," Shape Memory Applications, Inc.
- Hwang J.S., Tseng Y.S., (2005), "Design formulations for supplemental viscous dampers to highway bridges", Earthquake engineering and structural dynamics, Vol. 34, pp.1627-1642.
- Hwang J.S., Wu J.D., Pan T.C.; Yang G., (2002), "A mathematical hysteretic model for elastomeric isolation bearings", Earthquake engineering and structural dynamics, Vol. 31, pp.771-789.
- Ivshin Y., Pence T., (1994), "A thermo-mechanical model for a one-variant shape memory material", Journal of Intelligent Materials Systems and Structures, Vol. 5, pp.455–473.
- Jung H.-J., Park K.-S., Spencer Jr B.F., Lee I.-W., (2004), "Hybrid seismic protection of cable-stayed bridges". Earthquake Engineering and Structural Dynamics, Vol. 33, pp. 795–820.
- Kar R., Rainer J.H., (1996), "New damper for seismic control of structures", Proceedings of the first Struct. Spec. Conf., Canadian Society of Civil Engineering, Edmonton, Alta., Canada, 835–842.
- Kar R., Rainer J.H., Lefrançois A.C., (1996), "Dynamic properties of a circuit breaker with friction-based seismic dampers", Earthquake Spectra, Vol. 12, No. 2, pp. 297–314.
- Kartoum A., Constantinou M.C., Reinhorn A.M., (1992), "Sliding isolation system for bridges: analytical study", Earthquake Spectra, Vol. 8, No. 3, pp. 345–372.
- Kawashima, K., Hosoiri, K., Shoji, G., Watanabe, G., (2001), "Effect of Unbonding of Main Reinforcements at Plastic Hinge Region for Enhancing Ductility of RC Bridge columns", Proc. Structural and Earthquake Engineering, JSCE, 689/I-57, 45-64.
- Kawashima, K., Nagai, M., (2002), "Development of RC Pier with Rubber Layer in the Plastic Hinge Region", Proc. Structural and Earthquake Engineering, JSCE, 703/I-59, 113-128.
- Kawashima K., Shoji G., Saito A., (2002), "Effect of hysteretic behavior in an isolated bridge", 12th European Conference on Earthquake Engineering, Paper reference 108, Elsevier Science Ltd.
- Kawashima K., Watanabe G., (2005), "Seismic performance of unbonded columns and isolator built-in columns based on cyclic loading tests", 2nd International Conference on Urban Earthquake Engineering, pp. 63-70, Tokyo, Japan.
- Kikuchi M., Aiken I.D., (1997), "An Analytical hysteresis model for elastomeric seismic isolation bearings", Earthquake engineering and structural dynamics, Vol. 26, No. 2.

- Kurata N., Kobori T., Koshika N., (2002), "Performance-based design with semi-active structural control technique" *Earthquake engineering and structural dynamics*, Vol. 31, pp. 445-458.
- Kurata N., Kobori T., Takahashi M., Niwa N., Midorikawa H., (1999), "Actual seismic response controlled building with semi-active damper system". *Earthquake Engineering and Structural Dynamics*, Vol. 28, pp. 1427-1447.
- Yoshikawa M., Hayashi H., Kawakita S., Hayashida M., (2000), "Construction of Benten Viaduct, rigid-frame bridge with seismic isolators at the foot of the piers". *Cement and concrete composite*, Elsevier Science Ltd., Vol. 22, pp. 39-46.
- Lee T.Y., Kawashima K., (2004), "Effectiveness of supplemental dampers for isolated bridges under strong near-field ground motions", 13th World conference on earthquake engineering, Vancouver, B.C., Canada, 1-6 August, Paper No. 138.
- Liang C., Rogers C.A., (1990), "One-dimensional thermo-mechanical constitutive relations for shape memory materials", *Journal of Intelligent Materials Systems and Structures*, Vol. 1, No. 2, pp. 207-234.
- Makris N., (1997), "Rigidity-plasticity-viscosity: can electrorheological dampers protect base-isolated structures from near-field ground motions?", *Earthquake engineering and structural dynamics*, 26, No. 5, 571-591.
- Makris N., Burton S.A., Hill D. and Jordan M., (1996), "Analysis and design of an electrorheological damper for seismic protection of structures", *J. eng. mech. ASCE* 122, pp. 1003-1011.
- Makris N., Chang S., (2000), "Effect of viscous, viscoplastic and friction damping on the response of seismic isolated structures", *Earthquake engineering and structural dynamics*, Vol. 29, No.1, pp.85-107.
- MANSIDE Consortium, (1998), "Guidelines for the passive seismic protection of structures using shape memory alloy based devices", Report of the Brite/Euram Project BE95-2168, September.
- Marioni A., (1997), "Development of a new type of hysteretic damper for the seismic protection of bridges", *Proceedings of the fourth world congress on joint sealing and bearing systems for concrete structures*, American concrete institute, Sacramento, USA - 29 Sept-2 October, Vol. 2, pp.955-976.
- Marioni A., (1999), "The use of hydraulic dampers for the protection of the structures from the seismic risk: an outstanding example", *International Post-Smirt Conference Seminar on Seismic Isolation, Passive Energy Dissipation and Active Control of Vibration of Structures*, Cheju, Korea - 23/25 August.
- Marioni A., (2002), "The use of anti-seismic devices for the protection of the structures from the seismic risk", *Rose School Conference*, 22 January, Pavia.
- Nagarajaiah S., Ferrell K., (1999), "Stability of Elastomeric Seismic Isolation Bearings", *Journal of Structural Engineering*, ASCE, Vol.125, No. 9, pp.946-954.
- Nims D.K., Richter P.J., Bachman R.E., (1993), "The Use of the Energy Dissipation Restraint for Seismic Hazard Mitigation" *Earthquake Spectra*, Vol. 9, No.3, EERI, pp.467-487.
- Palermo A., "The use of controlled rocking in the seismic design of bridges". *Doctoral thesis*, Politecnico di Milano, 2004.
- Pall A.S., Marsh C., Fazio P., (1980), "A Friction joint for seismic control of large panel structures", *Journal of Prestressed Concrete Institute*, Vol. 25, No. 6, December, pp.38-61.
- Park J.G., Otsuka H., (1999), "Optimal yield level of bilinear seismic isolation devices", *Earthquake Engineering and Structural Dynamics*, Vol. 28, pp.941-955.
- Patten W.N., Sun J., Li G., (1999), "Field test of an intelligent stiffener for bridges at the I-35 Walnut Creek Bridge". *Earthquake Engineering and Structural Dynamics*, Vol. 28, pp. 109-126.

- Priestley M.J.N. and Calvi G.M., (2003), "Direct displacement-based seismic design of concrete bridges", Proceedings of the fifth International Conference on Seismic Bridge Design and Retrofit for earthquake resistance, La Jolla, California.
- Priestley M.J.N., Calvi G.M., (2002), "Strategies for repair and seismic upgrading of Bolu Viaduct 1, Turkey", JEE, Vol. 6 (SP1), pp. 157-184.
- Priestley M.J.N., Seible F., Calvi G.M., (1996), "Seismic design and retrofit of bridges", Jon Wiley, New York.
- Priestley M.J.N., Kowalsky M.J., (1998), "Aspects of drift and ductility capacity of rectangular cantilever structural walls". Bulletin, New Zealand Society for Earthquake Engineering, Vol. 31, No. 2, pp.73-85, July.
- Ribakov Y., Gluck J., (2002), "Selective Controlled Base Isolation System With MRDs", Earthquake engineering and structural dynamics, Vol. 31, pp.1301-1324.
- Sahasrabudhe S.S., Nagarajaiah S., (2005), "Semi-active control of sliding isolated bridges using MR dampers: an experimental and numerical study". Earthquake Engineering and Structural Dynamics, Vol. 34, pp. 965 –983.
- Shames I.H., Cozzarelli F.A., (1992), "Elastic and Inelastic Stress Analysis", Prentice-Hall: Englewood Cliffs, NJ, pp.120-122.
- Skinner R.I., Robinson W.H., Mc Verry G.H., (1993), "An introduction to seismic isolation", Wiley, England.
- Spencer B.F. Jr, Dyke S.J., Sain M.K., Carlson J.D., (1997), "Phenomenological model for magnetorheological dampers", ASCE Journal of Engineering Mechanics, 123(3), pp. 230-238.
- Spencer Jr B.F., (2001), "Advanced in semi-active control of civil engineering structures". Proceedings of the 2nd European Conference on Structural Control, Paris, 2001.
- Symans M.D. and Kelly S.W., (1998), "Seismic protection of bridge structures using hybrid isolation systems", Proceedings of the 6th U.S. Conference on Earthquake Engineering (6NCEE), Seattle, Washington.
- Symans M.D., Constantinou M.C., (1997), "Seismic testing of a building structure with a semi-active fluid damper control system". Earthquake Engineering and Structural Dynamics, Vol. 26, pp. 759 –777.
- Taylor A.W., Lin A.N., EERI M., Martin J.W., (1992), "Performance of elastomers in isolation bearings: a literature review", Earthquake Spectra, Vol. 8, No. 2, 1992.
- Tremblay R., Stiemer S.F., (1993), "Energy dissipation through friction bolted connections in concentrically braced steel frames", ATC 17-1 Seminar on Seismic Isolation, passive energy dissipation and active control, Vol. 2, 557-568.
- Tsai C. S., (1997), "Finite element formulations for friction Pendulum seismic isolation bearings", International Jour. for Num. Methods in Engineering, Vol. 40, pp. 29–49.
- Tsai C.S., Chiang T.-C., Chen, B.-J., Lin S.B., (2003), "An advanced analytical model for high damping rubber bearings", Earthquake engineering and structural dynamics, Vol. 32, pp.1373-1387.
- Wang Y., Chung L.L., Liao W.H., (1998), "Seismic response analysis of bridges isolated with friction pendulum bearings", Earthquake engineering and structural dynamics, 27, 1069–109.
- Wen Y.K., (1976), "Method for random vibration of hysteretic systems", ASCE Journal of Engineering Mechanics, 102(2), pp. 249-263.
- Xu Y.L., Qu W.L., Ko J.M., (2000), "Seismic response control of frame structures using Magnetorheological/ Electrorheological dampers", Earthquake engineering and structural dynamics, 29:557-575.
- Yang J.N., Wu J.C., Hsu S.Y., (1994), "Parametric control of seismic-excited structures". Proceedings of the 1st World Conference on Structural Control, Vol. 1, Los Angeles, WP1 88–97.

7 Design for spatial variation of ground motion

7.1 Introduction

Seismic design of bridges is in almost all cases done assuming that all contact points experience the same ground motion (rigid input), in spite of ample evidence proving that this is not the case. This evidence covers both ground motion per se, as well as its effect on structural response. As it regards the first, a number of strong-motion recorder arrays have been set up in the past twenty years in different parts of the world, the most renowned ones being Taiwan (Smart-1 array) and in California, from which the spatial variation of ground motion during seismic events has been observed and measured (Abrahamson et al. 1991). For what concerns the effects on structural response, it suffices to recall the large number of spectacular failures of simply supported bridges due to seating length inadequate to accommodate the relative displacements induced by spatial variation.

The spatial variation of seismic ground motion is commonly attributed to the combination of four different phenomena: a) the loss of correlation (incoherence effect) between the motions at separate points resulting from random reflections and refractions as the waves travel through the soil; b) the so-called wave-passage effect, that is the difference in the arrival times of the seismic waves at different stations; c) the attenuation effect, which is the selective decay of the amplitudes of the frequency components of the waves due to geometric spreading and energy dissipation of the medium; d) the site-response effect, which consists in the modification of the motion due to the specific stratigraphic and mechanical properties of the soil under each surface point of interest. Further, even in the ideal case of an identical input motion at all points at the free surface, the presence of the foundations and of the structure would alter locally (at each support foundation) the motion due to soil-structure interaction (SSI). This is due to the fact that the geometry and the stiffness of the foundation structure (that can be massive in the case of bridges) modify the free movement of the soil (kinematic interaction) and, also, to the fact that inertia forces from the superstructure are transmitted back into the soil (inertial interaction).

Obviously all of the above mentioned effects are interdependent, and, in principle, a comprehensive approach should take them simultaneously into consideration. Apparently there is only one such attempt available in the literature (Sextos et al. 2003), of which adequate mention is given in the following. Anyway, given the very large number of parameters entering the problem in its entirety, it is convenient to examine the effects a) to d), in order to gain an insight of their relevance on bridge response, disregarding their interaction with SSI effects. This approach is taken in this chapter.

The first pioneering studies on the effect of non-synchronism of the ground motion on bridge response date back to the '70s, though it is only from the '90s that this phenomenon has obtained more substantial attention. Since then, quite a few interesting studies have been produced (see, for example, among others, Zerva 1990 and Harichandran et al. 1996). These studies, however, still have a rather theoretical character, being based on linear elastic random vibration theory. In addition, none of them takes into account the effects of the local soil conditions on the variability of the motion.

Studies with a more practice-oriented aim try to provide a statistical basis adequate for detecting systematic trends, delimiting the magnitude of the effects, and possibly suggesting simplified measures for accounting of the phenomenon in design. A number of contributions belong to this category, as for example Monti et al (1996), Monti and Pinto (1998), Shinozuka et al. (2000) and Sextos et al. (2003). Even within the last category, however, spatial variability due to different subsoil conditions beneath the piers, an effect that most bridge

designers would readily indicate as an influential one based on intuition, has received limited attention.

From the review of a selection of the most relevant studies that is given in the following sections, it will be apparent, though, that the present state of knowledge is still far from a clear and simple vision of this admittedly complicated problem.

Starting with the tools necessary for investigating the phenomenon, the very idea of setting up a purely mechanical model is out of question. In fact, the complexities characterising the process of earthquake generation and propagation through the geologically inhomogeneous Earth's crust are such as to rule out any attempt at setting up a detailed mechanical model of soil motion variability at the scale of tens or hundreds of metres.

Alternatively, one might think of addressing the problem using recorded ground motions, as it is now frequently done for assessment or design verification of building structures. This possibility is, however, completely unrealistic, since it would require an enormous, practically uncollectible, database of simultaneously recorded motions for all the possible combinations of support point number and distances, local site conditions, magnitude, fault mechanism, etc.

As it is generally known, the approach pursued in practice to explore the phenomenon is to set up a probabilistic model, i.e. a random field, substantiated from the data collected from the strong-motion arrays installed worldwide. Further, since current seismic design philosophy relies on energy dissipation through non-linear behaviour, the random field model cannot be used in the framework of classical random vibration, but, rather, it needs to be employed to generate samples of spatially distributed motions to be used in non-linear time-history analysis. This latter is the only available tool for a meaningful study of the problem.

The second and perhaps most important obstacle to attaining a comprehensive vision of the problem and, hence, to being able to give indications on the combinations of the parameters values that affect negatively the response, resides in the almost uncountable situations regarding bridge geometry and materials, design criteria and underlying soil profile characteristics, combined with the many possible scenarios of ground motion variability. Available studies have explored only tiny portions of this vast space and not in a systematic fashion, which makes it quite difficult to draw general conclusions from them.

7.2 Analytical modelling

7.2.1 Model of spatial variability

Spatial variability is described in the literature by means of a second-order random field, discrete in space (i.e. defined in a discrete number of stations), and continuous, zero mean, in time.

The stationary version of this field is thus completely described by the $n \times n$ symmetric matrix of the auto- and cross-power spectral density (PSD) functions:

$$\mathbf{S}(\omega) = \begin{bmatrix} S_{11}(\omega) & S_{12}(\omega) & \Lambda & S_{1n}(\omega) \\ & S_{22}(\omega) & \Lambda & S_{2n}(\omega) \\ & & \mathbf{O} & \mathbf{M} \\ & & & S_{nn}(\omega) \end{bmatrix} \quad (7-1)$$

where n is the number of stations.

It is useful to introduce the following non-dimensional function called coherency function:

$$\gamma_{ij}(\omega) = \frac{S_{ij}(\omega)}{\sqrt{S_{ii}(\omega)S_{jj}(\omega)}} \quad (7-2)$$

The value of the modulus of $\gamma_{ij}(\omega)$ at all frequencies is bounded by zero and one, and it provides a measure of the linear statistical dependence of the two processes at the stations *i* and *j*. In this simplified model the combination of all the effects mentioned earlier is accounted for by this linear statistical dependence.

The following form of the coherency function is frequently adopted (Luco & Wong 1986, Der Kiureghian 1996):

$$\gamma_{ij}(\omega) = \exp\left[-\left(\frac{\alpha\omega d_{ij}}{v_s}\right)^2\right] \cdot \exp\left[i\frac{\omega d_{ij}^L}{v_{app}}\right] \cdot \exp[i\theta_{ij}(\omega)] \quad (7-3)$$

where v_s is the shear-waves velocity, d_{ij} and d_{ij}^L the distance and the projected distance along the direction of propagation of the waves between the stations *i* and *j*, respectively, v_{app} is the surface apparent velocity of waves, $\theta_{ij}(\omega)$ is defined subsequently and α is a constant.

The three factors in Eq.(3) describe the contributions to the coherency function due to reflections/refractions (decreasing with increasing values of v_s / α , often denoted as ‘loss of coherence’), due to the wave-passage (decreasing with increasing v_{app}), and due to the difference in soil conditions at support *i* and support *j*, respectively. In particular, the first factor decreases exponentially the correlation, proportionally to the square of the distance and the frequency of the waves, and inversely to the mechanical properties of the soil as represented by shear wave velocity. Zerva (1990) reports for the coherency parameter α values in the range 0.1 to 0.5, while Der Kiureghian & Neuenhofer (1992) use for $\alpha d_{ij} / v_s$ values in the interval 0-2, which can be shown to be consistent with the indicated range for α . Confirmation of the above ranges can be found in (Nuti & Vanzi, 2004), where they have examined data from a larger set of events and back-calculated values of α falling in the range 0.02-0.5.

Other formulations have been proposed in literature for the coherency function (see, for example, Harichandran & Vanmarke 1986, Hao et al. 1989). Differences deriving from the adoption of these and other alternative proposals rather than Eq.(3), however, are masked by the necessity of spanning wide ranges of the parameters entering all the models, due to the impossibility of their direct previous determination.

Local soil conditions are dealt with reference to the following topographical/geotechnical model. A rigid base beneath the bridge moves according to a white noise process of power S_0^b . Soil columns of different heights and mechanical properties respond to the excitation at the base giving surface motions at each considered point. The surface PSD’s correspond to the diagonal terms of the matrix in Eq.(1).

The common excitation introduces also a correlation among the surface motions, i.e. the third term in Eq.(3). Denoting by $H_i(\omega)$ the frequency transfer function of the *i*-th soil column, from basic random vibration theory one has for the off-diagonal terms of matrix in Eq.(1):

$$S_{ij}^s(\omega) = H_i(\omega)H_j(-\omega)S_0^b \quad (7-4)$$

From the definition of the coherency function one has:

$$\gamma_{ij}^s(\omega) = \frac{S_{ij}^s(\omega)}{\sqrt{S_{ii}^s(\omega)S_{jj}^s(\omega)}} = \frac{H_i(\omega)H_j(-\omega)}{|H_i(\omega)||H_j(-\omega)|} = \exp[i(\theta_i(\omega) - \theta_j(\omega))] = \exp[i\theta_{ij}(\omega)] \quad (7-5)$$

which shows that the effect of different soil properties for what concerns the correlation consist of a phase shift between the motions at points i and j at the surface equal to:

$$\theta_{ij}(\omega) = \tan^{-1} \left[\frac{\text{Im}(H_i(\omega)H_j(-\omega))}{\text{Re}(H_i(\omega)H_j(-\omega))} \right] \quad (7-6)$$

7.2.2 Generation of samples

Samples of the stationary field defined by the auto- and cross-PSD $\mathbf{S}(\omega)$ of Eq. (1) can be obtained by the following procedure (Shinozuka 1972). Matrix $\mathbf{S}(\omega)$ is first decomposed into the product:

$$\mathbf{S}(\omega) = \mathbf{L}(\omega)\mathbf{L}^{*T}(\omega) \quad (7-7)$$

between a matrix $\mathbf{L}(\omega)$ and the transpose of its complex conjugate $\mathbf{L}^*(\omega)$. If the Cholesky method is employed, $\mathbf{L}(\omega)$ is a lower triangular matrix:

$$\mathbf{L}(\omega) = \begin{bmatrix} L_{11}(\omega) & & & & \\ L_{12}(\omega) & L_{22}(\omega) & & & \\ \mathbf{M} & \mathbf{M} & \mathbf{O} & & \\ L_{n1}(\omega) & L_{n2}(\omega) & \Lambda & L_{nn}(\omega) & \end{bmatrix} \quad (7-8)$$

Writing the off-diagonal terms $H_{ij}(\omega)$ in the form:

$$L_{ij}(\omega) = |L_{ij}(\omega)| \exp[i\theta_{ij}(\omega)] \quad (7-9)$$

a sample motion at the generic station i is obtained from the series:

$$a_i(t) = 2 \sum_{m=1}^n \sum_{l=1}^N |L_{im}(\omega_l)| \sqrt{\Delta\omega} \cos[\omega_l t - \theta_{im}(\omega_l) + \phi_{ml}] \quad i = 1, K, n \quad (7-10)$$

where N is the total number of frequencies ω_i in which the significant bandwidth of $S_{ij}(\omega)$ is discretised, $\Delta\omega = \omega_{\max} / N$, and the angles ϕ_{ml} are, for any m , a set of N independent random variables uniformly distributed in the interval $[0, 2\pi)$.

It can be easily checked that the ensemble expected value of $a_i(t)$ $i=1,2,\dots,n$ is zero and that the ensemble auto/cross-correlation functions are the same as the corresponding ones of the given field, which are:

$$R_{ij}(\tau) = \int_{-\infty}^{\infty} \sqrt{S_{ii}(\omega)S_{jj}(\omega)} \gamma_{ij}(\omega) e^{i\omega\tau} d\omega \quad (7-11)$$

As an example, Eq.(10) has been used to generate set of samples characterised by different values of the two parameters v_s / α and v_{app} , and different local site conditions. Having in mind that the structural response is strongly influenced by the relative displacements between the support points it is of interest to observe the magnitude of the relative displacements provided by the generated samples.

Fig. 7-1 shows the latter displacements for four combinations of the velocity parameters and the indicated site conditions, for points located 50m apart. The maximum values observed are in the order of 10 centimetres for all the cases, a value which is consistent with empirical evidence for the considered distance between the points and intensity of motion.

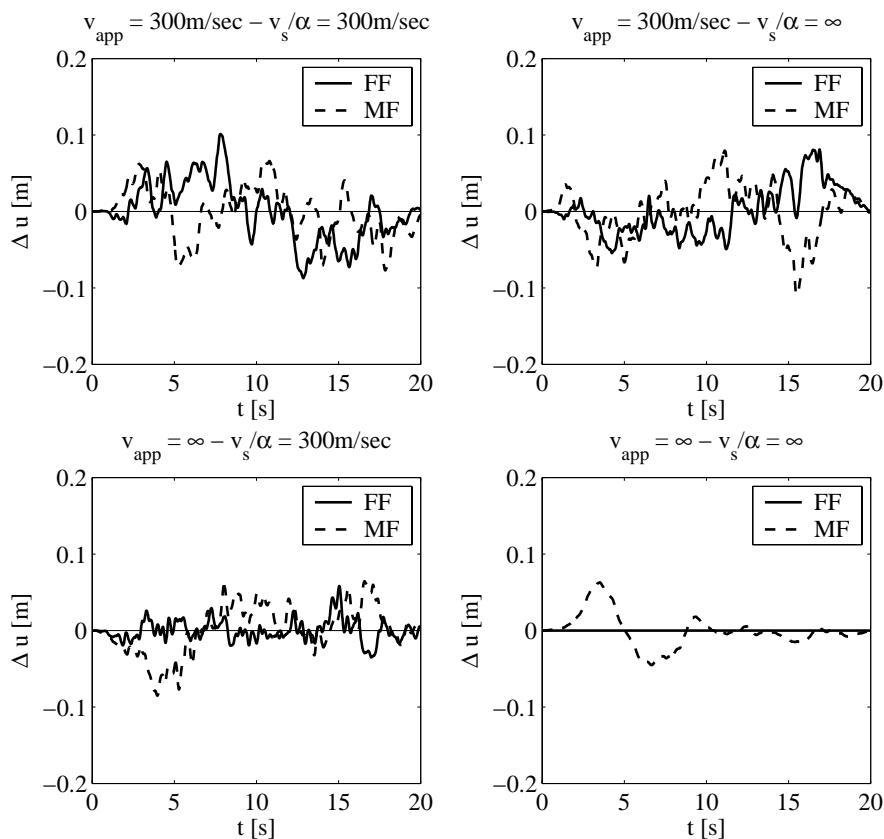


Fig. 7-1: Relative displacements time-histories between two points at 50m distance for a ground motion with PGA on firm soil of 0.35g. (F=firm type soil; M= medium type soil according to Eurocode 8)

		<i>Monti et al 1996</i>	<i>Lupoi et al 2005</i>	<i>Sextos et al 2003</i>	<i>Shinozuka et al 2000</i>	<i>Monti & Pinto 1998</i>
<i>Bridge geometry</i>	<i>Number of spans</i>	6	4	4, 6, 8	3, 5, 12	6
	<i>Span lengths</i>	50m	50m	50m, 100m, 150m		50m
	<i>Total length</i>	200m	200m	200m, 400m, 600m		200m
	<i>Configurations (²)</i>	3	27	13	7	1
	<i>Isolation</i>	NO	NO	NO	NO	YES
<i>Spatial variability parameters</i>	<i>Loss of coherence</i>	3 values	3 values	1 value	1 value	2 values
	<i>Wave-passage</i>	3 values	3 values	1 value	2 values	2 values
	<i>Site response⁽¹⁾</i>	N/A	4 scenarios	6 scenarios	8 scenarios ⁽³⁾	6 scenarios
	<i>SSI</i>	N/A	N/A	Kinematic, inertial	N/A	N/A
<i>Total cases analysed</i>		27	972	180	56	12
<i>Type of analysis</i>		NLTHA	NLTHA	LTHA, NLTHA	NLTHA	Random vibrations (with equivalent linearization)
<i>Type of results</i>		<i>Envelope of ductility demands on all piers</i>	<i>Fragility curves for the entire bridge</i>	<i>Ratios of non- synchronous to synchronous demands</i>	<i>Peak ductility demand on all piers</i>	<i>Envelope of isolator displacement demands</i>
<i>Direction of Seismic input</i>		Transverse	Transverse	Transverse (one case longitudinal)	Longitudinal	Transverse

Table 7-1: Summary of the reported studies. (1) Site response scenarios are defined as distinct sequences of soil profiles under the piers; (2) Configurations are defined as distinct combinations of sequences of pier heights and/or deck and abutment types; (3) 1 scenario is a uniform soil profile, the remaining 7 are the actual soil profiles under the considered (existing) bridges.

7.3 Review of relevant past studies

Of the non abundant literature devoted to investigating, with a design-oriented approach, the effects of spatial variability of seismic ground motion on structural response, few studies have sufficient width of scope for providing concrete indications. Those that have been selected are reported in Table 7-1, which summarises their main features in terms of bridge configurations, spatial variability scenarios, type of analysis performed and of results provided. An additional study is included in this survey, which focuses on the probabilistic description of the relative motion between two points, both at the ground level and at the top of two adjacent piers, due to different soil properties as well as the loss of coherence effect. The merit of the study is to provide a consistent formal derivation of differential

displacements, an open issue still subject of empirical contrasting proposals that have found their way into existing codes.

7.3.1 Monti, Nuti and Pinto 1996

7.3.1.1 Description of the study

The bridge configuration examined in the study is represented in Fig. 7-2. It is a 6-span continuous deck with 5 piers of the same height H and of 2.5 m diameter. The span length is 50.0 m. The deck, transversely hinged to the piers and the abutments, has a dead load of 200 kN/m. The piers (acting as cantilevers) are considered as fixed on the soil. The bridge has been designed according to Eurocode 8, using response spectra described in the following, reduced by three values of the behaviour factor q and scaled to a peak ground acceleration (PGA) of: $0.42 g/q$.

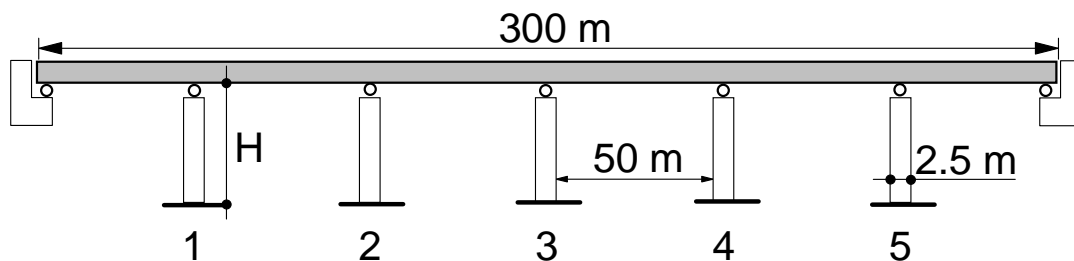


Fig. 7-2: Schematic view of bridge.

Fig. 7-3 and Fig. 7-4 report the spectral shapes used for design (soft soil has not been considered) and the corresponding power spectral densities (Clough-Penzien model).

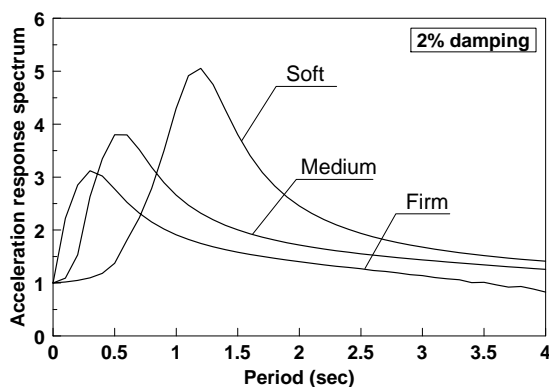


Fig. 7-3: Soil types F, M, S: response spectra.

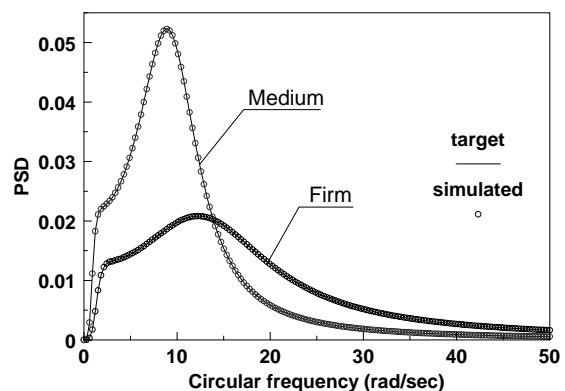


Fig. 7-4: Soil types F, M: power spectral density.

All the analyses of the bridge have been performed in transverse direction.

The parameters considered in the study are: a) the soil type, b) the structure stiffness, represented by the piers height H , c) the design level, given by the behaviour factor: q , and d) the coherency parameters: v_s/α and v_{app} . The numerical values assigned to the above

parameters are indicated in Table 7-2. By combining all the values of the parameters 216 cases are obtained. The three different pier heights are intended to produce three different degrees of bridge stiffness and have been chosen so as to get bridges with fundamental periods varying within rather large limits. The first three periods of vibration are listed in Table 7-3.

Parameter	Values			
Soil type	Firm (F)		Medium (M)	
Pier height H (m)	7.50	10.00	15.00	
Behavior factor q	2	4	6	
v_s/α (m/s)	300		600	∞
v_{app} (m/s)	300	600	1200	∞

Table 7-2: Values considered in the parametric study

Period	$H = 7.50$ m	$H = 10.00$ m	$H = 15.00$ m
T_1 (sec)	0.43	0.60	1.20
T_2 (sec)	0.40	0.57	0.84
T_3 (sec)	0.33	0.41	0.48

Table 7-3: Periods of vibration of the bridges.

In this study the coherency function in Eq.(3) has been used without the last factor, that accounts for different soil conditions at the supports. Fig. 7-5 shows the trend of the loss of coherence term in Eq.(3) as a function of circular frequency and for different distances d_{ij} , for the two values of v_s/α that have been adopted, which correspond to relatively soft and medium soil conditions.

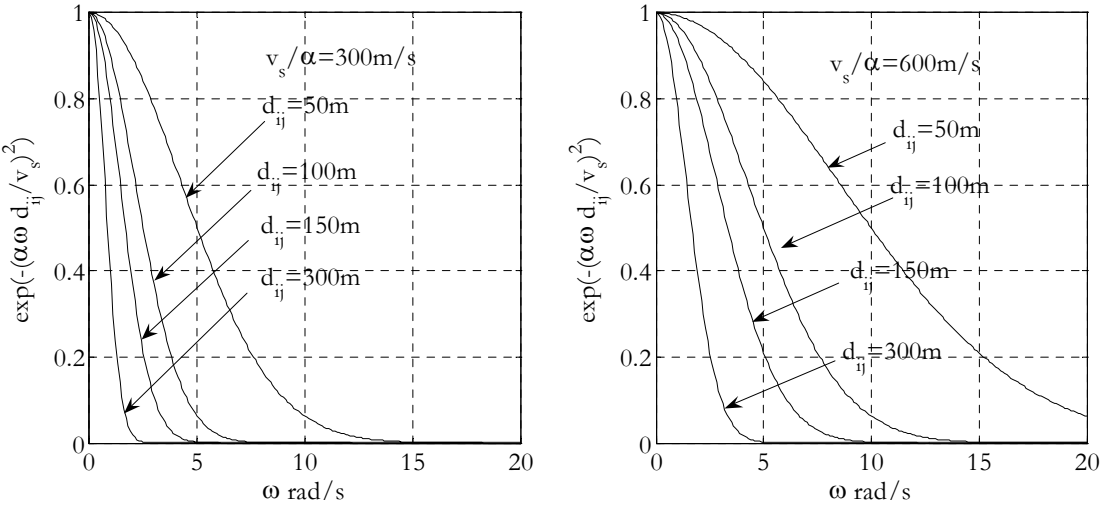


Fig. 7-5: Loss of coherence as a function of frequency, distance and v_s/α

7.3.1.2 Main results

The results are presented in terms of required pier displacement ductility demand, average over twenty sample ground motions for each case. The results of the bridge with $H= 10.0$ m

only are presented, on soil types F and M with values $v_s/\alpha = 300, 600$ and ∞ m/s for the loss of coherence term. In each diagram, for each value of the behaviour factor $q = 2, 4$ and 6 adopted in the design, three curves obtained for $v_{app} = 300, 600$ and ∞ m/s (the wave-passage effect) are represented. Curves relative to $v_{app} = 1200$ m/s are not represented, since they are almost coincident with those for $v_{app} = 600$ m/s.

We first comment on the top of Fig. 7-6, i.e., the ones containing the cases of largest loss of coherence. Since in this case the response is due mainly, when not exclusively, to the imposed pseudo-static differential displacements at the piers bases, wave-propagation effects are almost irrelevant, as confirmed by the closeness of the curves for different values of v_{app} .

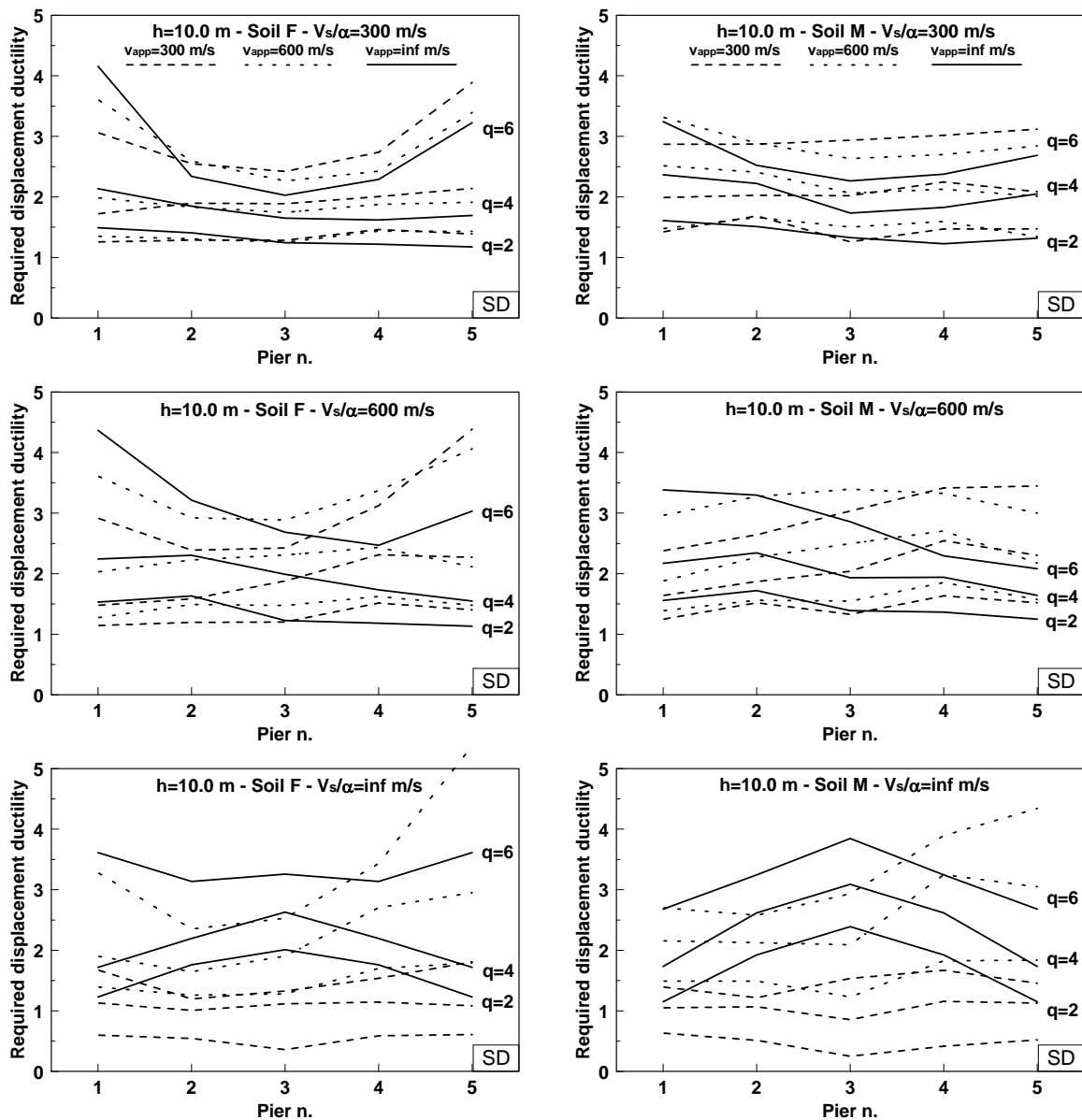


Fig. 7-6: Results for bridge with pier height $H=10$ m

The second extreme situation is when loss of coherence is absent and the lack of correlation is only due to wave propagation (see bottom of Fig. 7-6). In this case, contrary to

the previous one, the results show a significant sensitivity to the parameter v_{app} , for all values of q .

Overall the study concludes, as shown by the selected results presented, that the presence of the wave-passage and loss of coherence has, generally, a beneficial effect on the ductility demand. The highest reduction occurs for the highest level of loss of coherence ($v_s / \alpha = 300m/s$), which is more effective, for the more typical values of the parameters, in making the input motion un-correlated, thus reducing the net dynamic component of the excitation.

7.3.2 Lupoi, Franchin, Pinto and Monti 2005

7.3.2.1 Description of the study

The study provides a rather comprehensive parametric investigation on the interacting effects of different sources of spatial variability of ground motion, for a relatively wide number of bridge geometries, for a constant total length of 200m.

The bridges have all a continuous deck over three cantilever piers, with equal length spans of 50 m. Twenty configurations are obtained by combining two “basic” deck sections and two “basic” pier sections, which are shown in Fig. 7-7. The two deck sections are both pre-stressed concrete box girders.

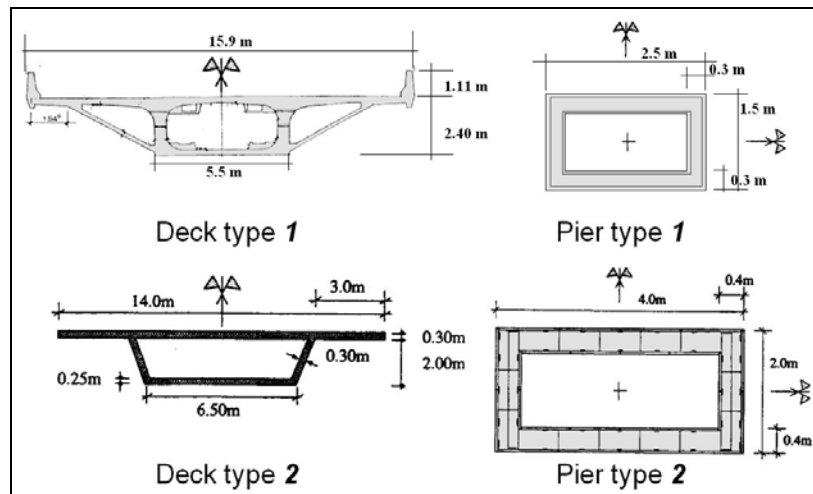


Fig. 7-7: Bridges analysed in Lupoi et al.: deck and pier section types.

Deck type 1 is associated with three concrete piers having the hollow core concrete section type 1 and heights of 8 m, 10 m and 12 m. These three piers have been combined to form two “regular” and two “irregular” bridge configurations: the former are 10-10-10 and 8-12-8, the latter 8-10-12 and 12-8-12. The layouts described above are illustrated in Fig. 7-7 (Left). Deck type 2 of Fig. 7-7 is associated with the concrete piers having the hollow core concrete section type 2 and heights of 7 m, 14 m and 21 m. These piers have been combined to form one “regular” and one “irregular” bridge configurations: the former is 14-21-14, the latter 14-7-21. The layouts described above are illustrated in Fig. 7-8 (Right).

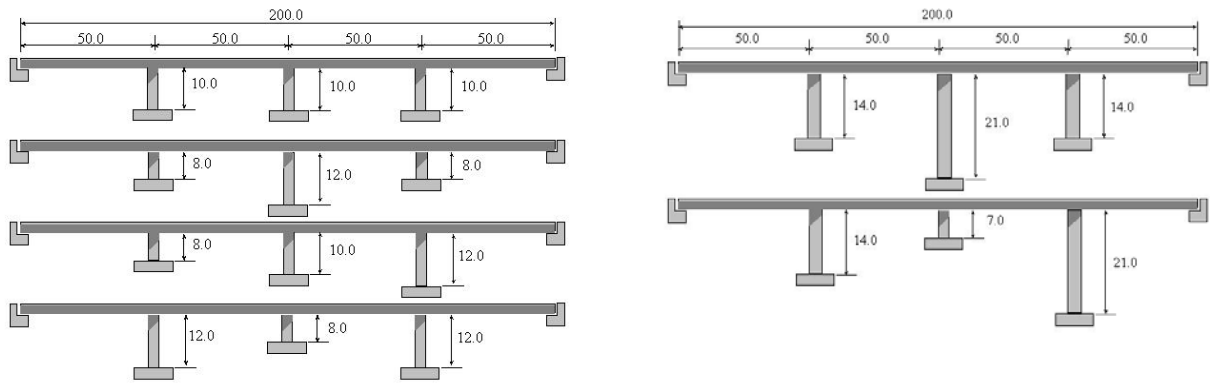


Fig. 7-8: Bridges analysed in Lupoi et al., pier profiles for deck type 1 (left) and 2 (right).

The relative stiffness between deck and piers influences the effects of the spatially varying ground motion on the bridge response, since the state of stress generated by differential displacements in the hyperstatic bridge system increases with the stiffness of the deck. To account for this effect, in addition to the configurations described above, further bridges have been generated by varying the decks transverse stiffness: in particular, the inertia of deck type 1 has been reduced by factors of 5, 10 and 20, while that of deck type 2 has been increased by a factor of 3. In total the bridge configurations considered amount to 27, and are summarised in Fig. 7-9.

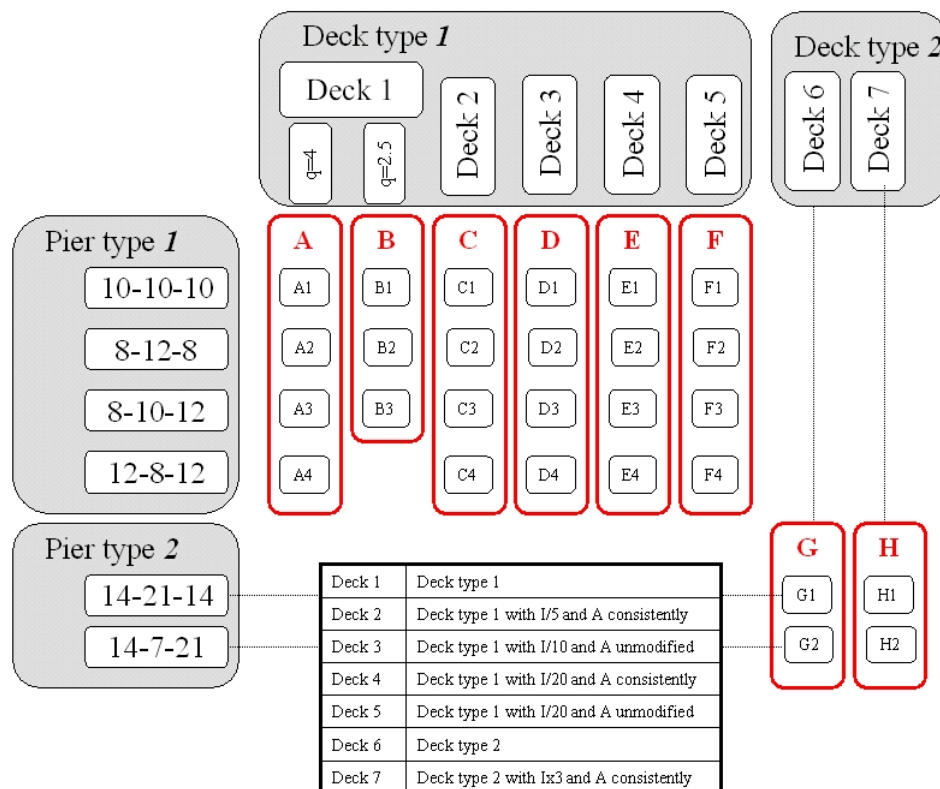


Fig. 7-9: Lupoi et al.: summary of bridge configurations analysed.

The bridges have been designed for synchronous ground motion using modal analysis with a “uniform” elastic response spectrum of intensity $S_e = 2.5 \times PGA$, where $PGA = 0.35g$, using two values of the behaviour factor: $q = 2.5$ and $q = 4$.

All the analyses of the bridges have been performed in transverse direction.

The soil at the supports is assumed to be either firm-type (F) or medium-type (M), according to the Eurocode 8 site classification. The following four combinations of local soil conditions are examined: FFFFF, FMMMM, FFMFF and FMFMF, where the first and the last letter indicate soil type underneath the abutments, while the three central ones indicate the soil underneath the piers. Three different levels of both loss of coherence and wave-passage are investigated, corresponding to the following values of v_s / α and v_{app} : 300m/s, 900m/s and infinity, the case in which both are infinity corresponding to synchronous motion (the coherency function used in this study is the one reported in Eq.(7-3)).

Combining all possible configurations, each bridge is subjected to 36 different cases of non-synchronous input motion. For each case, 20 sample ground motions have been generated and used in non-linear time-history analysis.

A particularity of the study is the recourse to a probabilistic approach, the outcome of which consists of a full fragility function (i.e. the probability of failure versus seismic intensity, as measured by PGA) for each bridge and each examined case. The choice is made in order to obtain a global measure of performance of each bridge, for easier comparison of the effects.

For the purpose of fragility analysis, bridge piers are assumed to fail in bending, and the bridge is considered as a series system.

7.3.2.2 Main results

The fragility curves for the regular bridge A1 are shown in Fig. 7-10. The fragilities are grouped by arrangement of local site conditions. The upper left figure, which refers to the FFFFF case, allows to separate the effect of site conditions from those of loss of coherence and wave-passage. The main evidence from the figure is summarised as follows: the case of full synchronism (FFFFF, $v_s / \alpha = \infty$, $v_{app} = \infty$) does not represent the worst condition; the most favourable case corresponds to the combination of complete coherence ($v_s / \alpha = \infty$) and slowest propagation of the waves ($v_{app} = 300$ m/s); on the other hand, as soon as the loss of coherence effect comes into play it tends to dominate, negatively, and to mask the effect of the second factor, as it can be noted from the fact that the three upper fragilities (maximum loss of coherence $v_s / \alpha = 300$ m/s for all values of v_{app}) are almost coincident. The same conclusion regarding the combined effect of loss of coherence and wave-passage can be stated independently from the arrangement of the local soil conditions examined. The effect of the latter is instead a “global” increment of demand on the bridge, and hence of the failure probabilities. This is partly due to the larger spectral ordinates of soil M and partly to the contrast between different soils.

The results for the three other bridges of set A are qualitatively analogous to those of bridge A1, therefore, their fragilities are not shown. With regard to the other sets of bridges, one can state, generally, that the effect of a spatially varying ground motion due to all sources is qualitatively maintained. For brevity, a detailed description of the fragilities for the other sets of bridges is omitted.

The results shown so far clearly indicate that the spatially varying ground motion significantly influences the response of the bridges. It is of interest to assess quantitatively the variation of the level of safety attained with respect to the case of uniform motion, assumed as reference case. To this end, for each bridge, the 36 values of the failure probability at the design PGA have been divided by the value for the reference synchronous case (P_{f_sync}) and the statistics of these ratios have been evaluated. These are represented in Fig. 7-11: it is noted that in the large majority of cases the mean is greater than one. The few cases of mean equal

to one correspond to the bridges for which the synchronous input is already such as to cause a close-to-collapse condition (i.e. $P_{f_sync} \approx 1$), thus limiting the margin for further increment of the failure probability. On the contrary, the few cases of mean amplification larger than one order of magnitude are not significant since the corresponding P_{f_sync} is particularly low.

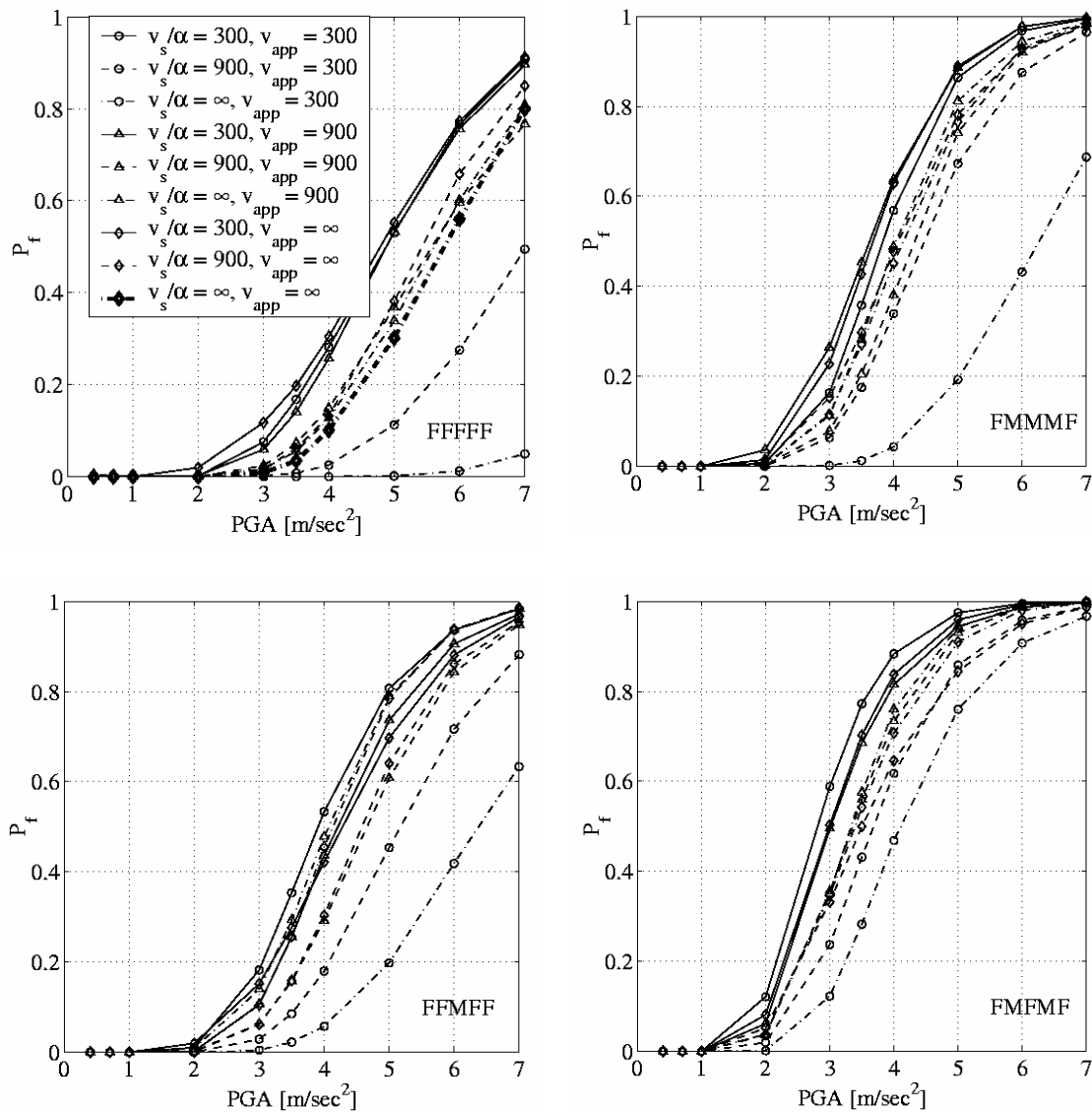


Fig. 7-10: Fragility curves

These results allow to conclude that, within the limits of the configurations and parameters considered in this study, the asynchronous input statistically decreases the level of safety with respect to that obtained in the assumption of rigid input motion.

A second important finding is that local soil condition play a major role with respect to that played by the wave passage and the loss of coherency. Evidence of this finding is achieved by comparing the maximum value of the amplification of P_f due to the soil profile variation only, i.e. among the four combinations FFFFF- ∞ - ∞ , FMMMMF- ∞ - ∞ , FFMFF- ∞ - ∞ , FMFMF- ∞ - ∞ , with the maximum amplification due to the combination of wave passage and loss of coherency only, i.e. the nine combinations FFFFF- ∞ - ∞ , FFFFF- ∞ -900, FFFFF- ∞ -300, FFFFF-900- ∞ , FFFFF-900-900, FFFFF-900-300, FFFFF-300- ∞ , FFFFF-300-900, FFFFF-

300-300. This ratio, given in Fig. 7-12 for all bridges, is always larger than one. The observed relevance of the soil profile variability is even more important in light of the relatively moderate inhomogeneity of the considered soil profiles.

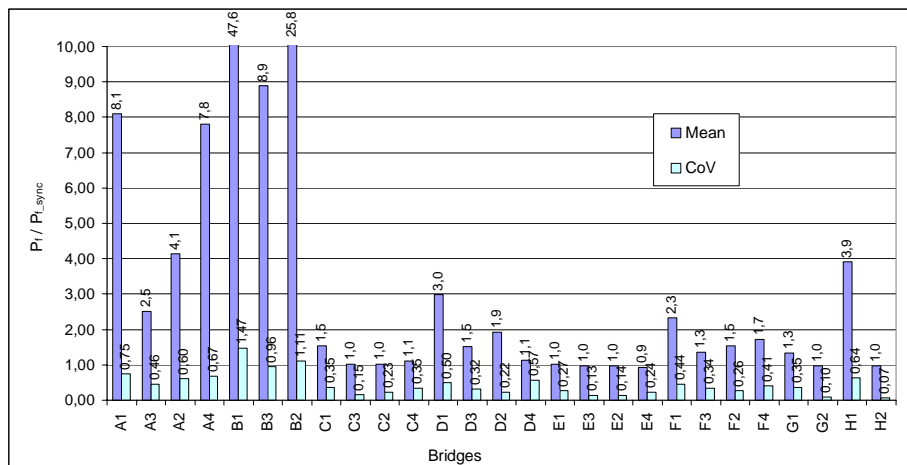


Fig. 7-11: Mean and coefficient of variation (from a sample of 36 values) of $P_j / P_{j, sync}$ for all 27 bridges.

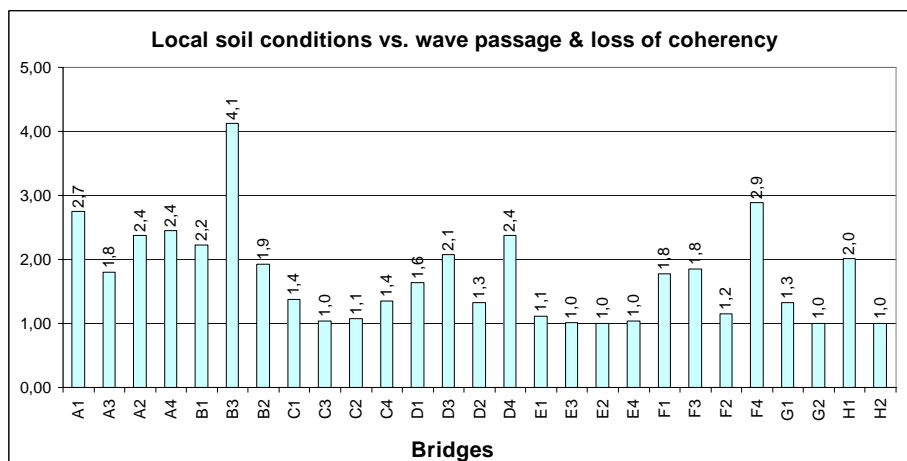


Fig. 7-12: Ratio of maximum P_j including different soil conditions but no wave-passage & loss of coherency effects over maximum P_j including wave-passage & loss of coherency but no difference in soil conditions.

7.3.3 Sextos, Kappos and Pitilakis 2003

7.3.3.1 Description of the study

This parametric study follows a companion work where a comprehensive methodology for inelastic dynamic analysis of bridges accounting for spatial variability, local site conditions and soil-foundation-superstructure interaction is presented.

The bridge typologies are shown in Fig. 7-13. The 200m-long one (Top) coincides with one of the bridge types analysed in Lupoi et al (2005), specifically that with Deck Type 2 and Pier Type 2. The longer ones, 400 and 600m total length (Middle and Bottom, respectively), are obtained as variations of the original one.

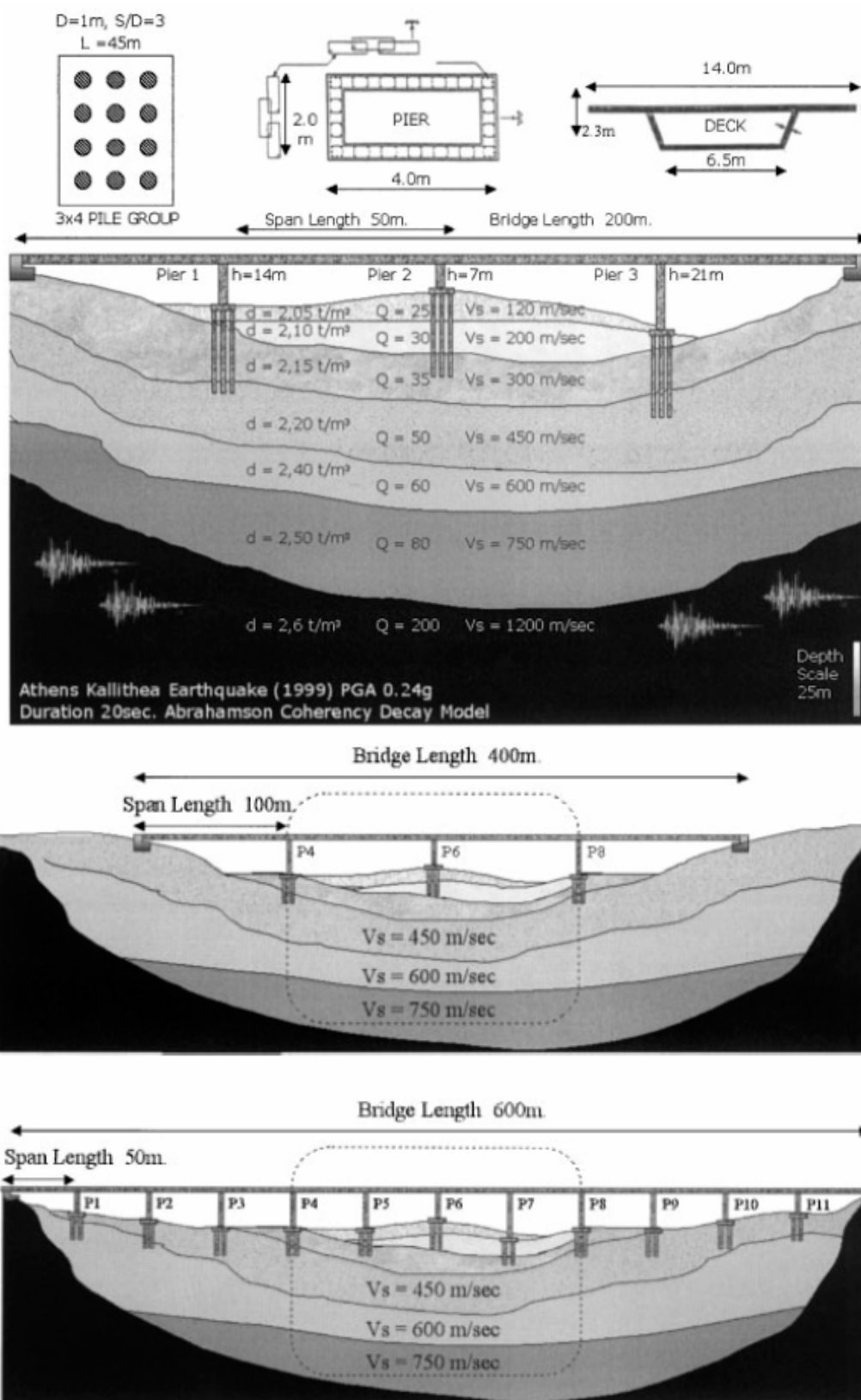


Fig. 7-13: Top: Model A (reference bridge), middle: Model G2, bottom: Model G3.

The actual cases examined in the study are reported in Table 7-4, where it is seen that, in addition to different geometric configurations, a number of alternatives are considered for what concerns cracked stiffness to be used when analysis is linear elastic, different direction of excitation, etc.

Model	Difference with respect to the reference bridge	T_{long} (s)	T_{transv} (s)
A	None (reference bridge)	0.60	0.58
B1	$EI_{eff} / EI_{gross} = 100\%$	0.42	0.40
B2	$EI_{eff} / EI_{gross} = 75\%$	0.50	0.48
B3	$EI_{eff} / EI_{gross} = 40\%$	0.67	0.64
B4	$EI_{eff} / EI_{gross} = 30\%$	0.74	0.70
C1	$H_1 = 14\text{m}, H_2 = 7\text{m}, H_3 = 14\text{m}$	0.61	0.46
C2	$H_1 = 14\text{m}, H_2 = 14\text{m}, H_3 = 14\text{m}$	0.80	0.61
C3	$H_1 = 14\text{m}, H_2 = 21\text{m}, H_3 = 14\text{m}$	0.92	0.77
D1	$H_1 = 11\text{m}, H_2 = 4\text{m}, H_3 = 18\text{m}$	0.59	0.51
D2	$H_1 = 17\text{m}, H_2 = 10\text{m}, H_3 = 24\text{m}$	0.85	0.68
E1	Monolithic abutment-deck connection	0.60	0.58
E2	Abutment-backfill interaction	0.61	0.59
E3	Transversely free abutment-deck connection	1.60	1.60
F1	Excitation in the longitudinal direction	1.98	0.86
F2	Excitation with alternative "target" frequency content	0.60	0.58
G1	Overall length 400m, span length 50m	0.70	0.70
G2	Overall length 400m, span length 100m	2.17	0.83
G3	Overall length 600m, span length 50m	0.69	0.69
G4	Overall length 600m, span length 100m	1.67	0.77
G5	Overall length 600m, span length 150m	3.05	1.13

Table 7-4: Cases considered in Sextos et al.

The reference bridge is assumed to be located on a hypothetical subsoil structure, whose geometry, stiffness, density and damping properties (quality factor $Q = \xi/2$) are also shown in Fig. 7-13. In order to explore the importance of total and span lengths, additional bridges are included (G1 to G5).

The frequency content of the input motion at the bedrock is described by the elastic response spectrum from the Kallithea record (1999 Athens earthquake). Twenty samples of ground motions having the desired degree of correlation (according to the Luco & Wong model) are generated at the bedrock, and then propagated to the surface through the soil profiles underneath the piers (one-dimensional site-response analysis).

For each one of the twenty cases reported in Table 7-4, the analysis is performed for 9 scenarios, characterised by a different level of completeness. For the purpose of the present review, which does not consider separately the effects of soil-structure interaction, only six of these scenarios are relevant. They are reported in Table 7-5.

Scenarios	SC1	SC2	SC3	SC4	SC8	SC9
Uniform excitation	X					X
Wave-passage		X	X	X	X	
Loss of coherence			X	X	X	
Site effects				X	X	
Fixed-base supports	X	X	X	X		X
Kinematic & Inertial SSI					X	
Elastic response of piers	X	X	X	X		
Inelastic response of piers					X	X

Table 7-5: Partial list of scenarios considered in Sextos et al.

7.3.3.2 Main results

Selected results are presented in figures from Fig. 7-14 to Fig. 7-16.

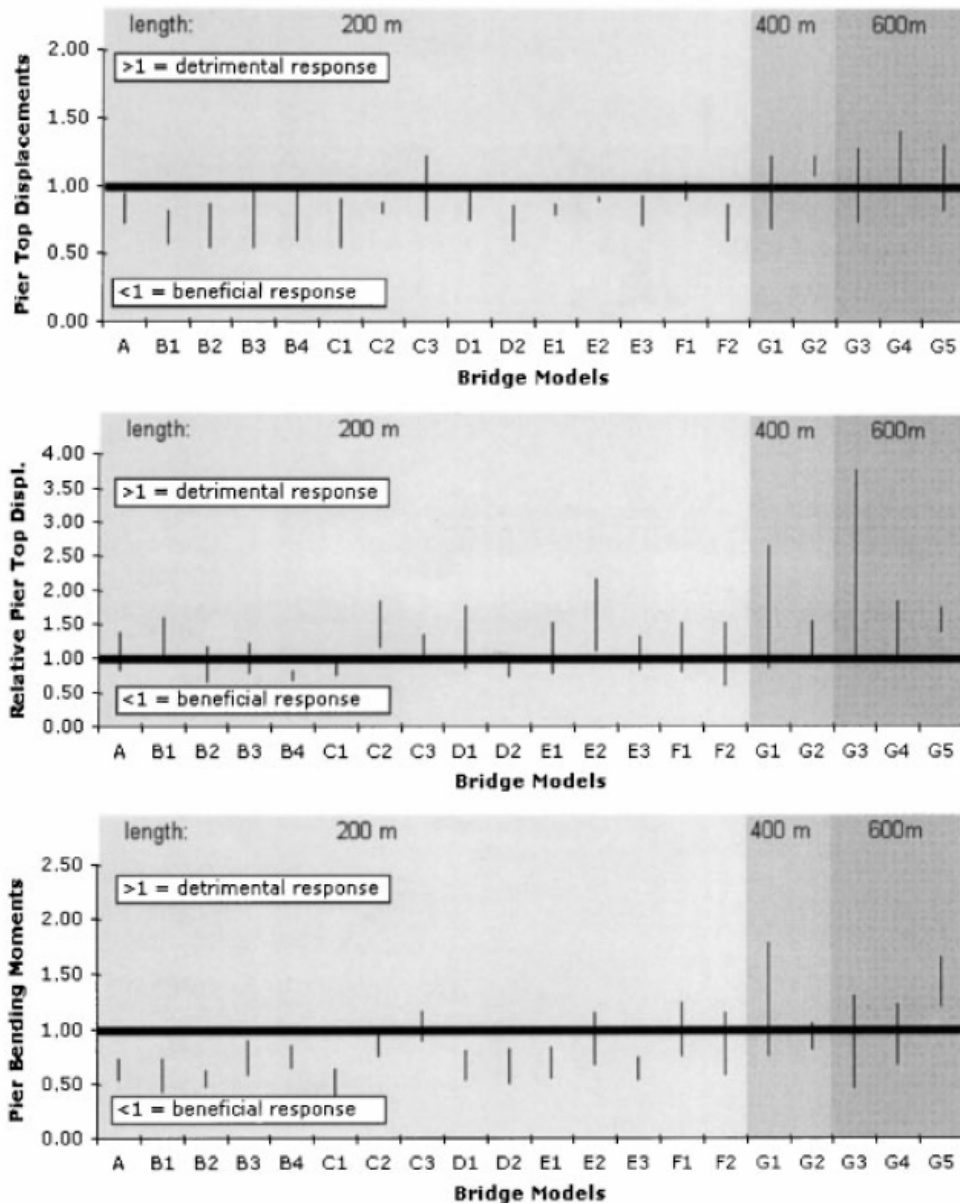


Fig. 7-14: Results of scenario SC3 (loss of coherence and wave-passage, no site effects) normalised to scenario SC1 (rigid-base input)

The response quantities shown in the figures are maximum displacement at the pier top, maximum relative displacement between pier tops and maximum bending moment at the piers base for the two elastic cases reported (SC3 and SC4). For scenario SC9, which considers inelasticity in the piers, the response quantity is maximum rotation ductility at the pier base.

Fig. 7-14 shows for each of the twenty bridge cases considered, the results from the scenario SC3, normalised by those of scenario SC1. For each bridge model the vertical bar represents the range of variation of the normalised responses over the twenty sample motion generated. The top and bottom plots contain correlated quantities, and in statistical terms over the entire population of bridge cases, one can see that the combined effects of loss of coherence and wave-passage have overall a mild favourable effect for the bridges of total length of 200m, which shows a tendency towards detrimental effects for increasing total length.

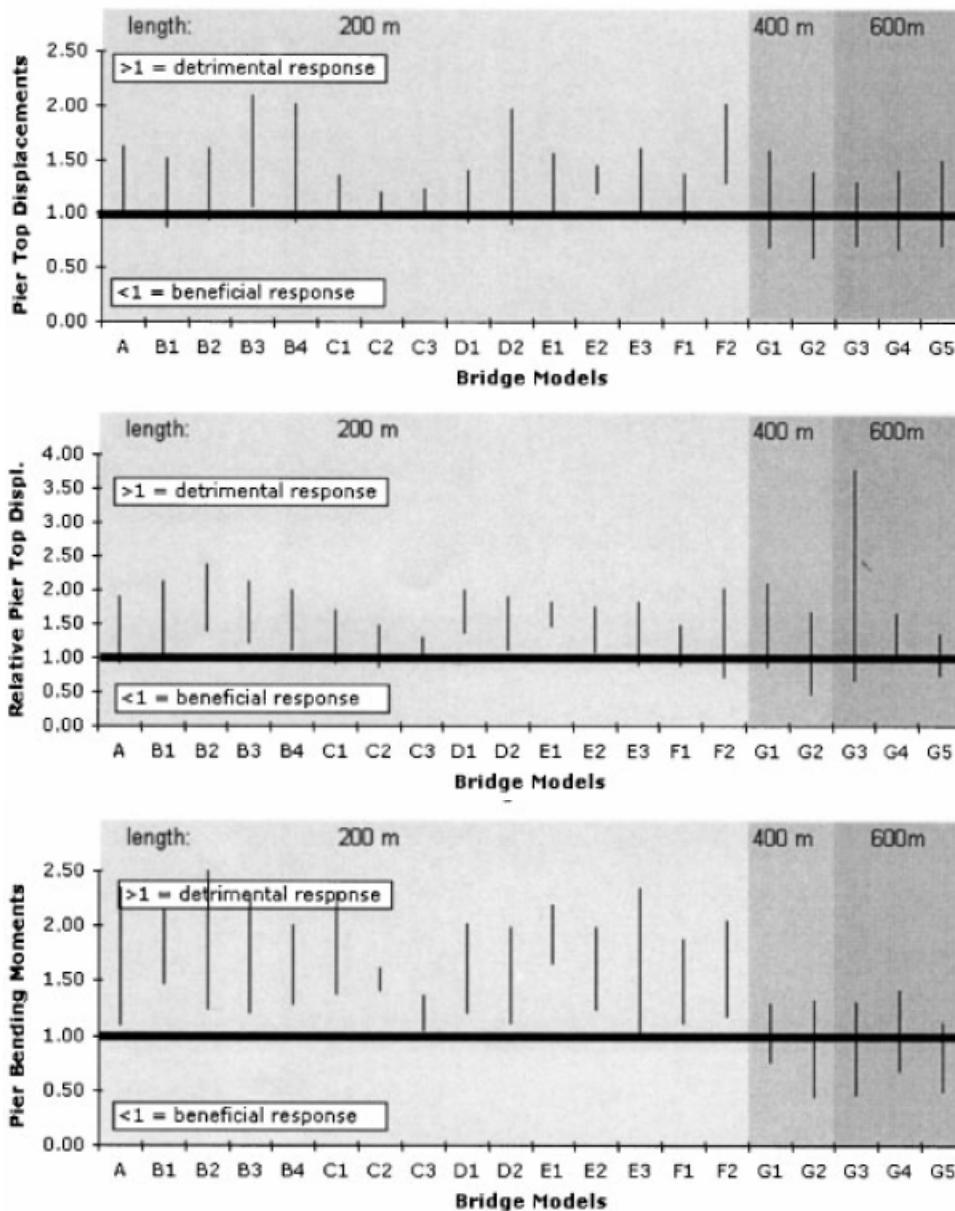


Fig. 7-15: Results of scenario SC4 (loss of coherence, wave-passage and site effects) normalised to scenario SC1 (rigid-base input)

Fig. 7-15 shows for each of the twenty bridge cases considered, the results from the scenario SC4, normalised by those of scenario SC1. It is apparent that the consideration of the actual local site conditions at the supports has a marked negative effect on the response, with average increases with respect to the uniform excitation case between 1.5 and 2.

Finally, the last results presented is a comparison between the response obtained with most realistic model, which includes all of the relevant effects and accounts for inelasticity in the structure, and that of an inelastic reference model, which is like scenario SC1 but for the pier behaviour which is inelastic. These results are shown in Fig. 7-16, where one can note that practically in all cases the response is amplified by factors ranging from 1 to 3.

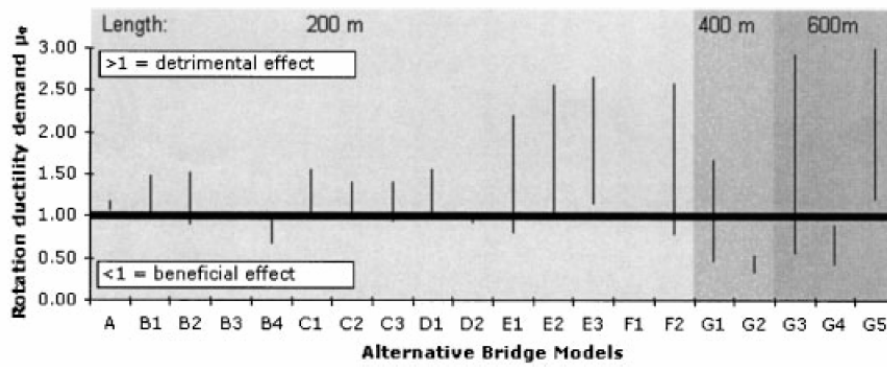


Fig. 7-16: Results of scenario SC8 (inelastic, loss of coherence, wave-passage, site effects, SSI) normalised to SC9 (inelastic, uniform motion, fixed-base)

7.3.4 Shinozuka, Saxena and Deodatis 2000

7.3.4.1 Description of the study

The study concerns the response of seven existing bridges, having the overall geometric properties reported in Table 7-6.

Bridge	Number of spans	Largest span (m)	Total length (m)	Number of expansion joints
Text	3	13.2	33.3	0
FHWA 2	3	45.6	120	0
TY0H	5	52.5	238.5	0
TY1H	5	52.5	238.5	1
TY2H	5	52.5	238.5	2
Gavin Canyon	5	62.4	222	2
Santa Clara	12	42.9	492	0

Table 7-6: Bridges analysed in the study by Shinozuka et al.

All bridges have been analysed considering the seismic input acting along the axis of the bridge.

The coherency function employed in this study accounts for loss of coherence effect only according to the expression (Harichandran & Vanmarke, 1986):

$$\gamma_{jk}(\omega) = A \exp \left[\frac{2\xi_{jk}}{\alpha\theta(\omega)} (1 - A + \alpha A) \right] + (1 - A) \exp \left[\frac{2\xi_{jk}}{\theta(\omega)} (1 - A + \alpha A) \right] \quad (7-12)$$

where ξ_{jk} is the distance between stations j and k , the frequency dependent function $\theta(\omega)$ has the form:

$$\theta(\omega) = k \left[1 + \left(\frac{\omega}{\omega_0} \right)^b \right]^{-1/2} \quad (7-13)$$

and $A, \alpha, k, \omega_0, b$ are model parameters.

Wave-passage effect is accounted for by means of the modulating function, which is dependent on wave-propagation velocity v_{app} , thus producing a time-shift ξ_{1j}/v_{app} between the motions at different stations:

$$A_{1j}(t) = \begin{cases} 0 & t < \frac{\xi_{1j}}{v_{app}} \\ a_1 \left(t - \frac{\xi_{1j}}{v_{app}} \right) \exp \left[-a_2 \left(t - \frac{\xi_{1j}}{v_{app}} \right) \right] & t \geq \frac{\xi_{1j}}{v_{app}} \end{cases} \quad (7-14)$$

A single set of values is adopted in the study ($A = 0.626, \alpha = 0.022, k = 19700m, \omega_0 = 12.7rad/s, b = 3.47$). The values are those estimated from data of the SMART-1 array by Harichandran and Wang. The parameters of the modulating function have been assigned the values $a_1 = 0.906$ and $a_2 = 1/3$. As an example, Fig. 7-17 shows on the left the modulating functions for three stations 50m apart and for $v_{app} = 1000m/s$, and on the right, the loss of coherence function for a discrete number of distances between distances.

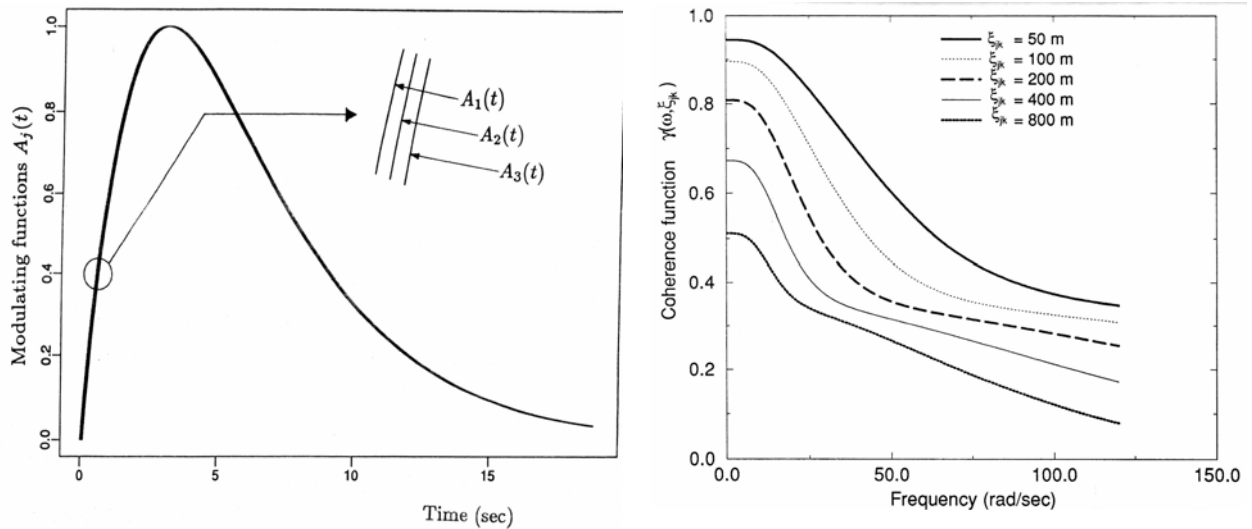


Fig. 7-17: Shinozuka et al: left, modulating functions, right, loss of coherence functions.

It is noted the large difference between the loss of coherence functions adopted in this and in the Monti et al 1996 study (Fig. 7-5 and Fig. 7-17), the former ones representing a much faster decrease in correlation with frequency.

For each bridge, eight cases of spatial variability have been considered, reported in Table 7-7. For each case 20 sample ground motion have been generated and used in the non-linear dynamic analyses. Further, an additional case has been considered for all bridges, i.e. a rigid-base input ($\gamma_{ij}(\omega) \equiv 1 \quad \forall i, j$), labelled as IDENT, so as to allow a direct comparison between the response for all possible sources of soil variability and that for the conventionally adopted synchronous input.

Case	Loss of coherence	Wave-passage v_{app} (m/s)	Soil conditions
1	Yes	1000	SAME
	Yes	300	SAME
	Yes	1000	DIFF
2	Yes	∞	SAME
	Yes	∞	DIFF
3	No	1000	SAME
	No	300	SAME
	No	1000	DIFF

Table 7-7: Cases considered (SAME= uniform soil conditions, DIFF= variable soil conditions).

The DIFF soil profile corresponds, for each bridge, to a simplification of the real profile under the bridge according to UBC site classification criteria, as reported in Table 7-8.

Bridge	Soil at abutments	Number of piers	UBC soil type II (medium) at piers	UBC soil type III (soft) at piers
Text	Medium	2	1	2
FHWA	Medium	2	-	1, 2
Gavin Canyon	Medium	4	1, 4	2, 3
TY0H	Medium	4	1, 4	2, 3
TY1H	Medium	4	1, 4	2, 3
TY2H	Medium	4	1, 4	2, 3
Santa Clara	Medium	11	1-4, 8-11	5-7

Table 7-8: Description of different local soil conditions for the seven bridges.

7.3.4.2 Main results

The response variable used to describe the effect of spatial variability is the peak flexural ductility demand at the base of each pier. The results are similar for all bridges. For two of them, the FHWA and the TY1H bridges, sample results are reported and commented.

Fig. 7-18 shows, on the left, the peak ductility demands for six out of the eight cases reported in Table 7-7 (the cases excluded are those with $v_{app} = 300\text{m/s}$), and on the right the ratio of peak ductilities for two cases of differential soil motions (Case 1 SAME, Case 1 DIFF), to that of rigid-input. One notes that the different combinations of loss of coherence and wave-passage effects do not produce appreciable differences in the response, with or without differential soil conditions at the supports. When soil conditions differ, however, the magnitude of the response is significantly increased. This can be more clearly appreciated from the plot on the right, where it is seen that addition of the actual, different, soil conditions doubles the ductility demand with respect to the case of wave-passage and loss of coherence alone. More importantly, the plot shows how the ductility demand increases about 2.5 times with respect to the rigid-input case, for this particular bridge, when all effects are present.

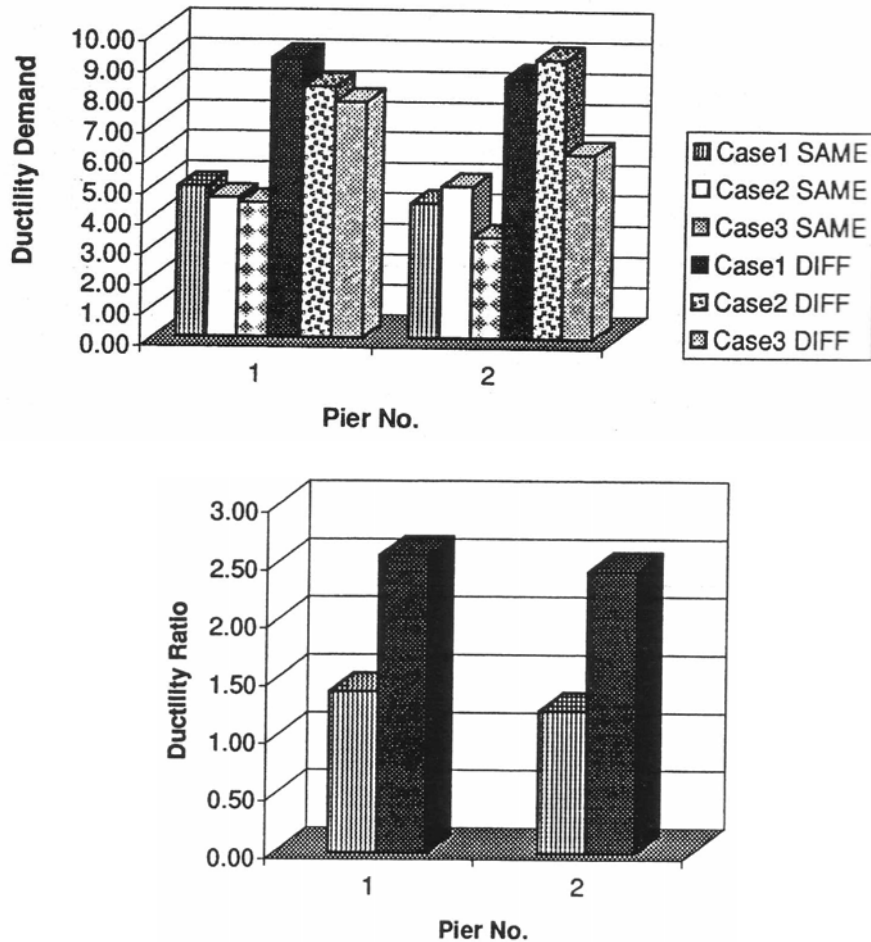


Fig. 7-18: Sample results for the FHWA bridge.

Fig. 7-19 shows selected results from the TY1H bridge case. The plots represent the same quantities as those in Fig. 7-18. Results, and observations, are entirely analogous to those already made for the previous bridge.

The consistent nature of the results obtained for all bridges, leads the authors to conclude that, whenever soil differences are present along the bridge axis, the commonly adopted, conventional, rigid input design procedure is unconservative. They suggest for this case to use, for design purposes, non-linear time-history analyses using as input correlated ground motions generated to match target response spectra appropriate for the specific site conditions at each support. Similar conclusions and recommendations can be found in the study by Monti and Pinto (1998), which refers to isolated bridges. This study is briefly outlined in the next section.

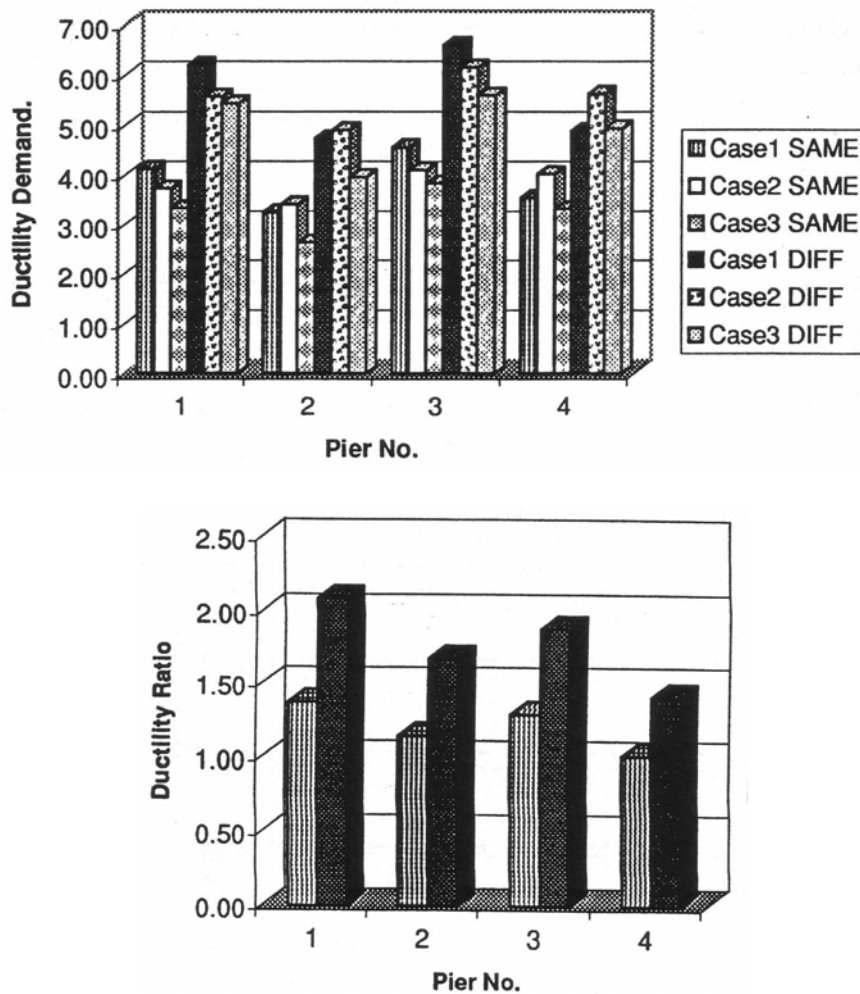


Fig. 7-19: Sample results for the TYIH bridge.

7.3.5 Monti and Pinto 1998

The study refers to a single bridge configuration, identical to that shown in Fig. 7-2, with the single pier height of $H = 10.0m$. In this case the deck is supported on isolator devices on top of both piers and abutments. All analyses are carried out in the transverse direction. Beside wave-propagation and loss of coherence effects, various combinations of soil properties beneath the supports are considered in this study. In particular, the six different sequences of firm (F) and medium (M) soil types considered are: FFFFF, FFMFF, MMFMM, MMMMM, MFFFM, FMMMM, with firm and medium are defined as in Section 0, and the abutments are assumed to be always on firm soil.

Response analyses are performed with a random vibration approach and equivalent linearization of the bilinear inelastic isolator devices. The response quantities considered are the medians from the distribution of the maxima of each isolator displacement. The main results and conclusions can be derived directly by observing the plots in Fig. 7-20 and Fig. 7-21.

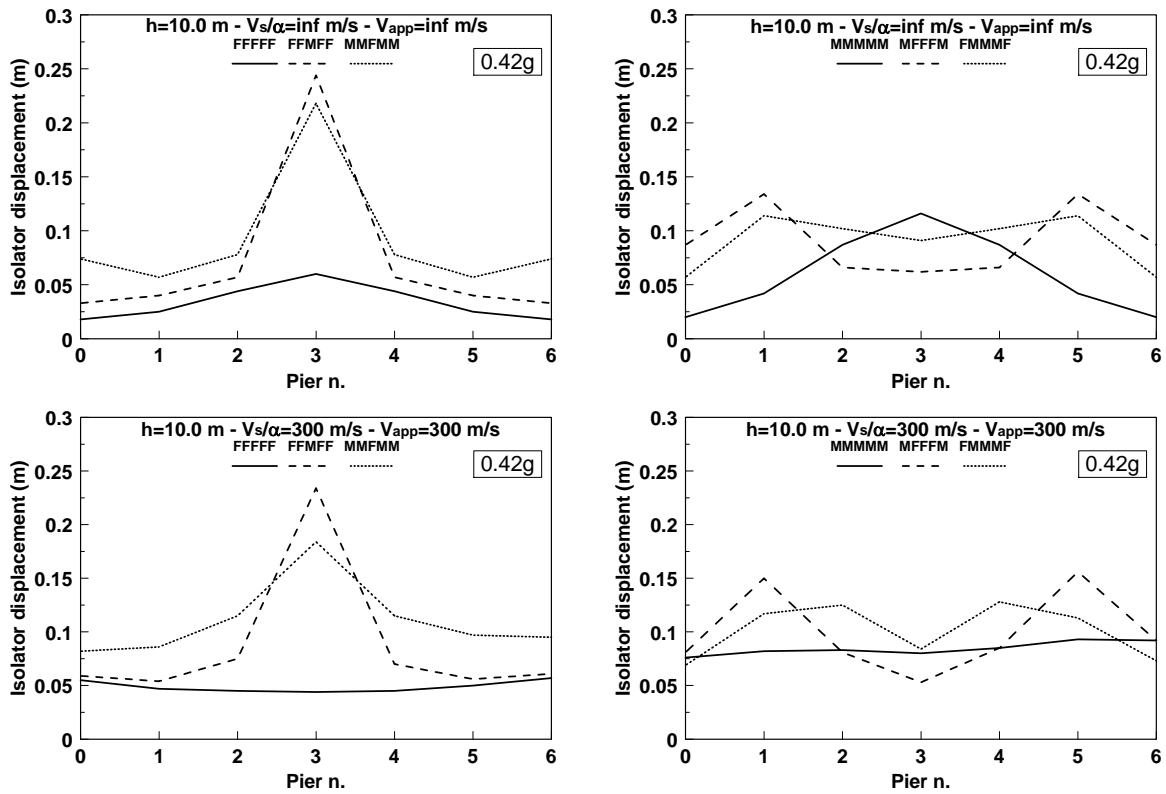


Fig. 7-20: Isolator displacement responses for varying soil profiles.

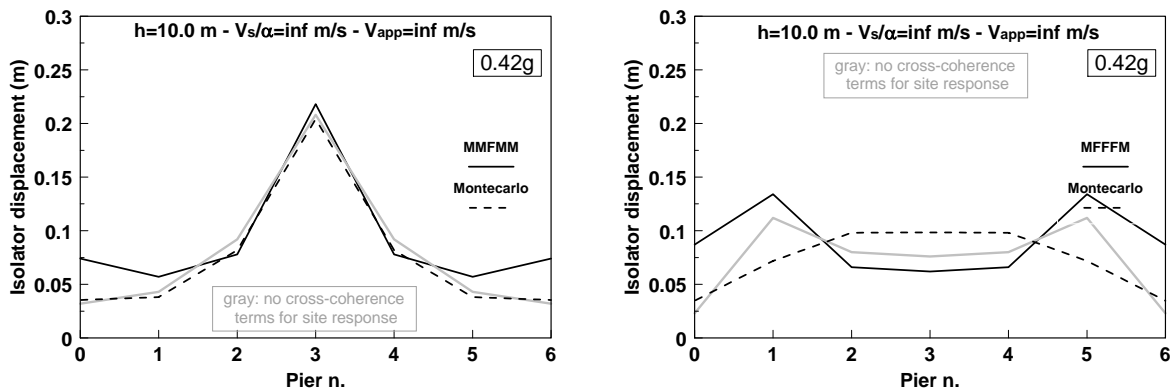


Fig. 7-21: Isolator displacement response obtained with Monte Carlo analyses (dashed lines), compared with random vibration analyses with complete ground motion model (black lines) and the simplified model with no coherence terms (grey lines).

Fig. 7-20 refers to the cases of just one pier having different soil condition (Left) and to that of three piers resting on a different soil type (Right). In both cases it is observed that the presence of non-homogeneous soil profile under the supports dominates over other sources of spatial variability, such as loss of coherence and wave-passage, suggesting the practical possibility of disregarding these latter altogether. Further, it is worth examining a further simplification consisting in setting to zero also the coherency term accounting for site effect (third factor in Eq.(7-3)). This simplification is acceptable, as shown in Fig. 7-21 by the comparison of random vibration analysis, with and without off-diagonal terms in the matrix (7-1). This, in accordance with the findings of Shinozuka et al (2000), opens the possibility of dealing with the problem by simply performing non-linear time-history analyses using as input independently generated ground motions matching target response spectra appropriate

for the specific site conditions at each support. This possibility is validated by the further comparison in Fig. 7-21, which includes median isolator displacements from numerical simulation.

7.3.6 Nuti and Vanzi 2004, 2005

As anticipated, this study differs from the previous ones in that it does not investigate the effect of the spatial variability of ground motion on the structural response of an entire bridge, but focuses instead on the determination, in probabilistic terms, of maximum differential displacements between two points, both at the ground level and at the top of cantilever piers resting on the two points.

Solution of the above problem is useful in the design of simply supported bridges, when sizing seating lengths and displacement capacity of moveable bearings, and, more generally, if a simplified analysis with imposed deformations is employed to account for spatial variability of ground motion.

7.3.6.1 Description of the study

The study includes two steps. The first one consists in the derivation, starting from the vector random process model presented in Section 7.2.1, of the power spectral density of the random process of relative displacement between two points at distance d_{ij} , denoted by X_{PQ} in the study. The sought PSD is obtained based on the individual PSD's of the displacement processes in P and Q . The variance of the relative displacement follows from its PSD and, using an appropriate peak factor, any desired fractile value of the distribution of maximum relative displacement can be obtained.

The second step consists of an exhaustive parametric analysis from which a simplified well-approximate expression for the fractile differential displacement is derived. The data used for this analysis are briefly summarised in the following.

Soil types at the two points are characterised in terms of power-spectral densities of ground displacement, consistent with three different displacement response spectra as specified in Eurocode 8 for soil types A, B-C-E and D. The consistent PSD is obtained as a modification, through a further frequency-dependent filter, of the Clough-Penzien two-filter model.

The value of the shear-wave velocity is uniquely associated to each of the above spectra, hence the loss of coherence parameter is only the factor α (the Luco-Wong model as represented in Eq.(7-3) is used). Values for the apparent wave velocity v_{app} are also given in the code for the three soil types. To account for large uncertainty associated with the estimate of v_{app} , the code values have been factored by a parameter θ with values 0.5, 1 and 1.5. The values given in EC8 for v_s and v_{app} for each soil type are reported in Table 7-9.

	A	B,C,E	D
Description	rock	gravel, sand, clay	gravel, sand, clay
v_s (m/s)	800	580	90
v_{app} (m/s)	3000	2000	1500

Table 7-9: Values of v_s and v_{app} specified in EC8.

The range of variation of all the considered parameters is reported in Table 7-10.

Variable	Value
Variables used to assess differential displacement at ground level	
Soil type in P	A,B and D as in EC8
Soil type in Q	A,B and D as in EC8
Distance between P and Q	0 – 10000m
Coherency parameter α	0.02 – 0.5
θ	0.5, 1.0, 1.5
Probability level	0.01 – 0.99
Additional variables for differential displacement between pier tops (only for $\alpha = 0.5, \theta = 1$)	
Period of first structure T_p	0.2s – 2.0s
Period of second structure T_Q	0.2s – 2.0s

Table 7-10: Values of the parameters used in parametric analysis.

7.3.6.2 Results

The most relevant final result for what concerns the maximum relative displacement between point P and Q at ground surface, as a function of their distance and for different coupling of local site conditions, is shown in Fig. 7-22. Values refer to a reference PGA value of 1 m/s^2 . The curves are obtained for the most unfavourable situation, i.e. for a value of α equal to 0.5. For this value of α the differential displacement is insensitive to θ .

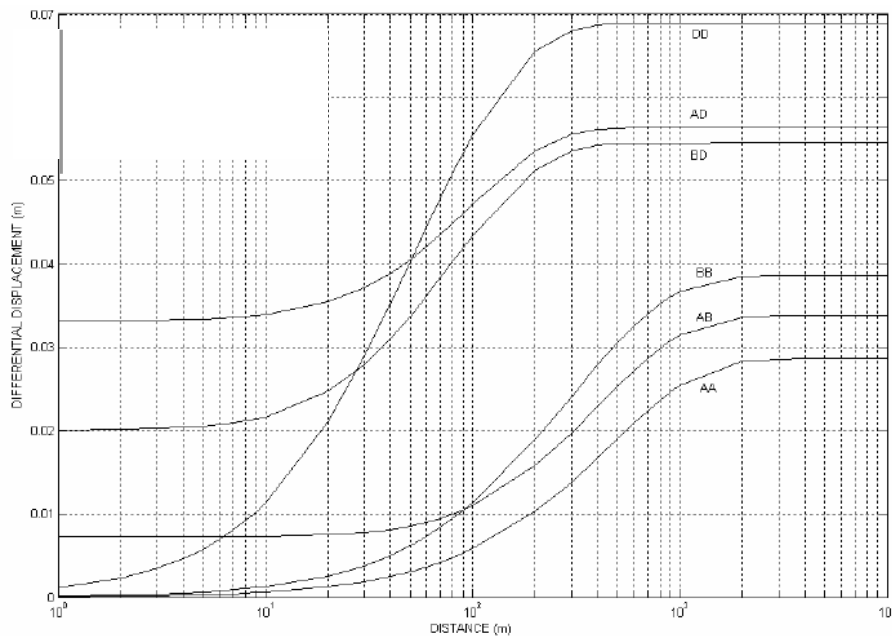


Fig. 7-22: Differential soil displacement as a function of soil-coupling and distance.

An approximate analytical expression for the curves in Fig. 7-22 is provided:

$$\Delta u(X_{PQ}) = q_1 + q_2 [\log(X_{PQ})]^{q_3} \leq \Delta u_{\max} \quad (7-15)$$

with values of q_1, q_2, q_3 and Δu_{\max} as given in Table 7-11.

	$100q_1$			$10^5 q_2$			q_3			Δu_{\max}		
	A	B	D	A	B	D	A	B	D	A	B	D
A	0	0.70	3.30	16.97	1.36	17.05	2.52	3.87	2.80	2.90	3.40	5.60
B	-	0	2.00	-	14.28	28.91	-	2.90	2.81	-	3.9	5.5
D	-	-	0	-	-	265.54	-	-	1.91	-	-	6.9

Table 7-11: Values to be used in Eq.

(7-15).

It is noted in the study that the value obtained for Δu_{\max} is also reasonably approximated by the commonly adopted code provision consisting in taking for Δu_{\max} the square root of the sum of the squares of the individual peak ground displacements in P and Q .

The study concludes with the analysis of the maximum relative displacement between the tops L and M of adjacent piers, resting on points P and Q . The analysis is carried out for fixed values of α and θ , i.e. 0.5 and 1 respectively. The total differential displacement between pier tops Δu_{LM} is cast in the form:

$$\Delta u_{LM} = D[\Delta u(X_{PQ}) + \Delta u(T_L, T_M)] \quad (7-16)$$

where $\Delta u(T_L, T_M)$ is the relative displacement between two SDOF systems of period T_L and T_M respectively, evaluated according to the CQC rule, and D is a correction factor.

It is found that the trend of the term D varies as a function of distance X_{PQ} and periods T_L and T_M , differently depending on whether the period separation $T_L - T_M$ is above or below 0.1s. The former case is considered first. The maximum and minimum values of the correction factor D have been calculated, as a function of distance and parametrised by soil coupling, by considering all possible pairs of periods T_L and T_M taken in the range 0.2s-2s, having difference $T_L - T_M \geq 0.1s$.

The authors comment that “no matter what the distance and the soil coupling is, the value of 1 is a reasonable upper bound for D . The correct value of D depends on soil coupling and the period distance, and ranges from about 0.6 to 0.98” (i.e. $D_m \pm D_e$).

The case of $T_L - T_M$ lower than 0.1s gives rise to a less regular trend and the authors provide an approximate analytical expression for D . They add, however, that period distances of such a small magnitude do not occur in practice, hence they suggest to retain the value of D equal to 1 for this case also.

7.4 Concluding remarks

The preceding sections contain a review of the most relevant studies on the effect of ground motion spatial variability on the maximum response of bridge structures. One cannot but confirm that the present state of the art is still rather inadequate for what concerns the physical modelling of the phenomenon and that the available studies, based on present

models, do not cover the whole range of cases that can occur in practice. In spite of the limited scope of each of these studies, a well-defined trend systematically emerges from all of them. The sources of ground motion spatial variability denoted as loss of coherence and wave-passage produce responses that, in statistical terms, are equal or slightly lower than those obtained by ignoring them. Of course, including these sources in an assessment procedure would lead to an increase of the global variability of the response. One has to note, however, that this variability is well within the resolution in controlling the response achievable with the present design procedure, which would lead logically to discard consideration of these effects for design purposes.

On the contrary, when ground motion spatial variability is due to differences in soil profiles beneath the supports the effect on the response can be quite substantial. Clearly, given the infinite variety of possible combinations of subsoil conditions and of bridge structures, no general design rules can be expected. The problem shifts on how to account for this phenomenon in a way that is practical and still reasonably accurate. From the (limited) evidence presented, it appears that such a solution might consist in performing time-history analyses of the bridge structure using as input at each pier independent ground motions generated according to the local soil conditions. Ignoring the actual correlation between the motion at the supports does not seem to introduce significant error in the estimate of the response.

References

- Abrahamson N.A., Schneider J.F. & Stepp J.C. 1991. Empirical spatial coherency functions for application to soil-structure interaction analyses. *Earthquake Spectra*, Vol.7(2) pp. 1-27
- Der Kiureghian A. & Neuenhofer A. 1992. Response spectrum method for multi-support seismic excitations. *Earthq. Eng. & Struct. Dyn.*, Vol.21 pp. 713-740
- Der Kiureghian A. 1996. A coherency model for spatially varying ground motions. *Earthq. Eng. & Struct. Dyn.*, Vol.25 pp. 99-111
- Hao H., Olivera C.S. & Penzien J. 1989. Multiple-station ground motion processing and simulation based on SMART-1 array data. *Nuclear Engineering & Design*. Vol. 111 pp.293-310
- Harichandran R.S. & Vanmarke E. 1986. Stochastic variation of earthquake ground motions in space and time. *ASCE Jnl Eng. Mech.*, Vol.112 pp.154-174
- Harichandran R.S., Hawwari A. & Sweidan B.N. 1996. Response of long-span bridges to spatially varying ground motions. *ASCE Jnl Struct. Eng.*, Vol.122(5) pp.476-484
- Luco J.E. & Wong H.L. 1986 Response of a rigid foundation to a spatially random ground motion. *Earthq. Eng. & Struct. Dyn.*, Vol.14 pp. 891-908
- Lupoi A., Franchin P., Monti G. & Pinto P.E. 2005. Seismic design of bridges accounting for spatial variability of ground motion. *Earthq. Eng. & Struct. Dyn.*, Vol.34 pp. 327-348.
- Monti G., Nuti C. & Pinto P.E. 1996. Nonlinear response of bridges under multisupport excitation. *ASCE Jnl Struct. Eng.*, Vol.122(10) pp.1147-1159
- Monti G. & Pinto P.E. 1998. Effects of multi-support excitation on isolated bridges. *Tech.Report MCEER 98/0015*, pp.225-247
- Nuti C. & Vanzì I. 2004. Influence of earthquake spatial variability on the differential displacement of soil and single degree of freedom structures. *Tech. Report DIS 1/2004*, Dept. of Structures, University of Roma Tre

- Nuti C. & Vanzi I. 2005. Influence of earthquake spatial variability on differential displacement of soil and SDF system response. *Earthq. Eng. & Struct. Dyn.*, Vol.34 pp. 1353-1374.
- Sextos A.G., Kappos A.J. & Ptilakis K.D. 2003. Inelastic dynamic analysis of RC bridges accounting for spatial variability of ground motion, site effects and soil-structure interaction phenomena. Part 1: Methodology and analytical tools & Part 2: Parametric study. *Earthq. Eng. & Struct. Dyn.*, Vol. 32 pp.607-627 and pp.629-652
- Shinozuka M. 1972. Monte Carlo solution of structural dynamics. *Computers & Structures*. Vol. 2 pp. 855-874
- Shinozuka M., Saxena V. & Deodatis G. 2000. Effect of spatial variation of ground motion on highway structures. Tech. Report MCEER 00-0013, December
- Zerva A. 1990. Response of multi-span beams to spatially incoherent seismic ground motions. *Earthq. Eng. & Struct. Dyn.*, Vol.19 pp. 819-832

8 Design for active fault crossing

8.1 Introduction

Surface rupture of active faults poses a significant risk to bridges or other structures crossing or constructed over the active fault zone. While this is a well known risk, until recently there had been relatively few instances of severe damage to bridges from such ground displacements. However, in 1999, the Kocaeli (Izmit) Earthquake on 17 August (M7.4), the Chi-Chi Earthquake of 21 September (M7.3) and the Duzce Earthquake on 12 November (M7.2) all produced major damage to bridges crossing surface ruptures of active faults. This clearly highlighted the need for bridge authorities and designers to ensure that the effects and risks posed by active faults beneath bridges are appropriately considered in the planning, siting, design and construction of such bridges.

Some jurisdictions have regulations or policies to address this risk. In California, construction across active fault zones is prohibited and Caltrans have a policy to avoid siting new bridges across or very near active faults [Mualchin (2004)]. However in some cases, for example bridges crossing active faults over major rivers or harbours, it may be necessary to construct the facility across the fault zone. Clearly, in the case of existing bridges crossing active faults, retrofitting will be the only risk mitigation solution in many situations. Hence where this hazard cannot be avoided, an appropriate assessment and mitigation of the risk needs to be made in the design or retrofit of the bridge.

In the 1999 Chi-Chi Earthquake in Taiwan, seven bridges were assessed to have collapsed due to large fault displacements of the fault beneath them [Chang et al. (2004)]. Surface ground displacements were significant varying from 2 m to 9 m along of the Chelungpu fault which they crossed [Unjoh & Kondoh (2000)]. One of the bridges severely damaged was the Wushi Bridge, a 625 m long river crossing, comprising two parallel bridges with simply supported I girder spans.



Fig. 8-1: Wushi Bridge - fault movement between piers 2 and 3



Fig. 8-2: Wushi Bridge - span collapse due to longitudinal movement at pier P2N

(Figures available electronically on fib website; see production note on p. ii)

The Chelungpu fault crossed the bridge diagonally (at almost 45°) between piers 2 and 3, leading to collapse of bridge spans in this area. The vertical fault scarp can be seen in Fig. 8-1 and was estimated as 2.1 m to 2.3 m high [Hsu & Chang (2000)]. The resultant horizontal displacements were estimated to be about 2 m transverse to the bridge longitudinal axis and 2 m along the bridge. This resulted in loss of spans and severe damage to the adjacent piers as illustrated in Figures 8-2, 8-3 and 8-4.



Fig. 8-3: Wushi Bridge - shear failure of pier P2S



Fig. 8-4: Wushi Bridge - settlement and shear cracks at pier P3N

(Figures available electronically on **fib** website; see production note on p. ii)

In the 1999 Duzce Earthquake in Turkey, the almost completed Bolu Viaduct was severely damaged leaving the superstructure in a precarious position with some longitudinal girders completely unseated and hanging by the deck link slab [Priestley & Calvi (2002)]. The Duzce fault crosses the bridge alignment at an acute angle (approximately 15° to the bridge longitudinal axis). In the earthquake, right-lateral slip of the fault of approximately 1.6 m occurred, resulting in shortening of the bridge length by about 1.5 m, concentrated over two spans of the bridge. Resultant displacements of the superstructure after the earthquake were in the order of 1.1 m longitudinal and 0.5 m transverse. The bridge comprises simple spans supported on pot bearings with a seismic isolation system using energy dissipating units (EDUs). The EDUs were destroyed and most pot bearings ejected. Significant damage to the piles in the fault zone was observed at the piers indicated in Fig. 8-6. The bridge is shown in Figures 8-5, and superstructure damage is illustrated in Figures 8-7 and 8-8. The bridge was able to be repaired and retrofitted.



Fig. 8-5: Bolu Viaduct - view from abutment S2

(Figure available electronically on **fib** website; see production note on p. ii)

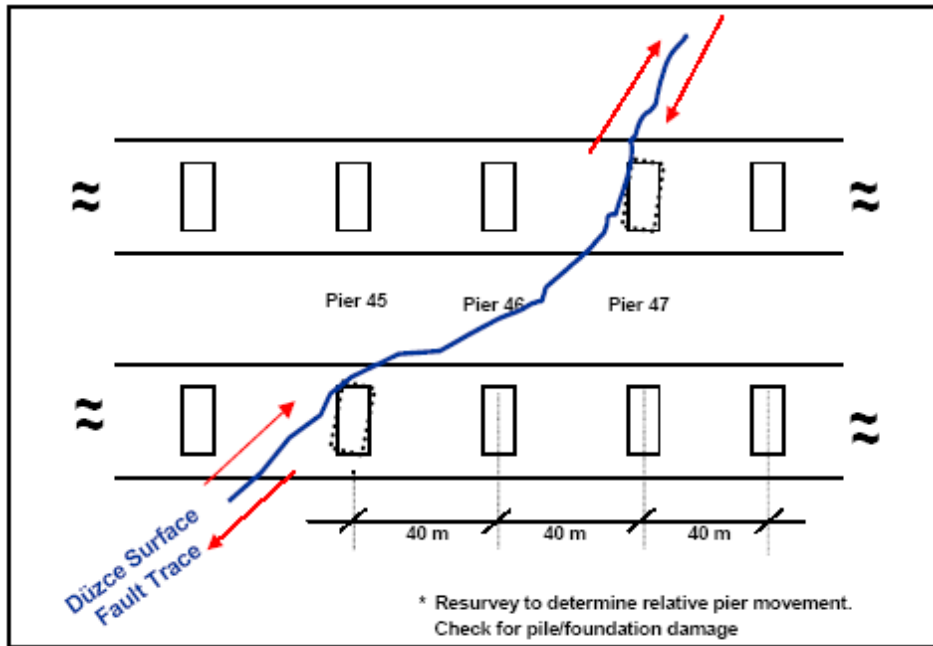


Fig. 8-6: Bolu Viaduct - fault trace between piers 45 and 47



Fig. 8-7: Bolu Viaduct - failure of an EDU



Fig. 8-8: Bolu Viaduct - unseating of beam end at pier cap

(Figures available electronically on **fib** website; see production note on p. ii)

There are a number of other examples of major bridges crossing active faults including the Vincent Thomas Suspension Bridge crossing the Palos Verde Fault in Los Angeles [Baker et al. (1998)], the San Diego-Coronado Bay Bridge crossing the Rose Canyon Fault Zone in California [Ashley et al. (2001)] and the Thorndon Overbridge crossing the Wellington Fault in New Zealand [Billings & Powell (1996)]. All these bridges have been seismically retrofitted. The Akashi Kaikyo Bridge was under construction in Japan when the M6.9 Great Hanshin (Hyogo-ken Nambu) Earthquake struck on 17 January 1995. Measurements after the earthquake showed the main span length had decreased by 3 m to 1997 m. Subsequent investigations indicated an active fault segment lies in the Akashi Strait under the bridge [Koketsu et al. (1998)].

8.2 Fault effects and ground displacements

Near fault ground motion hazards that influence bridge behaviour are:

- Dynamic displacements due to seismic wave generation; and
- Permanent displacement due to the static displacement field resulting.

Sommeville (2002) notes these need to be quantified in separate hazard analyses because they are not strongly correlated.

Dynamic displacement (or vibratory ground motion) hazard spectra for near fault motions are significantly higher than ‘far field’ motions and are commonly specified in many bridge design standards. Near fault ground motions have different characteristics from ‘far field’ motions and hence care is needed in choosing appropriate records for time history analyses.

The permanent displacement hazard at a site depends on both the characteristics of the fault and the probability that a rupture will affect the site under study. Permanent displacements and associated return periods are commonly assessed from geological studies of the fault characteristics and movement history. A methodology for the probabilistic hazard assessment of permanent displacements across faults has recently been developed by Trifunac and Todorovska (2005) for use in California. The use of this methodology and the fault displacement data shown in Fig. 8-9 resulted in the assessed hazard at a site lying on a Californian Class B Fault site as shown in Fig. 8-10.

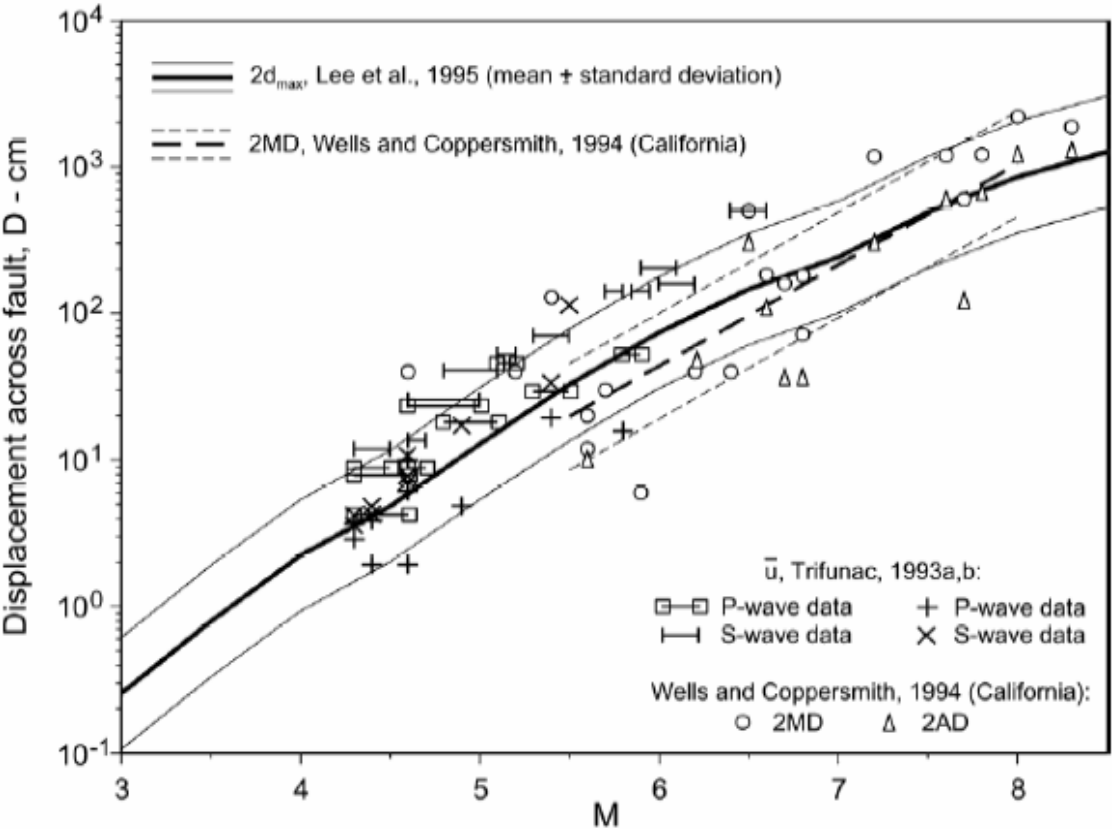


Fig. 8-9: Data on fault dislocation for earthquakes in California showing displacement at the ground surface across the fault, D , versus earthquake magnitude

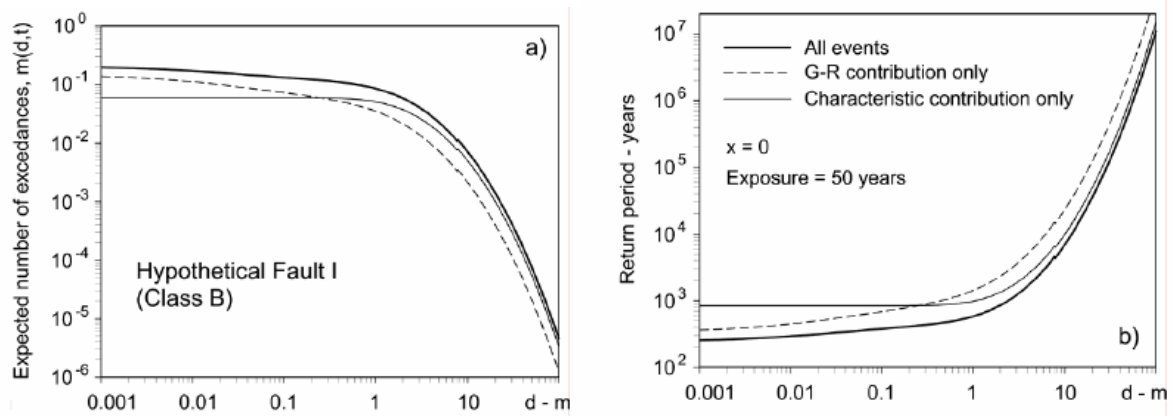


Fig. 8-10: Results at a site at the centre of the fault for hypothetical fault I (Class B): a) expected number of exceedances of level d during 50 years exposure, b) return period of exceedance of level d

The damage to a bridge crossing a fault rupture will be greatly influenced by the type of fault, the orientation of the bridge to the fault and the ground conditions. As can be seen from Figures 8-9, 8-10 and the damaged bridges described in 8.1 above, fault displacements of several metres can be expected to occur in a major earthquake. In general it is not possible for bridges to survive such movements without very special design measures and even then, for large displacements, major repairs of the bridge after the event are likely to be needed. For short or medium span bridges, reconstruction of the displaced portion of the bridge to correct the geometry is likely to be required.

8.3 Planning issues

In general, because of the risk posed to the transportation network by bridges crossing active faults, it is desirable to either avoid the fault crossing altogether or to cross the fault with lower risk alternatives [Mualchin (2004), Wu et al. (2004), Alexandris (2004)]. Typically this would involve embankments or mechanically stabilised earth retaining systems and for rail crossings would also involve guide walls.

Where there is no other feasible alternative and bridge crossing of the active fault cannot be avoided, the bridge should be designed to mitigate the risk to acceptable levels. The planning for the bridge should take into account the expected damage to the bridge in a fault rupture event and make appropriate allowance for the repair and reconstruction works necessary to reinstate the bridge.

In Taiwan, it is considered impractical to design an active fault crossing bridge to be free from damage in a fault rupture event and it is recognised that there remains, in many cases, a significant risk of collapse [Wu et al. (2004)]. For this reason, a hazard mitigation plan which includes repair methods, alternative route and construction of emergency access is required as part of the bridge planning and design process. In addition, a bridge collapse alarm system is required to be installed and maintained on the bridge. The planning and design procedure required in Taiwan is shown diagrammatically in Fig. 8-11.

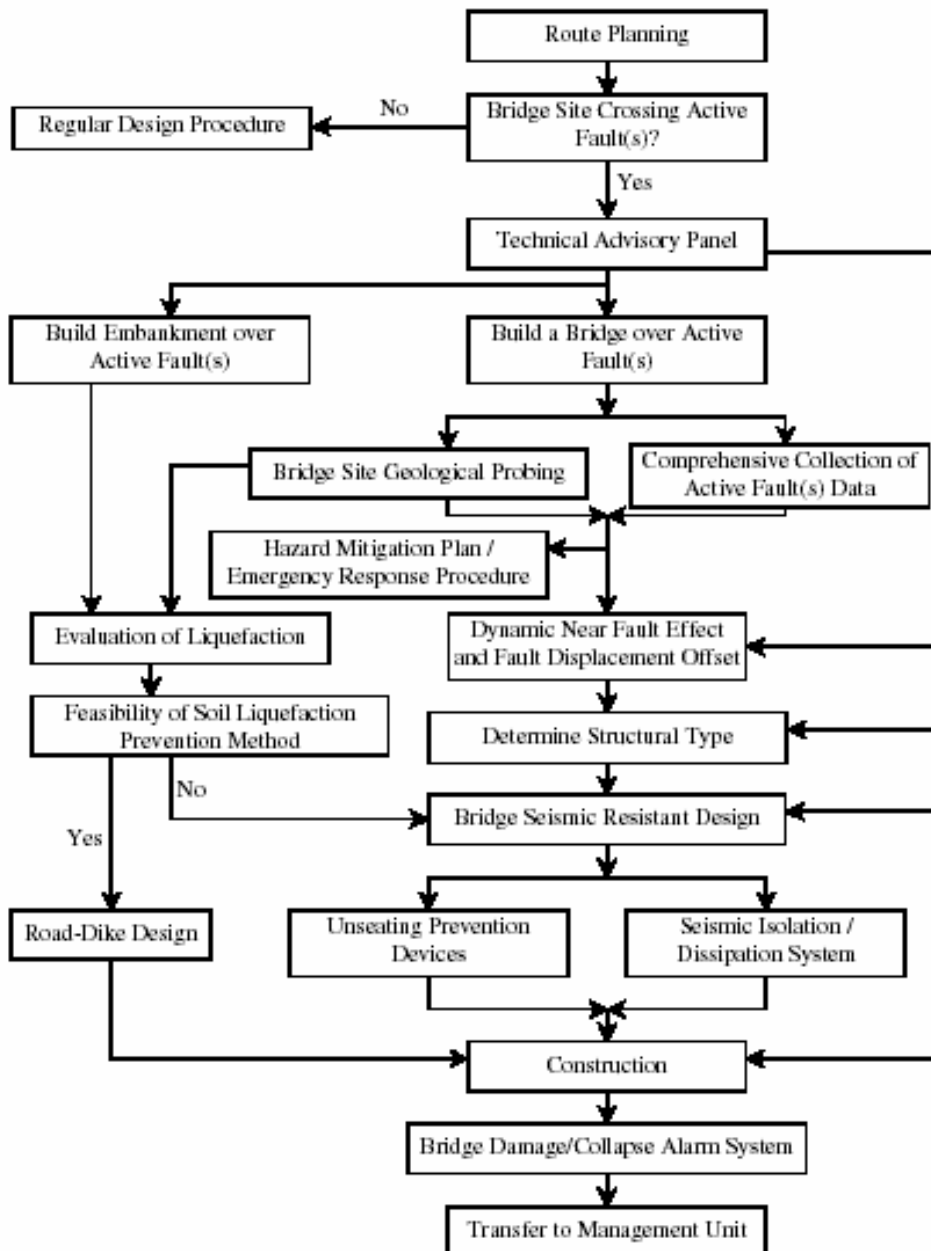


Fig. 8-11: Flowchart illustrating recommended planning and design procedure for fault crossing bridges in Taiwan

8.4 Performance requirements and design philosophy

Performance standards for the seismic design of bridges generally recognise two levels of required performance, as reported in Table 8-1.

In general, it is desirable that bridges crossing active faults meet the same performance standards as other bridges on the network so that the risk to the network is minimised and the fault crossing bridge does not become the most vulnerable ‘weak link’ in the system. It is convenient to divide fault crossing bridges into two categories.

Performance Level	Probability of occurrence of ground motion in bridge life	Performance Objective
Serviceability	High	- No loss of function - No damage
Safety	Low	- No collapse - No loss of life - Repairable damage

Table 8-1: Performance levels for the seismic design of bridges

Category I Bridges - those for which normal seismic code performance standards and risk levels are to be achieved. For bridges where the ratio of the fault displacement occurring between any two piers, to the length of the span concerned is very small, then it is likely that such a performance standard can be achieved. Typically the superstructures of these bridges are subject to relatively small permanent changes in angle between piers (measured along the bridge longitudinal axis). Examples of this would be the Bolu Viaduct, Turkey [Priestley & Calvi (2002)], the Vincent Thomas Bridge, USA [Baker et al. (1998)] and the San Diego-Coronado Bay Bridge, USA [Ashley et al. (2001)].

Category II Bridges - those for which specific seismic performance standards and risk levels must be formulated and agreed with the relevant bridge and network controlling authorities. For bridges crossing faults with large fault displacements occurring between any two piers and having relatively short length spans, then normal performance levels cannot be achieved. Meeting the serviceability performance level would not be practical for many bridges where the likelihood of significant fault displacement at this performance level is high. Furthermore, large fault displacements are likely to pose risks of collapse and to life which cannot be fully mitigated, and also likely to lead to damage which cannot be repaired, thus requiring reconstruction of some of the bridges and approaches. Examples of Category II bridges are the Taiwan High Speed Rail Active Fault Crossing Bridges [Empelmann et al. (2004)] and the Thorndon Overbridge, New Zealand [Billings & Powell (1996)].

Note that there are a number of bridges crossing faults or fault zones where slow but progressive fault displacements are expected to occur but no significant fault rupture in a major seismic event. For such bridges, normal design procedures and performance standards apply. However, provision for adjusting the bridge to accommodate such fault movements is likely to be required. Examples of this are the Rion Antirion Bridge, Greece [Infanti et al. (2004)] and the Katy Freeway Reconstruction Project IH-IO, Houston, USA [Zlotnik et al. (2004)].

8.5 Design steps

The design steps to be followed for a bridge crossing an active fault are summarised below.

- Site Conditions
Determine fault type and characteristics and geotechnical conditions of the site.
- Near Fault Ground Motions
Determine site specific (dynamic) ground motion hazard spectra.
- Fault Displacements
Determine site specific (static) permanent ground displacements. Probabilistic hazard assessment methodologies can be used. Refer discussion in 8.2 above.
- Design Concepts
Develop appropriate design concepts - refer 8.5.1 below.
- Design
Complete bridge design - refer 8.5.2 below.

8.6 Design concepts

For Category I bridges, base isolation systems have commonly been used together with continuous superstructures. Where superstructure joints occur, these have generally been provided with suitable lock up devices or restrainers to improve the performance of the structure.

For Category II bridges, simply supported spans with provision for the articulation expected in all directions due to fault displacements in the fault crossing area have typically been adopted. Where necessary, such systems may be provided with fuse mechanisms which fail at large displacements but provide appropriate restraint under serviceability conditions.

Where the design fault displacements are modest, then it is possible to provide for the bridge to be realigned at the piers and abutments, thus avoiding demolition and reconstruction. Such an approach was adopted for bridges on the Taiwan High Speed Rail Project.

The substructures of bridges in active fault zones may be subject to significant ground movements and appropriate concepts should be chosen. An example of this is the Bolu Viaduct mentioned earlier, where substantial pile damage and pier rotation occurred in the fault rupture area. In cases where the designer is confident that the fault rupture will not cause ground disturbance at the piers, no additional precautions are likely to be required. However, at some sites where the fault zone is not well defined or is known to be over a relatively wide area, then substructure types which will perform adequately should be chosen. For example, at the Taiwan High Speed Rail crossing of the Tuntzuchia Fault [Emplemann et al. (2004)], a monopile system was chosen instead of a multi-pile foundation to minimise the risk of foundation damage due to fault rupture passing directly through a pier.

8.6.1 Design of fault crossing bridges

Design of fault crossing bridges is relatively complex as it is necessary to take into consideration both the near fault dynamic ground motions and the permanent displacements as discussed in section 8.2 above.

For the assessment, design or retrofit of very large and critical lifeline structures, time history analyses using individual support displacement time histories are sometimes employed. In the case of bridges crossing active faults subject to major permanent displacements, the development of appropriate time history inputs is complex as they must:

- a) For vibrational ground motions:
 - Take account of the near fault dynamic displacement effects (including bridge/fault orientation);
 - Only include the characteristics of near fault earthquakes that result in surface rupture (see Sommeville (2002)); and
 - Recognise that the ground motions on each side of the fault will be different.
- b) For simultaneous permanent displacements:
 - Incorporate the relevant permanent fault displacement determined from the fault hazard assessment.

In general, it is not practical to carry out such analyses and normal practice for such major structures is to carry out an analysis incorporating the applicable near fault/surface rupture characteristics noted in a) above and to consider the fault rupture displacement effects noted in b) separately. As noted by Somerville (2002) the permanent ground displacements occur at about the same time as the large dynamic motions and hence a) and b) need to be considered as coincident effects. Conservatively, these effects can be added together. However, this will

be excessively conservative in many situations. The dynamic ground motions on each side of the fault may be very different and thus lead to a low vibrational response of the structure.

It is recognised that non linear time history analysis techniques are too onerous for most bridges and that development of a rational simplified method for fault crossing bridges is desirable. To this end, research is currently underway [Chopra (2005)]. The lack of guidance and need for further research into the design of active fault crossing bridges is also recognised in Japan [Japan Road Association (2002)].

For the design of most of the recent fault crossing bridges, common practice is to provide articulation to the bridge at the piers so that the permanent displacements can be accommodated without inducing significant forces in the superstructure or piers. Following this approach, the bridge is first designed for the near fault ground motions without consideration of fault displacement. A static application to the structure of the design fault displacement values is then carried out and any additional demands from the (relatively small) restraint provided by the articulation devices is also provided for by the piers. The static displacement application is a simple assessment of the displacement and force effects (if any) of imposing the fault displacement on the bridge. All joints are then designed to accommodate the necessary rotations and displacements.

Unjoh and Kondoh (2000) carried out an analytic study of the Wushi Bridge (described above), using a static displacement application and found that this simple model was appropriate to simulate and explain the damage and collapse observed in the Chi-Chi Earthquake.

A cautious approach should be taken to bridges crossing active faults with generous allowance for displacement and with careful ductile detailing using capacity design principles.

For Category I bridges which are major bridges and have continuous superstructures, it is likely that base isolation and response modification systems will be used. For such structures, regardless of the preliminary design procedures followed, it is commonly considered necessary to verify the design using non linear time history analyses. However, for fault crossing bridges, such analyses should be used with great caution.

For Category II bridges which have superstructures free to articulate at the piers, the design should proceed as described above for recent fault crossing bridges.

8.7 Retrofit design

A significant number of critical active fault crossing bridges have been assessed and subject to major seismic retrofits. In general, the principles outlined above equally apply to retrofit design. Examples of such retrofits include the Bolu Viaduct, Vincent Thomas Bridge, San Diego-Coronado Bay Bridge and Thorndon Overbridge.

8.8 Project examples

A number of project examples illustrating the principles described above are set out below.

8.8.1 Bolu viaduct retrofit, Turkey

The Bolu Viaduct is described in Section 8.1. It crosses the Duzce fault and was damaged in the 1999 Duzce Earthquake. The structure was subsequently assessed, repaired and subjected to a seismic retrofit. The retrofit concept was to make the bridge superstructure fully continuous over ten span bridge segments and to support it on large capacity (axial force and displacement) friction pendulum seismic isolation bearings [Priestley and Calvi (2002), Ghasemi (2004)].

The retrofit design was carried out on the basis of a 2000 year return period ground motion (which included for near fault effects) and the permanent ground deformation (of 500 mm) estimated to be possible during the life of the bridge. The seismic hazard assessment indicated a peak ground acceleration of 0.82 g. The bridge and isolation system was then subject to non linear time history analyses (NLTHA) using a set of fifteen appropriate earthquake records.

The bearings in the critical fault crossing ten span section were then designed for the sum of the peak displacement obtained from the NLTHA plus the permanent displacement estimated for the fault movement. The resulting bearings in the fault crossing section of the viaduct had a displacement capacity of 900 mm.

8.8.2 Thorndon overbridge retrofit, New Zealand

The Thorndon Overbridge comprises twin 1.3 km long elevated concrete bridges located in Wellington, an area of high seismicity. The bridges cross the Wellington fault, the dominant seismic hazard source for the site [Billings and Powell (1996)]. There is a significant risk of rupture on the fault taking place through the site with assessed permanent fault displacements of 5 m horizontal and 1 m vertical.

The overbridge carries six lanes of motorway and runs above the only rail corridor into Wellington City. The bridge has relatively short 27 m spans simply supported on concrete T heads. The retrofit comprised major strengthening of the pilecaps and jacketing of the piers to bring their performance up to an acceptable level. Capacity design procedures and scale model testing were carried out to confirm this. Fault rupture displacements were accommodated by allowing for movements to occur at the existing pin joints in the structure. To allow for the very large predicted fault displacements, large steel beams were placed under the joints to provide major seat extensions, thus reducing the risk of span collapse. The restrainer system across the joints at the beam ends was also designed so that the restrainers at the fault over the extended seatings would fracture and thus prevent fault rupture from pulling over the adjacent piers. In general, the assessment and retrofit design methodology described above for Category II bridges was followed. Typical details are illustrated in Figures 8-12, 8-13 and 8-14.

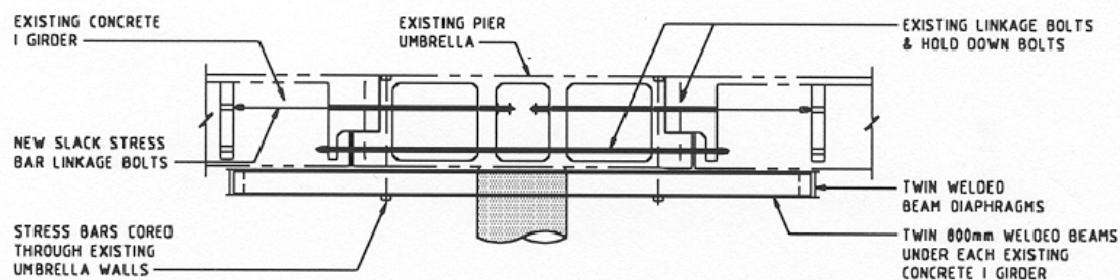


Fig. 8-12: Typical section at pier



Fig. 8-13: Extended seating frame



Fig. 8-14: Extended seating frame

(Figures available electronically on *fib* website; see production note on p. ii)

8.8.3 Taiwan high speed rail project - Tuntzuchiaio fault crossing

The Taiwan High Speed Rail Project is a new 345 km line designed for train speeds up to 350 kph. It crosses several active faults, one of these being the Tuntzuchiaio Fault [Empelmann et al. (2004)]. For the Safety Level earthquake, the bridge was designed for a 950 year return period ground motion (corresponding peak ground acceleration 0.4 g). The Serviceability Level design earthquake spectrum is one third of this. The bridge comprised a 55 m span steel truss with 30 and 35 m concrete approach spans. The spans were all simply supported and provided with articulation to allow for the design fault movement of 1.5 m horizontal and 0.5 m vertical. In general, the design methodology described above for Category II bridges of this type was used.

Interesting features included the use of large pier caps and abutment seatings to allow the bridge to be moved and resealed after a fault rupture and the use of large monopile foundations instead of multi piled caps. Typical details are shown in Figures 8-15, 8-16 and 8-17.



Fig. 8-15: Abutment with extended seating length and special bearings
(Figures available electronically on *fib* website; see production note on p. ii)



*Fig. 8-16: Piers with extended seating length and special bearings
(Figure available electronically on fib website; see production note on p. ii)*



*Fig. 8-17: Steel bridge and in-situ concrete bridges
(Figure available electronically on fib website; see production note on p. ii)*

8.8.4 Fujimi Dori Torii route bridge, Japan

This is a recently constructed 140 m long bridge which crosses an active fault [Watanabe et al. (2004)]. The fault crosses the southern end of the bridge almost at right angles to the bridge longitudinal axis and the estimated design displacement is 3 m vertical and 1 m horizontal. The assessed position of the fault is indicated in the southernmost span of the bridge.

The owner's preference was for a continuous bridge superstructure, however, this was assessed as being difficult to repair in particular against the vertical displacement and posing a significant risk of partial collapse. The target seismic performance criteria against the fault displacement were 1) to prevent span collapse, and 2) to make reasonable and practical provision for the permanent repair of the bridge after a fault rupture event. Accordingly, an articulated span was designed with the movement joints capable of absorbing the fault displacement. To prevent span collapse, wide seatings were provided and connections provided between the girders based on a series of simulation analyses.



*Fig. 8-19: Rion Antirion bridge
(Figure available electronically on fib website; see production note on p. ii)*

8.8.6 I10/I215 interchange ramp, California

One of the ramp bridges for the I10/I125 Interchange in San Bernadino crosses the San Jacinto fault, which is assessed to have a high probability of rupture in the next 30-50 years. The exact location of the fault is not known - it could be anywhere in a width of about 100m. The bridge was constructed before the fault location was known, so an assessment and retrofit design was carried out. The expected fault movement was about 1.5m strike-slip, with a smaller vertical component. The ramp is a typical Californian design with single column piers and a monolithic connection to a single-cell box. It has vertical and horizontal curvature and is quite high (about 20m average) and there are no movement joints in the region of concern. It was assessed that a time-history analysis would be meaningless, as the input motion on either side of the fault would be very different if fault rupture occurred, and this would thus be impossible to model, and could be expected to limit the vibrational response to low levels. Thus the assessment was for fault movement or vibrational response, but not the two combined. It was found that with column-base flexural retrofit the columns could be expected to retain adequate strength (i.e. no collapse), but that the damage might be such that the structure would need to be demolished and replaced after fault rupture.

References

- Alexandris A.P., Protopapa E.A. and Papastamatiou D.J. (2004). "A Highway Section Close to an Active Fault Seismic Risk Assessment and Design Considerations", *Geotechnical Engineering for Transportation Projects*, ASCE vol.2, Geotechnical Special Publication No. 126, pp.1729-1739
- Ashley M., Dougherty B., Jones R.M., Kompfner T.A. and Pourvahidi S. (2001). "Holding Steady", *Journal of Civil Engineering*, ASCE Vol.71, No.7, pp. 52-57, 85

- Baker G., Ingham T. and Heathcote D. (1998). "Seismic Retrofit of Vincent Thomas Suspension Bridge", Transportation Research Record
- Billings I.J. and Powell A.J. (1996). "Thorndon Overbridge Seismic Retrofit", 11th World Conference in Earthquake Engineering, Paper No.1477, Acapulco, Mexico
- Chang K.C., Kuo K.Y., Liu K.Y. and Lu C.H. (2004). "On Seismic Retrofit Strategies of Highway Bridges – Experiences Learned from Chi-Chi Earthquake", 13th World Conference on Earthquake Engineering, Paper No.639, Vancouver, B.C., Canada
- Chopra A.C. (2005). "Analysis of Bridge Structures Crossing Fault Rupture Zones", Current research project, UC Berkeley, California, USA
- Combault J., Morand P. and Pecker A. (2000). "Structural Response of the Rion-Antirion Bridge", 12th World Conference in Earthquake Engineering, Paper No.1609, Auckland, New Zealand
- Empelmann M., Whittaker D., Los E. and Dorgarten H. (2004). "Taiwan High Speed Rail Project – Seismic Design of Bridges Across the Tuntzuchiaio Active Fault", 13th World Conference on Earthquake Engineering, Paper No.140, Vancouver, B.C., Canada
- Ghasemi H. (2004). "Bolu Viaduct: Damage Assessment and Retrofit Strategy", The 36th Joint Meeting US-Japan Panel on Wind and Seismic Effects (UJNR), Session 1, National Institute of Standards and Technology, Gaithersburg, Maryland, USA
- Hsu Y.T. and Fu C.C. (2004). "Seismic Effect on Highway Bridges in Chi Chi Earthquake", Journal of Performance of Constructed Facilities, Vol.18, No.1, pp. 47-53
- Hsu Y.T. and Fu C.C. (2000). "Study of Damaged Wushi Bridge in Taiwan 921 Earthquake", Practice Periodical on Structural Design & Construction, ASCE Vol. 5, No.4, pp.166-171
- Infanti S., Papanikolas P., Benzoni G. and Castellano M.G. (2004). "Rion Antirion Bridge: Design and Full-Scale Testing of the Seismic Protection Devices", 13th World Conference on Earthquake Engineering, Paper No.2174, Vancouver, B.C., Canada
- Japan Road Association (2002). "Design Specifications of Highway Bridges", Maruzen, Tokyo, Japan
- Koketsu K., Yoshida S. and Higashihara H. (1998). "A fault model of the 1995 Kobe earthquake derived from the GPS on the Akashi Kaikyo Bridge and other datasets", Earth Planets Space, Vol. 50, No.10, pp. 803-811
- Mualchin L. (2004). "Seismic Hazard Assessment for Bridge Engineering in California", 13th World Conference on Earthquake Engineering, Paper No.2226, Vancouver, B.C., Canada
- Pecker A. (2004). "Design and Construction of the Rion Antirion Bridge", Geotechnical Engineering for Transportation Projects, ASCE vol.1, Geotechnical Special Publication No. 126, pp.216-240
- Priestley M.J.N. and Calvi G.M. (2002). "Strategies for Repair and Seismic Upgrading of Bolu Viaduct 1, Turkey", Journal of Earthquake Engineering, Vol.6, Special Issue1, pp.157-184
- Somerville P. (2002). "Characterizing Near Fault Ground Motion for the Design and Evaluation of Bridges", The 3rd National Conference & Workshop on Bridges & Highways, Session 5, Portland, Oregon, USA
- Trifunac M.D. and Todorovska M.I. (2005). "Methodology for Probabilistic Assessment of Permanent Ground Displacement Across Earthquake Faults for the Transportation System", School of Engineering/Department of Civil Engineering, University of Southern California, Los Angeles, California, USA

- Unjoh S. and Kondoh M. (2000). "Analytical Study on the Effect of Fault Displacement on the Seismic Performance of Bridge Structures", The 2nd International Workshop on Mitigation of Seismic Effects on Transportation Structures, Taipei, Taiwan
- Watanabe T., Yamamura N., Tokida K. and Hiraishi H. (2004). "Seismic Design of Bridges Considering Fault Displacement", Proceedings of Civil Structures and Materials, No. 20, Dec 2004 pp 99-109 (in Japanese)
- Wu C., Lin C.J. and Loh C. (2004). "Reliability-Based Seismic Design of Near-Fault Bridge Structures in Taiwan", 13th World Conference on Earthquake Engineering, Paper No.746, Vancouver, B.C., Canada
- Zlotnik E., Hasen M. and Milner D. (2004). "Growth Fault Design for Katy Freeway Reconstruction Project IH-10, Houston, Texas", Geotechnical Engineering for Transportation Projects, ASCE vol.2, Geotechnical Special Publication No. 126, pp.1747-1754

9 Screening of bridges for assessment and retrofit

9.1 Introduction

A network of bridges contains many different structures, which may be collectively identified by the term *bridge stock*. For a bridge stock, the issue of retrofitting usually derives from inadequacy with respect to structural national standards for new structures. Due to a lack of resources for generalised retrofitting, the decision maker is generally faced with the problem of selecting only a few bridges within the inadequate ones: the issue of prioritizing upgrading hence naturally arises.

In the present chapter we deal with the problem of how, within a bridge stock, one can make a rational choice in assessing a priority of intervention. The available literature is reviewed and indications are given.

One can consider this topic as preliminary to a detailed assessment and design for retrofitting of a single bridge. However the procedure allows to check, at the end of the assessment and/or design of retrofitting, whether a right choice has been done in prioritizing repeating the analysis after the detailed work has been completed.

It is a matter of fact that different views of the problem can be given if prioritization is done for the owner of the stock, for the one who maintains the stock (for example in Italy the highway system is owned by the state and given in concession to private companies) or by the final user of the stock. Therefore one cannot establish the absolute best solution. Moreover, not all the data are available to all subjects involved in prioritization, and therefore different methods can be used by different subjects.

The choice of the bridges to be retrofitted, and the retrofitting level, needs a clear definition of the goals to be achieved: safety, minimum cost, at the bridge or network level, minimum travel time within the network after an earthquake, are all reasonable and desirable aims; but obviously different goals lead to different upgrading priorities.

Furthermore, even after selecting a single goal, different evaluation methods may be employed. Each method often implies a considerable degree of subjectivity, in the form of engineering judgement, e.g. because of lack of data, to arrive at the final choices.

These considerations lead to issue an important initial warning: screening of bridges for prioritizing purposes is not a mature field of research, and generally accepted methods are not available. Thus, prioritization techniques need a cautious and critical user, because otherwise design choices “are entirely dependent on the procedure used as a basis for model development” [Small (1999)] irrespectively of the bridges stock. Furthermore, different issues can trigger seismic retrofitting, such as the need of intervention due to evident material deterioration, an increase of accidental load due to traffic issue, an increase of road transverse dimension etc.

In any case, prioritisation techniques, expertly used, can be of important help to the decision maker, giving a rational ranking among bridges, in order to detect the critical ones, and the best upgrading levels. These data should be considered to support choices among alternatives, usually not depending on seismic issues only.

Prioritisation has been already used in many cases in a more or less conscious way, and the methods are slowly consolidating.

The input data common to all prioritisation methods are two input information: action on the bridge F (seismic hazard), bridge fragility R (which increases as resistance decreases).

Some methods also consider the cost of failure C . Failure is defined as exceedance of a limit state, usually the ultimate limit state. C is the sum of the so-called direct costs (monetary value of the works to rebuild the bridge) and indirect costs (monetary value of the bridge failure effects on its surroundings, e.g. casualties and increase in travel time because of

detours). The cost of failure may be computed with reference to the single bridge or to the bridge within the transportation network. Often the cost of failure is expressed via the bridge importance.

As it will be shown, prioritisation methods lead to the priority value P_b for every bridge in a stock.

More formally P_b is expressed by all surveyed methods in the format:

$$P_b = f(F_b, R_b, C_b) \quad (9-1)$$

with f a method dependent function, F_b the force on the bridge (hazard), R_b the fragility of the bridge, C_b the cost of bridge failure (not always considered). Within each method, the values given by eq. (9-1), for all the bridges considered within a stock, must be considered comparatively: bridges with higher value of P_b deserve higher priority in seismic retrofitting.

In the following a classification of the methods and a short description of each is given. Many of the methods require solving a problem of functions minimization with respect to the independent variables. This classical problem for engineering is often referred to as optimization, be it constrained or not; in section 9.5 a brief summary of the different solution schemes and computational references for optimization problems is given.

9.2 Classification of the methods

The main issue the decision maker is interested in, is a thorough evaluation of the expected rate of failure due to seismic actions and, possibly, of the failure consequences. The computation of the rate of failure requires definition of the force on the bridge (hazard, F_b) and resistance of the bridge (fragility, R_b), while the failure consequences can be synthesised in terms of costs. Therefore, though many different methods exist in the literature, it has been considered effective, for classification purposes, to concentrate on the criteria used to evaluate the expected rate of structural failure, given bridge location, and consequences (essentially in terms of costs). A grouping may be made based on the following properties:

- (i) Model objectiveness in evaluating structural rate of failure via fragility and hazard. Models may be mainly based on: (A) engineering judgement (e.g. predefined criteria multiplied by subjective weights), or (B) on the outcome of a physically-based model
- (ii) Consequences of structural failure of the bridge (e.g. cost of retrofitting, structural failure consequence like interruption of traffic flow etc.). The consequences may be computed on the single bridge (A), for example the cost of failure, or on the bridge as part of a network (B), for example the time to go from a point to a different one.

Among the methods found in literature, it has been noticed that those based on engineering judgement, i.e. belonging to i.A, always consider failure consequences, property (ii); methods based on physically-based models, i.B, may or may not consider failure consequences also.

Property (i) is the basic one: each method is either based on engineering judgement (A) or on a physically-based model (B); on the other side, the choice of a model conditions the mathematical expression of f in eq. (9-1).

Methods mainly based on engineering judgement, (i.A), will retain subjective coefficients within the expression of f . Many of the so called bridge *check lists*, which are a collection of

seismic performance scores of bridge components, multiplied by subjective weights and summed up, are a typical example of (i.A).

When f is instead based on a physical model, the method is classified (i.B), such as evaluation of fragility of bridge typologies based on structural analyses or recorded data from past earthquakes, compared with the hazard at the site. Some of the (i.B) methods do not consider failure consequences, and therefore costs, and essentially give the priority as a direct function of structural failure rate, so that eq. (9-1) reduces to $P_b = f(F_b, R_b)$.

Property (ii) depends on the consideration of bridge failure costs. Quantities like bridge importance, traffic flow on the bridge, distance to destination in a net, can also implicitly be regarded as costs.

More generally, failure costs are a function of the bridge utility, U . Methods classified as (ii.A), consider the cost of the b -th bridge failure, C_b , as function of b -th bridge utility, U_b , only. Methods classified as (ii.B) consider costs as function of the utility of the b -th bridge within the network, U_B .

Formally, one can write:

$$\begin{aligned} C_b &= C_b(U_b) && \text{for methods within (ii.A)} \\ C_b &= C_b(U_B) && \text{for methods within (ii.B)} \end{aligned} \tag{9-2}$$

In the next sections the methods will be reviewed and commented. Methods are grouped and presented, depending on the combination of properties (i) and (ii). This choice leads to a classification in three groups :

- Methods based on direct or indirect evaluation of structural rate of failure, based on physical models, (i.B), without consideration of failure consequence
- Methods based on direct or indirect evaluation of structural rate of failure based on engineering judgement, (i.A), with consideration of the cost of failure
- Methods based on direct or indirect evaluation of structural rate of failure based on physical models, (i.B), with consideration of the cost of failure, (ii).

The methods classified according to properties (i) and (ii), presented in the following chapter, are briefly reviewed in Table 9-1.

9.3 Review of the methods

While all four combinations of properties (i) and (ii) are possible, in literature three main groups have been found, as already noticed in the previous section. The description of groups is repeated here for reading convenience:

- Methods based on direct or indirect evaluation of structural rate of failure, based on physical models, (i.b), without consideration of failure consequence
- Methods based on direct or indirect evaluation of structural rate of failure based on engineering judgement, (i.a), with consideration of the cost of failure
- Methods based on direct or indirect evaluation of structural rate of failure based on physical models, (i.b), with consideration of the cost of failure, (ii).

In this section, the methods belonging to each group are reviewed, following the order given above.

Reference and country	Property		Short description
	(i)	(ii)	
[Kawashima (1990)], Japan	B	-	Method based on regression on bridge damage data, with no consideration of failure costs. Bridges are prioritized according to their rate of failure. Vulnerability of i-th bridge, D_i , depends on properties derived from hazard and resistance. Each property is weighted and then summed up. Weights are derived from observation of damages from past earthquakes. The most influential properties are highlighted.
[Nielson (2003)], USA	B	-	Study solely based on bridge fragility curves. Priority for the i-th bridge is the median value of the bridge fragility curve with respect to a selected limit state (slight, moderate, extensive damage and collapse)
[ATC (1983)], USA	A	A	Procedure based on sum of physical variables, whose value is assigned via engineering judgement, with consideration of failure costs of the single bridge. Priority for i-th bridge, is computed as the sum of hazard, bridge resistance and bridge importance. Each item may vary between 0 and 10.
[FHWA (1995)], USA	A	A	Conceptually similar to ATC. Priority for the b-th bridge is computed as the product of hazard and bridge resistance. Resistance may vary between 0 and 10 and is computed based on engineering judgement. The authors suggest to further take into account “socio-economic” issues by subjectively increasing the priority.
WSDOT [Babei (1991)], USA	A	B	Conceptually similar to ATC, with consideration of the bridge network behaviour. Priority for the b-th bridge depends on hazard, bridge resistance, cost of failure. The latter is computed considering network behaviour. Bridge resistance may be computed with the provisions in ATC, 1983
[Basoz (1996)], USA	A	B	Conceptually similar to WSDOT. Priority for the b-th bridge is computed as the sum of vulnerability and importance. The network behavior is taken into account within the importance factor.
[Unjoh (2000)], Japan	B	A	Method based on regression on bridge damage data, with consideration of the single bridge failure costs. Priority for the b-th bridge depends on properties derived from hazard, resistance and cost. Weights are derived from observation of damages from past earthquakes.
[Chang (1996)], USA	B	A	Study based on cash flow of investments, with consideration of the single bridge. Analysis of alternatives is made with a life-cycle approach. By discounting all the costs and benefits pertaining to the bridge at the present time, seismic hazard related included, the most economical alternative may be chosen.
[Nuti (2003)], Italy	B	A/B	Study based on cash flow of investments, with consideration of the single bridge. May be easily extended to include network behaviour. Prioritization is done according to R_{max} , the maximum amount of money which can be exploited to retrofit the bridge, while doing an investment with a positive rate of return. Inputs are hazard and bridge resistance, before and after retrofitting
[Nojima (1998)], Japan	B	B	Montecarlo simulation of the bridge network behaviour. A whole road network is modeled, in a simplified way. Montecarlo simulations are used. The bridges which maximize the network flow are chosen for retrofitting.
[Werner (2000)] and [Werner (2004)], USA	B	B	Montecarlo simulation of the bridge network behaviour, via a GIS procedure. By comparing the results between with / without retrofit of a specific bridge, a prioritization can be made

Table 9- 1: Prioritization methods surveyed

9.3.1 Methods based on physical models only, (i.B): Kawashima (1990), Nielson (2003)

Kawashima and Unjoh (1990) developed a method to predict the rate of failure for bridges within a stock, using actual recorded damage data to fit the model parameters. The predicted rate of failure is then proposed as the bridge retrofitting priority (with respect to the other bridges).

The authors collected the damage data, for the ultimate limit state, relative to 124 bridges for four Japanese seismic events (Miyagiken-oki, 1978, Kanto, 1923, Fukui, 1948, Niigata, 1964). The data were screened using statistical techniques.

The authors preliminarily identified the N variables most likely to affect structural damage, with 1 variable for hazard, and $N-1$ variables for fragility. The index $j=1..N$, identifies a specific variable. Each variable is discretized into M_j intervals (from two to three); the index $k=1..M_j$, identifies a specific interval of the j -th variable. Damage to the i -th bridge is obtained as the sum of the weights relative to the values of the N variables for the i -th bridge. The model for damage, y_i , to the i -th bridge reads:

$$y_i = \sum_{j=1}^N \sum_{k=1}^{M_j} \delta_{ijk} \cdot w_{jk} \quad (9-3)$$

The damage scale varies from 0 (no damage) to 5 (falling-off of superstructure); w_{jk} quantifies the influence of the k -th interval of the j -th variable on the forecast damage y_i , while δ_{ijk} is a Boolean variable equal to 1 if, for the i -th bridge, the j -th variable falls within the k -th interval, and 0 otherwise.

The weights w_{jk} are obtained with the data bank of 124 bridges, using a statistical technique called *type II quantification analysis*, by comparing the forecast damage y_i to the historical recorded damage Y_i . The expected damage for a different bridge can then be computed using eq. (9-3).

The method has many positive aspects: it is physically sound, it may be expeditly employed, it allows to single out the variables that are most likely to affect structural failure, some of which can be modified via retrofitting (e.g. falling off of superstructure may be lowered via retrofitting), while other ones cannot (e.g. seismic hazard). The relative importance of the different variables on the predicted bridge rate of failure is shown in Table 9-2.

The difference between the maximum and minimum weights of the variables, which may be taken as their relative importance, ranges from about 1.2 to 0.3. The first eight have ranges between 1.2 and 0.7, then five variables have ranges equal to about 0.4 while the relative importance of the last variable, pier height, is equal to about 0.3.

It should be noticed that no initial test on the independence of the N variables is done; therefore the weights in Table 9- 2 may be correlated. For instance, the height of piers appears the least important among the variables considered (difference equal to 0.284) while ground condition and peak ground acceleration appear much more important. However, all three variables significantly influence the spectral acceleration on the bridge, and their relative importance cannot be estimated from the (correlated) values in Table 9- 2.

The authors propose a bridge check list, which includes the variables of Table 9- 2. However, if bridge ranking for prioritisation is made on the sole basis of the rate of failure y_i , aspects related to structural failure consequences and network behaviour (properties ii) are

disregarded. However, results given in Table 9- 2, suggests that check-lists and related models to estimate the rate of failure should include a considerable number of variables. Were the variables uncorrelated one should consider at least the first eight among the eleven proposed.

Variable	Minimum weight	Maximum weight	Difference
Intensity of peak ground acceleration	-0.283	0.936	1.219
Device to prevent falling off of superstructure	-0.647	0.459	1.106
Materials of substructure (plain or reinforced concrete)	-0.025	0.995	1.020
Ground condition	-0.461	0.522	0.983
Longitudinal slope in bridge axis	-0.023	0.918	0.941
Effect of soil liquefaction	-0.092	0.724	0.816
Design specification (1925, 1939, 1956, 1964, 1971, 1980)	-0.223	0.517	0.740
Type of substructure (r.c. or other materials)	-0.119	0.578	0.697
Shape of superstructure (skewed, straight)	-0.396	0.028	0.424
Irregularity of supporting ground	-0.024	0.396	0.420
Type of substructure (single pile, frame)	-0.119	0.292	0.411
Type of superstructure (simply supported, continuous, other)	-0.308	0.082	0.390
Height of piers (lower than 5m, between 5 and 10m, higher than 10m)	-0.112	0.172	0.284

Table 9- 1: Relative importance of the different variables on the predicted bridge rate of failure

Another drawback of the study, is that the method applicability is tested on the same data (124 bridges) used to initially calibrate the model. Although the reason why this is done is easily understood (data collecting is extremely expensive), the test is probably strongly biased.

The method proposed by Nielson and DesRoches (2003) is instead solely based on bridge fragility curves.

Using a sample of bridges from Central and Southeastern U.S., with four different multi-span deck types (continuous with pre-stressed concrete, continuous with steel, simply supported with pre-stressed concrete, simply supported with steel) they conducted non linear analysis and computed the fragility curves of each bridge type with respect to four different limit states, slight, moderate, extensive damage and collapse. They thus computed 16 fragility curves. Since the dispersion (measured by the coefficient of variation) of each fragility curve did not vary very much among the 16 curves, they chose the median value of the fragility curve as the key parameter. The result, the median value of each of the 4 fragility curves (one for each bridge type), is plotted versus the limit state considered in Fig. 9- 1. From the figure, they can single out the most fragile type for all limit states considered (the most fragile type is the multi-span bridges with continuous deck in steel), and therefore this type deserves priority in retrofitting. This criterion can be somehow reasonable if bridges are located in sites of similar seismic hazard and soil conditions.

The authors conclude indeed that this piece of information should be considered together with seismic hazard and indirect losses due to traffic flow reduction in order to prioritize bridges, but do not suggest quantitative model for these issues.

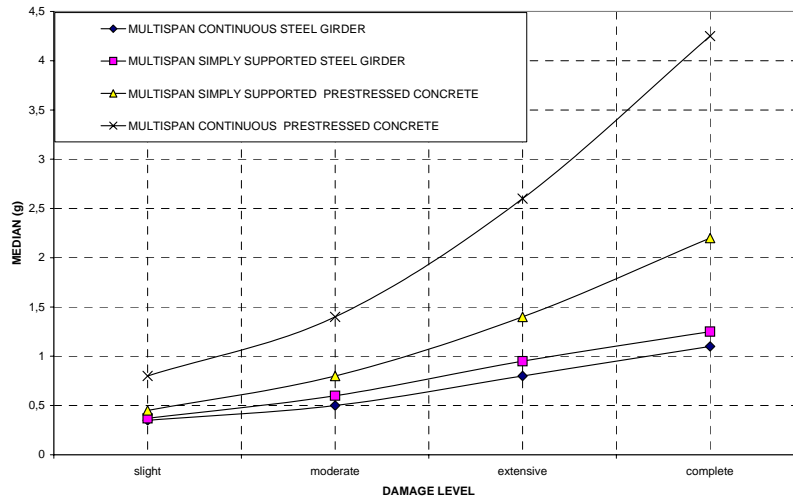


Fig. 9- 1: Fragility curves for four bridge types; each bridge type is represented by a single curve [Nielson and DesRoches (2003)]

9.3.2 Methods based on engineering judgement and cost of failure, (i.A) (ii,A,B): ATC (1983), FHWA (1995), WSDOT (1991), Basoz (1996)

The methods are similar in the approach. The priority in retrofitting of each bridge is computed via simple algebraic computations (sums and/or multiplications) of variables derived from bridge inspection and engineering judgement. Account is taken for failure consequences via an empirical approach.

The ATC (Applied Technology Council, USA) formulation reads:

$$P_b = f(F_b, R_b, C_b) = F_b \cdot w_F + R_b \cdot w_r + C_b (U_B) \cdot w_c \quad (9-4)$$

The priority of the b -th bridge, P_b , is expressed as the sum of bridge seismic hazard, F_b , fragility, R_b (which clearly increases as resistance decreases), cost of failure, C_b , with each input variable multiplied by a different weight w . Each of the input variables F_b , R_b , C_b , lies within the 0-10 range. The weights are all equal to 10/3. The final result, P_b , lies within the 0-10 range. Both the quantification of the input variables and of the weights is very subjective.

This is in fact explicitly recognized by the authors of the report. Seismic hazard, F_b , should be computed as 25 times the peak ground acceleration (contour maps for the peak ground acceleration in the U.S. are given). Fragility, R_b , is determined on the basis of a check list for bridge components, seatings, foundations, abutments, piles. The cost of failure is given via an importance classification (IC): essential bridges ($IC=1$) must continue to function after an earthquake and are assigned a score within 6-10; remaining bridges ($IC=2$) are assigned a score within 0-5.

It is worth noticing that the check list to determine bridge fragility R_b is very detailed and is, at least qualitatively, a useful guidance. A further interesting aspect is that the study acknowledges the need for a full cost-benefit analysis. In fact it states that, at least theoretically, design choices should be guided by the cost-benefit ratio:

$$BCR = \text{benefit cost ratio} = \frac{Loss_B - Loss_R}{\text{Retrofitting Cost}} \quad (9-5)$$

where $Loss_B$ and $Loss_R$ are the expected monetary loss before and after retrofitting. However, no guidance is given to compute the above quantities.

A very similar approach is followed by the FHWA, Federal Highway Administration, (1995). The formula for ranking bridges reads:

$$P_b = f(F_b, R_b, C_b) = F_b \cdot R_b + C_b(U_B) \quad (9-6)$$

Apart from the slight difference in the formulation of f , with hazard and fragility multiplied by each other, the terms within eq. (9-6) are computed nearly in the same way as with the ATC method. F_b is equal to 12.5 times the peak ground acceleration, with consideration of the local condition via a soil coefficient. R_b is the maximum value between V_1 , fragility of seatings, and V_2 , fragility due to structural behaviour of piles, abutments, foundations. Both V_1 and V_2 are computed with the ATC check-list. C_b should finally be added, based on subjective considerations “to include such factors as bridge importance, network redundancy, non-seismic deficiencies, remaining useful life, and the like”.

Similarly, the WSDOT (Washington State Department of Transport, USA) [Babey (1991)] approach to prioritisation can be expressed as:

$$P_b = f(F_b, R_b, C_b) = F_b \cdot R_b \cdot C_b(U_B) \quad (9-7)$$

F_b is expressed via the peak ground acceleration with a 10% probability of exceedance in 50 years: $F_b = 9.85 \text{ pga}^{0.41}$. In the original formulation, the figure 0.41 is the power for the product of F_b , R_b and one of the terms of C_b . Here, since these variables are quantified separately, the figure 0.41 appears at the power of each of them.

For R_b , the ATC formulation should be used. The value computed with the ATC check list, R_{b_ATC} , is introduced in eq. (9-7) as $R_b = R_{b_ATC}^{0.41}$.

C_b is accounted for via a “criticality factor” C_f , which lies in the 0-6 range and is computed in a subjective way considering traffic volume on or under the bridge, detour length, emergency route designation, bridge length, utilities carried on the bridge, route type on and under the bridge, and a “remaining life factor” K , which accounts for the remaining useful life. K is equal to 1, 0.91, 0.80, 0.67, 0.50 for, respectively, remaining life of more than 40 years, 30-40, 20-30, 10-20 and lower than 10 years. C_b is then computed as $C_f K^{0.41}$.

The method has the merit to also consider the length of time exposure to seismic risk, although in a simplified way.

Finally Basoz and Kiremidjian (1996), use an approach mathematically similar to what first proposed by ATC, but very much detailed as for hazard, structural fragility and costs are concerned.

The model may be recast in the form:

$$P_b = f(F_b, R_b, C_b) = F_b \cdot w_F \cdot R_b \cdot w_r + C_b(U_B) \cdot w_c \quad (9-8)$$

Structural behaviour is taken into account via computation of the structural rate of failure, $F_b \cdot w_F \cdot R_b \cdot w_r$, which is done in a traditional way comparing hazard and structural fragility.

To this term, the authors add a term for failure consequences; this depends on the bridge utility within the network it belongs to. The variables that define bridge utility (traffic flow, location within the network, highway type etc.) are recognised as not quantifiable in monetary values, since this step depends on the decision maker. The conceptual steps of their method is portrayed in the following figure.

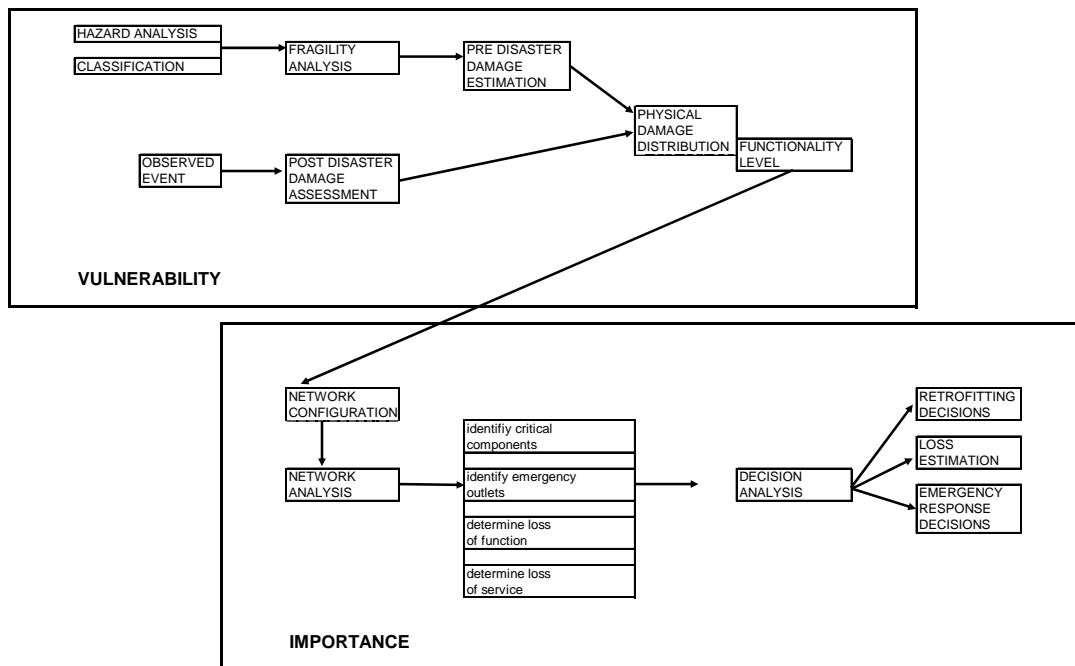


Fig. 9- 2: Conceptual steps of the Basoz (1996) and Kiremidjian method

The method is composed of two parts: for each bridge within the considered network, seismic vulnerability is first assessed (VULNERABILITY) and then compared with its importance within the network (IMPORTANCE). Based on these information, a decision, based on decision analysis, can be taken.

The methods described in this section can all be considered simplified approaches to the problem of prioritization, since they are essentially constructed based on common sense and empirical rules.

A weak point is the high degree of subjectivity which is inherent in the methods, both for the weights w quantification, and for the scores to assign to F_b , R_b , C_b ; this subjectivity may lead to results of little use.

Furthermore, since all methods require bridge data collection (type and current state of bridge components, seatings, foundations, abutments, piles, etc.), which is a very time consuming phase, their ease-of-use is more apparent than substantial, unless data are already available on data bases.

Both objections were confirmed by a study of Small (1999), of the Federal Highway Administration of the US. He applied five prioritisation procedures, all of the type (i.A, ii.A or B), among which the FHWA and WSDOT, described above, to a set of ten randomly selected bridges in California.

First of all, he found that the information required as input to the methods was generally not available within the Californian highway data bank.

He then collected the required information through surveys and best guesses.

Table 9- 2 shows the list of the bridges selected.

The final outcome of the analysis was disappointing: prioritisation of the bridges was strongly dependant on the method. On average, the ranking of each bridge might vary of almost six positions, out of ten, i.e. depending on the prioritisation method, a bridge might have been classified as the first or the seventh to retrofit.

All the methods employed by Small belonging to categories (i.A, ii.A or B), they had the common feature to be mainly based on engineering judgement, i.e. the bridge properties considered within the methods were scored in a subjective way and multiplied by expert

(subjective) weights. Thus the final outcome was that experts gave opinions which did not match the problem in a meaningful way. The next table shows the rank obtained by Small.

Bridge	Caltrans district	County	Feature carried	Owner	Service on	Service under
01 0024	01	Del Norte	U.S. Highway 101	State DOT	Highway	Waterway
04 0155	01	Humboldt	U.S. Highway 101	State DOT	Highway	Waterway
06C0108L	02	Shasta	Cypress Ave	City/Muni	HW + Ped.	HW – WW
08 0021	02	Tehema	State Route 36	State DOT	Highway	Waterway
10 0180	01	Mendocino	U.S. Highway 101	State DOT	Highway	Waterway
19C0062	03	Sonoma	Bowman Road	County	HW + Ped.	Railroad
23 0172	04	Sacramento	Vaca Valley Pkwy O	State DOT	Highway	Highway
50C0179L	06	San Bernardino	Gosford Road	City/Muni	HW + Ped.	Waterway
52 0274	07	Riverside	U.S. Highway 101	State DOT	Highway	Highway
58 0240L	11	Unknown	Intestate 8	State DOT	Highway	Waterway

Table 9- 2: Structures selected for examination from California Bridge Population, [Small, (1999)]

Bridge	Fhwa	Caltrans	Gilbert	Wadot	Odot	Kim	Average ranking	s.d.of ranking
01 0024	2	8	5	6	5	3	4.8	2.1
04 0155	5	1	1	5	2	7	3.5	2.5
06C0108L	7	3	7	3	7	2	4.8	2.4
08 0021	9	4	8	10	6	5	7.0	2.4
10 0180	1	2	2	4	4	1	2.3	1.4
19C0062	10	7	10	9	7	8	8.5	1.4
23 0172	5	9	4	2	7	10	6.2	3.1
50C0179L	8	10	9	8	7	4	7.7	2.1
52 0274	4	5	3	1	1	9	3.8	3.0
58 0240L	3	6	6	7	3	6	5.2	1.7

Table 9- 3: Prioritization ranking for different criteria and bridges [Small et al., (1999)]. Lower figures deserve higher priority. S.d. is the standard deviation.

Small concludes that, for the tested procedures, “the results ... are entirely dependent on the procedure ... Applicability is thus suspect ... A more quantitative approach is desired, which would ideally be based on rigorous engineering analysis”.

One may conclude that the outcome of models of the type (i.A) strongly depends on the experience of the engineer assigning the weights. This fact is well known, for example in all vulnerability assessment based on screening in the field. It is therefore recommended to use the methods in this section with caution.

9.3.3 Methods based on physical models and cost of failure, (i.B) (ii.A or B)

These methods can be further divided in two subgroups, depending on whether the road network behaviour, to which each bridge belongs, is accounted for or not. The first subgroup contains procedures which do not consider network behavior and, making reference to the initial properties classification, belong to (i.B) (ii.A). The methods in the second subgroup model the network behavior and therefore belong to (i.B) (ii.B).

9.3.3.1 Models without consideration of the network, (i.B) (ii.A): Unjoh (2000), Chang (1996), Nuti (2003)

This section contains the procedures proposed by Unjoh et al., Chang and Shinozouka, Nuti and Vanzi. In principle, their proposals are general enough to incorporate network behaviour, via a proper value of the model parameters. The authors, however, do not give indication on this issue and have developed the procedures taking into account single bridges: for this reason, the methods have been grouped in this section and categorized within the “no network” models.

The approach proposed by Unjoh, Terayama, Adachi, Hoshikuma, in 2000 can be considered as an evolution of the Kawashima (1990) and Unjoh method described in section 9.3.1. The method assumes the following equation for ranking bridges:

$$P_b = f(F_b, R_b, C_b) = F_b \cdot R_b \cdot C_b = \{S\} \cdot \{V_T \cdot V_v \cdot (V_{RP1} \cdot V_{RP2} \cdot V_{RP3}) \cdot (V_{MP} \cdot V_{FS} \cdot V_F)\} \cdot \{I\} \quad (9-9)$$

Item	Category	Evaluation Point
Importance of highway (I)	(1) Emergency Routes	1.0
	(2) Overcrossing with Emergency Routes	0.9
	(3) Others	0.6
Earthquake Force (S)	(1) Ground Condition Type I	1.0
	(2) Ground Condition Type II	0.9
	(3) Ground Condition Type III	0.8
Structural Factor (V_T)	(1) Viaducts	1.0
	(2) Supported by abutments at both ends	0.5
Weighting Factor on Structural Members (V_T)	(1) Reinforced Concrete Piers	1.0
	(2) Steel Piers	0.95
	(3) Unseating Prevention Devices	0.9
	(4) Foundations	0.8
Reinforced Concrete Pier (1), design specification (V_{RP1})	(1) Pre – 1980 design specification	1.0
	(2) Post – 1980 design specification	0.7
Reinforced Concrete Pier (1), pier structure (V_{RP2})	(1) Single Column	1.0
	(2) Wall – type column	0.8
	(3) Two – column bent	0.7
Reinforced Concrete Pier (1), aspect ratio (V_{RP3})	(1) $h/D < 3$	1.0
	(2) $3 < h/D < 4$ with cut – off section	0.9
	(3) $h/D > 4$ with cut – off section	0.9
	(4) $3 < h/D < 4$ without cut – off section	0.7
	(5) $h/D > 4$ without cut – off section	0.7
Steel Pier (V_{MP})	(1) Single Column	1.0
	(2) Frame Structure	0.8
Unseating Prevention Devices (V_{FS})	(1) Without unseating devices	1.0
	(2) With one devices	0.9
	(3) With two devices	0.8
Foundations (V_F)	(1) Vulnerable to ground flow (without unseating devices)	1.0
	(2) Vulnerable to ground flow	0.9
	(3) Vulnerable to liquefaction (without unseating devices)	0.7
	(4) Vulnerable to liquefaction	0.6

Table 9- 5: Prioritization factors [Unjoh (2000)]

In the eq. 9-9, the terms of expressions (9-1) and (9-2) may be recognized. P_b is the ranking of bridges, the function f is the product of the variables on the right hand side of (9-9), each of which retain values within the 0-1 range. Hazard is specified via S , the earthquake

force, costs $C_b(U_B)$ are given via the importance factor I , and the remaining variables quantify structural fragility.

By applying the same philosophy used to compute weights as in the previous study by Kawashima and Unjoh, but using the data of the Hyogo-Ken-Nambu earthquake, the values for the variables in eq. (9-9) are obtained as follows.

The most important difference between the results of this study (2000) and the previous one by Kawashima and Unjoh (1990), is that one of the major causes of collapse for the Japanese bridge stock of the '90s, excessive relative movement between the superstructure and substructure, had been eliminated by 2000 via installation of unseating devices. Hence, the weights in Table 9-5 are relative to bridges without this failure mode. Most problems are now relative to "the strengthening of substructures with inadequate strength, lateral stiffness and ductility". In this method, however, the monetary cost of bridge retrofitting is disregarded, and the consequences are estimated in a simplified way.

More precise analyses, on the cost side, can be made using life cycle cost analysis, as was done by Chang and Shinozuka (1996) and Nuti and Vanzi (2003).

Chang and Shinozuka compute the net present value of the different retrofitting choices (do nothing included) by discounting at time 0 all the costs the owner of the structure will incur in during the life of the structure,. Then the solution which gives the highest benefit-cost ratio can be used. This procedure applies both for a specific structure to discriminate among different retrofitting designs and among different structures to single out the one(s) with the highest retrofitting priority.

The study is interesting from a methodological point of view: all the costs within the life-cycle cost analysis are clearly highlighted and defined, together with the mathematical framework to discount them at time 0. The full list of costs and their categorizations are shown in the next figures.

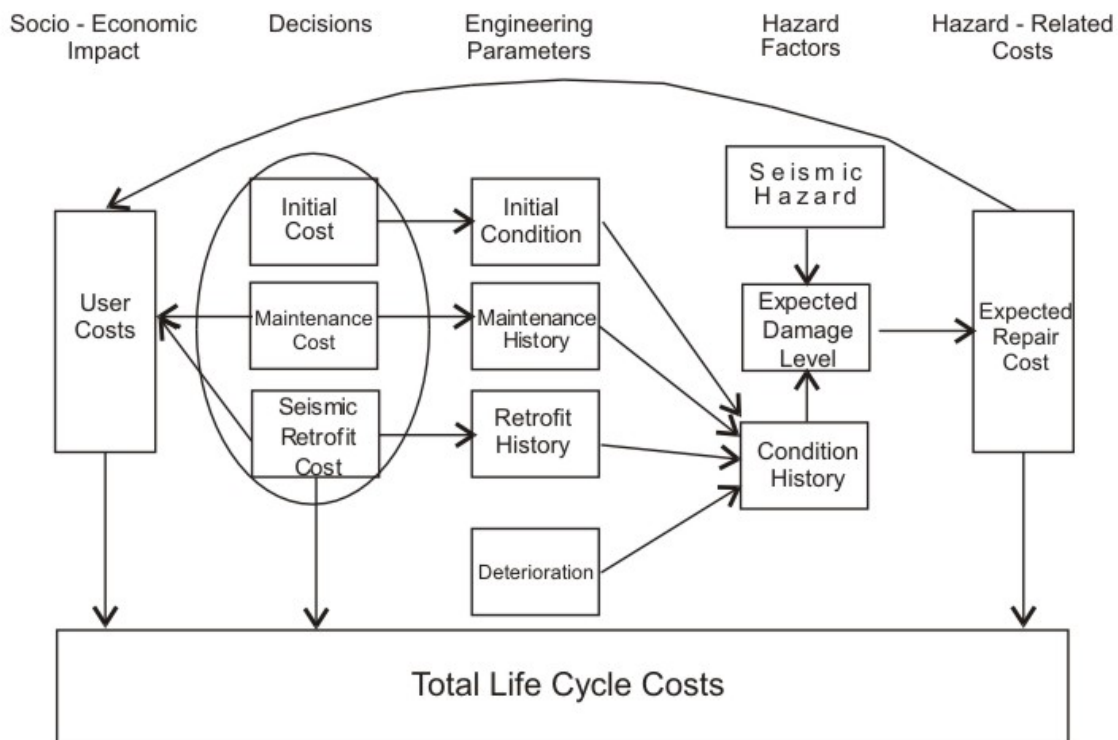


Fig. 9- 3: Categorization of life-cycle costs [Chang and Shinozuka (1996)]

The example application given in the paper is however too simplified with respect to the many parameters that must be included.

For an exhaustive and real world application, although in the different field of buildings, the reader could refer to [Smyth (2004)]. This paper deals with a five story reinforced concrete building in Istanbul and makes a prioritization among different retrofit designs. Among the merits of the study, is the high level of detailing the problem is dealt with (all the steps to compute direct and indirect costs are illustrated), thus making the paper a good starting point for a full real-world life cycle cost analysis.

However it must be noticed that application of life cycle cost analysis to structures is a lengthy method, requiring definition of all the structure-specific costs and thus not apt for fast bridge stock screening. The quantification of the structure related parameters (and of costs) is in fact the main obstacle in applying life-cycle approaches in prioritization.

The work by Nuti and Vanzi (2003) tries to overcome this problem. By means of a simplification of the cash-flow obtained with life-cycle cost analysis, the authors are able to compute the amount of money S_{max} which can be employed to retrofit a structure in order to have net present value of all the life cycle costs equal to 0. In other words, S_{max} is the retrofitting investment so as to break-even. Retrofitting designs whose cost is lower than S_{max} have positive net present value, and are thus economically sound.

If the investment cost S_{max} is divided by the expected cost of structural failure C (sum of direct and indirect costs), the non dimensional variable $R_{max} = S_{max} / C$ is obtained. R_{max} may be expressed in closed form as:

$$R_{max} = \left\{ \frac{\lambda}{\lambda + i} \cdot \frac{\exp[L \cdot (i + \lambda)] - 1}{\exp[L \cdot (i + \lambda)]} \right\} - \left\{ \frac{\Lambda}{\Lambda + i} \cdot \frac{\exp[L \cdot (i + \Lambda)] - 1}{\exp[L \cdot (i + \Lambda)]} \right\} \cong L \cdot (\lambda - \Lambda) \cong L \cdot \lambda \quad (9-10)$$

i is the net interest rate (without inflation), L the economic life of the structure, λ and Λ the pre and post-retrofitting annual rates of structural failure. The first expression on the right hand side of eq. (9-10) is exact; the second one is an approximation valid for low interest rates (below 1-2% annual, as is the case for EU, USA, Japan) and economic lives (below 50 years). The third expression is valid for retrofitting such that the rate of failure after upgrading (Λ) may be disregarded with respect to the rate of failure before upgrading (λ) (Albanesi 2004). A plot of the exact expression for R_{max} , for low interest rate i , is given in Fig. 9-4.

R_{max} can then be computed for a stock bridge once hazard and structural fragility are known; then the bridge stock can be prioritized according to the R_{max} value for each bridge. An example application, made on the 50 bridges belonging to the Naples – Canosa highway is shown in Fig. 9- 5. The bridge number is on the x-axis, the priority index R_{max} is on the y-axis. On the y-axis, the value of λ can also be read. The five different curves in the figure show λ and four curves for R_{max} , each relative to a different assumption for Λ , the post retrofitting rate of failure ($\Lambda = \lambda / 2$, $\Lambda = \lambda / 10$, $\Lambda = \lambda / 100$, $\Lambda = 1/1000$). One can notice that for $\Lambda \leq \lambda / 10$ all bridges having $\lambda > 1/100$ show $R_{max} > 0.1$, i.e. they should certainly be retrofitted.

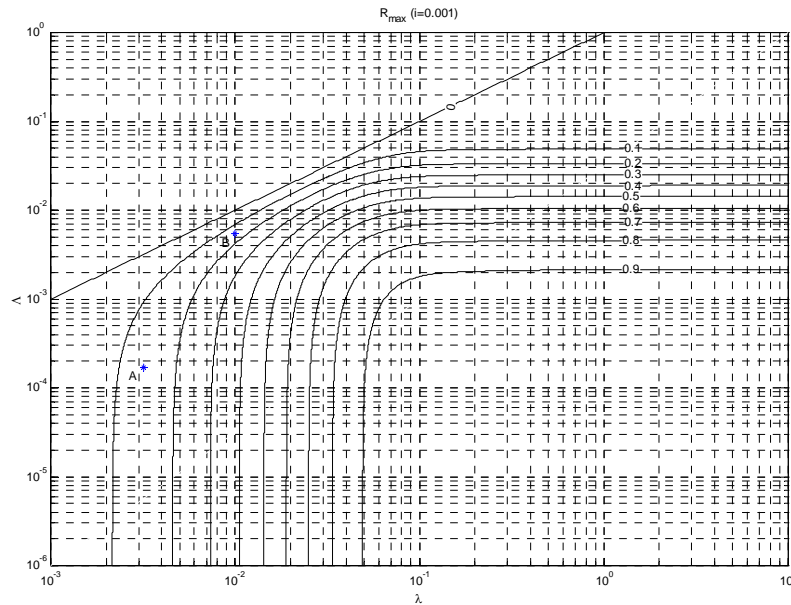


Fig. 9- 4: Maximum retrofitting cost to break even [Nutti and Vanzi (2003)]

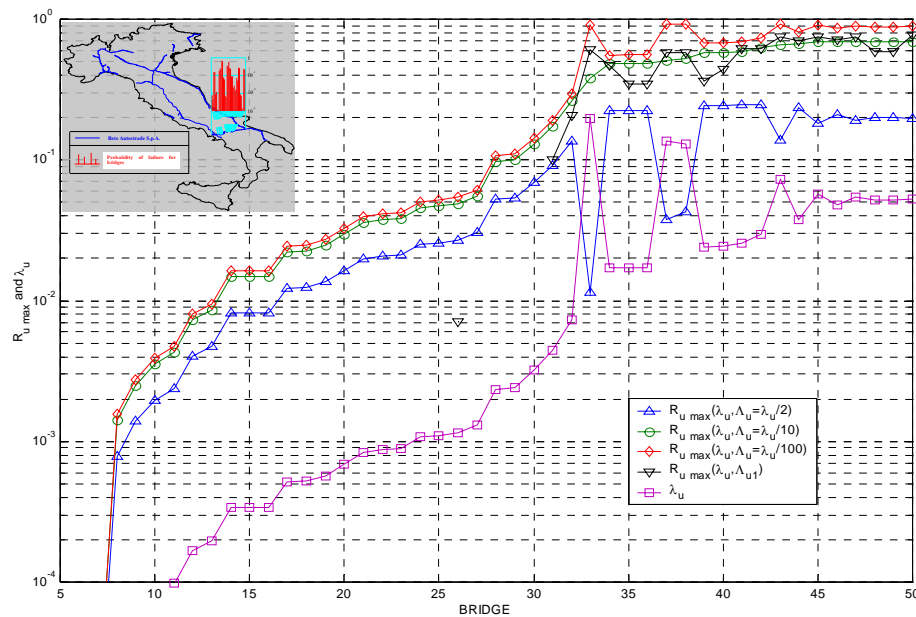


Fig. 9- 5: Priority index R_{max} for the bridges on the Napoli – Canosa highway [Nutti (2003)]

9.3.3.2 Models with consideration of the network, (i.B) (ii.B): Nojima (1998), Werner (2000)

This section groups the methods which explicitly deal with network behaviour. This implies increase in model complexity, in the number of model variables and in computational requirements. The most used mathematical method is Monte Carlo simulation which is powerful and flexible. Results of this mathematical method can be gathered at different levels of accuracy, ranging from mean values to full probabilistic distribution of the random variables.

Nojima presents a road network, which includes, composed of 25 nodes, under pre and post-earthquake conditions. The network considered is shown in the next figure.

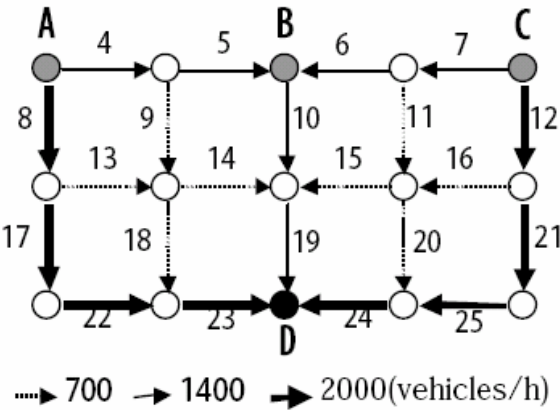


Fig. 9- 6: Example road network considered [Nojima (1998)]

A, B and C are nodes from which traffic departs; D is the destination node of all traffic. Each bridge, modeled as a link numbered from 4 to 25, is capacitive, i.e. may carry a finite amount of traffic, and seismically fragile. It is assumed that all the bridges have the same probability of survival p . The quality level r of the network is the flow exiting at D after the earthquake with respect to the flow before ($1400+2000+2000=5400$). The author identifies three levels of interest for r , 0.2, 0.5 and 0.8, respectively equal to 1080, 2700 and 4320 vehicles / hour exiting at D.

Using Montecarlo simulation, the author computes the probability of the quality level r as a function of bridge safety p . The result is shown in the next figure.

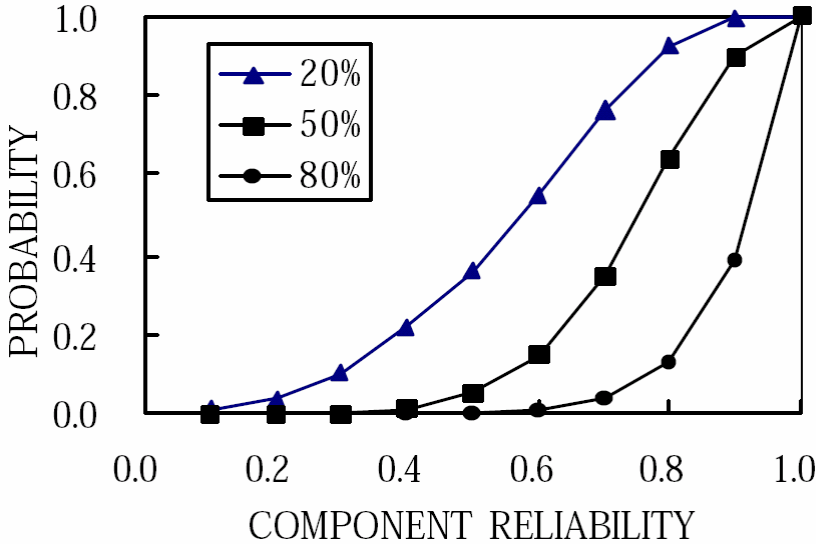


Fig. 9- 7: Traffic flow exiting at node D as a function of bridge safety [Nojima (1998)]

He then removes the bridges from the network one at a time, repeating the analysis each time. Comparing the results obtained with and without each bridge, he defines the priority of each bridge as the difference in the probability of r . This prioritization criterion is called

Birbaum's probabilistic importance and is one of the steps of the overall procedure, portrayed in Fig. 9- 8.

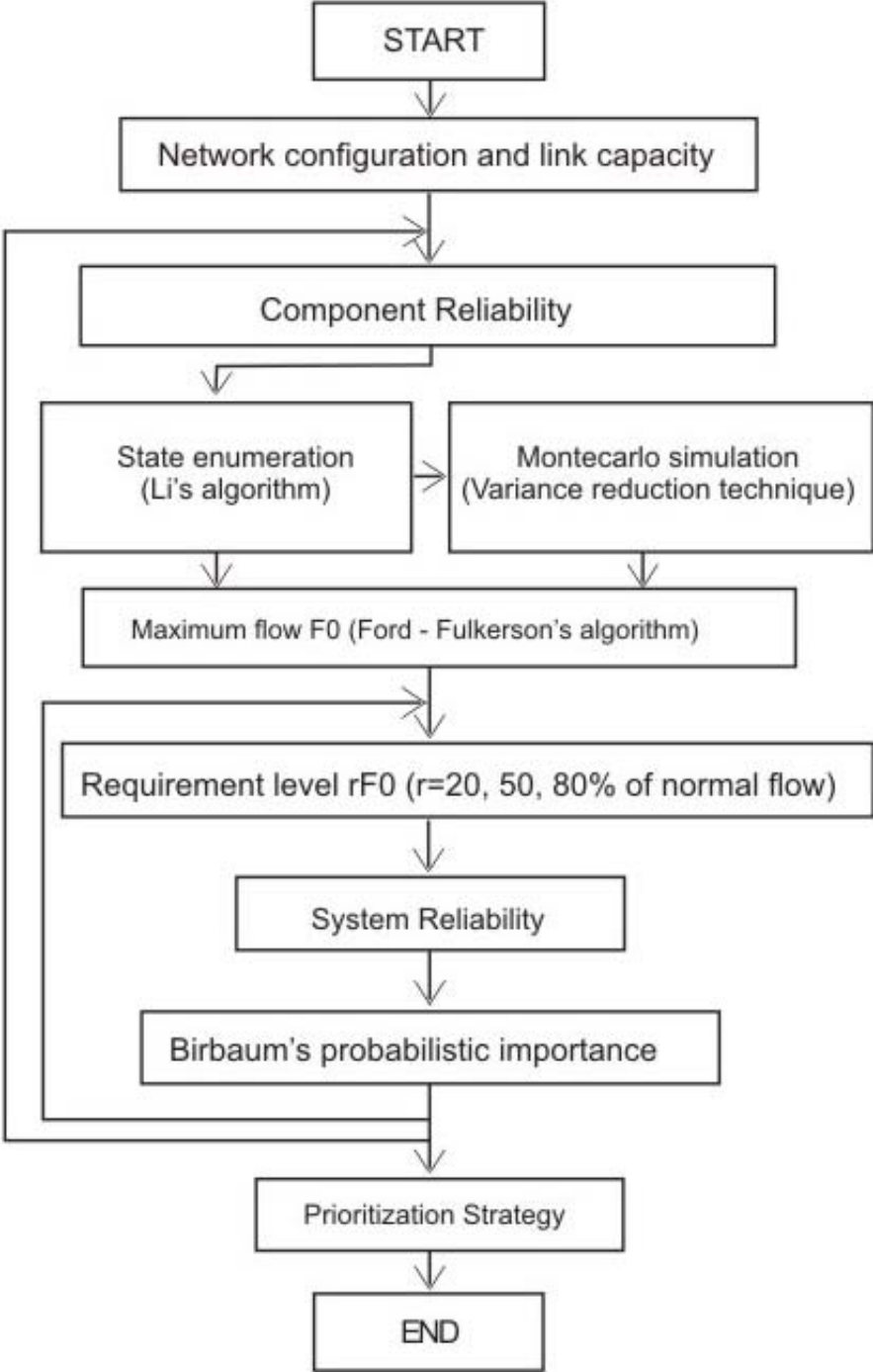


Fig. 9- 8: Steps of the procedure [Nojima (1998)]

The degree of accuracy and capability of detailed description of the system functioning is high, though assumptions on transportation demand after the earthquake, which is very uncertain and difficult to estimate, are needed.

The final results of the simulation, together with the example network studied, are shown in Fig 9-9.

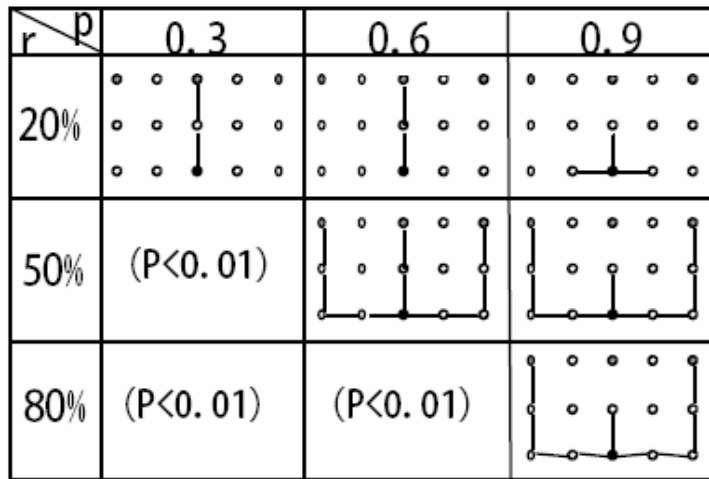


Fig. 9- 9: Most important links (=bridges) within the network [Nojima (1998)]

Each row is relative to a value of r , (0.2, 0.5, 0.8), flow exiting at node D; each column to an assumption for bridge safety, p , (0.3, 0.6, 0.9). It can be seen that, depending on the desired flow within the network and bridge safety, one would select totally different bridges within the network. This result is important in that it shows that different results, in terms of bridge priority, are obtained for different r and p . They could not have been forecast in qualitative terms or by methods that disregard the network problem.

A similar approach is used by Werner, on a real road network. By using traditional Montecarlo simulations and a GIS database of the road network of Shelby County in Tennessee, US, he obtains either scenarios or averaged system response. The road system analyzed is shown in Fig. 9-10 and is composed of about 8,000 links and 16,000 nodes.



Fig. 9- 10: Road system of Shelby County [Werner (2004)]
(Figure available electronically on *fib* website; see production note on p. ii)

By associating monetary losses to system damages, the author can compute the cumulative distribution function of monetary losses within selected return periods. This result is shown in the next figure.

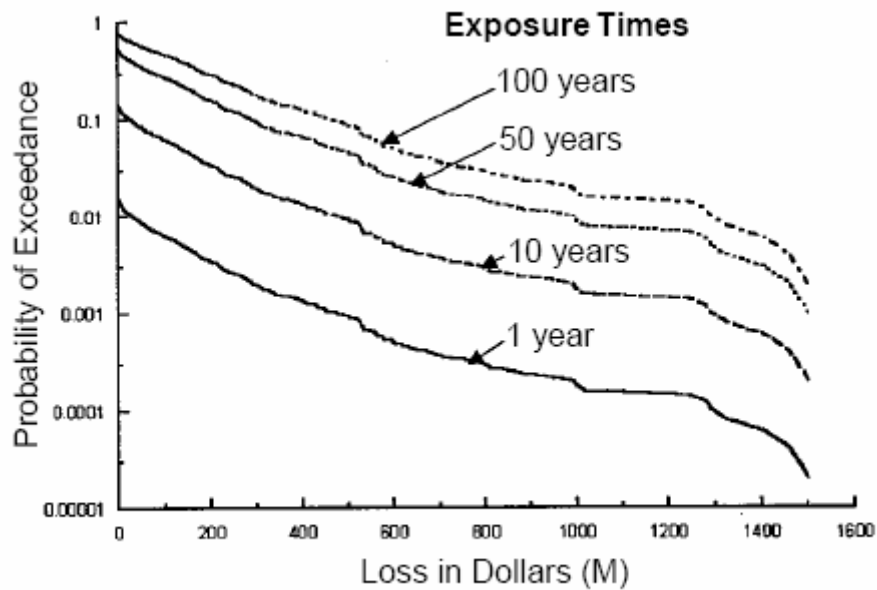


Fig. 9- 11: Cumulative distribution function of losses in the road system of Shelby County, in the current situation [Werner (2000)]

Since the damage state of each bridge within the network is known (see next figure) retrofitting prioritization is rather straightforward. On the other hand, the costs of the do-nothing option, i.e. current situation, are known from the results in Fig. 9-11.

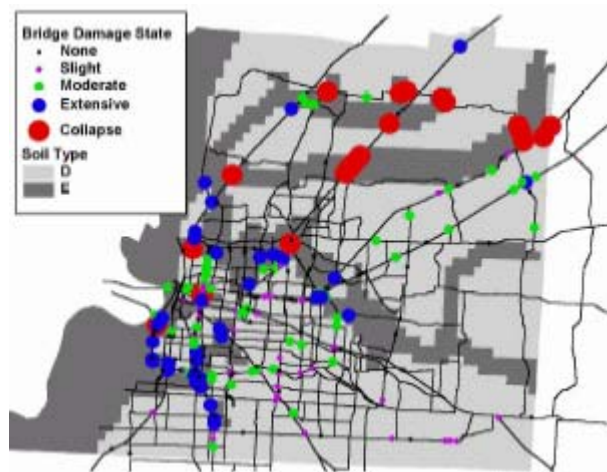


Fig. 9- 12: State of the bridges in the road system of Shelby County [Werner (2000)]
(Figure available electronically on fib website; see production note on p. ii)

9.4 Classification of minimisation problems

Prioritization often requires solution of a function minimization problem. A short summary on the class of problems variably known as minimization, maximisation, programming and optimization is given in this section.

These problems (minimization, maximisation, programming and optimisation), often heard of in engineering and economics, possibly coupled with the adjective (un)constrained,

are the same and single problem. In minimisation terms: find the point x , within a definition set X , such that the function f computed at x is lower than the value computed at any other point within X , i.e. is a minimum. More compactly:

$$\text{Find } x \in X : f(x) \text{ is min} \quad (9-11)$$

The mathematical procedures to solve the above equation are different depending on the definition set X (which is often defined via constraints), and the functional form of f . eq. (9-11) is termed accordingly.

X may be:

- unspecified (unconstrained minimization)
- specified as a region of the space within lines, or planes in multidimensional space (linear constraints)
- specified as a region of the space within paraboloids (quadratic constraints)
- more complex (generic constrained minimization).

Similarly, f may be linear or quadratic or more complex in x (linear, quadratic or nonlinear minimization).

If X and f are defined by same degree laws in x , eq. (9-11) is called programming and termed accordingly: for instance, linear programming is the problem in which X and f are linear in x , quadratic programming is the problem in which X and f are quadratic in x .

This classification is needed because the mathematical methods and computational routines are different, according to the type of the problem for which a solution is needed. Today, almost any problem is solved, due to high and cheap computer power.

Computer libraries for linear, quadratic or more complex minimisation problems are widespread and available in most programming language. Two excellent reviews of the mathematical methods, accompanied by the computer code, are [Press (1986)] relative to fortran, and available also in C, and [The Mathworks (2002)], relative to matlab.

Two examples, relative to the simplest and most complex forms of the problem (respectively linear programming and generically constrained minimization) are given in [Dodo (2005)] and [Vanzi (2000)]. The first example deals with prioritization for houses, the second with prioritization for electric networks substations.

If no specific mathematical and/or programming procedures are available for the problem at hand, approximate brute force solutions can always be obtained. By brute force solutions, here it is meant to discretize X and compute f at every single point of the discretized domain, i.e. span different $x_i \in X$, compute $f(x_i)$, retain $x_j : f(x_j) \leq f(x_i), \forall i \neq j$. With ever increasing computer power, and ever decreasing computer costs, brute force is becoming more and more applicable, while being the simplest mathematical methods and representing the only way for more complex or less common problems.

9.5 Conclusions

A review of the methods to prioritize the order of structural retrofitting of bridges within a stock is given. Methods are grouped and presented, depending on the combination of two main features: the criterion to evaluate the annual failure rate and the criterion to evaluate failure consequences. Three groups of methods have been obtained from state-of-the-art and of the practice:

- Methods based on physical models for failure rate evaluation, without consideration of failure consequence

- Methods based on engineering judgement for failure rate evaluation, with consideration of the cost of failure
- Methods based on physical models for failure rate evaluation, with consideration of the cost of failure.

Failure rate of each bridge may be estimated at different levels of accuracy, depending on available data, and all procedures, correctly applied, can lead to reasonable estimations. Failure consequences evaluation are strongly dependant on network effects. If the bridge is part of a network with many links, and therefore failure consequences may have effect well far from the bridge, results obtained taking into account the network cannot be forecast otherwise. More recent methods have shed some light on this aspect, which was disregarded in older applications. However, if bridges belong to a system which is essentially a serial one, network effects can be disregarded.

It is a matter of fact that the same set of bridges can be considered to belong to different systems, depending on who is looking at them. For instance, the owner of the highway which goes from town A to town B, will be interested on all the bridges of the highway (serial system); civil protection managers have instead to consider the entire regional transport system, therefore the highway from A to B is just a (possibly small) part of a much wider network. The priority of the bridges along A-B usually varies widely from the two perspectives.

References

- Albanesi T., Nuti C. and Vanzi I. 2004. Should we retrofit structures for earthquake protection?. 13th World Conference on Earthquake Engineering, Vancouver, B.C., Canada
- ATC-6-2 1983. Seismic retrofitting guidelines for highway bridges, Report ATC-6-2. Applied technology council, Palo Alto, California, August (Also report No. FHWA/RD 83/007)
- ATC-13 1985. Earthquake damage evaluation data for California. Report ATC-13, Applied technology Council, Redwood City, California
- Babei K. and Hawkins N. 1991. Bridge seismic retrofit prioritization. Proc. Of the 3rd US conference on Lifeline Earthquake Engineering, Los Angeles, California
- Basoz N. and Kiremidjian A.S. 1995. Prioritization of bridges for seismic retrofitting. Technical Report NCEER-95-0007, April
- Basoz N. and Kiremidjian A.S. 1996. Risk Assessment for Highway Transportation Systems. John A. Blume Earthquake Engineering Center, Department of Civil and Environmental Engineering, Stanford University, Report N°118, November
- Buckle I.G., Screening procedures for the retrofit of bridges, Proc. Third U.S. National Conf. On Lifeline Earthquake Engrg., Los Angeles, California, 156 – 165.
- California Department of Transportation (Caltrans), OSMI coding guide for sms, Division of Structure, Sacramento CA, 1993
- California Department of Transportation (Caltrans), The Northridge earthquake, Caltrans PEQUIT Report, Division of Structure, Sacramento CA
- Chang S.E. and Shinozuka M. 1996. Life-cycle Cost Analysis with natural hazard risk. journal of infrastructure systems, vol.2, n°2
- Cherng R. and Wen Y.K. 1992. Reliability based cost – effective retrofit of highway transportation system against seismic hazard. University of Illinois
- Dodo A., Xu N., Davidson R.A. and Nozick, L.K. 2005. Optimizing Regional Earthquake Mitigation Investment Strategies. Earthquake Spectra, Volume 21, No. 2, pp. 305–327, May
- Federal Highway Administration, FHWA 1995. Seismic retrofitting manual for highway bridges. Publication number, FHWA-RD-94 052, Virginia, USA

- Gilbert A.D. 1993. Developments in seismic prioritization of bridges in California. Proceeding of the 9th U.S. – Japan Bridge Engineering Workshop, May
- Haas C., Weissmann J. and Groll T. 1999. Remote bridge scour monitoring: a prioritization and implementation guideline. Report n°TX-00/0-3970-1, Texas Department on Transport
- Kanda J. and Shah H. 1997. Engineering role in failure cost evaluation for buildings. Structural Safety, vol.19, n.1
- Kawashima K. and Unjoh, S. 1990. An inspection method of seismically vulnerable existing highway bridges. Structural Engineering and Earthquake Engineering, Proc. JSCE, 416/I-13, pp. 143-150, Tokyo, Japan
- Kim S.H. 1992. A GIS-based Regional Risk Analysis Approach for bridges against earthquakes. Dissertation, State University of New York at Buffalo, Department of civil engineering, May
- King S.A., Adib H.R., Drobny J. and Buchanan J. 2003. Earthquake and terrorism Risk Assessment: Similarities and differences. Technical Council on Lifeline Earthquake Engineering, Monograph N°25, August, Advancing mitigation technologies and disaster response for lifeline systems, edited by J.E. Beavers
- Kiremidjian A.A. and Basoz N. 1997. Evaluation of bridge damage data from recent earthquakes. NCEER BULLETIN, volume 11, number 2, april
- Kusakabe T., Research on seismic retrofitting prioritization method, Report 2004 of Research center for disaster risk management, Japan
- Illinois DOT 1993, Ranks Risky Bridges, Civil Engineering Magazine 63, n°3:27
- Maffei, J. 1995. A new method for prioritizing bridges for seismic upgrading. Proc. Of the 4th US conference on lifeline earthquake engineering, San Francisco, USA
- Nielson B. and DesRoches R. 2003. Seismic Fragility Curves for Bridges: a Tool for Retrofit Prioritization. Technical Council on Lifeline Earthquake Engineering, Monograph N°25, August, Advancing mitigation technologies and disaster response for lifeline systems, edited by J.E. Beavers
- Nojima N. 1998. Prioritization in upgrading seismic performance of road network based on system reliability analysis. Third China-Japan-US Trilateral Symposium on Lifeline Earthquake Engineering, August, Kunming, China
- Nuti C. and Vanzi I. 2003. To retrofit or not to retrofit?. Engineering Structures 25, pp. 701 – 711
- Onoufriou T. and Frangopol D.M. 2002. Reliability – based inspection optimization of complex structures: a brief retrospective. Computers & Structures, 80, pp. 1133-1144
- Press W.H., Teukolsky S.A., Vetterling W.T. and Flannery B.P. 1986. Numerical recipes in fortran. Cambridge University Press
- Priestley M.J.N, Seible F. and Calvi G.M. 1996. Seismic Design and retrofit of bridges. John Wiley & sons
- Small E.P. 1999. Examination of Alternative Strategies for Integration of Seismic Risk Considerations in Bridge Management Systems. TRB Transportation Research circular 498, Presentation from the 8th international bridge management conference, Denver, Colorado, April 26-28
- Smyth A.W., Altay G., Deodatis G., Erdik M., Franco G., Gulkan P., Kunreuther H., Lus H., Mete E., Seeber N. and Yuzugullu O. 2004. Probabilistic Benefit – Cost Analysis for Earthquake Damage Mitigation: Evaluating Measures for Apartment Houses in Turkey. Earthquake Spectra, Volume 20, N°1, pages 171-203, February
- The Mathworks Inc. 2002. Optimization Toolbox for use with matlab, Version 2. Natick, Massachusetts
- Unjoh S., Terayama T., Adachi Y. and Hoshikuma J. 2000. Seismic retrofit of existing highway bridges in Japan. Cement & Concrete Composites, 22, 1

- Vanzi I. 2000. Structural upgrading strategy for electric power networks under seismic action. *Journal of Earthquake Engineering and Structural Dynamics*, John Wiley and Sons, U.S., vol. 29 (7), pp. 1053-1073
- Werner S.D., Taylor C.E., Moore J.E. II and Walton J.S. 2000. A Risk-Based Methodology for assessing the seismic performance of highway systems. Report MCEER-00-0014, Multidisciplinary Center for Earthquake Engineering Research, University at Buffalo
- Werner S.D., Taylor C.E., Cho S., Lavoie J.P., Huyck C.K., Eitzel C., Eguchi R.T. and Moore J.E. 2004. New developments in seismic risk analysis of highway systems. 13th World Conference on Earthquake Engineering, Vancouver, B.C., Canada, August 1-6, Paper No. 2189
- Woodward Clyde Consultants 1991. Report of seismic bridge condition survey, (prepared for Illinois Department of Transportation Bureau of bridges and structures), Oakland, California, vol.1

10 Fragility assessment

10.1 Introduction

This chapter is concerned with review of methods of assessment of bridge sensitivity to damage from earthquake ground motion, with emphasize on probabilistic fragility analysis. Response data necessary for fragility analysis may be collected from the field (observational) or generated by advanced analysis. The data assembled may be treated deterministically or probabilistically. The Chapter is designed to present a coherent and succinct overview of the rapidly emerging field of fragility assessment that is critical to the development and application of regional seismic loss assessment software. Table 10-1 summarizes the framework used to design the Chapter and a key to its scope and sections.

Response Data		Data Treatment		Limit State	
Type	Section	Type	Section	Type	Section
Observational	10.4.1	Deterministic	10.4.3	Observational	10.3.2/10.3.3
Analytical	10.4.2	Probabilistic	10.5.3	Analytical	10.3.4

Table 10-1: Overview of Chapter scope and contents

The scope is restricted to individual structures with some exceptions where the treatment of groups of structure serves the purpose of presenting widely used approaches. Emphasis is also placed on examples of probabilistic fragility analysis at the end of the Chapter where the various components outlined in earlier sections are brought together to provide an advanced tool for assessment of the probability of reaching a limit state of damage.

10.2 Structural deficiencies

Failure modes observed in existing RC bridges during past earthquakes world-wide have been caused by a number of member, connection and/or system deficiencies. It is difficult to categorize these structural deficiencies and generalizations by definition are fraught with omissions. However, most of the cases of damage and collapse surveyed in the aftermath of major seismic events may be attributed to the following defects (Priestley et al., 1996):

- i. The earthquake-induced deformations were underestimated because gross sections were considered in the computation of displacements instead of cracked-sections;
- ii. Serious underestimation of the combined effects of seismic and gravity loads. Bridges with few or no seismic requirements are unlikely to survive seismic loading;
- iii. Foundation movements due to local soil conditions. Potential liquefaction and differential settlements may undermine the global stability of the bridge or impair its functionality;
- iv. The requirements of ductility in the plastic hinge areas (also known as ‘dissipative zones’) were not satisfied. The ductility capacity is of primary importance if structures are to survive high level of inelastic deformation demands.

Examples of bridge failures during recent earthquakes are outlined hereafter. The observed damage or failure of structural elements can often be related to one or more of the aforementioned deficiencies. Common structural failures of existing bridges include:

- i. Flexural failures in plastic hinges with inadequate confinement;
- ii. Shear failures in short single columns, piers, multicolumn bents, columns with flares and other accidental restraints and columns in skewed bridges;
- iii. Inappropriate location of lap splices in pier members, causing shear failure;
- iv. Compressive failures of columns and piers with corresponding rebar buckling and stirrups openings and/or ruptures;
- v. Overstressing of seismic restrainers leading to local failure;
- vi. Uplifting and overturning of bridge foundations and/or piers with inadequate anchorages at base;
- vii. Pounding and unseating at hinge seats and girder supports.
- viii. Footing failures caused by soil liquefaction and/or differential settlements.

High magnitude earthquakes may also cause severe damage to bridge abutments; however, the latter are generally over-designed and hence their failure does not endanger the structural safety of the bridge as a whole.

The following paragraphs present the most common damage patterns, show examples of impressive collapses of RC bridge structures world-wide and discuss their likely causes.

10.2.1 Span failure

A direct consequence of underestimation of displacements is that the bridge spans may fail due to unseating at the movement joints. This effect is particularly frequent for slender structures. Figure 10-1 shows an example of collapse which occurred at the I-5 (Golden State) and C-14 (Antelope Valley) interchange in the San Fernando Valley in California. The collapse of interior bridge spans was observed in the 1971 San Fernando and 1994 Northridge earthquakes. Extensive damage to lifelines during previous earthquakes, especially in the 1971 San Fernando and 1989 Loma Prieta earthquakes, caused the Transportation Agency (Caltrans) to initiate and develop a program of designed to strengthen the vulnerable features of existing structures (Elnashai *et al.*, 1989). While this program was far from complete at the time of the Northridge earthquake, retrofitted structures, as well as those of more recent construction, displayed superior seismic performance (Broderick *et al.*, 1994; EERI, 1994). The portion of the highway in Figure 10-1, which was designed to pre-1974 seismic standards, had not been retrofitted when the seismic event (Northridge) occurred in 1994. It is evident that seismic restrainers provided at joints were incapable of resisting the demand imposed. The displacement amplification is aggravated for skewed spans as a consequence of the imposed combination of longitudinal and transversal motion.

Punching of piles through the road bed is another typical example of inadequate resistance of decks of RC bridges to withstand punching shear. During the 1989 Loma Prieta earthquake, several bridge spans collapsed because of punching of supporting piers as displayed in Fig. 10-2.

During strong earthquakes severe pounding damage may also take place at joints between adjacent spans (Fig. 10-3). This type of damage can be localized both between adjacent bridge spans and at abutments.



Figure 10-1: Span collapses at the Golden State-Antelope Valley interchange collectors during the 1971 San Fernando (left) and the 1994 Northridge (right) earthquakes (courtesy of USGS).
(Figure available electronically on **fib** website; see production note on p. ii)

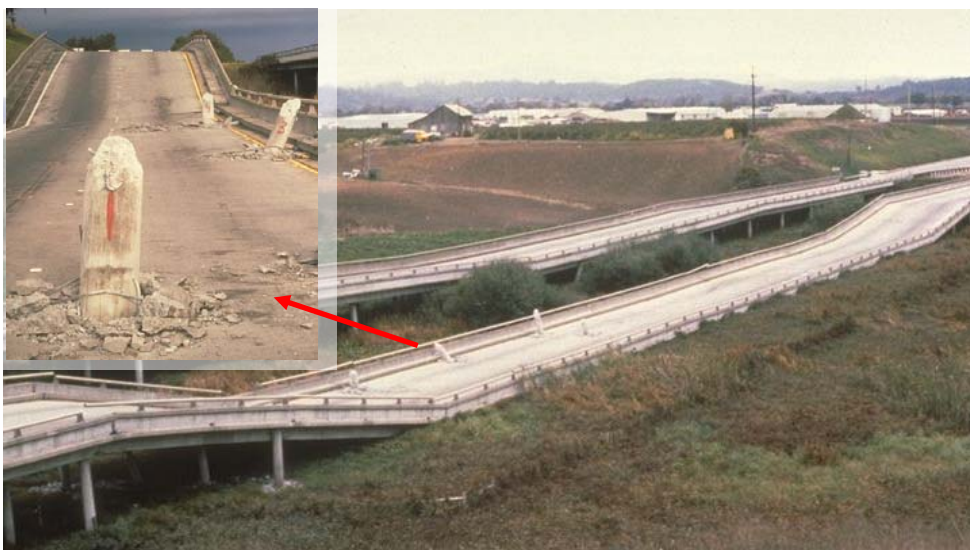


Fig. 10-2: Punching of piles through the road bed of the State Route 1, Watsonville area, span during the 1989 Loma Prieta earthquake (after NISEE, 2000).
(Figure available electronically on **fib** website; see production note on p. ii)



Fig. 10-3: Pounding damage: between adjacent spans at the Interstate-5 at Santa Clara River in Los Angeles County during the 1994 Northridge earthquake (left) and at the abutment of a bridge near Nishinomiya Port in the 1995 Kobe earthquake (after NISEE, 2000).
(Figure available electronically on **fib** website; see production note on p. ii)

10.2.2 Pier failure

RC pier failures during past earthquakes have often been a consequence of using elastic design (force as opposed to displacements). Strength design may be successful if the demand is estimated accurately, which has been repeatedly shown to be an onerous requirement. The strength is frequently insufficient to guarantee the elastic response of the bridge even though the real resistance is higher than the design value, as a consequence of overstrength. Hence to survive intense shaking, structures must exhibit an adequate ductility capacity. The most common damage patterns for bridge piers are outlined below.

10.2.2.1 Column flexural failure

The lack of ductility in flexural failure mechanism is due to inadequate confinement of the plastic hinge zone. Unless the concrete is well confined by closed transverse stirrups, crushing rapidly extends into the core, buckling of longitudinal reinforcement occurs and loss of strength is observed (Goltz, 1994). In extreme conditions the columns become unable to sustain gravity loads. There are several examples of failure in plastic hinge zones, such as top column failure, as shown in Fig. 10-4.



*Fig. 10-4: Confinement failure at bridge pier top during the 1994 Northridge earthquake (after NISEE, 2000).
(Figure available electronically on **fib** website; see production note on p. ii)*

Another common design deficiency is highlighted by discontinuity of longitudinal reinforcement leading to weak sections at which unexpected inelastic deformations are imposed. The above design deficiency caused spectacular cases of collapse during the 1995 Kobe earthquake as for example in the case of the Hanshin expressway shown in Fig. 10-5.

Failure may also occur without yielding of vertical reinforcement, due to an inadequate lap-splice length or failure in welded bars.



*Fig. 10-5: Flexural failure above column base of columns of the Hanshin expressway, due to premature termination of longitudinal reinforcement and inadequate confinement in the 1995 Kobe earthquake (courtesy of Kawashima). (Figure available electronically on **fib** website; see production note on p. ii)*

10.2.2.2 Column shear failure

Elastically designed structures may suffer failure by shear, since the shear strength corresponding to the maximum (not design) flexural strength would not have been considered. Shear failure mechanisms are not usually (with a few exceptions) suitable for ductile seismic response, because of the low levels of deformation corresponding to failure. Short columns are particularly susceptible to such effects. A high percentage of bridges collapsed during recent earthquakes because of shear failure (Fig. 10-6).

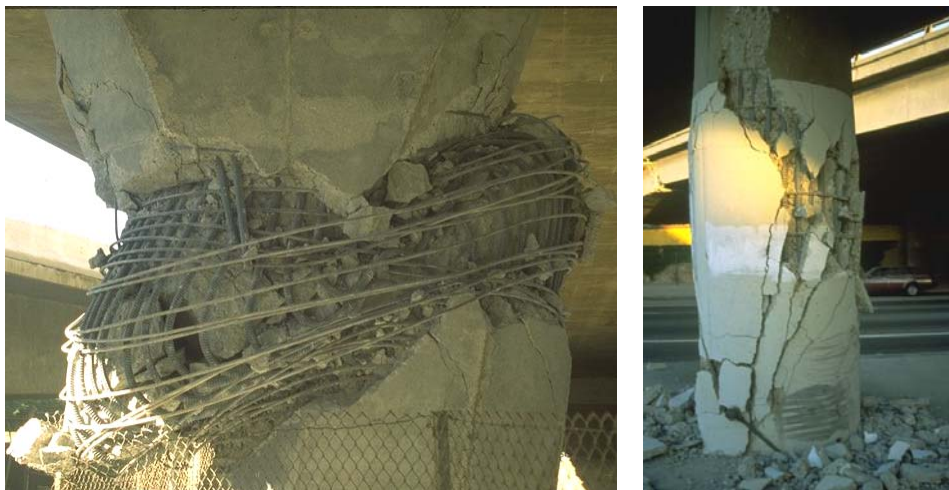


*Fig. 10-6: Shear failure within (left) and outside (right) the plastic hinge region in San Fernando Mission Blvd-Gothic Avenue Bridge and I-10 Freeway at Venice Blvd, respectively, during the 1994 Northridge earthquake (after NISEE, 2000). (Figure available electronically on **fib** website; see production note on p. ii)*

In particular, Fig. 10-6 shows a case in which flexural and shear failure mechanisms were combined. The reduced contribution of concrete to the shear resistance in the plastic hinge area, after the concrete was damaged, led to shear failure.

10.2.2.3 Column buckling

Several cases of symmetric buckling of reinforcement and compressive failure of piers may be, at least in part, attributable to high vertical earthquake forces both in Kobe and Northridge (Broderick *et al.*, 1994; Elnashai *et al.*, 1995). Three out of four RC piers supporting the I10 (Santa Monica freeway) collector-distributor 36 suffered varying degrees of shear failure due to the short shear span that resulted from on-site modification of the original design (Fig. 10-7).



*Fig. 10-7: Different shear damage patterns for RC piers at the under-crossing of the Santa-Monica Interstate 10 during the 1994 Northridge earthquake: Piers # 5 with inadequate detailing for plastic hinge (left), Piers # 6 with symmetric buckling (middle) and Pier # 8 with typical shear failure (right) (after Broderick *et al.*, 1994). (Figure available electronically on **fib** website; see production note on p. ii)*

10.2.3 Joint failure

Beam-column connections (or pier-cross beam connections) are subjected to high levels of shear. It was, however, the heavy damage inflicted on several RC bridges in the San Francisco area during the Loma Prieta earthquake that brought this problem to the fore (Elnashai *et al.*, 1989; Astaneh *et al.*, 1989). Current design philosophy is to attempt to over-design connections in order to force inelastic action in beams and columns. Without adequate transverse reinforcement, concrete diagonal cracks are opened in the joint regions, where shear stresses produce excessive tension cracks. A further factor that may precipitate joint failure is insufficient anchorage of the reinforcement in the end regions. Sliding shear at intentional flexural hinges has also been observed, and is possibly the main reason for the collapse of the Cypress Viaduct (Fig. 10-8).



Fig. 10-8: Sliding shear at top columns of the Cypress viaduct in the 1989 Loma Prieta earthquake (after NISEE, 2000). (Figure available electronically on fib website; see production note on p. ii)

10.2.4 Abutment failure

The failure of abutments is typically due to slumping of the soil, which produces a global rotation of the structure. This is due to a pressure increase in the infill soil as a consequence of longitudinal response. The sketch and the picture in Fig. 10-9 show a failure mechanism of this type that caused the abutment collapse of the Rio Bananito Bridge during the 1990 Costa Rica earthquake.

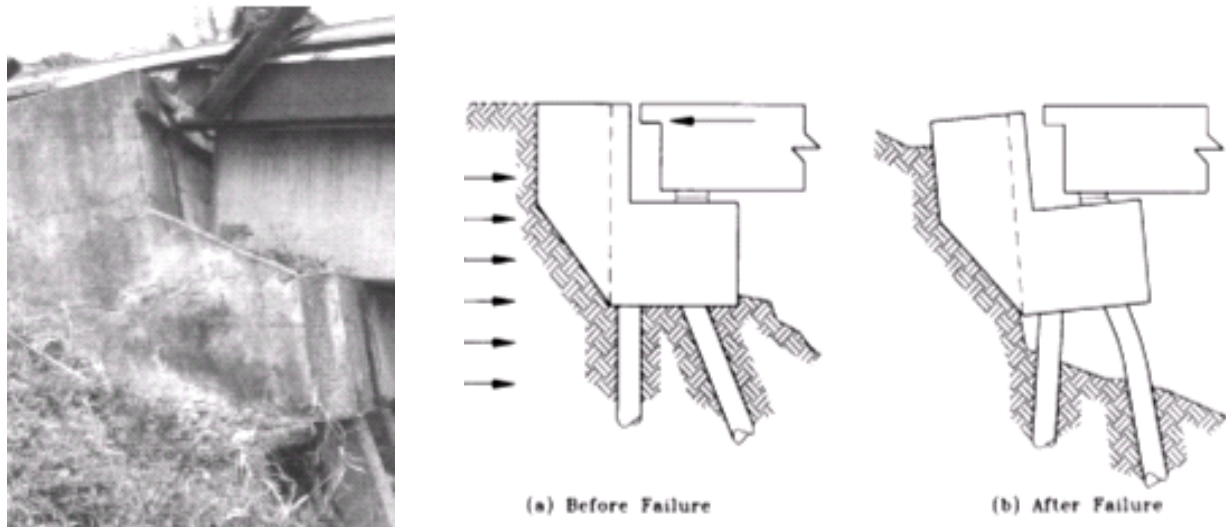


Fig. 10-9: Abutment slumping and rotation failure of the Rio Banano Bridge during the 1990 Costa Rica Earthquake: post-earthquake site observation (left) and sketch of failure mechanism (right) (after Priestley et al., 1996).

The rotation of the abutment produced shear collapse of the foundation piles. Furthermore, the pounding of span and back wall may induce damage to the back wall itself. Even if abutment failure carries heavy consequences for bridges, this is not a commonly observed mechanism because these components are usually over-dimensioned.

10.2.5 Footing failure

Compared to other effects there are few cases of failures caused by footing damage for both RC and steel bridges. Since it is more likely that piers will suffer damage due to inadequate design, actions transmitted to the foundations are limited by the capacity of piers. The rocking of the footing may also have contributed to safeguarding of the foundation system, limiting the level of seismic forces. However, analysis of typical footing detailing points towards several inadequacies, such as:

- i. Footing flexural resistance, mainly due to omission of top reinforcement;
- ii. Footing shear resistance;
- iii. Joint shear resistance;
- iv. Inadequate anchorage of the longitudinal reinforcement of the columns;
- v. Inadequate connection between tension piles and footings.

In the 1995 Kobe earthquake, a number of investigated cases showed damage to footings, which cracked mainly in shear. Several piles were also damaged. It is relatively difficult to ascertain the cause of failure of sub-grade structures, but it is likely that such failures are due to underestimations of the actions transmitted from the piers to the foundations. Also, the point of contra-flexure of the pile-footing-pier system is often mis-placed, hence the critical sections are not treated as such. The paucity of damage data generally may be due to limited investigations, which are typically time-consuming and onerous.

10.3 Limit states

10.3.1 Requirements for comprehensive limit states for assessment

A realistic and usable definition of *limit states* (LS), usually referred to in the US as *performance levels* (PL), and a viable procedure for identifying them by visual inspection and/or by analytical methods, is at the heart of all bridge assessment procedures and is also the basis for deriving fragility curves, as described in Section 10.5. As a general rule, LS are defined in terms of (acceptable) degree of damage and associated implications on the functionality of the bridges, which are a vital component of a transportation network, and disruption of their use can have grave consequences on the function of the network (with economic implications that far outweigh the cost of repairing the bridges).

The proposed number of LS to be verified varies significantly in the various documents (whether code-type or not), depending mainly on the objectives and limitations of each work. For instance, in the damage assessment of bridges carried out by Caltrans engineers following the 1989 Loma Prieta earthquake, only two damage states, minor and major, were used (Basöz and Kiremidjian, 1998), whereas in analytical studies (*see* Section 10.3.4) five, or even more, states were proposed. This interestingly points to the difficulties in classifying damage in a consistent way using visual inspection, as opposed to the relative easiness in specifying a large number of ranges of analytical damage parameters and/or indices, each corresponding to a (conveniently named) LS.

In the following sections the various proposals are briefly described for defining LS of bridge behaviour in three different ways, i.e.

- Observational LS (by visual examination) (*see* Section 10.3.2);
- Functionality LS (according to intended service after the earthquake) (*see* Section 10.3.3);
- Analytical LS (by calculation) (*see* Section 10.3.4).

Prior to describing the above LS, it is appropriate to refer to the general requirements regarding the seismic *performance* of bridges, as set forth in a recently published set of

guidelines for the seismic design of bridges (ATC/MCEER, 2004):

- Loss of life and serious injuries due to unacceptable bridge performance should be minimized;
- Bridges may suffer damage and may need to be replaced but they should have low probabilities of collapse due to earthquake motions;
- The function of essential (critical lifeline) bridges should be maintained even after a major earthquake;
- Upper level event ground motions used in design should have a low probability (usually 15%) of being exceeded (PE) during the conventional design life of the bridge (usually 75 years).

The AASHTO (1998) provisions have three *implied* performance objectives for small, moderate and large earthquakes, with detailed design provisions for a 10% PE in 50 year event (approximately 15% PE in 75 year event) to achieve the stated performance objectives (a performance *objective* is the association of a certain level of seismic action with a PL or LS). Explicit consideration of the “Collapse Limit State” only is prescribed in the current seismic criteria by Caltrans (2004).

The ATC/MCEER (2004) Guidelines provide more definitive performance levels and damage states for *two* design earthquakes, with *explicit* design checks to ensure the performance objectives are met, as described in the following sections. In line with standard European practice, the Eurocode 8 Part 2 for Bridges (EC8, 2004) specifies *two* limit states, the *Ultimate* (or no-collapse) Limit State and the *Serviceability* (or minimisation of damage) LS; both limit states are described in terms of the amount and type of damage that can be sustained.

The aforementioned code-type documents refer to new bridges, nevertheless the performance objectives prescribed in them can also be applied to existing bridges; serviceability, and even damage limitation, requirements might be relaxed in this case, particularly for non-critical bridges. However, it is not permitted to accept higher probability of collapse for existing bridges (Priestley *et al.* 1996).

10.3.2 Observational limit states

Visual examination of seismically damaged bridges permits assigning each bridge to a LS defined by a number of criteria relating to the observed type and extent of damage. This can then be used in a number of ways, notably for deriving statistical vulnerability (fragility) curves (e.g. Basöz & Kiremidjian 1998, Shinozuka *et al.* 2000). A detailed system for defining LS in terms of observed damage after an earthquake was suggested by Basöz and Kiremidjian (1998). Based mainly on damage in concrete bridges during the 1994 Northridge earthquake, as illustrated in Section 10.4.1, a set of preliminary damage states for components of concrete bridges were defined. The system included a total of four damage states (minor, moderate, severe, and collapse), plus the no damage state. The description of this set of damage states was given to experts as a questionnaire in order to capture their opinion on damage definitions for components of concrete bridges. In Table 10-1, the detailed description of damage for each state is given for three key components of the bridge, i.e.

- Abutments;
- Substructures (column bents and/or pier walls);
- Connections and bearings.

While reflecting the collective judgement of a significant number of engineers, some of the descriptions of damage in Table 10-1 are not necessarily representative of the current state of the practice; for instance, “spalling at column faces” is usually considered as (at least) moderate damage, and “buckling of longitudinal reinforcement” is more than “moderate” damage, whereas “shear cracks” are not indicators of moderate damage unless they are wide.

A similar, slightly less detailed, set of damage state definitions was set forth by Kawashima and Unjoh (1997) based on observed damage during the 1995 Hyogo-ken Nanbu (Kobe) earthquake. The system considers description of damage in the following components of the bridge: (i) Piers; (ii) Foundations; (iii) Superstructure, and (iv) Bearing supports. Damage to “superstructure” refers to items such as unseating, which is addressed as damage to “connections and bearings” in Table 10-1, and others such as cracking and spalling of concrete members of the deck, which are not directly addressed in the system described in Table 10-1.

Looking now at a code-type document, the various performance objectives in the ATC/MCEER (2004) Guidelines are described in terms of degree of damage (as well as in terms of functionality, *see* Section 10.3.3). The correspondence between earthquake level and performance level is given in Table 10-1, wherein the three damage states (none, minimal, and significant) are defined as follows:

- *None*: Evidence of movement may be present, but no notable damage;
- *Minimal*: Some visible signs of damage. Minor inelastic response may occur, but post-earthquake damage is limited to narrow flexural cracking in concrete and the onset of yielding in steel. Permanent deformations are not apparent, and any repairs could be made under non-emergency conditions with the exception of superstructure joints;
- *Significant*: Although there is no collapse, permanent offsets may occur and damage consisting of cracking, reinforcement yield, and major spalling of concrete and extensive yielding and local buckling of steel columns, global and local buckling of steel braces, and cracking in the bridge deck slab at shear studs on the seismic load path is possible. For sites with lateral flow due to liquefaction, significant inelastic deformation is permitted in the piles, whereas for all other sites the foundations are capacity-protected and no damage is anticipated.

It is seen that (as expected in a code-type document) the definition of LS in terms of (observational) damage states in the Guidelines is more condensed than the one proposed in Table 10-2. It is also noted that the aforementioned *three* damage states are used for defining *two* performance levels, which are associated with two levels of seismic action.

Probability of Exceedance For Design Earthquake Ground Motions		PERFORMANCE LEVEL	
		LIFE SAFETY	OPERATIONAL
Rare Earthquake (MCE) 3% PE in 75 years/1.5 Median Deterministic	Service	Significant disruption	Immediate
	Damage	Significant	Minimal
Expected Earthquake 50% PE in 75 years	Service	Immediate	Immediate

Table 10-1: Design earthquakes and seismic performance objectives in ATC/MCEER Guidelines (2004).

DAMAGE STATE		DESCRIPTION
1	MINOR	<p>Columns: a) hairline cracks in columns, b) cracks at column top and bottom (1.4 to 1.6mm) and minor spalling, c) spalls at column faces, spalled column flares ($\{\text{flare height/column height}\}$ ratio $<1/3$ or adequate reinforcement exists), e) cracks at bent cap connection.</p> <p>Abutments: a) cracks in shear keys, b) cracks in barrier rail, c) minor wing wall (WW) cracking, d) cracks in closure wall, e) minor curb spalling, f) minor crack and spalling at the abutment, g) cracked slope paving</p> <p>Connections and Bearings: a) railing cracks, b) slight movement, c) settlement at hinges ($\sim 13\text{mm}$), d) minor spalling, e) cracks in hinges</p>
2	MODERATE	<p>Columns: a) shear cracks, b) spalled column flares ($\{\text{flare height/column height}\}$ ratio $>1/3$ or inadequate reinforcement exists), c) flexural failure (formation of plastic hinges, buckling of longitudinal reinforcement over a length of one column diameter), d) cracks exposing core</p> <p>Abutments: a) spalling of soffit ($500\text{mm}\times 200\text{mm}\times 13\text{mm}$), b) pile cap damage, c) diaphragm crack, d) curtain wall cracking, e) end diaphragm damage, f) moderate WW cracking and spalling, g) minor settlement of the approach slab ($\sim 150\text{mm}$), h) small movement of the abutment ($\sim 25\text{-}50\text{mm}$), i) extensive cracking and spalling of shear keys, j) cracks and spalls in the abutment seat, k) backwall cracking, l) anchor bolt damage (no breaks), m) shear key damage (no failures)</p> <p>Connections and Bearings: a) shear key failure, b) keeper bar failure without unseating, c) damage to restrainers hardware, d) longitudinal restrainers failure, e) rocker bearing failure due to breaking of keeper plates, f) bearing pedestal and anchorage failure, g) rotation and displacement of the rocker bearings ($\sim 50\text{mm}$), h) misalignment of finger joints, i) tearing of anchorage and fastenings out of the deck, j) shattering of rail and overhang spalling at hinges, k) residual movements at the expansion or movement joints (less than half of available seat width), l) cracking of girder seats, m) soffit spall, n) joint seal damage (no breaks)</p>
3	SEVERE	<p>Columns: a) shear failure, b) flexural failure (without formation of a plastic hinge due to inadequate confinement steel-due to steel rupture or broken welds-, inadequate anchorage of the steel, inadequate lap splices), c) vertical pull of the longitudinal column reinforcement, d) ground displacement at column base, e) tilting of substructure due to foundation failure</p> <p>Abutments: a) shear key failure, b) WW backwall separation $>60\text{mm}$, c) pull out of restrainers from the backwall, d) damage to restrainer hardware, e) longitudinal restrainer failure, f) rocker bearing failure due to breaking of keeper plates, g) bearing pedestal and anchorage failure, h) rotation and displacement of the rocker bearing ($\sim 50\text{mm}$), i) moderate movement of the abutment ($\sim 50\text{-}250\text{mm}$), j) approach slab rotation, k) WW breakage, l) large approach settlement ($\sim 300\text{mm}$), m) large spalls under girders, n) joint seal failure</p> <p>Connections and Bearings: a) residual movements at the expansion or movement joints (more than half of available seat width), b) tearing of modular joints, c) large spalls (concrete broken due to pounding), d) joint seal failure, e) differential settlement ($\sim 50\text{mm}$)</p>
4	COLLAPSE	<p>Abutments: a) vertical and/or lateral offsets, b) tilting and movement ($>250\text{mm}$) of abutments implying foundation problems, c) foundation failure (e.g. tilting, severe pile damage), d) settlement of backfills ($>300\text{mm}$), e) large crack or broken concrete at the abutments</p> <p>Connections and Bearings: a) span drop due to insufficient seat width, b) hinge restrainer or equalizing bolt failure</p>

Table 10-2: Definition of observational damage states (after Basöz and Kiremidjian, 1998)

10.3.3 Limit states of functionality

As noted earlier in this section, bridges are a vital component of a transportation network, and disruption of their use can have grave consequences on the function of the network, with economic implications that far outweigh the cost of repairing the bridges. Hence, most codes and documents advocating performance-based design and assessment of bridges try to correlate the

limit states described in Section 10.3.2 to the intended function of the bridge *during* and immediately *after* the earthquake, the main emphasis being on whether the bridge will remain in service, either fully or for emergency traffic only. Referring to Table 10-2, where the LS prescribed in ATC/MCEER (2004) are summarised, the Performance Levels are defined in terms of functionality (Service Levels) as follows:

- *Immediate*: Full access to normal traffic shall be available following an inspection of the bridge;
- *Significant Disruption*: Limited access (reduced lanes, light emergency traffic) may be possible after shoring, however the bridge may need to be replaced.

A total of *three* performance levels, each corresponding to a different level of functionality, were proposed by Lehman *et al.* (2004) and are summarised in Table 10-3, where the corresponding damage level descriptions and required repair techniques are also given. The third (and lower) performance level “stability” might be appropriate for a number of existing old bridges, which do not constitute critical lifelines (i.e. alternative routes to reach the nearby urban centres *do* exist), hence upgrading them to a higher performance objective, i.e. to remain functional after the 3% (or even 10%) in 75 yr. earthquake, would generally be not cost-effective. The guidelines by ATC/MCEER (2004) refer to the design of new bridges, for which such a low performance objective is in principle not desirable (although one might argue that it could be appropriate for some small and unimportant bridges).

PERFORMANCE LEVEL	SERVICE	DAMAGE	REPAIR
Fully operational	Full service of bridge after earthquake	Minimal damage: Hairline cracks	Limited epoxy injection required
Delayed operational	Limited service (emergency vehicles)	Moderate damage: Open cracks Concrete spalling	Epoxy injection Concrete patching
Stability	Bridge is not useable after earthquake	Severe damage: Bar buckling/Fracture Core crushing	Replacement of damaged section

Table 10-3: Description of Performance Levels in terms of service level, damage level, and required repair technique (after Lehman *et al.* 2004)

10.3.4 Analytical limit states

For analytical assessment purposes, limit states and/or damage states have to be defined in terms of damage parameters (e.g. drifts, plastic rotations, ductility factors, strength ratios, etc.) and/or damage indices, which involve one or more damage parameters, and are preferably expressed on a scale from 0 to 1 (or 100%), as discussed in more detail in a report by CEB (1997) and a state-of-the-art paper by Kappos (1997), among others. Some proposals, specifically intended for bridges, are briefly summarized in the following.

For assessing the serviceability LS, Priestley *et al.* (1996) recommend strain values of $\epsilon_c=0.004$ for concrete and $\epsilon_s=0.015$ for steel, suggesting that the latter value would lead to residual crack widths of about 1mm (which would not require repair, unless environmental conditions would dictate otherwise); residual crack widths were assumed to be about one third the maximum width. Code limits for strains are generally much stricter than the aforementioned values. It is noted that checking inelastic strains is not a very convenient procedure in analysis of reinforced concrete structures, unless other (more conveniently calculated) response parameters are checked in a way that the strain limitations are met; for instance, Priestley *et al.* (1996) propose to calculate the member rotations corresponding to the above strain limits and carry out

the serviceability check in terms of rotations.

A “dual-phase” damage index, i.e. considering separately concrete and reinforcement damage by monitoring strain in each material, was proposed by Lehman and Moehle (2000); it is defined as:

$$DI = \sum_i \frac{1}{N_f} = \sum_i \frac{1}{a(\varepsilon/\varepsilon_0) + c} \quad (10.1)$$

where N_f is the number of cycles to failure (low-cycle fatigue under seismic loading), $\varepsilon/\varepsilon_0$ is the normalized strain (defined separately for concrete and steel), and a and c are experimentally calibrated constants; e.g. for steel, whose fracture should always be avoided (complete spalling of concrete could be tolerated if the performance objective is not very high), the equation proposed by Lehman *et al.* (2004) is:

$$(N_f)_s = 0.08(\varepsilon_s/\varepsilon_{su})^{-5.5} + 0.92 \quad (10.2)$$

The correlation of the index $(DI)_c$ for concrete and $(DI)_s$ for steel reinforcement with physical damage and recommended repair technique is shown in Table 10-4.

NUMERICAL EXPRESSION		PHYSICAL DAMAGE	REPAIR
Tensile Strain in Steel		Cracking	Epoxy Injection
Compressive Strain in Cover		Initial Spalling	Patching
Residual Drift		Residual Drift	Plumb Structure
Dual-Phase Damage Index	$(DI)_c = 1$ $(DI)_s = 1$	Complete Spalling	Concrete Replacement
	$(DI)_s = 0.9$	Bar/Spiral Failure	Replacement Only

Table 10-4: Limit states for different levels of repair.

A number of proposals have been made for analytically defined LS at the member level. Karim and Yamazaki (2001) have proposed the use of the damage index by Park and Ang (1985) for bridge piers, in the form

$$DI = \frac{\mu_d + \beta \cdot \mu_h}{\mu_u} \quad (10.3)$$

where μ_d and μ_u are the displacement and ultimate ductility of the bridge piers, μ_h is the cumulative energy ductility, defined as the ratio of the hysteretic energy (obtained from dynamic analysis) to the energy at yield point (obtained from static analysis), and β is the cyclic loading factor taken as 0.15, which is not an appropriate value for well-detailed piers (Kappos 1997), but rather corresponds to non-ductile detailing. The suggested correlation of the Park & Ang DI with the damage state of the pier is as shown in Table 10-5; it is based on a limited calibration using results from dynamic analysis for increasing levels of ground motion and cross-correlation with other response parameters such as drifts (which are better calibrated against test data). In fact, drift (relative displacement of pier top with respect to its base) is a good candidate for defining LS in bridges (as well as in buildings). It is much more reliably estimated during tests, compared to local quantities like strains or curvatures, and it is not very sensitive to the details of the model used for estimating it, except for the effective stiffness to be assumed in member-type models (CEB, 1997). However, when attempting to define appropriate drift limits, special care is required to properly account for a number of important parameters that affect drift capacity, such as pier aspect ratio (related to potential for shear failure) and foundation flexibility effects (which

might significantly increase the total drift).

DAMAGE STATE	DI
No damage	DI < 0.14
Slight damage	0.14 ≤ DI ≤ 0.40
Moderate damage	0.40 ≤ DI ≤ 0.60
Extensive damage	0.60 ≤ DI ≤ 1.0
Collapse	DI > 1.0

Table 10-5: Relationship between the Park-Ang damage index (DI) and pier damage state

In a recent study, Erduran and Yakut (2004) correlated damage with pier drift, by defining a damage index (DI) as a (rather complicated) function of the pier drift, the slenderness of the pier, and the steel grade. The empirical parameters used for the definition of the damage functional based on pier drift, were derived combining test results (for the “heavy damage” LS) and nonlinear finite element analysis of piers with the computer program ANSYS (for the other three damage LS, see Table 10-5); steel strains derived from FE analysis were converted to crack widths using an empirical relationship and then correlations of crack width and mean DI values were introduced. The finally proposed relationship between pier drift and the damage functional DI is shown in Fig. 10-10.

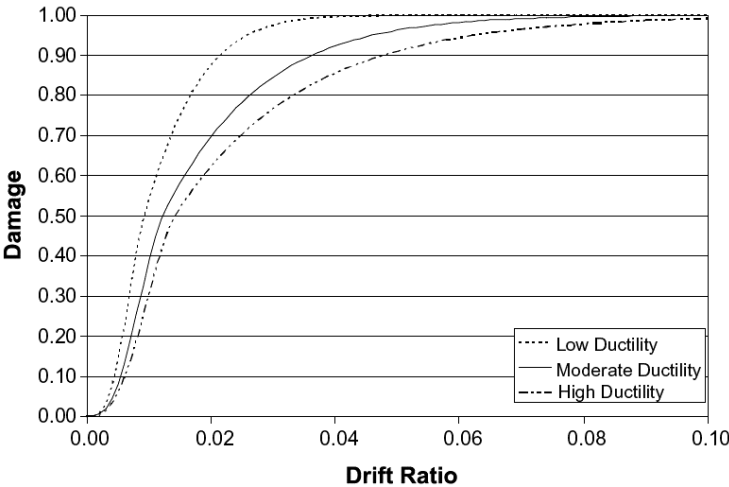


Fig. 10-10: Relationship between drift and damage state for piers (after Erduran-Yakut, 2004).

Although relationships of the type shown in Fig. 10-10 are conceptually attractive, it is essential for them to be based on realistic assumptions as to what constitutes damage. From this point of view, the curves shown in Fig. 10-10 are considered over-conservative (i.e. they tend to over-predict damage); the main reason for this appears to be the unrealistically low crack widths used for describing damage; e.g. ‘light’ damage was associated with crack widths of 0.2 to 1.0mm, and ‘heavy’ damage to widths greater than 2mm, apparently referring to maximum, not residual, values. It is instructive to recall that Priestley *et al.* (1996) consider 1mm residual crack width, i.e. about 3mm maximum width, as the onset of damage.

Another analysis-based proposal for the definition of LS in bridges is that by Choi *et al.* (2004), involving correlation of damage with the curvature ductility factor μ_ϕ calculated for the pier, as well as steel (fixed and expansion rocker) bearing deformations, and elastomeric bearing deformations (d). These bearings are deemed as typical in old concrete bridges in the Central and Southeastern United States, and are considered as the most vulnerable ones (FHWA, 1995). The definition of the various damage states in terms of these parameters is shown in Table 10-6. Damage state definitions used were based on recommendations from previous studies and results from experimental tests at SUNY Buffalo (on non-seismically designed columns, hence the low values for μ_ϕ in Table 10-6).

DAMAGE STATE	SLIGHT DAMAGE	MODERATE DAMAGE	EXTENSIVE DAMAGE	COMPLETE DAMAGE
Columns (μ_ϕ)	$1 < \mu_\phi < 2$	$2 < \mu_\phi < 4$	$4 < \mu_\phi < 7$	$\mu_\phi > 7$
Steel bearings (d , mm)	$1 < d < 6$	$6 < d < 20$	$20 < d < 40$	$40 < d$
Expansion bearings (d , mm)	$d < 50$	$50 < d < 100$	$100 < d < 150$	$150 < d < 255$
Fixed dowels (d , mm)	$8 < d < 100$	$100 < d < 150$	$150 < d < 255$	$255 < d$
Expansion dowels (d , mm)	$d < 30$	$30 < d < 100$	$100 < d < 150$	$150 < d < 255$

Table 10-6: Definition of damage states for non-ductile bridge components.

For seismically designed ductile bridge piers, significantly higher ductility factors than those given in Table 10-6 are in order. Priestley *et al.* (1996) recommend that for the damage control LS (roughly corresponding to the moderate damage state in Tables 10.5 and 10.6) the structural ductility factor range (for the entire bridge) should be between 3 and 6; i.e. assuming $\mu_\delta = (2\div 3)\mu_\phi$, the range for μ_ϕ would be from 6 to 18 (contrasted to 2 to 4 in Table 10-6). The foregoing comparisons strongly point to the need for selecting appropriate limits of the parameters used to analytically define the limit states in seismic assessment of bridges and the derivation of fragility curves.

10.4 Methods of assessment

Assessment of the vulnerability of structural systems subjected to earthquake actions is an essential component of evaluating losses after an earthquake to direct repair efforts. It is equally important prior to the occurrence of earthquakes in order to draw emergency plans and strengthen the potentially exposed stock. There are several levels and approaches for assessment of structural systems, ranging from physical inspections or using a code expression to compare ‘supply’ and ‘demand’, to the derivation of regionally applicable probabilistic vulnerability functions. Such probabilistically-based vulnerability relationships may also be applicable to a type of construction regardless of the region; this depends on the variables and input motion characteristics used in the derivation. Deterministic and probabilistic approaches may be viewed as shown in Fig. 10-11. Methods based on deterministic assessments are represented by the lines [D], whilst [P1] and [P2] represent different levels of variability (Wen *et al.*, 2004).

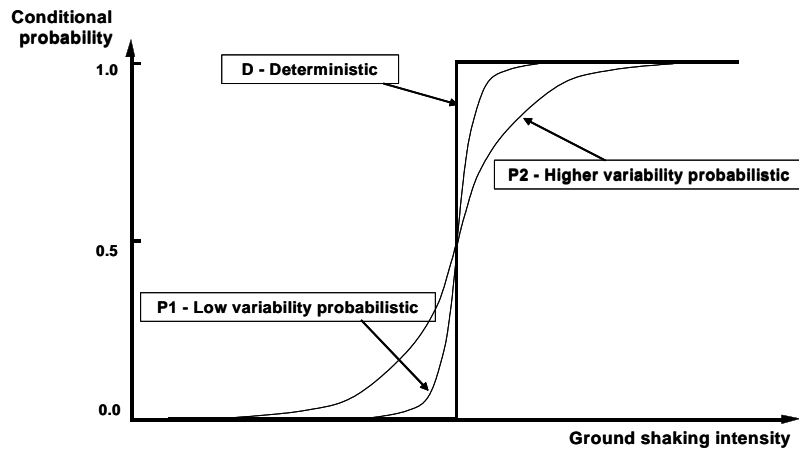


Fig. 10-11: Schematic depiction of deterministic and probabilistic assessment methods (after Wen *et al.*, 2004).

The seismic vulnerability or fragility function of bridges is the conditional probability (vertical axis in Fig. 10-11) that a given intensity of earthquake input (horizontal axis in Fig. 10-11) will cause a limit state criterion (*see* Section 10.3.4) to be achieved or exceeded. Probabilistic vulnerability studies are in general undertaken employing relationships that express the probability of damage as a function of a ground motion parameter, since neither the input motion nor the structural behaviour can be described deterministically. The two widely used forms of motion-versus-damage relationships are ‘vulnerability curves’ and ‘damage probability matrices’ (DPM). A plot of the computed conditional probability versus the ground motion parameter is defined as the vulnerability curve for the damage state, whilst the discrete probability of reaching or exceeding a damage state for a certain input motion severity represents an element of the DPM. The damage level is randomly described corresponding to random input variables. Out of the large number of parameters, which affect the behaviour of structures under seismic action, only those considered to influence significantly the response are assumed as random variable. The principal steps for the evaluation of vulnerability curves and DPMs are as follows:

- i. Identification of random input variables and hence likely scenarios of systems based on a prototype structure;
- ii. Quantification of potential earthquake ground motion(s);
- iii. Evaluation of structural response;
- iv. Comparison between demand, corresponding to the seismic hazard, and limit states of the considered structural system.

Vulnerability analyses may be either empirical or analytical depending on whether observational or analytical results are utilised, respectively. In the first case the information available on structures similar to those for which the seismic vulnerability is sought must be selected (e.g. Basöz, and Kiremidjian, 1998; Yamazaki *et al.*, 1999, Elnashai *et al.*, 2004). On the other hand, inelastic (static and/or dynamic) analyses are generally utilised to compute analytically the seismic vulnerability of structural systems. The following sections provide an overview of existing observational and deterministic analytical methods to perform the assessment of seismic vulnerability of bridge structures. Approaches for fragility assessment are discussed in detail in Section 10.5.1.

10.4.1 Observational methods

Ultimately, only through the collection and archiving of comprehensive and representative field damage data, coupled with relevant hazard definition from destructive earthquakes, would loss predictions with a quantifiable reliability be available. This target, however, is not even on

the earthquake engineering horizon. Damaging earthquakes striking heavily developed areas, as regrettable as they are, furnish an opportunity to improve the statistical representation of the relationship between shaking intensity and damage limit state attainment. The data collected, however, may or may not be useful. There are several important considerations that dictate the quality and usefulness of the observational data intended for seismic vulnerability assessment. To provide a vivid expose of the issues pertinent to field data, the bridge damage data sets of Basöz and Kiremidjian (1998) and Yamazaki *et al.* (1999) are assessed. The former utilised a dataset compiled for the 1994 Northridge earthquake, whilst the latter employed data from the 1995 Hyogo-ken Nanbu (Kobe) earthquake of 1995. The damage data presented by the two research groups is given in Tables 10.7 and 10.8.

DAMAGE	PEAK GROUND ACCELERATION (G)										Total
	0.15-0.2	0.2-0.3	0.3-0.4	0.4-0.5	0.5-0.6	0.6-0.7	0.7-0.8	0.8-0.9	0.9-1.0	>1.0	
NONE	318	502	234	50	34	29	24	29	16	16	1252
MINOR	2	10	25	2	6	4	6	1	7	3	66
MODERATE	1	15	13	11	10	9	5	4	9	4	81
MAJOR	0	10	2	6	7	3	2	5	11	1	47
COLLAPSE	0	0	1	0	0	0	0	2	2	1	6

Table 10- 7: Observational Damage Data of Basöz and Kiremidjian (1998) - 1994 Northridge Earthquake.

It is clear that the damage data usable to define the collapse state is totally unsuitable, being 6 and 4 sampling points only. Moreover, the distribution amongst the ‘hazard’ intervals, represented by peak ground acceleration, is not viable for statistical treatment. There is clearly a long way to go before observational data on its own is reliably used in probabilistic damage assessment. Below are some of the requirements to arrive at a reliable observational data base.

DAMAGE	PEAK GROUND ACCELERATION (G)										Total
	0.15-0.2	0.2-0.3	0.3-0.4	0.4-0.5	0.5-0.6	0.6-0.7	0.7-0.8	0.8-0.9	0.9-1.0	>1.0	
NONE	80	34	23	28	12	3	3	1	0	0	184
MINOR	0	0	2	1	0	4	0	1	0	0	8
MODERATE	0	0	1	3	3	6	0	0	0	0	13
MAJOR	0	0	0	1	0	5	1	0	0	0	7
COLLAPSE	0	0	0	2	0	2	0	0	0	0	4

Table 10-8: Damage Data of Yamazaki *et al.* (1999) - 1995 Hyogo-ken Nanbu Earthquake

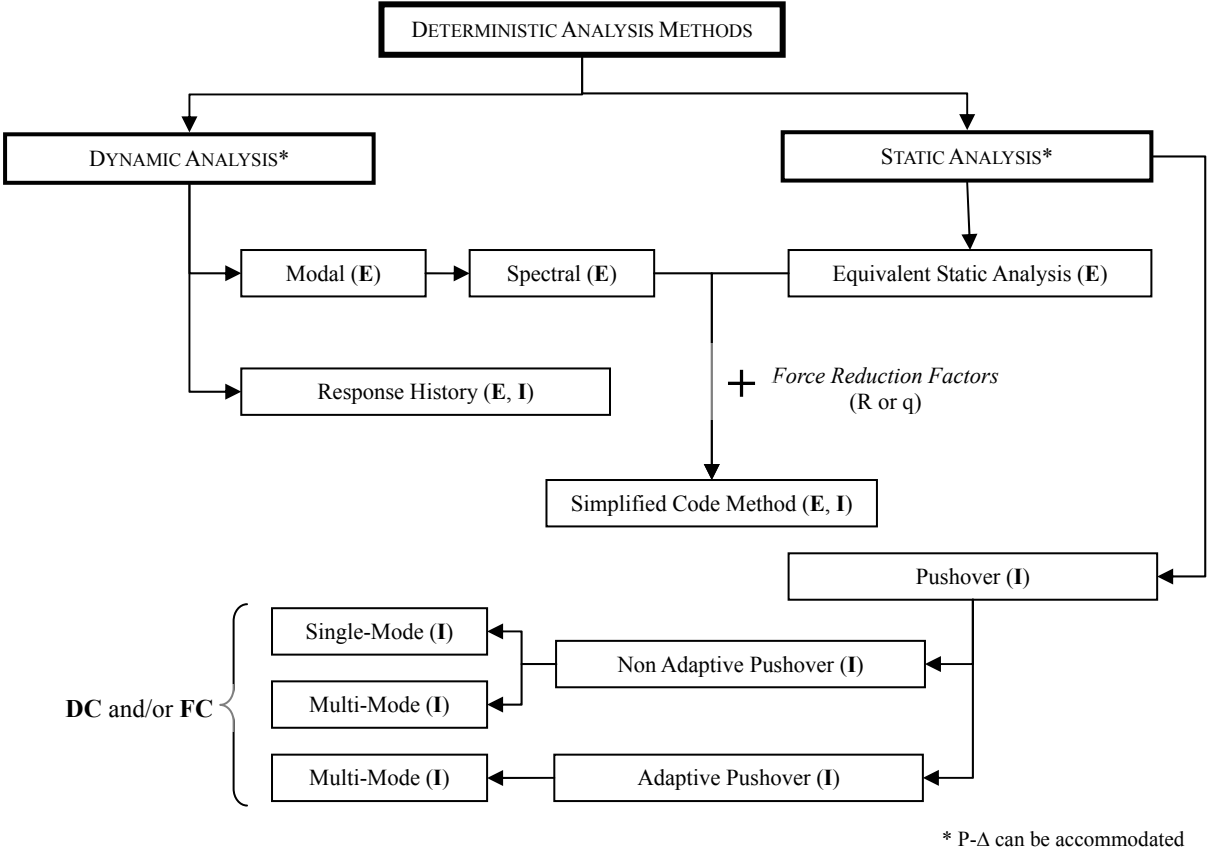
Firstly, the collection of data from the field should be carefully directed and controlled; the quality of data is locked-in once the inspection teams leave the site. Thereafter, it is not possible to improve the quality of data but through methods of dealing with uncertain data that invariably increase the uncertainty level in the fragility analysis. Moreover, it is clear that the number of data points associated with low levels of damage is significantly more than for higher damage states. Indeed, the vulnerability curves could be extrapolated in a number of different shapes even if they have fitted the observational data. Finally, attempts at fitting the data collected with normal or lognormal functions, or any other interpolation function, may yield poor correlations. It is concluded that for seismic risk analysis tool to be developed it is essential that empirical observations are supplemented by analytically-simulated damage statistics. The standardization of inspection forms used to collect damage data, and high-level training of engineers who are entrusted with collecting the data, are essential to the needed improvement of the world-wide damage data. Verification and deployment of advanced inventory collection methodologies are also issues of priority for the improvement of damage data. Such data remain the only viable

means of calibrating analytical vulnerability formulations, which are in turn the only viable means of describing damage to many different forms of system, while maintaining a consistent confidence level.

10.4.2 Analytical methods

Many existing bridges in earthquake-prone regions world-wide were not designed in compliance with seismic provisions; therefore the assessment of their level of safety is crucial to minimize economic and societal losses.

The seismic design of new bridges is routinely based on elastic response spectrum (multi-modal) analyses or even equivalent static analyses (Fig. 10-12); both methods rely on force-based formulations. More advanced displacement-based design methodologies are under development (e.g. Bozorgnia and Bertero, 2004); further improvements are, however, required to enhance the reliability of methods of earthquake response analysis. On the other hand, procedures to assess seismic performance of existing bridges are lacking.



Key: E = Elastic; I = Inelastic; DC = Displacement-Controlled; FC = Force-Controlled.

Fig. 10-12: Common methods of analysis used in structural earthquake engineering.

Inelastic analyses, either static (pushover) or dynamic (time-history) are the most appropriate tool to investigate the deformation capacity of existing bridges and to provide estimate of their seismic vulnerability. The use of time-history analyses, however, requires several assumptions regarding the selection of the suite of earthquake ground motions and is also generally time-consuming because of the high number of calculations involved. Conversely, inelastic pushovers are more efficient tools to assess the earthquake response of bridges. Although originally formulated for single degree of freedom (SDOF) systems (e.g. Freeman *et al.*, 1975;

Shibata and Sozen, 1976; Saiidi and Sozen, 1981; Fajfar and Fischinger, 1988, among many others), pushover analyses are extensively utilized for the displacement-based assessment of regular and irregular multi-storey buildings. Recently, the application of pushovers has been extended also to existing bridge structures (e.g. Kappos *et al.*, 2004; Aydinoglu, 2004; Casarotti, 2005; Kappos *et al.*, 2005; Isakovic and Fischinger, 2005). Different formulations have been suggested for this type of analysis; a comprehensive review along with pros and cons of each formulation can be found in FEMA 440 (ATC, 2005). The following section provides an overview of the most common procedures of non-adaptive and adaptive pushover analyses (see also Fig. 10-12).

10.4.2.1 Inelastic static (pushover) analysis: non-adaptive approaches

Single-mode methods

This method of non-linear static analysis was formulated by Freeman *et al.* (1975) to assess earthquake response of structural systems. Over the years, a number of variants have been proposed and also implemented in international design codes and recommendations. For example, in the USA, ATC 40 (1996) and FEMA 356 (2000) employ the capacity spectrum and the displacement-coefficient methods to evaluate the seismic performance of existing buildings. Similarly, in Europe, the non-linear static N2 method (Fajfar and Fischinger, 1988; Fajfar and Gasperic, 1996) has been recently included in the Eurocode 8 Part 2 (EC8, 2004) which deals specifically with bridge structures. The latter procedure is outlined below.

The N2 method encompasses three fundamental steps: (i) definition of equivalence between the MDOF system and an ‘equivalent SDOF’; (ii) evaluation of nonlinear response and limit states of the equivalent SDOF; (iii) evaluation of demand/capacity ratios of all members in the MDOF corresponding to the limit states computed through the equivalent SDOF. In so doing, it is assumed that:

The applied load pattern is invariant and proportional, through the mass matrix \mathbf{M} , to the first mode shape Φ - normalised to unit displacement at the building top;

The displacement pattern of the structure is assumed to be invariant and described by the first mode shape Φ .

Based on the above assumptions, the applied forces \mathbf{f} and the lateral displacements \mathbf{u} for the MDOF can be written as:

$$\mathbf{f}(u) = \mathbf{M}\Phi\lambda(u) \quad (10.4)$$

$$\mathbf{u} = \Phi u \quad (10.5)$$

where u is the displacement of the ‘monitoring point’, i.e. lateral displacement of the equivalent SDOF system, and $\lambda(u)$ is a load multiplier, with $\lambda > 1.0$. While for buildings, the monitoring point corresponds to the centroid of mass of the roof, for bridges natural choices are the deck mass centre (EC8, 2004) or the top of the pier nearest to it. However, it has been demonstrated that the location of such point in bridge structures is not always straightforward, especially when multi-modal pushover analyses, illustrated later, are carried out (Aydinoglu, 2004; Kappos *et al.*, 2005).

If viscous damping forces are ignored, the equations of dynamic equilibrium of the system are:

$$\mathbf{M}\ddot{\mathbf{u}} + \mathbf{f}(u) = -\mathbf{M}\mathbf{1}a(t) \quad (10.6)$$

where $\mathbf{1}$ is a unitary vector and $a(t)$ is the input acceleration ground motion.

Substituting in eq.(10.6) the relationships for \mathbf{u} and \mathbf{f} given in eq.(10.4) and (10.5), respectively, and pre-multiplying both sides by Φ^T , it follows:

$$(\Phi^T \mathbf{M} \Phi) \ddot{u} + (\Phi^T \mathbf{M} \Phi) \lambda(u) = -\Phi^T \mathbf{M} \mathbf{1} a(t) \quad (10.7)$$

The modal participation factor can be expressed as given below:

$$\Gamma = (\Phi^T \mathbf{M} \mathbf{1}) / (\Phi^T \mathbf{M} \Phi) \quad (10.8)$$

thus, eq.(10.7) becomes:

$$(\Phi^T \mathbf{M} \mathbf{1}) \frac{\ddot{u}}{\Gamma} + (\Phi^T \mathbf{M} \mathbf{1}) \frac{\lambda(u)}{\Gamma} = -\Phi^T \mathbf{M} \mathbf{1} a(t) \quad (10.9)$$

where $\Phi^T \mathbf{M} \mathbf{1} \lambda(u) = \sum_i f_i(u) = V_b(u)$ is the base (seismic) shear.

By setting $m^* = \Phi^T \mathbf{M} \mathbf{1} = \sum_i m_i \phi_i$, $u^* = u/\Gamma$ and $V^*(\Gamma u^*) = V_b(u)/\Gamma$, the equation of dynamic equilibrium of the ‘equivalent SDOF system’ is given by:

$$m^* \ddot{u}^* + V^*(\Gamma u^*) = -m^* a(t) \quad (10.10)$$

The function $V^*(\Gamma u^*) = V_b(u)/\Gamma$, which quantifies the nonlinear restoring forces of the system, can be plotted with regard to the horizontal displacement of the monitoring point (*pushover* or *capacity curve*). The pushover curve is computed through non-linear analysis under monotonically increasing forces $\mathbf{f}(u) = \mathbf{M} \Phi \lambda(u)$ until failure is attained or the global stiffness matrix becomes singular.

The evaluation of the structural response of the equivalent SDOF system requires some assumptions on the cyclic behaviour, e.g. shape of hysteresis loop including strength and/or stiffness degradation, if any. Thus, the response of the SDOF can be computed either by numerical integration of eq. (10.10) employing a suitable set of earthquake records, or by utilizing inelastic response spectra available in the literature (e.g. Bozorgnia and Bertero, 2004, among others). In the N2 method, formulated by Fajfar and his co-workers (Fajfar and Fischinger, 1988; Fajfar and Gasperic, 1996) chiefly for the seismic performance assessment of buildings, the inelastic spectral displacement $S_d = u_{\max}^*$ is given as a function of the elastic spectral displacement $S_{de}(T^*)$ in the form:

$$S_d(T^*) = \frac{\mu}{R_\mu} S_{de}(T^*) \quad (10.11)$$

where μ is the displacement ductility, given by:

$$\begin{cases} \mu = 1 + (R_\mu - 1) \frac{T_0}{T^*} & T^* < T_0 \\ \mu = R_\mu & T^* \geq T_0 \end{cases} \quad (10.12)$$

and the period T_0 is equal to the corner period T_C , which marks the transition between the constant acceleration and constant velocity regions of the spectrum.

On the other hand, Eurocode 8 Part 2 (EC8, 2004) recommends, for inelastic static

(pushover) analysis of bridges to employ as target displacement (d_T) - of the monitoring point - the maximum displacement (d_E) at the centre of the mass of the deck (*monitoring point*) estimated through response spectrum analysis employing behaviour factor $q=1.0$ (*elastic response spectrum*). Combinations of the seismic action along two orthogonal directions should be considered if three-dimensional structural models are assessed.

Once the SDOF maximum response u_{\max}^* is known, the actual maximum displacement at the top of the building is given by $u_{\max} = \Gamma u_{\max}^*$. The latter is used to compute the demand in all members of the structure and hence to perform the check of the demand/capacity ratios.

Multi-mode methods

This type of static analysis is a refinement of the single-mode non adaptive method presented earlier. The horizontal force pattern is invariant; however, a set of patterns are applied to the structure, each distribution corresponds to a single mode of vibration (Chopra and Goel, 2002; Goel and Chopra, 2004, Kappos *et al.*, 2005). The response parameters are evaluated by employing probabilistic combinations rules, either SRSS or CQC, for the effects computed with the pushover analyses corresponding to the significant modes considered. The fundamental steps of this method of analysis are outlined below.

The equations of dynamic equilibrium of the system, neglecting the damping forces, are:

$$\mathbf{M}\ddot{\mathbf{u}} + \mathbf{f}(\mathbf{u}) = -\mathbf{M}\mathbf{1}a(t) \quad (10.13)$$

where the internal forces \mathbf{f} depend on the total displacement vector \mathbf{u} . The term on the right-hand side is the vector of earthquake-induced forces. The invariant pattern of these forces can be expanded using the initial modal shapes according to:

$$\mathbf{M}\mathbf{1} = \sum_j \Gamma_j \mathbf{M}\Phi_j \quad (10.14)$$

as it can be verified by substituting for $\Gamma_j = (\Phi_j^T \mathbf{M}\mathbf{1}) / (\Phi_j^T \mathbf{M}\Phi_j)$ and pre-multiplying by Φ_j^T .

If the behaviour of the bridge structure is linear elastic, when excited by a generic component of the summation in eq.(10.14), the structure would respond in compliance with the corresponding mode, i.e.:

$$\mathbf{u}_j(t) = \Phi_j q_j(t) \quad (10.15)$$

where the modal response $q_j(t)$ is the solution of the SDOF equation:

$$m_j \ddot{q}_j + k_j q_j = -\Gamma_j m_j a(t) \quad (10.16)$$

in which $m_j = \Phi_j^T \mathbf{M}\Phi_j$ and $k_j = \Phi_j^T \mathbf{K}\Phi_j$ are the modal mass and stiffness, respectively.

When the structure oscillates in the inelastic range one cannot uncouple the equations of motion using modal shapes, as it can be seen from the j -th modal equation:

$$m_j \ddot{q}_j + \Phi_j^T \mathbf{f}(\mathbf{u}) = -\Gamma_j m_j a(t) \quad (10.17)$$

where the internal resisting force is still a function of the whole displacement vector

$$\mathbf{u} = \sum \Phi_j q_j .$$

The approximation used in this method is that of assuming that when the excitation is proportional to the j -th mode, the response is still predominantly contributed by the same mode ($\mathbf{u}(t) \cong \Phi_j q_j(t)$), which in turn implies that the modal equations are uncoupled:

$$m_j \ddot{q}_j + \Phi_j^T \mathbf{f}(q_j) = -\Gamma_j m_j a(t) \quad (10.18)$$

The non-linear force-displacement relation $\Phi_j^T \mathbf{f}(q_j)$ should be determined by non-linear static analysis of the structure under increasing imposed displacements $\mathbf{u} = \Phi_j q_j$. Chopra and Goel (2002) suggested to conduct a force-controlled inelastic static analysis with a distribution of lateral forces with invariant pattern $\mathbf{M}\Phi_j$ - since this is what can be done with most of the commercially available software. Substituting in eq.(10.18) for $\mathbf{f}(q_j)$ the forces $\mathbf{M}\Phi_j \lambda(q_j)$ and dividing and multiplying all terms by $\Phi_j^T \mathbf{M}\mathbf{1}$ one has:

$$\Phi_j^T \mathbf{M}\mathbf{1} \frac{\ddot{q}_j}{\Gamma_j} + \Phi_j^T \mathbf{M}\mathbf{1} \frac{\lambda(q_j)}{\Gamma_j} = -\Phi_j^T \mathbf{M}\mathbf{1} a(t) \quad (10.19)$$

which is the same as eq.(10.9) but for the fact that it refers to the generic j -th mode.

Further steps of the multi-mode non adaptive pushover analysis are similar to those illustrated earlier for the N2-method (Fajfar and Fischinger, 1988; Fajfar and Gasperic, 1996). In particular, maximum modal displacements $q_{j,max}$ are estimated either directly by numerical integration or by using inelastic response spectra. Response quantities from each mode are then computed and combined with either SRSS or CQC combination rules. These rules, although formulated for linear elastic systems, are employed in this method of analysis to combine effects in the inelastic range. In addition, multi-mode analyses combine responses from inhomogeneous structure states since different levels of inelasticity are attained in each mode; it is like combining response of different structures. Notwithstanding, comparisons between values of response quantities computed through non-adaptive single-mode, multi-mode pushover and inelastic time-history analyses have demonstrated the applicability and relative accuracy of multi-mode (non-adaptive) approaches to perform seismic assessment of RC bridges (e.g. Kappos *et al.*, 2005).

10.4.2.2 Inelastic Static (Pushover) Analysis: Adaptive Approaches

Adaptive is the term used to indicate those approaches that while constructing the pushover curve, modify the pattern of the applied forces (or applied deformations) so as to follow more or less closely the change of the (instantaneous) mode shapes, change due to the varying stiffness properties of the structure. Several proposals of adaptive procedures have been formulated in the last decade (e.g. Reinhorn, 1997; Gupta and Kunnath, 2000; Elnashai, 2001; Aydinoglu, 2003, 2004; Antoniou and Pinho, 2004-a, 2004-b, among others). Most of these proposals, however, possess common pitfalls relative to the adaptive force patterns, as discussed hereafter.

It was observed earlier in Section 10.4.2.1 that even non-adaptive multi-modal approaches incur in the inconsistency of combining responses from inhomogeneous structure states. This problem becomes more evident for adaptive procedures. The latter require, - to perform eigenvalue analysis at each step - the evaluation of the structure state at the end of previous step. Such state cannot be estimated through combination of (inelastic) modal response employing

either SRSS or CQC.

Formulations for adaptive pushovers employ generally a unique force pattern derived by means of the (SRSS or CQC) combination of modal forces. However, combining actions rather than action-effects represents a large source of approximation, even in the elastic range, due to the sign-loss. Modal contributions can only add to the global force patterns, which, in turn, may lead to significant errors in the estimation of action- and/or deformation-response quantities. Proposals for alternative weighted vector combinations of modal forces have been proposed by Kunnath (2004) for building structures; the proposed formulation is, however, still far from maturity.

Multi-mode methods

Adaptive multi-mode inelastic analyses have been formulated either in terms of force- (Elnashai, 2001; Antoniou and Pinho, 2004-a) or displacement-patterns (Antoniou and Pinho, 2004-b). The fundamental steps of the force-base adaptive method are summarised below.

The applied forces at time t are given by the following incremental expression:

$$\mathbf{p}_t = \mathbf{p}_{t-\Delta t} + \Delta\lambda_t \cdot \bar{\mathbf{p}}_t \quad (10.20)$$

where $\Delta\lambda_t$ is the load-factor increment at time t and the ‘normalised scaling vector’ $\bar{\mathbf{p}}_t$ is a unit-norm vector; it corresponds to the force increment shape. The load-factor increment ($\Delta\lambda$) can be either load- or displacement-control.

The vector $\bar{\mathbf{p}}_t$ is the normalised SRSS/CQC combination of the modal force vectors given by:

$$\mathbf{p}_j = \Gamma_j \mathbf{M} \Phi_j S_a(\omega_j) \quad j = 1, K, n \quad (10.21)$$

In particular, the j -th modal force at the i -th degree of freedom can be computed as:

$$p_{ij} = \Gamma_j m_i \phi_{ij} S_a(\omega_j) \quad (10.22)$$

and the corresponding normalised scaling vector component, using the SRSS-combination, is given by:

$$\bar{p}_i = \frac{p_i}{|\mathbf{p}|} = \frac{\sqrt{\sum_j p_{ij}^2}}{|\mathbf{p}|} \quad (10.23)$$

Frequencies and mode-shapes, required to update the normalised scaling vector $\bar{\mathbf{p}}$, can be either calculated at each time-step, or - to optimize the computational effort - at a finite number of intermediate discrete states.

The application of this analytical method may give rise to inaccurate results in the equivalence with the SDOF system; the latter may undermine the reliability of the assessment procedure as it relies on the demand computed through a response spectrum.

Incremental response spectrum analysis (IRSA)

Incremental response spectrum analysis (IRSA) is a displacement-based procedure

formulated by Aydinoglu (2003, 2004) for the seismic assessment of regular and irregular building and bridge structures. It can accommodate second order P-D effects, which are relevant in slender RC bridge piers. This method of inelastic (static) analysis employs elastic design spectrum and relies on equal-displacement rule. The latter implies that inelastic spectral displacements associated with the instantaneous configuration of the structure ($S_{den}^{(i)}$), at any pushover step can be assumed equal to the initial elastic spectral displacement estimated at the first step ($S_{den}^{(1)}$).

The analysis stages to be applied at each pushover step of the IRSA are summarised below:

- (i) Run a linear response spectrum analysis corresponding to the current plastic hinge configuration. Include a sufficient number of modes and second order (P- Δ) effects, if any. Use the same elastic spectral displacements at all pushover steps as seismic input ($S_{den}^{(1)}$). These displacements are defined only once at the first pushover step as elastic spectral displacements.
- (ii) Compute the structural response parameters ($\tilde{r}^{(i)}$) through a modal combination rule, e.g. SRSS or CQC. For example, the use of CQC-rule gives rise to the following expression for $\tilde{r}^{(i)}$:

$$\tilde{r}^{(i)} = \sqrt{\sum_{m=1}^{N_s} \sum_{n=1}^{N_s} (\tilde{r}_m^{(i)} \rho_{mn}^{(i)} \tilde{r}_n^{(i)})} \quad (10.24)$$

where N_s indicates the total number of modes considered and $\rho_{mn}^{(i)}$ is the cross-correlation of the CQC-rule. The response quantity $\tilde{r}_n^{(i)}$ are computed from:

$$\tilde{\mathbf{u}}_n^{(i)} = \Phi_n^{(i)} \Gamma_{xn}^{(i)} S_{den}^{(1)} \quad (10.25)$$

- (iii) Specialize the following expression relative to the generic response quantity at the end of the i -th pushover step for the response quantity that defines the coordinates of yield surfaces of all potential plastic hinges in the bridge structural system:

$$\mathbf{r}^{(i)} = \mathbf{r}^{(i-1)} + \Delta \mathbf{r}^{(i)} = \mathbf{r}^{(i-1)} + \tilde{r}^{(i)} \Delta \tilde{\mathbf{F}}^{(i)} \quad (10.26)$$

where $\Delta \tilde{\mathbf{F}}^{(i)}$ is an incremental scale factor, which is applicable to all modes at the i -th step in the pushover analysis. Response quantities corresponding to gravity loads are assumed as $\mathbf{r}^{(0)}$ in the first pushover step.

- (iv) Compute the incremental scale factor $\Delta \tilde{\mathbf{F}}^{(i)}$ according to the yield conditions of all potential plastic hinges and identify the occurrence of new hinges. The section that yields with the minimum positive incremental scale factor $\Delta \tilde{\mathbf{F}}^{(i)}$ is assumed to be the new plastic hinge.
- (v) Compute the cumulative scale factor $\tilde{\mathbf{F}}^{(i)}$ given by:

$$\tilde{\mathbf{F}}^{(i)} = \tilde{\mathbf{F}}^{(i-1)} + \Delta \tilde{\mathbf{F}}^{(i)} \quad (10.27)$$

- (vi) Check if the cumulative scale factor $\tilde{\mathbf{F}}^{(i)} \leq 1$. If so, continue with the next stage. Conversely ($\tilde{\mathbf{F}}^{(i)} > 1$), calculate the incremental scale factor corresponding to this final pushover step (indicated by superscript p) through the relationship:

$$\Delta \tilde{F}^{(p)} = 1 - \tilde{F}^{(p-1)} \quad (10.28)$$

- (vii) Estimate all the response quantities at the end of the pushover step by employing eq.(10.26). If the final pushover step has been reached, the analysis terminates. If not, continue to the next stage and repeat steps (i) to (vii).

The analysis presented above is very useful for practical bridge applications which are generally characterised by significant higher modes effects and/or structural irregularities (Aydinoglu, 2004, Kappos *et al.*, 2004; Kappos *et al.*, 2005). It is also a reliable tool to assess geometrical nonlinearities, i.e. P- Δ effects, in slender structural systems. Moreover, IRSA requires neither transformations to equivalent SDOF systems nor computations of pushover curves. Finally, it is an innovative displacement-controlled displacement procedure and hence can be implemented in the framework of the performance-based design and assessment of bridges.

10.4.3 Example applications

Applications of pushover-based assessment methods for bridge structures in the literature are rather scarce. The few existing case studies comprise generally bridge systems with special features (e.g. Une *et al.*, 1999; Zheng *et al.*, 2003; Kappos *et al.*, 2004, Kappos *et al.*, 2005). Comprehensive parametric studies by Isakovic and Fischinger (2005) and Casarotti (2005) have been recently carried out and results applicable to a wide range of design cases have been derived. These results are outlined below to illustrate pros and cons of the analytical methods for earthquake response assessment of bridges presented in the previous section.

Four RC viaducts (Fig. 10-13) were assessed by Isakovic and Fischinger (2005) through inelastic static (pushover) and dynamic (time-history) analyses. In Fig. 10-13, the labels used for the sample bridges indicate the height of the piers, from left to right, as multiple of the reference length of 7m, and the support conditions at abutments (P and R stands for pin and roller, respectively). For example, V213P indicates the RC viaduct (V) with piers of 14m (2), 7m (1) and 21m (3) high and pinned (P) abutments.

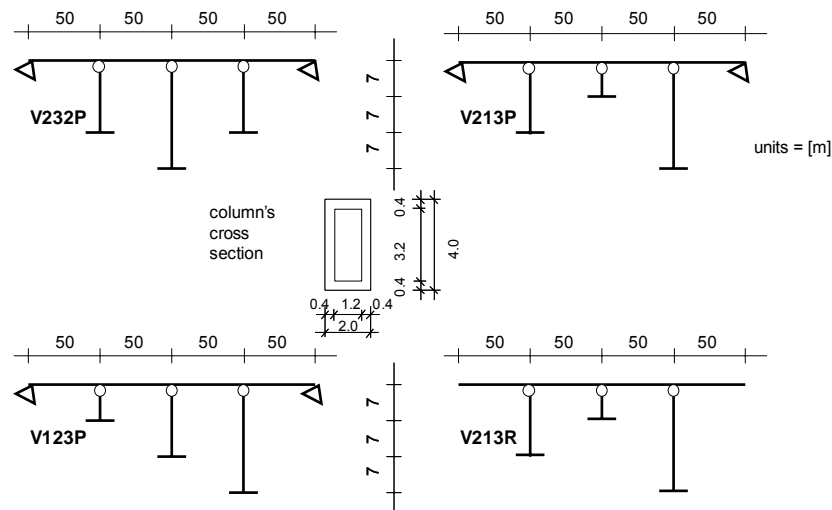


Fig. 10-13: Sample RC viaducts assessed by Isakovic and Fischinger (2005).

The three pinned bridges (V232P, V213P and V123P) were employed as benchmark structures in previous studies (e.g. Fischinger and Isakovic, 2003); these structures were

designed and pseudo-dynamically tested in the framework of a EU-funded project in support of Eurocode 8 Part 2 Bridges (Calvi and Pinto, 1996). The sample viaduct V213R is a further case study employed by Isakovic and Fischinger (2005) as an example of ‘highly’ irregular bridge. The deck, continuous over the piers is the same for all assessed viaducts; it was modelled through elastic elements in the performed analyses.

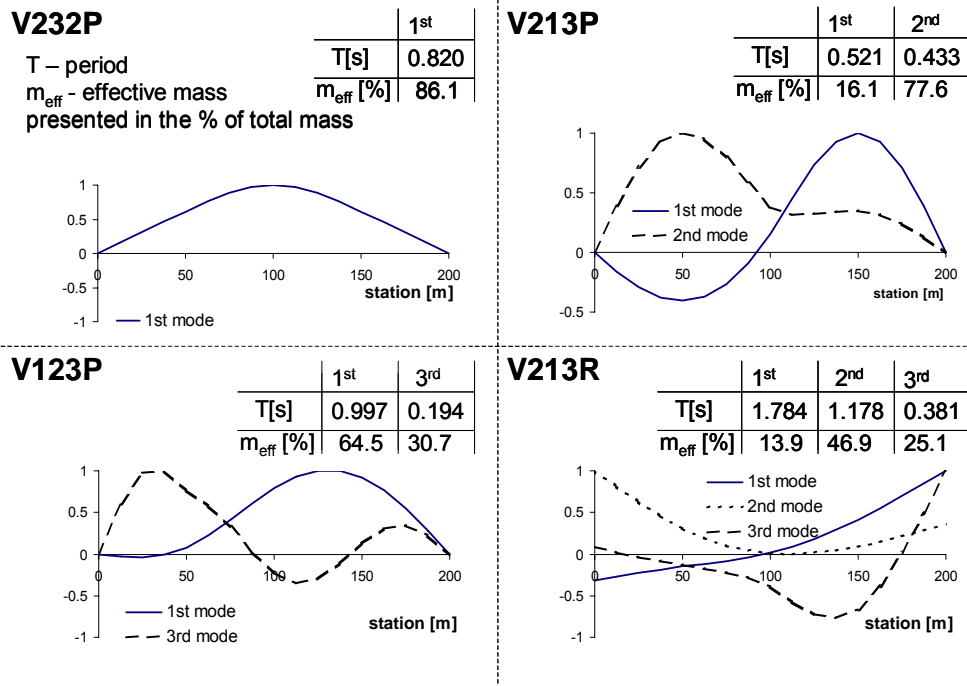


Fig. 10-14: Mode shapes, periods and participation factors of the sample viaducts (after Isakovic and Fischinger, 2005).

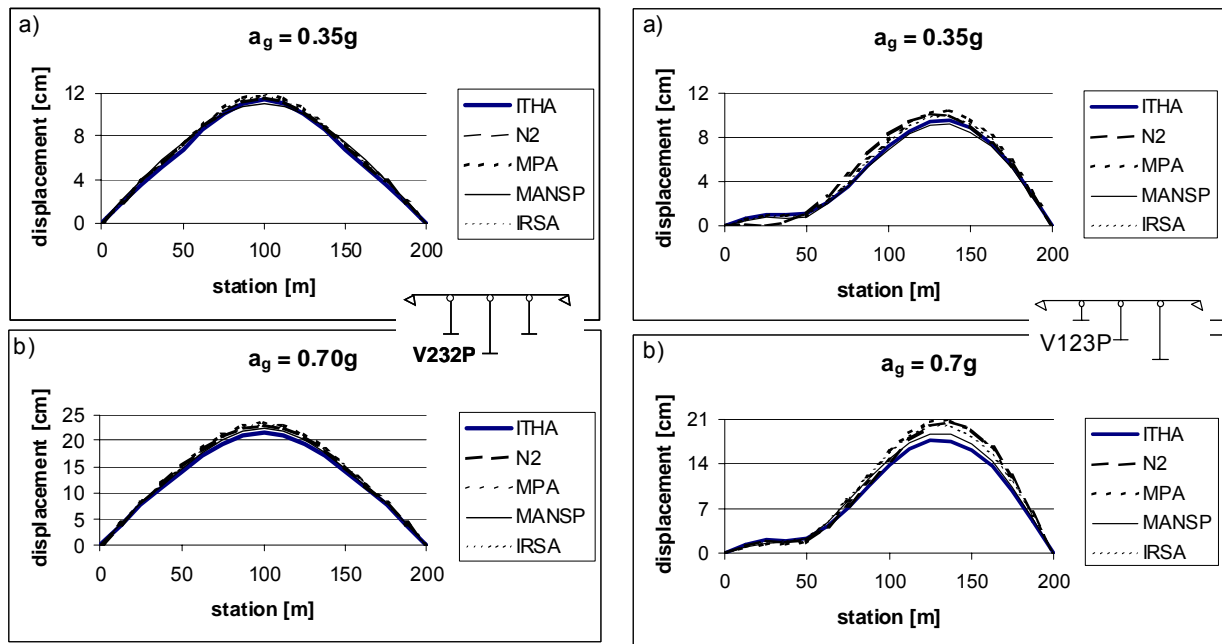
Fig. 10-14 shows the initial elastic mode shapes, periods and participating mass ratios of the four sample bridges. The latter may be grouped as ‘regular’, ‘slightly irregular’ and ‘highly irregular’ depending on their mode shapes in Fig. 10-14. Viaduct V232P is ‘regular’ since its response is governed by a single mode (first mode) whose shape is not expected to change significantly upon entering in the inelastic range. Viaduct V123P is ‘slightly irregular’ since its response is partially sensitive also to the second mode, though the variation of the stiffness properties is progressive. Viaducts V213P and V213R are ‘highly irregular’ because of the sharp contrast of stiffness between supports.

The seismic action is represented in terms of the Eurocode 8 Soil B Type I spectrum (EC8, 2004); two values of PGA, i.e. 0.35g and 0.70g, were employed. Inelastic time-history analyses were carried out by using three natural earthquake records modified to match the afore-mentioned spectrum. The results of inelastic time-history analyses (ITHAs) were used as benchmark to investigate the reliability of (inelastic) pushover analyses (POAs). The latter included both single-mode (non adaptive) and multi-mode (adaptive and non adaptive) formulations:

- Single-mode N2 method (Fajfar and Fischinger, 1988; Fajfar and Gasperic, 1996);
- Modal pushover analysis (Chopra and Goel, 2002);
- Modal adaptive nonlinear static procedure (Reinhorn, 1997);
- Incremental response spectrum analysis (Aydinoglu, 2005).

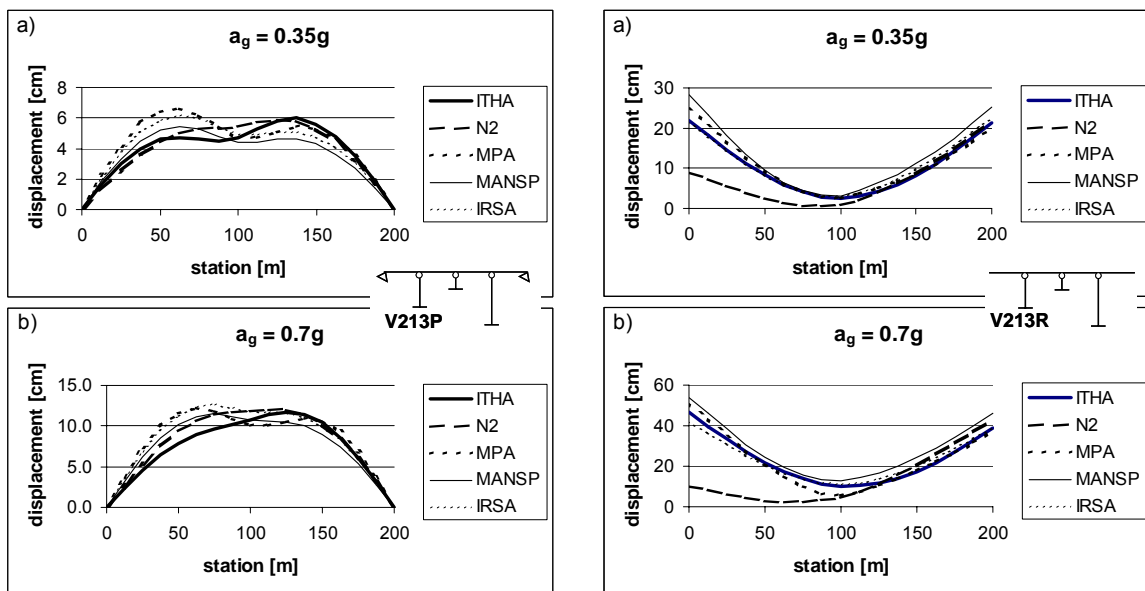
Horizontal displacements for the regular viaduct V232 are shown in Fig. 10-15. As expected, since the response is contributed by a single mode which does not vary appreciably with increasing inelastic behaviour, differences between the various methods are negligible. All

inelastic static methods provide estimates of inelastic deformations which match the results - average of the three records - computed through ITHAs.



Keys: ITHA = Inelastic time-history; N2= single-mode pushover; MPA = Multi-modal pushover; MANSP = Modal adaptive nonlinear static procedure; IRSA= Incremental response spectrum.

Fig. 10-15: Comparisons between inelastic static (pushover) and dynamic analyses: V232P (left) and V123P viaducts (right) (after Isakovic and Fischinger, 2005).



Keys: ITHA = Inelastic time-history; N2= single-mode pushover; MPA = Multi-modal pushover; MANSP = Modal adaptive nonlinear static procedure; IRSA= Incremental response spectrum.

Fig. 10-16: Comparisons between inelastic static (pushover) and dynamic analyses: V213P (left) and V213R viaducts (right) (after Isakovic and Fischinger, 2005).

Fig. 10-15 provides also the results computed for the (slightly irregular) viaduct V123P. There is still close agreement between the results of static and dynamic approaches, although, for this bridge two modes are contributing to the overall response (*see* also Fig. 10-14). It can be demonstrated that the scatter between the predictions of POAs and ITHA is of the same order of the variations between the response history computed for each of the three (spectrum-matching) records. The seismic behaviour of both highly irregular bridges (V213P and V213R) is displayed in Fig. 10-16. For both bridges, multi-mode (pushover) methods give rise to sufficiently reliable estimates of horizontal drifts. The single-mode N2 method was applied by employing force patterns compliant with the predominant mode of vibration, i.e. the 2nd mode for both V213P and V213R (*see* also Fig. 10-14). While the N2-method exhibits accuracy either similar or even superior to multi-mode approaches for viaduct V213P, it gives rise to large underestimations of lateral displacements for the sample bridge V213R.

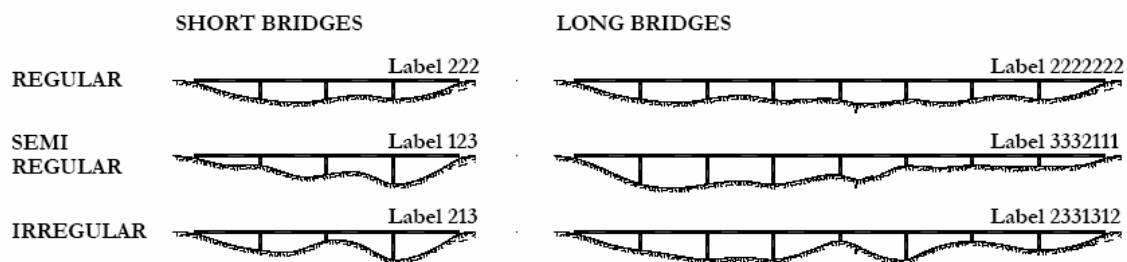


Fig. 10-17: Sample RC viaducts assessed by Casarotti (2005).

Further comparative analyses were carried out by Casarotti (2005) on a set of twelve RC bridges with span lengths multiple of 50m (Fig. 10-17). The sample structures include short (4-spans, total length of 200m) and long (8-spans, total length of 400m) bridges; these can be regular, semi-regular and irregular. The desk-to-abutment connection is assumed either continuous (clamped) or simply supported (pinned). The labels of sample viaducts (*see* Fig. 10-17) are similar to those in the work by Isakovic and Fischinger (2005). The sequence of numbers indicates the height of piers, from left to right, as multiple of the reference length of 7m. Thus, ‘222’ means, for example, that the viaduct employs three piers of 14m high. The semi-regular (123) and the irregular (213) short bridges (Fig. 10-17) analysed by Casarotti (2005) coincide with viaducts V123P and V213P (Fig. 10-13) in Isakovic and Fischinger (2005).

Methods of POAs in the work by Casarotti (2005) comprise:

- Single-mode non-adaptive method employing either first-mode or uniform force patterns;
- Multi-mode force-controlled adaptive pushover analysis (Antoniou and Pinho, 2004-a);
- Multi-mode displacement-controlled adaptive pushover analysis (Antoniou and Pinho, 2004-b);

The accuracy of the results computed through the above inelastic static methods is compared with the structural response (action and deformation) parameters evaluated by means of ITHAs. The latter are performed by using an ensemble of 14 historical earthquakes. The sample records are scaled to produce an average spectrum matching the uniform hazard spectrum for high seismicity zones in the USA, i.e. Los Angeles (California), with 10% probability of exceedence in 50 years. Comparative analyses of the bridge structural performance are carried out by means of the following deformation- and action-based response parameters:

- Global bridge index (BI);
- Normalized base shear (\bar{V}_b).

The above parameters quantify the deviation of the static from the “exact” dynamic

prediction of the lateral displacement and base shear of each pier, respectively.

The global bridge index (BI) is defined as given below:

$$BI = \hat{\Delta}_i \quad (10.29)$$

where $\hat{\Delta}_i$ is the median over the supports of the lateral displacement Δ_i , which is computed through the relationship:

$$\Delta_i = \frac{\Delta_{i,static}}{\hat{\Delta}_{i,dynamic}} \quad (10.30)$$

with $\Delta_{i,static}$ the displacement demand evaluated through POA and $\hat{\Delta}_{i,dynamic}$ the median over the supports of the lateral displacements estimated using ITHA. In eq. (10.29) and (10.30) the index i denotes the i -th support of the sample bridge assessed. The median values are computed with reference to the suite of 14 earthquake records.

The normalized base shear (\bar{V}_b) is computed as the ratio between the total base shear from POA and the median value from ITHA.

The values of BI and \bar{V}_b computed for the sample RC bridges are summarised in Table 10-9. Values of BI close to the unity indicate small differences between the predictions of inelastic displacements derived using either POAs or ITHAs. The dispersion of Δ_i is estimated through the coefficient of variation (δ).

	BRIDGE INDEX (BI)			DISPERSION (δ)			NORMALIZED BASE SHEAR (\bar{V}_b)		
	MEAN	MIN	MAX	MEAN	MIN	MAX	MEAN	MIN	MAX
FSPm	0.74	0.57	0.92	0.79	0.58	1.00	0.80	0.69	0.95
FSPu	0.87	0.75	1.03	0.24	0.17	0.34	1.03	0.92	1.18
FAP	0.88	0.78	1.01	0.22	0.13	0.34	0.99	0.89	1.10
DAP	0.87	0.78	0.99	0.19	0.14	0.27	1.03	0.95	1.13

Key: FSPm = Single-mode non-adaptive (1st mode force pattern); FSPu = Single-mode non-adaptive (uniform force pattern); FAP = force-adaptive pushover; DAP = displacement-adaptive pushover.

Table 10-9: Comparisons between inelastic analyses for the sample RC bridges assessed in Casarotti (2005).

The results in Table 10-9 demonstrate that all but the FSPm method of inelastic static analyses give rise to the same values of bridge index and normalized base shear. The latter exhibit mean values ranging between 0.87 and 1.03, which implies that the deviations of the static from the “exact” dynamic predictions of the lateral displacement and base shear of each pier are negligible. Therefore, single-mode non-adaptive (with uniform force-pattern) and multi-modal adaptive (either force- or displacement-based) approaches provide equivalent results.

The example applications discussed above show that the various formulations of inelastic static (pushover) analyses - especially with increasing irregularity of system layouts - provide results which are appreciably similar as well as of acceptable accuracy compared to those derived from ‘exact’ non-linear dynamic analysis. It can therefore be argued that non-linear static procedures, albeit lacking theoretical rigour, do constitute sufficiently accurate and reliable tools for the assessment of earthquake structural response of RC bridge structures.

10.5 Fragility assessment

10.5.1 Approaches for fragility assessment

Vulnerability curves introduced in Section 10.4 play a critical role in regional seismic risk and loss estimation as they give the probability of attaining a certain damage state when a structure is subjected to a specified demand. Such loss estimations are essential for the important purposes of disaster planning and formulating risk reduction policies.

Vulnerability functions exhibit considerable variability (*see* Fig. 10-11) depending on the approaches used in their derivation. The factors that influence the vulnerability functions are input ground motion sets, performance limit states, source of structural damage data, structural modelling method, analysis platform characteristics, analysis method, and consideration of uncertainty. Fig. 10-18 depicts the flow chart for the derivation of typical analytical fragility or vulnerability functions. Five aspects of the derivation process mainly affect vulnerability curves: structure, hazard definition, performance criteria, simulation method and vulnerability analysis. Each component can be divided into a number of sub-components. By definition, vulnerability analysis is probabilistic, as discussed in Section 10.5.2, since each of the constituent components is uncertain: uncertainties are present in the hazard (demand) as well as in structural supply (capacity). Some of the uncertainties are inherently random (referred to as aleatoric uncertainty) while others are consequences of lack of the knowledge (referred to as epistemic uncertainty). Sources of uncertainty that may affect the fundamental components of the fragility assessment are indicated along with proposals to treat them analytically. The scheme outlined in Fig. 10-18 is generic and can be employed for any type of structural system.

Based on the sources of data available, vulnerability curves may be sub-divide into four categories as summarised in Table 10-10. A class of curves is based on observational data from post-earthquake surveys, while others are based on analytical simulation.

CATEGORY		CHARACTERISTICS
EMPIRICAL	<i>Feature</i>	Based on post-earthquake survey Most realistic
	<i>Limitation</i>	Highly specific to a particular seismo-tectonic, geotechnical and built environment The observational data used tend to be scarce and highly clustered in the low-damage, low-ground motion severity range Include errors in building damage classification Damage due to multiple earthquake may be aggregated
JUDGMENTAL	<i>Feature</i>	Based on expert opinion The curves can be easily made to include all factors
	<i>Limitation</i>	The reliability of the curves depends on the individual experience of the experts consulted A consideration of local structural types, typical configurations, detailing and materials inherent in the expert vulnerability predictions
ANALYTICAL	<i>Feature</i>	Based on damage distributions simulated from the analyses Reduced bias and increased reliability of the vulnerability estimate for different structures
	<i>Limitation</i>	Substantial computational effort involved and limitations in modeling capabilities The choices of the analytical method, idealization, seismic hazard, and damage models influence the derived curves and have been seen to cause significant discrepancies in seismic risk assessment
HYBRID	<i>Feature</i>	Compensate for the scarcity of the observational data, subjectivity of judgmental data, and modeling deficiencies of analytical procedures Modification of analytical or judgment based relationships with observational data and experimental results
	<i>Limitation</i>	The consideration of multiple data sources is necessary for the correct determination of vulnerability curve reliability

Table 10-10: Categorization of vulnerability curve (adapted from Kwon and Elnashai, 2005).

Empirical vulnerability curves are more representative of reality than their analytical counterparts should, since they are based on the observed damage of actual structures subjected to real strong motion. They have, however, limitations in general application since the curves are derived for a specific seismic region and a sample that is not necessarily similar to that sought. On the other hand, analytical vulnerability curves can be derived for general purposes, but the choice of analytical model, simulation method, and required computational power pose challenges for the development of the required relationship. The aforementioned vulnerability approaches summarised in Table 10-10 are compared in terms of accuracy, time and computational effort and application in Table 10-11.

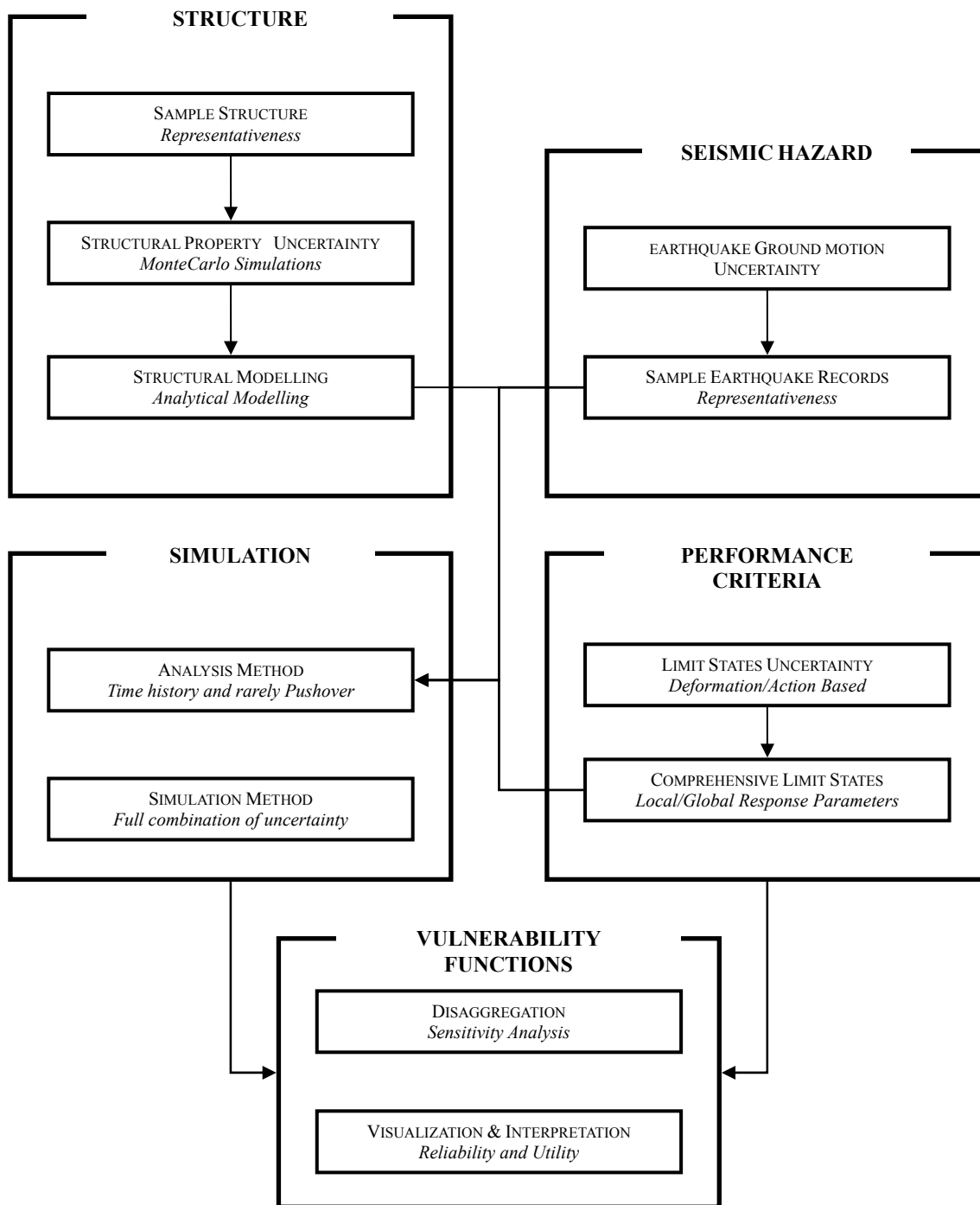


Fig. 10-18: Flow chart for the derivation of analytical vulnerability functions.

One of the main criteria for the selection of the method is the availability of the structural damage data; either the observation of post-earthquake losses or the analytical simulation (refer to Table 10-10). Observational data are realistic, but are often neither statistically viable nor homogeneous. The data from simulation, on the other hand, is constrained by computational power and reliability of analytical tools. With the expansion of computational power and the development of reliable analysis tools, the limitations in the analytical derivation of vulnerability curves are diminishing.

Vulnerability Assessment Methods	Hybrid functions		
	Empirical Functions	Judgmental Functions	Analytical Functions
Effort / Precision	Time and Computation Effort / Accuracy of the Assessment 		
Application	Structure Stock	Individual/Stock	Individual Structure

Table 10-11: Comparison between typical vulnerability assessment methods.

10.5.2 Background to probabilistic fragility assessment

The term fragility function or simply fragility was defined in Section 10.4 as the probability of exceeding a given state of structural performance (*probability of failure*, P_f), as a function of (conditional to) one parameter describing the intensity of the ground motion, typically peak (PGA) or spectral (S_a) accelerations. Since the states of interest (*see* limit states illustrated in Section 10.3) are mostly in the inelastic range of behaviour, evaluation of fragilities normally requires some form of simulation, i.e. performing a set of inelastic analyses to obtain the statistics of maximum response. In particular, one set of analyses may be performed for each ground motion intensity as also illustrated in the flow-chart in Fig. 10-18.

The probabilistic assessment of structural systems with a single mode of failure necessitates suitable probabilistic models to describe reliably the structural behaviour (*demand*, D) and cumulative distribution functions of the corresponding response (*capacity*, C). The fragility is thus computed through the expression:

$$P_f(i) = \int_0^{\infty} f_D(\alpha|i)F_C(\alpha)d\alpha \quad (10.31)$$

where i indicates the generic value of the selected intensity measure (I).

Eq. (10.31) shows that the probability of failure P_f depends on the intensity i ; however, it is significantly influenced by other characteristics of earthquake ground motion, notably frequency content and duration, and by mechanical properties of the assessed structure(s). The fragility thus depends both on structural system and earthquake scenario.

The unconditional probability of exceeding a given limit state is referred to as ‘risk’. Its evaluation requires the fragility and the probabilistic characterisation of the conditioning variable I . The latter is usually given as the complementary distribution of I for time interval of one year, i.e. the annual probability of exceeding any value i of I (*hazard function*, H). The hazard function H is thus given by:

$$H(i) = \Pr\{I \geq i | 1 \text{ year}\} \quad (10.32)$$

The risk can be estimated through the total probability theorem as follows:

$$P_f(1 \text{ year}) = \int_0^{\infty} P_f(i) \left| \frac{dH(i)}{di} \right| di \quad (10.33)$$

The above separation between ‘fragility’ and ‘hazard’ was introduced as a convenient means to sub-divide the task of risk evaluation between two disciplines, namely structural engineering and engineering seismology, traditionally, albeit wrongly, considered separate.

The definition of fragility extends directly to the case in which the state of the structural system depends on a combination of the states of its components. The system function, that translates a given set of component states into the system state, reflects the logical arrangement of the components of the system, be it a simple one such as series or parallel, or any more general combination. General system combinations can be re-arranged in one of two forms: the cut-set and the link-set formulations. With probabilistic models of both capacities and demands in each failure mode established, the fragility function, in a general cut-set formulation, can be expressed as:

$$P_f(i) = \Pr \left\{ \bigcap_{j=1}^{N_c} \bigcap_{k \in I_{C_j}} C_k \leq D_k(i) \right\} \quad (10.34)$$

where N_c is the number of cut-sets and I_{C_j} the set of indices of failure-modes belonging to the j -th cut-set. The above probability of failure can be evaluated by the methods of time-invariant system reliability.

10.5.3 Example applications

10.5.3.1 Example 1 – Innovative procedure for fragility assessment

Description of the bridge

An innovative procedure for fragility analysis proposed by Lupoi *et al.* (2004) is employed for the seismic assessment of a highway viaduct crossing a mountainous area of high seismicity in Southern Italy (Fig. 10-19). The bridge consists of eleven spans with length varying between 40m and 110 m. The structural system is a continuous beam over cantilever piers. Typical deck and piers cross-sections are shown in Fig. 10-19. The deck has a composite steel-concrete box section; the deck is haunched in the three longest spans and its height is constant over most spans. The RC piers have rectangular hollow-core cross-sections; on the creek sides polygonal-shaped piers are used for reasons linked to hydraulic issues. The bridge is designed for a value of PGA equal to 0.35g.

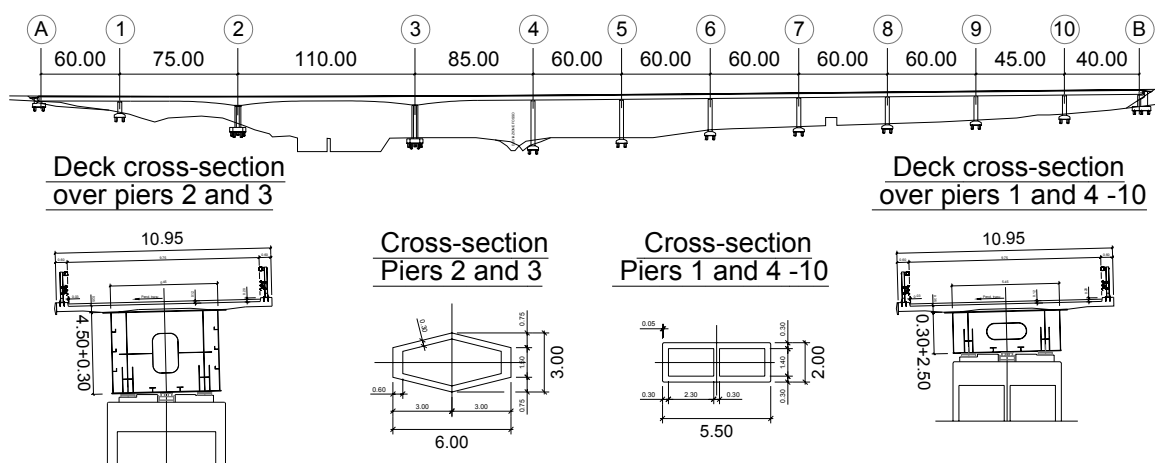


Fig. 10-19: The viaduct over the Lordo creek on state road SS106, Italy.

Limit states and system behaviour

Fragility analysis is carried out for the case of earthquake ground motion acting in the transverse of the viaduct. Both damage and ultimate limit states (LSs) are investigated.

The structural response is modelled through a series system, i.e. collapse of any pier gives rise to total interruption of traffic and implies global failure of the bridge. Series system idealisation is adopted also for the damage limit state. The structure of the bridge is capacity-designed and adequate seismic details were utilized in the construction. Brittle failure modes are prevented and it suffices to monitor merely flexural response. Damage and ultimate LSs are assumed correspondent respectively to the onset of yield (ϕ_y) and ultimate (ϕ_u) curvatures at any pier base. It is assumed that, for any level of axial load, $\phi_u = 5 \phi_y$.

Seismic input model

A vector random process model is employed to describe earthquake ground motion at bridge supports. This model is defined by a cross power spectral densities matrix, with off-diagonal terms accounting for loss of correlation between motions at distinct points caused by waves-scatter, finite propagation velocity and difference in surface geology (Lupoi *et al.*, 2005). A power spectral density function compatible with the Eurocode 8 spectrum (EC8, 2004) is selected for diagonal terms of the matrix; the latter terms influence the frequency content of earthquake ground motions.

Two spatial variability scenarios are studied: uniform or synchronous motion and non-uniform motion. For both scenarios twenty sets of ground motion time histories are generated for the ‘preliminary simulation phase’ discussed later. To derive fragility curves it is necessary to scale earthquake records to increasing seismic intensities; in this example application the scaling is carried out reference to the PGA at the left abutment.

Uncertainty in the system

Seven random variables are employed to characterise the uncertainty of the system (randomness) and its model (epistemic). Five variables describe the randomness of material

properties; these include: concrete strength f_c , concrete ultimate strain ϵ_{cu} , steel yield stress f_y , steel ultimate strain ϵ_{su} and hardening ratio b . The Kent-Park model is used for concrete, while steel reinforcement is modelled through bilinear stress-strain relationship. Two variables are utilized to quantify model errors. In particular, the parameter ϵ_{Lp} accounts for the relatively large dispersion associated with formulae used to estimate plastic hinge length L_p . The latter may influence significantly the evaluation of curvature demands in inelastic zones. In this study, L_p is assumed equal to 8% of the pier height (H), and the mean value is computed as:

$$L_p = 0.08H\epsilon_{Lp} \quad (10.35)$$

The random variable ϵ_ϕ is the error term of the curvature capacity model adopted. The basic random variables with their respective distribution type and parameters are reported in Table 10-12.

A linear response surface $C(\mathbf{x})$ is employed to model yield curvature capacity of RC members; it is a function of material variables and is computed through the following expression:

$$C(\mathbf{x}) = \ln[\phi_y(f_c, f_y, b)] \cdot \epsilon_\phi = \ln[a_0 + a_1f_c + a_2f_y + a_3b] \cdot \epsilon_\phi \quad (10.36)$$

Model parameters in eq. (10.36) are obtained by linear regression of the results of fibre-section analysis. The standard error from the regression is used as the standard deviation of the random variable ϵ_ϕ .

VARIABLE	TYPE	MEAN	CoV
f_c	Lognormal	43 MPa	0.2
ϵ_{cu}	Lognormal	0.006	0.25
f_y	Lognormal	513 MPa	0.1
ϵ_{su}	Lognormal	0.1	0.2
b	Lognormal	0.006	0.2
ϵ_{Lp}	Lognormal	1	0.2
ϵ_ϕ	Normal	1	0.025

Table 10-12. – Random variables used in the study of the viaduct in Fig. 10-19.

Preliminary simulation phase

The probabilistic characterisation of seismic demands is based on results of a preliminary numerical simulation phase. The computational effort associated with this simulation is by far the most important contributor to the overall cost of reliability analysis. A complete characterisation of the demands vector D , in terms of its joint density function $fD(d)$, would require a number of inelastic time-history analyses which are cumbersome even for moderately complex models. Some simplifications are hence introduced. In so doing, input and system uncertainties, which are two sources of uncertainty in x , are considered to be independent. Additionally, it is assumed that demands vary linearly with x , while the variability induced in the demands by the seismic action is evaluated for the mean value of x . These assumptions lead to a

drastic reduction of analyses to perform: N structural analyses, with different earthquake time-histories, are carried out for the ‘mean’ structure, i.e. $\mathbf{x} = \boldsymbol{\mu}_x$, and the second moments of seismic demands are:

$$\mu_{Di} = E[D_i(\boldsymbol{\mu}_x)] \cong \frac{1}{N} \sum_{k=1}^N D_{ik}(\boldsymbol{\mu}_x) \quad (10.37)$$

$$\sigma_{Di} = E[(D_i(\boldsymbol{\mu}_x) - \mu_{Di})^2] = \frac{1}{N-1} \sum_{k=1}^N (D_{ik}(\boldsymbol{\mu}_x) - \mu_{Di})^2 \quad (10.38)$$

$$Cov(D_i, D_j) = E[(D_i(\boldsymbol{\mu}_x) - \mu_{Di})(D_j(\boldsymbol{\mu}_x) - \mu_{Dj})] = \frac{1}{N-1} \sum_{k=1}^N (D_{ik}(\boldsymbol{\mu}_x) - \mu_{Di})(D_{jk}(\boldsymbol{\mu}_x) - \mu_{Dj}) \quad (10.39)$$

where $D_{ik}(\boldsymbol{\mu}_x)$ is the *maximum* of the i -th demand in the k -th run:

$$D_{ik}(\boldsymbol{\mu}_x) = \max_t [D_{ik}(\boldsymbol{\mu}_x, t)] \quad (10.40)$$

within the same analyses, *response-sensitivities*, i.e. first-order partial derivatives of the response with respect to \mathbf{x} , are evaluated in the mean, $\boldsymbol{\mu}_x$. This can be evaluated either numerically by a finite difference scheme, e.g. repeating the analysis for perturbed values of the parameters, or, more efficiently, by means of the direct differentiation method (Franchin, 2004). A response-sensitivity value is obtained for each analysis; the computed values are then averaged to obtain the sensitivity of the mean demand, i.e. unconditional on the earthquake record:

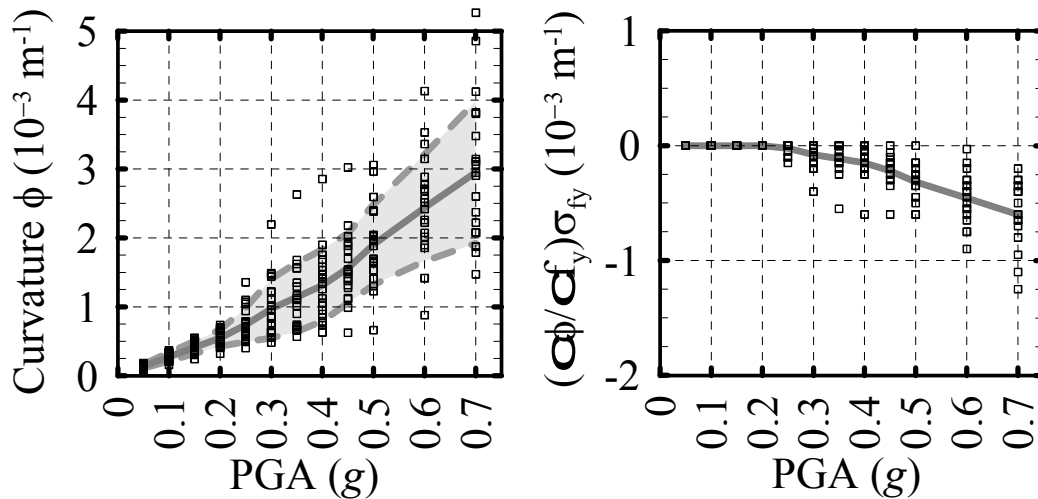
$$\left. \frac{\partial D_i}{\partial x_j} \right|_{\boldsymbol{\mu}_x} = \frac{\partial}{\partial x_j} \left(\frac{1}{N} \sum_{k=1}^N D_{ik}(\boldsymbol{\mu}_x) \right) = \frac{1}{N} \sum_{k=1}^N \frac{\partial D_{ik}(\boldsymbol{\mu}_x)}{\partial x_j} \quad (10.41)$$

Demand-derivatives are used to establish a linear expansion of demands around the mean of \mathbf{x} . The resulting approximate expression for the i -th demand is:

$$D_i(\mathbf{x}) = \mu_{Di}(\boldsymbol{\mu}_x) \varepsilon_{Di} + \nabla D_i \Big|_{\boldsymbol{\mu}_x} (\mathbf{x} - \boldsymbol{\mu}_x) \quad (10.42)$$

where ε_{Di} is a random variable with unit mean, standard deviation equal to the coefficient of variation δ_{Di} of $D_i(\boldsymbol{\mu}_x)$, and correlation coefficient ρ_{ij} with ε_{Dj} equal to that between $D_i(\boldsymbol{\mu}_x)$ and $D_j(\boldsymbol{\mu}_x)$.

The effectiveness of the method presented above may be investigated through the minimum number of analyses required to obtain sufficient stability in the evaluation of demand statistics. Variations of mean, coefficient of variation and pair-wise correlation coefficients of curvature demands with increasing number of analyses are thus monitored at all piers. Fig. 10-20 shows results for Pier 3 (see Fig. 10-19), under both input scenarios. It is noted that ten time-history analyses give rise to adequate stability for all parameters. Similar results are found for all piers of the sample viaduct. In Fig. 10-20, maximum curvatures versus seismic intensity are plotted for Pier 3; results of the sensitivity analysis carried out for the maximum curvature with respect to yield of steel (f_y) are also included in the same figure. As expected, the sensitivity of the curvature demand with respect to f_y is null before first yielding of the pier; subsequently, it becomes negative.



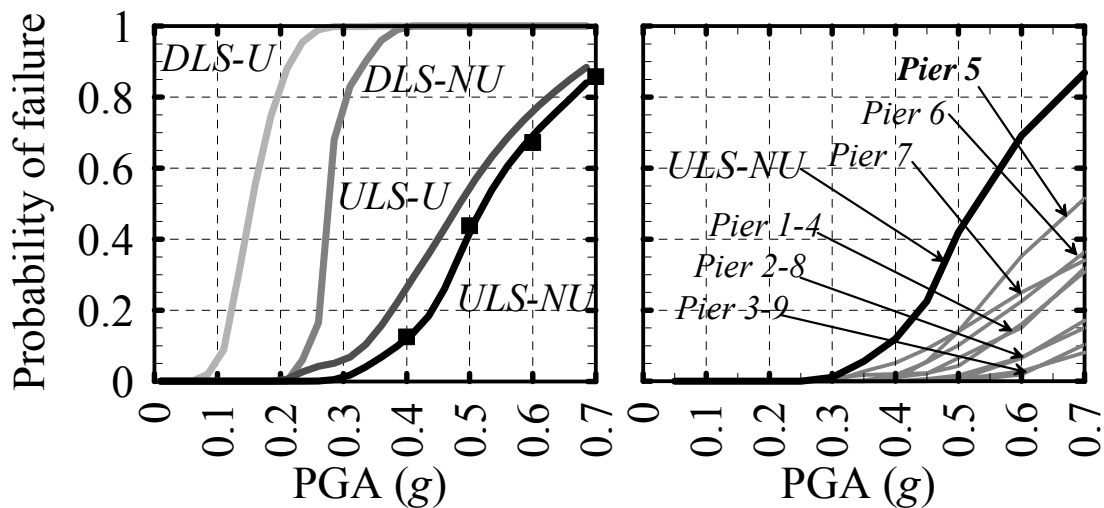
Key: Markers denote individual analyses results; Solid and dashed lines indicate mean and mean plus/minus one standard deviation, respectively.

Fig. 10-20: Variation of maximum curvature demand (left) and of its derivative with respect to f_y (right) at the base of Pier 3 (see Fig. 10-19).

Collecting stable statistics for seismic demand parameters and their sensitivities ends the preliminary simulation phase. Limited computational effort is required: about ten inelastic analyses are necessary for the derivation of fragility curves. To complete the fragility assessment, the problem of reliability dealing with time-invariant systems is solved by means of simple Monte Carlo simulation, sampling from the distribution of \mathbf{x} . The results of the fragility analysis are discussed in the next section.

Fragility analysis

Fragility curves for damage and ultimate LSs and disaggregation of fragility relative to the ultimate limit state are provided in Fig. 10-21. The disaggregation is used to estimate the contribution to the system fragility curves of all single piers. Comparisons between system and component fragilities show that the contribution to the total probability of failure is similar for all but Pier 5. Fig. 10-21 shows that fragility curves relative to the LS of damage are steeper than ULS counterparts; this result reflects the larger dispersion in the prediction of earthquake response of systems which exhibit high inelastic deformations. When the input motion is non-uniform, the failure probabilities are lower. However, this outcome can not be generalised since failure is governed by numerous parameters related to structural configuration and type and amount of loss of coherence (Lupoi *et al.*, 2005). The example application discussed in the previous paragraphs demonstrates that the probabilistic approach employed for the seismic assessment of bridges is efficient also for structures which do not possess a single predominant mode of vibration modes. The proposed methodology is found cost-effective also for cases with small correlations between the maxima of response quantities.



Key: Black markers on fragility curves are Monte Carlo comparison points; DLS and ULS indicate damage and limit states, respectively; U and NU correspond to uniform and non-uniform input motion.

Fig. 10-21: Fragility curves for two limit-states and two types of input motion (left) and disaggregation of fragility relative to ULS and non-synchronous input (right).

Finally, a limited validation of the method is carried out, with reference to non-uniform input motion scenario and ultimate LS. A large number of time-history analyses were performed by using random sampling of the variables x and of the ground motion from the vector random process described earlier (ordinary Monte Carlo simulation). The points computed through the Monte Carlo simulation fit almost exactly the counterparts of the fragility curves obtained by means of the proposed method. The associated cost, however, for the target confidence in the estimate (coefficient of variation equal to 0.05), is in the order of 3000 time-history analyses.

10.5.3.2 Simplified vulnerability assessment of viaducts with rectangular hollow section piers

i. Background

Viaducts having piers with rectangular hollow sections are prevailing highway bridge structures in Europe (Fig. 10-22). With notable exception of experiments done at ELSA, Ispra (Pinto, 1996), limited research has been done related to seismic vulnerability of such structures. Further analytical work is required to provide accurate modelling of inelastic cyclic behaviour of hollow piers, especially under shear. Effects induced by deck/pier interaction and shear deformations should be implemented in sound models to achieve reliable prediction of earthquake response of bridges with rectangular hollow section piers. Moreover, influence due to regularity/irregularity of structural configuration should be investigated.

In the study case presented in the following sections, the probabilistic seismic performance assessment method proposed by Cornell *et al.* (2002) is employed. The latter was originally derived for buildings but it can also be adopted to analyses bridge systems.



Fig. 10-22. – Typical European viaduct. (Figure available electronically on fib website; see production note on p. ii)

ii. Analysed structures

Two bridges with four 50 m spans were analyzed. Decks were pinned at the abutments. Concrete piers have constant rectangular hollow cross section and were designed according to the Eurocode standards (e.g. EC8, 2004). In order to address regularity issues with reference to the behaviour of bridges in the transverse direction, two sets of piers were considered in this study. The former set is representative of typical regular bridges, with fundamental mode shape similar to that of the deck alone; the second pier set represents an irregular bridge structure. The configuration of regular bridge is symmetrical, with the tallest pier in the middle: side piers are 14 m high, central pier is 21 m high; this system is referred to as B232. The other bridge, labelled as B213, is highly irregular: side piers are 14 and 21 m high, central pier is 7 m high.

iii. Modelling

OpenSees (Mazzoni *et al.*, 2003) computer code was used to model the sample bridges. The superstructure was assumed to respond elastically to all earthquake intensities. Abutments were modeled as infinitely rigid. Piers were pinned at the level of the superstructure and fixed to their footings. The piers were modelled using a nonlinear line element with distributed plasticity which employed force-based formulation. For steel fibres, Menegotto-Pinto (Filippou *et al.*, 1983) stress-strain relationship was used, to account for Bauschinger effect. Concrete was modeled using a standard envelope, taking into account compression softening and tension stiffening. Effect of confinement of the concrete core was also considered, according to the recommendations of Mander *et al.* (1986). To model the response of the shortest pier of B213 bridge, which is expected to respond in a predominantly shear mode during earthquake loading, shear force-deformation envelopes were determined for each section, using the modified compression-field theory (Vecchio and Collins, 1986). Hysteretic and shear strength degradation parameters were calibrated according to experimental results (Pinto, 1996). Numerical models of both bridges were verified by comparing analytical results to experimental data from large-scale PSD test (1:2.5) of the same type of bridges (Pinto, 1996).

iv. Mean probability of exceeding the limit state

In order to estimate mean probability of exceeding a limit state of described bridges a set of recorded ground motions, corresponding to good soil conditions according to Eurocode 8 (EC8, 2004), was first selected from the ESMD database (Ambraseys *et al.*, 2002). The elastic spectra of the 14 records are presented in Fig. 10-23. It can be seen, that the average spectra corresponds rather well to the elastic spectra suggested by Eurocode 8 (EC8, 2004). However, it is important to note the large scatter in spectral values.

Mean annual probability of exceeding a limit state was assessed through the method formulated by Cornell *et al.* (2002). The ground motion records were first normalized and then scaled, performing a nonlinear dynamic analysis at each step. Peak ground acceleration (PGA) was chosen as intensity measure. The hazard function defined for the region of Krško Nuclear Power Plant, Slovenia, was used (Fajfar *et al.*, 1994). The function and its approximation in the PGA interval of interest are shown in Fig. 10-23.

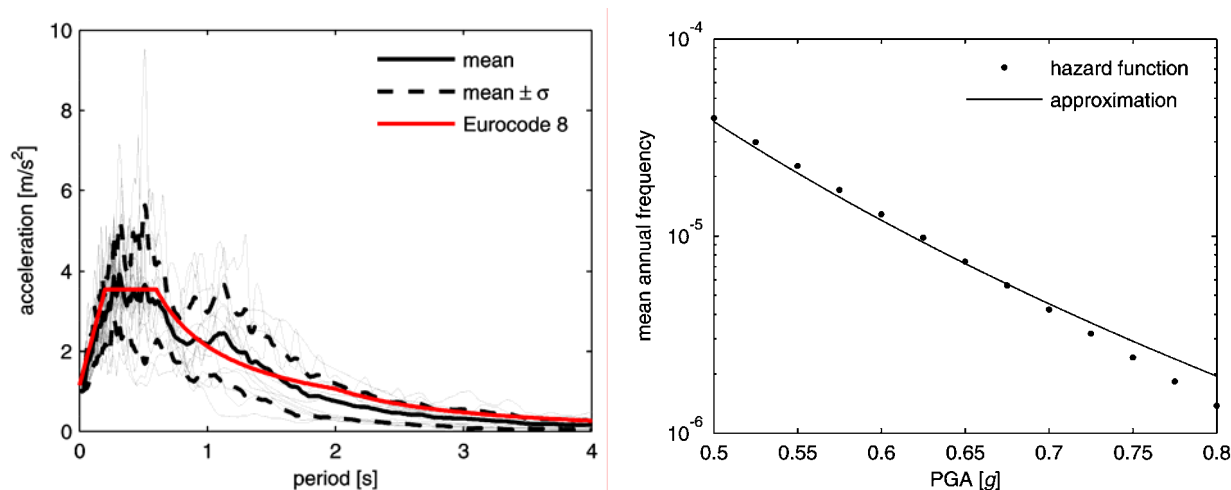


Fig. 10-23. – Elastic spectra (left) and hazard function (right).
 (Figure available electronically on **fib** website; see production note on p. ii)

Two sets of analyses were performed for each bridge: one with model taking into account nonlinear shear behaviour and one considering only linear shear behaviour. As expected, nonlinear shear properties do not change the response of the regular bridge, and therefore risk assessment for this bridge yields the same results, regardless of the model under consideration.

The capacity of the bridges was assumed to be deterministic at this stage ($\sigma_{CR} = 0$). Uncertainties related to demand calculation and bridge capacity were estimated according to recommendations implemented in FEMA350 (2000), i.e. $\sigma_{DU} = \sigma_{CU} = 0.25$. Uncertainties related to the hazard function were calculated as a mean value from the actual data ($\sigma_H = 1$). The capacity of the piers was determined on the basis of experimental data (Pinto, 1996). Several engineering damage parameters were considered during the study with an attempt to choose an optimal one, which could be used for all types of structures (regular and irregular ones). The parameters tested were global (such as pier top displacement) and local (section curvature, section shear deformation) ones. It is obvious, that shear structural elements are not compatible with damage parameters such as section curvature, and also that shear deformation is not the right parameter to monitor for columns, where flexure dominates the response. Therefore the obvious choice in both cases would be displacement at the top of the pier, which combines both the contribution of shear and flexure to the total response. On the other hand, for piers governed by flexural modes, the curvature of the section at the pier footing and displacement of the top of the pier were selected as damage indicators. Both were constrained to the value corresponding to 9.4 % deformation in longitudinal steel, which was the maximum steel strain, obtained during calibration to experimental results. The displacement was taken as an damage parameter in case of the short pier (0.129 m, according to the experimental data). An example of results, demonstrating the influence of inelastic shear behavior in short column on the mean probability of failure in 50 years is included below.

10.5.3.3 Fragility analysis of bridges with soil-structure interaction

i. Introduction

Response of structures under earthquake loading is highly sensitive to soil-foundation response characteristics. The effect of soil-structure interaction could be either detrimental or beneficial depending on the input motion and natural frequency of the system (Mylonakis and Gazetas, 2000). Consideration of site effects in seismic risk evaluation of structures primarily consists of two components; (i) propagation of the ground motion from bedrock to

soil-foundation system, and (ii) features of soil-structure interaction. Soil-structure interaction (SSI) may have one or more of the following effects:

- *Structural period elongation*: compared to the fixed foundation assumption, foundation flexibility elongates the system periods resulting in changes in the seismic force and displacement demand.
- *Energy dissipation*: the semi-infinite soil medium supporting a structure dissipates seismic energy by hysteretic soil behaviour and through wave radiation effects.
- *Inertial soil-structure interaction*: when the mass and stiffness of structures are significant compared to the supporting soil, inertial soil-structure interaction modifies the foundation input motion. Hence applying free-field motion on the base of the structure is inappropriate.
- *Permanent soil deformation*: Interaction between soil and foundations impose large demand on the soil that may lead to large permanent deformations and failure.

The example provided hereafter, using new coupled analysis approach (Elnashai and Kwon, 2005) utilizes a simplified SDOF system which accounts for soil-structure interaction (SSI). Several modelling issues are still controversial in fragility assessment of bridges including SSI effects. Therefore, the following case study is employed also to lay the ground for further research needs.

ii. Simplified SSI -models

The existence of a soil media under a structure decrease the lateral stiffness and increases damping of the part of the structure above ground (termed ‘super-structure’). These effects are caused by radiation of seismic waves and hysteretic energy dissipation of soil material. Several formulations have been provided in the literature to account for the above changes in the earthquake response of structures. In particular, simplified lumped mass models with springs and dashpots have been suggested by Newmark and Rosenblueth (1971), Gazetas (1991) and Wolf (1994). In such models, the soil is assumed elastic half-space medium and the foundation is massless. These lumped systems are easy to implement in common computer programs for structural analysis because they employ finite elements already available in the analysis package. The model proposed by Gazetas (1991) is utilized for the present analytical study due to its versatility and reliability. The configuration of simplified SDOF system utilized to simulate a sample bridge pier is displayed in Fig. 10-24. The latter is extracted from an actual bridge in which the given pier is supported by pile cap with 25 piles. In the model in Fig. 10-24 the SDOF rests on a footing having the sample dimension in plan of the pile cap, i.e. 4.57m by 4.57m. This rough approximation does not account for the response of the pile group. However, the above assumption is acceptable for the target of the present analytical study, i.e. estimation of the influence of SSI on vulnerability curve using simplified soil-structure systems.

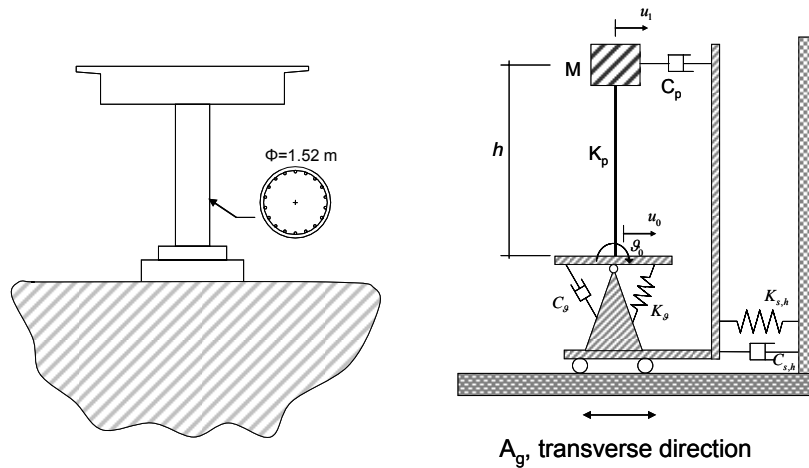


Fig. 10-24: Simplified SSI model.

iii. Dynamic soil properties for SSI study

Numerical soil-foundation models requires dynamic soil parameters such as shear modulus (G), density (ρ), Poisson's ratio (ν), hysteretic damping (β), and footing dimensions. Among these parameters, the shear modulus and the hysteretic damping are conventionally assumed to be a function of a shear strain of soil (Kramer, 1996). The lumped soil spring and dashpot coefficients of the adopted simplified model by Gazetas (1991) were derived assuming that the soil is linear elastic homogeneous half space, as mentioned earlier. However, soil is inelastic material in which shear modulus G decreases and hysteretic damping β increases as shear strains increase in the soil. Thus, using shear modulus and hysteretic damping at low strains to characterize the simplified SDOF model gives rise to very stiff soil with small damping. Therefore, effective strains for given surface ground motion intensities were computed. In so doing, three sample sites were selected, i.e. soft, stiff and very stiff soil, and equivalent linear site response analyses were performed to derive the relationship between effective strain, surface PGA, and soil type. Fig. 10-25 shows, for example, the proposed relationship for soft soil site with mean and ± 1 standard deviation bounds. Fig. 10-25 also compares the proposed relationship in terms of G/G_0 with the relationship implemented in FEMA 368 (2001).

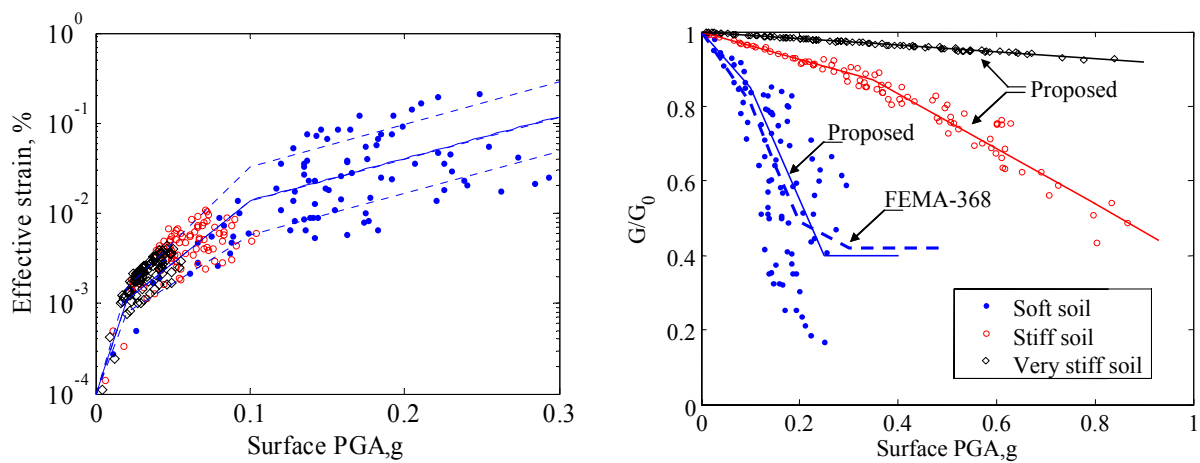


Fig. 10-25: Surface PGA and effective strain of the soft soil deposit (left) and surface PGA versus G/G_0 (right). (Figure available electronically on **fib** website; see production note on p. ii)

iv. Uncertainties in the soil-structure system

Shear modulus (G), density (ρ), and hysteretic damping parameters (β) are assumed as random variables for soil properties. Studies by Jones et al. (2002) have shown that the coefficient of variation (COV) of soil density ρ is equal to 0.09. Uncertainties relative to shear wave velocity have been suggested by Romero and Rix (2001) on the basis of in situ geotechnical investigations in three sites. The latter were characterized by values of shear wave velocity of about 250 m/sec, which is higher than that of the soft soil considered for this case study. The average of COV of shear wave velocity along the depth of the test holes for the three sites is employed; the adopted value of COV is 17.8%. Darendeli (2001) reported uncertainties in the shear modulus reduction, G/G_0 , and hysteretic damping. The latter are employed for the assessment of the SDOF system with SSI. On the other hand, the uncertainties relative to structural parameters are very small compared to those in soil material properties and ground motion. Hence, it is assumed that the geometry of footing is deterministic. The uncertainties of random variables employed in the performed analyses are summarised in Table 10-13.

VARIABLE	MEAN	COV	REFERENCE
Shear wave velocity	112 m/sec	0.178	Romero and Rix (2001)
Density	1600 kg/m ³	0.09	Jones <i>et al.</i> (2002)
G/G_0 and β	Refer Darendeli (2001)		Darendeli (2001)
PGA - strain	Fig. 10-25		Proposed in this study

Table 10-13: Uncertainties of random variables.

v. SSI effect on the fragility curve

The response of the SDOF system with and without SSI is compared in Fig. 10-26. The comparisons are provided in terms of mean lateral drifts and fragility curves. As expected, the system with SSI experiences higher lateral displacement than the fixed base structure because of the lengthening of the fundamental period of vibration. The results in Fig. 10-26 show that the effect of radiation damping is not large enough to compensate for the increase in spectral displacement demand from period elongation. In other reference applications, it was found that the effect of radiation damping overshadowed the period elongation effect, a rather unexpected situation. Vulnerability curves derived with and without soil-structure interaction are also displayed in Fig. 10-26. These curves are computed for drift limit state of 0.46%.

It is observed that the vulnerability curve for the system with SSI is less steep than that of fixed-base structure. The 'steepness' of probabilistic vulnerability curves is a measure of uncertainty: for deterministic systems, the vulnerability curve will be a vertical straight line (Wen *et al.*, 2004). Thus, results computed for the system with SSI prove that the response of the latter is affected by larger uncertainty than the fixed base model. In addition, Fig. 10-25 shows that the contribution of soil deformation on total drift of the pier may be significant. Finally, it is of paramount importance, when performing seismic assessment with SSI, to account for a complete set of limit states, e.g. those reflecting the effect of deck tilt on the functionality of the bridge structure for the case study discussed above.

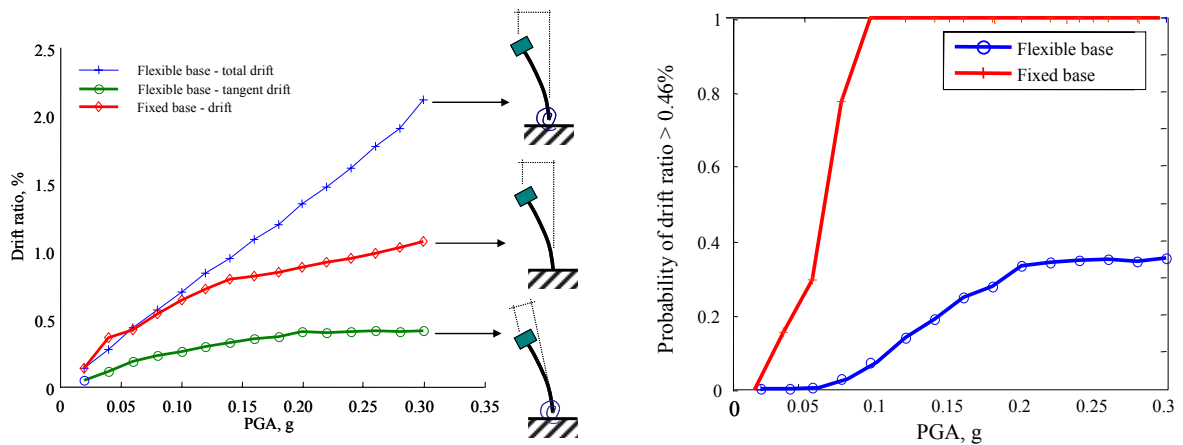


Fig. 10-26: Drifts of the SDOF system with and without SSI effects (left) and fragility curves of the SDOF (right).

References

- AASHTO (2004) LRFD Bridge Design Specifications (3rd edition), Washington D.C.
- Astaneh-Asl, A., Bertero, V.V., Bolt, B., Mahin, S.A., Moehle, J.P. and Seed, R.B. (1989). Preliminary report on the seismological and engineering aspects of the October 17, 1989 Santa Cruz (Loma Prieta) earthquake. Earthquake Engineering Research Centre, University of Berkeley, Report No.UCB/EERC-89/14, California, USA.
- Ambraseys, N., Smit, P., Sigbjornsson, R., Suhadolc, P. and Margaris, B. (2002). Internet-Site for European Strong-Motion Data. European Commission, Research-Directorate General, Environment and Climate Programme.
- Antoniou, S. and Pinho, R. (2004-a). Advantages and limitations of adaptive and non-adaptive force-based pushover procedures. *Journal of Earthquake Engineering*, 8(4), 497-522.
- Antoniou, S. and Pinho, R. (2004-b). Development and verification of a displacement-based adaptive pushover procedure. *Journal of Earthquake Engineering*, 8(5), 643-661.
- Applied Technology Council (1996). Seismic evaluation and retrofit of concrete buildings. (ATC-40), Redwood City, California, USA.
- Applied Technology Council (2005). Improvement of Nonlinear Static Seismic Analysis Procedures, FEMA Report No. 440, California, USA.
- ATC/MCEER Joint Venture (2004) Recommended LRFD Guidelines for the Seismic Design of Highway Bridges. Part I: Specifications, Part II: Commentary and Appendices. MCEER / ATC 49, ATC, Redwood City, California.
- Aydinoglu, M.N. (2003). An incremental response spectrum analysis procedure based on inelastic spectral deformation for multi-mode seismic performance evaluation. *Bulletin of Earthquake Engineering*, 1(1), 3-36.
- Aydinoglu, M.N. (2004). An improved pushover procedure for engineering practice: incremental response spectrum analysis (IRSA). Proceedings of the Workshop "Performance-based seismic design. Concepts and implementation" Krawinkler and Fajfar Eds., PEER Report No.2004/05, 345-356.
- Basöz, N. and Kiremidjian, A.S. (1998). Evaluation of bridge damage data from the Loma Prieta and Northridge, CA earthquakes. Multidisciplinary Center for Earthquake Engineering Research, Technical Report MCEER-98-0004, Buffalo, New York.
- Bozorgnia, Y. and Bertero, V.V. (2004). *Earthquake Engineering. From Engineering Seismology to Performance-Based Engineering*. CRC Press, Boca Raton, Florida, USA.
- Broderick, B.M., Elnashai, A.S., Ambraseys, N.N., Barr, J.M., Goodfellow, R.G. and Higazy, E.M. (1994). The Northridge (California) Earthquake of 17 January 1994: Observations,

- Strong Motion and Correlative Response Analysis. Engineering Seismology and Earthquake Engineering, Research Report No.ESEE 94/4, Imperial College, London.
- California Department of Transportation (1994). Initial and Supplementary Bridge Reports for the Northridge Earthquake. Caltrans, Division of Structures, Sacramento, CA.
- California Department of Transportation (2004) Seismic Design Criteria (version 1.3), California Caltrans, Division of Engineering Services, Sacramento, CA.
- Calvi, G.M. and Pinto, P.E. (1996). Experimental and Numerical Investigations on the Seismic Response of Bridges and Recommendations for Code Provisions. ECOEST-PREC8 Report No. 4, LNEC, Lisbon.
- Casarotti, C. (2005). Adaptive pushover-based methods for seismic assessment and design of bridge structures. PhD thesis, European School for Advanced Studies in Reduction of Seismic Risk (ROSE School), Pavia, Italy.
- Comite Euro-International Du Beton (1997). Seismic Design of Reinforced Concrete Structures for Controlled Inelastic Response - Recent advances in design concepts and codes, CEB Bulletin d'Information No. 236, Lausanne, Switzerland.
- Choi, E., DesRoches, R., Nielson, B. (2004) Seismic Fragility of Typical Bridges in Moderate Seismic Zones. *Engineering Structures*, 26 (2), 187-199.
- Chopra, A.K. and Goel, R.K. (2002). A modal pushover analysis procedure for estimating seismic demands for buildings. *Earthquake Engineering and Structural Dynamics*, 31 (3), 561-582.
- Cornell, C. A., Fatemeh, J., Hamburger, R.A., Foutch, D.A. (2002). Probabilistic Basis for 2000 SAC Federal Emergency Management Agency Steel Moment Frame Guidelines., *Journal of Structural Engineering*, ASCE, 128(4), 526-533.
- Darendeli, M.B. (2001). Development of a New Family of Normalized Modulus Reduction and Material Damping Curves. Ph.D. Dissertation, The University of Texas at Austin, Austin, TX.
- Earthquake Engineering Research Institute (1994). Northridge Earthquake January 17, 1994. Preliminary Reconnaissance Report. Hall, J.F. Editor, EERI, California.
- Elnashai, A.S. (2001). Advanced inelastic static (pushover) analysis for earthquake applications. *Structural Engineering and Mechanics*, 12(1), 51-69.
- Elnashai, A.S., Bommer, J.J. and Elghazouli, A.Y. (1989). The Loma Prieta (Santa Cruz, California) Earthquake of 17 October 1989. *Engineering Seismology and Earthquake Engineering*, Report No. ESEE/98-9, Imperial College, London.
- Elnashai, A.S., Bommer, J.J., Baron, I., Salama, A.I. and Lee, D. (1995). Selected Engineering Seismology and Structural Engineering Studies of the Hyogo-ken Nanbu (Kobe, Japan) Earthquake of 17 January 1995. *Engineering Seismology and Earthquake Engineering*, Report No. ESEE/95-2, Imperial College, London.
- Elnashai, A.S., Borzi, B. and Vlachos, S. (2004). Deformation-based vulnerability functions for RC bridges *Journal of Structural Engineering and Mechanics*, 17(2), 215-244.
- Elnashai, A.S. and Kwon, O-S. (2005). Multi-platform earthquake analysis of geotechnical-structural systems, Keynote Lecture no. 2, ASCE International Conference on Computing in Civil Engineering, Cancun, Mexico, 12-15 July.
- Erduran, E., Yakut, A. (2004) Drift Based Damage Functions for Reinforced Concrete Columns. *Computers and Structures*, 82 (2-3), 121-130.
- Eurocode 8 (2004). Design of structures for earthquake resistance - Part 2: Bridges. PrEN1998-2: 2003, Comité Europeen de Normalization, Brussels, Belgium.
- Fajfar, P. et al. (1994). Probabilistic assessment of seismic hazard at Krško Nuclear Power Plant. Revision 1 prepared for Nuclear Power Plant Krško.
- Fajfar, P. and Fischinger, M. (1988). N2 - A method for non-linear seismic analysis of regular buildings. *Proceedings of the 9th WCEE, Tokyo-Kyoto, Japan, Vol. V*, 111-116.
- Fajfar, P., and Gaspersic, P. (1996). The N2 method for seismic damage analysis of RC buildings. *Earthquake Engineering and Structural Dynamics*, 25(1), 31– 46.

- Federal Emergency Management Agency (2000). Recommended seismic design criteria for new steel moment frame buildings. Report No.FEMA-350, SAC Joint Venture, Federal Emergency Management Agency, Washington, D.C.
- Federal Emergency Management Agency (2000). NEHRP guidelines for the seismic rehabilitation of buildings. FEMA 356. Buildings Seismic Safety Council, Washington D.C., USA.
- Federal Emergency Management Agency (2001). NEHRP recommended provisions for seismic regulations for new buildings and other structures, Part 1 - Provisions. Report No. FEMA 368, Washington, D.C., USA.
- FHWA (1995) Seismic Retrofitting Manual for Highway Bridges (FHWA-RD-94-052), Buckle I.G and Friedland, I.M. (Editors), Turner-Fairbank Highway Research Center, McLean, Virginia.
- Fischinger, M. and Isakovic, T. (2003). Inelastic seismic analysis of reinforced concrete viaducts. *Structural Engineering International, IABSE*, Vol. 2, 111-118.
- Franchin, P. (2004). Reliability of uncertain inelastic structures under earthquake excitation, 2004, *Journal of Engineering Mechanics, ASCE*, 130(2), 180-191.
- Freeman, S.A., Nicoletti, J.P. and Tyrell, J.V. (1975). Evaluations of Existing Buildings for Seismic Risk – A Case Study of Puget Sound Naval Shipyard, Bremerton, Washington. Proceedings of the 1st U.S. National Conference on Earthquake Engineering, Oakland, California, 113-122.
- Gazetas, G. (1991). Foundation Vibrations. *Foundation Engineering Handbook*. Edited by Fang, H. Y., Van Nostrand Reinhold, New York, 553-593.
- Goel, R. and Chopra, A.K. (2004). Evaluation of modal and FEMA pushover analyses: SAC buildings, *Earthquake Spectra*, 20(1), 225-254.
- Goltz, J.D. (1994). The Northridge, California Earthquake of January 17, 1994: General Reconnaissance Report. National Centre for Earthquake Engineering Research, Report No. NCEER-94-0005, Buffalo.
- Gupta, B. and Kunnath, S. K. (2000). Adaptive spectra-based pushover procedure for seismic evaluation of structures. *Earthquake Spectra* , 16(2), 367-391.
- Kappos, A.J. (1997) Seismic damage indices for R/C buildings: Evaluation of concepts and procedures, *Progress in Structural Engineering and Materials*, 1(1), 78-87.
- Kappos, A.S., Paraskeva, T.S. and Sextos, A.G. (2004). Seismic assessment of a major bridge using modal pushover analysis and dynamic time-history analysis. Proceedings of the International Conference on Computational and Experimental Engineering and Sciences, Madeira, Portugal
- Kappos, A.S., Paraskeva, T.S. and Sextos, A.G. (2005). Modal pushover analysis as a means for the seismic assessment of bridge structures. Proceedings of the 4th European Workshop the Seismic Behaviour of Irregular and Complex Structures, Thessaloniki, Greece, Paper No.49.
- Karim, K.R., and Yamazaki, F. (2001) Effect of Earthquake Ground Motions on Fragility Curves of Highway Bridge Piers Based on Numerical Simulation, *Earthquake Engineering and Structural Dynamics*, Vol. 30, 839-1856.
- Kawashima, K. and Unjoh, S. (1997) The Damage of Highway Bridges in the 1995 Hyogo-ken Nanbu Earthquake and Its Impact to Japanese Seismic Design, *Journal of Earthquake Engineering*, 1(3), 505-541.
- Kramer, S.L. (1996). *Geotechnical earthquake engineering*. Prentice Hall, Upper Saddle River, NJ, USA.
- Kunnath, S.K. (2004). Identification of modal combinations for non-linear static analysis of building structures. *Computer-aided Civil and Infrastructure Engineering*, 19, 246-259.
- Kwon, O.S., Elnashai, A.S. (2005). The effect of material and ground motion uncertainty on the seismic vulnerability curves of RC structure. *Engineering Structures* (in press).

- Isakovic, T. and Fischinger, M. (2005). Higher modes in simplified inelastic seismic analysis of single-column bent viaducts. *Earthquake Engineering and Structural Dynamics*, (submitted).
- Jones, A., Kramer, S., Arduino, P. (2002). Estimation of uncertainty in geotechnical properties for performance-based earthquake engineering. Pacific Earthquake Engineering Research Center PEER Report No.2002/16, University of California at Berkeley, USA.
- Lehman, D.E. and Moehle, J.P. (2000) Performance-based seismic design of reinforced concrete bridge columns, Proceedings of the 12th World Conference on Earthquake Engineering, Auckland, New Zealand, Paper No. 2065, CD-ROM.
- Lehman, D.E., Moehle, J.P., Mahin, S., Calderone, A. and Henry, L. (2004) Experimental Evaluation of the Seismic Performance of Reinforced Concrete Bridge Columns. *Journal of Structural Engineering*, ASCE, 130(6), 869-879.
- Lupoi, G., Franchin, P., Lupoi, A. and Pinto, P.E. (2004). Seismic fragility analysis of structural systems. Proceedings of the 13th WCEE, Vancouver, Canada, Paper No.4008, CD-ROM.
- Lupoi A., Franchin P., Pinto P.E. and Monti G. (2005). Seismic design of bridges accounting for spatial variability of ground motion. *Earthquake Engineering and Structural Dynamics*, 34(4-5). 327-348.
- Mylonakis, G. and Gazetas, G. (2000). Seismic Soil-Structure Interaction: Beneficial or Detrimental? *Journal of Earthquake Engineering*, 4(3), 277-301.
- Mander, J. B., Priestley, M. J. N, and Park, R. (1986). Theoretical Stress-Strain Model for Confined Concrete. *Journal of Structural Engineering*, 114(8), 1804-1826.
- Mazzoni, S., McKenna, F., Scott, M. H., Fenves, G. L. and Jeremic, B. (2003). Open System for Earthquake Engineering Simulation (OpenSees) [Command Language Manual]. University of California, Berkeley, USA.
- National Information Service for Earthquake Engineering (2000) - Image Database. <http://www.nisee.org>
- Newmark, N. M., and Rosenblueth, E. (1971). *Fundamentals of Earthquake Engineering*. Prentice-Hall, Englewood Cliffs, NJ.
- Park, Y.-J. and Ang, A.H.-S. (1985) Mechanistic seismic damage model for reinforced concrete. *Journal of Structural Engineering*, ASCE, 111(4), 722-739.
- Pinto, A. V. (Ur.). (1996). Pseudodynamic and Shaking Table Tests on R. C. Bridges (Report No. 5). Ispra: The European Laboratory for Structural Assessment (ELSA).
- Priestley, M.J.N., Seible, F. and Calvi, G.M. (1996). *Seismic design and retrofit of bridges*. John Wiley, New York.
- Reinhorn, A. (1997). Inelastic analysis techniques in seismic evaluations. Proceedings of the International Workshop “Seismic design methodologies for next generation of code”, Krawinkler and Fajfar Editors, Bled Slovenia, Balkema, 277-287.
- Romero, S., Rix, G.J. (2001). Regional variation in near-surface shear wave velocity in the greater Memphis area. *Engineering Geology*, 62(1-3), 137-158.
- Saiidi, M. and Sozen, M. (1981). Simple Nonlinear Seismic Analysis of R/C Structures. *Journal of the Structural Division*, ASCE, 10(ST5), 937-952.
- Shibata, A. and Sozen, M.A. (1976). Substitute Structure Method for Seismic Design in Reinforced Concrete. *Journal of Structural Division*, ASCE, 102(ST1), 1-18.
- Shinozuka, M., Feng, M.Q., Lee, J., and Naganuma, T. (2000) Statistical Analysis of Fragility Curves. *Journal of Engineering Mechanics*, ASCE, 126 (12), 1224-1231.
- Une, H., Kawashima, K. and Shoji, G. (1999). Pushover analysis of a frame bridge. *Journal of Structural Engineering (JSCE)*, 45A, 947-956.
- Vecchio, F. J. and Collins, M. P. (1986). The Modified Compression-Field Theory for Reinforced Concrete Elements Subjected to Shear. *ACI Journal*, 83(2), 219-231.
- Wen, Y.K., Ellingwood, B.R. and Bracci, J. (2004). Vulnerability function framework for Consequence-Based Engineering. MAE Center Project DS-4 Report, Department of Civil and Environmental Engineering, University of Illinois, Urbana, IL, USA.

- Wolf, J.P. (1994). Foundation vibration analysis using simple physical models. Prentice-Hall, Englewood Cliffs, NJ, USA.
- Yamazaki, F., Hamada, H., Motoyama, H. and Yamauchi, H. (1999). Earthquake Damage Assessment of Expressway Bridges in Japan. Optimizing Post-Earthquake Lifeline System Reliability, ASCE Proceedings of the 5th U.S. Conference on Lifeline Earthquake Engineering, Seattle, Washington, 361-370.
- Zheng, Y., Usami, T. and Ge, H. (2003). Seismic response predictions of multi-span steel bridges through pushover analysis”, Earthquake Engineering and Structural Dynamics, 32 (8), 1259-1274.

11 Seismic retrofit

11.1 Introduction

Seismic retrofit of bridges which do not satisfy the current design requirements is increasingly becoming important worldwide. A large amount of scientific knowledge on the seismic performance of structures has been accumulated in the last three decades. Seismic requirements have been upgraded and a large number of bridges which fail to meet the current level of seismic requirements need to be retrofitted.

Seismic retrofit of existing bridges is generally more difficult than design of new bridges because of the various restrictions in the seismic retrofit. Main structural components cannot be changed or replaced in seismic retrofit, which narrows possible options of design and construction. Because bridges are often required to be retrofitted in a short period without suspension of traffic, this imposes difficult restrictions on design criteria and retrofit methods. It should be noted that bridges can be retrofitted only when it is technically, economically and socially feasible. The bridges which fail to satisfy these requirements have to be replaced with new bridges.

Seismic performance levels and goals have to be clearly determined in seismic retrofit. It is always an argument at which level a bridge should be retrofitted. Satisfying the current high seismic performance requirements is generally difficult for bridges which were designed and built in the early days. Even if the retrofit is feasible, it may be virtually equivalent to reconstruction of substructures in such bridges. In the determination of seismic performance levels and goals, it should be noted that the cost of construction of an access road, retaining wall, dry-up of foundations and treatment of soils or water for preventing pollution is more or less the same with or even higher than the cost of the repair itself. It should be also noted that criticism from the public will be very strong if a retrofitted bridge suffers extensive damage in a future earthquake.

An important aspect of seismic retrofit is that difficult restrictions and requirements in retrofit design sometimes validate the use of new materials and construction methods. Consequently, seismic retrofit is a good opportunity and a challenge for engineers and researchers to use new and high performance materials and to develop new construction methods.

Seismic retrofit follows the standard seismic design and construction procedures for a new bridge. The only difference with design of a new bridge is that actual strength and capacity instead of nominal values should be used in retrofit design. Options of seismic retrofit depend on materials and construction methods available.

This chapter introduces retrofitting of bridges with an emphasis on the various examples of seismic retrofit.

11.2 Retrofit of columns and piers

11.2.1 Introduction

Reinforced concrete columns which were designed in accordance with the practice which did not take account of the importance of plastic deformation and ductility capacity are commonly deficient in flexural ductility, shear strength and flexural strength under strong seismic excitation. Lap splices in critical regions, premature termination of longitudinal

reinforcement and lack of lateral confinement are the common practices which affects the deficiency.

A number of column retrofit techniques have been developed and clarified based on loading tests. Column retrofit techniques include steel jacketing, composite materials jacketing involving fiberglass, carbon fiber reinforced plastics, aramid fiber reinforced plastics and other fibers, and jacketing with reinforced concrete and pre-cast concrete. Of these, the most common retrofit technique implemented to date has been steel jacketing and reinforced concrete jacketing, with lesser amount of retrofit involving pre-cast concrete segment jackets and composite materials jackets. Retrofit, with emphasis on the four approaches is introduced as follows.

11.2.2 Steel jacketing

11.2.2.1 Steel jacket for circular columns

Providing a jacket around an existing column which has insufficient ductility and strength capacity is effective to prevent premature failure. The jacket is fabricated such that its radius is 12.5 to 25 mm larger than the column radius. After being positioned over the areas to be retrofitted, the jacket is site-welded up the vertical seams to provide a continuous tube. With a small annular gap around the column, the gap is grouted with epoxy resin or a pure cement grout.

The jacket resists not only tension and compression but also shear of the column. Lateral confinement to the core concrete can also be provided by the jacket. Because a jacket cannot sufficiently provide lateral confinement to a rectangular column if special details are not included, steel jacketing is more appropriate to circular columns than rectangular columns. However restriction exists for hollow circular columns in which confinement from inside cannot be well provided. Furthermore, because columns with much larger radius are used in bridges than in buildings, effectiveness of the steel jacket for confining columns with large radius (over 4 m) still needs to be clarified.

Smooth setting of a steel jacket and availability of structural steel plates restrict the minimum thickness of the jacket. Because steel plate with thickness in the range of 6-12 mm is generally used for the jacket, the amount of steel of the jacket is very large compared to the existing longitudinal and tie bars.

A steel jacket enhances the shear and flexural strength and the ductility capacity of the column. Generally the enhancement of shear and flexural strength of the column increases the moment and shear demand of the foundation. Because redundancy of the moment and shear capacity of a foundation designed in the early days is limited, and because retrofit of a foundation is much costly than the retrofit of a column, the increase of the moment and shear demand of the foundation is not most likely preferable.

Consequently, there are essentially two practices in the steel jacketing. The first practice is to restrict the amount of increase of moment and shear demand of the foundation as small as possible. For this purpose, it is recommended to provide a space between the jacket and the footing or cap beam to avoid excessive flexural and shear strength enhancement of the plastic hinge. The gap depends on the radius of the column, but a 50-100 mm gap is generally recommended so that stable plastic hinge can be formed at the plastic hinge.

The other practice is to allow a certain amount of increase of moment and shear demand of the foundation. If the foundation has some redundancy on the moment and shear capacity, it is effective in restricting excessive plastic displacement of the column. In particular, it is appropriate to avoid excessive residual displacement of the column.

The jacket is effective in passive confinement. The level of lateral confinement induced in the concrete by flexible restraint as the concrete attempts to expand laterally in the compression zone depends on the hoop strength and stiffness of the steel jacket. A similar action occurs in resisting the lateral column dilation associated with development of diagonal shear cracks. In both the confinement of flexural hinges or potential shear failures, the steel jacket can be considered equivalent to continuous hoop reinforcement.

Fig. 11-1 shows lateral force-displacement hysteresses of a retrofitted circular column [Priestley, Seible and Calvi (1996)]. Flexural response of the columns is typically limited by the effective ultimate tension strain of the longitudinal reinforcement. This may be taken as $0.75 \varepsilon_{su}$, where ε_{su} is the strain at maximum stress.

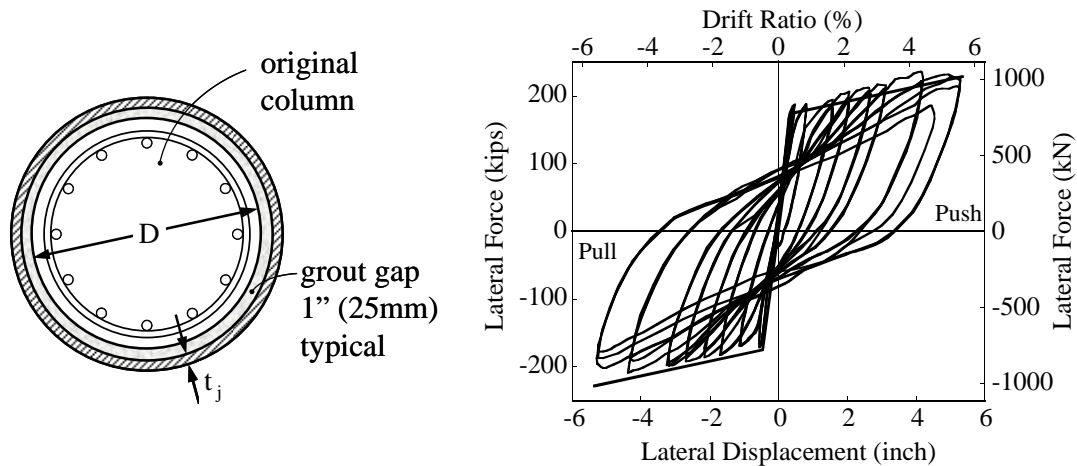


Fig. 11-1: Lateral force-displacement response of columns retrofitted with steel jackets for enhanced ductility: (a) circular column with circular jacket, (b) Lateral force vs. lateral displacement [Priestley, Seible and Calvi (1996)]

Steel jacketing has been widely used in California for lap splice retrofit as shown in Fig. 11-2 as the major retrofit technique for bridge columns, with several thousands column thus retrofitted. Extensive experimental studies have been conducted to develop steel jacketing technique [Chai et al. (1990)]. During the 1994 Northridge earthquake, some 50 bridges with steel jacketed columns were subjected to peak ground acceleration of 0.3g or higher. None of these bridges suffered damage to columns requiring subsequent remedial work.

Steel jacketing has been also used in Japan for retrofit of premature shear failure which resulted from termination of longitudinal reinforcement having inadequate development length. After this problem was first recognized in the 1982 Urakawa-oki earthquake, extensive studies were initiated. In particular, a series of experiment in 1987 [Kawashima (1990)] led to the retrofit of nearly 50 columns since 1989 [Akimoto et al. (1990)]. Steel jackets with 9 or 12 mm thick plates were used as shown in Figs. 11-3 and 11-4 depending on the column radius. Some columns which were retrofitted in 1989 (Fig. 11-4) were subjected to ground accelerations with nearly 0.8g PGA during the 1995 Kobe earthquake. None of the columns retrofitted suffered damage but the columns which were not retrofitted and were next to the retrofitted columns suffered extensive damage. Since the 1995 Kobe earthquake, over 40,000 columns and piers were retrofitted in roads and railways in Japan although the number of circular columns is much smaller than rectangular columns.



(a)



(b)

Fig. 11.2: Steel jacket retrofit of columns: (a) Los Angeles, and (b) San Francisco
(Figure available electronically on **fib** website; see production note on p. ii)



Fig. 11-3: Steel jacket retrofit at Metropolitan Expressway



Fig. 11-4: Steel jacket retrofit at Hanshin Expressway in 1989, which was effective during the 1995 Kobe earthquake

(Figures available electronically on **fib** website; see production note on p. ii)

11.2.2.2 Steel jacket for rectangular columns

A rectangular steel jacket is effective for enhancing the shear and moment capacity of a rectangular column, but it cannot provide sufficient lateral confinement in critical region as the size of the column increases.

Extensive studies have been conducted for retrofit of rectangular columns. For example, Figs. 11-5 and 11-6 show the effect of elliptical jacket, built-up steel channels, and stiffened rectangular jacket on lap splices in critical regions [Chai et al. (1990)]. With an elliptical jacket, the column showed subsequent improved behavior compared to the as-built-column. Bond failure at the lap-splice of the longitudinal reinforcement resulted in the final failure. The elliptical jacket restrained the spalling of covering concrete, and therefore allowed more gradual deterioration of strength. The bolted system of retrofit using built-up steel channels shows stable response up to 6 times yield displacement, after which bond failure at the lap-splice was again the cause for strength deterioration. Stiffened rectangular jacket indicated an earlier and more rapid deterioration of strength.

Based on the studies, rectangular steel jackets on rectangular columns are not generally recommended although they can be expected to be fully effective for shear strength enhancement. An elliptical jacket is recommended to a rectangular column.

On the other hand, because rectangular columns are mostly used and because enlarging the size of the columns using elliptical jackets is not generally allowed, an extensive study has been conducted in Japan for retrofit of rectangular columns. Based on various attempts, a rectangular jacket which was confined by a stiffened lateral beam at the bottom as shown in Fig. 11-7 was proposed. Stiffness of the lateral beam must satisfy a requirement depending on a ratio of the wider and shorter widths of the section. Generally H-shape beams are used for the lateral beams. Either 9 mm or 12 mm thick steel plates are used for rectangular jacket. Non-Shrinkage mortar or epoxy resin is grouted between the jacket and the column. Generally a 50-100 mm gap is provided between the jacket and the footing for ductility retrofit.

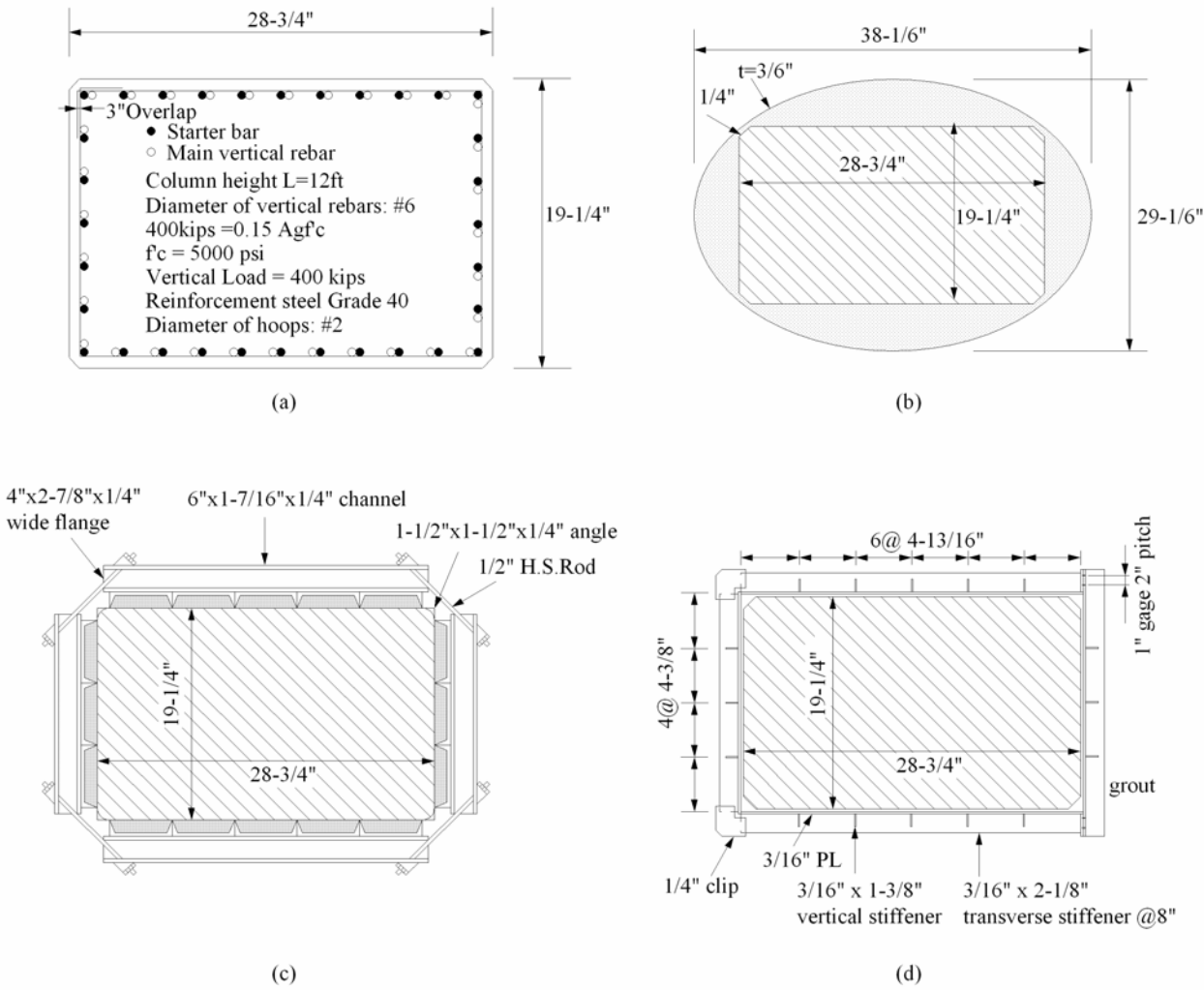


Fig. 11-5: Retrofit for rectangular columns; (a) Column 1 - 'As-built' (b) Column 2 - Elliptical retrofit (c) Column 3 - 'Built-up' steel channels (d) Column 4 - Stiffened rectangular jacket [Reproduced from Chai et al. (1999)]

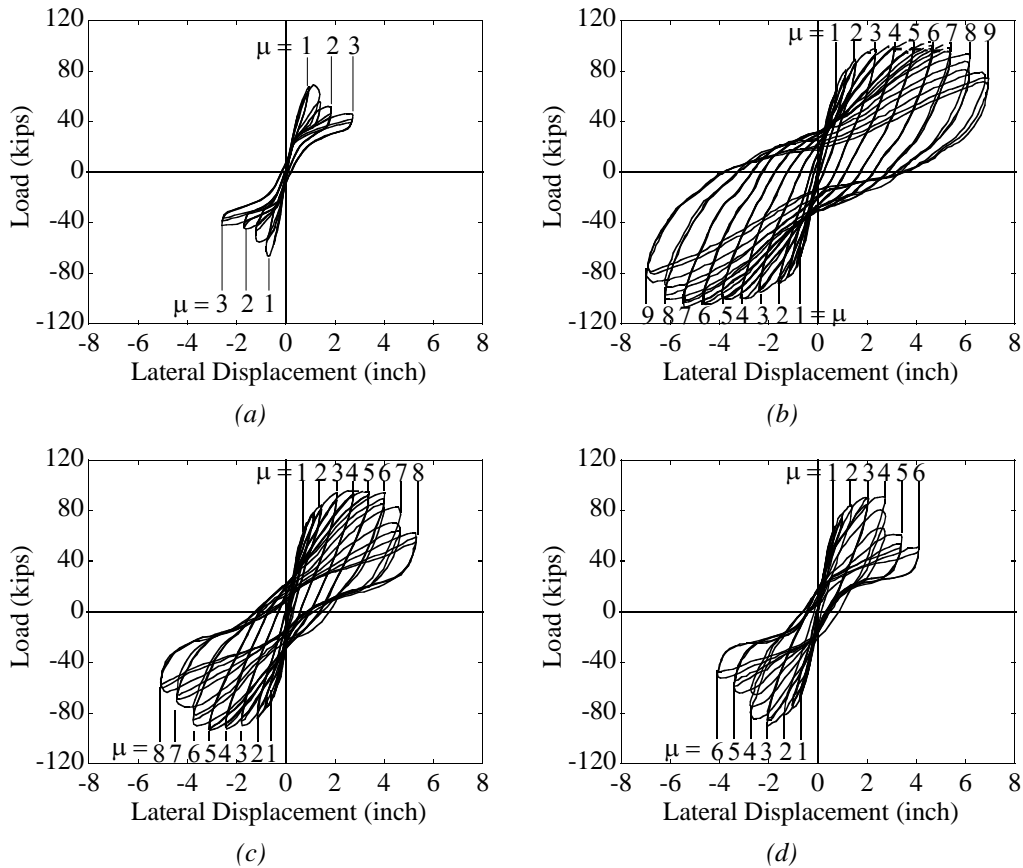


Fig. 11-6: Hysteretic response of rectangular flexural columns; (a) Column 1 - 'As-built' (b) Column 2 - Elliptical retrofit (c) Column 3 - 'Built-up' steel channels (d) Column 4 - Stiffened rectangular jacket [Reproduced from Chai et al. (1999)]

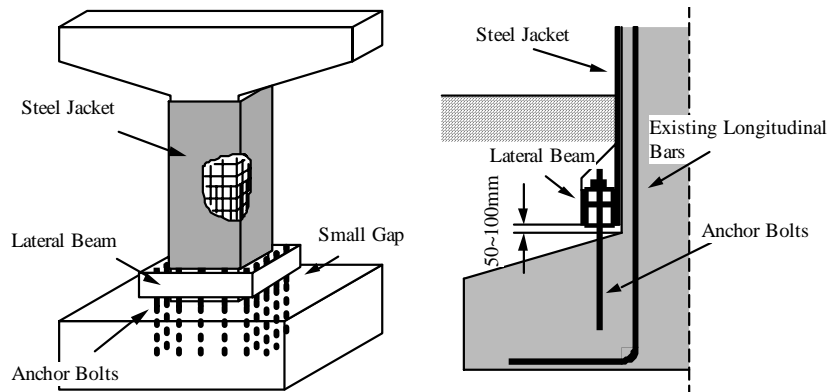


Fig. 11-7: Rectangular steel jacket with controlled enhancement of flexural capacity

Because enhancement of the flexural capacity of a column is in favor of mitigating the residual displacement after an earthquake, the flexural capacity of the column can be enhanced under a level that does not result in excessive damage to the foundation. For this purpose, the lateral beam welded to the jacket is constrained to the footing by anchor bolts. The level of constraint depends on the redundancy of the moment and shear demand of the foundation. Consequently, radius and number of the anchor bolts are decided depending on the redundancy of the foundation. Because this retrofit allows a certain enhancement of flexural capacity of a column, it is called steel jacket with controlled enhancement of flexural capacity.

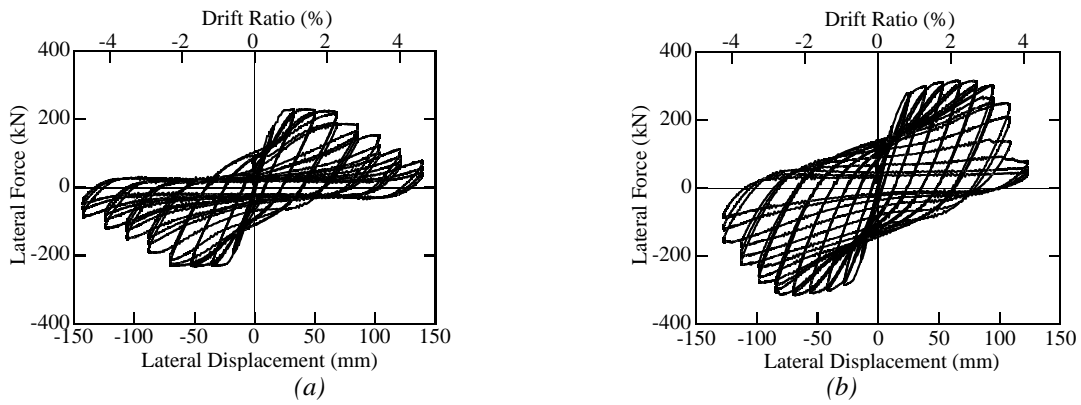


Fig. 11-8: Effect of steel jacket with controlled enhancement of flexural capacity for rectangular piers : (a) As-Built, (b) Retrofitted [Reproduced from Unjoh et al. (1997)]



Fig. 11-9: Test models (9m tall and 2.5m x 2.5m section) for steel jacketing with controlled enhancement of flexural capacity (Figure available electronically on **fib** website; see production note on p. ii)

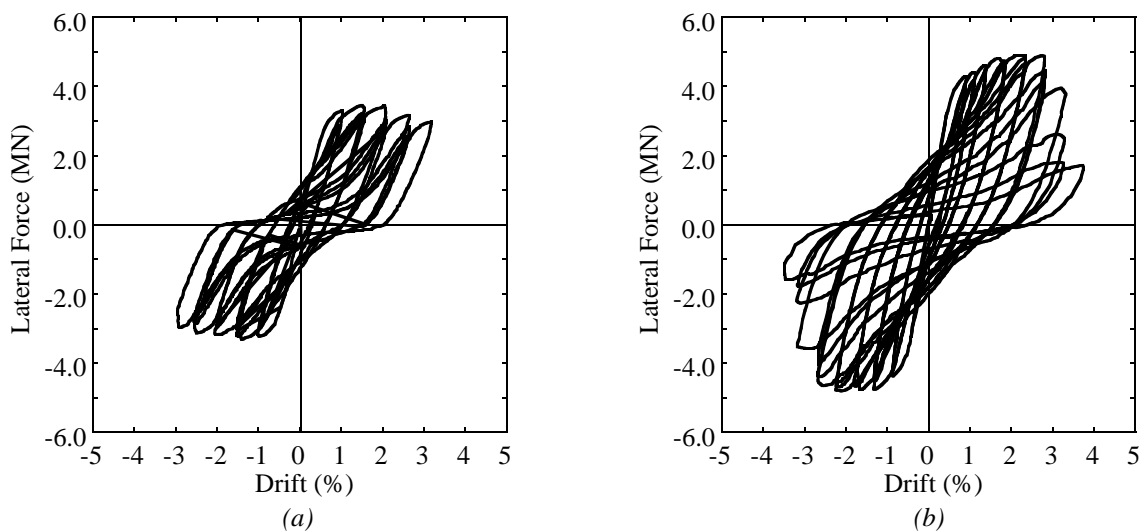


Fig. 11-10: Effect of steel jacket with controlled enhancement of flexural capacity for full-scale square column: (a) As-built, and (b) Retrofitted [Reproduced from Unjoh et al. (1997)]

Fig. 11-8 shows a verification test on the steel jacket with controlled enhancement of flexural capacity using a 3.01 m high rectangular column with a section of 600x600 mm [Unjoh et al. (1997)]. Flexural capacity and displacement ductility capacity of the as-built column were enhanced by a factor of 1.39 and 1.4, respectively, by the retrofit. A verification test was also conducted to a full scale square column (9 m tall and 2.5 m wide) as shown in Fig. 11-9. Fig. 11-10 shows the effectiveness of the steel jacketing with controlled enhancement of flexural capacity.

Fig. 11-11 shows an example of retrofit by steel jacket with controlled enhancement of flexural capacity for a 7.5 m tall column. The column had premature termination of longitudinal bars at 4.7 m from the bottom. Consequently premature shear failure was anticipated. Furthermore because the flexural capacity was insufficient, an excessive residual displacement was anticipated. Nine mm thick steel plates and H-shape beams with a section of 300x300x10 mm were used for the jacket and the lateral beam, respectively. Thirty two 35 mm radius anchor bolts were used to enhance the flexural capacity [Japan Road Association (1997)].

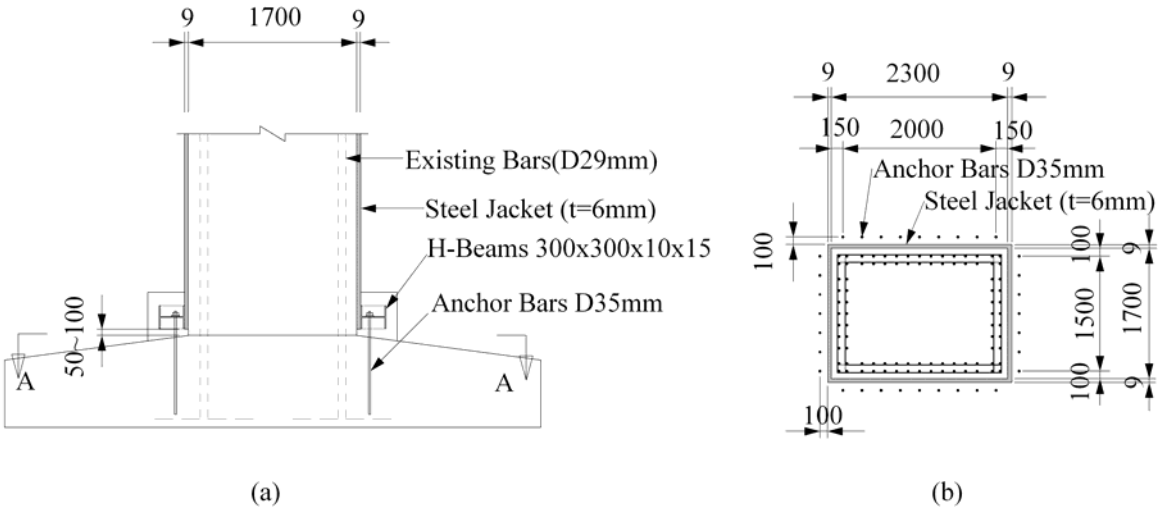


Fig. 11-11: Retrofitted section and anchor bolts



Fig. 11-12: Steel jacket retrofit for frame piers, Metropolitan Expressway, Japan
(Figure available electronically on fib website; see production note on p. ii)

Fig. 11-12 shows another example of rectangular jackets on rectangular columns. Steel jackets were temporarily attached to columns in position by bolts, and then were welded.

Steel jacket is generally assembled by welding at site. However not only the quality of the site-welding depends on workmanship and weathering condition but also welding takes time. Therefore an engagement joint as shown in Fig. 11-13 was developed to eliminate site-welding. The engagement joints were effectively used to retrofit railway viaducts as shown in Fig. 11-14.

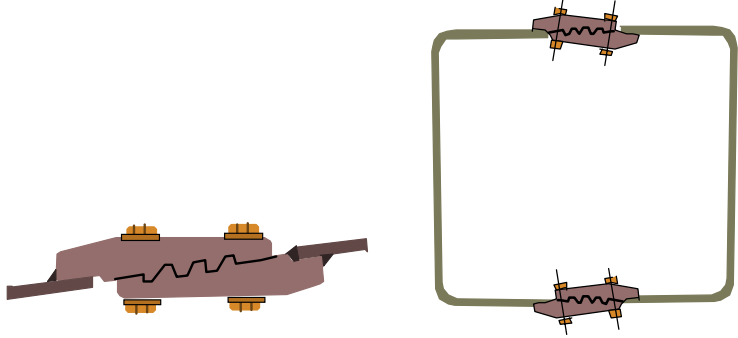


Fig. 11-13: Engagement joint (Courtesy of JR Research Institute)



Fig. 11-14: Effective use of engagement joint for retrofit at a railway viaduct (JR Research Institute) (Figure available electronically on fib website; see production note on p. ii)

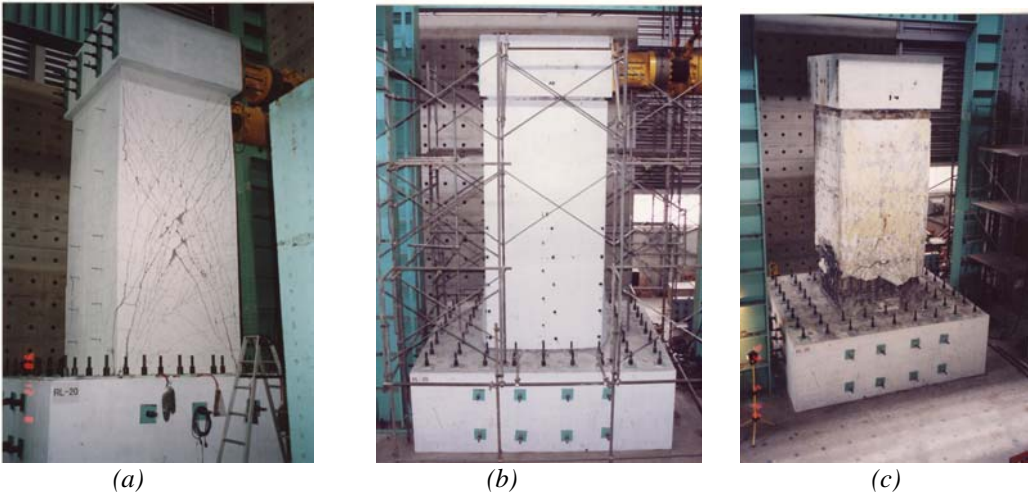


Fig. 11-15: Steel jacket repair and retrofit for shear; (a) shear failure after loaded, (b) repaired by steel jacketing, and (c) flexural failure of retrofitted column (after steel jacket was removed) [Iwata et al. (2001)] (Figure available electronically on fib website; see production note on p. ii)

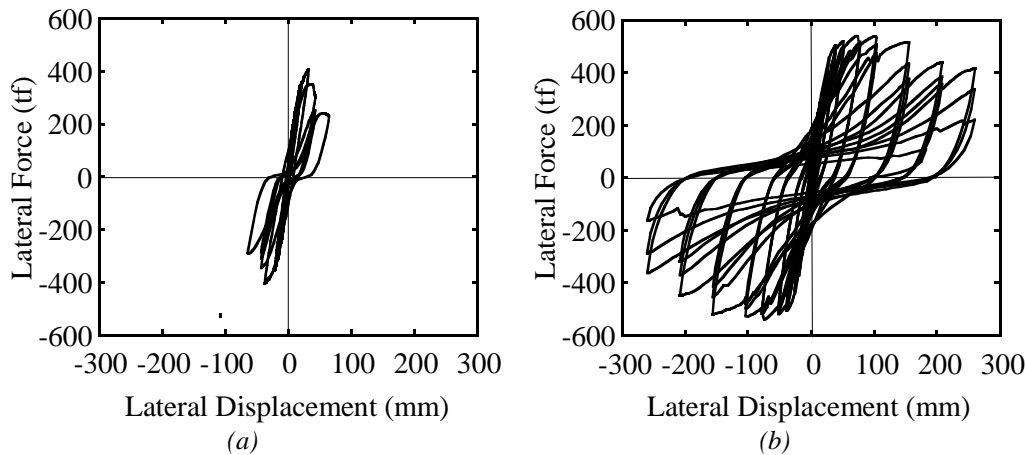


Fig. 11-16: Effect of steel jacket for shear enhancement: (a) as-built, and (b) steel jacketing [Iwata et al. (2001)]

Steel jackets are used not only for retrofit but also for repair of damaged columns. For example, Fig. 11-15 shows a test conducted to verify the effectiveness of a rectangular steel jacket to repair a rectangular column which failed in shear [Iwata et al. (2001)]. The column was first loaded to fail in shear. After shear cracks were grouted with epoxy resin, the column was repaired by a rectangular jacket. The repaired column was loaded again to fail in flexure. Significant enhancement of ductility and strength capacity was achieved by the steel jacketing as shown in Fig. 11-16.

11.2.3 Reinforced concrete jacket and shear wall

11.2.3.1 Reinforced concrete jacket

In reinforced concrete jacketing, new reinforced concrete section is constructed around the existing columns and piers to enhance the strength and ductility capacities. The new section and the existing section have to be well connected together. For this purpose, anchor bolts are generally inserted and grouted with a cement mortar after chipping out the covering concrete and drilling holes at the section of connection. Because the new section is at least 200 mm thick and most likely 300 mm, the flexural capacity is generally much enhanced. As a consequence, redundancy of the foundation due to an increase of flexural demand has to be well clarified in the reinforced concrete jacketing.

Reinforced concrete jacketing is frequently used based on two reasons. First, it is generally cheaper than other retrofit measures. However because direct cost for retrofit is only a part of the total cost, selection of an appropriate retrofit method has to be decided based on various other considerations. Second, the reinforced concrete jacketing is favorable in retrofit of columns in water. Based on this reason, the reinforced concrete jacket is much widely used than the steel jacketing for columns in river and sea.

Similar to the steel jacketing, there are essentially two strategies in flexural enhancement depending on redundancy on the demand of a foundation. First is to provide a gap between the jacket and the footing. The other is to anchor new rebars into the footing.

Same with the steel jacketing, reinforced concrete jacketing is effective for circular columns but not for rectangular columns as the cross section increases. Consequently required are ties or anchors which are provided crossing the section in the weak (mostly longitudinal) direction. Because cross ties are more important in wall piers, retrofit by reinforced concrete jacket is

described below for wall piers. The same methods can be used to square columns.

Wall piers are widely used in various regions worldwide. Wall piers which were designed and constructed in the early days were generally insufficiently reinforced. Volumetric tie reinforcement ratio was sometimes less than 0.1%. As a result, they have essentially insufficient flexural and shear strengths and ductility capacity.

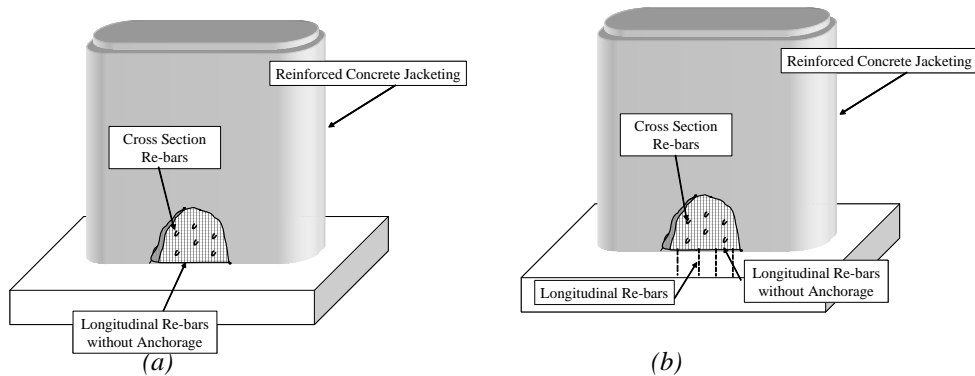


Fig. 11-17: Reinforced concrete jacket for wall piers: (a) longitudinal reinforcement is not anchored into footing, and (b) longitudinal reinforcement is anchored into footing

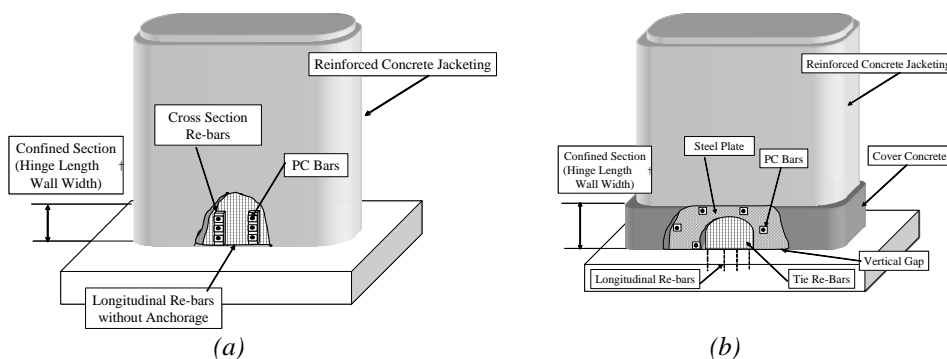


Fig. 11-18: Reinforced concrete jacket for wall piers: (a) cross PC strands, and (b) reinforced concrete jacket + steel jacket at the bottom

Fig. 11-17 shows a typical reinforced concrete jacket which is not anchored to the footing. A gap of 100-150 mm is generally provided between the jacket and the footing. PC strands are provided and grouted in drilled holes to enhance the lateral confinement. PC strands are generally provided at every 300 mm and 1m spacing in the vertical and transverse directions, respectively. Prestress is not generally provided in the PC strands because passive confinement is expected. Based on a loading test, a prestressing force in PC strand makes the plastic hinge of the pier shorter resulting in smaller ductility capacity.

Drilling holes crossing a pier is always difficult because drilling most likely cuts the existing reinforcements. Although razor sensors, sound echo sensors and other devices are used, it is always troublesome to drill holes crossing a pier. Consequently, technologies which eliminate or use rods with smaller radius are being developed as will be described later. Cutting of concrete by high water pressure was developed to split a pier into several segments so that cross ties can be easily set.

Fig. 11-18 shows a reinforced concrete jacket which is anchored to the footing. Because the pier responds almost elastically, this can be used only when the foundation has sufficient flexural and shear capacities. In addition to a reinforced concrete jacket, a 1-2 m high steel jacket is sometimes provided at the base for protection.

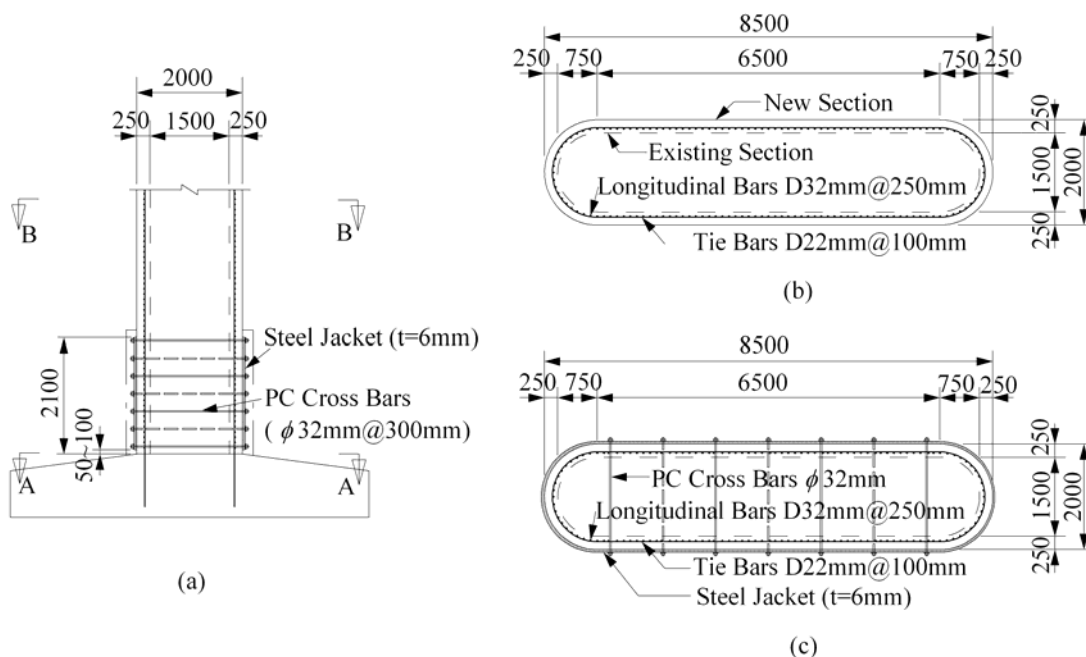


Fig. 11-19: Reinforced concrete jacket with steel jacket at the plastic hinge for a 5.3 m tall wall pier

Fig. 11-19 shows an example of the reinforced concrete jacket with a steel jacket at the plastic hinge. It is a 5.3 m high wall pier with a 8.5 m and 2.5 m section in the transverse and longitudinal directions, respectively. New longitudinal rebars with a radius of 32 mm were provided at an interval of 125 mm along the existing pier. Half of the longitudinal rebars were anchored in the footing, while the rest were not anchored. New ties with a radius of 22 mm were placed at every 100 mm interval. Six mm thick and 2.1 m high steel jacket was set surrounding the new reinforced concrete jacket. Forty nine PC strands with a radius of 32 mm were provided crossing the section at 300 mm and 1000 mm interval in the vertical and transverse directions, respectively.

Aramid fiber reinforced plastics rods which will be described in 11.2.4.3 b) can be used as cross bars in the retrofit of wall piers. Aramid fiber reinforced plastics rods have several advantages as cross bars compared to normal steel bars or PC strands. First, the aramid fiber reinforced plastics rods have lower elastic modulus than PC strands. Consequently, it is easier to introduce a prestressing force with lesser deterioration of the prestressing force due to creep. Second, because bond strength between the aramid fiber reinforced plastics rods and concrete section is higher than steel bars or PC strands, a large anchor device is not required. Therefore, anchoring of aramid fiber reinforced plastics bars with reinforced concrete section is much easier than PC strands. Third, lateral confinement of the existing RC section can be achieved using the aramid fiber reinforced plastics rods with smaller radius. This makes the drilling easier and faster than the rebars or PC strands.

Effectiveness of aramid fiber reinforced plastics rods as cross bars was clarified based on a series of cyclic loading test as shown in Fig. 11-20 [Tamaoki et al. (1996)]. Seven 2 m tall wall piers with a section of 2.5 m and 0.5 m were retrofitted by 2.3 mm thick steel jacket at the entire height. They were further retrofitted by 100 mm thick reinforced concrete jacket at the plastic hinge zone to enhance the flexural strength of the piers. Because the prototype piers had insufficient flexure strength (refer to Fig. 11-20 a), enhancement of the flexural strength and the ductility capacity was required. Effect of steel rebars, PC strands and aramid fiber reinforced plastics rods (Refer to Fig. 11-20 b) as cross bars were clarified. Aramid fiber reinforced plastics rods with a radius of 6 mm were provided at 500 mm and 250 mm interval in the lateral and vertical directions, respectively. Effect of introducing prestressing force in the aramid fiber reinforced plastics rods was also studied.

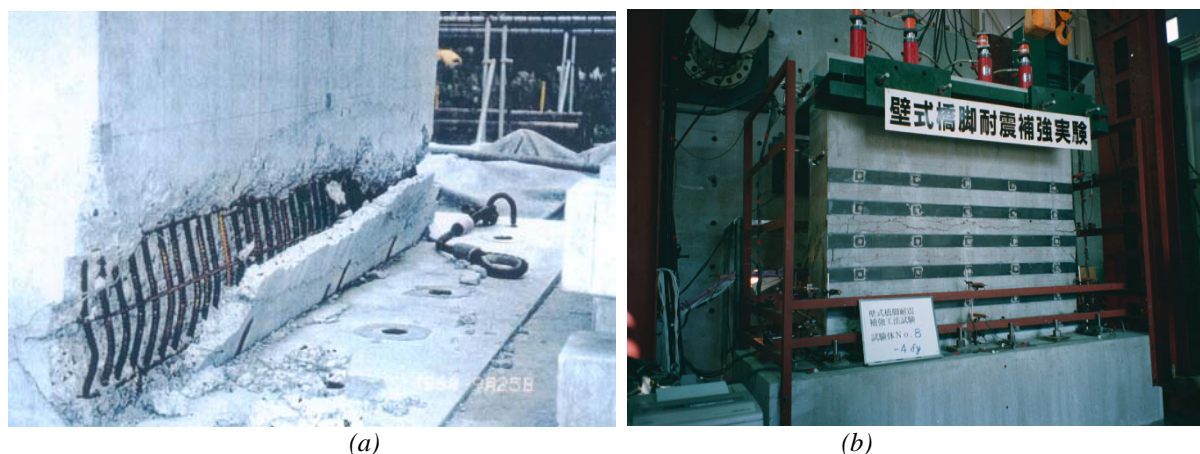


Fig. 11-20: Cyclic loading test on the retrofit of wall pier by steel jacket covered by reinforced concrete jacket with cross aramid fiber reinforced plastics rods: (a) As-built pier, and (b) Pier retrofitted using cross aramid fiber reinforced plastics rods [Tamaoki et al. (1996)]
(Figure available electronically on **fib** website; see production note on p. ii)

Lateral Confinement in the Weak (Longitudinal) Direction	Maximum Restoring Force (kN)	Ductility Factor
As-built	609	5.1
Steel jacket at the entire height covered by RC jacket at the plastic hinge zone (standard model)	616	8.1
Standard model + cross bars (steel bars with a radius of 16 mm) at the plastic hinge zone	626	11.8
Standard model + cross bars (PC bars with a radius of 7.1 mm) at the plastic hinge zone	603	12.0
Standard model + cross bars (PC bars with a radius of 11 mm) at the plastic hinge zone	614	12.6
Standard model + cross bars (aramid fiber reinforced plastics bars with a radius of 6 mm without prestress) at the plastic hinge zone	606	14.0
Standard model + cross bars (aramid fiber reinforced plastics bars with a radius of 6 mm with prestress) at the plastic hinge zone	702	12.9

Table 11-1: Effectiveness of cross aramid rods for retrofit of wall piers based on a cyclic loading test [Tamaoki et al. (1996)]

Table 11-1 summarizes the effect of retrofit in terms of the maximum restoring force and the ductility capacity. It is obvious that the ductility capacity of the pier without lateral confinement in the weak direction is insufficient. The aramid fiber reinforced plastics rods were effective in enhancing the ductility capacity as well as the flexural strength by well confining the piers in the weak direction.

The cross aramid fiber reinforced plastics rods were implemented to several bridges. For example, Fig. 11-21 shows retrofit of wall piers based on the experimental clarification described above. After steel jacket was provided (refer to Fig. 11-21 a), aramid fiber reinforced plastics rods were set in drilled holes in the weak direction (refer to Fig. 11-21 b). After prestressing force was introduced in the aramid fiber reinforced plastics, a reinforced concrete jacket was further provided at the plastic hinge zone (refer to Fig. 11-21 c).



(a)



(b)



(c)

Fig. 11-21: Retrofit using cross aramid fiber reinforced plastics rods to wall piers: steel jacketing, (b) set of cross aramid fiber reinforced plastics rods, and (c) after retrofitted (courtesy of Sumitomo Mitsui Construction)

(Figure available electronically on *fib* website; see production note on p. ii)

11.2.3.2 Infill shear walls

Infill shear walls are frequently used to retrofit framed piers. Because infill wall provides high shear and flexural capacity in the direction parallel to the wall (most likely in the transverse direction), it increases flexural and shear demand of the foundation. Therefore seismic performance of the foundation has to be carefully evaluated.

Frame piers which were designed in the early days are often vulnerable for shear because shear capacity of beams and columns as well as their joints is insufficient. Similar to wall piers, they are very lightly reinforced and lateral confinement is insufficient. Basic strategy for retrofit of frame piers is to retrofit all columns, lateral beams and joints. Another strategy is to build a new infill shear wall.

Fig. 11-22 shows an example of an infill shear wall for an 8.7 m tall reinforced concrete frame pier. The shear wall was 400 mm thick. The covering concrete of the existing substructures was chipped-out, and holes with a radius of 26mm were drilled. Anchor bars with a radius of 16mm were set and grouted with epoxy resin at every 300 mm interval.

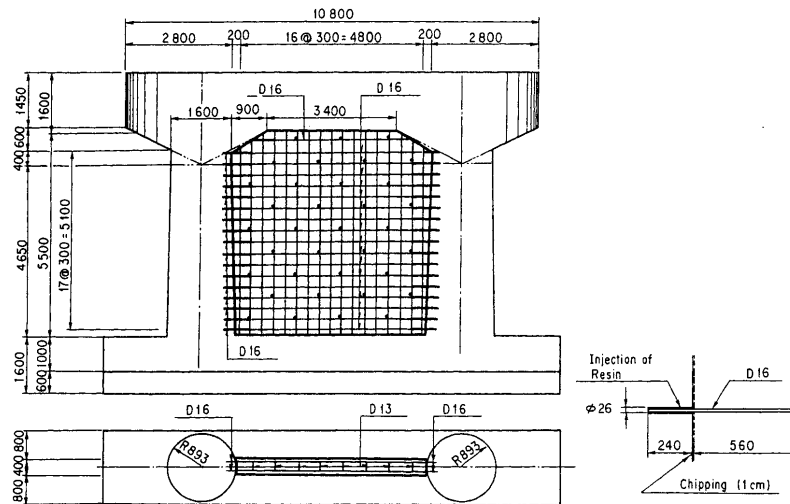


Fig. 11-22: Seismic retrofit of frame pier by new infill wall [Kawashima et al.(1994)]

11.2.4 Composite material jackets

11.2.4.1 Introduction

Composite-materials such as carbon fiber reinforced plastics, aramid fiber reinforced plastics jackets and fiber glass have been used for retrofit of existing bridges. How and under what form these materials are used for retrofit of bridges depends on their properties. Strength and the elastic modulus are in particular important to determine how and what form a material is used. Some materials have nearly elastic behavior until failure while the others have inelastic property from small strain. Carbon fibers have similar elastic modulus with steel, but most composite materials have lower elastic modulus than steel. Rupture strain is another important parameter for retrofit. In addition to the mechanical properties, durability under various natural environments is the most crucial requirement.

Composite materials are generally expensive, but the cost of material is only a part of the total retrofit cost. If retrofit can be conducted shortly without interruption of traffic by using composite materials, it can be validated from the total cost and performance point of view. Because composite materials are generally light and easy to handle at site, it is useful at a bridge where construction space for other retrofit measures such as reinforced concrete jacketing and steel jacketing are limited. Composite materials are provided in various shapes and forms. The following paragraphs introduce some examples of column retrofit using composite materials.

11.2.4.2 Carbon fiber jacketing

A carbon fiber consists of a number of carbon atoms continuously connected in the direction of the fiber. This is called monofilament. Carbon atoms are composed of more than 90% carbon. A carbon strand generally consists of 1000 to 2000 monofilaments, and they are glued or wound on the surface of concrete structures similar to the wire strand presented above. A special device is required to wind carbon strands around a column.

Carbon strands which are impregnated with resin in the form of sheet are available. This is called carbon fiber sheet. Because carbon strands are generally set in one direction in a sheet, the sheet has strength in that direction. Carbon fiber sheets in which carbon strands are

impregnated with resin in two directions are available. Because carbon fiber sheet can be easily cut by knife in any size and shape, it is easy to handle and glue on the surface of a concrete structure as shown in Fig. 11-23. Consequently, among several forms of carbon fiber reinforced plastics, carbon fiber sheets have been most extensively used for seismic retrofit of columns.

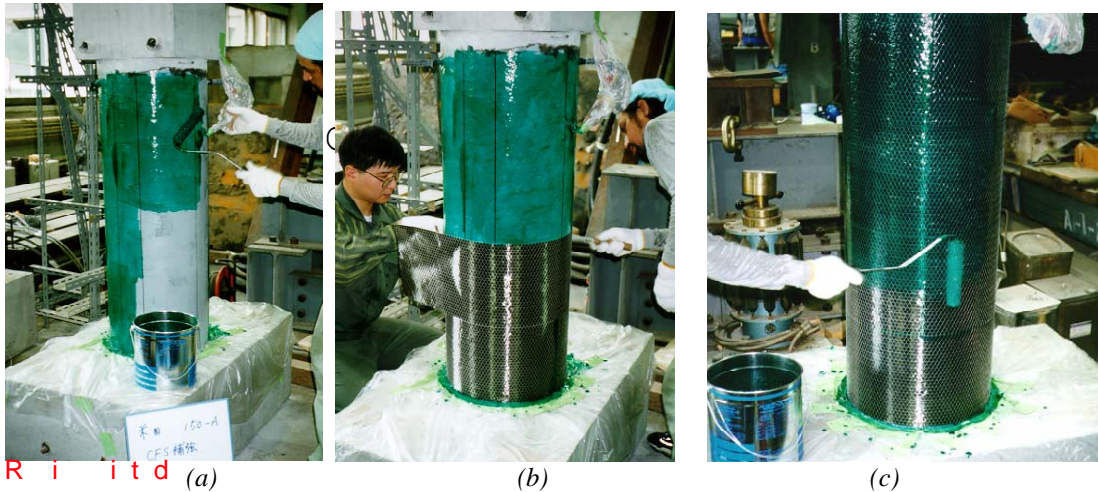


Fig. 11-23: Wrapping of carbon fiber sheet: (a) pasting glue, (b) wrapping the first layer, and (c) bonding on the first layer
(Figure available electronically on fib website; see production note on p. ii)

The elastic modulus and strength of standard carbon fibers are nearly the same with and about 10 times larger, respectively, than those of reinforcing bars. Carbon fibers have essentially linear stress-strain characteristics up to failure. Rupture strain is about 2%. As a consequence, when the core concrete is laterally confined by carbon fibers, residual plastic strains do not remain in the carbon fiber jacket such that the strength of the core concrete is maintained until rupture of the jacket in the subsequent cycles of response. Therefore, carbon fiber is more effective than steel rebars in the flexural retrofit and in resisting shear in the shear retrofit. There are special carbon fibers with higher elastic modulus and strength. Because the elastic modulus of carbon fiber is the largest among the composite materials currently available, it is effective for lateral confinement of a column. Carbon fiber was first introduced to repair damage of concrete structures, and it has been extended to seismic retrofit of columns since 1980s [Matsuda et al. (1990)].

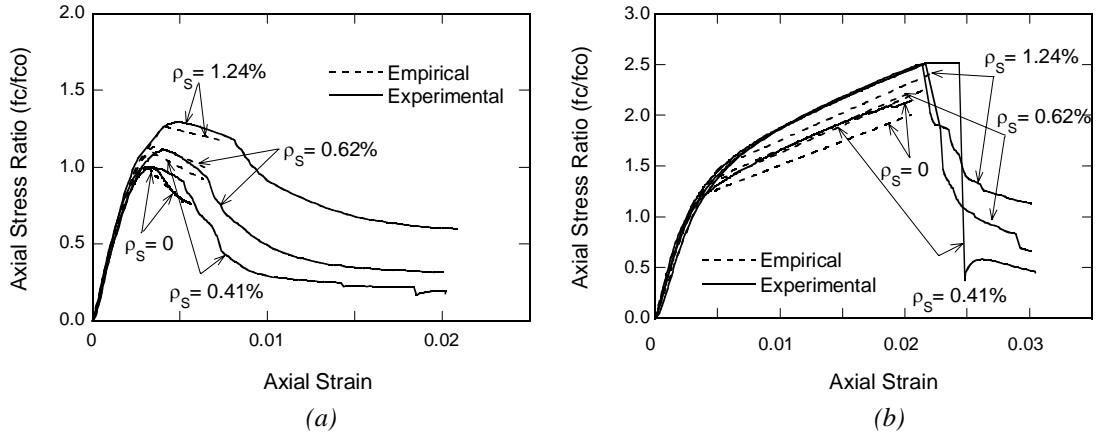


Fig. 11-24: Stress vs. strain hysteresis of circular concrete columns confined by ties and carbon fiber sheets [Kawashima et al. (2000)]

Because a standard carbon fiber sheet has nearly 10 times the strength of tie bars, mechanism of the lateral confinement is different with that of tie bars. The lateral confinement provided by ties does not increase after yield of ties, but it builds up nearly ten times the yield strength of ties in the confinement by carbon fiber. As a consequence, if the concrete is confined by a sufficient amount of carbon fiber, concrete stress continues to increase with limited stiffness deterioration as concrete strain increases. The lateral confinement of existing columns is developed by both existing ties and carbon fiber.

Several empirical confinement models which represent the lateral confinement for arbitrary combinations of ties and carbon fiber are available. For example, Fig. 11-24 shows a stress vs. strain relation of concrete confined by ties and carbon fiber sheets for volumetric carbon fiber sheet ratio of 0.056% and 0.111%. Sudden deterioration of stress occurs when carbon fiber sheet ruptures.

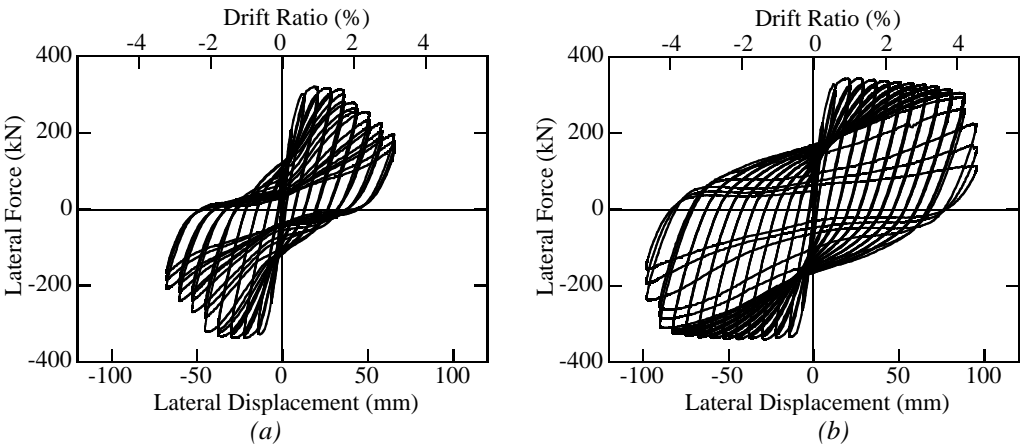


Fig. 11-25: Effect of carbon fiber sheet jacketing for a 2.1 m tall circular column: (a) as-built, (b) retrofitted [Unjoh et al. (1997)]

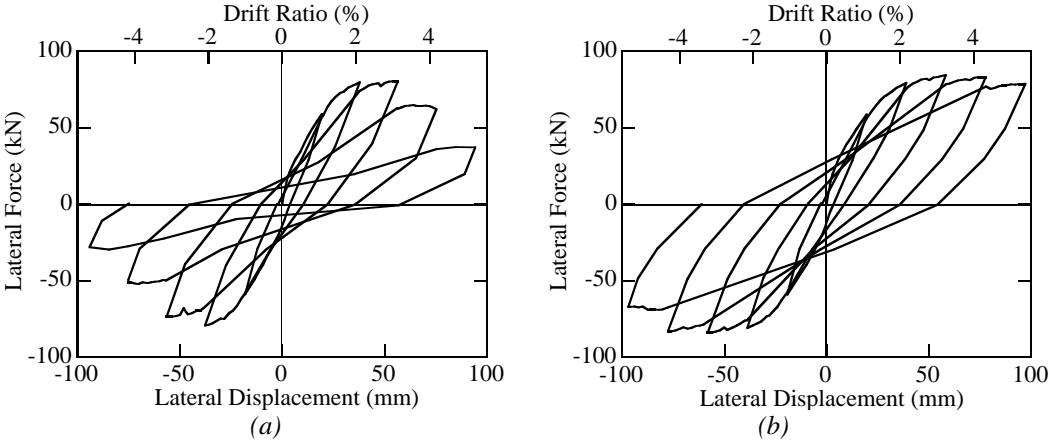


Fig. 11-26: Effect of carbon fiber sheet jacketing for piers in Sakawa-gawa bridge: (a) As-built, and (b) Retrofitted [Ogata et al. (1999), Osada et al. (1999)]

Fig. 11-25 shows a cyclic loading test on carbon fiber sheet jacket for 2.1m high circular columns with a radius of 700 mm [Unjoh et al. (1997)]. The carbon fiber sheet was wrapped in two ways; lateral direction alone and both lateral and vertical directions. The carbon fiber sheets wrapped along column height were used to enhance the flexural strength. They were

anchored at the upper surface of the footing by steel plates. The carbon fiber sheet wrapped in the lateral direction alone and the lateral + vertical directions enhanced the displacement ductility capacity by a factor of 200% and 300%, respectively.

One of the most extensive seismic retrofits of highway bridges using the carbon fiber sheet was implemented at the Sakawa-gawa Bridge, Japan. The bridge consisted of a 5-span continuous steel girder supported by five 42-65 m high hollow reinforced concrete piers. Before the retrofit, a series of cyclic loading tests was conducted to verify the effectiveness [Ogata et al. (1997), Osada et al. (1999)]. Fig. 11-26 shows the effect of retrofit. Stable flexural capacity range increases from 3% drift (as-built) to over 5% drift (retrofitted). The seismic retrofit by carbon fiber sheet was implemented as shown in Fig. 11-27. Right column was under wrapping while surface treatment was completed at the left columns.

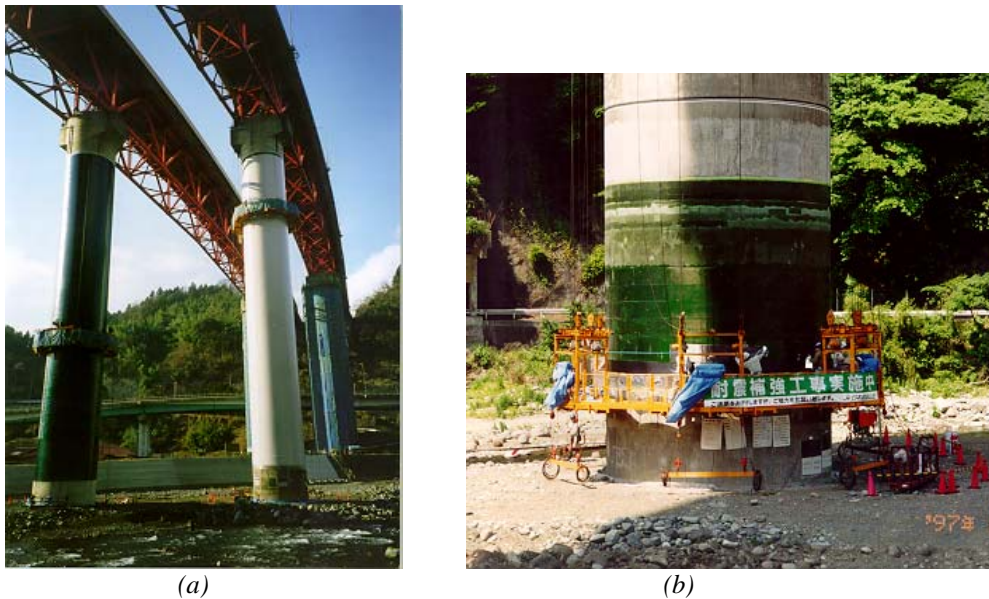


Fig. 11-27: Carbon fiber sheet jacketing of hollow reinforced concrete columns, Sakawa-gawa bridge, Tomei expressway; (a) Retrofitted east- and west-bound bridge, and (b) Wrapping of carbon fiber sheets [Ogata et al. (1999), Osada et al. (1999)]

(Figure available electronically on **fib** website; see production note on p. ii)

11.2.4.3 Aramid fiber reinforced plastics jacketing

Aramid fiber reinforced plastics jacketing has benefit similar to the carbon fiber jacketing. It is light and easy to wrap without use of heavy machines. Elastic modulus is generally in the range of $(0.8-1.2) \times 10^5$ MPa which is smaller than that of the carbon fiber. Nominal strength and rupture strain are generally in the range of 2.1-2.4 GPa and 1.8-3%, respectively.

Aramid fiber is essentially available in four forms; 1) braided tape, 2) unidirectional tape, 3) sheet and 4) rods. Braided tape is typically 20 mm wide, and consists of aramid fibers woven in a braided form. Unilateral tape and sheet are fabric woven in a tape form typically 75 mm wide and sheet, respectively, and consists of aramid fibers in the axial direction and glass fibers in the transverse direction. Strength of the aramid fiber depends on the quantity of fiber per cross section. Tensile strength of a braided tape and unidirectional tape with 307,200 deniers (1 denier=1 g/9,000 m) and 34.5 mm^2 impregnated with epoxy resin is 54.7 kN and 36.0 kN, respectively.

Among the above four forms, aramid fiber sheets and aramid fiber rods are well used for seismic retrofit of existing columns and piers. Aramid fiber sheets are used for aramid fiber sheet jacket. Aramid fiber rods are used to confine a pier as cross ties, and to retrofit a footing

by providing prestressing force. Examples of the retrofit will be described in the later section.

Effectiveness of aramid jacketing has been clarified based on cyclic loading tests. For example, 625 mm high square columns with a width of 250 mm, which were designed to fail in shear, were retrofitted by aramid braided tape, unidirectional tape and sheet as shown in Fig. 11-28. Smoothing of square section at corners was not conducted. Braided tape and directional tape were helically placed at a 100mm interval. A sheet was cut into 160 mm wide strip, and 4 to 5 sheets were superposed to have the same total fiber quantity with braided tape and unidirectional tape. As shown in Fig. 11-29, as-built column failed in shear, while retrofitted columns failed in flexure. Aramid fiber did not rupture until final loading except the column retrofitted by sheets where sheet ruptured at a corner at a drift of 20/625.

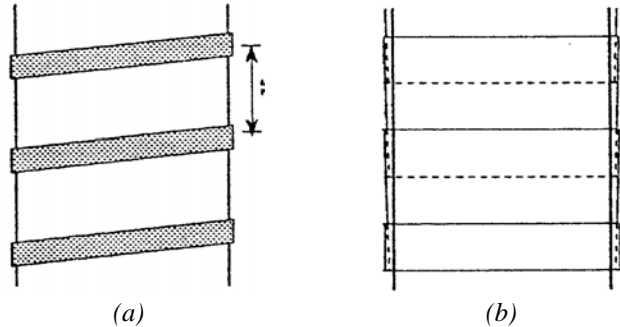


Fig. 11-28: Retrofit by aramid fiber reinforced plastics: (a) braided tape and unilateral tape, and (b) sheet [Okamoto et al. (1994)]

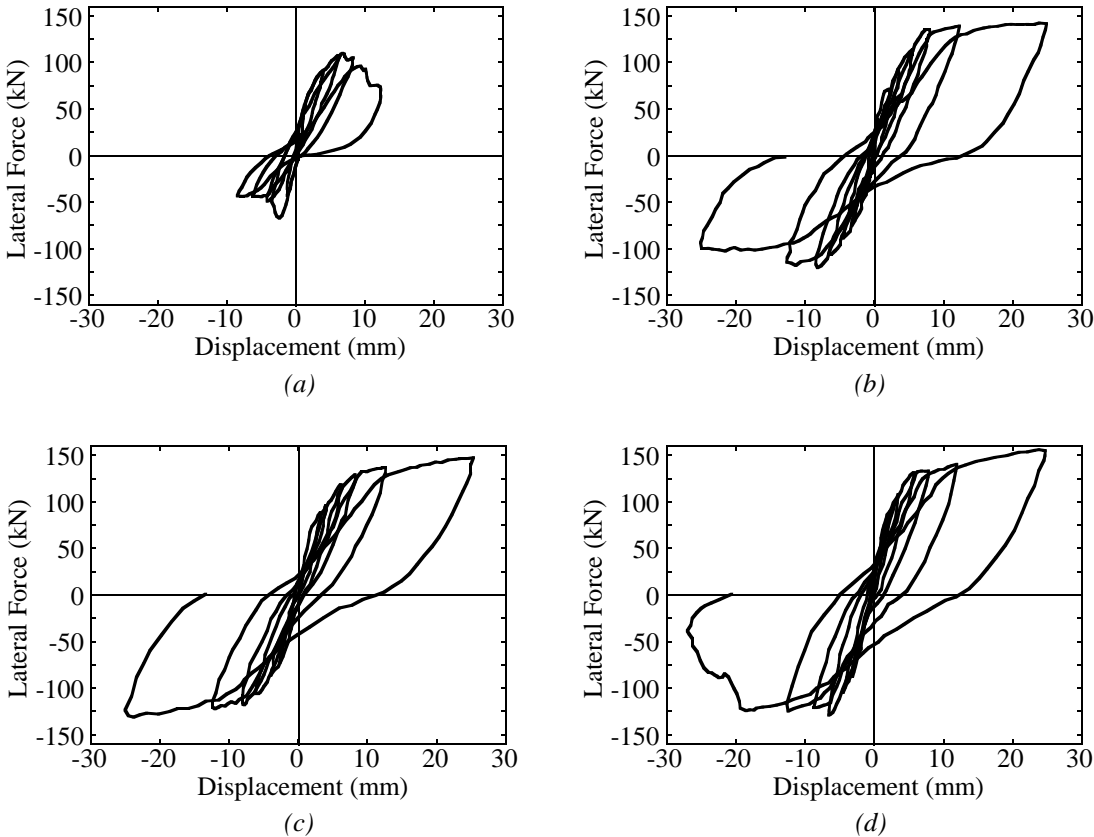


Fig. 11-29: Effect of retrofit by aramid fiber: (a) no reinforcement, (b) braided tape, (c) UD tape, and (d) sheet [Okamoto et al. (1994)]

Aramid fiber jackets have been implemented at the sites where steel jackets and reinforced concrete jackets cannot be used because of space limitation. Because aramid fiber sheets are more flexible than carbon fiber sheets, aramid fiber jackets are superior for retrofitting columns of varying sections.

Fig. 11-30 shows seismic retrofit of a reinforced concrete column in a railway viaduct by aramid fiber jackets. Aramid fiber sheet jacketing was used at this site because the columns were located high without sufficient space for retrofit. Mortar cover was provided on the aramid fiber jacket for protection. A series of cyclic loading tests verified the effectiveness of this method on enhancing the ductility and shear capacity.



Fig. 11-30: Aramid fiber reinforced plastics jacketing for a railway viaduct [courtesy of JR Research Institute] (Figure available electronically on *fib* website; see production note on p. ii)



Fig. 11-31: Piers retrofitted by aramid fiber sheet [Kato et al. (2001)] (Figure available electronically on *fib* website; see production note on p. ii)

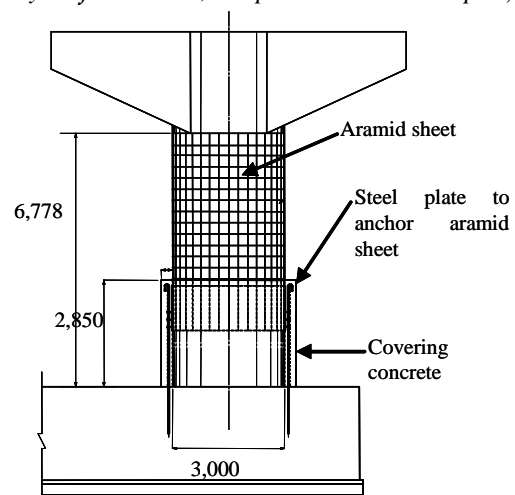


Fig. 11-32: Anchor of aramid fiber to the footing [Kato et al. (2001)]

Fig. 11-31 shows another implementation of aramid fiber jacket to 8-12.5 m tall circular reinforced concrete columns with a radius of 3 m [Kato et al. (2001)]. Because the flexural and shear strength was insufficient in the columns, enhancement of the strength and the ductility capacities were required at this bridge. Since aramid fiber jacket less increased the demand to foundations, it was adopted here. Aramid fiber sheets with a strength of 4.4 MN per meter were wrapped along the column axis (vertical direction) to enhance the flexural capacity. These were not anchored to the footing so that flexural demand of the footing does not significantly increase. Aramid fiber sheets with a strength of 0.88 MN were wrapped around columns in the spherical direction to enhance the shear capacity. However aramid fiber sheets with a strength of 4.4 MN were wrapped at the bottom to confine the plastic hinge region for enhancing the ductility capacity. Aramid fiber sheets as many as 8 layers were wrapped without any problem

because of the high impregnation of epoxy resin in the aramid fiber sheets.

Because the flexural capacity of a pier and footing system was still insufficient in the above retrofit at some tall piers, the vertical aramid fiber sheets were anchored to the footing as shown in Fig. 11-32. Steel jacket was provided at the plastic hinge region, and the vertical aramid fiber sheets were bonded to the steel jacket. Detailings of the bond between the steel jacket and the aramid fiber sheets were clarified based on a cyclic loading test.

In addition to the aramid fiber sheets, aramid fiber rods are effective for retrofit of foundations and piers. This will be described later.

11.2.4.4 Glass fiber reinforced plastics jacket

Glass fiber is used for seismic retrofit of columns. Fig. 11-33 shows a rectangular glass fiber-epoxy jacket placed to enhance shear strength of a short rectangular column [Priestley, Seible and Calvi (1996)]. Although it was not expected that the jacket would provide significant enhancement to ductility, it is seen in Fig. 11-33 b that the column sustained displacement ductility up to 8, corresponding to a drift angle of 4% before jacket failure.

Fig. 11-34 shows another implementation of glass fiber to a railway bridge column. Glass fiber with resin mixture was blasted by a spray gun. Steel cross-mesh was used together with the glass fiber to enhance the strength and ductility of the columns. From a cyclic loading test, it was confirmed that the glass fiber and steel cross-mesh jacket enhanced the ductility capacity.

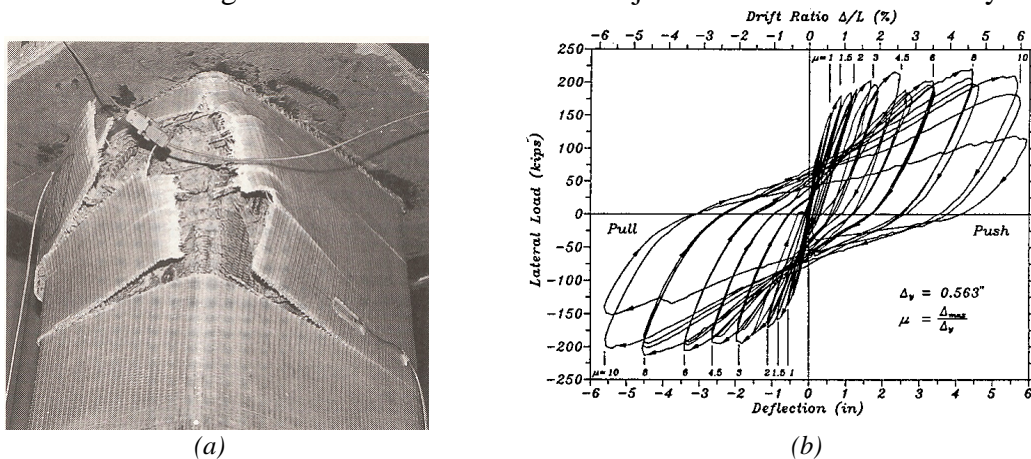


Fig. 11-33: Rectangular column with glass fiber-epoxy rectangular jacket: (a) failure by jacket fracture, (b) lateral force-displacement response [Priestley, Seible and Calvi (1996)]
(Figure available electronically on **fib** website; see production note on p. ii)



Fig. 11-34: Glass fiber jacketing (courtesy of JR Research Institute)
(Figure available electronically on **fib** website; see production note on p. ii)

11.2.5 Precast concrete segment jacket

Because steel jacket is vulnerable to corrosion, it is not generally used for retrofit of columns under water in river, lake and sea. As described in 11.2.3, reinforced concrete jacket is used for retrofit of columns in water, however it generally takes longer construction period. Setting a new reinforced concrete jacket requires drying up the top of footing and piers. Therefore, reinforced concrete jacketing is costly.

As a consequence, a jacketing method which uses precast concrete segments is now increasingly used for columns in water. There are at least three reasons for the wide acceptance of the precast concrete segment jacketing. The first is the technical development which enables setting of precast concrete segments without drying up of foundation under water. The second is the speedy construction compared to the standard reinforced concrete jacketing. Use of prefabricated concrete segments significantly reduces the construction period. Special joints for connection of segments are sometimes used to further reduce construction period. The third is the cost saving. Because size of the columns is generally more or less the same at a bridge, fabrication of segments in a factory and setting them at the site saves cost compared to the reinforced concrete jacketing. However, the use of precast concrete segments is not feasible for bridges which are supported by irregular columns with different cross-sections.



Fig. 11-35: Precast concrete segment jacket [courtesy of PS Concrete]
(Figure available electronically on [fib](#) website; see production note on p. ii)

Early implementation of the precast concrete segment jacketing started after the 1995 Kobe, Japan earthquake as shown in Fig. 11-35. Because enhancement of flexural strength as well as shear strength was required in this bridge, precast concrete segments were set after longitudinal bars were installed around the existing columns. The longitudinal bars were anchored into the footings by grouting with epoxy resin. Because the retrofit had to be completed in winter with lower water level, it was beneficial to adopt the precast concrete segment jacketing due to the shortened construction period. Segments were tied together around the existing columns by high-strength cable strands. Small amount of prestressing force was introduced to fasten the segments and assure contact between the segments and existing columns. Non-shrinkage mortar was grouted between the segments and the existing columns.

The effectiveness of precast concrete segment jacketing was clarified by testing half-scale models at the site (refer to Fig. 11-36) and at the laboratory. It was found that this method was effective in enhancing the strength and ductility capacity of reinforced concrete columns. Based on loading tests, lateral confinement effect by strands with high strength as well as existing ties was clarified.

Fig. 11-37 shows another example of seismic retrofit of rectangular columns.



Fig. 11-36: On-site loading test on the effectiveness of PC segment jacketing (Figure available electronically on **fib** website; see production note on p. ii)



(a) before retrofit



(b) after retrofit

Fig. 11-37: Columns retrofitted by PC segment jacket: (a) as-built and (b) after retrofit (courtesy of Kawada Construction)

(Figure available electronically on **fib** website; see production note on p. ii)

Various new technologies have been developed since the early implementation of the precast concrete segment jackets. There are several directions of technical development. The first is anchoring of segment jackets into the footing without drying up of the foundation. Because drying up of foundations is costly, it is always a problem in the implementation of seismic retrofit of columns under water. Limiting construction only during seasons with low water level makes the total management difficult. Therefore, a method which enables retrofitting of existing columns without drying up of foundations is required. The second is the extension of this method to wall piers. Because lateral confinement in a wall pier is insufficient as the width increases, cross ties are necessary to provide lateral confinement. However drilling holes in a pier to set cross ties is likely to cut the existing longitudinal bars.

A new precast concrete segment jacketing was therefore developed and is now increasingly used. This method has several features. The first is the use of vinyl-ester epoxy resin to anchor the anchor bolts in the footing after holes are drilled. Because the resin stably anchors bolts in the footing even under water, drying up of the foundations is not required. After drilling and anchoring by divers, precast concrete segments can be set and slid down. The second is to provide lateral confinement by anchor bolts with extended radius at the bottom as show in Fig. 11-38. These anchor bolts, which mechanically extend radius after they are set in drilled holes passes through the core concrete, confining the precast concrete segments. Therefore drilling of

cross-holes to set the cross ties is not required. This avoids the risk of cutting longitudinal bars during the drilling stage and significantly saves the construction period. The third is to connect precast concrete segments together by mechanical joints as shown in Fig. 11-39. After temporarily connecting by working joints, mechanical joints are set from the top. This significantly improves the construction efficiency.

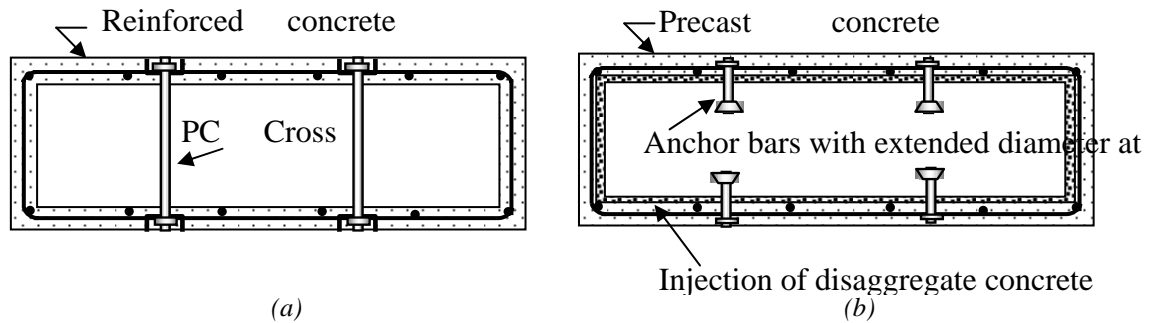


Fig. 11-38: PC segment jacket which does not require drying-up of foundations: (a) retrofit using standard reinforced concrete jacket and cross bars, and (b) retrofit using precast concrete segments with anchors with extended diameter at bottom (courtesy of Maeda Construction)

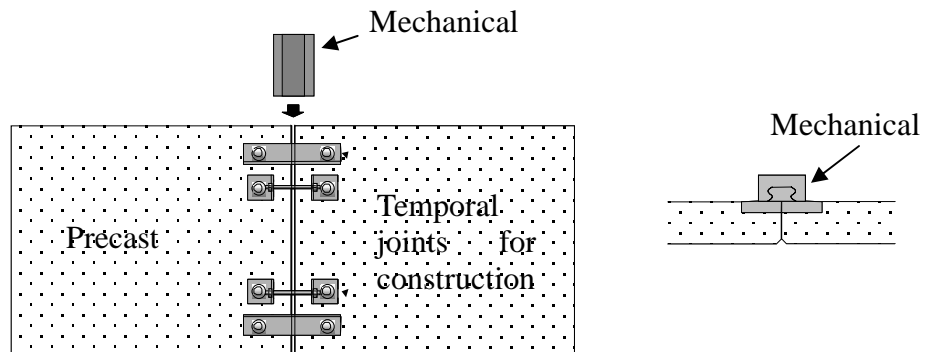


Fig. 11-39: Mechanical joint of pre-cast concrete segment jacket (courtesy of Maeda Construction)

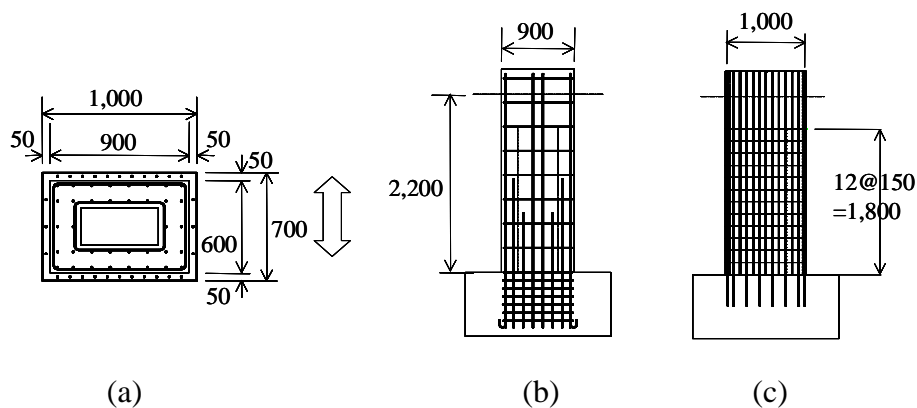


Fig. 11-40: Loading test on the retrofit of hollow rectangular column: (a) section, (b) as built and (c) retrofitted (courtesy of Maeda Construction)

Several series of tests were conducted to confirm the performance of this retrofit method. For example, Fig. 11-40 shows a loading test to show the effectiveness of this method on a hollow rectangular column. Because longitudinal reinforcements were terminated at

mid-heights with insufficient development length (refer to Fig. 11-40 b), the premature shear failure occurred in the as-built column. The column was retrofitted by precast concrete segments as shown in Fig. 11-40 c. Fig. 11-41 shows the lateral force vs. lateral displacement hysteresis of the retrofitted column.

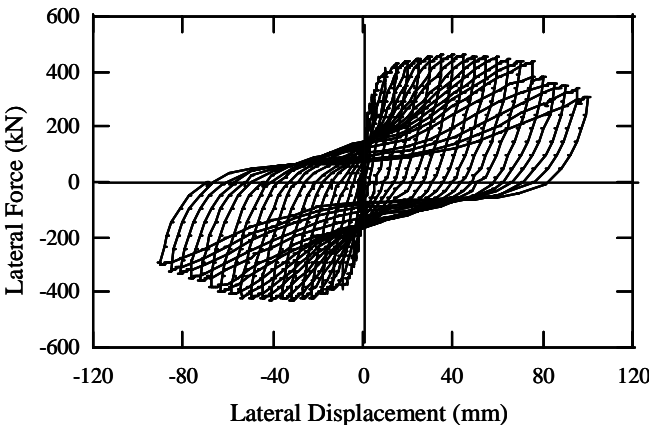


Fig. 11-41: Lateral force vs. lateral displacement hysteresis of a column retrofitted by PC segment jacket (courtesy of Maeda Construction)

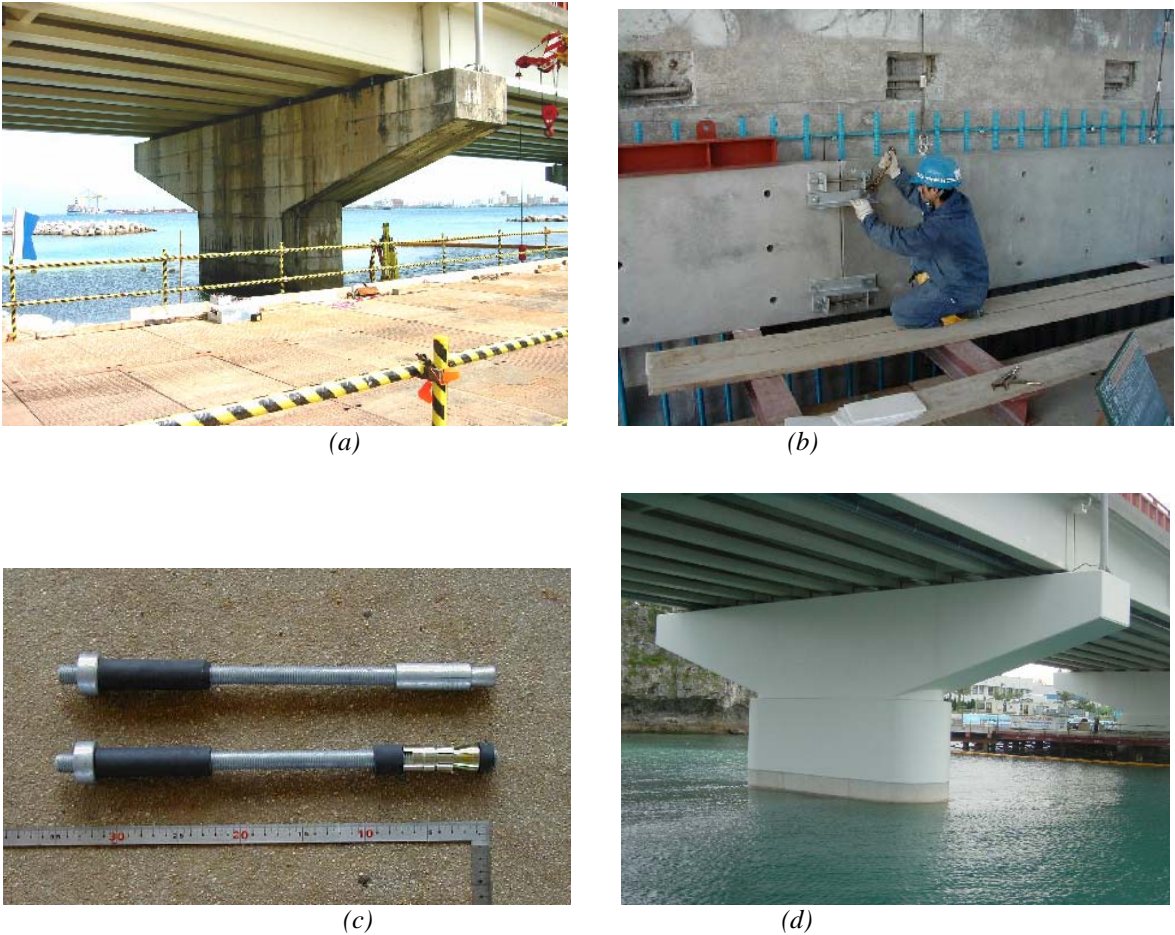


Fig. 11-42: Retrofit of wall pier by PC segment jacket: (a) as-built pier, (b) set of a precast segment using temporary joints, (c) anchor bolt for confinement (up) and anchor bolt for footing (bottom), and (d) after retrofitted (courtesy of Maeda Construction)
 (Figure available electronically on fib website; see production note on p. ii)

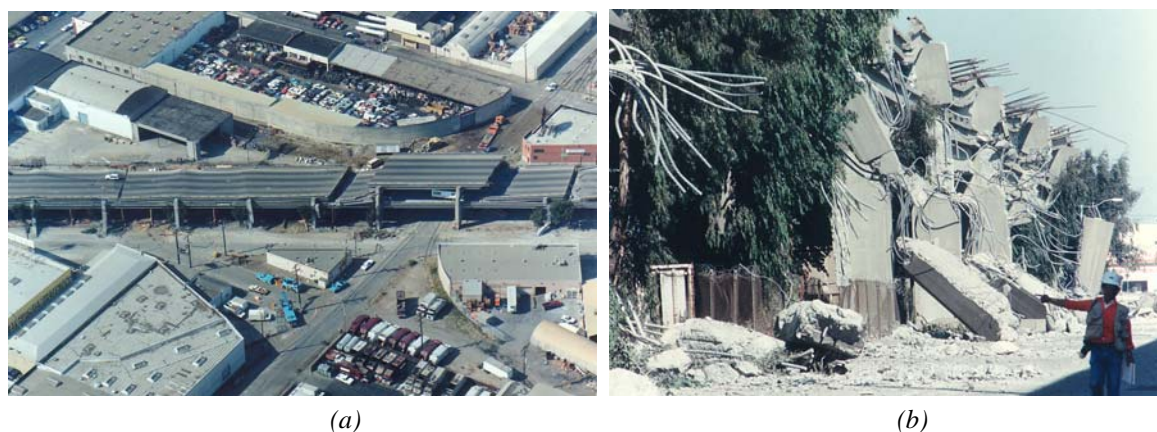
Fig. 11-42 shows an implementation of this method to a bridge which was supported by 4.5-6.2 m high and 8.6 m wide hollow reinforced concrete wall piers. The piers were retrofitted using 150 mm thick precast concrete segments. Anchor bolts with a radius of 16 mm (refer to Fig. 11-42 c) were set to provide the lateral confinement at every 1.63m and 300 mm in the horizontal and vertical directions, respectively. New longitudinal bars with a radius of 32 mm (SD295 D32) were set around the existing piers and were anchored in the footings with a development length of 0.96m. After segments were set together as shown in Fig. 11-42 b, they were slip sown. Fig. 11-42 d shows one of the retrofitted piers.

11.3 Retrofit of beam-column joints

11.3.1 Retrofit of cap beams

Multi column bents and framed columns are widely used for bridges. Extensive damage occurred due to deficiencies of those columns, cap beams and column/cap beam joints as shown in Fig. 11-43.

Cap beams provide the link in force transfer between the superstructure and columns. The cap beams of multicolumn bents will be subjected to flexure and shear. Deficiencies in flexural strength are common, particularly as a consequence of low positive reinforcement ratios at column faces and premature termination of negative reinforcement. Inadequate shear strength of cap beams is also common. Under longitudinal response, cap beams supporting superstructures via bearings are unlikely to have problems, but monolithic superstructure/cap beams/column designs may develop cap beam torsional problems, particularly when the columns are located outside the superstructure.



(a) (b)
 Fig. 11-43: Collapse of Cypress viaduct (Courtesy of Caltrans)
 (Figure available electronically on *fib* website; see production note on p. ii)

Cap beam deficiencies can be difficult and expensive to alleviate. Two basic approaches may be adopted: The cap beam strength can be increased to the level required to sustain the column plastic hinges, or the seismic forces developed in the cap beam can be reduced by a number of means. When cap beams and particularly column/cap joint forces induced by seismic action severely exceed capacity, it may be worth considering means for cap beam force reduction. As shown in Fig. 11-44, if located high on the columns, the link beam is effective in reducing seismic force in the cap beam. The link beam should be constructed by removing the column cover concrete over the height of the link beam and using a link beam width sufficient to place the longitudinal reinforcement outside the column core.

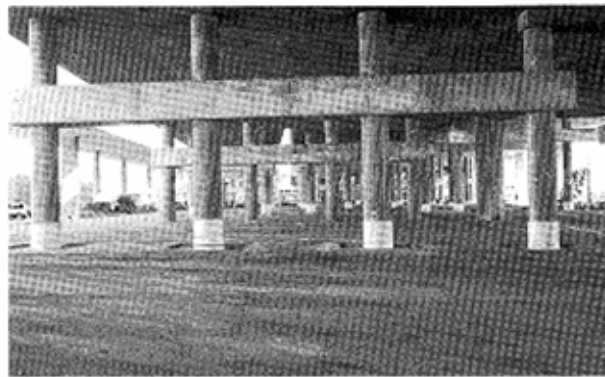
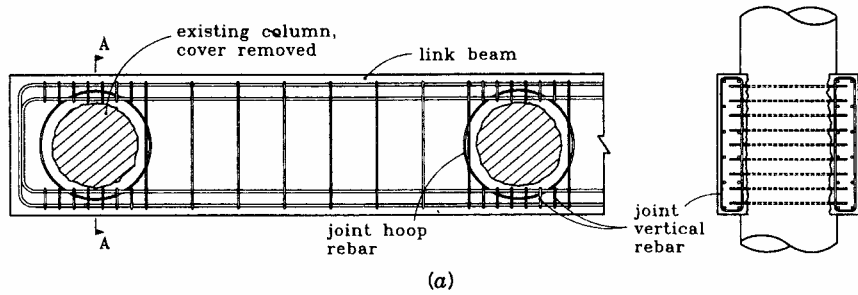


Fig. 11-44: Retrofit using link beams: (a) Link beam reinforcement details; (b) Link beam implementation on I-10 Santa Monica viaduct [Priestly, Seible and Calvi (1996)]

Generally, the retrofit philosophy of cap beams will be to increase the cap beam flexural strength sufficiently to force plastic hinge into the columns. With a separate cap beam supporting the superstructure via bearings, as shown in Fig. 11-45 a, flexural strengthening can be achieved by adding reinforced concrete bolsters to the sides after roughening the interface. The new and old concrete should be connected by dowels, preferably passing right through the existing cap beam.

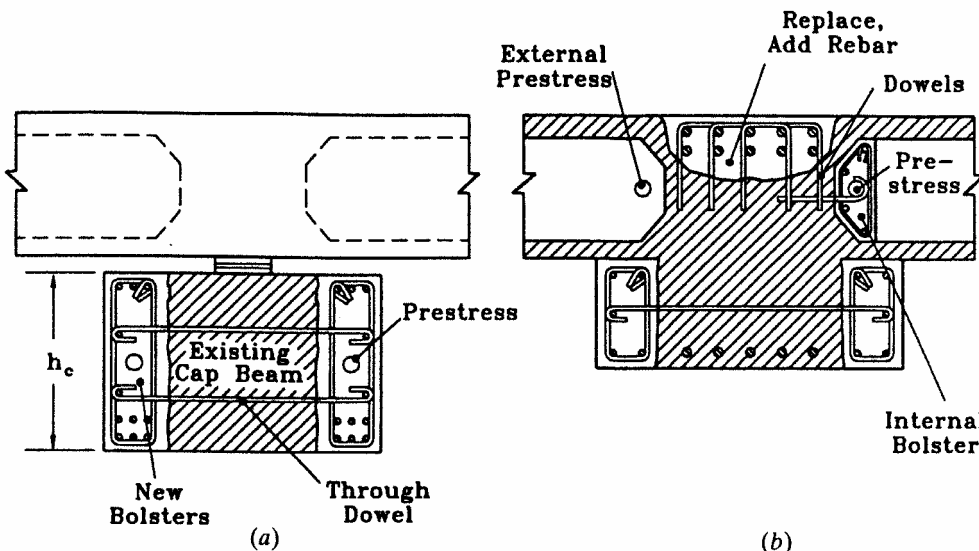


Fig. 11-45: Flexural and shear retrofit of cap beam: (a) Bearing-supported superstructure; (b) Integral cap beam [Priestley, Seible and Calvi (1996)]

An alternative or supplemental means of flexural strength enhancement is to prestress the cap beam using strong-backs at the cap beam ends. The prestress may be inside bolsters as shown in Fig. 11-45 a, or using external prestressing without bolsters. Enhancing the flexural capacity of integral cap beam as shown in Fig. 11-45 b is more difficult because of physical constraints

imposed by the existing superstructure. Bolsters may be added at the bottom to enhance positive moment capacity, and negative moment capacity can be increased by removing the top concrete and adding additional reinforcement. Full or partial-depth bolsters can be reinforced with transverse reinforcement to enhance cap beam shear strength as indicated in Fig. 11-45. Prestressing will also enhance the cap beam shear strength. Tests on a large-scale model of a retrofit concept for the San Francisco double-deck viaducts following the Loma Prieta earthquake [Priestley et al. (1993a), Priestley et al. (1993b)], which incorporated cap beam prestressing to enhance flexural and shear strength of the existing cap beam and edge beams as shown in Fig. 11-46, indicated that the approaches for flexure and shear enhancement were dependable and conservative. Fig. 11-47 shows cap beam retrofit details.

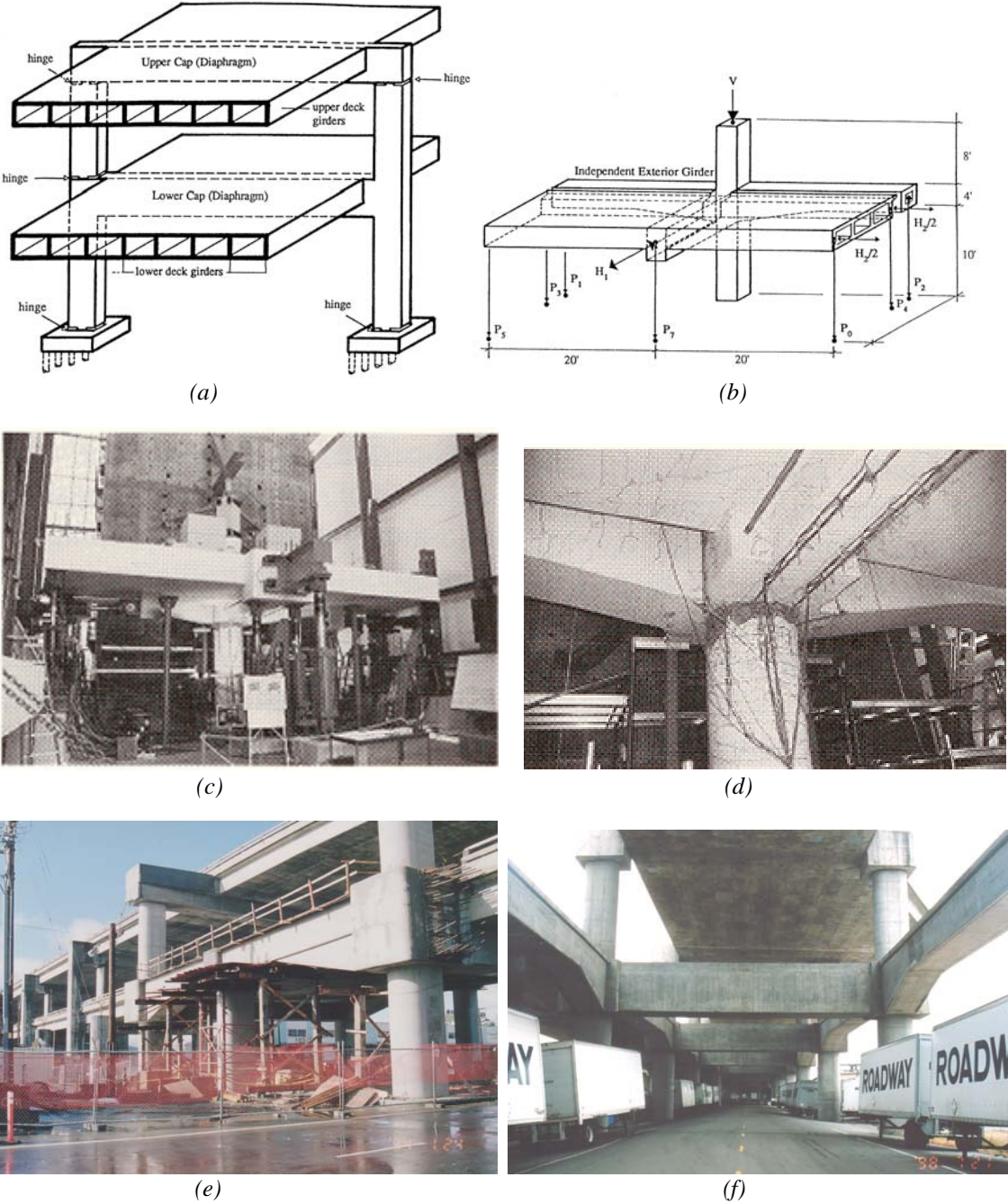


Fig. 11-46: Retrofit of San Francisco double-deck viaducts using edge link beams: (a) as-built viaduct, (b) proof test model, (c) proof test, (d) column damage in the proof test, (d) retrofit, and (e) edge beams [(a)-(d): Priestley, Seible and Calvi (1996)]
 (Figure available electronically on fib website; see production note on p. ii)

Cap beam shear strength may also be enhanced by composite materials bonded to the sides of the cap beam. This will be most effective when the composite layer can be wrapped around the top and soffit of the cap beam, as will be generally the case for bearing-supported superstructures.

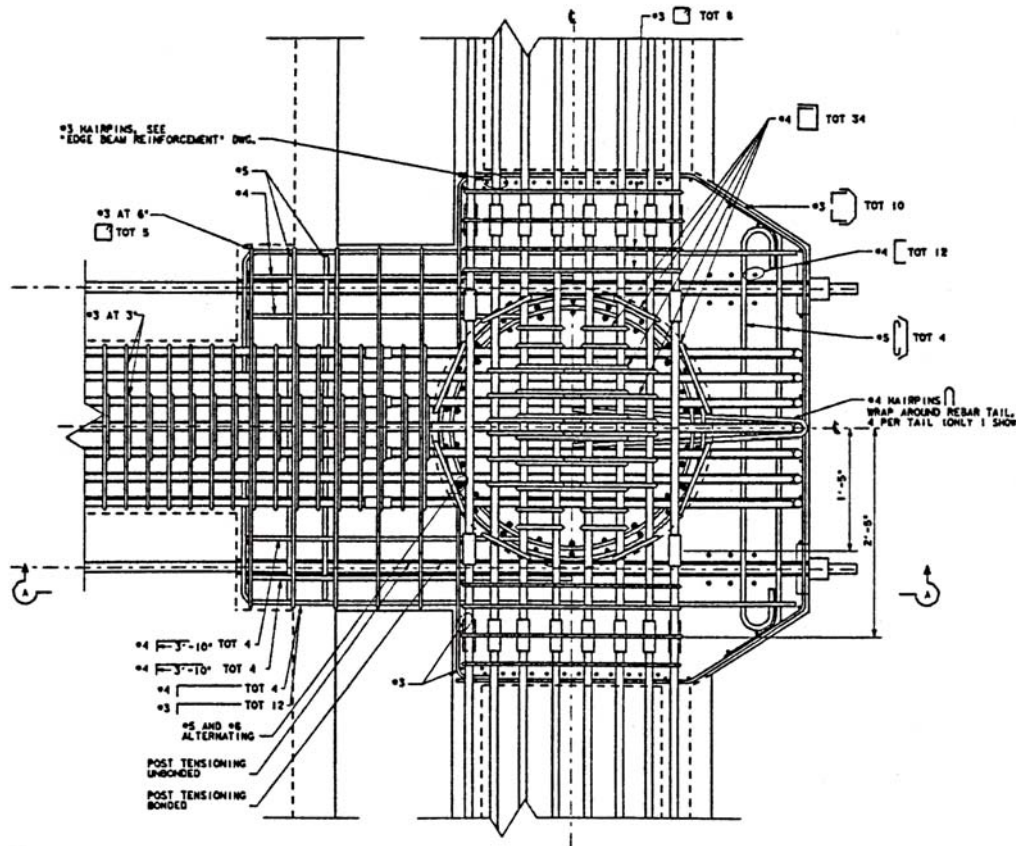


Fig. 11-47: Seismic retrofit of a cap beam for San Francisco double-deck viaduct [Priestley, Seible and Calvi (1996)]

11.3.2 Retrofit of cap beam/column joint regions

As with cap beam retrofit, a number of options are available, including joint force reduction, damage acceptance with subsequent repair, joint prestressing, jacketing, and joint replacement.

The means discussed in 11.3.1 to reduce cap beam forces will also, naturally, reduce column-cap beam joint forces. If it can be shown in the assessment phase of the as-built structure that joint failure will not lead to entire collapse under the design earthquake, an option to be considered is to accept the probability of damage in a major earthquake, with subsequent joint repair or replacement. In such cases there must be certainty that the joint failure will not jeopardize the gravity-load capacity of the structure, and the possibility of punch-through failures, where columns have penetrated the deck surface.

In many cases unacceptable joint performance can be improved by addition of prestressing. As well as increasing the flexural and shear strength of the cap beam, it will reduce the tendency for joint cracking. However there will often be a need for more effective retrofitting measures. In such cases, jacketing of the joint by concrete, steel, or composite-materials jackets should be considered.

With concrete jacketing, the necessary reinforcement to satisfy the load-path mechanism is placed in the concrete jacket, which is connected to the existing concrete by dowels and by roughening the surface of the existing joint. Typically, the jacket will extend beyond the

original joint dimensions into the cap beam and column, utilizing a haunch, as indicated in Fig. 11-48 a, which shows a retrofit example for an outrigger knee joint. Jacketing also increases the joint thickness, thus reducing joint stress level. As shown from the lateral force vs. displacement response in Fig. 11-48 b, this form of retrofit can be completely effective. In this knee-joint example, plastic hinging formed in the column, and the limit to the response was caused by a confinement failure in the column at moderately high curvature ductility factors.

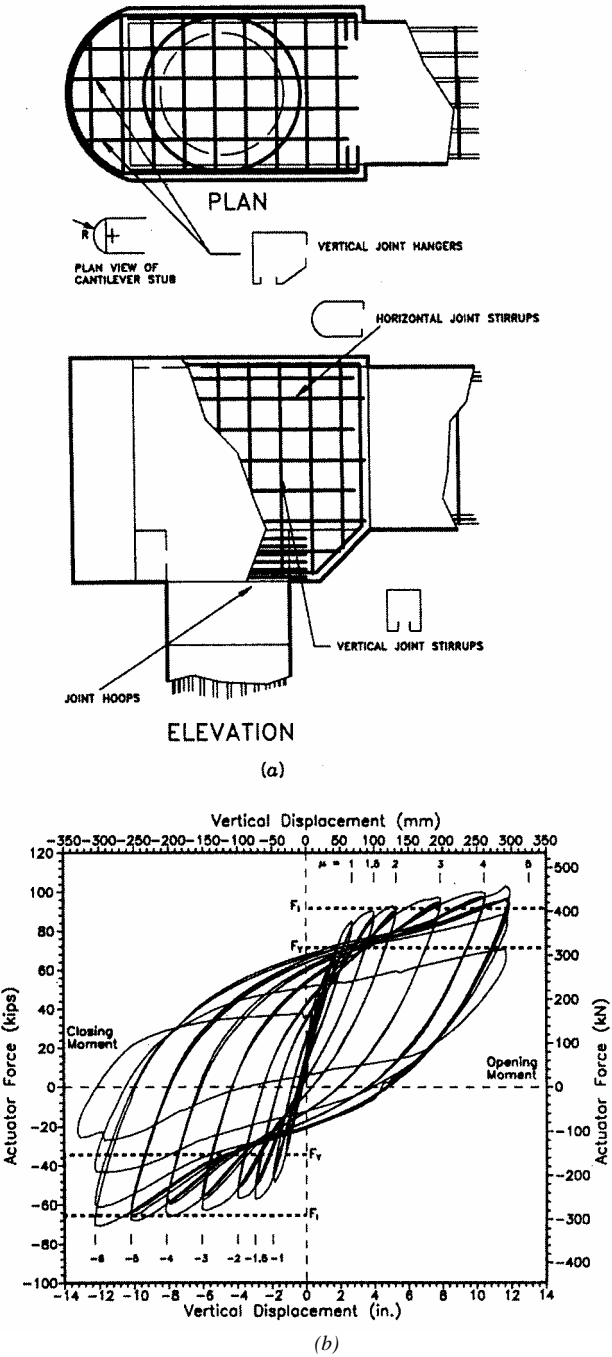


Fig. 11-48: Concrete jacketing of a deficient knee joint: (a) concrete jacket with a haunch, and (b) lateral force vs. displacement hysteresis [Priestley et al. (1996)]

Similar improvement in joint behavior have been obtained with steel jackets epoxy bonded to the concrete surface connected through the joint thickness with through-bolts to assist in the transfer of the joint force resistance mechanism from the outer steel plates to the beam and column stress resultants.

11.4 Retrofit of foundations

11.4.1 Introduction

Because retrofit of a foundation is much costly than the retrofit of a column and a pier, a strategy of seismic retrofit which does not require the retrofit of the foundation should be sought first. Retrofit measures which do not increase the demand of a foundation are most appropriate for this purpose. However foundations have to be properly retrofitted if this is inevitable. Retrofit strategy for enhancing only the capacity of piers and columns which results in unbalance of total bridge system should be avoided.

Similar to the practice to columns and piers, there are several deficiencies in design of foundations. Because driving force of piles was limited at the early days, radius and lengths of piles were generally insufficient based on the current design criteria. Large radius cast-in-place piles were not yet developed. Connection of piles to footing was always weak or insufficient, and this results in overturning or excessive uplift of the footing during an earthquake. Similar to columns insufficient lap splices are often used in piles.

Footings designed in the early days have generally insufficient shear and flexural strength. Because seismic force was not regarded as a main design force prior to the 1971 San Fernando, USA earthquake, footings were not adequately reinforced along the top surface [Xiao et al. (1994)].

Instability of soils around the foundations results in extensive failure during an earthquake. Failure of clayey soils and soil liquefaction are major sources of threat to foundations. In past earthquakes, lateral spreading associated with soil liquefaction resulted in extensive damage.

Because retrofit of foundations has to be mostly conducted under water, construction works become considerable. Construction of an access road to the foundations is sometimes as costly as the retrofit jobs. Because enhancing the shear and flexural capacity of piles by jacketing is difficult, additional piles are generally driven around the existing footings. Because piles have to be driven under the deck, space limitation results in narrowed selection of construction procedure.

Compared to the retrofit of columns and piers, retrofit of foundations is so far limited. However various new technologies are being developed.

11.4.2 Retrofit of foundations to instability of surroundings soils

In past earthquakes, instability of soils surrounding footings resulted in extensive damage. Effect of soil liquefaction and lateral spreading was not known and was not considered in the design of bridges in the early days. The bridges which were designed at the early days without taking those effects into account and were built at the sites where extensive soil liquefaction and lateral spreading are likely to occur are particularly vulnerable.

Retrofit of foundations under such a condition is extensively difficult, because all components including shear, flexural and ductility capacity of piles and footings are mostly insufficient. Consequently, whole foundations have to be retrofitted in most cases.

Fig. 11-49 shows an example of seismic retrofit of pile foundations in a 238 m long 14-span simply supported bridge. Footings were supported by 24 pre-cast concrete piles with a radius of 250 mm. Because bearing capacity of soils around the foundations was insufficient, two methods were clarified for retrofit. The first was to construct new piles by extending the existing footing. The other was to improve soils around the foundation so that the level of seismic risk due to soil liquefaction can be mitigated. Because soil improvement was more costly and risk reduction was difficult to ascertain, the first option was appropriate. However

space limitation made it difficult for driving new piles in the first option. Consequently, a combination of new pile construction and soil improvement was adopted in this bridge.

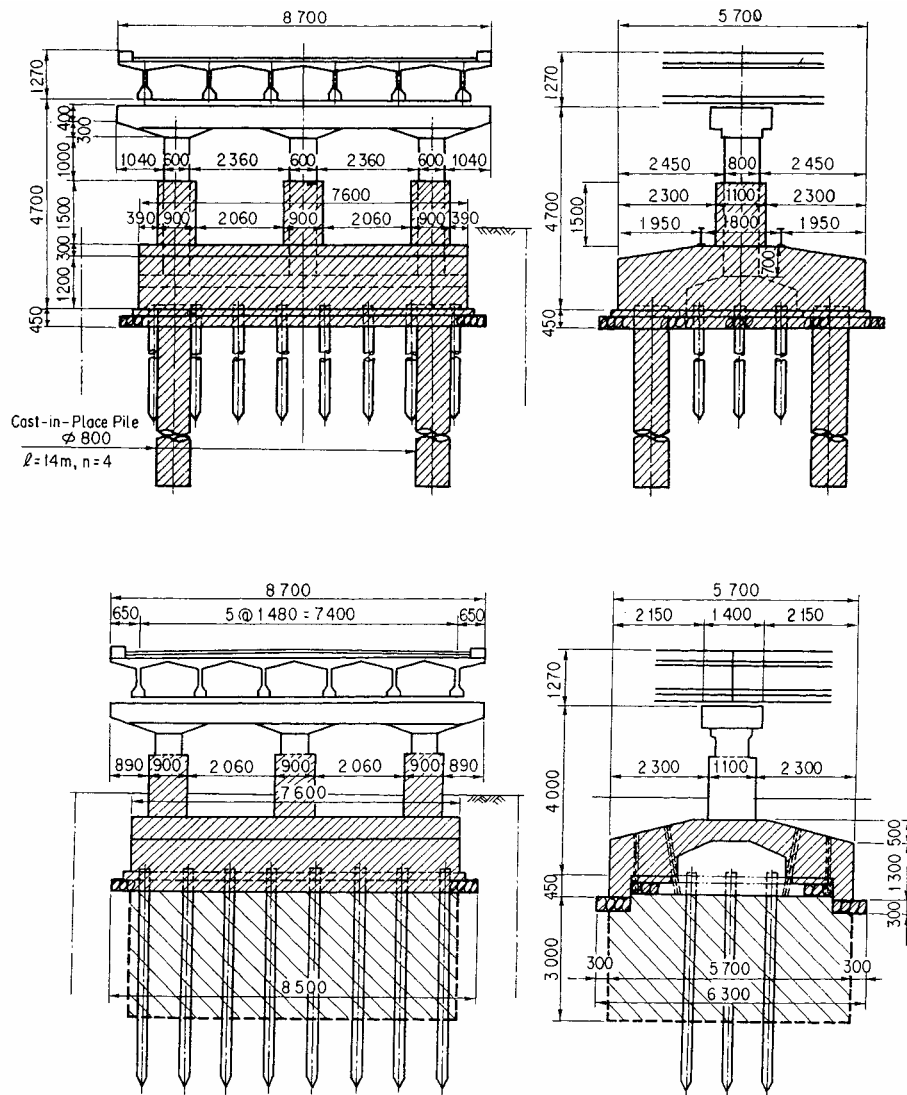


Fig. 11-49: Seismic retrofit of a pile foundation by new piles and an extension of footing [Kawashima et al. (1994)]

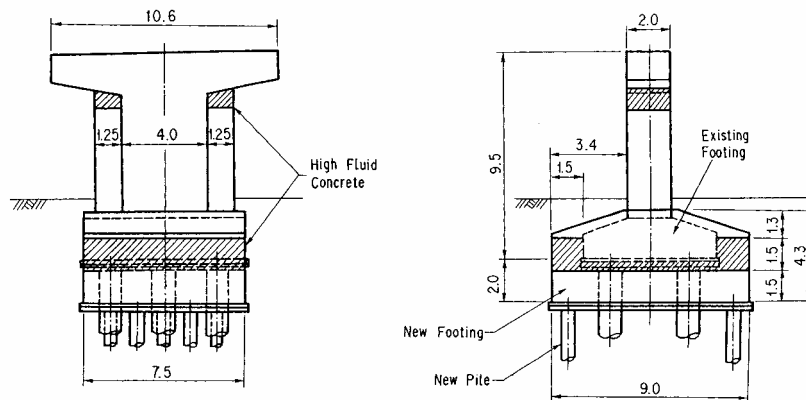


Fig. 11-50: Seismic retrofit of a pile foundation by new piles and an extension of footing [Kawashima et al. (1994)]

Four new 14-m long cast-in-place piles with a radius of 800 mm were built at the corners of the footing. To extend the footing, the covering concrete of existing footings was chipped out and anchor bars with a radius of 22 mm were inserted into drilled holes with epoxy resin grouting. Cement milk was grouted into the surrounding ground up to 3m deep below the bottom of the footing to improve the soil strength. The footing was extended almost twice the original, in thickness and length along the longitudinal direction.

Fig. 11-50 shows another example of seismic retrofit of pile foundations in 30m thick soft clayey soils. Because the bearing capacity of clayey soils was insufficient, six new piles were constructed by expanding the footing. A difficult point of this retrofit was the space limitation on the upper level of the footing. Because of river flow, the thickness of overlay on the upper surface of the footing was limited. Consequently, the footing expansion was built not only on the existing footing but also under the footing. Special excavation under the existing footing was needed and was costly.

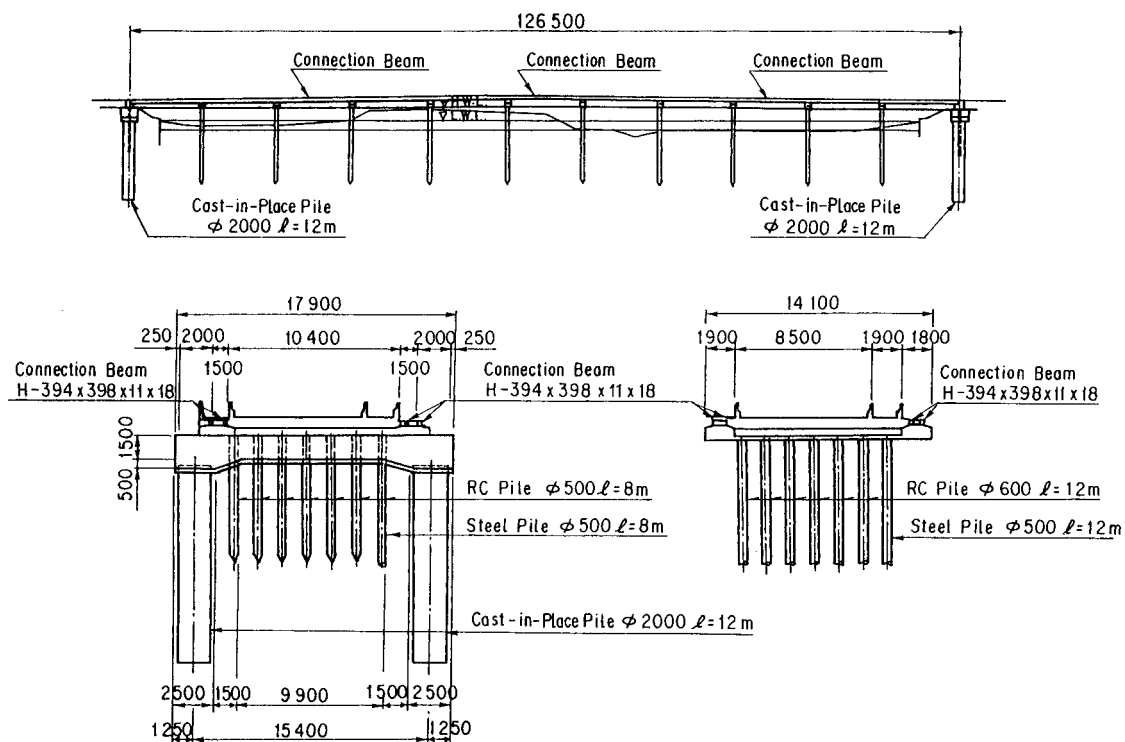


Fig. 11-51: Seismic retrofit of an 11-span simply supported bridge in liquefiable sandy soils by edge beams [Kawashima et al. (1994)]

In addition to direct retrofit of foundations, there are alternative approaches for retrofit of bridges on unstable soils. Fig. 11-51 shows a seismic retrofit of an 11-span simply-supported pre-tensioned concrete slab bridge. Used were reinforced concrete bent piles, 12 m long and 600 mm in radius, which were vulnerable to soil liquefaction.

Five approaches were clarified for retrofit; (1) retrofit all 12 substructures, (2) retrofit every other substructures (3) retrofit abutments at both ends and connect all bent piers to the abutments by two edge beams, (4) replace soils vulnerable to liquefaction, and (5) improve liquefiable soils by chemical grouting. Because options (4) and (5) were costly in spite of unreliable effectiveness, they were eliminated. Among the remaining three options, (3) was finally adopted because the cost vs. performance was most appropriate.

The bridge was designed so that all seismic lateral force of the decks in the longitudinal direction is supported by two abutments. Two edge beams were built along the bridge and the inertia force of the decks were transferred by the edge beams to the end abutments. The edge

beams were connected to the top of each bent pile by fixed bearings. The edge beams were used as pedestrian paths.

11.4.3 Shear and flexure retrofit of footings

Retrofit of columns and piers mostly results in an increase of the demand in the footings. As a consequence, enhancement of the shear and flexural capacities of the footings is required. Construction of a new footing surrounding the existing footing, as shown in Figs. 11-49 and 11-50, can accommodate this requirement. Fig. 11-52 shows examples of footing retrofit. An alternative method of shear and flexural retrofit of a footing is to introduce a prestressing force into the footing.



Fig. 11-52: Footing retrofit: (a) extension of footing and new piles (California, USA), (b) extension of footing and new piles (Japan), and (c) Overlay of footing (Japan)
(Figure available electronically on fib website; see production note on p. ii)

Shear and flexural retrofit of 2.5 m thick footings was conducted using aramid fiber reinforced plastic rods at a bridge supported by 8-12.5 m tall circular reinforced concrete columns with a radius of 3m [Kato et al. (2001)]. Flexural yield and shear failure were anticipated if the footings were subjected to compression from the piles. Extension of the footings with new piles was costly and overlaying of the footings at their tops was restricted due to space limitation for ship transportation. As a consequence, the footings were retrofitted by introducing prestressing force in the vertical and lateral directions as shown in Fig. 11-53. The vertical prestressing was required to enhance the shear capacity while the lateral prestressing was required to enhance both the shear and flexural capacities of the footings.

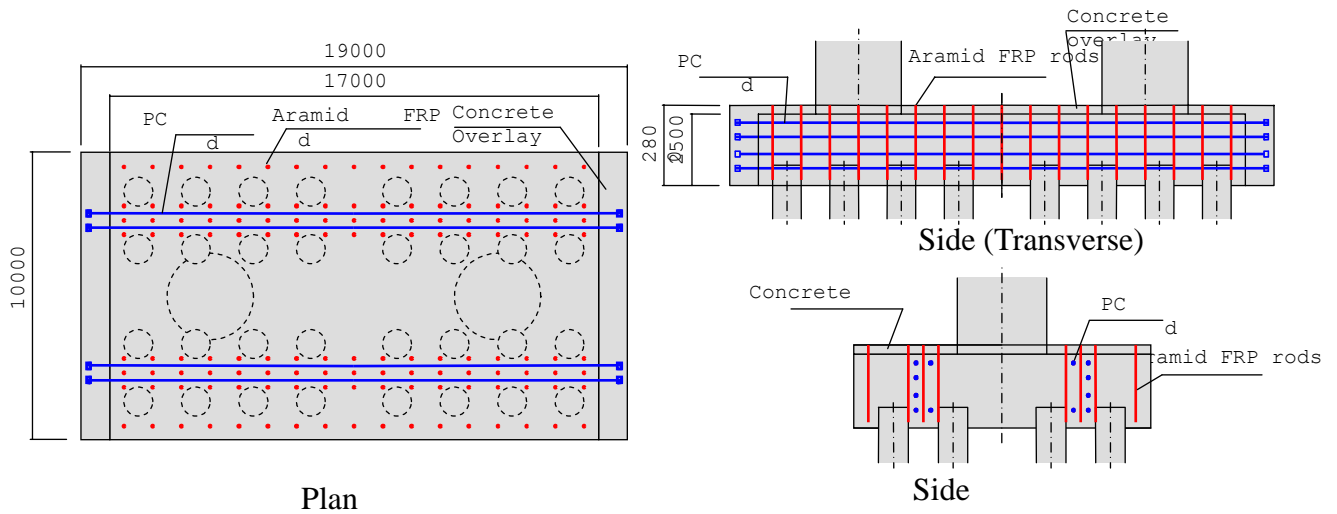


Fig. 11-53: Retrofit of a footing using aramid fiber reinforced plastics rods [Kato et al. (2001)]



Fig.11-54: Retrofit of a footing using aramid fiber reinforced plastic rods: (a) as-built bridge, (b) aramid fiber reinforced plastic rods, and (c) aramid fiber reinforced plastic rods installed in the footing in the vertical direction [courtesy of Sumitomo Mitsui Construction] (Figure available electronically on fib website; see production note on p. ii)

The lateral prestressing was provided by PC strands. On the other hand, aramid fiber reinforced plastic rods were used for the vertical prestressing. There were three reasons in the adoption of the aramid fiber rods. The first is lower elastic modulus of aramid fiber rods than PC strands. It was appropriate to stably introduce and maintain the prestressing force in the 2.5 m thick footings. The second was smaller radius of drilled holes required to set aramid fiber rods which reduced risk of cutting existing rebars by drills. The third is that aramid fiber rods are durable under sea.

Fig. 11-54 shows the setting of aramid fiber rods in the retrofit of the footings. After the foundations were dried up, holes with a radius of 60 mm were drilled 2.3 m deep from the surface of the footings. Nine aramid fiber rods with a radius of 7.4 mm were set per hole and were anchored by a special resin. Pretension force was introduced in the aramid fiber rods.

11.4.4 Cost-effective dry-up construction method

As shown in the above retrofit examples, a major obstacle for the retrofit of columns and foundations under water is the high cost involved in drying up around the foundations. Dry up is generally very costly and its cost is sometimes more or less the same with the cost for retrofit. Because foundations have to be retrofitted under the deck, only limited space is usually available which narrows the option of retrofit methods. Long construction period for construction is also a problem of the dry up method.

Several attempts are being conducted to reduce the cost and construction period of drying up of foundations. For example, prefabricated steel segments which can be easily transported at the site for assembly around the columns make the construction period and cost much reduced. Fig. 11-55 shows an example of the implementation of this method to a bridge supported by 12.2 m tall circular RC columns with a radius of 4.4m. Steel segments were transported to the site and were assembled around the columns. Construction cost at this site was nearly half compared to the standard dry-up method. The segments can be re-used at other construction sites.



Fig. 11-55: Implementation of steel segment dry-up method: (a) assembling test, and (b) assembling the segments around the foundation [courtesy of Obayashi Construction]
(Figure available electronically on fib website; see production note on p. ii)

11.4.5 Micro piles

Limited space under the deck generally makes it difficult to drive new piles for retrofit of foundations. Micro piles as shown in Fig. 11-56 are increasingly used for retrofit of foundations where only limited space is available. Various types of micro piles are available [Nishitani et al.

(2002)]. Deformed rebars are used for micro piles which carry less heavy load while steel tubes with and without deformed rebars are used for micro piles which carry heavy load. If a space of 3.5 m high and 2.5 m wide is available, micro piles as long as 50 m with a radius of 150-300 mm can be driven. Bearing capacity of micro piles can be as large as 1 MN per pile.

Fig. 11-57 shows an example of driving micro piles for retrofit of foundations [Nishitani et al. (2002)]. In addition to the space limitation, there were two other reasons for adopting the micro piles in this bridge. The first is that micro piles can be constructed without suspending the traffic of this bridge. Because this was an important bridge in the region, this condition was extremely important in the selection of this retrofit method. The other is the minimal water pollution. Any other alternative retrofit methods such as extension of footings and driving new large radius cast-in-place piles can pollute the water.

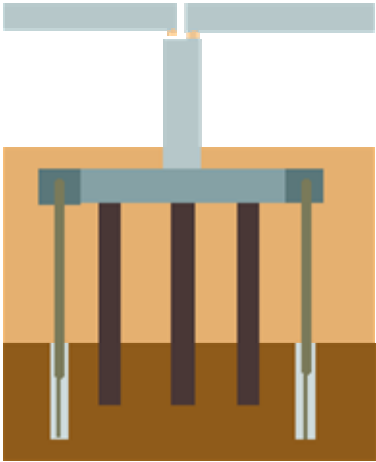


Fig. 11-56: Micro pile retrofit of pile foundation



(a)



(b)

Fig. 11-57: Micro piles for retrofit of foundations: (a) drilling and (b) micro piles after installation [Nishitani et al. (2002)]
 (Figure available electronically on fib website; see production note on p. ii)

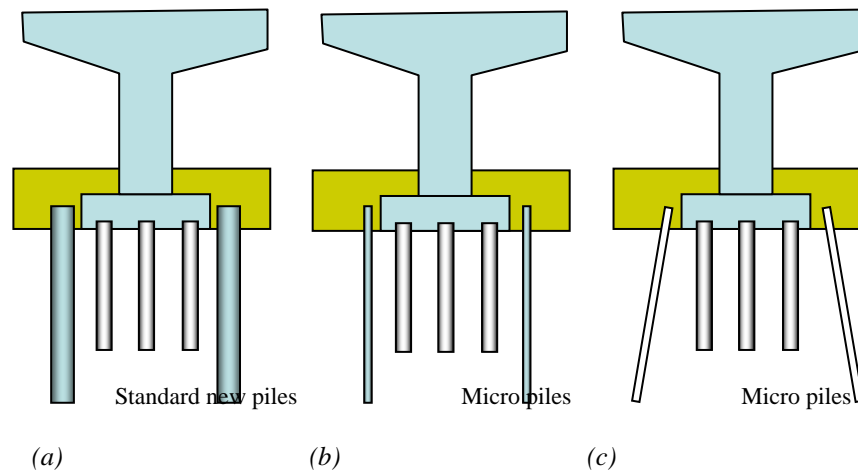


Fig. 11-58: Comparison of retrofit cost: (a) standard new pile & footing extension, (b) micro-piles (straight), and (c) micro-piles (inclined) [Nishitani et al. (2002)]

Table 11-2 shows an evaluation of construction cost and retrofit period of a bridge for the 3 options shown in Fig. 11-58. Because radius of micro piles is much smaller than the radius of cast-in-place piles, savings in cost and construction period for micro pile retrofit is acceptable.

Properties and cost	Cast-in-place piles	Straight micro piles	Inclined micro piles
Radius of piles	1000m	178mm	178mm
Number of piles	8	26	14
Length of piles	16m	21m	21m
Cost of piles relative to cast-in-place piles	100%	90%	80%
Total cost of retrofit including dry-up and footing retrofit	100%	81%	72%
Construction period relative to cast-in-place piles	100%	80%	65%

Table 11-2: Cost evaluation of retrofit using micro piles [Nishitani et al. (2002)]

11.4.6 Retrofit of abutments

Because abutments are subjected to the soil-pressure from the back-fill side to the front side, abutments are likely to be mobilized on the front side which may result in residual tilt and displacement after an earthquake. Essentially there are two types of abutment movement as shown in Fig. 11-59. One is lateral movement of an abutment at the top, resulting in tilt on the front side. This failure typically results from the dynamic earth-pressure acting on the abutment from the back-fill. Because a deck resists the abutment movement by strut action, unseating of the deck does not occur by this failure. However bearings, expansion joints and girders at the end face as well as parapet wall of the abutment suffer extensive damage. In particular, because parapet wall is generally very lightly reinforced, it suffers various levels of damage, and sometimes breaks into several segments. Similar damage occurs when the deck oscillation becomes excessively large which results to pounding of the decks with the parapet walls.

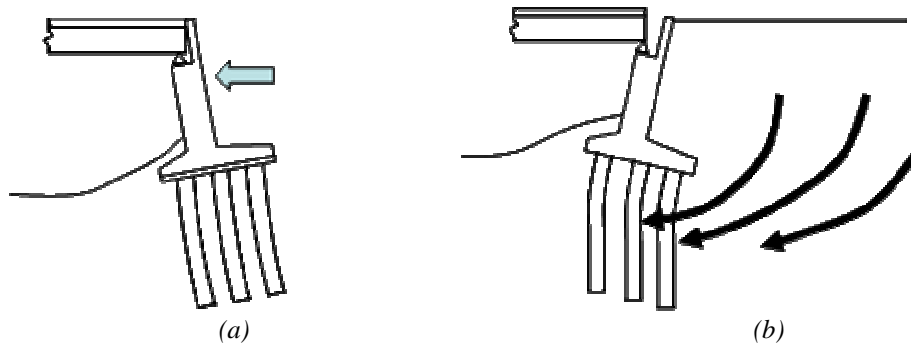


Fig. 11-59: Damage of abutments: (a) tilt in the river side, and (b) tilt in the back-fill side due to instability of ground

The other is the lateral movement of an abutment under the footing which results in tilt of the abutment to the back-fill side. This damage is likely to occur when sliding of the back-fill as well as underlying ground occurs which results from instability of underlying ground. Liquefaction of sandy soil or sliding of soft clayey soils is a typical cause of the instability of underlying ground. Bearings mostly suffer extensive damage. If the tilt of the abutment is large, unseating of the deck from the abutment occurs.

In the past, the first type damage was dominant with several examples of the second damage. Because damage which results from failure of abutment is generally restricted to the ends of the girder, expansion joints, bearings and parapet wall, it has been regarded as a secondary damage compared to the damage of columns and piers and deck. However once abutments suffer damage, the function of a bridge to carry traffic deteriorates or becomes lost and takes long period for repair.

Similar to retaining walls, the most essential retrofit of abutments is enhancement of its strength. Retrofit is conducted by enlarging the footing and constructing new piles. Enhancement of soil strength by soil replacement or cement mixing is also widely accepted for tilt resulting from instability of underlying ground. Earth-anchors are frequently used to mitigate tilt of abutments in the front direction.

A unique retrofit for tilt of an abutment in the front direction is to partly replace the back-fill with expanded polystyrene (EPS) blocks as shown in Fig. 11-60. Because use of EPS blocks reduces the dynamic earth-pressure of the back-fill to the abutment, damage of the abutment during an earthquake can be mitigated. For example, 1.75 m high and 13 m long EPS blocks replaced the back fill behind an abutment to decrease the dynamic earth-pressure.

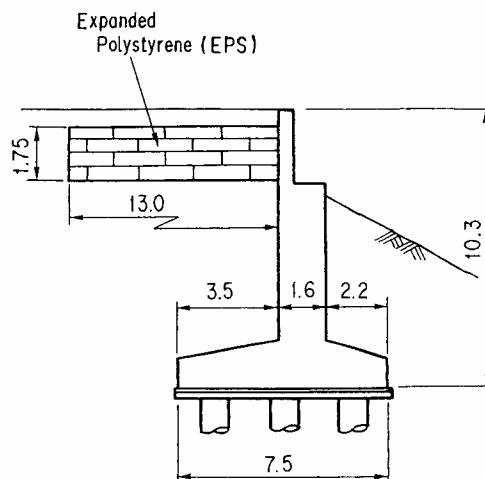


Fig. 11-60: EPS retrofit of abutments

11.5 Retrofit of superstructures

Because superstructures are designed for dead load and traffic load considering large safety factors, their direct damage which results from the seismic effect is not generally as severe as the substructures. However the members in the vicinity of the bearing and at the end of the superstructures are vulnerable. For example, Fig. 11-61 shows damage of decks at an intermediate hinge resulting to pounding.

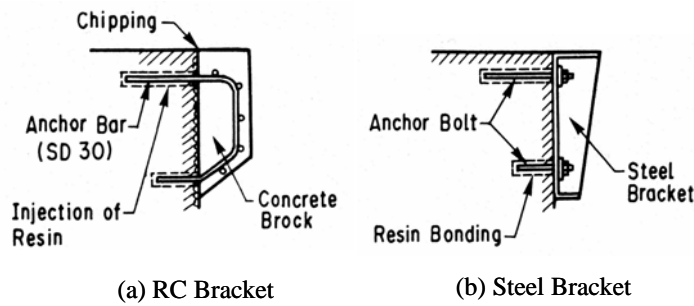
The most common retrofit for superstructures is installation of unseating prevention devices. Unseating prevention devices were first developed after the 1964 Niigata earthquake [Kawashima (1990)]. Various unseating prevention devices are now used worldwide [Yashinsky (19979)]. They may be classified into four groups; (1) extension of a seat, (2) connection of decks to substructure, (3) connection between decks at the edges, and (4) connection of decks at an intermediate hinge. There are connectors which resist only tension such as cable restrainers, and connectors which resist both tension and compression. Fig. 11-62 and Fig. 11-63 show typical unseating prevention devices.



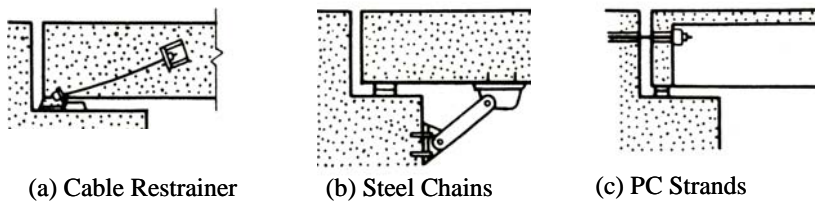
*Fig. 11-61: Damage of intermediate joint due to pounding (1994 Northridge earthquake)
(Figure available electronically on fib website; see production note on p. ii)*



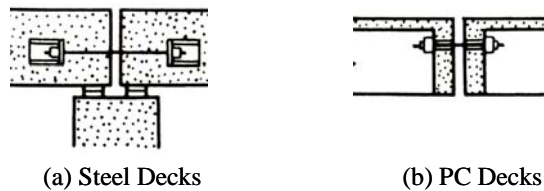
*Fig. 11-62: Installation of cable restrainers (courtesy of California Department of Transportation)
(Figure available electronically on fib website; see production note on p. ii)*



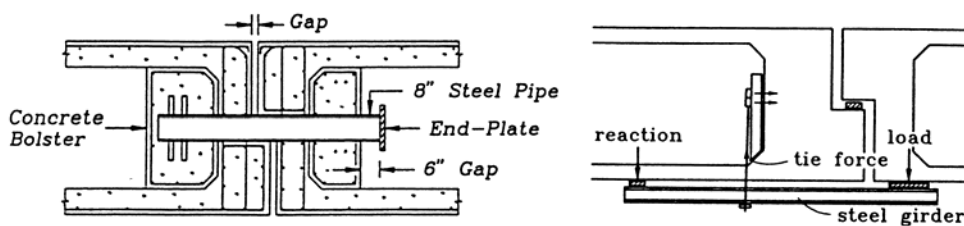
(1) Extension of Seat



(2) Connection of Deck to Substructures



(3) Connection between Decks



(4) Device for Support Following Unseating at Internal Movement Joints

Fig. 11-63: Typical unseating prevention devices [(1), (2) and (3): Kawashima et al. (1994), (4) Priestley et al. (1996)]

11.6 Retrofit using dampers and isolation

11.6.1 Introduction

Mitigation of seismic response of bridges using dampers and seismic isolation is an alternative approach to seismic retrofit. If the seismic response of a bridge can be mitigated by using dampers to a level which does not require any direct retrofit of structural components under the design ground motions, there must be tremendous benefit in the cost and period of seismic retrofit. No matter how the use of dampers and seismic isolation does not bring the bridge response to the level which does not require any seismic retrofit, benefit still exists if reasonable amount of mitigation of seismic response can be achieved. Because direct retrofit of foundations is costly, development of appropriate measures which avoid direct retrofit of foundations is expected. This can be through the use of dampers and seismic retrofit.

There are various applications of dampers and seismic isolation for seismic retrofit. Some are direct application based on the original concept of seismic isolation, and the others are indirect application. Some examples of retrofit using dampers and seismic retrofit are presented here.

11.6.2 Retrofit using seismic isolation

Seismic isolation is effective not only for new bridges but also for existing bridges. However, there are several restrictions in the implementation of isolation technologies to existing bridges. The first is the restriction on the leveling of bridge surface. Replacing the existing steel bearings with new elastomeric bearings with energy dissipating capacity such as the lead rubber bearings and high damping rubber bearings is likely to increase the leveling of the bridge. Because change of leveling of bridge surface is generally restricted, alternative approaches have to be sought. The second is the restriction on the amount of gap between adjacent decks. Because larger deck displacement which results from the period shift is needed to dissipate energy in the seismic isolation, gaps between two adjacent decks must be large enough. However this is mostly difficult in the existing bridges.

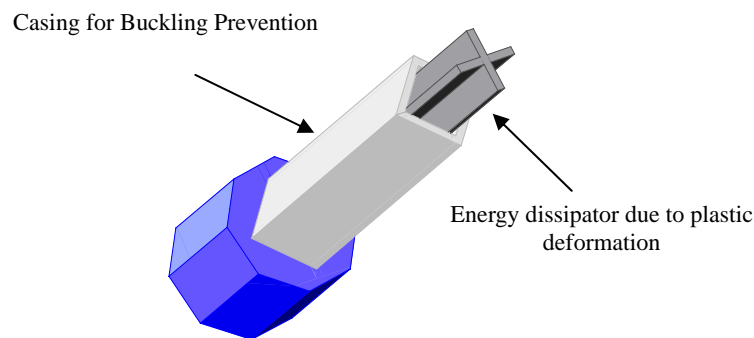


Fig. 11-64: Unbond brace damper

An analytical study on the effectiveness of seismic isolation for retrofit was conducted to three span simply supported bridges with a span length of 26m each which were subjected to the JMA Kobe ground acceleration ($PGA=0.87g$) measured during the 1995 Kobe, Japan earthquake. The bridge was supported by four 7.5-11.3 m tall reinforced concrete columns. The bridges were originally supported by steel fixed and movable bearings, but they were replaced with high damping rubber bearings. Because deck displacement increased in the seismic isolation, unbonded brace dampers as shown in Fig. 11-64 were installed at every support. The unbonded dampers consisted of an energy dissipating unit and a casing which constrained the buckling of the energy dissipating unit. As shown in Fig. 11-65, the 7.5 m tall column in the as-built bridge exhibits extensive hysteretic response while the same column shows linear response when the bridge is retrofitted using isolation and unbonded brace dampers. The peak shear force at the foundation decreases to 91% of the response of the existing bridge. The peak deck displacement of the retrofitted system is 164 mm which is 72% of the unretrofitted system peak deck displacement of 227 mm.

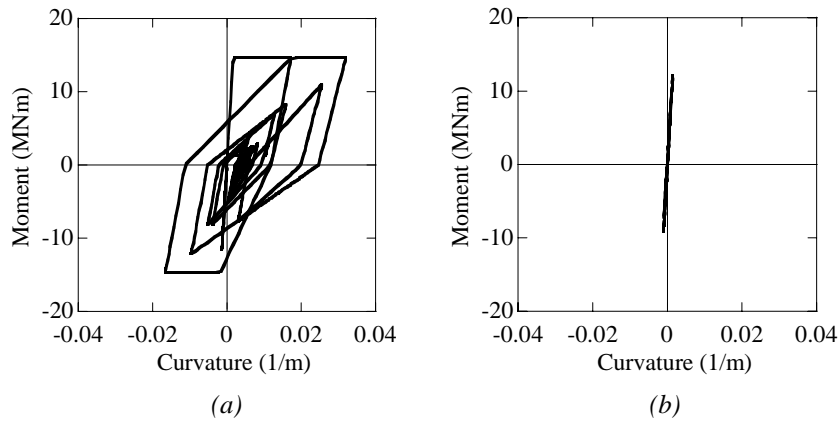


Fig. 11-65: Effect of isolation and unbonded brace dampers: (a) as-built bridge, and (b) isolated bridge with unbonded brace dampers

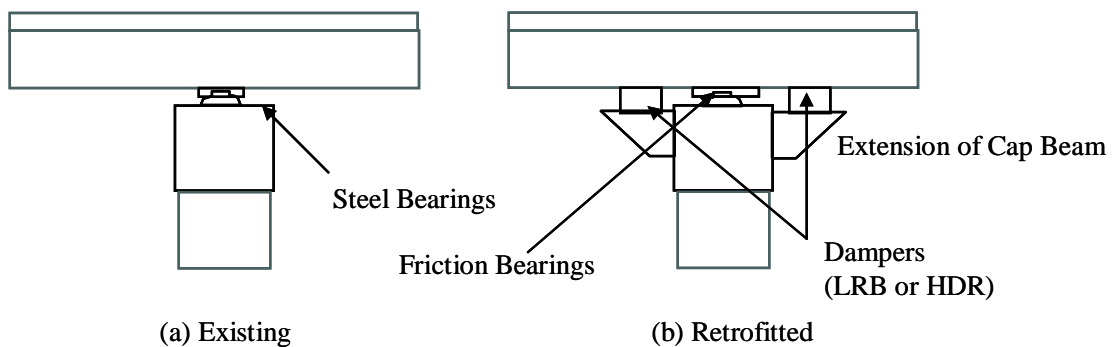


Fig. 11-66: Seismic retrofit using isolation



Fig. 11-67: Seismic retrofit using isolation: (a) installation of lead rubber bearings and sliding bearings, and (b) after retrofit (courtesy of Japan Highway Public Corporation)
(Figure available electronically on *fib* website; see production note on p. ii)

Fig. 11-66 shows an implementation of seismic isolation for retrofit of existing bridges. Because existing steel bearings were vulnerable to damage they were replaced with lead rubber bearings. The existing steel bearings were made to carry the dead weight of the superstructure by removing stoppers so that they functioned as sliding bearings. The lead rubber bearings were installed to provide the lateral restoring force and energy dissipation capability.

Several bridges supported by frame piers were retrofitted using this method. Only a part of the existing steel bearings was replaced with new sliding bearings so that the deck can move in

the longitudinal direction as shown in Fig. 11-67. After extending the seat, lead rubber bearings were installed. Fig. 11-67 b shows the bridge after retrofit.

Fig. 11-68 shows another application of lead rubber bearings to change the bridge supporting system from several-span simply-supported bridge to a multi-span continuous bridge. There are a number of simply supported bridges which have maintenance problem at expansion joints due to traffic load. Consequently, connecting adjacent decks together is beneficial for reducing maintenance cost. Because unseating of deck occurs at the ends of the deck, the connection of adjacent decks reduces the risk of unseating of a bridge during an earthquake.

Therefore existing steel fixed and movable bearings were replaced by lead rubber bearings or high damping rubber bearings as show in Fig. 11-68. Simply supported decks were tied together after removing the existing expansion joints so that the bridge responds as a multiple-span continuous bridge during an earthquake.



Fig. 11-68: Connection of decks and retrofit: (a) removal of existing steel bearings, and (b) set of new lead rubber bearing (courtesy of Hanshin Expressway Public Corporation)
(Figure available electronically on fib website; see production note on p. ii)

11.6.3 Retrofit using brace dampers

Installation of new dampers mitigates the seismic response of a bridge during an earthquake. Various dampers can be effective for this purpose. Because a bridge substructure is much larger in section and stiffer than buildings, deformation in a substructure is smaller. Therefore stiffer dampers are required for retrofit of a bridge. Brace dampers and unbonded brace dampers are increasingly used in recent years for this reason.

For example, single frame piers have been used for standard viaducts in railways including Shin-kansen (bullet train) in Japan. Because this type of viaduct suffered extensive shear and flexural failure in the past earthquakes, seismic retrofit is required. However space limitation around the viaducts sometimes does not allow retrofitting the viaducts by steel or composite materials jacketing. Consequently, a compression brace damper which consists of four steel shear panel dampers and four X-shape braces as shown in Fig. 11-69 was developed and has been successfully implemented for retrofit [Yoshida et al. (2005)]. The panel dampers were designed so that they dissipate energy once they yield in shear. When shear panels deform, the damper consisting of four shear panels, which is so designed to have an identical shape with the retrofitted viaduct frame, deforms to form a parallelogram by following the deformation of the viaduct as shown in Fig. 11-70. Consequently, anchoring of the braces to the viaduct in tension is not required because only compression force applies to the braces, which allows use of simpler connection between the braces and the viaducts.

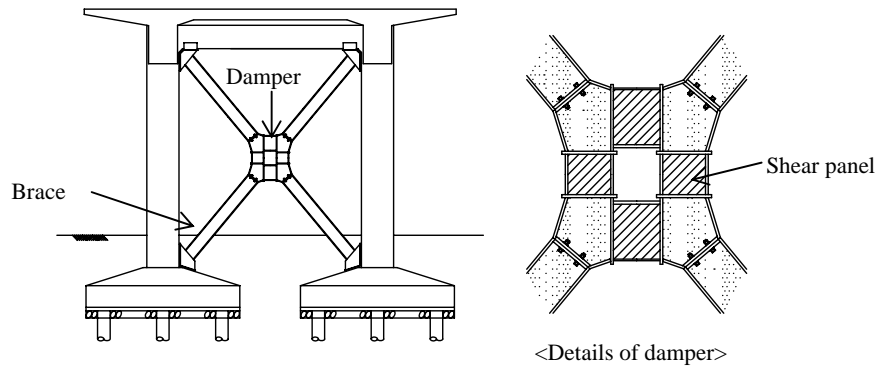


Fig.11-69: Steel brace damper system [Yoshida et al. (2005)]

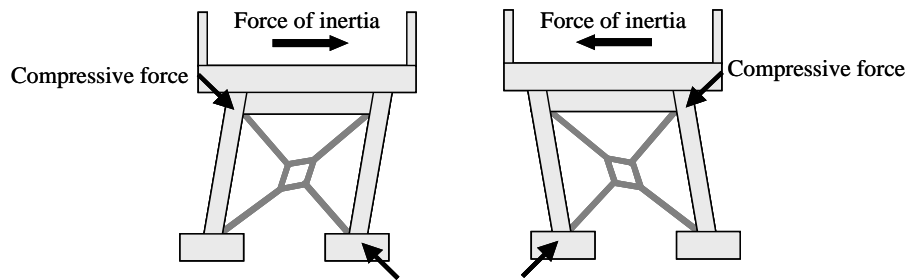


Fig. 11-70: Compression damper braces [Yoshida et al. (2005)]



Fig. 11-71: Shake table test for the effectiveness of compression damper brace [Yoshida et al. (2005)]
(Figure available electronically on fib website; see production note on p. ii)

Effectiveness of the compression brace damper was clarified using a 1/5 scale model based on a shake table test as shown in Fig. 11-71. A 5.8 m tall standard viaduct of Shinkansen was scaled down to a model, and was excited using several ground motions. Fig. 11-72 shows one of the results on the hysteretic response of the viaduct model. The models which were not accommodated with a compression brace damper suffered extensive shear failure at the columns. The damage of the columns resulted in extensively large deck displacement which is dangerous for the safety of Shinkansen. However the models which were accommodated with a compression brace damper did not suffer shear failure.

Fig. 11-73 shows an implementation of the compression brace damper to a Shinkansen viaduct in Tokyo.

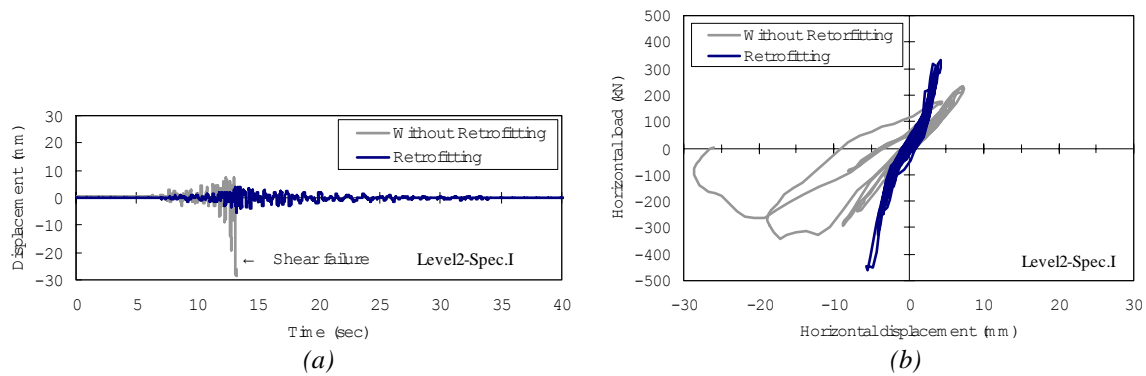


Fig.11-72: Hysteretic response of a viaduct model with and without compression brace damper: (a) displacement response in the transverse direction, and (b) lateral force vs. lateral displacement hysteresis [Yoshida et al. (2005)]



Fig. 11-73 Viaduct retrofitted using compression brace damper [Yoshida et al. (2005)]
(Figure available electronically on fib website; see production note on p. ii)

11.7 Other measures for seismic retrofit

Flexural deformation of a column is mitigated if the decks are restrained by cables as shown in Fig. 11-74. Because a part of the deck inertia force is transferred to the foundations, the moment demand of the columns decreases. Contribution of cables for transferring the deck inertia force can be varied by appropriately choosing the stiffness and strength of the cables. However because the system becomes stiff after retrofit, the shear demand is likely to increase due to the decreased natural period. Consequently this system can be implemented to mitigate the shear and flexural demand only when shear capacity of the footings is sufficient. The connections between cables and decks or foundations must be well designed so that premature failure does not occur.

Effectiveness of the cable-restrained system was clarified for the bridge presented in 10.6.2. Fig. 11-75 shows the moment vs. curvature hysteresis at the shorter column (P2). The peak ductility factor of the column in the cable-restrained system decreases to 8.1 which is 43% of the unretrofitted bridge. Thus, the cable-restrained system is effective in mitigating the flexural demand of the column. However the peak shear force of the foundation increases to 7.3 MN which is 292% of the unretrofitted system. Therefore the cable-restrained system can be implemented when the foundation has sufficient shear capacity.

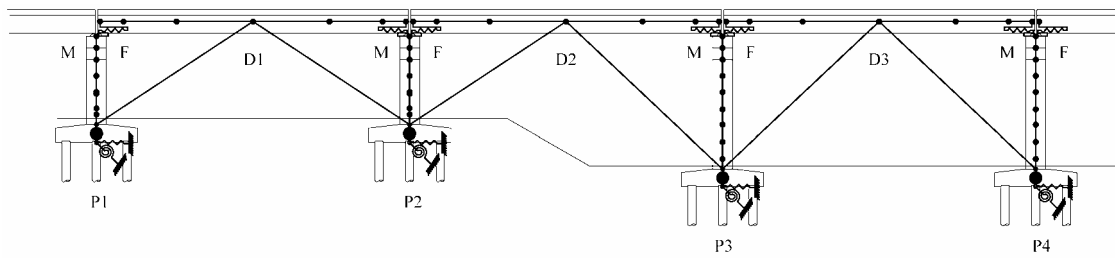


Fig. 11-74: External cable-restrained system

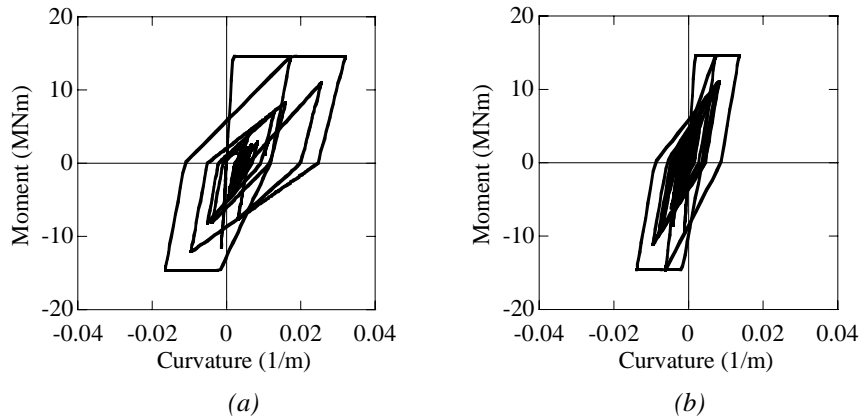


Fig. 11-75: Effect of external cable-restrained system on the plastic curvature at P2: (a) as built and (b) retrofitted by external cable-restrained system



(a)



(b)



(c)



(d)

Fig. 11-76: Retrofit of a simply supported bridge using pipe arches: (a) before retrofit, (b) after retrofit, (c) pipe arches, and (d) connection between arches and a foundation [Mizuta and Hashimoto (2001)]

(Figure available electronically on fib website; see production note on p. ii)

A 232 m long bridge consisting of 14.15 m long simply-supported decks was retrofitted by steel pipe arches which were built under the decks as shown in Fig. 11-76 [Mizuta and Hashimoto (2001)]. This arch-restrained system transfers the deck inertia force to the foundations by arches.

The effectiveness of this method was clarified for the four-span simply-supported bridge shown above. Unbonded brace dampers which are shown in Fig. 11-64 were installed between the deck and the crown of the arch at every span. The deck displacement is only 23 mm which is 10% of the as-built bridge. Consequently, the column stays in elastic range as shown in Fig. 11-77. However, similar to the cable-restrained system, the peak shear force at the foundation increases to 4.23 MN which is 169% of the as-built bridge. Therefore the arch-restrained system is effective in mitigating the moment and ductility demand of the columns if the foundations have sufficient shear capacity.

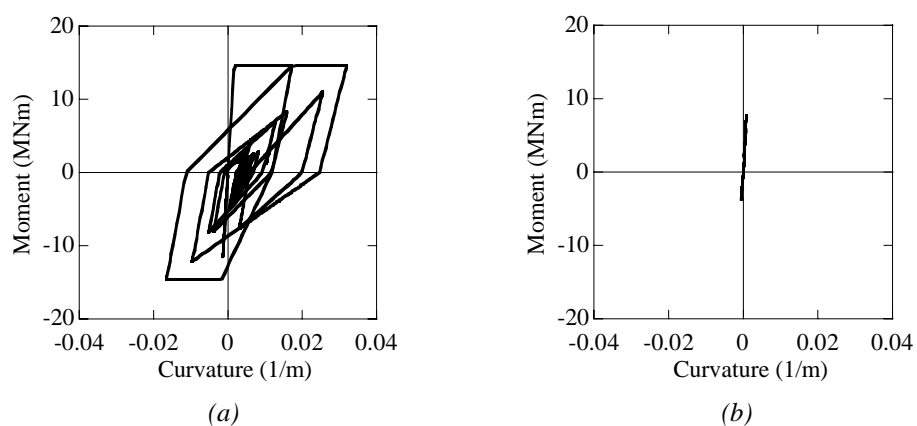


Fig. 11-77: Effect of pipe arch system: (a) as-built an (b) retrofitted by pipe arches

Acknowledgements

Invaluable materials and information were provided by many personnel and organizations. Special appreciation is conveyed to Dr. Ikeda, S. (Professor Emeritus, Yokohama National University), Drs. Unjoh, S. and Fukui, J. (Public Works Research Institute), Dr. Fujimoto, Y. (Fuji PS), Drs. Ando, N. and Fujiwara, Y. (Mitsui Sumitomo Construction), Dr. Mizuta, Y. (Professor, Kyusyu Sangyo University), Dr. Mori, T. (PS Mitsubishi), Drs. Iida, Y. and Okano, M. (Obayashi Construction), Dr. Watanabe, H. (Kawada Kensetsu), and Dr. Tabata, M. (Maeda Construction).

References

- Akimoto, T., Nakajima, H. and Kogure, F., 1990. "Seismic Strengthening of Reinforced Concrete Piers on Metropolitan Expressway," Proc. 1st US-Japan Workshop on Seismic Retrofit of Bridges, Tsukuba Science City, Japan, 280-298.
- Chai, Y.H., Priestley, N.M.J., and Seible, F., 1990. "Retrofit of Bridge Columns for Enhanced Seismic Performance," Proc. First US-Japan Workshop on Seismic Retrofit of Bridges, Tsukuba Science City, Japan, 321-340,
- Iwata, S., Otaki, K. and Iemura, H., 2001, "Experimental Study on the Seismic Retrofit and Repair of Large-scale Reinforced Concrete Columns," 26th Earthquake Engineering Symposium, JSCE, 1393-1396.

- Kato, S., Sato, H., Nakai, H. and Fujita, M., 2001. "Seismic Retrofit of Oga Bridge Using Aramid Fiber Reinforced Plastics," *Civil Engineering Construction*, 17-22.
- Kawashima, K., 1990. "Seismic Design, Seismic Strengthening and Repair of Highway Bridges in Japan," *Proc. 1st US-Japan Workshop on Seismic Retrofit of Bridges*, Tsukuba Science City, Japan, 3-61.
- Kawashima, K., Unjoh, S. and Mukai, H., 1994. "Seismic Strengthening of Highway Bridges," *2nd US-Japan Workshop on Seismic Retrofit of Bridges*, Earthquake Engineering Research Center, University of California, Berkeley, USA, Report No. UCB/EERC 97/09, 1-36.
- Kawashima, K., Hosotani, M. and Yoneda, K., 2000. "Carbon Fiber Sheet Retrofit of Reinforced Concrete Bridge Piers," *Proc. International Workshop on Annual Commemoration of Chi-Chi Earthquake, Vol. II-Technical Aspect*, National Center for Research on Earthquake Engineering, Taipei, Taiwan, R. O. C., 124-135.
- Matsuda, T., Sato, T., Fujiwara, H. and Higashida, N., 1990. "Effect of Carbon Fiber Reinforcement as Strengthening Measure for Reinforced Concrete Bridge Piers," *Proc. 1st US-Japan Workshop on Seismic Retrofit of Bridges*, Tsukuba Science City, Japan, 356-374.
- Mizuta, Y. and Hashimoto, A., 2001. "A Reinforcing Method for Earthquake-Proof of Bridge with Many Spans and High Piers Using the Pipe Arches," *Journal of Structural Engineering*, Japan Society of Civil Engineers, 47A, 1063-1074.
- Nishitani, M., Umebara, T. and Fukui, J., 2002. "Development of Seismic Retrofitting Technologies for Existing Foundations," *Proc. 18th US-Japan Bridge Engineering Workshop, Panel on Wind and Seismic Effects*, UJNR, Vol. 18, 284-297.
- Ogata, T. and Osada, K., 1999. "Seismic Retrofitting of Expressway Bridges," *Cement and Concrete Composites*, UK, Vol. 19, 185-192.
- Osada, K., Yamaguchi, T. and Ikeda, S., 1999. "Seismic Performance and Strengthening of Hollow Circular RC Piers Having Reinforced Cut-off Planes and Variable Wall Thickness," *Concrete Res. and Tech.*, Vol. 10, No. 1, 13-24.
- Okamoto, T., Tanigaki, M., Oda, M. and Asakura, A., 1994. "Shear Strengthening of Existing Reinforced Concrete Column by Winding with Aramid Fiber," *Proc. 2nd US-Japan Workshop on Seismic Retrofit of Bridges*, Earthquake Engineering Research Center, University of California, Berkeley, USA, Report No. UCB/EERC 97/09, 337-344.
- Tamaoki, K., Wada, N., Kawakami, T., Sasaki, K. and Fujiwara, Y., 1996. "Experimental Study on the Seismic Retrofit of Wall RC Piers," *51st Annual Convention*, Japan Society of Civil Engineers, Tokyo, Japan, 1064-1065.
- Unjoh, S., Terayama, T., Adachi, Y. and Hoshikuma, J., 1997. "Seismic Retrofit of Existing Highway Bridges in Japan," *Proc. 29th Joint Meeting, U.S.-Japan Panel on Wind and Seismic Effects*, UJNR, 161-178.
- Priestley, M.J.N, Seible, F. and Anderson, D.L., 1993a. "Proof Test of a Retrofit Concept for the San Francisco Double-Deck Viaducts, Part I: Design Concept, Details and Model," *ACI Structural Journal*, Vol. 90, No. 5, 467-479.
- Priestley, M.J.N, Seible, F. and Anderson, D.L., 1993b. "Proof Test of a Retrofit Concept for the San Francisco Double-Deck Viaducts, Part II: Test Details and Results," *ACI Structural Journal*, Vol. 90, No. 6, 616-631.
- Priestley, N.M.J., Seible, F., and Calvi, M., 1996. "Seismic Design and Retrofit of Bridges," John Wiley & Sons, New York.
- Watanabe, H., 2002. "Precast Concrete Segment Jacket for Seismic Retrofit of Columns Under Water," *Journal of Japan Society of Civil Engineers*, Tokyo Japan, Vol. 87, No. 12, 50-52.
- Xiao, Y., Priestley, N.M.J. and Seible, F., 1994. "Evaluation of Retrofitting of Existing Bridge Footing," *Proc. 2nd US-Japan Workshop on Seismic Retrofit of Bridges*, Earthquake Engineering Research Center, University of California, Berkeley, USA, Report No. UCB/EERC 97/09, 287-300.

- Yashinsky, M., 1997. "Caltran's Bridge Restrainer Retrofit Program," Proc. 2nd US-Japan Workshop on Seismic Retrofit of Bridges, Earthquake Engineering Research Center, University of California, Berkeley, USA, Report No. UCB/EERC 97/09, 39-61.
- Yoshida, K., Kita., N., Okano, M. and Seki, M., 2005. "Shaking Table Tests on Seismic Performance of Railway Bridges with Compression Type Braces," AESE, Nagoya, Japan, 481-488.